Modern Approaches in Solid Earth Sciences

Trong-Hoa Tran · Gleb V. Polyakov
Tuan-Anh Tran · Alexander S. Borisenko
Andrey E. Izokh · Pavel A. Balykin
Thi-Phuong Ngo · Thi-Dung Pham

Intraplate Magmatism and Metallogeny of North Vietnam

Springer

Modern Approaches in Solid Earth Sciences

Volume 11

More information about this series at http://www.springer.com/series/7377

Trong-Hoa Tran • Gleb V. Polyakov
Tuan-Anh Tran • Alexander S. Borisenko
Andrey E. Izokh • Pavel A. Balykin
Thi-Phuong Ngo • Thi-Dung Pham

Intraplate Magmatism and Metallogeny of North Vietnam

Springer

Trong-Hoa Tran
Vietnam Academy of Science
and Technology
Institute of Geological Sciences
Hanoi, Vietnam

Tuan-Anh Tran
Vietnam Academy of Science
and Technology
Institute of Geological Sciences
Hanoi, Vietnam

Andrey E. Izokh
Russian Academy of Science
Institute of Geology and Mineralogy
Novosibirsk, Russia

Thi-Phuong Ngo
Vietnam Academy of Science
and Technology
Institute of Geological Sciences
Hanoi, Vietnam

Gleb V. Polyakov
Russian Academy of Science
Institute of Geology and Mineralogy
Novosibirsk, Russia

Alexander S. Borisenko
Russian Academy of Science
Institute of Geology and Mineralogy
Novosibirsk, Russia

Pavel A. Balykin (deceased)

Thi-Dung Pham
Vietnam Academy of Science
and Technology
Institute of Geological Sciences
Hanoi, Vietnam

Responsible Series Editor: F. Pirajno

This is a revised and updated version of the book in Vietnamese "Intraplate Magmatism and Metallogeny of North Vietnam" by the same authors, published by the Publishing House for Science and Technology for the Vietnam Academy of Science and Technology (VAST) in the series of monographs on Vietnam Natural Resources and Ecology in 2010 (no ISBN is available).

ISSN 1876-1682 ISSN 1876-1690 (electronic)
Modern Approaches in Solid Earth Sciences
ISBN 978-3-319-25233-9 ISBN 978-3-319-25235-3 (eBook)
DOI 10.1007/978-3-319-25235-3

Library of Congress Control Number: 2015953432

Springer Cham Heidelberg New York Dordrecht London

Printed on acid-free paper

Springer International Publishing AG Switzerland is part of Springer Science+Business Media (www.springer.com)

Preface

The study of intraplate magmatism with the aim to reconstruct geodynamic settings and estimate related endogenic mineralization has significant scientific and practical meanings. These allow to consider the role of deep mantle and mantle – lithosphere interaction processes in the formation of large-scaled intraplate rift systems, collision and shear zones, and their associated magma – ore formations having high potentials of gold, gold-copper, precious platinum group metal (PGM), rare earth and radioactive metals (REE–U–Th), and gemstones (ruby, sapphire, etc.).

The clearest expression of intraplate magmatism is mantle plume-induced large igneous provinces (LIP) in Asia during the Permian–Triassic (Dobresov 1997; Nikishin et al. 2002). The mantle plume-related magmatic activities were widely developed in the Asian continent in rift and trap environments forming the Siberian craton and Emeishan LIP, which have been well studied. However, intraplate magmatic activities during the period of Permian–Triassic in Viet Nam have not been detailedly studied with focus on their identification and role in southeastern Asian geodynamic evolution as a whole, as well as their associated mineralization.

This monograph is a combined report of petrological and metallogenic studies of late Paleozoic–early Mesozoic and Cenozoic magmatism in northern Viet Nam in the past several decades by the authors through collaboration between the Institute of Geological Sciences, Vietnam Academy of Science and Technology, and the Institute of Geology and Mineralogy, Siberian Branch of the Russian Academy of Sciences, on magma–metallogeny. Two intraplate magmatic–metallogenic stages in northern Vietnam are being introduced in this monograph; these were associated with two important tectonic events in the evolution of the southeastern Asian continent including Emeishan-type mantle plume during ca. 260–250 Ma and India-Eurasian collision ca. 60–55 Ma.

The Emeishan mantle plume-related impact produced magmas which occurred in wide areas in western and southern margins of the Yangtze craton (China) forming a series of mafic–ultramafic and felsic along with alkaline felsic associations in the craton's peripheral terrains (e.g., Cathaysian multi-cycle folded belt) including the northeastern terrain of Vietnam. Depending on particular structurally geological

positions within the then-northern Viet Nam regional structure – tectonic framework and the geochemistry according to the lithospheric mantle source – the mantle dynamics and nature of mantle–lithosphere interaction of the Permian–Triassic magmatism formed a number of chemically diversified magmatic–metallogenic associations in northern Viet Nam. Among the ore minerals, clearly high potential associations include Cu–Ni–PGM, Ti–Fe–V, Cu–Au, Sn–Pb–Zn–Ag, Sb–Hg–(Au), and others that occurred in industry-rated ore fields that are being exploited to serve the nation's needs. Among the Permian–Triassic magmatic formations, this monograph will focus only on volcano-plutonic mafic–ultramafic and felsic magmas in the Song Da–Song Hien rift zone and Song Chay anticlinoria. With the new understanding of mantle plume and its role in generating mantle and lithospheric mantle magmatic melts, the Permian–Triassic volcano-plutonic mafic–ultramafic–felsic and alkaline mafic–felsic associations and accompanying metallogeny in northern Viet Nam may be explained by the impact of the Emeishan mantle plume on the lithospheric mantle under different lithospheric structures in southwestern and southern margins of the Yangtze craton. This is the first time that genetic relation between the magmatism and mineralization has been proven using geochemical and isotopic data.

The India-Eurasian collision in the Cenozoic is considered as the major force that changed the form in the southeast Asian tectonic map, forming intercontinental shear zones such as the Ailao Shan–Red River. Along both sides of the shear zone, there are a series of intraplate extended belts containing typical Mediterranean-type mafic and felsic magmatic associations and their accompanying ore mineralization of Cu–Au, Cu–Mo–Au porphyry, REE–Th–U, and others, starting from Tibet to Vietnam. This is also the first time that the formation of Cenozoic magma–metallogenic associations is associated with the evolution of the shear zone.

The monograph contains nine chapters included in three parts: Part I introduces general regional geological structures in northern Viet Nam; Part II is about Permian–Triassic magmatic–metallogenic associations; and Part III dedicates to Cenozoic (Paleogene) magmatic ore mineralization formations, corresponding to the abovementioned geological events. Each chapter describes geological features, principles of dividing magmatic associations in different structures, and compositional characteristics, including geochemical, mineralogical, isotopic, and chronologic compositions analyzed using the latest analyzing methods in world well-known laboratories. In explaining formation conditions of magmatic ore associations and related geodynamic settings, the authors have employed with selection the concept of plate tectonics and plume-related kinematics from the world's most recent geological literature. Many of the research results being introduced in this monograph have been reported in international and domestic reputed journals, as well as appeared in a number of master's and doctorate theses. Besides, the monograph also contains newly achieved results that have not been reported elsewhere.

Materials being introduced in this monograph may be useful for both domestic and international geologists in exploring the history of geological and metallogenic evolution in Vietnam as an important marginal region of the Asian continent. One of the most practical contributions offered by the monograph is providing new criteria on prediction and potential evaluation of magmatic metallogenesis,

directly helping in exploring and finding new and valuable mineral resources for national use. The introduced monograph is useful for science and technology projects and may be used as university teaching materials in the field of petrology and metallogeny.

After the first monograph entitled *Permian–Triassic mafic and ultramafic magmatic formations in Northern Vietnam* published in 1996 in the occasion of the 20th Anniversary of the Institute of Geological Sciences, Vietnam Academy of Science and Technology (1976–1996), this monograph is the second being introduced as a result of a 25-year Vietnam–Russia research collaboration (1984–2009).

During the preparation of the monograph, the authors have constantly received support from the leaders of Vietnam Academy of Science and Technology (VAST), Institute of Geological Sciences (IGS), and Science and Technology Publishing House. Discussions with and suggestions by colleagues helped improve the contents of the monograph. Contributors from the Magma Department (IGS), direct or indirect, include Drs. Hoang Huu Thanh, Vu Van Van, Bui An Nien, Tran Quoc Hung, Phan Luu Anh, and other researchers including Tran Viet Anh, Hoang Viet Hang, and Tran Hong Lam; international colleagues from the Russian Institute of Geology and Mineralogy (Siberian Branch, Russian Academy of Science) include Petrov V.G., Petrova T.I., Ponomarchuc V.A., Gaskov I.V., Shelepaev R., Telesev A.E., and many others. Many of the geochemical and isotopic data being introduced here were analyzed at the National Taiwan University and Institute of Earth Sciences, Academia Sinica (Taiwan) thank to Drs. Chung S-L., Lo C-H., and Lan C.Y.

All are gratefully acknowledged.

This monograph is a result of the International Collaboration Research Protocol entitled "Investigation of origin and formation conditions of magma – metallogenic formations having high potentials of Pt, Au and Ti-V in Vietnam" (2007–2009) and Basic Research project coded 70.87.06 "Geodynamics, origin and formation conditions of magmatic – metallogenic formations of high potentials of Cu-Au, Cu-Mo-Au porphyry in Vietnam" with support from the Viet Nam–Russian research collaboration fund № 08-05-90304Viet_a (2008–2009) and Basic Research Project "Permian – Triassic magmatism and metallogeny of Tu Le and Phan Si Pang structures in relation to mantle plume" of the National Foundation for Science and Technology Development (NAFOSTED) coded 105.06.73.09.

Last, regardless of our best effort, there must be shortcomings in the monograph's preparation and edition, the authors kindly appeal to readers for suggestions in order to improve the quality of the monograph.

Hanoi, Vietnam — Trong-Hoa Tran
Novosibirsk, Russia — Gleb V. Polyakov
Hanoi, Vietnam — Tuan-Anh Tran
Novosibirsk, Russia — Alexander S. Borisenko
Novosibirsk, Russia — Andrey E. Izokh
Novosibirsk, Russia — Pavel A. Balykin
Hanoi, Vietnam — Thi-Phuong Ngo
Hanoi, Vietnam — Thi-Dung Pham

Contents

Part I
Structure: Tectonics and Magmatic Activities in Northern Vietnam

Chapter 1
An Overview on the Structures, Tectonics and Magmatic Activities in North Vietnam

Abstract Reconstruction of paleo-geodynamic framework of Vietnam in the relation to major tectonic events in southeast Asia reveals that Paleozoic structures in Northern Vietnam (from northeastern Song Ma suture zone northward) were developed in the southern and southeastern margins of the Yangtze Block. Northern Vietnam is divided into two major folding systems, based on their positions relative to the Song Hong fault zone.

The most important structural elements in northern Vietnam are Precambrian massifs including the Phan Si Pan uplift, the Late Paleozoic – Early Mesozoic Song Da – Tu Le continental rift. Many of the volcanic basins previously determined as Mesozoic have been added to Paleozoic Song Da rift volcanic groups as newly evidence of Permian – Triassic age from sedimentary, volcanic and subvolcanic formations in the Tu Le Basin coming to light. Meanwhile several major tectonic units are classified in Northeastern Vietnam. These include the Song Chay dome – outcrop of Yangtze massif's basement that was reactivated during the Permian – Triassic, and the surrounding Paleozoic folding structures such as Lo Gam and Phu Ngu. The latter are viewed as various erosion terraces of the Song Chay dome. The Paleozoic structures are surrounded by the Masozoic Song Hien and An Chau basins, and by the circle-shaped Yen Minh – Phu Luong fault zone.

1.1 Vietnam in the Southeast Asian Tectonic Framework

History of SE Asian geological formation and evolution is related to a number of complex geological events, starting from the Archean to the present time. In the present tectonic framework Vietnam belongs to two major geo-blocks, e.g., the Indochina in the southwest and North Vietnam – South China block in the northeast (Tung and Tri 1992) (Fig. 1.1). The two blocks are divided by the Ailao Shan – Red River Shear Zone (RRSZ) (e.g. Tapponnier et al. 1982).

The RRSZ, originating in Tibet (China) running to the continental shelf of the Vietnam East Sea with more than 1000 km. There are four narrow high-grade metamorphic belts located within the ARRSZ. One is the Day Nui Con Voi (DNCV) in Vietnam, the other three including Ailao Shan, Diancang Shan and Xuelong are in Yunnan, China (Leloup et al. 1995; Harrison et al. 1996). The DNCV belt is less

T.-H. Tran et al., *Intraplate Magmatism and Metallogeny of North Vietnam*,
Modern Approaches in Solid Earth Sciences 11,
DOI 10.1007/978-3-319-25235-3_1

than 10 km wide and more than 250 km long, spreading from Lao Cai to Viet Tri province. To the northwest the belt gradually join the Ailao Shan fault zone, while in the south the DNCV is covered by Red River Neogene – Quaternary sediments. The DNCV fault zone is divided from the other northern Vietnam structures by the Song Hong and Song Chay deep fault systems. Both fault systems show a steep, northeasterly dip angle (ca. 70°), and reach down to depths between 30 and 50 km. Proterozoic is the oldest age determined based on the levels of metamorphism (such as almandine – amphibolite – granulite facies) in the Song Hong fault zone (Geological Map of Northern Vietnam 1967, 1977, 1989). However, recent studies have shown that metamorphic and deformed activities in the Song Hong fault zone occurred in the Paleogene, mostly Oligocene (Tapponnier et al. 1990). The metamorphic complexes include amphibole-bearing gneiss, kyanite-schist, surrounded by various mafic and ultramafic bodies. The RRSZ plays an important role in the history of Southeast Asian tectonics. Recent radiometric age data have shown that cooling time of anatexis melts in the regional metamorphic complexes occurred between 24 and 26 Ma (Schaerer and Tapponnier 1990, 1994), most in agreement with the timing of India – Eurasian collision induced continental extrusion (e.g. Tapponnier et al. 1990). The magnitude of extrusion was estimated between 330 ± 60 km (e.g. Lacassin and Leloup 1993) or 500 and 700 km (after Tapponnier et al. 1990; Leloup et al. 1995).

Another important tectonic structure in the northern Vietnam geology is the Song Ma suture zone, that is named for the presence of Paleozoic ophiolite association (Tran Van Tri 1977; Bach 1986). Many researchers believe that the Indochina and

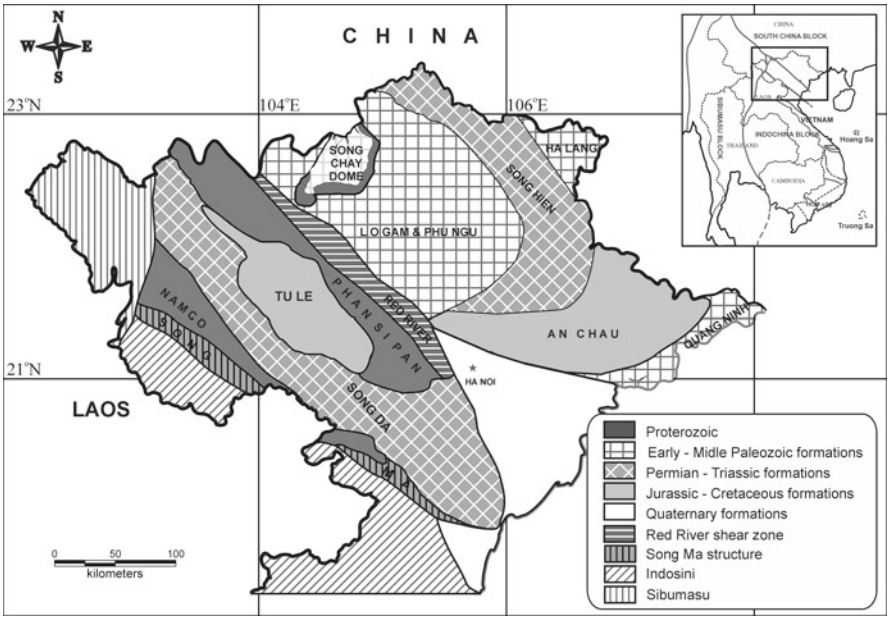

Fig. 1.1 Distribution scheme of major tectonic structures in northern Vietnam

South China (the Yangtze basement and surrounding folded structures) blocks were amalgamated during the late Paleozoic that led to the formation of Truong Son Indosinian orogeny that spans about 1000 km along the margin of Indochina block from the border between China and Vietnam in the north to the Kontum massif in south Central Vietnam (Fig. 1.1). Within this orogeny belt several magmatic types have been identified such as ophiolitic, orogeny, post-orogeny comprising pluton-volcanic magmatic associations; therefore, this structure is termed as Truong Son pluton-volcanic belt (Hoa et al. 2008). To the southeast the orogenic belt is detached by a Mesozoic pluton-volcanic belt that is developed in the northeast direction and termed as Dalat segment (Thi 1995; Hoa et al. 2005). The formation and evolution of the Dalat segment was thought to relate to the subduction of Pacific plate under the Asian continent (Tung and Tri 1992; Bao 2001; Hoa et al. 2005).

1.2 Major Structural Factors in Northern Vietnam

Reconstruction of paleo-geodynamic framework of Vietnam in the relation to major tectonic events in southeast Asia reveals that Paleozoic structures in Northern Vietnam (from northeastern Song Ma suture zone northward) were developed in the southern and southeastern margins of the Yangtze Block. Northern Vietnam is divided into two major folding systems, based on their positions relative to the Song Hong fault zone, being identified as Northwest Northeast. In turn, in each folding system a series of structural units are identified such as facies, zones (Dovjikov 1965; Tri 1977) or terrains (Bach 2001).

The most important structural elements in northern Vietnam are Precambrian massifs including the Phan Si Pan uplift, the Late Paleozoic – Early Mesozoic Song Da – Tu Le continental rift (Fig. 1.1). Many of the volcanic basins previously determined as Mesozoic have been added to Paleozoic Song Da rift volcanic groups as newly evidence of Permian – Triassic age from sedimentary, volcanic and subvolcanic formations in the Tu Le Basin coming to light. This will be described in detail in the subsequent chapters. Meanwhile several major tectonic units are classified in Northeastern Vietnam. These include the Song Chay dome – outcrop of Yangtze massif's basement that was reactivated during the Permian – Triassic, and the surrounding Paleozoic folding structures such as Lo Gam and Phu Ngu. The latter are viewed as various erosion terraces of the Song Chay dome. The Paleozoic structures are surrounded by the Masozoic Song Hien and An Chau basins, and by the circle-shaped Yen Minh – Phu Luong fault zone.

A brief description of the major structures listed above and embedded intraplate magmatic associations, which are the focus of this monograph, is given below.

The Phan Si Pan Uplift block is an elongated lens-shaped of about 200 km running in the north-southeast direction, from northern tip of Lao Cai province to the northern margin of Song Da structure in Hoa Binh province. To the west the block is separated from the Song Da – Tu Le rift by a system of regional faults, while in the east, is bordered by the RRSZ. The Phan Si Pan is consisted mostly of

Precambrian and Paleozoic metamorphosed sediments and various plutonic associations having diversified compositions and occurrence ages. These include Archean calc-alkaline granitoids such as Ca Vinh type (Lan et al. 2001; Nam 2001), Meso- Proterozoic metagabro of Bao Ha type (Hoa et al.1999a), high K-granitoids of Xom Giau type and calc-Neoproterozoic alkaline granitoids of Po Sen type (Nam 2003). Permian alkaline granitoids such as Muong Hum, Phu Sa Phin and Phan Si Pan complexes and Cenozoic Ye Yen Sun granitoids, respectively, are widely spread elsewhere in the block.

Permian – Triassic Song Da – Tu Le continental rift system is a trough-like structure containing terrigenous – volcanic formations. The rift system extends over 300 km long (within Vietnam) and more than 100 km wide. To the west, the Song Da – Tu Le rift is circled by the Nam Co platform system West Bac Bo Paleozoic intracontinental orogenic belt showing outcrops of Precambrian rocks (Tri and Khuc 2011); to the east is bordered by the Phan Si Pan uplift block. There are a number of mafic pluton- volcanic associations of tholeiitic and sub-alkaline types whose geochemistry is closely similar to continental rifting-induced magmas such as East African, Emeishan (China) and Siberian trap basalts. Subalkaline and alkaline felsic pluton – volcanic associations are also widely occurred, especially, in the Tu Le basin. The formation and evolution Song Da – Tu Le continental rift during the Permian – Triassic contemporaneous with the amalgamation of Indochina and Vietnam – South China paleo-continental blocks are viewed as an important geological event. However, the nature of tectonic setting of the Song Da – Tu Le structure remains controversial. Those hypothetical settings include inner-continental rift (Tri 1977; Gatinsky 1986; Hoa 1995, 1998, 2002; Polyakov et al. 1996), ophiolitic belt (Chuong 1996, 2001), and newly formed oceanic crust (Bach and Thang 1995). Discussions and explanations in Chap. 2, Part II of this work may help clarify this matter.

The Song Chay metamorphic dome located in northeastern Vietnam contains Precambrian fragments of Yangtze basement's origin that were involved in early Paleozoic tectonic activities, especially in the Triassic (e.g. 236 Ma) (after Maluski et al. 2001). U – Pb ages determined for gneiss, crystalline schist and migmatite yielded values between 2500 Ma and 1000 Ma (Tri 1977). On the other hand, protolite age of some metamorphic rocks gave a value of 428 ± 5 Ma (Leloup et al. 1999) contemporaneous with the formation age of granite (Ordovician) in the Song Chay block (Ponomareva et al. 1997). U – Pb (SHRIMP) age dating on zircon in lherzolite and gabbrodolerite (266–262 Ma) in the Suoi Cun block (Song Hien belt) showed evidence of 2900 Ma, 1000 Ma and, especially, 480–460 Ma evolution (Hoa et al. 2008). This suggests that the formation and development of geological structures in northeastern Vietnam are closely related to the formation and evolution of marginal terrains of Yangtze basement.

Lo Gam belt, located to the northeast of RRSZ along the southeastern margin of Song Chay done, is comprised mainly of early- middle Paleozoic sedimentary – metamorphic formations, being penetrated by Ordovician – Silurian high-Al granite of the Song Chay complex (Ponomareva et al. 1997). Magmatic activities in this belt are considered as complicated with the earliest occurrence comprising ophiolite-type mafic and ultramafic associations in the southern margin of Song Chay dome.

The magmatic associations also include strongly- serpentinized dunite and harzburgite of the Nam But, and amphibole gabbro, gabbro-dolerite of the Bach Sa complex (Xuyen 2001). Study of actinolite – epidote – chlorite assemblages in an early Cambrian sedimentary – volcanic formation in Ha Giang complex had led several researchers to believe that they are metabasalt belonged to an ophiolite association (Tri, personal comm.). Besides, according to Lien et al. (2005), meta-andesite outcrops elsewhere along a cross-section toward Hoang Su Phi. Within the Lo Gam belt, to the east of Song Chay dome, observed are Permian – Triassic gabbo – syenite plutons with major compositions being monsogabbro, monsogabbro-dolerite. These magmas show a close temporal, spatial as well as geochemical relationship with the syenite; in turn, the this syenite has genetic relation with the gabbro (Hoa et al. 1999b, 2004b). To the east of Lo Gam belt well-developed are trachy-rhyolite, rhyolite and granosyenite magmas having typical intraplate geochemical characteristics (T.T. Hoa unpublished). Permian age of these rocks were determined by U-Pb, LA-ICP-MS for zircon (Tri, personal comm.). High-Al granite is widely observed in the Phia Bioc complex, having a close spatial connection with the above mentioned gabbro- syenite plutons. This high-Al granite was previously determined as Late Triassic (Dovjikov 1965; Tri 1977; Thuc and Trung 1965); however, latest radiometric age dating of a high-Al granite in the Tam Tao pluton of Phia Bioc complex yielded a value of 250 ± 0.5 Ma (Permian) (Anh and Hang 2005; Hoa et al. 2008), suggesting that the granite may be contemporaneous with the above Permian – Triassic gabbro – syenite pluton.

The Phu Ngu Zone, to the northeast, is bordered by Song Hien Late Paleozoic – Early Mesozoic terrigenous – volcanic depression and An Chau Late Mesozoic superimposed depression. In nature, the Phu Ngu belt is a structure showing deeper erosion as compared to the encircled Song Chay arc-shaped fold zone. Early – Middle Paleozoic (Ordovician, Silurian and Devonian) terrigenous formations as well as mafic and ultramafic blocks, such as Nui Chua formation, are widely spread in the Phu Ngu zone. These plutons are known as potential resources for Ti – Fe, Cu – Ni and accompanying PGE mineralization. Age of the Nui Chua gabbro-norite formation was determined to be 251 ± 4 Ma (Hoa et al. 2008). The Nui Chua magmas show closely spatial and temporal relation to the high-Al granite of the Phia Bioc complex and alkaline pyroxenite, gabbro and syenite in this area. These alkaline gabbroids were previously classified as Nui Chua Late Triassic formation (Dovjikov 1965; Tri 1977; Thuc and Trung 1965); whereas the syenite in Cho Don complex was Paleogene. Recent studies revealed that the gabbroids showed significantly different petrology and geochemistry compared to those of Nui Chua formation, therefore these magmas may be viewed as a separate magmatic association (Hoa et al. 2004c). Among the alkaline magmas, pyroxenite, gabbroids and syenite are known to contain nepheline (jacupirangite); Rb – Sr isotopic age dating of a nepheline-bearing syenite yielded a value of 230 Ma (Chi 2003), suggesting that these magmas are part of the regional Permian – Triassic magmatic activities.

The Song Hien structure, located in the northeast of the Lo Gam – Phu Ngu structure (for this monograph terms Lo Gam or Lo Gam – Phu Ngu are used hereafter to indicate this duo-structure) is a terrigenous – volcanic depression with more than 200 km long, running in the northwest – southeast direction, from Meo Vac

(Ha Giang province to Loc Binh (Lang Son province)). To the northeast the structure is bordered by Ha Lang Paleozoic structure belonged North East Bac Bo orogenic belt (Tri and Khuc 2011), while in the northeast is covered by the An Chau Late Mesozoic sedimentary superimposed depression. The Song Hien depression is filled mostly by Triassic terrigenous sediments, among these organic-rich shale is dominant. Other formations including Devonian terrigenous, Permian – Triassic bimodal basalt – rhyolite as well as mafic (gabbro-dolerite) and felsic (granite – granophyre) sub-volcanic bodies are widely developed. Mafic – ultramafic plutonic (such as) lherzolite, picrite, gabbro-norite, gabbro-dolerite bodies making the Cao Bang complex are outcropped elsewhere in the depression. Whereas, Cretaceous Sn-W –bearing high-Al granite of Pia Oac formation is distributed in the northwest of the Song Hien structure.

The An Chau late- Mesozoic superimposed depression is a terrigenous – volcanic depression closely similar to that of Song Hien. The terrigenous sediments are Early Triassic and Jurassic accompanied by a minor amount of Early-Middle Triassic felsic sub-volcanic rocks such as rhyo-dacite and rhyolite (Geological Map of Vietnam 1989). The products are commonly crisscrossed by porphyric granite sub-volcanic bodies.

The Red River Shear Zone (RRSZ) in Vietnam is a southeastern extension of the Ailao Shan – Red River Shear Zone (ARRSZ), starting from Tibet (China) spanning to Vietnam East Sea. The extension is exposed for more than 250 km in the northwest – southeast direction before being buried under the current Red River Trough. The RRSZ is comprised majorly of paragneiss of biotite – silimanite – almandine – cordierite assemblages, and a subsidiary amount of marble, crystalline shale, paraamphibolite and quartzite. Based on the biotite – garnet thermobarometry and the presence of biotite – garnet – cordierite – K-feldspar assemblage the highest metamorphic grade in the Red River zone may be consistent with almandine – amphibole and granulite facies (Thang and Anh 2000).

Within the RRSZ's gneiss strata mantle derived mafic and ultramafic such as lherzolite, pyroxenite and gabbro-amphibole are outcropped elsewhere. Products of re-metamorphosed of gneiss including aplitic and pegmatite granites, and crystalline shale produced by shear motion along the Red River fault zone in the Cenozoic are also well developed. Besides, bright colored magma-origin high-Al and high alkaline granite bodies are commonly occurred. Ages of the mafic and ultramafic bodies vary between 35 and 25 Ma (Izokh et al. 2004), and between 24 and 22 Ma were determined for bright colored granite (Hoa et al. 2000, 2004b).

1.3 Magmatic Activities in Northern Vietnam

Study of the interaction between the lithosphere and mantle, and among the mantle layers has become a new way in geological and mantle geodynamic research (Kuz'min 2003). Given specific tectonic settings different mantle plume with different scales are defined, for example, hotspot (Hawaii, Iceland..), plume and super

plume (Zonenshan and Kuzmin 1983; Flower and Russo 2001; Kuz'min et al. 2001; Yarmolyuk et al. 2000; Dobresov 2003). Melts resulted from the interaction of deep mantle plumes with the crust and lithospheric mantle may form contrast magmas (bimodal) (Yarmolyuk et al. 2000), gabbro – granite series (Litvinovsky et al. 2001) and flood basalt (trap). Large igneous provinces (LIP) comprising pluton-volcanic mafic magmas are believed to intrude into the crust within a short time span by mantle (and lithospheric mantle) melting under the impact of deep-rooted, thermally anomalous mantle plumes. LIPs can be continental (trap) and oceanic: oceanic plateau, seamount groups, passive marginal volcanic activity (Coffin and Eldholm 1994). Many LIPS show temporal relation to some certain continental plate separation events in particular the Gondwana. This period is characterized by thermally anomalous mantle flows expressed by widely spread picrite magmatic activities and high temperature – low pressure metamorphism; strong lithospheric mantle – crust interaction; formation of massive platinum, gold, rare metal and rare earth deposits.

Mantle plume-related magmas appeared in many parts of Asia as continental rift or trap activity (Siberian craton, Emeishan…). The most important LIP occurrence in Asia was in the Permian – Triassic time (Dobresov 2003; Nikishin et al. 2002). For this reason, the monograph will present data of Permian – Triassic mafic –ultramafic and felsic magmas as well as other intraplate magmas occurred in other time periods in northern Vietnam.

Major stages of geological evolution and magmatic activities in northern Vietnam may be listed as follows Precambrian, early – middle Paleozoic, late Paleozoic – early Mesozoic (Indosinian), late Mesozoic (Pacific or Yen Son stage) and Cenozoic (Himalayan stage). The Precambrian formations include granitoidic, metagabbro, gabbrodolerite together with a minor amount of olivine gabbro. Ar-Ar radiometric age dating yielded a value that is no younger than 1700 Ma (Hoa et al. 1999a; Tran Ngoc Nam and Itaya 1998). The Precambrian granitoids being the major component of Phan Si Pan Uplift are divided into the following complexes (1) Archean tronjdemite – tonalite – granodiorite (metagranitoids) of Ca Vinh complex (2834–2936 Ma), (2) high-K biotite granite as of Paleoproterozoic Xom Giau complex (2264 Ma), and (3) Neoproterozoic Po Sen calc-alkaline granitoid complex (760 Ma) (Lan et al. 2001; Nam 2001; Nam et al. 2003).

Early-middle Paleozoic magmatic activity are observed in the Song Ma suture zone, northwest Vietnam, and in marginal structures of the Song Chay dome in form of ophiolitic mafic – ultramafic associations (Bach et al. 1982; Hung et al. 1985; Phuong et al. 1999; Nien et al. 2005). Citing from their position among Cambrian and Cambrian – Ordovician sedimentary – metamorphic layers as well as their corresponding radiometric ages the age of the mafic – ultramafic associations may be about 540–460 Ma (Tung and Tri 1992; Thang et al. 1999; Vuong et al. 2006). These formations were extruded to upper lithological strata, in case of the Song Ma ophiolitic associations, for example, during the late Paleozoic. In the Song Chay dome area there was a report on meta-volcanic rocks with andesitic composition in early Paleozoic sedimentary – metamorphic formations (Lien et al. 2005), suggesting the existence of an ancient (early Paleozoic) subduction zone in the region.

By the Ordovician – Silurian period granitoidic magmatic activity (ca. 460 Ma) was recorded in the Song Chay dome. The granitoids show the geochemistry compatible with those of synchronous collision setting (Ponomareva et al. 1997).

In general, there has none representative pre-Indosinian intraplate magmatism been established in any geological structure in entire northern Vietnam.

Magmatic activity in the Permian – Triassic (Indosinian stage) occurred in most of the structures in northern Vietnam. Magmas in northwestern segment of Truong Son orogeny (west wing of the Song Ma suture zone), in the Muong Te – Dien Bien area, are late Paleozoic (Carboniferous – early Permian) calc-alkaline although Permian – Triassic granitoids (diorite – granodiorite of Dien Bien complex) are the major constituent. These granitoids show geochemical signatures that are mostly similar to subduction-related or active marginal magmas (Anh and Hoa 1996; Anh et al. 2005b). High-Al granite (259–265 Ma by Rb-Sr age dating after Thanh et al. 2005; 260 Ma by U-Pb after Tam 2008) and collision-induced pluton-volcanic associations are also observed in this area (Hoa 1995; Hoa et al. 2008). It has been determined that magmatic complexes in the northwest segment within the Truong Son fold zone was related to the Indosinian orogeny (Anh et al. 2005; Hoa et al. 2008).

Meanwhile Permian – Triassic magmatic activity in other tectonic settings in northern Vietnam shows totally different characteristics. The Song Da – Tu Le rift region in the northwest is characterized by contrast intraplate ultramafic – mafic – alkaline felsic; whereas in the Song Hien rift, arc-like mafic – felsic magmas are dominant. The geochemistry of these Permian pluton – volcanic magmas is corresponding to mantle plume melting interacting with different geological blocks having different lithospheric structures (Hoa et al. 2004a; Izokh et al. 2005). In this same period, gabbro – syenite, layered gabbro-peridotite intrusive bodies and subduction-like high-Al granite occurred in marginal structures around the Song Chay dome (Lo Gam and Phu Ngu) (Hoa et al. 2004b). These occurrences are mostly similar to Permian – Triassic representative magmas in the Song Hien zone.

Magmatic activity in Vietnam during the Mesozoic, according to recent investigations, is much less developed. Since the (Mesozoic) subalkaline and alkaline pluton- volcanic rocks in the Tu Le basin were reconsidered to be Permian – Triassic, late Mesozoic (Jurassic – Cretaceous) magmatic activity in northern Vietnam is even more sporadic, most concentrated only in the northeastern region. To the southeastern Lang Son within Song Hien zone among the terrigenous – (rhyolitic) volcaniclastic Tam Lung formations (J_3tl) (Thanh and Khuc 2005) found are Sn – W- bearing two-mica granite classified as late Cretaceous Pia Oac complex (Thuc and Trung 1995). Besides, according to Dovjikov (1965) felsic intrusive and effusive rocks in the Binh Lieu and Mong Cai area, on the border between late Mesozoic An Chau and Paleozoic Quang Ninh, are late Mesozoic. However, Binh Lieu volcanic formations were determined by stratigraphic correlation to be mid-Triassic (Tuyen et al. 1992), and their Anisian age has been kept since. The new isotopic data (U-Pb, LA-ICP-MS, zircon) of rhyolite from Binh Lieu area showed early Triassic age (246 Ma, unpubl. data). Based on latest mineralogical and geochemical studies, Jurassic volcanic rocks in the Tam Lung formation and Cretaceous two-mica granite in the Song Hien basin are produced during the late Mesozoic (Yanshanian) orogeny.

Therefore, according to the most recent studies there is no intraplate magmatic activity in the Mesozoic being observed in northern Vietnam.

Cenozoic magmatic activity in Vietnam may be divided into two sub-stages: Paleogene and Neogene – Quaternary. The first sub-stage is complicated in terms of appearances as well as chemical compositions. They occurred in various structural settings, and their formation is related to the tectonic collision between India and Eurasia; these are pluton – volcanic associations classified as pre-, syn- and post-collision based on the major tectonic activities in the Red River Fault zone during the Paleogene (Hoa 2007). End of the Cenozoic magmatic activity is marked by small-scaled Neogene – Quaternary basaltic eruption in the Phan Si Pan zone (northwestern tip of Lao Cao province) and Muong Te zone (Dien Bien Province). These Neogene – Quaternary magmas are not described in this monograph.

References

Bui An Nien, Tran Trong Hoa, Ngo Thi Phuong, Hoang Huu Thanh, Tran Tuan Anh, Pham Thi Dung (2005) Mafic and ultramafic magmatic formations in the Ha Giang and north Pho Rang areas. J Earth Sci 27(2):103–114 (in Vietnamese with English abstract)

Coffin MF, Eldholm O (1994) Large igneous provinces – crustal structure, dimensions and external consequences. Rev Geophys 32(1):1–36

Đao Đinh Thuc, Huynh Trung (eds) (1995) Geology of Viet Nam, P. II: magmatic formations. Department of Geology and Minerals of Viet Nam Publication, Hanoi

Dobresov (2003) Mantle plume and their role in formation of the anorogenic granitoids. Geol Geophys 44(12):1243–1261 (in Russian)

Dovjikov (ed) (1965) Geology of Northern Viet Nam. Science and Technology Publication, Hanoi, 668 p

Flower MFJ, Russo RM (2001) Mantle contamination and the Izu-Bonin-Mariana (IBM) 'high-tide mark': evidence for mantle extrusion caused by Tethyan closure. Tectonophysics 333(1–2):9–34

Gatinsky YG (1986) Geodymanics of Southeast Asia in relation to the evolution of ocean basins. Palaeogeogr Palaeoclimatol Palaeoecol 55:127–144

Geology of Viet Nam, P I. Stratigraphy. Science and Technology publ (1989) Hanoi (in Vietnamese)

Harrison TM, Leloup PH, Ryerson FJ, Tapponnier P, Lacassin R, Chen Wenji (1996) Diachronous initiation of transtension along the Ailao Shan-Red River Shear Zone. Yunnan and Vietnam, Tectonic evolution of Asia. World and regional geology series. Cambridge University Press, New York, pp 208–226

Izokh AE, Tran Trong Hoa, Polyakov GV, Ngo Thi Phuong, Tran Tuan Anh, Travin AV (2004) Syn-kinematic ultramafic-mafic magmatism in the Red River shear zone. J Geol B 23:26–41

Izokh AE, Polyakov GV, Tran Trong Hoa, Balykin PA, Ngo Thi Phuong (2005) Permian-Triassic ultramafic-mafic magmatism of Northern Vietnam and Southern China as expression of plume magmatism. Russ Geol Geophys 46(9):942–951

Kuz'min MI, Iarmoluk VV, Kovalenko VI, Ivanov VG (2001) Evolution of Central- Asian's "Hot" field in phanerozoic and some problems of plume-related tectonic. Ir.GTU, Irkutsk, pp 246–262

Lacassin R, Leloup PH (1993) Bounds on strain in large Tertiary shear zones of SE Asia from boundinage restoration. J Struct Geol 15(6):677–692

Lan CY, Chung SL, Lo cH, Lee TY, Wang PL, Li H, Dinh Van Toan (2001) First evidence for Archean continental crust in northern Vietnam and its implications for crustal and tectonic evolution in Southeast Asia. Geology 29(3):219–222

Le Duy Bach (1986) Tectonic evolution of Earth crust in the Indochina. J Geol A 176–177:29–39 (in Vietnamese)

Le Duy Bach (2001) Composite terrane: theory and reality. J Earth Sci 23(1):1–15 (in Vietnamese with English abstract)

Le Duy Bach, Ngo Gia Thang (1995) Phanerozoic ophiolites in Indochina. In: Proceedings of the international symposium geology of SEA and adj. areas, J Geol B 5–6:212–221

Le Duy Bach, Vu Minh Quan, Tran Quoc Hùng, Ngo Gia Thang, Hoang Huu Thanh (1982) Song Ma ophiolite. J Earth Sci 4:97–106 (in Vietnamese with English abstract)

Leloup PH, Ricard Y (1999) Shear heating in continental strike-slip shear zones: model and field examples. Geophys J Int 136(1):19–40

Leloup PH, Tapponnier RLP, Scharer U, Zhong Dalai, Liu Xaohan, Zhang Shan, Ji Shaocheng, Phan Trong Trinh (1995) The Ailao Shan – Red river shear zone (Yunnan, China), Tertiary transform boundary of Indochina. Tectonophysics 251:3–84

Litvinovsky BA, Yarmolyuk VV, Voronsov AA, Zhuravlov DZ, Vosokhov VF, Sandimirova GP, Kuz'min DV (2001) Late Triassic stage of formation of the Mongolo-Transbaikalian alkaline granitoid province: data of isotope-geochemical studies. Russ Geol Geophys 42(3):445–455

Maluski H, Lepvrier C, Jolivet L, Carter A, Roques D, Beyssac O, Ta Trong Thang, Nguyen Duc T, Avigad D (2001) Ar-Ar and fission track ages in the Song Chay massif: early Triassic and Cenozoic tectonics in northern Vietnam. J Asian Earth Sci 19:233–248

Ngo Thi Phuong, Tran Trong Hoa, Hoang Huu Thanh, Tran Tuan Anh (1999) Geochemical significances of Paleozoic igneous rocks of Song Ma belt – Northwest Vietnam. J Sci Earth 21(1):51–56

Nguyen Xuan Bao (ed) (2001) Tectonics and metallogeny of south Viet Nam. Final report to the Ministerial project (Ministry of Natural Resources and Environment), Archives of the Center for Geology Information and Literature, Hanoi (in Vietnamese)

Nguyen Trung Chi (ed) (2003) Petrology and mineralization of alkaline magma formations in northern Viet Nam. Final report of Ministerial Project (Ministry of Natural Resources and Environment), Center for Information and Literature Archives, Dept. Geology and Minerals, Hanoi (in Vietnamese)

Nguyen Xuan Tung, Tran Van Tri (eds) (1992) Geological and geodynamic formations of Viet Nam. Science and Technology Publication, Hanoi (in Vietnamese)

Nguyen Duc Thang, Pham Dinh Truong, Bui Cong Ha (1999) Chemical compositions of ophiolite association in the Song Ma belt. Geol Nat Miner Resour III:117–141 (in Vietnamese)

Nguyen Ngoc Lien, Tran Van Tri, Pham Binh, Pham Hoe (2005) Meta-andesite in the Bac Ha area, Lao Cai province. 60-Anniversary of Geology of Viet Nam 122–125 (in Vietnamese)

Nguyen Van Thanh, Pham Huy Hoc, Le Hung (2005) New results of Rb-Sr age dating of the Pu Si Lung granitoid. In: Proceedings of science symposium on the 60th anniversary of the Vietnamese Geology, pp 221–225 (in Vietnamese)

Nguyen Van Vuong, Mai Hong Chuong, Ta Trong Thang (2006) Radiometric ages and evolution of thermal tectonics of ophiolites along the Song Ma deformed belt. J Earth Sci 28(2):165–173 (in Vietnamese with English abstract)

Nikishin AM, Zieler PA, Abbott D, Brunet M-F, Cloetingh S (2002) Permo-Triassic intraplate magmatism and rifting in Eurasia: implications for mantle plumes and mantle dynamics. Tectonophysics 351:3–39

Phan Truong Thi (1995) Indosinian block and Indosinian movement in the Indochina and East Sea in Cenozoic. In: Proceedings of 3-rd geological conference of Vietnam: geology, mineral resources and petroleum, Hanoi, pp 137–147

Phan Luu Anh, Hoang Viet Hang (2005) Crust-origin of the Tam Tao granite block: evidence of late Permian age. J Earth Sci 27(2):115–124 (in Vietnamese with English abstract)

Polyakov GV, Nguyen Trong Yem, Balykin PA, Tran Trong Hoa, Hoang Huu Thanh, Tran Quoc Hung, Ngo Thi Phuong, Petrova TE, Vu Van Van (1996) Permian – Triassic mafic and ultra-

mafic formations in northern Viet Nam. Science and Technology Publication, Hanoi, 172 p (in Vietnamese)
Ponomareva AP, Vladimirov AG, Phan Luu Anh, Kruk NN, Rudnev SN, Ponomarchuk VA, Bibikova EV, Juravlov DJ (1997) High-aluminous granites of Song Chay massif (North Vietnam): Ordovician age, petrogenes, tectonic position. Geol Geophys 38(11):1792–1806 (in Russian)
Schaerer U, Tapponnier P (1990) Intraplate tectonics in Asia: a precise age for large-scale Miocene movement along the Ailao Shan-Red River shear zone. China Earth Planet Sci Lett 97:65–77
Schaerer U, Zhang LS (1994) Duration of strike-slip movements in large shear zones: the Red River belt, China. Earth Planet Sci Lett 126:379–397
BM Tam (2008) Magmatism in Vietnam according to Global Tectonic Theory. Project Report of Research Institute of Geology and Mineral Resources
Tapponnier P, Peltzer G, Le Dain AY, Armijio R, Cobbold P (1982) Propagating extrusion tectonics in Asia: new insights from simple experiment with plasticine. Geology 7:611–616
Tapponnier P, Lacassin R, Leloup H, Scharer U, Zhong Dalai, Liu Xaohan, Shaocheng J, Zhang Lian Shang, Zhong Jiayou (1990) The Ailao Shan – Red River metamorphic belt: left-lateral shear between Indochina and China. Nature 343:431–437
Tong Duy Thanh, Vu Khuc (eds) (2005) Stratigraphic divisions of Viet Nam. National University Publication, Hanoi, 504 p (in Vietnamese)
Tran Trong Hoa (ed) (1995) Study of Mesozoic – Cenozoic magmatism and its mineralization potential. Final report for National project KT- 01–04 (1992–1995). Archives of the National Center for Science and Technology Information, Hanoi (in Vietnamese)
Tran Xuyen (ed) (2001) Geology and mineral resources of the Ma Quan – Bac Quang area (geological map, sheet Ma Quan – Bac Quang, scale 1: 200.000)
Tran Ngoc Nam (2001) SHRIMP U-Pb isotopic age dating on zircons of the Ca Vinh and Xom Giau complexes. J Geophys Res 262:1–11 (in Vietnamese with English abstract)
Tran Trong Hoa (2002) Subdivision and correlation of Permian-Triassic basaltoid associations in the Song Da Structure (NW Vietnam). J Geol B, No 19-20/2002, pp 22–30
Tran Ngoc Nam (2003) 750 Ma U-Pb age of zircon from Po Sen granite and its tectonic significance. J Geophys Res 274:1–2 (in Vietnamese with English abstract)
Tran Trong Hoa (2007) Intraplate magmatism in North Vietnam and related metallogeny. Dissertation of Dr. of Science, Institute of Geology and Mineralogy, Siberian Branch, RAS, Novosibirsk, 382 p
Tran Ngoc Nam TM, Itaya T (1998) P-T-t paths and post-metamorphic exhumation of the Day Nui Con Voi shear zonein Vietnam. Tectonophysics 290:299–318
Tran Tuan Anh, Tran Trong Hoa (1996) Permian – Triassic calc-alkaline granitoids in the marginal areas of Truong Son micro-continent, vol 2. Geology and Natural Resources, Science and Technology Publication, Hanoi, pp 100–108 (in Vietnamese)
Tran Tat Thang, Tran Tuan Anh (2000) Indications of granulite metamorphic facies in the Red River zone. J Earth Sci 22(4):410–419 (in Vietnamese with English abstract)
Tran Van Tri TKT, Truong Cam Bao (eds) (1977) Geology of Vietnam, northern part. Explanation to geological map of Northern Vietnam at the scale 1: 1.000.000. Institute of Geology and Mineral Resources (in Vietnamese), 357 pp
Tran Van Tri, Vu Khuc (eds) (2011) Geology and natural resources of Vietnam. Science and Technology Publication, Hanoi, 645 p
Tran Quoc Hung, Bui An Nien, Hoang Huu Thanh (1985) Petro-chemical characteristics and genesis of intrusive rocks in the Song Ma Zone. J Earth Sci 7(1):6–11 (in Vietnamese)
Tran Thanh Tuyen, Vu Khuc, Luu Lan (1992) New findings on Song Hien structure in the Binh Lieu area, Tien Yen. J Geol A212–213:68–70 (in Vietnamese with English abstract)
Tran Trong Hoa, Hoang Huu Thanh, Tran Tuan Anh, Ngo Thi Phuong, Hoang Viet Hang (1998) High-Ti basaltoidic formations in the Song Da rift zone: chemical compositions and geodynamic conditions of magma genesis. J Geophys Res 244:7–15 (in Vietnamese with English abstract)
Tran Trong Hoa, Ngo Thi Phuong, Hoang Huu Thanh, Vu Van Van, Bui An Nien, Tran Tuan Anh, Hoang Viet Hang (1999a) Magmatic complexes in the Cao Bang – Dong Khe area. Geological

map of Cao Bang – Dong Khe sheet of 1:50,000. Archives of the Center for Geological Information and Literature, Department of Geology and Minerals of Viet Nam (in Vietnamese)

Tran Trong Hoa, Ngo Thi Phuong, Tran Tuan Anh, Nguyen Van The, Nguyen Đuc Thang (1999b) New findings of Proterozoic ultramafic intrusive magmas in the Phan Si Pang belt. J Earth Sci 21(2):159–170 (in Vietnamese with English abstract)

Tran Trong Hoa, Tran Tuan Anh, Ngo Thi Phuong, Phan Luu Anh, Hoang Huu Thanh (2000) Origin of ultramafic rocks in the Red River zone on the basis of new results of mineralogical, geochemical and isotopic analyses. J Geol B 15–16:62–75

Tran Trong Hoa, Tran Tuan Anh, Ngo Thi Phuong, Pham Thi Dung, Tran Viet Anh (2004a) Permian – Triassic basalt – rhyolite associations in the Song Hien structure, northeast Viet Nam. J Earth Sci 26(4):392–405 (in Vietnamese with English abstract)

Tran Trong Hoa, Tran Tuan Anh, Ngo Thi Phuong, Pham Thi Dung, Tran Viet Anh, Izokh AE (2004b) Mesozoic – Cenozoic magmatic formations in the Phan Si Pang – Red River uplift block, northwest Viet Nam. In: The Red River fault zone, geodynamics, mineralization and natural hazards. Science and Technology Publication, Hanoi, pp 297–372 (in Vietnamese)

Tran Trong Hoa, Tran Tuan Anh, Ngo Thi Phuong, Izokh AE, Polyakov GV, Balykin PA, Ching-Ying Lan, Hoang Huu Thanh, Bui An Nien, Pham Thi Dung (2004c) Gabbro-syenite associations of East Bac Bo structures: evidences of intra- plate magmatism?. J Geol B 23:12–25, Hanoi

Tran Trong Hoa, Hoang Huu Thanh, Ngo Thi Phuong, Vu Van Van, Bui An Nien, Hoang Viet Hang, Tran Tuan Anh, Pham Thi Dung, Tran Hong Lam, Tran Viet Anh, Phan Luu Anh (2005) Survey and evaluation of accompanying minerals in Pb – Zn and Cu mines in Viet Nam. Final report of National project on mineral resources (2002–2004). Archives of the Center for Information and Literature, Viet Nam Academy of Science and Technology (in Vietnamese)

Tran Tuan Anh, Tran Trong Hoa, Hoang Huu Thanh (2005) Geochemical significances of Carboniferous – Permian intermediate volcanism of South Vietnam. J Geol B 26:18–27

Tran Trong Hoa, Tran Tuan Anh, Ngo Thi Phuong, Pham Thi Dung, Tran Viet Anh, Izokh AE, Borisenko AS, Lan CY, Chung SL, Lo CH (2008) Permo-Triassic intermediate-felsic magmatism of the Truong Son belt, eastern margin of Indochina. C R Geosci 340:112–126

Van Đuc Chuong (1996) The ophiolite belts in Viet Nam. Geogr Nat Resour Viet Nam Monogr 2:41–52

Van Đuc Chuong, Van Đuc Tung, Tran Van Thang (2001) Mafic and ultramafic magmas in ophiolite belts in Viet Nam. J Earth Sci 23(3):231–238 (in Vietnamese with English abstract)

Yarmolyuk VV, Kovalenko VI, Kuzmin MI (2000) North-Asian's super-plume in the Phanerozoic: magmatism and deep dynamics. Geotectonica 5:3–29 (in Russian)

Zonenshan LP, Kuzmin MI (1983) Intraplate magmatism and their significance for understanding earth mantle processes. Geotectonica 1:28–45 (in Russian)

Part II
Permian: Triassic Magmatic Activity

The Permian – Triassic is a special period in the history of geological development in Asian continent and Vietnam, especially. WIDe magmatic activities in a number of tectonic settings at this stage including the Siberian trap, Emeishan large igneous province (LIP), basalt and picrite in northern Vietnam and other LIPs are thought to relate to mantle super-plumes resIDed under the Asian lithosphere (Dobresov 2005). This stage was characterized by anomalous heat flows evIDenced by picritic magmatism, high T-P metamorphism, significant interaction between mantle, mantle lithosphere and crust, and the occurrence of platinoID, gold, rare metal and rare earth deposits elsewhere in the region (Izokh et al. 2005).

Within the Indochina block and composite terrain in northern Vietnam – south China in the Permian – Triassic, as described in Chap. 1, magmas of various origins are wIDely spread. Permian – Triassic orogenic pluton – volcanic associations were recognized in the east and southeast of Indochina Block, while in the southwest of north Vietnam – south China composite terrain intraplate pluton- volcanic and plutonic formations are commonly encountered (Hoa 2005, 2007, 2008). Intraplate magmatic associations are developed in rift-origin structures such as Song Da – Tu Le rift in the northwest and Song Hien in the northeast as well as in other areas in conjunction with rifting domains such as Song Hien – Lo Gam and Phu Ngu. Distribution scheme of the Permian – Triassic magmatic formations are shown in Fig. 1. Petrology, geochemistry and isotope geochemistry of these magmas showed that they are related to different mantle lithosphere sources. Permian – Triassic intraplate magmas described in the following sessions are Song Da, Tu Le, Song Hien and Lo Gam.

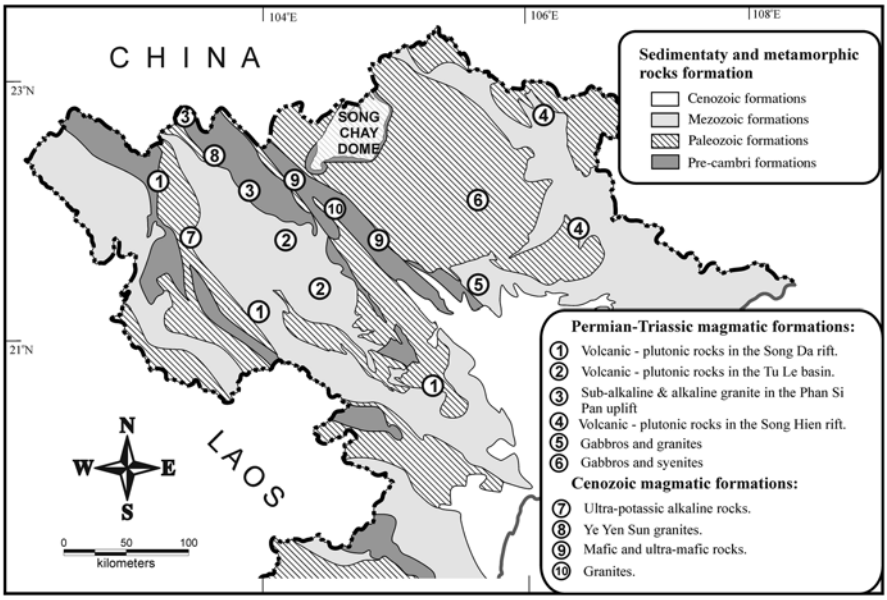

Fig. 1 Distribution scheme of intraplate magmas on a simplified geological background

Chapter 2
Permian – Triassic Magmatic Activity in the Song Da Structure

Abstract Late Permian mafic-ultramafic volcanic and sub-volcanic rocks in the Song Đa Rift include four different associations in terms of low-Ti and high-Ti types. Low-Ti, high-Mg volcanic and sub-volcanic rocks are composed of komatiite, komatiitic basalt and basalt and are divided into three groups according to their petrological and geochemical features. Chemical composition of rocks of the komatiite-basalt association is alkali-low (but rather Na-high), very Ti-low, varying from Al-high komatiite to Al-low basalt. They are characterized by high content of Mg, Al, Ni, Co, Cu and Cr, and low of Ti, Fe, Na, K, P, Rb, Ba, Sr, Nb, Ta, Nd, Hf, Zr and REE. In general, based on geochemical and isotopic characteristics the Song Đa mafic-ultramafic rocks of the komatiite-basalt association may be products of a melt derived from depleted mantle suffering the impact of mantle plume. Digital modeling showed that the initial melt composition was correspondent to komatiitic basalt. Eruption ages of the magmas are 257 ± 24 Ma (by Rb/Sr age dating), and 270 ± 21 Ma (by Re/Os age dating).

High-Ti basalts (and picrite) and gabbro-dolerites are widely distributed in marginal areas as well as in the center of the Song Đa Rift and belong to three associations: andesite-basalt, andesite-picrite-basalt and trachybasalt-trachyandesite-trachydacite. The chemical compositions of high-Ti basalts are characterized by having high Ti content, moderately low Al, medium to low Mg, relatively low alkalinity, but high K, high Rb, Sr, Zr and LREE, but Nb and Ta varies from low- to hight. The high-Ti basalts have relatively restricted ranges of $(^{87}Sr/^{86}Sr)_i$ (0.7048–0.7079) and $\varepsilon Nd(t)$ values (−5.7 to +3.1) indicating weak lithospheric signature that may be related to their trace element-rich nature and this is consistent with abundant earlier studies suggesting that the high-Ti basalts at Song Da or elsewhere in the ELIP formed from low degrees of partial melting.

T.-H. Tran et al., *Intraplate Magmatism and Metallogeny of North Vietnam*,
Modern Approaches in Solid Earth Sciences 11,
DOI 10.1007/978-3-319-25235-3_2

2.1 Song Da Permian – Triassic Mafic and Ultramafic Pluton – Volcanic Formations

2.1.1 Magma Classification

Intracontinental rifting in northwest – southeast direction was commonly developed in Southeast Asia during the Permian – Triassic (Gatinsky 1986; Khain and Balukhovsky 1993; Metcalfe 1996). The activity was accompanied by strong ultramafic – mafic magmatism. The Song Da rift is located between the Ailao Shan – Red River shear zone to the northeast and the Song Ma suture zone in the southwest. Although rifting structure features in an intracontinental setting are well described and defined (Gatinsky and Thuc 1982; Toat 1987; Hoa 1995; Polyakov et al. 1996, and references therein) the formation and evolution of this rifting structure is a focus of hotly debate in many geological forums.

The Song Da rift, according to up-to-date geological concerns, includes other structural facies such as Son La, Song Da, Ninh Binh and part of Thanh Hoa zone in the tectonic scheme presented by Dovjikov (1965). There are a number of areas and ultramafic – mafic magmatic associations in this structure such as Cam Thuy, Vien Nam – Ba Vi, Kim Boi – Hoa Binh, Son La Pass, Bac Yen – Van Yen, Deo Chen (Chen Pass), Nam Muoi, Nam So and Sin Ho (Fig. 2.1).

The classification of Permian – Triassic ultramafic – mafic magmatic rocks in northwestern Vietnam have been done in a number of igneous studies; however, up to the present the matter is not conclusive. Based on the petrology, recent studies have shown that the Permian mafic and ultramafic volcanic rocks may be divided into two distinct complexes, e.g., Cam Thuy (P_3) and Vien Nam (P_3). These are described in the monograph 'Geological stratigraphic divisions of Vietnam' edited by Tong Dzuy Thanh and Vu Khuc (2005). However, due to lack of radiometric age data the above division may be inappropriate in terms of geochemical compositions of the magmatic associations. The Cam Thuy volcanic rocks comprises mostly homogeneous high – Ti basalt and andesitic basalt (andesite – basalt association); while volcanic (and sub-volcanic) rocks in the Vien Nam complex are geochemically heterogeneous that include both high- and low- Ti mafic and ultramafic types. Among the high- Ti mafic magmas (mostly basalt) of Vien Nam complex there are two distinct magmatic associations picrite – andesite – basalt (Nam So type) and trachybasalt – trachyandesite – trachydacite (Nam Muoi – Suoi Chat type) (Hoa 2002). In general, among the magmas in Vien Nam complex aside from ultramafic – mafic rock types termed as komatiite – basalt association volcanic and sub-volcanic subalkaline felsic rocks are also common (Polyakov et al. 1991, 1996; Phuong 1994). Sources to form the high- and low- Ti magmas in the Song Da structure are obviously different: the low-Ti magma was formed by melting of MORB-like depleted mantle, whereas the high- Ti type was produced by melting of an enriched mantle (Hoa 2002, 2005, 2007). Therefore, classifying both the magmas to a single formation may not be appropriate. Based on the geochemical characteristics the magmas in these areas may belong to two series, e.g., low- and high- Ti where the high-Ti is dominant (Hoa et al. 1998; Hoa 2002). On the other hand, mineralogical

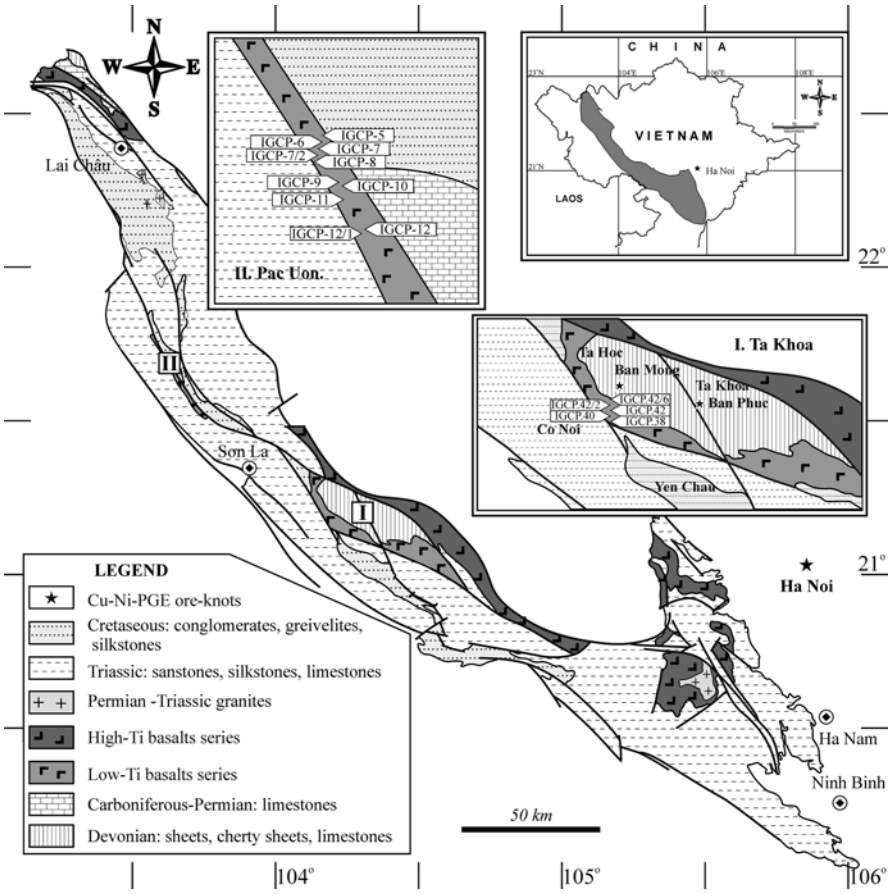

Fig. 2.1 Distribution scheme of Permian – Triassic magmatic formations within the Song Da structure

and geochemical studies (e.g. Polyakov et al. 1991, 1996; Hoa et al. 1998; Hoa 2002, 2005) distinguish the ultramafic – mafic rocks in the Song Da structure into various magmatic associations:

- Low-Ti series: including komatiite – basalt associations distributed in the center of Song Da rift, in the Nam Muoi and Ta Khoa areas.
- High-Ti series: with two different volcanic associations, one in the southeast and the other to the northwest along the alignment of Song Da zone. In the southeast andesite – basalt (and rhyolite – basalt) association is widely observed sometimes with a minor amount of sub-alkaline felsic (rhyodacite and rhyolite) rock types. These rock associations occur in the areas of Cam Thuy, Kim Boi, Vien Nam – Ba Vi, and Bac Yen – Van Yen. In contrast, in the northwest, the following volcanic associations are well-spread: andesite – basalt (Son La), picrite – andesite – basalt (Nam So) and trachydacite – trachyrhyolite – trachybasalt. Except for sub-alkaline volcanic rocks in the Nam Muoi area which is at the center of Song Da structure the other magmatic associations are distributed at the margins of this structure.

The formation ages of the Song Da ultramafic – mafic pluton-volcanic magmas are subjects to clarify. Age of the komatiite – basalt magmas in the Nam Muoi area was dated to be Permian – Triassic based on stratigraphic correlation and radiometric determination (Polyakov et al. 1991, 1996). Basaltic and komatiitic lavas in the Nam Muoi area are, on the one hand, overlain by carbonate terrigenous (shale) containing late Triassic fossils, and on the other, komatiitic subvolcanic bodies in the Nam Muoi and Ta Khoa areas penetrate Carboniferous and Permian terrigenous sediments. These observations were also reported by Pham Duc Luong (2005). Radiometric age dating (Rb-Sr) conducted on a basaltic komatiite (MgO = 18 wt%) yielded a value of 257 ± 24 Ma (Hoa 1995; Polyakov et al. 1996) (Fig. 2.2a). Re-Os age dating on 12 komatiite samples in the Nam Muoi area yielded a number of 270 ± 21 Ma (Hanski et al. 2004); Nguyen Hoang et al. (2004) reported a Rb-Sr age for Doi Bu high- Ti basalts at 280 Ma and 256 Ma for trachytes. Except for the age of 280 Ma that must be independently checked, other reported age data for the Song Da ultramafic – mafic magmas are rather consistent and closely similar to the reported eruption age of Emeishan basalts. Emeishan magmas aged about 260 Ma were thought to erupt within a short time span, from one to two million years (Zhong et al. 2007).

2.1.2 Komatiite – Basalt Associations in Nam Muoi and Ta Khoa Areas

2.1.2.1 Spatial Distribution Characteristics and Geological Structure

Up to date Song Da Rift high-Mg, low-Ti and low-alkali komatiite – basalt rocks have been convincingly defined in the two following areas Nam Muoi (Polyakov et al. 1991, 1996; Phuong 1994) and Ta Khoa (Hoa 1995) and more evidence was subsequently added later (e.g. Hoa 2005, 2007).

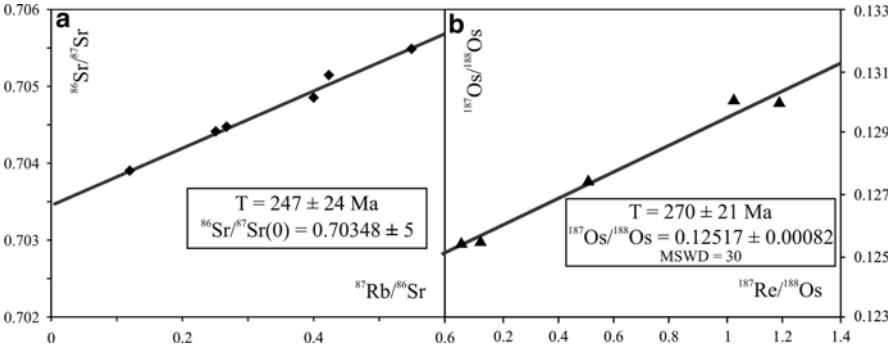

Fig. 2.2 Rb – Sr and Os – Re age dating for komatiitic basalt in the Nam Muoi area, (**a**) after Hoa 1995; Polyakov et al. 1996) and (**b**) after Hanski et al. 2004

Photo 2.1 Stratified structure between komatiite and low-Ti basalt. Outcrop nearby Pa Uon bridge cross Da river (By Hoa et al. 2013)

In the Nam Muoi area, high-Mg volcanic and sub-volcanic ultramafic – mafic rocks are described in two cross-sections Pac Uon- Muong Giang and Chieng Ngam (Fig. 2.1). In both two cross-sections bi-compositional, lower and upper, structures were defined. The lower structure is thicker and comprised of high-Mg volcanic rocks (olivine basalt, komatiitic basalt) and small bodies of pluton-volcanic ultramafic rocks. The upper unit the komatiitic basalt magma is replaced by sub-alkaline high-Ti mafic – felsic volcanic rock, a component of trachyandesite – trachydacite – trachybasalt association (Fig. 2.1, Photo 2.1).

In the Ta Khoa area high-Mg komatiitic basalts and peridotitic komatiites are distributed mainly to the southwest wing of the Ta Khoa anticline, in a shape of elongated lens, running in the northwest-southeast direction from Ta Hoc-Nong Xang in the northwest to Ban Tang village in the southeast. In difference to volcanic strata in the Nam Muoi area, accompanying Ta Khoa olivine basalt and komatiitic basalt are doleritic dykes, sometimes sub-volcanic komatiitic bodies. These sub-volcanic bodies appear either as conform lenses among the leucobasalt or dykes that cut through metamorphosed quartzite and mica shale. The most representative cross-section containing a variety of volcanic, sub-volcanic and plutonic komatiite – basalt association in the Ta Khoa area is Co Noi- Deo Chen – Ta Khoa. Olivine basalt, basalt with spinifex pyroxene, leucobasalt (andesitic basalt) and komatiitic and komatiitic peridotite sub-volcanic bodies may be observed long this cross-section (Photo 2.2).

In northwestern wing of the Ta Khoa anticlinorium, aside from volcanic and sub-volcanic rocks as mentioned above commonly observed are small-sized ultramafic bodies (dunite, lherzolite and pyroxenite) and dykes having compositions and structures similar to komatiic peridotite and olivine-bearing pyroxenite. In the Nam Chin area also encountered are zoned dykes comprising komatiic peridotite and olivine-bearing pyroxenite in the center and doleritic mafic magma in the marginal zone.

Photo 2.2 Komatiite lenses in low-Ti basalt in the Deo Chen area

PGE bearing Ni-Cu mineralization forming mid- (Ban Phuc) to small-sized industrial deposits (Ban Mong) are associated with these intrusive bodies and dykes.

Komatiite – Basalt associations in the Nam Muoi and Ta Khoa areas are distributed in the center of the Song Da structure. According to Bùi Minh and Tô Văn (1995) hi-Mg basalt of komatiite – basalt association also occurred in the Sin Ho area, northwest edge of the Song Da rift (Bùi Minh and Tô Văn 1995). Olivine basalt, a typical representative of the komatiite – basalt association (e.g. hi-Mg and low-Ti) is also observed in the Hoa Binh hydro-reservoir area as well as in the Doi Bu area. These volcanic rocks may be members comparable with those sub-volcanic magmas of Ba Vi-type. This suggestion needs further investigation to clarify. The Doi Bu and Hoa Binh hi-Mg and low-Ti volcanic rocks are not described in this monograph.

2.1.2.2 Petrographic and Mineralogical Characteristics

The hi-Mg (low-Ti series) volcanic rocks are classified into different groups according to their petrographic and geochemical characteristics. The first group includes ultramafic magmas having composition, structure and texture features similar to plagioclase-bearing wehrlite (MgO >30 wt.%), comprising coarse-grained olivine and a minor amount of pyroxene and plagioclase. These are the major component of the small sub-volcanic-like intrusive bodies occurred in komatiite – basalt volcanic layers in the Nam Muoi area, and among the small peridotite intrusive bodies (dunite, lherzolite) in the Ta Khoa area.

The second group includes magmas that show a chemical composition correspondent to komatiite (MgO = 22–30 wt.%) and occur in the form of sub-volcanic bodies as well as porous pillow-lavas in the Nam Muoi area. In the Ta Khoa area, these magma types are major constituents of sub-volcanic bodies in the Deo Chen volcanic cross-section. The magmas also occur as dykes in Nam Chim, Ta Hoc, and

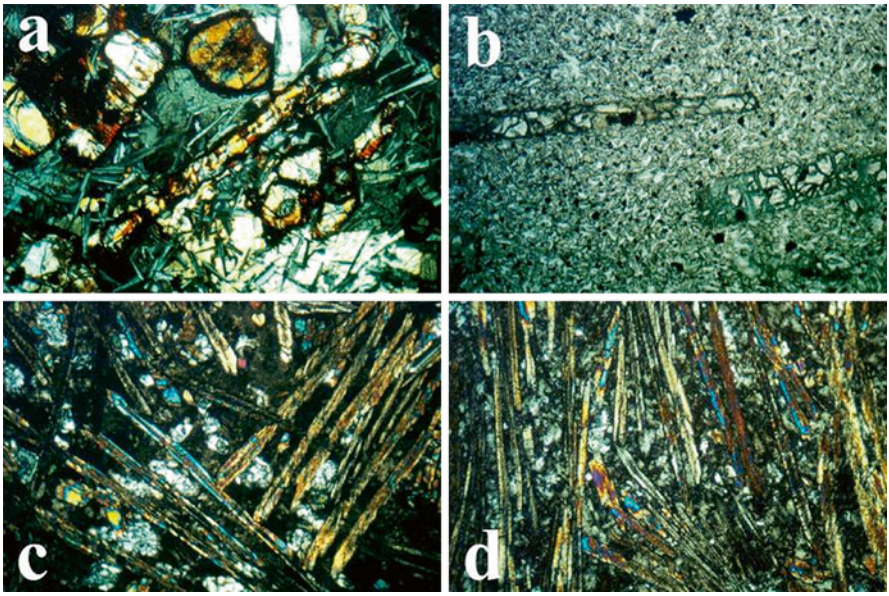

Photo 2.3 Porphyry (**a–b**) and spinifex (**c–d**) texture of pyroxene in Nam Muoi komatiitic basalt (After Polyakov et al. 1996)

Ban Mong areas. Most typical characteristics of this second group are that the mafic and ultramafic rocks show porphyry or porphyritic texture having elongated olivine phenocryst, and needle-shaped, spinifex-structured pyroxene (Polyakov et al. 1991) (Photo 2.3a–d).

The third group includes olivine basalt, olivine-free basalt, and transitional to andesitic basalt type. The olivine basalt and komatiitic basalt show elongated olivine and pyroxene phenocrysts in the ground masses of different level of crystallization. Among the phenocrysts, nearly rounded or anhydral olivine and pyroxene are commonly observed.

In association with magmatic intrusion and dyke activities in the Ta Khoa area, PGE bearing Ni-Cu mineralization is frequently occurred where Ban Phuc mine and Ban Mong ore site are most representatives (Hoa 1995; Hoa et al. 1998; Poliyakov et al. 1996; Phuong et al. 2001).

Major phenocryst minerals in the komatiitic basalt pluton volcanic associations are olivine, clinopyroxene and plagioclase, and the minor minerals are Cr-spinel and ilmenite. Aggregates of sulfur, sulfurarsenide, native copper, and PGM are also commonly occurred. Evolutional trend from dunite, peridotite and komatiite to olivine basalt is expressed by increasing the iron oxide in olivine from forsterite to chrysolite, decreasing the calcium oxide from bytownite to andesine in plagioclase, increasing the iron oxide in clinopyroxene and the Ti-, Fe- contents in Cr-spinel (Polyakov et al. 1996) (Tables 2.1, 2.2, 2.3 and 2.4). In general, mineralogical compositions of the komatiitic basalt associations of Song Da structure are closely

Table 2.1 Chemical compositions of olivine in komatiite and komatiitic basalt in the Nam Muoi and Ta Khoa areas. (EPMA analysis conducted at the Analytical Center, Institute of Geology and Mineralogy, Siberian Branch, Russian Academy of Sciences)

Sample ID	FeO	MgO	CaO	NiO	Ni (ppm)	f(*)
Nam Muoi						
Komatiite						
B6822	12.62	46.24	0.3	0.32	2476	13.3
B6825	8.1	49.03	0.27	0.4	3129	8.5
B6834	13.24	45.08	0.31	0.31	2437	14.1
B6854	11.87	46.25	0.29	0.33	2608	12.6
B6859	11.64	46.75	0.33	0.32	2476	12.3
B6860	12.06	46.5	0.23	0.3	2358	12.9
B6875	13.67	45.08	0.3	0.33	2608	14.5
B6885	13.54	44.79	0.34	0.3	2358	14.5
B7310	8.83	48.59	0.57	0.38	2985	9.3
B7329	12.27	46.91	0.37	0.35	2759	12.8
P250	11.36	46.58	0.36	0.27	2130	12
P260	12.88	45.16	0.32	0.24	1893	13.8
G1435	12.69	45.45	0.33	0.29	2278	13.1
G1441	12.65	45.22	0.3	0.33	2608	13.5
G1442	12.45	45.82	0.34	0.31	2437	13
G1444	12.49	46.07	0.33	0.29	2278	13.2
G1452	12.53	46.12	0.3	0.34	2670	13.2
G1453	18.51	40.77	0.32	0.26	2028	20.3
G1458	14.52	43.55	0.52	0.27	2130	15.8
G1461	12.52	43.25	0.27	0.33	2608	13.2
1/86	11.7	46.1	0.35	0.3	2358	12.5
9/86	13.44	45.22	0.33	0.3	2358	14.3
15/86	11.84	46.19	0.29	0.35	2759	12.5
34c/86	12.39	46	0.29	0.31	2437	13.2
43/86	12.55	45.91	0.32	0.32	2476	13.2
48a/86	11.64	46.55	0.32	0.3	2358	12.4
Pyroxenite						
B6842	14.38	44.2	0.3	0.31	2437	15.4
B6865	11.85	46.23	0.34	0.33	2608	12.6
B6888	13.17	45.14	0.31	0.29	2278	14.1
B6890	12.04	46.26	0.3	0.32	2476	12.7
B6892	13.62	44.88	0.35	0.27	2130	14.6
P272	8.1	49.33	0.28	0.3	2358	8.4
G1448	11.7	46.87	0.27	0.36	2812	12.3
G1456	11.49	46.49	0.3	0.31	2437	12.2

(continued)

Table 2.1 (continued)

Sample ID	FeO	MgO	CaO	NiO	Ni (ppm)	f(*)
7/86	8.17	49.5	0.26	0.41	3218	8.5
8/86	8.29	49.41	0.27	0.39	3074	8.6
33a/86	16.37	43	0.31	0.25	1987	17.8
48b/86	11.65	45.86	0.31	0.32	2476	12.5
Basalt- komatiite						
B6821	10.63	47.36	0.3	0.36	2812	11.2
B6830	12.29	46.48	0.33	0.34	2670	13
B6871	12.74	46.02	0.3	0.31	2437	13.4
B6889	12.53	45.26	0.32	0.29	2278	13.5
B6891	11.58	46.5	0.3	0.32	2476	12.3
Nam Muoi						
P247	16.96	42.16	0.33	0.12	943	18.4
48c/86	11.19	46.58	0.3	0.36	2812	11.8
G944	7.53	51.4	0.32	0.38	2985	7
48/86	12.13	45.54	0.32	0.32	2476	13
Ta Khoa						
T1631	11.28	46.09	0.26	0.38	2985	12
T1645	11.86	46.99	0.32	–	–	12
T1646-1	12.98	46.88	0.2	–	–	13

(*) ferrous content, $f = 100 \times FeO/(FeO + MgO)$

Table 2.2 Chemical compositions of pyroxene in komatiite and komatiitic basalt in the Nam Muoi and Ta Khoa areas

	Nam Muoi						Ta Khoa	
Sample ID	P67	B7329	B7335	P131Á/89	B7310	B7243	B5213	T1638
SiO_2	52.40	52.7	50.36	48.15	50.36	48.23	51.16	51.65
TiO_2	0.33	0.39	0.44	1.2	0.96	1.56	0.63	0.39
Al_2O_3	4.08	1.78	3.52	5.5	3.64	4.90	3.33	3.21
Cr_2O_3	0.11	0.17	0.28	0.12	0.23	0.01	0.77	0.01
FeO	6.61	7.32	7.6	9.29	10.21	9.71	6.83	12.34
MgO	18.18	18.68	16.92	14.77	14.97	12.25	17.78	13.65
CaO	17.39	18.05	19.72	19.89	19.35	22.35	18.15	16.70
Na_2O	0.13	0.25	0.37	0.34	0.26	0.48	0.26	0.54
Total	99.23	99.34	99.21	99.26	99.98	99.49	98.91	98.49
f	17	18	20.6	26	27.7	30.7	17.7	33.7
Wo.%	36.3	36.3	40.8	41.7	40.1	47.6	38.4	44.8
En.%	52.9	52.3	47.8	43.1	43.3	36.3	52.5	39.4
Fs.%	10.8	11.4	12.1	15.2	16.6	16.1	9.1	15.8

Table 2.3 Chemical compositions of plagioclase in komatiite and komatiitic basalt in the Nam Muoi and Ta Khoa areas

Sample ID	SiO_2	Al_2O_3	FeO	CaO	Na_2O	K_2O	An. %	Ab. %	Or. %
Komatiite									
B6842	52.29	29.53	0.77	13.3	3.82	0.09	65.2	34.2	0.6
B6859	47.58	32.83	0.39	17.2	1.81	0.01	85.4	14.6	0
B6865	49.14	31.56	0.5	16.0	2.21	0.01	80.3	19.6	0.1
B6888	52.39	30.02	0.09	12.5	4.18	0.26	61.4	37	1.6
B7310	51.79	28.02	1.07	12.1	4.42	0.12	59.8	40	0.2
B7329	51.73	28.94	0.83	13.3	3.81	0.24	66.4	32	1.6
P260	47.99	33.3	0.05	16.3	2.17	0.03	81	19	
G1442	54.97	27.78	0.47	10.7	5.1	0.28	52	46.2	1.8
G1458	49.51	31.39	0.58	15.3	2.65	0.1	76	23.6	0.4
1/86	50.8	30.59	0.13	13.3	3.8	0.15	66	33	1
9/86	53.27	29.31	0.23	12.0	4.45	0.38	58.6	39	2.4
15/86	49.91	30.38	0.74	15.1	2.9	0.03	74.4	25.5	0.1
43/86	50.49	30.71	0.59	14.5	3.04	0.11	72.5	27	0.5
Pyroxenite									
B6842	52.29	29.53	0.77	13.3	3.82	0.09	65.2	34.2	0.6
B6865	49.14	31.56	0.5	16.0	2.21	0.01	80.3	19.6	0.1
B6888	52.39	30.02	0.09	12.5	4.18	0.26	61.4	37	1.6
P272	50.73	31.33	0.14	14.1	3.41	0.06	69.4	30.5	0.1
8/86	54.24	28.63	0.34	11.4	4.98	0.34	56.2	41.8	2
Basalt komatiite									
B6891	55.66	27.99	0.18	10.3	5.29	0.26	51.8	46.4	1.8
B7335	50.93	28.54	1.56	12.8	3.93	0.06	64.6	35.2	0.2
P247	50.45	31.52	0.12	14.3	3.22	0.05	71.2	28.6	0.2
Olivine basalt									
P129/89	49.26	30.3	1.41	14.6	2.88	0.05	72.8	26.8	0.4
P131A/89	49.13	29.7	1.67	14.5	2.93	0.08	72.4	26.6	1
P131B/89	53.45	27.68	1.01	10.8	5.07	0.08	53.6	45.8	0.6

similar to those typical type occurred elsewhere in the world, in that: (1) the plagioclase, showing range between labrador – bytownite, is poor in orthoclase component but relatively high FeO contents (up to 1.7 %); (2) the olivine, varying between forsterite and chrysolite ($Fo_{78–93}$), is rich in Ni and Ca (NiO =0.1–0.4 %; CaO =0.2–0.6 %); the clinopyroxene, showing composition between augite and diopside, is poor in Ca, Ti, Ba, and average Cr contents ($En_{36-53}Fs_{9-17}Wo_{36–48}$, TiO_2 = 0.21.56 %, Cr_2O_3 up to 0.3 %); 4) the Cr-spinel shows composition correspondent to low-Ti, Al-chromite (Cr_2O_3 = 34–51 %, Al_2O_3 = 17–31 %, TiO_2 = 0.3–0.6 %) (Polyakov et al. 1996; Phuong et al. 2001).

Table 2.4 Chemical compositions of Cr-spinel in komatiite and komatiitic basalt in the Nam Muoi and Ta Khoa areas

Sample ID	SiO_2	Al_2O_3	FeO	CaO	Na_2O	K_2O	An. %	Ab. %	Or. %
Komatiite									
B6842	52.29	29.53	0.77	13.3	3.82	0.09	65.2	34.2	0.6
B6859	47.58	32.83	0.39	17.2	1.81	0.01	85.4	14.6	0
B6865	49.14	31.56	0.5	16.0	2.21	0.01	80.3	19.6	0.1
B6888	52.39	30.02	0.09	12.5	4.18	0.26	61.4	37	1.6
B7310	51.79	28.02	1.07	12.1	4.42	0.12	59.8	40	0.2
B7329	51.73	28.94	0.83	13.3	3.81	0.24	66.4	32	1.6
P260	47.99	33.3	0.05	16.3	2.17	0.03	81	19	
G1442	54.97	27.78	0.47	10.7	5.1	0.28	52	46.2	1.8
G1458	49.51	31.39	0.58	15.3	2.65	0.1	76	23.6	0.4
1/86	50.8	30.59	0.13	13.3	3.8	0.15	66	33	1
9/86	53.27	29.31	0.23	12.0	4.45	0.38	58.6	39	2.4
15/86	49.91	30.38	0.74	15.1	2.9	0.03	74.4	25.5	0.1
43/86	50.49	30.71	0.59	14.5	3.04	0.11	72.5	27	0.5
Pyroxenite									
B6842	52.29	29.53	0.77	13.3	3.82	0.09	65.2	34.2	0.6
B6865	49.14	31.56	0.5	16.0	2.21	0.01	80.3	19.6	0.1
B6888	52.39	30.02	0.09	12.5	4.18	0.26	61.4	37	1.6
P272	50.73	31.33	0.14	14.1	3.41	0.06	69.4	30.5	0.1
8/86	54.24	28.63	0.34	11.4	4.98	0.34	56.2	41.8	2
Komatiitic basalt									
B6891	55.66	27.99	0.18	10.3	5.29	0.26	51.8	46.4	1.8
B7335	50.93	28.54	1.56	12.8	3.93	0.06	64.6	35.2	0.2
P247	50.45	31.52	0.12	14.3	3.22	0.05	71.2	28.6	0.2
Olivine basalt									
P129/89	49.26	30.3	1.41	14.6	2.88	0.05	72.8	26.8	0.4
P131A/89	49.13	29.7	1.67	14.5	2.93	0.08	72.4	26.6	1
P131B/89	53.45	27.68	1.01	10.8	5.07	0.08	53.6	45.8	0.6

2.1.2.3 Geochemical Characteristics

Chemical compositions of the komatiitic basalt associations are characterized by having low alkalis (but relatively high Na), very low Ti and by evolution trend from hi-Al komatiite to low-Al basalt. They are characteristically high Mg, Al, Ni, Co, Cr and low Ti, Fe, Na, K, P, Rb, Ba, Sr, Nb, Ta, Nd, Hf, Zr, REE (Table 2.5).

Primitive mantle normalized trace element (LILE, HFSE and REE) patterns (after Sun and McDonough 1989) show a weak differentiation among the elements whose concentrations exceed those of the primitive mantle from one to ten times (Fig. 2.3). The plagioclase basalts and serpentinized peridotites show relatively high Cr, Rb, U, La and Ce, while the peridotites, komatiites and komatiitic basalts have Th, Nb, Zr, Ba, Sr, Nd, Hf, Y and REE contents closely matching with the primitive mantle (e.g. Sun and McDonough 1989). These geochemical features are character-

Table 2.5 Chemical compositions (wt. %) and trace element contents in the low-Ti volcanic rocks in the Nam Muoi and Ta Khoa areas (Nam Muoi area, after Hanski et al. 2004)

Sample ID	IGCP-42	IGCP-42/1	IGCP-42/6	IGCP-38	IGCP-40
	Komatiite		Olivine basalt		Andesite
SiO_2	40.1	43.2	47.7	43.8	59.0
TiO_2	0.33	0.76	0.62	0.94	0.70
Al_2O_3	5.34	10.30	13.20	10.50	14.20
Fe_2O_3	9.85	10.38	9.21	11.98	7.04
MnO	0.14	0.17	0.14	0.19	0.12
MgO	29.10	15.90	8.45	12.50	4.28
CaO	4.46	10.04	12.93	11.14	7.56
Na_2O	0.00	0.99	1.78	1.94	1.83
K_2O	0.09	0.02	0.44	0.02	1.38
P_2O_5	0.07	0.17	0.07	0.20	0.08
CO_2	0.04	0.04	0.04	0.07	0.04
H_2O	9.39	4.71	2.49	4.47	2.48
V	131	209	214	277	171
Cr	3118	1516	509	965	102
Ni	1630	672	45	396	15
Cu	54	102	81	105	33
Zn	72	79	67	97	72
Ga	9	16	16	16	24
Sr	10	139	167	52	127
Zr	16	48	64	43	162
Ba	36	28	132	38	168
Pb	10	11	12	14	19
Bi	1	4	0	1	4
Ce	3.77	12.5	16.9	9.47	46.3
Dy	1.65	3.58	3.83	4.49	5.02
Er	1.23	2.49	2.75	2.51	3.78
Eu	0.51	1.03	0.82	1.09	1.26
Gd	1.6	3.3	3.82	3.23	5.5
Ho	0.38	0.96	0.77	0.83	1.27
La	1.82	6.05	7.98	4.51	21.8
Lu	0.35	0.66	0.45	0.72	0.55
Nd	4.23	8.45	10.8	9.09	23.4
Pr	0.7	1.98	2.35	1.54	5.48
Sm	1.53	3.56	2.7	4.18	5.55
Tb	0.39	0.57	0.54	0.74	0.9
Tm	0.33	0.51	0.51	0.61	0.65
Yb	1.35	3.4	3.03	3.58	3.51
Sc	22.7	37.5	34.1	51.2	28
Y	6.79	16.2	17.1	19.2	29.7

(continued)

Table 2.5 (continued)

Sample ID	IGCP-42	IGCP-42/1	IGCP-42/6	IGCP-38	IGCP-40
U	0.55	0.68	0.94	0.97	1.82
Th	0.69	2.37	3.04	1.96	7.83
Hf	1.18	2.16	2.49	2.35	3.88
Nb	2.25	8.04	4.59	7.18	8.84
Rb	9.56	1.36	7.11	1.39	29.3
Ta	0.3	0.71	0.46	0.74	0.86

Sample ID	IGCP-6	IGCP-5	IGCP-7	Sample ID	IGCP-6	IGCP-5	IGCP-7
Rock type	Komatiite		Basalt	Rock type	Komatiite		Basalt
SiO_2	41.50	45.50	46.60	Pb	12	16	9
TiO_2	0.55	0.61	1.01	Ce	1.93	2.16	7.03
Al_2O_3	9.48	9.55	14.40	Dy	3.02	2.86	6.23
Fe_2O_3	10.79	8.64	11.88	Er	2.11	1.78	3.51
MnO	0.15	0.14	0.19	Eu	0.78	0.73	1.6
MgO	20.80	12.30	8.30	Gd	2.55	2.5	4.91
CaO	7.60	14.25	9.55	Ho	0.6	0.57	1.3
Na_2O	0.56	0.38	2.54	La	0.76	0.47	2.77
K_2O	0.02	0.01	1.09	Lu	0.37	0.28	0.74
P_2O_5	0.03	0.03	0.11	Nd	3.85	3.72	7.54
CO_2	0.13	0.24	0.04	Pr	0.64	0.48	1.64
H_2O	5.50	5.61	2.60	Sm	2.54	2.03	4.41
S	0	0.0009	0	Tb	0.57	0.44	0.85
Cl	0.004	0.0042	0.0058	Tm	0.37	0.32	0.8
V	183	182	321	Yb	2	2	4
Cr	1890	961	397	Sc	31	31.9	45.2
Ni	1044	379	189	Y	13.5	15	25.3
Cu	105	51	513	U	0.55	0.22	0.76
Zn	73	71	89	Th	0.61	0.5	1.22
Ga	12	18	19	Hf	1.37	1.05	2.85
Sr	42	23	220	Nb	0.69	0.66	2.49
Zr	24	25	49	Rb	3.97	0.68	32.7
Ba	28	20	117	Ta	0.56	0.2	0.45

Sample ID	IGCP-6	IGCP-5	IGCP-7	Sample ID	IGCP-6	IGCP-5	IGCP-7
Rock type	Komatiite		Basalt	Rock type	Komatiite		Basalt
SiO_2	41.50	45.50	46.60	Pb	12	16	9
TiO_2	0.55	0.61	1.01	Ce	1.93	2.16	7.03
Al_2O_3	9.48	9.55	14.40	Dy	3.02	2.86	6.23
Fe_2O_3	10.79	8.64	11.88	Er	2.11	1.78	3.51
MnO	0.15	0.14	0.19	Eu	0.78	0.73	1.6
MgO	20.80	12.30	8.30	Gd	2.55	2.5	4.91
CaO	7.60	14.25	9.55	Ho	0.6	0.57	1.3
Na_2O	0.56	0.38	2.54	La	0.76	0.47	2.77

(continued)

Table 2.5 (continued)

Sample ID	IGCP-6	IGCP-5	IGCP-7	Sample ID	IGCP-6	IGCP-5	IGCP-7
K_2O	0.02	0.01	1.09	Lu	0.37	0.28	0.74
P_2O_5	0.03	0.03	0.11	Nd	3.85	3.72	7.54
CO_2	0.13	0.24	0.04	Pr	0.64	0.48	1.64
H_2O	5.50	5.61	2.60	Sm	2.54	2.03	4.41
S	0	0.0009	0	Tb	0.57	0.44	0.85
Cl	0.004	0.0042	0.0058	Tm	0.37	0.32	0.8
V	183	182	321	Yb	2	2	4
Cr	1890	961	397	Sc	31	31.9	45.2
Ni	1044	379	189	Y	13.5	15	25.3
Cu	105	51	513	U	0.55	0.22	0.76
Zn	73	71	89	Th	0.61	0.5	1.22
Ga	12	18	19	Hf	1.37	1.05	2.85
Sr	42	23	220	Nb	0.69	0.66	2.49
Zr	24	25	49	Rb	3.97	0.68	32.7
Ba	28	20	117	Ta	0.56	0.2	0.45

Sample	G1456	B6889	B6865	B6859	B6891	B6892	P12/86	P46/89	P8/86	P9/86	G1436
SiO_2	43.41	44.68	44.55	40.89	40.60	42.28	46.80	44.90	43.54	41.86	47.90
TiO_2	0.52	0.56	0.39	0.36	0.53	0.54	0.46	0.47	0.58	0.44	0.61
Al_2O_3	10.41	9.84	9.55	7.11	10.19	9.77	10.97	9.90	9.40	8.79	13.42
Fe_2O_3	11.78	11.54	10.85	11.02	11.12	12.04	8.49	11.23	11.52	11.57	9.54
MnO	0.17	0.17	0.17	0.16	0.16	0.17	0.16	0.16	0.17	0.17	0.15
MgO	20.78	22.08	22.60	27.44	21.05	22.37	11.39	21.36	22.13	24.85	8.20
CaO	8.17	8.57	8.77	6.55	7.90	8.80	15.25	8.04	7.39	7.09	12.88
Na_2O	0.85	0.99	0.77	0.10	0.95	0.61	0.44	0.77	0.70	0.33	2.76
K_2O	0.03	0.02	0.01	0.07	0.04	0.04	0.00	0.09	0.02	0.02	0.02
P_20_5	0.04	0.04	0.02	0.02	0.05	0.04	0.03	0.03	0.04	0.03	0.05
LOI	2.88	1.79	2.08	6.08	2.48	3.07	3.95	2.38	4.30	4.69	3.96
Total	99.05	100.28	99.76	99.80	99.06	99.73	97.94	99.33	99.79	99.83	99.47
Cr	2034	1930	2519	3022	1763	1844	3687	2072	1804	2575	316
Ni	926	908	971	1382	1030	908	313	1072	1099	1259	123
Co	79.7	80	79	92.5	77.3	74.4	42.6	75	80.7	87.8	36.1
Sc	36.1	32.9	33.3	28	33	34.6	38.4	34.9	28.7	24.6	42.1
V	193	222	200	141	185	193	221	181	178	152	251
Zr	21.3	21.9	12.8	11.1	20.9	22.3	14.9	17.2	23.6	15.2	28
Hf	0.78	0.67	0.38	0.5	0.64	0.64	0.59	0.59	0.83	0.56	0.91
Nb	0.69	0.64	0.43	0.33	0.6	0.57	0.74	0.52	0.45	0.47	1.26
Th	<0.5	0.076	0.040	<0.5	<0.5	<0.5	<0.5	<0.5	<0.5	<0.5	0.87
U	<0.2	0.020	0.014	<0.2	<0.2	<0.2	<0.2	<0.2	<0.2	<0.2	<0.2
Rb	5.02	1.35	1.20	2.85	3.06	1.39	0.08	5.99	3.05	1.81	0.52
Sr	39	43.3	29.7	27	57	47	18	35	41	71.4	72
Ba	19	5.17	6.56	23	29	16	33	23	21	25	27

(continued)

Table 2.5 (continued)

Sample	G1456	B6889	B6865	B6859	B6891	B6892	P12/86	P46/89	P8/86	P9/86	G1436
Y	13.9	12.5	8.8	8.5	14.2	14.1	12.4	11.5	12.5	9.8	16.5
Cu	89	101	85	76	88	82	148	105	95	85	141
Zn	80	69	65	67	72	76	70	90	78	73	78
La	0.7	0.64	0.36	0.49	1.24	0.68	<0.8	0.89	0.66	<1.0	2.91
Ce	2.08	0.2.05	1.18	1.12	3.20	2.03	1.57	2.00	2.05	2.39	6.51
Pr	0.33	0.39	0.22	0.20	0.50	0.38	0.27	0.31	0.40	0.35	0.82
Nd	2.25	2.37	1.36	1.34	2.70	2.34	1.61	1.69	2.45	1.82	4.00
Sm	0.99	1.11	0.35	0.51	1.08	1.07	0.71	0.72	1.01	0.71	1.22
Eu	0.38	0.48	0.30	0.22	0.47	0.45	0.32	0.32	0.49	0.33	0.51
Gd	1.78	1.84	1.12	1.03	1.79	1.93	1.32	1.46	1.74	1.25	1.90
Tb	0.31	0.36	0.23	0.19	0.33	0.36	0.25	0.24	0.32	0.24	0.36
Dy	2.39	2.33	1.58	1.37	2.23	2.35	1.77	1.79	2.17	1.67	2.47
Ho	0.49	0.53	0.37	0.31	0.51	0.51	0.41	0.40	0.45	0.37	0.58
Er	1.48	1.55	1.14	0.90	1.44	1.50	1.27	1.30	1.29	1.01	1.90
Tm	0.20	0.22	0.17	0.15	0.19	0.22	0.19	0.19	0.19	0.16	0.28
Yb	1.43	1.41	1.07	0.93	1.36	1.42	1.38	1.26	1.23	1.02	1.76
Lu	0.23	0.21	0.17	0.15	0.19	0.20	0.21	0.21	0.19	0.16	0.27

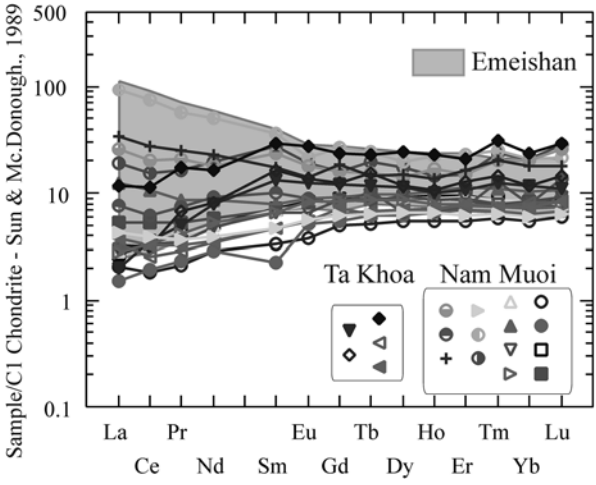

Fig. 2.3 Primitive mantle normalized patterns for Nam Muoi and Ta Khoa low-Ti magma series

ized for mantle plume-related magmas and melt inclusions in Iceland Hawaiian basalts (Sobolev et al. 2000; Breddam 2002). Basing on the REE contents and their distribution patterns (Table 2.5; Fig. 2.4) the komatiitic basalt associations may be divided into 4 groups: (1) peridotite, komatiite and komatiitic basalt group with a chondritic REE normalization pattern inclining to the left shows light-(L)REEs being up to 7 times higher, whereas, the heavy- (H)REEs being even higher, up to 9 times compared with the chondrite (Sun and McDonough 1989); (2) olivine basalts have REE contents 8–10 times higher than the given chondrite values, and show a

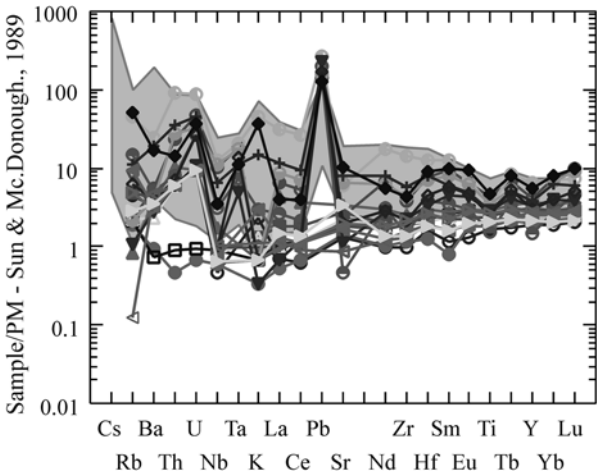

Fig. 2.4 Chondrite normalized patterns for Nam Muoi and TaKhoa low-Ti magma series

relatively flat normalizing curve; (3) Na-rich plagioclase basalt group has REE concentrations 20–40 times higher than the chondrite, showing Eu characteristically negative anomalies; (4) serpentinized peridotites of Ban Phuc massif as well as komatiitic pyroxenite in Nam Chim and Ban Mong dykes show clear differentiated rare earth element distribution, whose concentrations normally exceed those of the chondrite (e.g. Sun and McDonough 1989) 5–25 times with regard to LREEs and 3–9 times for HREEs. The Ban Phuc peridotite chondrite normalized distribution pattern is characterized by clearly Eu negative anomaly (Polyakov et al. 1996). This distribution feature may be related to secondary mineralization such that primary pyroxenes being replaced by serpentine, tremolite, chlorite as well as the appearance of biotite and magnetite. The $(Ce/Yb)_N$ ratios vary between 0.3 and 0.6 indicating a depleted mantle source. In addition, REE concentrations and Gd_N/Yb_N varying within 0.8–1.2 suggest a melting depth equivalent to spinel peridotite field. The olivine basalts show low Nb_N/La_N (0.31–0.42), falling in the field of oceanic island basalt (OIB) (Hanski et al. 2004). Similar geochemical features are also reported for Carboniferous picrites in the Shagin-Menglin ophiolite belt which were suggested to relate Paleotethyan oceanic plateau (Fang Nianqiao and Nin Gaoling 2003).

2.1.2.4 Re-Os and Sm-Nd Isotopic Compositions

14 whole rock Nam Muoi komatiitic samples were chosen for Re-Os and among these, 9 were chosen for Sm-Nd analysis. The samples being komatiite porphyry with olivine (samples G1448, G1456, 8/86, 11/86, 46/89, B6889, B6891, B6892) and needle-shaped clinopyroxene phenocrysts show MgO varying from 20.8 to 29.8 wt%. Other samples such as B6887, B6889 and B6865 were olivine cumulates having MgO between 22.6 and 30.9 wt% and showing such structural features to

Table 2.6 Representative Sm – Nd isotopic compositions of Nam Muoi komatiitic basalt associations (Hanski et al. 2004)

Sample ID	Rock type	Sm (ppm)	Nd (ppm)	$^{147}Sm/^{144}Nd$	$^{143}Nd/^{144}Nd$	ε_{Nd} (250)
B6887	Komatiite	0.6	1.48	0.2466	0.512957 ± 19	4.6
B6889	Komatiite	1.32	2.87	0.278	0.513184 ± 20	8
B6891	Komatiite	1.12	2.77	0.2446	0.513082 ± 10	7.1
B6892	Komatiite	1.2	2.65	0.274	0.513152 ± 10	7.5
G1456	Komatiite	1.13	2.45	0.2778	0.513112 ± 15	6.6
PI 1/86	Komatiite	0.7	1.8	0.2348	0.512869 ± 12	3.2
P9/86	Komatiite	0.8	1.97	0.2464	0.512883 ± 12	3.2
G1436	Ol-basalt	1.4	4.28	0.1972	0.512602 ± 30	−0.8
P73/89	Ol-basalt	2.95	13.06	0.1366	0.512158 ± 10	−7.5

suggest that their temperatures dropped slower while compared with other olivine-bearing porphyry magmas mentioned above. Sample 12/86 is komatiitic basalt (MgO =11.4 wt%); one of the other two samples has MgO lower than 10 wt% and spinifex texture for clinopyroxene, the other is a low-Ti basalt. Being sampled in a strongly metamorphosed zone (up to green schist facies) the collected samples were undeformed. The olivine-rich volcanic rocks are mostly well-reserved. Percentage of olivine being serpentinized and iddingsitized in 8/86 and 11/86 samples is about 50 % while in the other samples this secondary modification process occurs only about 25 % of the olivine grains. Cpx and Pl were not altered in most of the samples (Hanski et al. 2004).

Results of Sm-Nd and Re-Os isotopic compositions are shown in Table 2.6. Analytical procedure was described in detail in Hanski et al. (2004). Below are major comments from this report.

The initial $\varepsilon_{Nd(250)}$ data for komatiites and komatiitic basalts range from 3.2 to 8.0, whereas, for the low-Ti basalts the values are low, varying between −0.8 and −7.5. The high $\varepsilon_{Nd(250)}$ closer to 8 fall in the present depleted mantle field (DePaolo 1981; Goldstein et al. 1984). Correlation between the $\varepsilon_{Nd(250)}$ and the REEs is positive. Komatiites have the highest $^{147}Sm/^{144}Nd$ and the highest ε_{Nd}, the latter decreases as the corresponding $^{147}Sm/^{144}Nd$ decreases. This tendency explains basaltic lavas contaminated by high REE crust. Osmium contents are high in the komatiites, from 1.4 to 7 ppb, low in the komatiitic basalts, 1.2 ppb, and lowest in the basalts, at 0.12 ppb. There is apparent relationship between Os and MgO observed in the Song Da rift and Gorgona komatiites (Fig. 2.5). There is also close relationship between Os and Cr being observed in the Song Da rift volcanics except for Cr-spinel-bearing komatiitic basalts with almond-like structure. Rhenium contents in the Song Da rift volcanic magmas are low, from 0.07 to 0.96 ppb that show no clear relationship with MgO. Rhenium contents in the Song Da basalts are much lower compared with Gorgona basalt (1–3 ppb). In fact, Re contents in Song Da komatiites are also lower than those in Gorgona komatiites. Re and Cr in the two komatiite types do not show any clear relationship (Fig. 2.5). As a result of having high Os and low Re contents

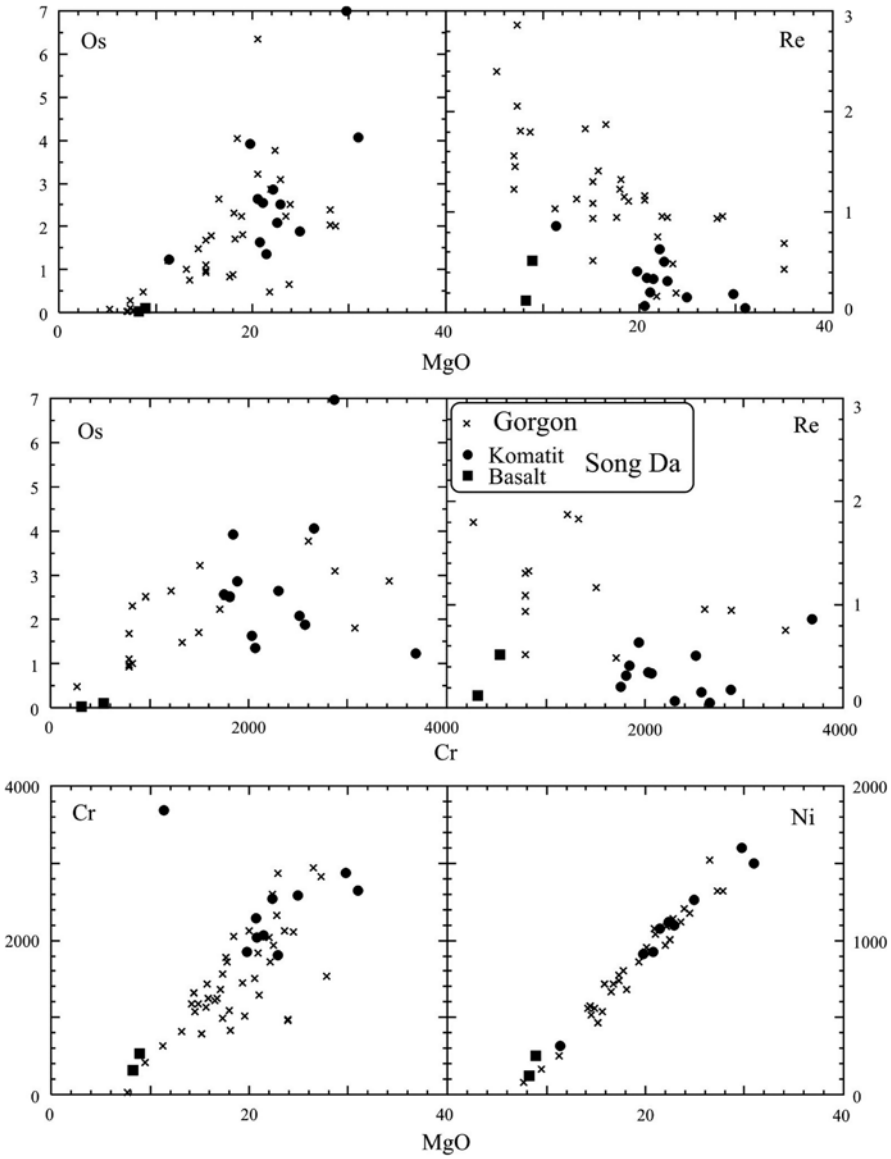

Fig. 2.5 Plots of Ni, Cr, Re and Os against MgO in Song Da rift komatiites (*circle*) and basalts (*square*) in comparison with Gorgona basalt – komatiite complex (*cross*) (The Song Da data are from Hanski et al. 2004)

$^{187}Re/^{188}Os$ ratios in komatiites are low (<1.2 to 0.05; Table 2.7). Among the samples analyzed for Re-Os isotopes 12 samples formed an isochron that yielded an age of 270 ± 21 Ma and an initial $^{188}Os/^{187}Os$ =0.12506 ± 0.00041 (γ_{Os} = +0.02 ± 0.4) (Fig. 2.5). Regardless of large uncertainty the age is consistent with previous Rb-Sr age at 257 ± 24 Ma (Hoa 1995; Polyakov et al. 1996), also consistent with age reported for basalts in the Emeishan large igneous province in China (Zhou et al. 2002).

Table 2.7 Representative of Re-Os isotopic compositions of Nam Muoi komatiitic basalt associations (Hanski et al. 2004)

Sample	Rock type	Re (ppb)	Os (ppb)	MgO (%)	$^{187}Os/^{188}Os$	$^{187}Re/^{188}Os$	Initial 7/8	γ0s
8/86	Komatiite	0.3168	2.511	22.13	0.12764	0.6078	0.12511	–0.2
11/86	Komatiite	0.18	6.995	29.76	0.12549	0.1239	0.12498	–0.3
9/86	Komatiite	0.1476	1.874	24.85	0.12769	0.3795	0.1261	0.6
B6865	Komatiite	0.5111	2.082	22.6	0.12995	1.1833	0.12501	–0.3
B6887	Komatiite	0.0421	4.075	30.94	0.12546	0.0498	0.12525	–0.1
B6892	Komatiite	0.4125	3.915	22.37	0.12752	0.5077	0.1254	0.1
B6889	Komatiite	0.6265	2.8413	22.08	0.1298	1.0627	0.12501	–0.1
B6891	Komatiite	0.2102	2.5286	21.05	0.12668	0.4004	0.12487	–0.3
G1456	Komatiite	0.3456	1.625	20.78	0.13005	1.0249	0.12577	0.4
46/89	Komatiite	0.3378	1.366	21.64	0.12962	1.192	0.12464	–0.5
G1448	Komatiite	0.0674	2.626	20.53	0.1255	0.1236	0.12498	–0.3
12/86	Komatiitic basalt	0.8586	1.238	11.39	0.14043	3.348	0.12645	0.9
G1436	Basalt	0.1188	0.0338	8.2	0.22075(7)	17.156	0.14914	19
	Basalt	0.0648	0.033	8.2	0.23833(7)	9.588	0.19831	58.2
P73/89	Basalt	0.5149	0.1166	8.93	0.26805	21.659	0.17765	41.8

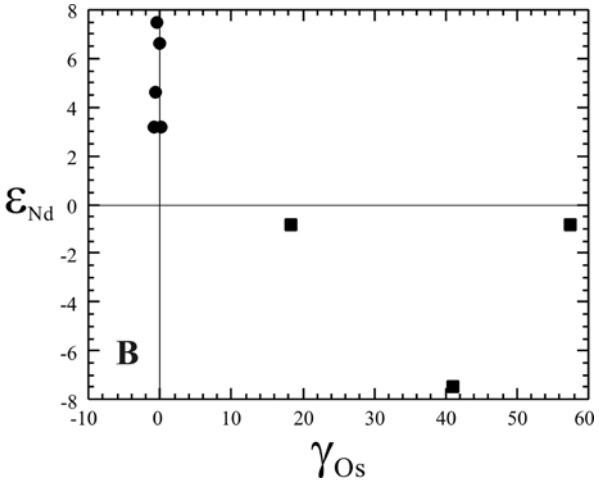

Fig. 2.6 Plots of 250 Ma initial γ_{Os} against ε_{Nd} for Song Da rift komatiites (*circle*) and basalt (*square*)

In contrast to the initial Nd isotopic ratios those vary widely from +3 to +8 the initial $^{187}Os/^{188}Os$ in komatiites change in a small interval from 0.1246 to 0.1264 (γ_{Os} = −5 – +0.9) and 0.1243 to 0.1260 (γ_{Os} = −0.7 – +0.6) (Table 2.7), calculated based on 250 Ma and 270 Ma, respectively. Two basaltic samples, G1436 and P73/89, show higher Os isotopic ratios compared with the initial γ_{Os} from +18 to +58. The initial γ_{Os} data in komatiites are nearly unchanged thus do not correlate with the correspondingly variable initial ε_{Nd} (Fig. 2.6). The basalts have higher γ_{Os} and lower ε_{Nd} compared with the komatiites.

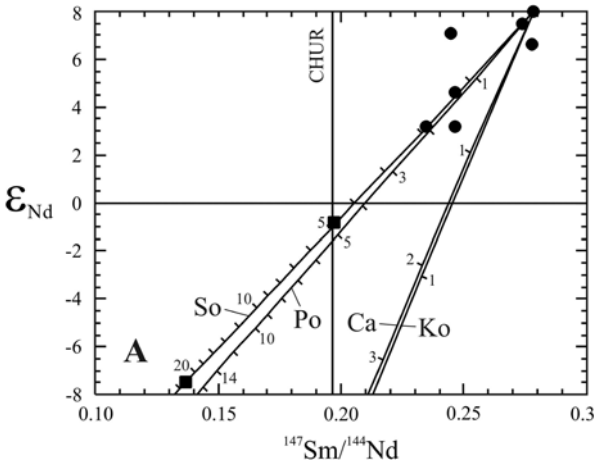

Fig. 2.7 Plots of $\varepsilon_{Nd(250Ma)}$ against $^{147}Sm/^{144}Nd$ for Song Da komatiites (*filled circle*) and basalts (*filled square*)

2.1.2.5 Isotopic Analytical Results

Geochemically Song Da rift komatiites are closely similar to Gorgona Cretaceous komatiites. Possibly they both were generated from long-term REE depleted mantle sources although the Gorgona komatiites show slightly higher ε_{Nd} (ca. +10) than Song Da rift komatiites (max. +8). Initial $^{87}Sr/^{86}Sr$ ratios of Song Da komatiites are 0.70348 (Hoa 1995; Polyakov et al. 1996) accompanied by high ε_{Nd} values, suggesting their being derived from a depleted mantle source. The strontium isotopic ratios are less radiogenic compared with those continental intraplate basalts, for example, the Siberian trap, while only slightly higher than those of Gorgona komatiites (at 0.7027, after Revillion et al. 2002). Majority of osmium isotopic ratios in komatiites from both Song Da and Gorgona are mostly similar to those reported for chondrite. As mentioned above, the geochemical similarity between Song Da and Gorgona komatiites suggests that their mantle sources may show many similar features in geochemistry and thermal state as well as melt generation (Herzberg and O'Hara 2002).

However, it is noteworthy that Song Da komatiitic basalt melts must have been through a continental crust having more heterogeneous compositions compared with the crust where Gorgona komatiitic melts having gone through. Song Da geochemically and isotopically enriched characters suggest the magmas may have been crustally contaminated. Plots of ε_{Nd} vs. $^{147}Sm/^{144}Nd$ show the komatiites lie between a depleted mantle and enriched Proterozoic and Archeanozoic sources suggesting a possible binary mixing (Fig. 2.7). For this mixing model, Archean basement may be Ca Vinh-type granito – gneiss (2800–2900 Ma) (Lan et al. 2001; Nam 2001), whereas gneiss of Song Chay formation and Po Sen-type calc-alkaline granite in northwestern Vietnam may serve as Proterozoic basement (Lan et al. 2000, 2001; Qui et al. 2000).

Proterozoic and Archean crustal contamination eventually leads to significantly decrease in ε_{Nd} and $^{147}Sm/^{144}Nd$, even at as a small percentage as 1–2 % involvement of crustal material. Isotopic results of the Song Da pluton- volcanic associations are not ready to tell what their true, uncontaminated mantle source was; for REE budgets in komatiitic magmas are sensitive to crustal input, therefore, the last eruptive Song Da komatiites may represent their true mantle source most similar to that of Gorgona source (for example, having $\varepsilon_{Nd}=+10$). If this is true the uncontaminated mantle of Song Da depleted komatiites may have $^{147}Sm/^{144}Nd$ ratios about 0.315 and their LREE concentrations may have been even smaller than the acquired results. Basalts in the komatiite – basalt associations having low $\varepsilon_{Nd,}$ high γ_{Os}, low Nb and Ta, aside from undergoing fractional crystallization and melt differentiation, may have been contaminated by crustal material as much higher percentage as 5–20 %. However, in contrast to Sm – Nd isotopic systematics, Re-Os system in komatiites is not affected by a small input of continental crust material, this possibly because Os concentration is very high in komatiites (>1 ppb) compared with that in continental crust (ca. 0.05 ppb) (Walker and Nisbet 2002). Therefore, osmium isotopic ratios possibly reflect the true mantle source signature even there is evidence of crustal involvement. Notice that as because Os content in komatiitic basalts is much smaller (ca. 0.03 ppb) than in komatiites, they, therefore, may be affected by crustal contamination more than the latter; as a result their primary osmium isotopic ratios may be higher.

Mixing model using initial isotopic compositions of komatiitic magmas and basement rocks represented by Ca Vinh (Ca) Archean granite in northwestern Vietnam and Conglin (Ko) granite in southwest China is illustrated in Fig. 2.7. Mesoproterozoic basement is represented by Song Hong (So) and Po Sen (Po) complexes (Lan et al. 2000, 2001; Qui et al. 2000). Values participating in the mixing model include $\varepsilon_{Nd(250)}$, Sm, Nd, respectively, for komatiite: +8, 1 ppm, 2.2 ppm; Ca: −33.4, 13.6 ppm, 78.7 ppm; Ko: −44.9, 3.02 ppm, 27.6 ppm; So: −10.3, 7.5 ppm, 41.1 ppm, Po: −131.1, 5.2 ppm, 32.9 ppm.

Apparently, the Nd and Os isotopic compositions of Song Da rift and Gorgona komatiite – basalt indicate that mantle sources of these two Phanerozoic komatiitic series were most similar to the presently defined depleted MORB mantle (DMM). Recent studies have shown that komatiitic magma can be produced by highly depleted mantle such as DMM under hydrous pressure. Based on experimental and geochemical data Grove et al. (1999) and Parman et al. (2001) suggested that Barberton 3.49 Ma komatiites were generated by hydrous melting of peridotite at a subduction zone. They observed that geochemical features of Barberton komatiitic basalt are mostly similar to boninites produced by melting of depleted peridotites which experienced previous melting events at an Archean mid-ocean ridge or a back-arc spreading axis. Shimizu et al. (2001) suggested that late Archean Belingwe komatiite was produced by mantle plume melting containing about 0.5 % water evidenced by high water contents in melt inclusions in Cr-spinel. Experimental studies of high pressure melting with or without water showed that anhydrous melting of mantle plume may also be a potential generation of komatiites (Asahara and Ohtani 2001).

Anhydrous melting of a DMM source may be considered as melting temperature for komatiitic generation in the upper mantle is rather low relative to that required for an anhydrous melting. High MgO in komatiites have been produced by anhydrous melting at melting temperatures that are 140–320 °C higher than a MORB melt (Herzberg and O'Hara 2002). This thermal state is difficult to present in the depleted upper mantle condition (Arndt and Christensen 1992). Hydrous melting mechanisms may be best explanation for Song Da rift komatiites for there are expressions of crustal contamination being explained by the input of highly incompatible elements from subducted lithospheric slab into the komatiite upper mantle source. Although Song Da komatiites can be produced by H_2O-saturated DMM source; but this is less likely for the LREE depletion nature of the komatiites. Mantle plume-related magmas, for example, OIB types, are more hydrous compared with MORB. The OIB magmas are thought not only being produced by hotspots but also by 'wet'-spot (Shilling et al. 1980; Wallace 1998; Nichols et al. 2002). Water contents in plume-related magmas depend on the magmatic composition; the more enriched in incompatible elements is the richer water magma (Danyushevsky et al. 2000). It has been explained that during OIB magma melting and crystallization water behaves as a lithophile element whose incompatibility may be comparable to that of La or Ce (Michael 1995). Melt inclusions in underwater volcanic rocks and in primary minerals from arc magmas show a positive correlation between H_2O/Y and Ce_N/Yb_N (r =0.99) (after Danyushevsky et al. 2000; Dixon and Clague 2001; Saal et al. 2002). If geochemical behavior of water in Song Da komatiitic melts was as mobile as any incompatible element most of their depleted primary magmas with Ce_N/Yb_N around 0.3 must have H_2O/Y lower than 200; meaning that the water concentration was no more than 0.03 wt%. Because there is no other evidence on the relationship between water and LREE in non-arc basaltic magmas, it may suggest that highly depleted Song Da komatiites may be produced by anhydrous melting of a primarily depleted mantle source. However, it is noteworthy that if Rb, Ba and Sr enrichment was inherited from their respective mantle source this phenomenon has to be expressed by slight increase in H_2O/Ce ratio and high water content in their mantle source.

Sub-continental lithosphere mantle (SCLM) can be source mantle for komatiites; however, like the DMM, thermal factor required for melting is not adequate. Although some komatiites may be produced in SCLM by metasomatism (Walker and Stone 2001); however, this possibility is ignored for the osmium isotopic data do not provide such evidence.

In the recent years there have been opinions that some mantle plume show geochemically and isotopically depleted characters therefore depleted mantle, not necessary DMM, can play a major component in a mantle plume source (Hart et al. 1992; Arndt et al. 1997; Fitton et al. 1997). However, the nature of depleted mantle and its role in a (mantle) plume are subject for wide debates (Kerr et al. 1995). Depleted mantle plume and DMM occur in Iceland where plume overlies Atlantic mid-ocean ridge. Highly variable geochemical and isotopic characteristics in Iceland and Reykenes basalts may be viewed as consequences of mixing between DMM and enriched Iceland mantle plume (Sun et al. 1975). However, based on

geochemical and isotopic (especially Pb) properties of the Iceland basalts several researchers stated that basalts and picrites that were depleted in incompatible elements may be produced by mantle other than DMM (Kerr et al. 1995; Kempton et al. 2000; Chauvel and Hémond 2000). Using Nb/Y vs. Zr/Y correlation diagram (Fitton et al. 1997) Iceland depleted magma is different from N-MORB. This opinion has not been shared by many. For example, Hanan et al. (2000) suggested that geochemical variations in Iceland and Reykjanes basalts and picrites may reflect mixtures of enriched mantle plume and surrounding mantle similar to N-MORB.

Determination of mantle sources for continental flood basalts (CFB) is even more difficult given the fact that if the magmas were produced by sub-lithospheric source, this may be obscured either by crustal assimilation or interaction with SCLM. In reality, geochemical and isotopic N-MORB-like magmas are rare in CFB (Thomson et al. 1983; Carlson 1991). The most depleted magmas are commonly observed for highly primitive lavas, for example, picrite from North Atlantic magmatic province (Saunders et al. 1997) and Horing Bay dykes in Namibian coastal areas (Thomson and Gibson 2000), and perhaps these Song Da rift komatiites.

Addition of a small amount of crustal material does not affect the Os isotopic compositions in komatiites; therefore, Os isotope can be the most important signature of the mantle source. Komatiites are the major component of Gorgona magma, their chondritic Os isotope composition plots in DMM field, mixture of peridotite, MORB glass and ophiolitic chromite (Walker et al. 2002). This combination is not compatible with any theoretically known average DMM. Whereas, Song Da komatiites show twice lower radiogenic values compared with a DMM at 250 Ma, whose radioactive evolution is estimated based on an average composition of chromite of ultramafic magmas in a Phanerozoic ophiolitite formation (Walker et al. 2002).

If mantle source for the Song Da komatiites is not DMM their chondritic Os component may be residual portions of oceanic lithosphere having depletion history closely similar to that of DMM. Kerr et al. (1995) presented that ultramafic lava in Caribbean large igneous province may be formed by depleted sources introduced from lower mantle. They argued that highly refractory (and depleted) oceanic lithosphere subducted to core mantle boundary was later brought up by a plume.

Therefore, geochemical and isotopic features of the Song Da high-Mg, low-Ti magmas suggest that they may be closely associated with mantle plumes which originated from the core mantle boundary. This southeast Asian magmatic province is not the only example, Permian – Triassic Siberian trap may also be another plume-related. Given the fact that Norinsk-type Ni-Cu-PGE mineralization is well developed in the Siberian trap; naturally, this potential resource can also be discovered in the Song Da rift region.

2.1.2.6 Composition of Primitive Melts and T-P Parameters

Experiments show that low-Al komatiite partial melts are formed under hydrous condition at depths between 500 and 650 km, while high-Al komatiites are formed by higher melting degrees, at depths lower than 450 km (Ohtani et al. 1989). Other

Table 2.8 Chemical compositions (wt%) of primitive melts for Nam Muoi and Ta Khoa komatiitic basalt associations

No	1	2	3	4	No	1	2	3	4
SiO_2	46.99	44.17	47.48	46.21	Na_2O	1.08	0.32	1.17	0.86
TiO_2	0.61	0.56	0.92	0.70	K_2O	0.11	0.11	0.57	0.26
Al_2O_3	11.54	10.36	11.09	11.00	P_2O_5	0.10	0.08	0.10	0.09
FeO	11.37	12.28	11.59	11.75	P_1	0.0	0.0	0.0	0.0
MgO	17.58	23.24	17.03	19.28	P_2	25	50	22	30
CaO	10.62	8.88	10.05	9.85	T°C	1510	1660	1500	1560

Remark: P_1, P_2 are crystallizing (P_1) and melting (P_2) pressures. T°C: melting temperature. 4 is average of 1, 2, and 3

experiments (e.g. Ryabchikov and Bogachikov 1984) showed that Iilgar-type primitive komatiitic melt was produced by 50 % partial melting of primitive mantle lherzolite at P = 35–37 kb and T = 1775–1825 °C. According to these authors Barberton-type komatiitic melt may be produced by 60–65 % partial melting of lhezolite at higher pressure and temperature, ca. 50 kb and 1875–1975 °C, respectively. They suggested that the difference between picrite – basalt and komatiite – basalt rock types depends on the variation and nature of fluids; komatiite – basalt melts are associated with 'dry' fluids while picrite – basalt and picrite – dolerite melts being produced under hydrous condition. Our recent studies may be used to expand the latter explanation. Our results showed that komatiite – basalt, in comparison to picrite – basalt and picrite – dolerite associations, are more enriched in Al, Mg, Ca, Ni, Co, Cr, Yb and Lu, while they are poorer in Ti, Fe, P, Rb, Sr, V, Nb, Ta, Zr and REEs (Balykin and Petrova 2000). Besides, we have found that evolution trend from Precambrian komatiitic basalt associations to Phanerozoic komatiitic basalt and picritic basalt associations is expressed by gradual decrease in of normative hypersthene (Balykin 2004). Primitive composition extrapolation of low-Ti ultramafic – mafic rocks shows result that is correspondent to komatiitic basalt (Table 2.8).

Calculation of normative co-existing minerals for the komatiitic basalt association shows a high pressure assemblage of Ol-Px-Gr while the total of accessory minerals such as apatite, ilmenite and phlogopite does not exceed 1–2 %, the latter amount is about 5–7 % in picritic basalt and dolerite associations. This may mean that the mantle source for picritic basalt associations is more enriched in incompatible elements and fluids compared with that of the komatiitic basalt. The above explanation is in favor to a suggestion that komatiitic melt is produced by progressive melting of a depleted mantle source, which had undergone previous melting to produce basaltic melt enriched in incompatible elements (Arndt 1976). Plots of Song Da high- and low-Ti magmas on a Fo-Di-Py diagram (Davies and Schairer 1965) show that the primitive komatiitic basalt melt is closely similar to observed komatiitic basalt, whereas the primitive melt of picritic basalt and dolerite is similar to that of melanobasalt (Balykin et al. 2001; Balykin 2004).

Modeling crystallization of primitive melts of komatiite, komatiitic basalt, olivine basalt was conducted using software program 'Comagmat-3.3' (Ariskin et al.

1993). This program allows for selecting initial melt compositions (among the given hypothetical melts) which provide co-existing mineral assemblages that are best fit for both calculated (normative composition) and real mineral assemblages as well as their crystallizing order. Comagmat 3.3 program can determine liquidus temperatures with accuracy within ±10 °C of more than 70 % of mineral cases; while accuracy of phase compositions is within ±2 % (for plagioclase us ±2.8 %).

In general, the composition of Song Da komatiitic basalt initial melt is MgO = 17.0–23.2 wt%. High aluminum content in clinopyroxene indicates that the initial crystallization pressure of Ol and Cpx was not lower than 10 kb (Balykin et al. 2001).

2.1.2.7 General Remark on the Komatiitic Basalt Associations

The Song Da komatiite – basalt associations in northwestern Vietnam may be viewed as part of Emeishan large igneous province, formed by melting of the top of a mantle plume under the Yangtzi craton during Permian – Triassic time (Chung et al. 1998). Following India- Eurasian collision during the Pliocene – Miocene (ca. 27–22 Ma) left lateral movement to the northeast of Ailao Shan – Red River shear zone displaced the now Song Da rift magmatic associations from the main basaltic province in southwest China. The komatiitic basalt associations currently are distributed within the axial area of the rift zone, comprising lava flows, dykes as well as lenses of pluton-volcanic mafic rocks. Komatiites intercalated with komatiitic basalts are dominant in the lower section, while upper sections are comprised by komatiitic basalt, olivine basalt being overlain by plagiobasalt. Eruption ages of the magmas are 257 ± 24 Ma (by Rb/Sr age dating), and 270 ± 21 Ma (by Re/Os age dating). The magmas, varying from high-Al komatiites to low-Al basalts, are characterized by having low alkalis, very low titanium and high Mg. They are rich in Ni, Co, Cr, Cu and poor in Fe, Rb, Ba, Sr, Nb, Ta, Nd, Hf, Zr and REEs. The komatiites and komatiitic basalts are relatively low in REE concentrations; however, their LREE contents are 2–7 times higher, and HREE are 5–9 times higher than those of the chondrite. Song Da rift komatiitic basalt associations are rare phenomena for Phanerozoic komatiitic basalt activity, not to mention the presence of Ni-Cu and PGE ore-formation is believed to associate with the komatiites. Digital modeling showed that the initial melt composition was correspondent to komatiitic basalt.

Song Da komatiites show many geochemical indexes similar to Gorgona Island's Cretaceous komatiites. They both are high-Al (compared with Archean komatiites), low incompatible elements and low LREE/HREE ratios. In difference from Gorgona komatiitic melts formed as part of oceanic magmatic plateau of Caribbean type, Song Da magmas were mantle derived interacted with continental lithosphere. This is evidenced by the presence of Proterozoic sialic signature in Nd isotopic systematics and LILE concentrations in high-Mg Song Da magmas; while their accompanying Os isotopes show signatures which are closer to a DMM source. Moreover, initial isotopic features and depletion of incompatible elements (e.g., Ce/Sm $\leq$0.3) of the Song Da komatiitic basalt magmas are closely similar to chondrite values.

This may mean that, the Song Da source had been depleted in incompatible and light rare earth elements for long period while showing Re/Os isotopic ratios similar to that of chondrite. In summary, Song Da komatiites may serve as a rare example of continental plateau basalts which contain geochemical and isotopic signatures of their primary source mantle.

Systematic variation of water and incompatible elements in present oceanic island basalts is not related to a subduction zone, therefore, we may assume that Song Da primitive komatiitic melts being depleted in water and incompatible elements were generated at the anhydrous topmost part of a mantle plume. High Mg in their primary melts indicate deep rooted origin and that melting temperature was about 200 °C higher than average potential temperature of a MORB primary source (Herzberg and O'Hara 2002). This unusual high temperature can only be expected at the hottest center of an initial plume. Geochemical and isotopic properties of the Song Da magmas and those from Caribbean oceanic plateau and North Atlantic large igneous provinces provide more evidence to support that plume-related melts may be formed at the boundary between lower mantle and core.

2.1.3 High-Ti Basalt Associations

2.1.3.1 Spatial Distribution and Geology

As mentioned above, high-Ti mafic volcanic and accompanying sub-volcanic magmas belong to three association-types: andesite – basalt (with rhyolite), picrite – basalt and trachyandesite-trachydacite – trachybasalt. They are widely distributed in marginal areas of the Song Da structure. Andesite – basalt associations outcrop mainly in the Cam Thuy and Son La Pass areas, southwestern wing of the structure (Fig. 2.1). Picrite – andesite – basalt associations have only been discovered in Nam So, northeastern tip of Song Da structure; while rhyolite – basalt associations are popular in Kim Boi, Vien Nam (Doi Bu), Ba Vi and Van Yen – Phu Yen (Suoi Chat). Trachyandesite – trachydacite – trachybasalt associations have only been found in the Nam Muoi area, northwestern side of Song Da structure. Outcrops of felsic rocks of various sizes and chemical compositions are being found in each high-Ti basalt field. Felsic magmas are rarely encountered among andesite – basalt and picrite – andesite – basalt associations, but highly common among rhyolite – basalt and trachyandesite-trachydacite – trachybasalt formations. Felsic volcanic and sub-volcanic rocks associated with rhyolite – basalt rock type show calc-alkaline geochemical character; while those found in trachyandesite – trachydacite – trachybasalt associations are sub-alkaline type.

Basalts and andesitobasalts in the Cam Thuy area are characterized by aphanitic sometimes doleritic texture, almond-shaped structure; albitization, actinolitization and chloritization (greenization), previously termed as spilite, are strongly developed. Basalts in the Kim Boi, Ba Vi (Vien Nam – Doi Bu), Phu Yen – Van Yen (Suoi Chat) show similar petrologic characteristics.

High-Ti basalts (andesite – basalt association) in the Son La Pass area are geochemically homogenous, showing aphanitic texture, almond-shaped structure filled with chlorite, epidot, albite and chalcedony. The basaltic groundmass is microdiabas, pilotaxitic texture with main microlites being uralitized plagioclase and clinopyroxene. No olivine is being observed in andesite – basalt associations, but fine-grained, diffused titanomagnetite is common. In many geological cross-sections aside from basalts encountered also are andesitobasalt and andesite. Among the basalt, andesitobasalt and andesite outcrops found also are small sub-volcanic bodies or dykes of diabase or gabbro-diabase.

Basaltoids belonged to the picrite – andesite – basalt associations in northwestern margin of the Song Da structure form an elongate belt running in the northwest – southeast direction from upstream of Nam So, south of boundary between China and Vietnam, in the north. A full cross-section for this association can be observed in an area northwest of Tam Duong town, Lai Chau province. Major constituents of the cross-section are mafic volcanic magmas, including picritodolerite (melanobasalt), dolerite, basalt and andesitobasalt (leucobasalt); picrite and andesite types are minor. Picrite is found in picritodolerite and other mafic volcanic cross-sections in the Nam So upstream area. The magma is fine-grained aphanitic texture and dark colored. Among the major rock-forming minerals are Cpx microlites in the groundmass, serpentinized or talcized olivine phenocrysts and altered plagioclase. Titanomagnetite is widely found. Picrite is chemically sub-alkaline and picritobasalt (ankaramite), having high Mg, low Al but high potassic alkalinity. The magma is also relatively high in Ti and P oxides. Picrite having high Mg and Ti contents has so far been found in the Nam So area. This picrite type is chemically different from ultramafic magmas in picrite – diabase association outcropped in the Ba Vi area although the picrite shows closely spatial connection with high-Ti volcanic magmas in this area (Polyakov et al. 1996). Chemically ultramafic magmas in the picrite – dolerite association are low-Ti and relatively low-alkaline type.

Picritodolerites (melanobasalt) are wider spread compared with picrites, and show spatial relation to basalts and andesitobasalts. The magmas are dark-colored, aphyric or porphyritic texture with Cpx and Pl in the phenocryst; the groundmass is ophitic, microdoleritic or taxitic. They are high in Mg and Ti, relatively high in alkalis, including K. Chemically they are close to sub-alkaline picritobasalt although their MgO contents are slightly lower.

Sub-alkaline basalts and andesitobasalts (leucobasalts) are dominant in Nam So and Phong Tho cross-sections. Chemical compositions of the leucobasalts are high variable; among these porphyritic basalts are most common with Cpx and Pl being in the phenocryst. The minerals present at various proportions forming different rock types such as pyroxene basalt or plagio-basalt. The groundmass is hialopilitic or microdoleritic. Almond-shaped structure is sometimes occurred where almonds are filled with epidote and calcite. The basalt and andesitobasalt rock types show relatively high T, K and P oxides. Besides, andesitodacites are also found but at a minor scale. Found also are sub-volcanic bodies comprised of diabase and dolerite.

Structurally volcanic cross-sections in the areas of Cam Thuy, Bac Yen – Van Yen (Suoi Chat), Hoa Binh, Kim Boi – Ba Vi, Vien Nam (Doi Bu) show distinct features

compared with those in the Son La Pass, Nam So and Nam Muoi areas. Firstly, commonly found are high-Ti and alkaline basalts equivalent to trachybasalt (Na-type), sub-alkaline felsic, and (Na-rich) alkaline magma types. Secondly, bright-colored lava flows and dyke-bodies are spread in, respectively, Kim Boi and Vien Nam – Bac Yen. Chemically the basalts are similar to basalts in andesite – basalt association in the Cam Thuy area (described above), in that they are high in TiO_2, relatively high Na_2O and P_2O_5. Small lherzolite, pyroxenite intrusive bodies and diabase dykes are commonly discovered in Ba Vi within the Song Da structure, Chim Thuong in southern margin of the Tu Le basin, and Dong Nghe – Suoi Can – Nga Hai belonging to the Phan Si Pan uplift and neighboring areas. At an outcrop in the Chim Thuong area there are a number of small-sized intrusive bodies comprising a chemically complex rock types including picrite and diabase, where picrite being distributed at the center and diabase being located at the periphery. These bodies normally cut conformably Paleozoic sediment-metamorphic (including shale, quartzite) strata. Other small intrusive bodies of peridotite (and picrite) are observed in the Ba Vi area, these bodies show closely spatial relationship with the above high-Ti mafic volcanic magmas and were previously grouped to Ta Khoa ultramafic magmas as Ban Xang complex (Tran Van Tri and Truong Cam Bao 1977). These Ba Vi and Dong Nghe – Suoi Can ultramafic bodies together with high-Ti diabase dykes were later grouped as picrite-diabase and viewed as sub-volcanic formations in affiliated with trachyandesite – trachydacite – trachbasalt associations in the Ba Vi area (Polykov, Yem et al. 1996). These are also high-Ti (relatively to low-Ti ultramafic volcanics), Mg, low- Al and relatively low alkalis. Phenocryst minerals include Ti-augite and kaersutite. The diabase is high-Ti and sub-alkaline (Na-K alkaline).

The intrusive ultramafic magmas are Pl-bearing wehrlite and lherzolite with a minor amount of clinopyroxenite, tremolitite, serpentinite and asbestos lenses. Main rock-forming minerals are Ol (f_{Ol} = 14.1–16.5), Cpx and small amount of highly basic Pl. Accessory minerals include of biotite, Cr-spinel and magnetite. In some intrusive olivine gabbro, gabbro-norite and gabbro are also found.

It is noteworthy that a meimechite (high magnesian alkaline) variation was found in the Hoa Binh hydropower dam area. Based on petrologic and chemical compositions this magma is equivalent to volcanic picrite. This picrite rock type was also found in the Doi Bu area but was described as olivine basalt (Lu 2004). Details of the magma so far have not yet been studied; but there is possibility that the magma is volcanic counterpart of intrusive peridotite being commonly observed in the Ba Vi area. Typical volcanic picrite is porphyritic with phenocryst of variously serpentinized olivine and pyroxene, and glassy groundmass.

2.1.3.2 Mineralogical and Geochemical Characteristics

Chemical compositions of major rock-forming minerals and ores of the studied pluton – volcanic series are shown in Tables 2.9, 2.10, 2.11, and 2.12. The olivines are highly magnesian, equivalent to forsterite – chrysolite. Olivines in mafic rocks are high ferrous (up to 22.5 %). The clinopyroxenes are low-Ti and alkaline, although

Table 2.9 Chemical compositions (wt%) of olivines in mafic-ultramafic intrusives, Dong Nghe – Suoi Can area (Polyakov et al. 1996)

Sample ID	FeO	MgO	CaO	NiO	Ni. ppm	f_{Ol}
Picrite. lherzolite and wehrlite						
B6185	16.01	43.6	0.3	0.09	707	17.1
B6187	17.75	41.53	0.24	0.08	644	19.3
B6809	14.59	44.08	0.33	0.27	2130	15.7
G1414	9.19	48.55	0.25	0.39	3074	9.6
G1415	10.35	47.91	0.15	0.36	2812	10.8
G1417	8.55	48.97	0.24	0.37	2907	8.9
G1418	12.51	45.55	0.29	0.26	2028	13.4
Clinopyroxenite and melagabbro-dolerite						
G1419	14.9	43.69	0.3	0.29	2278	16.1
G1420	20.49	39.37	0.27	0.24	1893	22.5

Table 2.10 Chemical compositions of clinopyroxenes in high-Ti mafic volcanic in Song Da structure (EPMA analyzed at IGM, SB-RAS)

Sample ID	T1552	H608	P-9	H616	H614	B6816
	Nam So area					
SiO_2	51.34	49.74	50.63	51.72	50.49	49.31
TiO_2	0.57	0.95	0.92	0.85	1.1	1.64
Al_2O_3	3.26	5.42	3.12	1.9	2.75	2.6
Cr_2O_3	0.58	1	0.1	0.81	0.01	0.02
FeO	4.73	5.2	7.58	6.52	11.13	10.56
MgO	16.08	14.48	14.9	17.1	15.76	14.48
CaO	21.49	22.2	21.17	19.49	17.08	20.78
Na_2O	0.28	0.44	0.44	0.38	0.39	0.36
f_{Cpx}	15.6	16.8	22.2	17.7	29.9	29
Wo	44.8	47.9	44.3	40.4	34.4	42.2
En	46.6	43.3	43.4	49.2	46	41
Fs	8.6	6.9	12.3	10.4	19.6	16.8

Sample ID	H669	47/88	52/88	51/88	57/88	G1414	P156	P163	G1405
	Vien Nam area					Suoi Can area			
SiO_2	47.73	51.75	50.69	50.06	52.91	52.19	50.12	50.19	52.02
TiO_2	2.45	0.46	0.91	1.46	0.34	0.46	1.38	0.75	0.75
Al_2O_3	4.4	2.72	1.8	2.99	1.29	3.03	3.82	4.22	2.46
Cr_2O_3	–	1.13	–	0.09	0.57	0.63	0.17	0.99	0.01
FeO	10.37	3.82	13.14	10.13	5.21	6.88	6.77	5.12	10.16
MgO	13.24	17.08	14.27	14.65	18.52	18.02	15.42	15.86	16.31
CaO	19.95	22.06	17.75	19.31	20.12	18.11	20.9	21.69	17.26
Na_2O	0.72	0.27	0.37	0.4	0.16	0.26	0.38	0.24	0.19
f_{Cpx}	30.5	11.2	34.1	28	13.7	17.6	19.7	15.7	25.9
Wo	42.9	45.2	37.1	40.5	40.3	37.3	45.6	45.2	36
En	39.7	48.7	41.5	42.8	51.6	51.7	46.8	46.2	47.4
Fs	17.4	6.1	21.4	16.7	8.1	11	7.6	8.6	16.6

Table 2.11 Chemical compositions of plagioclases in high-Ti mafic volcanics in Song Da structure (Polyakov et al. 1996)

Sample ID	SiO_2	Al_2O_3	FeO	CaO	Na_2O	K_2O	An	Ab	Or
Nam So area									
H608	54.71	27.68	0.14	9.49	5.91	0.28	48	51	1
P-9	61.75	21.11	0.73	3.97	7.88	3.91	20	60	20
Son La area									
B6816	52.95	27.94	0.97	11.78	4.8	0.4	58.6	39	2.4
T1687	58.65	21.63	3.42	10.13	5.69	0.05	50	50	
H668	54.63	28.06	0.34	9.69	5.73	0.16	49	50.5	0.5
H675	56.99	26.75	0.34	8.54	7.04	0.09	40	60	-
H676	52.83	23.17	2.99	10.46	6.95	0.09	51	49	-

Table 2.12 Chemical compositions of Cr-spinel in high-Ti lherzolite in Song Da structure (Polyakov et al. 1996)

Sample ID	TiO_2	Al_2O_3	Cr_2O_3	Fe_2O_3	FeO	MgO	MnO	NiO	ZnO
	Đồng Nghê – Suối Cẩn area								
G1417	0.33	16.22	48.93	4.34	18.42	10.19	0.54	0.1	0.06
G1418	0.29	16.64	48.37	4.56	18.08	10.42	0.53	0.16	0.03
T509	0.39	15.78	49.39	4.43	17.31	10.85	0.53	0.12	0.07
P156	0.33	17.42	49.37	4.03	14.82	12.76	0.48	0.1	0.05
T510	0.27	15.3	49.2	5.15	19.98	9.16	0.56	0.1	0.05

some are high-Ti and –Na. Chemical compositions of ore minerals such as Cr-spinel and sub-Fe-Cr-picotite are nearly invariable. Detailed descriptions are given in (Hoa 1995; Polyakov et al. 1996).

Representative chemical compositions of the sub-volcanic pluton and volcanic rocks are given in Tables 2.13 and 2.14. Plots of TiO_2 vs. SiO_2 and P_2O_5 vs. SiO_2 (Fig. 2.8) of Song Da samples in comparison with Emeishan representatives suggest the following.

Except for metabasalts from Cam Thuy, Hoa Binh, Vien Nam, Suoi Chat and picrite from Nam So, the samples are high in Ti and K that vary in large intervals (TiO_2 = 2.1–3.5 wt%; K_2O = 1.1–1.8 wt%). Their P_2O_5 contents are also high that vary between 0.2 and 0.55 wt%. These geochemical features are closely similar to those of Emeishan, East African rift and Oslo Paleo-rift. Dark-colored picrite, picritobasalt (pircritodolerite) in the Nam So area also show Ti, Mg and alkaline geochemical similarity to Emeishan picrite and picritobasalt.

Judging the behavior of major elements, especially characteristic elements such as Ti, K and P, Song Da high-Ti ultramafic – mafic magmas are comparable with corresponding magmatic types in large igneous provinces (LIP) such as Emeishan. Plots of MgO vs. TiO_2, Na_2O and K_2O among the Song Da magmatic associations show that Ti, Na and K increase from andesite – basalt (Cam Thuy and Son La areas) to picrite – andesitobasalt – basalt and trachyandesite – trachydacite – trachybasalt

Table 2.13 Major (%wt) and trace element (ppm) compositions in high-Ti basalts in the Nam Muoi area (1–4: analyzed in Finland; 5–7: analyzed at IGM, SB-RAS)

	IGCP-11	IGCP-12/1	IGCP-7/2	IGCP-8	16/86	P141/89	P142/89
Sample ID	1	2	3	4	5	6	7
SiO_2	47.6	47.4	48.2	50.2	50.33	47.85	48.52
TiO_2	2.14	3.51	3.54	4.26	4.04	2.64	2.56
Al_2O_3	13.9	11.6	13.9	13.4	13.18	15.03	12.97
Fe_2O_3	13.32	14.4	13.93	15.09	13.85	11.4	12.66
MnO	0.2	0.14	0.19	0.08	0.18	0.16	0.2
MgO	5.57	5.31	5.66	4.48	3.49	6.04	6.96
CaO	8.23	3.65	5.66	3.91	6.74	8.96	6.7
Na_2O	4.34	3.66	2.8	5.72	2.77	3.25	2.14
K_2O	0.61	0.73	1.62	1.56	3.24	1.07	1.09
P_2O_5	0.23	0.55	0.6	0.65	0.58	0.37	0.35
V	352	407	386	390			
Cr	170	29	40	6			
Ni	78	46	57	38			
Cu	222	188	490	193			
Zn	117	130	154	86			
Ga	20	27	33	29			
Sr	400	281	408	79			
Zr	151	263	395	424			
Ba	305	101	467	200			
Ce	45	73.7	115	153	112.2	52.3	40.4
Dy	5.68	7.98	6.91	7.87			
Er	3.18	4.73	3.73	3.91			
Eu	1.75	3.78	3.03	3.17	3.9	2.5	2.1
Gd	5.92	11.1	10.5	12	11.6	8.9	5.6
Ho	1.12	1.51	1.33	1.38			
La	20.1	32.2	51.1	68.2	59.3	24.8	19.1
Lu	0.29	0.84	0.46	0.26	0.4	0.4	0.3
Nd	23.6	46	57.3	66.3	58.3	30.6	23.8
Pr	5.39	9.97	14	17.5			
Sm	5.09	12.8	11.2	11.5	14.3	8.2	6.4
Tb	0.99	1.67	1.41	1.61	1.7	1.4	0.9
Tm	0.41	1.09	0.54	0.4			
Yb	2.62	4.54	3.03	2.63	3.4	2.9	2.3
Sc	44	25.6	20.9	25.2			
Y	33.4	34.9	36.7	42.3			
U	0.71	1.71	2.09	1.71			
Th	3.22	4.19	8.1	8.47			
Hf	4.01	6.59	7.87	8.82			
Nb	15	27.7	41	53.2			
Rb	18.2	29.6	27.7	24.8			
Ta	0.88	2.14	2.15	3.31			

Table 2.14 Major (%wt) and trace element (ppm) compositions of high-Ti picrite and basalt in the Nam So (1–5) and Son La (7–8) areas

	H615	H617	P18	T1495	T1648	H639	B6816	B6817
Sample ID	1	2	3	4	5	6	7	8
SiO_2	46.07	50.09	43.89	44.99	48.47	46.27	46.31	48.47
TiO_2	2.35	2.69	2.14	4.44	1.58	2.31	3.38	3.41
Al_2O_3	14.02	11.36	6.55	13.10	14.64	9.04	14.09	13.60
Fe_2O_3	13.87	12.34	12.76	15.64	13.93	13.23	14.12	13.37
FeO	0.00	0.00	0.00	0.00	0.00	0.00	0.00	0.00
MnO	0.24	0.18	0.19	0.24	0.23	0.22	0.23	0.25
MgO	7.32	7.72	22.91	4.67	7.40	12.16	5.06	4.61
CaO	8.24	8.85	10.22	9.98	10.31	12.78	10.55	8.80
Na_2O	3.29	3.06	0.21	2.26	2.39	2.49	2.98	3.29
K_2O	1.25	0.82	0.17	1.16	0.79	0.63	1.03	1.81
P_2O_5	0.20	0.30	0.27	0.56	0.18	0.25	0.60	0.72
Ce	43	64	49	113	29	68	58.90	78.50
Eu	1.80	2.30	1.70	3.30	1.39	2.20	2.90	3.40
Gd	4.90	6.60	4.50	9.30	5	5.40	8.70	11.60
La	20.40	31.30	23.60	56.20	13.60	33.00	27.40	37.80
Lu	0.20	0.30	0.20	0.50	0.45	0.20	0.30	0.40
Nd	24	34	26	55	17	36	35.20	45.20
Sm	5.60	7.80	5.60	11.70	4.50	7.40	9.60	12.00
Tb	0.80	1.00	0.70	1.50	0.85	0.80	1.30	1.70
Yb	1.80	2.20	1.20	3.30	3	1.70	2.30	2.30

H615 – H617: dolerite; P19: picrite; T1495: basalt; H639: picritodolerite; B6816-6817: basalt (Hoa 1995; Polyakov et al. 1996)

(Tables 2.13 and 2.14; Fig. 2.8). Note that K_2O/Na_2O ratios in Vien Nam – Doi Bu and Suoi Chat dacites and rhyodacites are usually <1; whereas the ratios are >1 in trachyandesite-trachydacite in the Nam Muoi area. Regardless of having difference K/Na ratios all the felsic magmas show high Nb (74–126 ppm), Ta (5–9 ppm), La (71–140 ppm), Ce (135–259 ppm). Primitive mantle normalized trace element distribution patterns for alkaline felsic magmas are intraplate in character (Fig. 2.9).

According to the chemical compositions picrite-diabase sub-volcanic – volcanic associations may be divided into three groups: ultramafic (plagioperidotite, olivine plagiopyroxenite); sub-ultramafic (dark-colored pyro-xenite) and mafic (gabbro and diabase). The pyroxenite, gabbro and diabase being usually high in Ti, relatively high alkalis, especially K, are viewed as typical high-Ti mafic magmas. The wehrlite and lherzolite are low in Ti and alkalis, in general, but relatively high when compared with ultramafic magmas in komatiite – basalt associations having the same MgO concentrations mentioned earlier. Cu, Ni, Co and Cr are relatively low in the basaltoids (including picrite and picritodolerite), lower compared with mafic magmas in the komatiite – basalt associations; whereas these elements are high in lherzolite and wehrlite in the Ba Vi and Nam Chim areas. The enrichment is similarly observed in Permian mafic magma in the Cao Bang area, northeast Vietnam (see below).

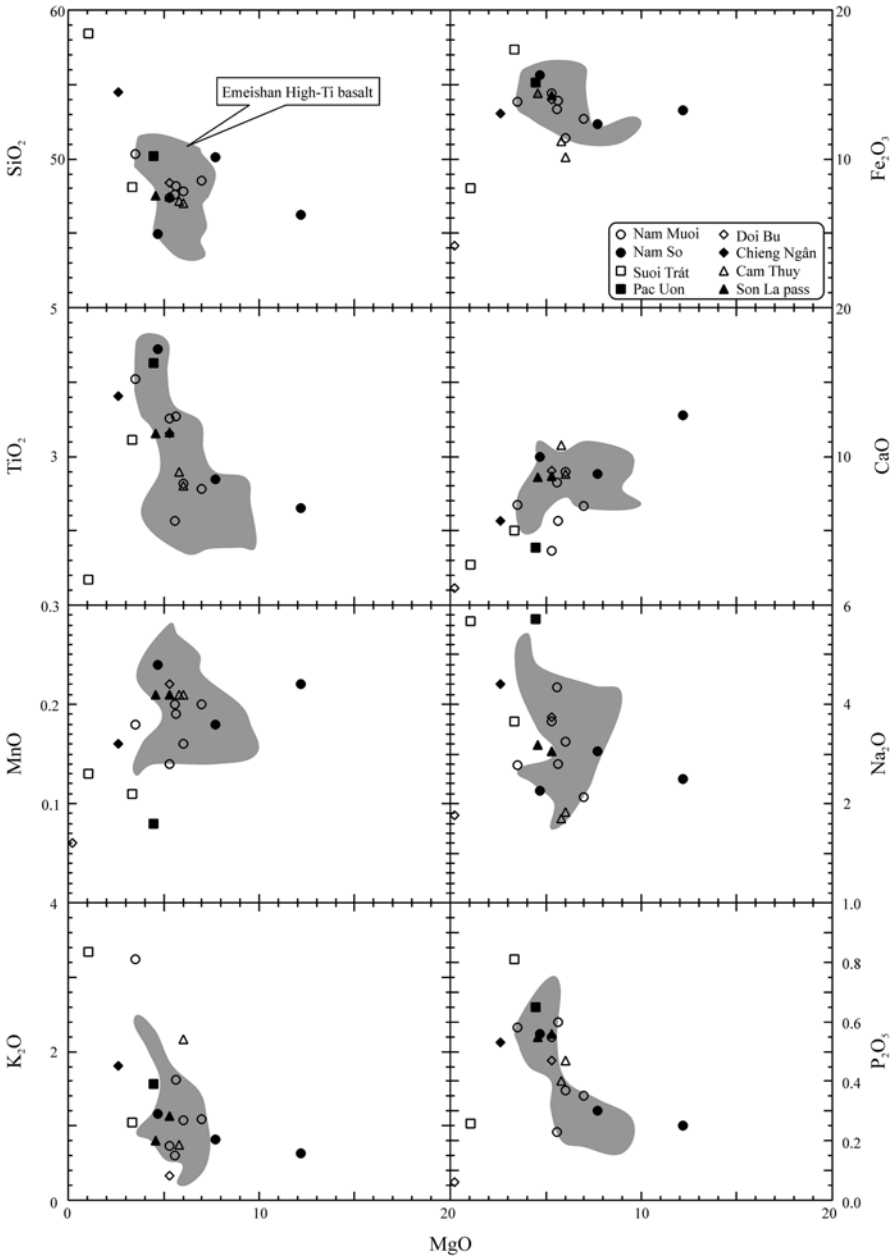

Fig. 2.8 Harker diagram for Song Da high-Ti basaltoids in comparison to high-Ti Emeishan (China) basalts

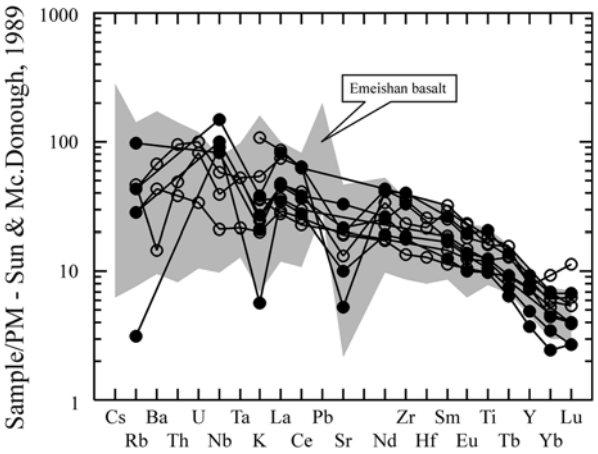

Fig. 2.9 Primitive mantle normalized trace element distribution patterns of Song Da Nam Muoi and Nam So high-Ti volcanics (Emeishan data are from Chung et al. (1998))

Song Da Permian basaltoids in the Nam So and Nam Muoi areas are high in Nb (26–53 ppm), Zr (151–424 ppm) and the rare earths, especially LREE (Tables 2.13 and 2.14). Primitive mantle normalized distribution patterns reveal positive anomalies at Nb, Ta, Rb, Zr, Ce and Th, while some samples show slightly negative anomalies at Nb and Zr, and strongly negative anomaly at Sr (Fig. 2.9); these are typical geochemical features of sub-alkaline continental rift-related basaltoids. Enrichment of Nb, Th, Zr and LREE is clearly observed in trachybasalt, trachyandesite and trachydacite in the Nam Muoi area where some sub-alkaline felsic magmas show high enrichment is Nb (97–164 ppm), Ta (6 ppm) and Zr (622–896 ppm) (Polykov et al. 1996). Primitive mantle normalized patterns of the trachyandesite and trachydacite magmas (Figs. 2.9 and 2.10) are intraplate in nature, mostly similar to Permian – Triassic trachyte and trachyrhyolite magmas in the nearby Tu Le structure. Absolute values of (for example) Nb and Zr in the basalts and bright-colored volcanic rocks are usually 20–100 (for Nb) or 10–40 times higher compared with given primitive mantle values (e.g. Sun and McDonough 1989). Dark-colored picrites and picritedolerites in the Nam So area are also characterized by high Nb, Ta, Th, Ce and Zr; these features distinguish the magmas from lhezolites in the picrite-diabase associations. In classification plots of Zr/Y vs. Zr most of the high-Ti Song Da basaltoids fall in field of intraplate magmatism (Hoa et al. 1998; Hoa 2002).

Basalt and trachybasalt in the Suoi Chat, Van Yen, Vien Nam, Kim Boi and Doi Bu areas show oceanic island basalt-like primitive mantle normalized distribution patterns similar to that observed for basalt and picritobasalt in the Nam So and Nam Muoi areas, in that they both are enriched in Rb, Nb, Ta and the rare earths (Figs. 2.11 and 2.12). Having different in K/Na ratios the felsic magmas of magma associations in these areas show high Nb (74–126 ppm), Ta (5–9 ppm), La (71–140 ppm), and Ce (135–259 ppm). Primitive mantle normalized distribution patterns of

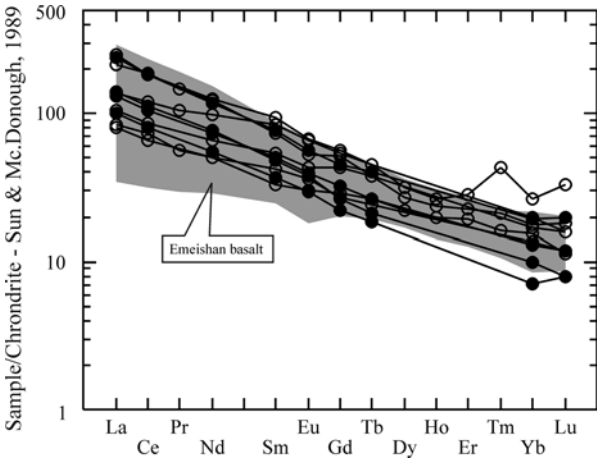

Fig. 2.10 Primitive mantle normalized trace element distribution patterns of Song Da high-Ti basalts in the Nam Muoi and Nam So areas (Emeishan basalts are after (Chung et al. 1998))

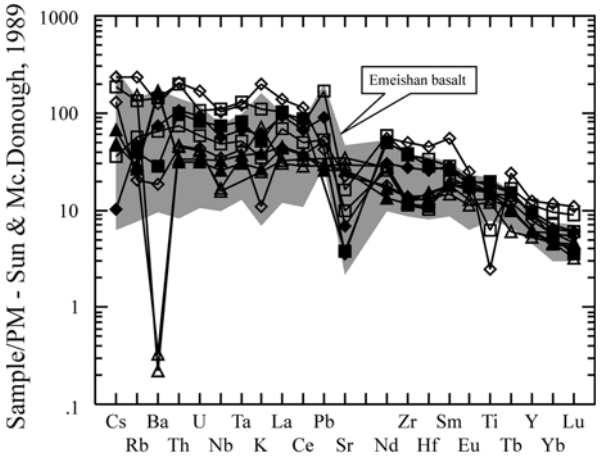

Fig. 2.11 Primitive mantle normalized trace element distribution patterns of Song Da high-Ti basalts in the Cam Thuy, Vien Nam, Suoi Chat and Doi Bu areas (Emeishan basalts are after (Chung et al. 1998))

the alkaline felsic volcanics are typical intraplate (Fig. 2.11). Note that lherzolite in the Thu Cuc area are low in Rb (3.99–4.77 ppm), Sr (40.88–57.97 ppm), Zr (20.49–25.69 ppm), Nb (1.76–2.26 ppm) and the rare earth elements (Table 2.15). Except for having slightly higher LREE, these geochemical compositions are mostly similar to low-Ti ultramafic magmas (komatiites) (Fig. 2.13). Gabbro associated with high-Ti basalts in the Suoi Chat area is characteristically high Rb (31.4 ppm), Sr (437.9 ppm), Zr (57.49 ppm), Nb (18.01 ppm) and the rare earths, similar to those in high-Ti basalts in the area (Figs. 2.11, 2.12).

Table 2.15 Geochemical compositions of lherzolite and picrite in the Ba Vi and Thu Cuc areas

Sample ID	10-123	10-124	10-126	IGCP-47	IGCP-48		IGCP-47	IGCP-48
SiO_2	42.5	42.1	39.3	44.46	41.67	Zr	25.69	20.49
TiO_2	0.73	0.81	0.66	0.52	0.41	Nb	2.26	1.76
Al_2O_3	5.4	6.4	5.8	8.59	5.9	Ba	33.12	26.27
Fe_2O_3*	10.46	9.32	10.57	11.45	11.55	La	2.25	1.81
MnO	0.11	0.12	0.13	0.17	0.17	Ce	4.91	3.82
MgO	25.97	25.58	27.37	23.09	28.52	Pr	0.67	0.53
CaO	5.44	5.41	4.18	8.44	6.3	Nd	2.26	1.76
Na_2O	0.09	0.13	0.07	0.49	0.02	Sm	1.03	0.79
K_2O	0.05	0.05	0.13	0.08	0.05	Eu	0.35	0.27
P_2O_5	0.11	0.1	0.07	0.03	0.02	Gd	1.28	0.97
Mkn	8.2	8.57	10.65			Tb	0.26	0.19
Total	99.7	99.35	99.68			Dy	1.72	1.37
Cu	24	32	4			Ho	0.39	0.29
Ni	1493	1415	1336	934.4	1250	Er	1.13	0.87
Co	85	86	83			Tm	0.17	0.12
V	190	196	78	191.9	150.8	Yb	1.12	0.87
Cr	2390	2388	2941	2417	3176	Lu	0.17	0.13
Sc				30.72	24.23	Hf	0.69	0.55
Cs				0.3	0.15	Ta	0.15	0.12
Rb				4.77	3.4	Pb	0.47	0.1
Sr				57.97	40.48	Th	0.52	0.45
Y				10.85	8.25	U	0.12	0.11

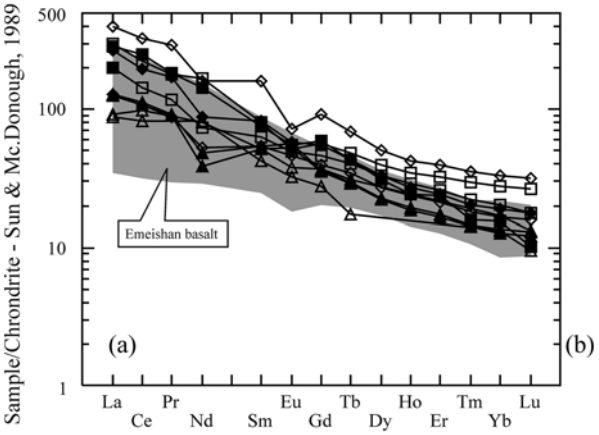

Fig. 2.12 Primitive mantle normalized trace element distribution patterns of Song Da high-Ti volcanics in the Cam Thuy, Vien Nam, Suoi Chat and Doi Bu areas (Emeishan data are after (Chung et al. 1998))

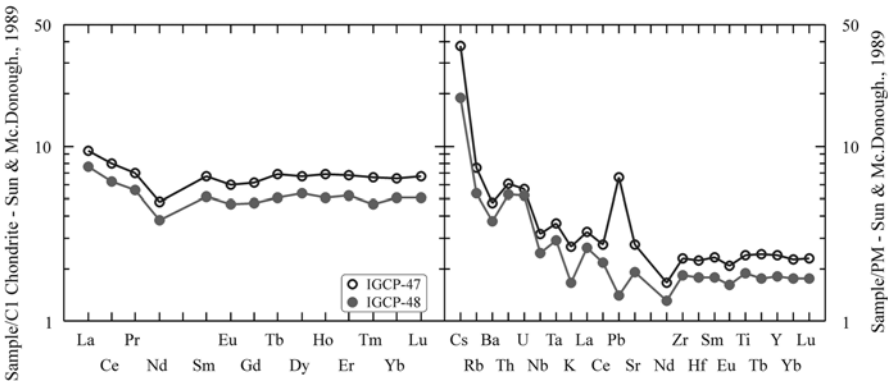

Fig. 2.13 Chondrite and primitive mantle normalized rare earth and trace element distribution patterns of Ba Vi lherzolites (Sun and McDonough 1989)

Initial $^{87}Sr/^{86}Sr$, $^{143}Nd/^{144}Nd$ and $^{206}Pb/^{204}Pb$ isotopic ratios of high-Ti basalts, rhyodacite in the Doi Bu and Suoi Chat areas vary, respectively, between 0.706–0.709, 0.5119–0.5124, and 18.32–23.5, indicating involvement of crustal material in the magma source (Hoang et al. 2004). Crustal involvement in the Song Da magma source or during magmatic melt evolution may be possible for the northwestern rim of the Song Da rift is bordered by the Truong Son mountain range where marginal pluton-volcanic magmas are wide-spread.

2.1.3.3 Source and Melt Generation Characteristics

The geochemical and isotopic compositions of Song Da mafic and ultramafic volcanic rocks indicate that their mantle source or magmatic melts were contaminated by crustal materials. However, questions remained are whether crustal involvement happened in the source mantle or after melt generation, e.g. wall-rock assimilation. Assuming dacite (and trachydacite) and rhyolite (trachyrhyolite) being formed by fractional crystallization of basaltic melts generated in the lithospheric mantle, therefore involvement of any crustal material must be related to previously subducted slab into the mantle. The difference in elemental enrichment of Nb, Ta, Zr and other incompatible elements in the high-Ti volcanic magmas, as well as geochemical signatures of sub-oceanic lithospheric mantle in the low-Ti magmas may be explained by specific Song Da rift magmatic evolution in the Permian and lithospheric mantle source heterogeneity under South China craton's marginal continents. Besides, the formation of (high field strength elements: HFSE) Nb-, Ta-, Zr-rich trachybasalts and their fractional sub-alkaline felsic magmas in the Nam Muoi, Suoi Chat and Doi Bu areas may be explained by low-degree partial melting of sources having been depleted by previous melting events to form high-Ti magmatic melts in the Cam Thuy, Son La and Nam So areas (Polyakov et al. 1996).

However, this model is lacking of formation order of basaltic melts in northwestern and southeastern Song Da rift. Up to date, there only a few relative reliable age data have been reported including 257 ± 24 Ma for komatiitic basalt in the axial area of Song Da rift (Hoa 1995; Polyakov et al. 1996) and 270 ± 21 Ma (Hanski et al. 2004); whereas Carboniferous (283 ± 21 Ma) (Hoang et al. 2004) may need additional evidence. It is interesting that Rb/Sr age dating on dacite whole rocks believed to genetically related to Song Da basalts yielded a Permian – Triassic age of 256 ± 15 Ma (e.g. Hoang et al. 2004).

The above description of regional geochemical features of Song Da high-Ti basaltic associations suggests that mantle sources from where high-Ti melts being generated may be locally 'independent' present. There was also possibility that during the HFSE-rich magma generation additional alkaline and incompatible elements having been introduced by a mantle plume. This remark is supported by (Anh et al. 2011) showing that the high-Ti basalts have relatively restricted ranges of $(^{87}Sr/^{86}Sr)_i$ (0.7048–0.7079) and ƐNd(t) values (−5.7 to +3.1) indicating weak lithospheric signature that may be related to their trace element-rich nature and this is consistent with abundant earlier studies suggesting that the high-Ti basalts at Song Da or elsewhere in the ELIP formed from low degrees of partial melting (Xu et al. 2001; Wang et al. 2007). The silisic rocks (trachyandesite, trachydacite) which occur in high-Ti basalts of the Song Da structure having ƐNd(t) values from −0.1 to 0.6, was formed by fractional crystallization of the associated high-Ti basalts.

References

Ariskin AA, Frenkel MY, Barmina GS, Nielsen RL (1993) COMAGMAT: a Fortran program to model magma differentiation processer. Comput Geosci 19:1155–1170

Arndt NT (1976) Melting relations of ultramafic lavas (komatiites) at 1 atm and high pressure. Carnegie Inst Wash Yearb 75:551–561

Arndt NT, Christensen U (1992) The role of lithospheric mantle in continental flood volcanism; thermal and geochemical constraints. J Geophys Res 97(10):967–10981

Arndt NT, Kerr AC, Tarney J (1997) Dynamic melting in plume heads; the formation of Gorgona komatiites and basalts. Earth Planet Sci Lett 146:289–301

Asahara Y, Ohtani E (2001) Melting relations of the hydrous primitive mantle in the CMAS-H2O system at high pressures and temperatures, and implications for generation of komatiites. Phys Earth Planet Inter 125:31–44

Balykin PA (2004) Composition and PT-conditions of melting of parental magmas for komatiite-basalt, picrite-basalt, and picrite-dolerite complexes. 32nd IGC, Florence

Balykin PA, Petrova TE (2000) Petrological types and genesis of komatiite-basalt, picrite-basalt and picrite-dolerites complexes. Russ Geol Geophys 41:1098–1111

Balykin PA, Polyakov GV, Petrova TE, Shelepaev PA, Tran Trong Hoa, Ngo Thi Phuong, Hoang Huu Thanh (2001) Composition of initial melts for Permo-Triassic and Triassic-Jurassic ultramafic-mafic complexes in North Vietnam. Rep RAS 378(2):225–229 (in Russian)

Breddam K (2002) Kistufell: primitive melt from the Iceland mantle plume. J Petrol 43:345–373

Bùi Minh Tâm, Tô Văn Thụ (1995) New report on volcanic and dyke phased magmas in the Phong Tho (Lai Chau) area. Geology – mineral resources and oil and gas of Viet Nam I, pp 89–96 (in Vietnamese with English abstract)

Carlson RW (1991) Physical and chemical evidence on the cause and source characteristics of flood basalt volcanism. Aust J Earth Sci 38:525–544

Chauvel C, Hémond C (2000) Melting of a complete section of recycled oceanic crust: trace element and Pb isotopic evidence from Iceland. Geochem Geophys Geosyst 1, 1999GC000002

Chung SL, Jahn BM, Genyao W, Lo CH, Bolin C (1998) The Emeishan flood basalt in SW China: a mantle plume initiation model and its connection with continental breakup and mass extinction at the Permian-Triassic boundary. In: Flower MFJ, Chung SL, Lo CH, Lee TY (eds) Mantle dynamics and plate tectonics in East Asia, vol 27, AGU geodynamics series. American Geophysical Union, Washington, DC, pp 47–58

Danyushevsky LV, Eggins SM, Falloon TJ, Christie DM (2000) H_2O abundance in depleted to moderately enriched mid-ocean ridge magmas; part I: incompatible behaviour. Implications for mantle storage and origin of regional variations. J Petrol 41:1329–1364

Davies BTC, Schairer JF (1965) Melting relations in the join diopside-forsterite-pyrope at 40 kilobars and at one atmosphere. Carnegie Inst Wash Yearb 64:123–126

De Paolo DJ (1981) Neodymium isotopes in the Colorado Front Range and crust – mantle evolution in the Proterozoic. Nature 291:684–687

Dixon JE, Clague D (2001) Volatiles in basaltic glasses from Loihi Seamount, Hawaii: evidence for a relatively dry plume component. J Petrol 42:627–654

Do Dinh Toat (1987) Petrology of Upper Permian and Upper Permian – Lower Triassic effusives in Cam Thuy – Ba Vi area. PhD dissertation, Hanoi University of Geology and Mining

Dobresov NL (2005) The Asian's large igneous provinces (250Ma): Siberian's and Emeishan's traps (plateau-basalts) and associated granitoids. Geol Geophys 46(9):870–890

Fang Nianqiao, Nin Gaoling (2003) Late paleozoic ultramafic lavas in Yunnan, SW China. J Petrol 44(1):141–157

Fitton JG, Saunders AD, Norry MJ, Hardarson BS, Taylor RN (1997) Thermal and chemical structure of the Icelandic plume. Earth Planet Sci Lett 153:197–208

Gatinsky YG (1986) Geodymanics of Southeast Asia in relation to the evolution of ocean basins. Palaeogeogr Palaeoclimatol Palaeoecol 55:127–44

Gatinsky YG, Thuc DD (1982) Geological structure and development of the Song Da peleorift zone in Vietnam. Bull Mineral Soc (Vietnam) 57:12–25

Goldstein SL, O'nions RK, Halmington PJ (1984) A Sm-Nd isotopic study of atmospheric dusts and particulates from major rive systems. Earth Planet Sci Lett 70:221–236

Grove TL, Parman SW, Dann JC (1999) Conditions of magma generation for Archean komatiites from the Barberton Mountainland, South Africa. In: Fei Y, Bertka CM, Mysen BO (eds) Mantle petrology: field observations and high pressure experimentation: a tribute to Francis R. (Joe) Boyd, vol 6, The geochemical society, special publication. Geochemical Society, Houston, pp 155–167

Hanan BB, Blichert-Toft J, Kingsley R, Schilling JG (2000) Depleted Iceland mantle plume geochemical signature: artifact of multicomponent mixing? Geochem Geophy Geosyst 1, 1999GC000009

Hanski E, Walker RJ, Hubma H, Polyakov GV, Balykin PA, Tran Trong Hoa, Ngo Thi Phuong (2004) Origin of the Permian-Triassic komatiites Northwestern Vietnam. Contrib Miner Petrol 147:453–469

Hart SR, Hauri EH, Oschmann LA, Whitehead JA (1992) Mantle plumes and entrainment; isotopic evidence. Science 256:517–520

Herzberg C, O'Hara MJ (2002) Plume – associated ultramafic magmas of Phanerozoic age. J Petrol 43:1857–1883

Izokh AE, Polyakov GV, Tran Trong Hoa, Balykin PA, Ngo Thi Phuong (2005) Permian-Triassic ultramafic-mafic magmatism of Northern Vietnam and Southern China as expression of plume magmatism. Russ Geol Geophys 46(9):942–951

Kempton PD, Fitton JG, Saunders AD, Nowell GM, Taylor RN, Hardarson BS, Pearson G (2000) The Iceland plume in space and time: a Sr-Nd-Pb-Hf study of the North Atlantic rifted margin. Earth Planet Sci Lett 177:255–271

Kerr AC, Saunders AD, Tarney J, Berry NH, Hards VL (1995) Depleted mantle-plume geochemical signatures: no paradox for plume theories. Geology 23:843–946

Khain VE, Balukhovsky AN (1993) Geotectonic. Mesozoi and Cenozoic. AVIAR, 451 p

Lan CY, Chung S-L, Jason Jiun-San Shen, Lo CH, Wang PL, Tran Trong Hoa, Hoang Huu Thanh, Mertzman SA (2000) Geochemical and Sr-Nd isotopic characteristics of granitic rocks from Northern Vietnam. J Asia Earth Sci 18:267–280

Lan CY, Chung SL, Lo cH, Lee TY, Wang PL, Li H, Dinh Van Toan (2001) First evidence for Archean continental crust in Northern Vietnam and its implications for crustal and tectonic evolution in Southeast Asia. Geology 29(3):219–222

Metcalfe I (1996) Pre-Cretaceous evolution of SE Asian terranes. In: Hall R, Blundell D (eds) Tectonic evolution of Southeast Asia. Geological Society Special Publications 106, London, pp 97–122

Michael P (1995) Regionally distinctive sources of depleted MORB: evidence from trace elements and H_2O. Earth Planet Sci Lett 131:301–320

Ngo Thi Phuong (1994) Permo-Triassic high-Magnesium volcano-plutonic associations in the Song Da structure. PhD dissertation. Thesis, Institute of Geology and Mineralogy, SB RAS, Novosibirsk, 24 pp

Ngo Thi Phuong, Tran Trong Hoa, Tran Tuan Anh (2001) Petro-minerallogical characteristics of the P2-T1 basalts-komatiite association in the Ta Khoa Anticline, Song Da Zone (NW Vietnam. J Geol Ser B, No 17–18, pp 10–19

Nguyen Dac Lu (2004) The relationship between volcanic rocks of Da River and Viet Nam areas and copper-gold mineralization. North Vietnam Geol Mapp Div, Geol Miner of Vietnam 4:166–174 (in Vietnamese)

Nguyen Hoang, Nguyen Đac Lu, Nguyen Van Can (2004) Paleozoic volcanics in the Song Da structure: Rb-Sr age of Doi Bu volcanics. J Geol A281:11–17 (in Vietnamese with English abstract)

Nichols ARL, Carroll MR, Höskuldsson A (2002) Is the Iceland hot spot also wet? Evidence from the water contents of undegassed submarine and subglacial pillow basalts. Earth Planet Sci Lett 202:77–87

Ohtani E, Kawabe I, Moriyama J, Nagata Y (1989) Partitioning of elements between majorite garnet and melt and implication for petrogenesis of komatiite. Contrib Mineral Petrol 103:263–269

Parman SW, Grove TL, Dann JC (2001) The production of Barberton komatiites in an Archean subduction zone. J Geophys Res Lett 28:2513–2516

Polyakov GV, Balykin PA, Glotov AI et al (1991) High-magnesian volcanites in Da river zone. In: Proceedings of the second conference on geology of Indochina, HN, 11–13 Nov 1991, vol 1, pp 247–261

Polyakov GV, Nguyen Trong Yem, Balykin PA, Tran Trong Hoa, Hoang Huu Thanh, Tran Quoc Hung, Ngo Thi Phuong, Petrova TE, Van Van V (1996) Permian – Triassic mafic and ultramafic formations in northern Viet Nam. Science and Technology Publ, Hanoi, 172 p (in Vietnamese)

Qiu YM, Gao S, McNaughton NJ, Groves DI, Ling W (2000) First evidence of >3.2 Ga continental crust in the Yangtze craton of South China and its implications for Archean crustal evolution and Phanerozoic tectonics. Geology 28:11–14

Révillon S, Chauvel C, Arndt NT, Pik R, Martineau F, Fourcade S, Marty B (2002) Heterogeneity of the Caribbean plateau mantle source: Sr, O and He isotopic compositions of olivine and clinopyroxene from Gorgona Island. Earth Planet Sci Lett 205:91–106

Ryabchikov ID, Bogachikov OA (1984) Physico-chemical conditions of formation and differentiation of Karelsk's komatiites. Geochemistry, No 5, pp 625–638 (in Russian)

Saal AE, Hauri EH, Langmuir CH, Perfit MR (2002) Vapour undersaturation in primitive mid-ocean-ridge basalt and the volatile content of Earth's upper mantle. Nature 419:451–455

Saunders AD, Fitton JG, Kerr AC, Norry MJ, Kent RW (1997) The North Atlantic igneous province. In: Mahoney JJ, Coffin MF (eds) Large igneous provinces: continental, oceanic and planetary flood volcanism. American Geophysical Union, Washington, DC, pp 45–93

Schilling J-G, Bergeron MB, Evans R (1980) Halogens in the mantle beneath the North Atlantic. Phil Trans Roy Soc Lond A297:147–178

Shimizu K, Komiya T, Hirose K, Shimizu N, Maruyama S (2001) Cr-spinel, an excellent micro-container for retaining primitive melts – implications for a hydrous plume origin for komatiites. Earth Planet Sci Lett 189:177–188

Sobolev AV, Hofmann AW, Nikogosian IK (2000) Recycled oceanic crust observed in 'ghost plagioclase' within the source of Mauna Loa lavas. Nature 404:986–990

Sun SF, McDonough WF (1989) Chemical and isotopic systematics of oceanic basalts: implication for mantle composition and processes. In: Saunders AD, Norry NJ (eds) Magmatism in ocean basins. Geol. Soc. Spec Pub 42, London, pp 313–345

Sun SS, Tatsumoto M, Schilling JG (1975) Mantle plume mixing along the Reykjanes Ridge axis; lead isotopic evidence. Science 190:143–147

Thompson RN, Gibson SA (2000) Transient high temperatures in mantle plume heads inferred from magnesian olivines in phanerozoic picrites. Nature 407:502–506

Thompson RN, Morrison MA, Dickin AP, Hendry GL (1983) Continental flood basalts … arachnids rule OK? In: Hawkesworth CJ, Norry MJ (eds) Continental basalts and mantle xenoliths. Shiva, Nantwich, Cambridge, MA, pp 158–185

Tong Dzuy Thanh, Vu Khuc (eds) (2005) Stratigraphic divisions of Vietnam. National University Publ, Hanoi, 504 p (in Vietnamese)

Tran Ngoc Nam (2001) SHRIMP U-Pb isotopic age dating on zircons of the Ca Vinh and Xom Giau complexes. J Geol A262:1–11 (in Vietnamese with English abstract)

Tran Trong Hoa (ed) (1995) Study of Mesozoic – Cenozoic magmatism and its mineralization potential. Final report for national project KT- 01–04 (1992–1995). Archives of the National Center for Science and Technology Information, Hanoi (in Vietnamese)

Tran Trong Hoa (2002) Subdivision and correlation of Permian – Triassic basaltoid associations in the Song Da structure (NW Vietnam). Geol Ser B 19–20:22–30

Tran Trong Hoa (ed) (2005) Intraplate magmatism in Viet Nam and related mineral resources. Final report for Viet Nam – Russian collaboration protocol (2002–2004). Archives of the National Center for Science and Technology Information, Hanoi, 333 p (in Vietnamese)

Tran Trong Hoa (2007) Intraplate magmatism in North Vietnam and related metallogeny. Dissertation of Dr. of Science. Institute of Geology and Mineralogy, Siberian Branch, RAS, Novosibirsk, 382 p

Tran Trong Hoa, Hoang Huu Thanh, Tran Tuan Anh, Ngo Thi Phuong, Hoanh Viet Hang (1998a) High – Ti Permian-Triassic basaltoid of Song Da rift. Material composition and geodynamic forming conditions. J Geol Ser A 244:7–15

Tran Trong Hoa, Hoang Huu Thanh, Tran Tuan Anh, Ngo Thi Phuong, Hoang Viet Hang (1998b) High-Ti basaltoidic formations in the Song Da rift zone: chemical compositions and geodynamic conditions of magma genesis. J Geol A244:7–15 (in Vietnamese with English abstract)

Tran Trong Hoa, Tran Tuan Anh, Ngo Thi Phuong, Pham Thi Dung, Tran Viet Anh, Izokh AE, Borisenko AS, Lan CY, Chung SL, Lo CH (2008) Permo-Triassic intermediate-felsic magmatism of the Truong Son belt, eastern margin of Indochina. Compt Rendus Geosci 340:112–126

Tran Trong Hoa, Tran Tuan Anh, Pham Thi Dung, Lan Ching-Ying, Usuki Tadashi, Polyakov GV, Izokh AE (2013) Permian plume-related magmatic associations in the Song Da – Tu Le rift system and Phan Si Pan uplift, Northwest Vietnam. Extend. Abstract volume of international symposium large igneous provinces of Asia: mantle plume and metallogeny, LIPs, Hanoi, 7 Nov 2013 pp 57–61

Tran Van Tri TKT, Truong Cam Bao (eds) (1977) Geology of Vietnam, northern part. The explanation to geological map of North Vietnam, scale 1: 1.000.000. Institute of Geology and Mineral Resources (in Vietnamese)

Tran Viet Anh, Pang KN, Chung SL, Lin HM, Tran Trong Hoa, Tran Tuan Anh, Yang HJ (2011) The Song Da magmatic suite revisited: a petrologic, geochemical and Sr–Nd isotopic study on picrites, flood basalts and silicic volcanic rocks. J Asian Earth Sci 42:1341–1355

Walker RJ, Nisbet E (2002) ^{187}Os isotopic constraints on Archean mantle dynamics. Geochim Cosmochim Acta 66:3317–3325

Walker RJ, Stone W (2001) Os isotope constraints on the origin of the 2.7 Ga Boston Creek Flow, Ontario, Canada. Chem Geo 175:567–579

Walker RJ, Prichard HM, Ishiwatari A, Pimentel M (2002) The osmium isotopic composition of convecting upper mantle deduced from ophiolite chromites. Geochim Cosmochim Acta 66:329–345

Wallace PJ (1998) Water and partial melting in mantle plumes: inferences from the dissolved H2O concentrations of Hawaiian basaltic magmas. J Geophys Res Lett 25:3639–3642

Wang CY, Zhou MF, Qi L (2007) Permian flood basalts and mafic intrusions in the Jinping (SW China)–Song Da (Northern Vietnam) district: mantle sources, crustal contamination and sulfide segregation. Chem Geol 243:317–343

Xu YG, Chung SL, Jhan BM, Wu GY (2001) Petrologic and geochemical constraints on the petrogenesis of Permian-Triassic Emeishan flood basalts in South Western China. Lithos 58:145–168

Zhong H, Zhu WG, Chu ZH, He DF, Song XY (2007) Shrimp U-Pb geochronology, geochemistry, and Nd-Sr isotopic study of contrasting granites in the Emeishan large igneous province, SW China. Chem Geol 236:112–133

Zhou MF, Malpas J, Song XY, Kenedy AK, Robinson PT, Sun M, Lesher CM, Keays RR (2002) A temporal link between Emeishan large igneous province (SW China) and the end-Guadalupian mass extinction. Earth Planet Sci Lett 196:113–122

Chapter 3
Plutonic: Volcanic Associations in the Tu Le Basin and Phan Si Pan Uplift, Northwest Vietnam

Abstract Major and trace elements and whole rock Sr–Nd isotope data of Late Permian silicic plutonic and volcanic rocks from the Phan Si Pan–Tu Le region in NW Vietnam were studied in order to establish their petrogenetic relationship with the magmatic rocks of the Song Da zone (NW Vietnam) and the alkaline silicic rocks of the Panxi area of the Emeishan large igneous province (ELIP) in SW China. The granites and rhyolites have geochemical characteristics of anorogenic granites (e.g. high Fe# and high Ga/Al) and are further subdivided based on mineralogy. The Phu Sa Phin and Muong Hum granites contain sodic to sodic–calcic amphiboles and sodic pyroxene, while the Phan Si Pan granite does not. The Phu Sa Phin and Muong Hum granites occasionally show peralkaline to metaluminous compositions, while the Phan Si Pan granites and the Tu Le rhyolites have metaluminous to peraluminous compositions. The chondrite-normalized REE patterns and the primitive mantle-normalized spidergrams (enrichment in high field strength elements) are similar to those of the Song Da silicic rocks. The eNd(t) values range from weakly negative to moderately positive values (−2.2 to +2.2), suggesting the silicic rocks may be assimilated by basement rocks during magma emplacement. Permian magmatic rocks in the Phan Si Pan–Tu Le region are petrologically, geochemically and geochronologically comparable to those of the inner zone of ELIP.

3.1 Problem of Permian: Triassic Age for Volcanic and Subvolcanic Magmas in the Tu Le Basin and Alkaline Granites in the Phan Si Pan Uplift

Permian – Triassic pluton-volcanic and pluton magmatic associations in the Tu Le Basin include sub-alkaline and alkaline volcanic and sub-volcanic pluton felsic magmas which were previously classified as products of late Mesozoic (Jurassic-Cretaceous) magmatic activities (Dovjikov 1965; Tri 1977; Thuc and Trung 1995; Chi 2003; Anh et al. 2004; Hoa et al. 2005). Position of Muong Hum alkaline granites in the geological evolution history of northwest Vietnam is rather complicated. They were considered as Archean orthogneiss being metamorphosed (Fromaget 1932), Proterozoic alkaline granite complex (Thuc and Trung 1995), late Mesozoic alkaline granite formed in relation to the formation and evolution of Tu Le Basin

T.-H. Tran et al., *Intraplate Magmatism and Metallogeny of North Vietnam*,
Modern Approaches in Solid Earth Sciences 11,
DOI 10.1007/978-3-319-25235-3_3

(Chi 2003; Hoa et al. 2003, 2005), or even being classified as Cenozoic (Paleogene) alkaline granitoids of Phan Si Pan series (Dovjikov 1965). The large mismatch in systematic classification between Tu Le basin and Phan Si Pan uplift sub-alkaline and alkaline granites is vastly due to the lack of up-to-date reliable radiometric age data for magmatic formations in both structures. Most of isotopic ages were K/Ar, Rb/Sr or Ar/Ar based, but many should be repeated to check the consistency. Some data show that activity of felsic magmatism in the Tu Le basin may last from 144 Ma till 79 to 59 Ma; the length is equivalent to two magmatic periods (Anh et al. 2004) which is hard to explain. Because of the lack of reliable age data, available evidence has been taken to suggest that the magmatic activity was late Mesozoic.

A series of evidence supporting rhyolite and sub-volcanic granites in the Tu Le Basin to view as Permian – Triassic magmas include: (1) the presence of volcanic-origin terrigenous sediment in the Tram Tau formation established in 2000 was determined to be Permian using flora fossil (Dong 2000); (2) U/Pb age dating on zircon in rhyolites (Tu Le rhyolite) and granite (Phu Sa Phin complex) from Tu Le Basin yielded 262–252 Ma (rhyolite) and 260–256 Ma (granite) respectively (LA-ICP-MS, Usuki et al. 2015); (3) Pb/Pb age dating on Pb-Zn ore from the Tu Le area which has genetic relation with the regional magmatic activity yielded an age of 250 Ma (Nhan 2002). In summary, within the acceptable errors the ages were determined between 261 and 256 for Tu Le sub-volcanic and volcanic magmas, which show mostly similar geochemical properties to Song Da sub-volcanic 256 Ma trachytes (e.g. Hoang et al. 2004). Alkaline granitoids in the Phan Si Pan uplift were previously viewed as a Palegene independent alkaline series (Phan Si Pan series, after Dovjikov 1965), while French geologists described as Archean orthogneiss being subsequently metamorphosed in the Huron age (Fromaget 1932). These Phan Si Pan alkaline granitoids were later grouped to Proterozoic Muong Hum complex and the occurrence of the magmas was marking the end of Proterozoic magmatic circle (Thuc and Trung 1995). Recent studies on the Phanerozoic granites of Phan Si Pan Uplift revealed that they belong to three associations according to colored minerals as riebeckite ± aegirine (Phu Sa Phin granite), arfvedsonite + aegirine (Muong Hum granite) and hornblend + biotite (Phan Si Pan granite) (Hoa et al. 2015). U/Pb age dating on zircons (LA-ICP-MS) in Phu Sa Phin, Muong Hum and Phan Si Pan granites yielded 260 ± 7 Ma, 259 ± 3 Ma, and 261 ± 4 and 257 ± 3 Ma respectively (Usuki et al. 2015). Slightly younger zircon U-Pb ages (251–253 Ma) are also reported from some Phu Sa Phin and Phan Si Pan granites (Hieu et al. 2013).

3.2 Mafic- Felsic Pluton-Volcanic Associations in the Tu Le Basin

Located between Phan Si Pan Uplift to the east and Song Da Rift in the west, Tu Le Basin is viewed as an independent Mesozoic structure (Fig. 3.1) (Tri 1977; Hutchison 1989). The basin is filled with volcanic terrigenous sediments mostly of Permian – Triassic and Jurassic – Cretaceous ages, and sub-alkaline and alkaline felsic volcanic rocks described as Tu Le formation (Vinh 1977; Thanh and Khuc

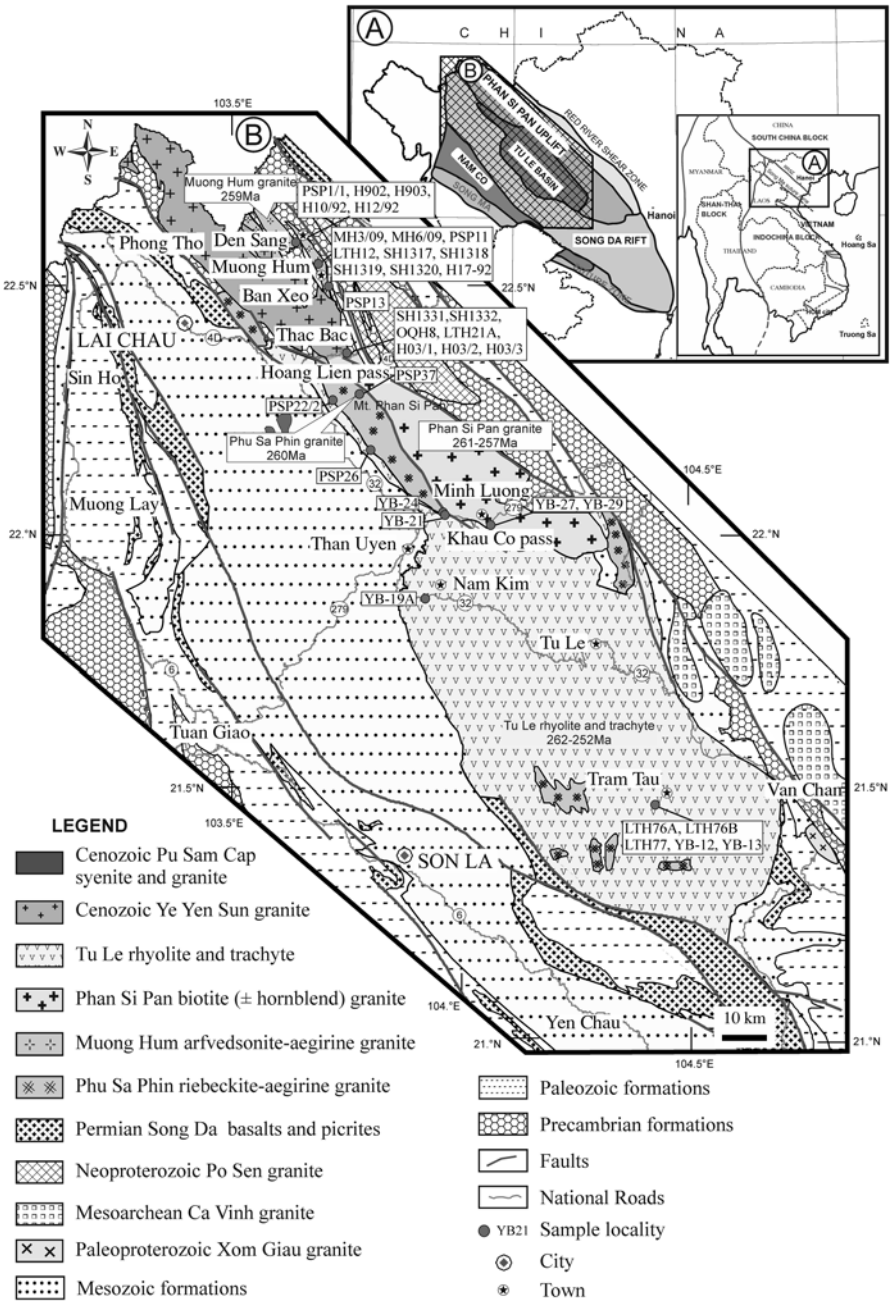

Fig. 3.1 Simplified geological scheme of northwest Vietnam Distribution of the Permian rhyolite in the Tu Le basin and alkaline granitoids in Phan Si Pan

2005) or Van Chan complex (Vinh 1978). There are a few basaltic layers observed not only in the Jurassic Suoi Be complex in the marginal areas (Bao 1978) but also in the central areas of the basin (e.g. Chi 2003). Geochemically the mafic volcanics are essentially similar to those of high-Ti Song Da basalts. Sub-volcanic mafic magmas previously grouped as Nam Chien complex were also highly developed (Tri 1977); however, basing on their compositional characteristics these sub-volcanic formations may be considered as intrusive products accompanying the volcanism to form a typical pluton-volcanic association.

3.2.1 Geological Characteristics

As mentioned above Tu Le Basin is filled with volcanic and terrigenous and accompanying sub-volcanic intrusive formations. Mafic volcanic magmas are located mainly in the south marginal of the basin, having homogenously petrologic compositions including trachybasalt and trachyandesite. They show similar geochemical compositions with contemporaneous sub-volcanic (intrusive) mafic magmas although their spatial distribution is vastly apart. The sub-volcanic magmas commonly appear as small bodies, or form wall-shaped exposure. The rock types are mostly gabbrodolerites and high-Ti and high-alkali dolerites. The largest gabbrodolerite blocks are Ban Hat and Nam Chien previously described as Mu Cang Chai complex in Tu Le Basin (Tri 1977). The Ban Hat gabbrodolerites are reported in this monograph. Basically the magmas may be viewed as monzogabbroids. Trachydacite, trachyrhyolite, rhyolite, granosyenite and syenite are the most abundant rock types among the sub-volcanic and volcanic felsic magmas. Other truly alkaline rock types such as comendite and pantelerite are exclusively minor. In previous studies, felsic magmas in the Tu Le Basin were classified into three different formations, including Nam Qua, Tu Le and Ngoi Thia basing on petrologic and textural features (Vinh 1978). These magmas are normally cut by Phu Sa Phin granite. In the 1:500 000 geological map of Vietnam published 1989 both mafic and felsic magmas were described as Jurassic – Cretaceous Van Chan formation. In a recent monograph of Stratigraphy of Vietnam, mafic volcanic magmas were left with the Suoi Be formation in southern margin of the Tu Le basin, whereas the felsic types, which are the major Jurassic – Cretaceous component of Tu Le basin, were not described as separate magmatic layers (Thanh and Khuc 2005). In this monograph silisic volcanic magmas in the Tu Le basin are named Tu Le rhyolite.

In all studied cross-sections there are two clear lithological divisions as follows: lower division includes volcanic-siltstone and shale, and intercalated sandstone and tuff layers; upper division contains layers of rhyodacite, trachyrhyolite, trachyte, and pockets of agglomerated tuff (Hoa 1995). Representative intrusive counterparts, showing spatial and compositional relationship to the volcanic magmas, appear in small bodies less than 1–2 km^2, rarely reaching 10–20 km^2. These intrusive magmas are described in the Phu Sa Phin complex (Phu Sa Phin granite).

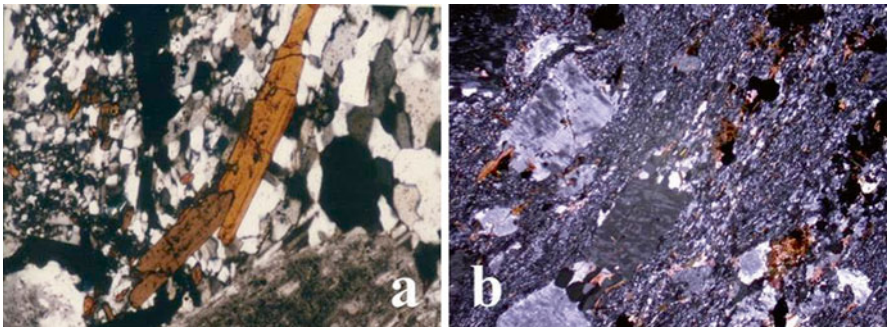

Photo 3.1 (**a**) Comendite in Lang Chang – LY-918 and (**b**) trachydacite in Tram Tau, Tu Le Basin – TLH-4, crossed nicols

3.2.2 Petrologic, Mineralogical and Geochemical Characteristics

As mentioned above, mafic volcanic magmas are trachybasalts in compositions. The basalts are aphyric or dolerite-like porphyritic. Aphyric basalts with rare phenocrysts of pyroxene and plagioclase and volcanic glass groundmass are found in lower layers of the cross-section. Porphyritic basalts are found the middle part of the cross-section, having phenocrysts of plagioclase, pyroxene together with a small amount of ore minerals such as ilmenite, magnetite and sulfur. The groundmass is doleritic containing up to 20 vol% of volcanic glass.

Monzogabbro and (mozo-) dolerite are porphyritic with pyroxene as major phenocryst and plagioclase. The pyroxenes are tablet or short prismatic with compositions varying between diopsite-augite and augite, forming typical ophitic texture. The dolerite is differentiated from gabbro by having smaller grain sizes. The groundmass contains mostly pyroxene, subsidiary plagioclase and sometimes K-feldspar. Accessory minerals in gabbro are ilmenite and apatite; sometimes take up to 0.5–1 vol%.

The Tu Le-type felsic magmas include porphyritic trachydacite, trachyrhyolite and rhyolite. Felzite, comendite and pantelerite are also present. The phenocrysts include quartz, K-feldspar, sometimes plagioclase. Euhedral arvedsonite is being observed in alkaline magma (such as comendite) (Photo 3.1a). Rhyolites with phenocrysts of quartz and K-feldspar are common. The groundmass is microfelzite, highly crystalline groundmass contains microlites of quartz, feldspar and sometimes biotite. Sub-volcanic magma shows higher crystalline rate compared with the accompanying volcanic type; they both have flow structure and in different from highly deformed magmas their groundmass contains euhedral feldspar or amphibole which are aligned by lava flow orientation (Photo 3.1b).

Chemical composition of biotite in the trachyrhyolite was determined by electron probe microscopic analysis (EPMA) shows high TiO_2 (2.69–4.28 wt%), low Al_2O_3 (13.36–14.46 wt%) and high FeO (21.81–25.08 wt%) representing biotite in highly alkaline felsic magma. In plots of Al^{IV} vs. Fe/(Fe + Mg) the rhyolitic biotite

Table 3.1 Chemical compositions (wt%) of amphibole and biotite in Tu Le trachrhyolite (Hoa 2005)

Sample	SiO_2	TiO_2	Al_2O_3	FeO	Cr_2O_3	MnO	MgO	CaO	Na_2O	K_2O
LY-918/1	49.43	0.15	1.36	35.06	0.05	0.54	0.28	0.44	6.44	0.46
LY-918/2	50.88	0.07	0.96	37.39	0.01	0.46	0.29	0.22	6.50	0.28
LY-905/1	35.21	4.28	13.36	21.81	0.03	0.27	9.01	0.01	0.50	9.24
LY-905/2	35.28	2.69	14.16	25.08	0.03	0.37	6.99	0.01	0.09	9.71

is closely similar to a mineral in group annite-siderofilite (Table 3.1). Amphiboles are observed only in the groundmass of trachydacite, trachyrhyolite and comendite. Having Na_2O ca. 6.45 wt% high-Ti, -Fe and low-Al the mineral is viewed as arvedsonite in composition (Table 3.1).

Chemical compositions and trace element abundances of the volcanic magmas are given in Table 3.2, and their positions in the SiO_2 vs. ($Na_2O + K_2O$) classification diagram are shown in Fig. 3.2. The sub-volcanic and volcanic mafic rocks are highly alkaline, while the rhyolite, trachydacite and trachyrhyolite rock types are also high alkalinity. Plotting in two contrast fields of the mafic and felsic magmas and linear configuration of felsic rocks are clearly recognizable in the Harker diagram for various chemical and geochemical indexes (Fig. 3.3). Moreover, correlation relationship between SiO_2 and Rb, Sr, Nb, Th, Y and Zr in felsic magmas is well-observed (Figs. 3.4, 3.5). The Tu Le rhyolites are characterized by low Al_2O_3 and CaO. The total alkaline oxides ($Na_2O + K_2O$) are variable with K_2O/Na_2O ratios between 0.9 and 2.2. The High Fe# values (0.9–1.0) of Tu Le rhyolite correspond to ferroan alkali granitoid (Frost et al. 2001). They are also metaluminous to peraluminous in ASI versus (Na + K)/Al diagram (not showed here).

Although being different many of petrologic and mineralogical features the dacite, rhyolite and sub-volcanic granitoid magmas are relatively similar in geochemical and isotopic characteristics. The volcanic and sub-volcanic granitoidic magmas are characteristically high in K, Rb, Zr, Nb, Ta, Th, U and REE, and low in Ba, Sr, P and Ti. These characteristics are expressed in chondrite and primitive mantle trace element normalized patterns in, respectively, Figs. 3.6 and 3.7. The light REEs in the magmas are 200–1000 times higher compared with the C1 Chondrite values in Sun and McDonough (1989). All the studied magmas show a similar trace element distribution configuration, including the negative anomalies at Eu, Ba, Sr, P, Ti. The geochemical homogeneity in felsic volcanics and sub-volcanic granitoids in the Tu Le basin suggests that they are co-magmatic and the magmas may be produced by fractional crystallization from a common partial melt source. In addition, enrichment of alkalis, the REE and other incompatible elements, including the high field strength elements makes the magmas most comparable to continental rift or oceanic island magmas. In diagrams of classification of magmatic systems using correlation among Rb-(Nb + Y) and Zr-Y, the granitoids are non-orogenic (A-type granite) (Figs. 3.8, 3.9, 3.10).

Table 3.2 Chemical compositions (wt%) and REE and trace element abundances of Tu Le magmas (After Anh et al. 2004)

Complex	Ngoi Thia							Phu Sa Phin		
Sample	H152	H187	H198	T929*	T962*	T985*	TLH-6	H178	H182*	V188*
SiO_2	75.07	77.56	72.69	77.06	77.23	74.68	75.73	62.87	72.90	74.50
TiO_2	0.24	0.22	0.31	0.25	0.22	0.23	0.28	1.00	0.33	0.34
Al_2O_3	11.90	12.26	12.25	11.21	11.02	12.33	11.58	16.06	12.77	11.88
Fe_2O_3	0.79	1.07	1.16	0.79	1.22	1.09	3.01	2.36	1.19	0.97
FeO	2.19	1.14	2.11	2.30	1.07	1.96		2.82	2.32	1.78
MnO	0.11	0.04	0.11	0.12	0.05	0.05	0.09	0.19	0.08	0.12
MgO	0.36	0.34	0.23	0.08	0.24	0.20	10.17	0.93	0.45	0.13
CaO	0.07	0.07	0.80	0.21	0.36	0.17	0.28	2.03	1.11	0.07
Na_2O	1.39	1.84	3.91	1.10	2.63	3.07	3.29	5.21	3.65	2.63
K_2O	5.43	3.43	4.05	5.32	4.12	4.78	4.57	4.97	4.21	6.27
P_2O_5	0.01	0.01	0.02	0.01	0.00	0.00	0.02	0.27	0.02	0.01
L.O.I.	2.04	1.81	1.88	2.14	1.24	0.81		1.13	1.58	1.66
Total	99.60	99.79	99.52	100.59	99.40	99.37	109.02	99.84	100.61	100.36
Sc	1	<1	2	1	1	1	17.45	8	3	2
V	5	<1	<2	<2	5	3		33	<2	6
Cr	7	4	6	23	8	11		7	23	4
Co	<1	3.6	<1	2	4	1	2.398	5	<1	1
Ni	4	3	2	3	4	6		3	4	4
Cu	2	<1	1	3	1	1		5	2	16
Zn	58	74	40	180	42	170	74.99	164	54	295
Ga	28.8	31.2	32.8	23.1	34.1	30.5	31.83	26	28	21.4
Rb	190	168	139	176	209	97	143.3	98	108	202
Sr	9.2	9.4	14.6	15	13	18	13.75	196	26	7

(continued)

Table 3.2 (continued)

Complex	Ngoi Thia							Phu Sa Phin		
Sample	H152	H187	H198	T929*	T962*	T985*	TLH-6	H178	H182*	V188*
Y	84	114	89	107	101	156	109.5	42	100	124
Zr	929	1023	818	1038	1002	975	916.7	320	877	1187
Nb	114.7	117.3	113.5	112.1	116.9	125.4	140.8	47.3	106.2	133.6
Ba	105	81	73	43	69	211	331.8	1245	277	91
La	167.13	191.63	149.66	207.60	88.70	185.7	110.7	62.4	120.7	166.7
Ce	287.33	326.48	272.73	419.80	190.60	321.8	228.3	128.7	248.9	327.8
Nd	204.24	185.65	202.62	243.30	121.80	209.40	97.35	78.7	134.90	160.60
Sm	23.00	27.55	24.26	28.80	16.90	29.70	18.7	10.6	20.40	21.40
Eu	0.82	1.23	1.39	0.72	0.76	1.67	0.968	2.95	2.07	1.20
Tb	2.37	2.99	2.78	3.17	2.44	3.76	2.907	1.20	2.78	3.60
Dy							18.04			
Ho							3.706			
Er							10.62			
Tm							1.754			
Yb	10.65	15.14	10.18	12.00	11.00	9.29	10.55	4.06	12.20	13.20
Lu	1.40	1.59	1.42	1.43	1.52	1.43	1.577	0.54	1.33	1.74
Hf	25.67	29.43	24.04	25.60	27.80	23.90	25.2	8.42	24.90	31.50
Ta	7.89	9.35	8.99	8.13	10.50	8.99	11.07	2.93	7.58	12.10
Pb	2	6	3	11	4	3	7.472	9	4	2
Th	24	27.7	23.1	29	23.4	28.4	26.15	7	24.6	38.3
U	4.1	6	3.6	5	5.8	5.3	6.34	2.8	4.3	7.7

SiO_2	46.50	36.82	44.79	48.98	45.56	46.58	47.45	48.27	44.78
TiO_2	3.13	2.75	3.15	3.47	2.02	3.30	2.66	3.63	2.78
Al_2O_3	15.05	20.76	12.37	11.86	15.65	12.85	13.36	11.78	12.10
Fe_2O_3	8.97	15.27	8.58	4.72	2.77	4.61	4.34	4.72	2.42
FeO	5.93	4.39	6.82	10.59	8.42	10.76	9.38	10.28	10.93
MnO	0.31	0.29	0.34	0.24	0.18	0.22	0.19	0.21	0.20
MgO	4.97	3.12	5.85	2.98	7.28	4.76	5.34	3.66	4.44
CaO	5.27	3.45	7.16	7.98	11.22	9.47	9.47	8.62	9.22
Na_2O	4.78	0.05	3.30	1.77	2.33	2.80	3.26	2.16	2.24
K_2O	1.70	7.24	0.08	3.00	0.16	0.59	0.88	1.80	1.57
P_2O_5	0.70	0.52	1.31	1.47	0.36	0.69	0.45	1.48	0.55
L.O.I.	2.76	5.40	6.69	2.77	3.79	3.20	2.81	2.88	8.90
Total	100.07	100.06	100.44	99.83	99.74	99.83	99.59	99.49	100.10
Sc	25	32	28	25	29	34	38	29	43
V	395	353	236	204	264	433	436	258	347
Cr	34	139	84	11	155	44	106	13	73
Co	49	43	43	27	60	43	43	45	39
Ni	19	121	34	7	146	23	35	9	27
Cu	9	72	13	17	108	19	36	68	45
Zn	201	343	167	149	112	151	129	138	162
Ga	24.3	35.8	19	22.6	15.7	20.1	19	23.2	17.9
Rb	45.4	358	2.1	152	3.4	21.1	22	79	96
Sr	250	18	97	408	276	299	401	387	169

(continued)

Table 3.2 (continued)

Complex	Suoi Be			Ban Hat					
Sample	T931331	T931344	T931352	H154	H155	H156	H158	H161	H167
Y	45	19	44	71	24	43	37	70	40
Zr	304	230	159	370	113	194	169	325	206
Nb	33	25.4	18.8	32.1	13.4	17.5	15.5	28.9	17.4
Ba	858	654	37	1884	78	228	369	1015	240
La	66.53	18.69	30.05	68.67	18.81	30.45	28.67	61.32	32.08
Ce	147.57	37.77	67.88	122.27	35.34	59.07	55.50	121.52	66.16
Pr	14.45	4.41	9.29						
Nd	58.30	18.54	41.59	74.73	23.33	34.86	29.62	64.59	33.75
Sm	10.58	4.13	9.18	15.92	4.91	8.03	7.26	14.43	7.94
Eu	3.32	1.62	3.66	5.17	1.82	2.80	2.30	5.09	2.65
Gd	10.89	4.63	9.95						
Tb	1.55	0.73	1.47	2.38	1.26	1.25	1.14	1.95	1.16
Dy	8.13	4.22	7.89						
Ho	1.69	0.98	1.63						
Er	4.92	3.16	4.57						
Tm	0.66	0.48	0.59						
Yb	4.38	3.43	3.77	5.89	2.00	3.71	4.28	6.77	4.61
Lu	0.63	0.56	0.54	1.16	0.37	0.67	0.60	0.84	0.59
Hf	6.67	4.81	3.28	9.98	3.04	4.45	4.51	8.11	5.15
Ta	2.02	1.59	1.17	1.81	1.11	0.97	1.07	1.81	1.04
Pb	11	15	8	7	6	5	6	10	7
Th	8.5	5.3	2.8	9.8	<0.5	2.9	4.1	8.10	3.2
U	0.5	2.4	0.7	1.2	<0.5	<0.5	0.6	<0.5	0.6

SiO_2	72.10	75.18	76.19	66.89	70.68	71.03	75.15
TiO_2	0.38	0.38	0.44	0.77	0.37	0.49	0.28
Al_2O_3	14.06	13.28	11.61	14.41	13.37	13.48	12.84
Fe_2O_3	0.69	0.13	1.71	1.51	4.04	4.15	3.05
MnO	0.01	0.01	0.02	0.18	0.11	0.07	0.07
MgO	0.07	0.06	0.42	0.5	0.08	0.05	0.00
CaO	0.14	0.05	0.09	1.4	0.70	0.24	0.22
Na_2O	2.11	2.38	1.85	4.54	4.37	3.29	1.63
K_2O	8.88	8.03	5.21	5.43	4.57	5.28	6.03
P_2O_5	0.03	0.02	0.05	0.14	0.04	0.07	0.02
L.O.I.	0.59	0.34	1.45	1.24			
Total	99.88	100.18	99.97	98.32	98.32	98.16	99.28
Sc					19.41	19.22	20.08
V	18	5	2	33			
Cr	13	3	8	14	0.485	2.036	
Co	1	1	1	2	3.085	3.629	
Ni	4	2	6	3		10.38	
Cu	4	1	3	5	3.89	12.98	2.521
Zn	79	20	34	121	172.9	60.7	43.49
Ga	28.8	25.6	23.4	26.7	32.95	28.66	27.59
Rb	232	202	135	128	122.4	183.4	177.3
Sr	16	9	14	88	61.91	24.55	22.81
Y	111	60	84	63	102.3	68.18	101.9

(continued)

Table 3.2 (continued)

Complex	Van chan						
Sample	RR-34A	RR-34B	RR38	RR-39	TLH-1/1	TLH-9	TLH-9/1
Zr	922	628	1011	677	952.7	749.9	960.5
Nb	116	99	116.4	81	112.1	99.41	132.1
Ba	145	117	462	933	527.1	315.8	106.9
La	167	120	139	82	124.5	173.4	137.6
Ce	213	168	248	149	251.6	343.8	274.2
Pr					26.86	35.75	33.17
Nd					106.1	138.1	117.3
Sm					19.45	21.8	21.56
Eu					2.376	1.715	0.65
Gd					16.57	16.61	18.29
Tb					2.856	2.337	3.038
Dy					17.48	12.49	17.39
Ho					3.562	2.401	3.369
Er					10.18	6.875	9.752
Tm					1.662	1.107	1.574
Yb					9.941	6.936	9.611
Lu					1.481	1.077	1.54
Hf					25.27	18.42	25
Ta					8.786	7.104	9.624
Pb					2.365	3.578	9.847
Th	19.6	15.9	24.9	15.6	22.38	18.44	26.28
U	5.1	3.5	5	5.646	2.8	3.829	6.09

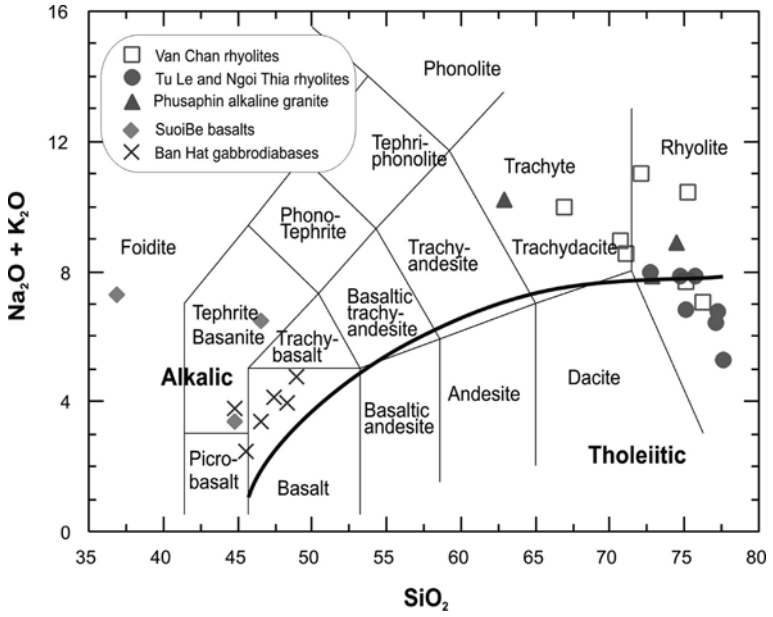

Fig. 3.2 Plots of Si_2O vs. $Na_2O + K_2O$ (After Le Bas, 1986) showing compositional positions of magmas in the Tu Le Basin

3.2.3 Isotopic Characteristics

Strontium and neodymium isotopic ratios of the Tu Le magmas are given in Table 3.3 and plots of $\varepsilon_{Nd(T)}$ vs. $^{87}Sr/^{86}Sr(i)$ are shown in Fig. 3.11. Difference between the neodymium and strontium isotopic ratios for the felsic and mafic magmas are obviously seen. For example, trachybasalt and monzogabbroid have $^{87}Sr/^{86}Sr$ ratios varying from 0.7061 to 0.7115 and $\varepsilon_{Nd(T)}$ from −7.32 to −0.47. Note that $^{87}Sr/^{86}Sr$ ratios in the Tu Le felsic magmas vary in a wide interval, from 0.7061 to 0.9101 while their $\varepsilon_{Nd(T)}$ changing between −2.8 and −1.5 (Fig. 3.11). The recent isotopic study of Tu Le rhyolite showed the similar characteristics with slightly higher $\varepsilon_{Nd(T)}$ values ranging from +2.2. to −0.3 (Hoa et al. 2015).

The above isotopic compositions of Tu Le volcanic and sub-volcanic mafic and silisic magmas may indicate that basalt and gabbro are comagmatic and they were formed from strongly crustal assimilated magma; in contract, Tu Le rhyolite were derived from fractionation of the high-Ti Song Da basaltic magma (Hoa et al. 2015).

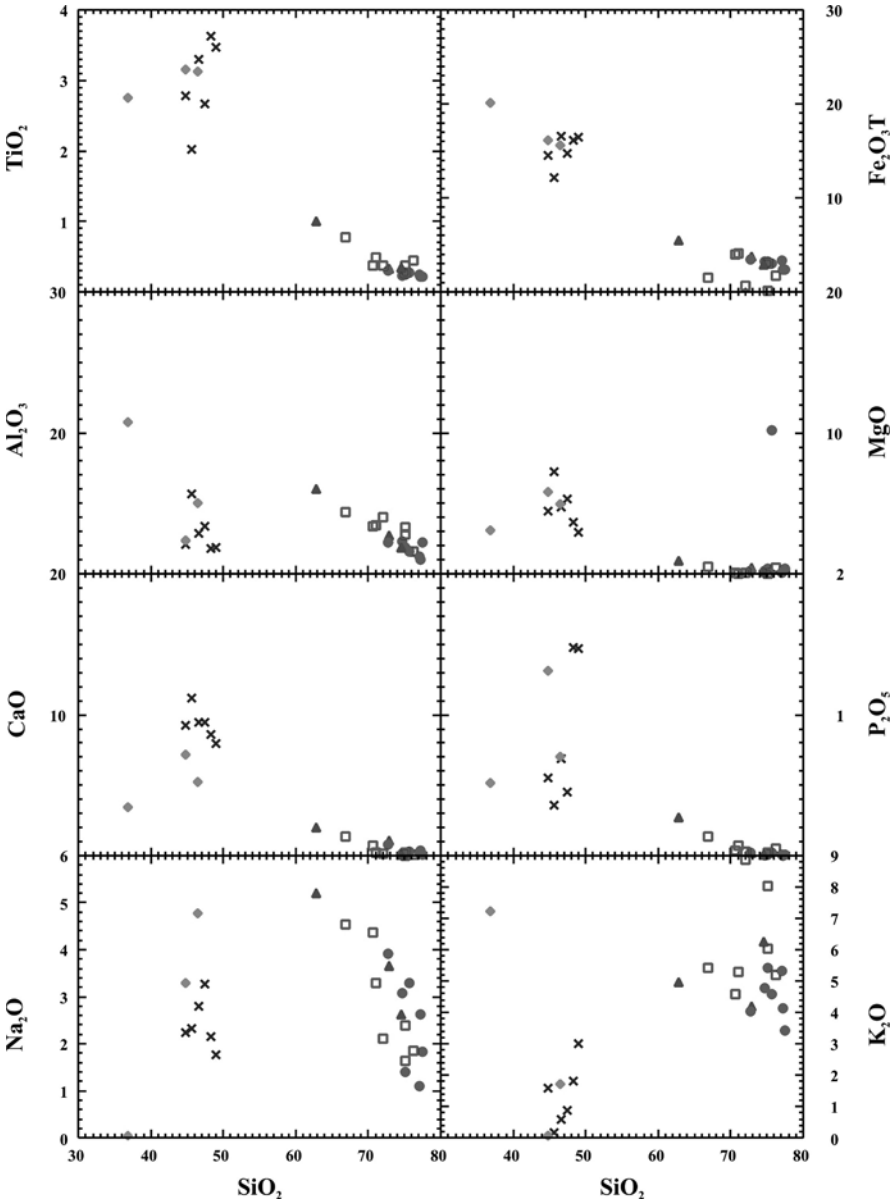

Fig. 3.3 Harker diagram for rock-forming oxides in Tu Le volcanic and sub-volcanic magmas in the Tu Le basin; *symbols* as in Fig. 3.1

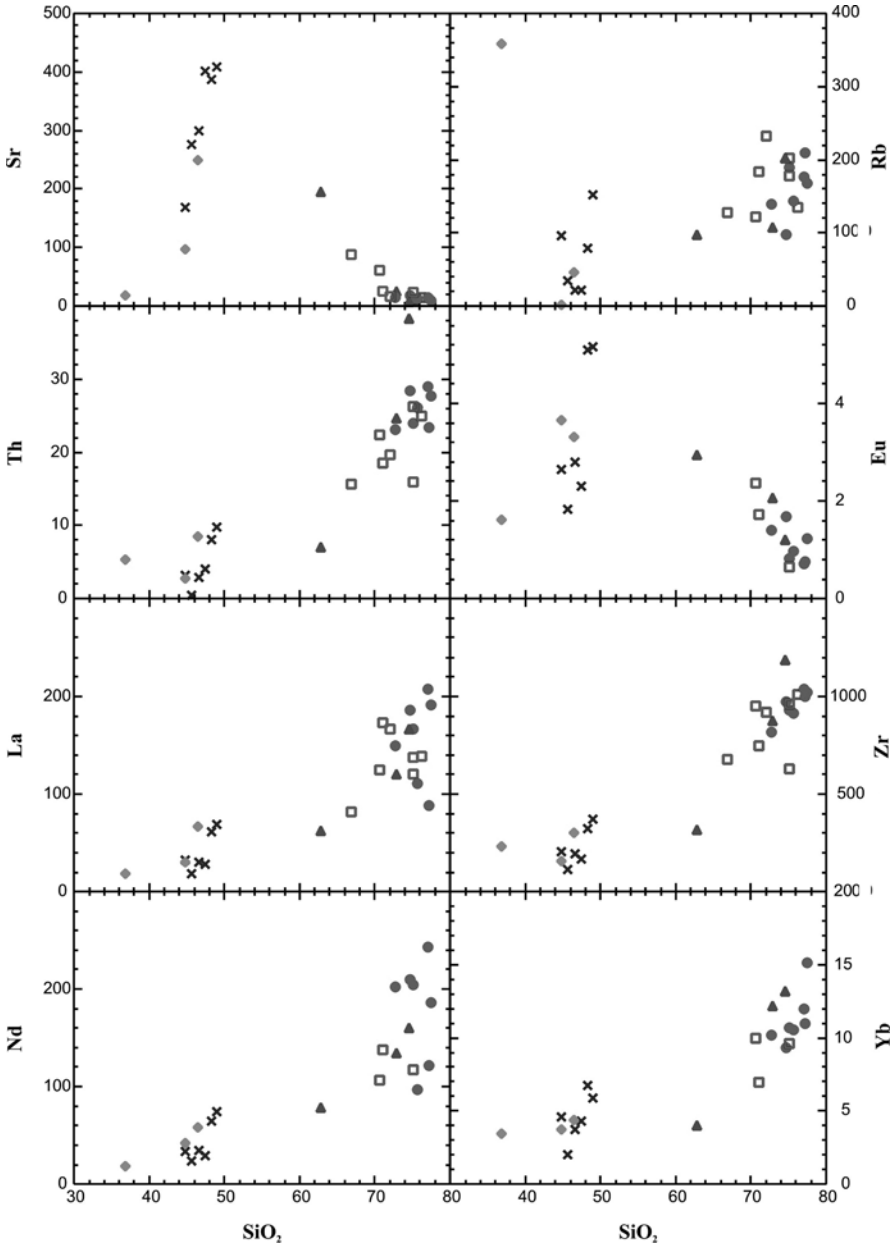

Fig. 3.4 Harker diagram for incompatible elements in Tu Le volcanic and sub-volcanic magmas; *symbols* as of in Fig. 3.1

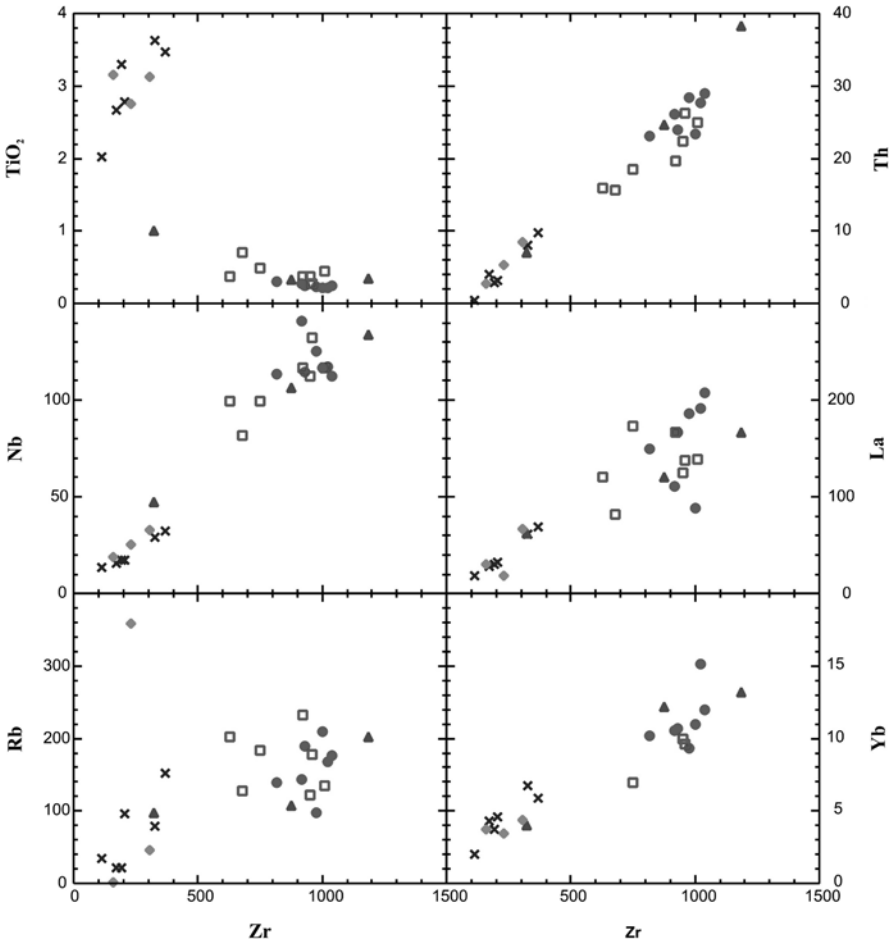

Fig. 3.5 Plots of Zr versus Rb, Nb, Th, La, and Y of the Tu Le magmas; *symbols* as of in Fig. 3.1

3.3 Permian Granitoids in the Phan Si Pan Uplift

3.3.1 Geology, Petrology and Mineralogy

As above mentioned, the granite in the Phan Si Pan Uplift are divided into three associations as riebeckite – aegirine (Phu Sa Phin), arfvedsonite – aegirine (Muong Hum) and hornblend – biotite according to the colored-mineral assemblages.

The Phu Sa Phin granite, beside presenting in south of Tu Le basin as above mentioned, are also exposed in the western side of Phan Si Pan mountain range (Fig. 3.1). They are separated from cenozoic Ye Ye Sun granite complex (massif) of the previous studies (e.g. Thuc et al. 1995) after U-Pb age dating on zircon in granite samples collected from western side of Phan Si Pan mountain (253–251 Ma,

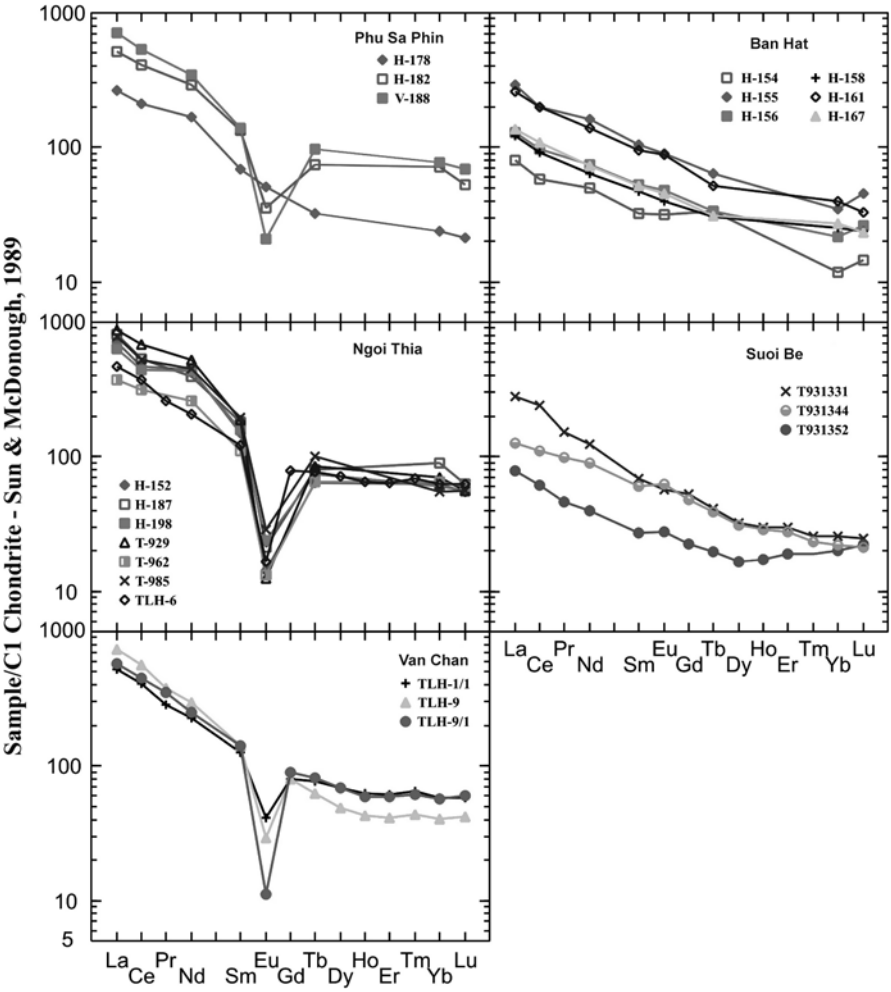

Fig. 3.6 Chondrite rare earth element normalized patterns of the Tu Le volcanic and sub-volcanic magmas (After Sun and McDonough 1989)

Hieu et al. 2013) and directly at the Phan Si Pan summit – altitude 3143 m which yielded 256 ± 6 Ma (Usuki et al. 2015). The Phu Sa Phin granites are medium to coarse-grained granular rocks which contain K- feldspar (40–50 %), quartz (25–30 %), plagioclase (20–30 %), riebeckite (1–3 %) ± aegirine (<1 %) and biotite (<1 %). The granite is generally isotropic but has localized banding structure. Accessory minerals include apatite, zircon, titanite and Fe-Ti oxides. Aegirine is occasionally observed around the riebeckite (Hoa et al. 2015). Chemical composition of aegirine, riebeckite and K-feldspar in Phu Sa Phin granite is presented in Tables 3.4, 3.5 and 3.6.

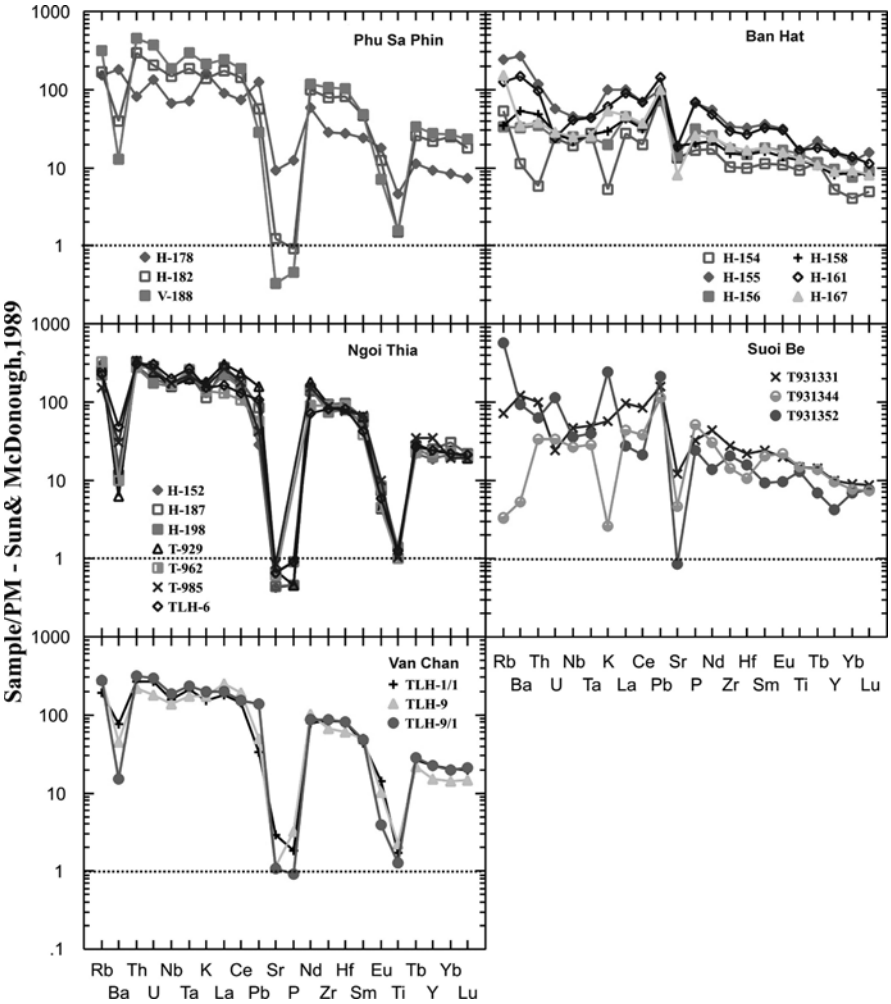

Fig. 3.7 Primitive mantle trace element normalized patterns (After Sun and McDonough 1989) of volcanic and sub-volcanic magmas in the Tu Le basin

Muong Hum-type alkaline granite represents the major component of five to six separate intrusive massifs within the Phan Si Pan Uplift (mostly to the northeast of Ye Yen Sun granite massif). Among the massifs Muong Hum, located to the east of Muong Hum town, Bat Xat district Lao Cai province, is the largest and most intensively studied (Fig. 3.12).

The Muong Hum granitoids are mostly granites with a minor amount of syenite. They are comprised of quartz (25–35 %) + K-feldspar (29–49 %) + plagioclase (19–36 %) + arfvedsonite (3–5 %) + aegirine (1–3 %) + biotite (<1 %). Typical accessory minerals are apatite, titanite and magnetite. The rocks are fine to medium grained and generally have banding structure, which likely formed during regional displace-

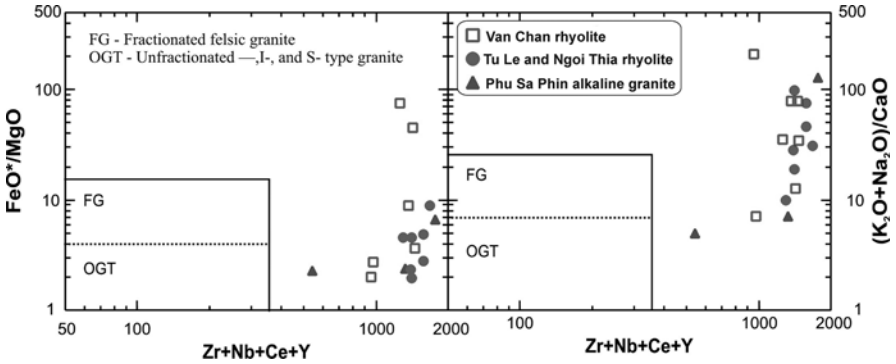

Fig. 3.8 Compositional positions of Tu Le volcanic and sub-volcanic magmas in coordination of $(K_2O+Na_2O)/CaO$ vs. (Zr + Nb + Ce + Y) and FeO*/MgO vs. (Zr + Nb + Ce + Y)

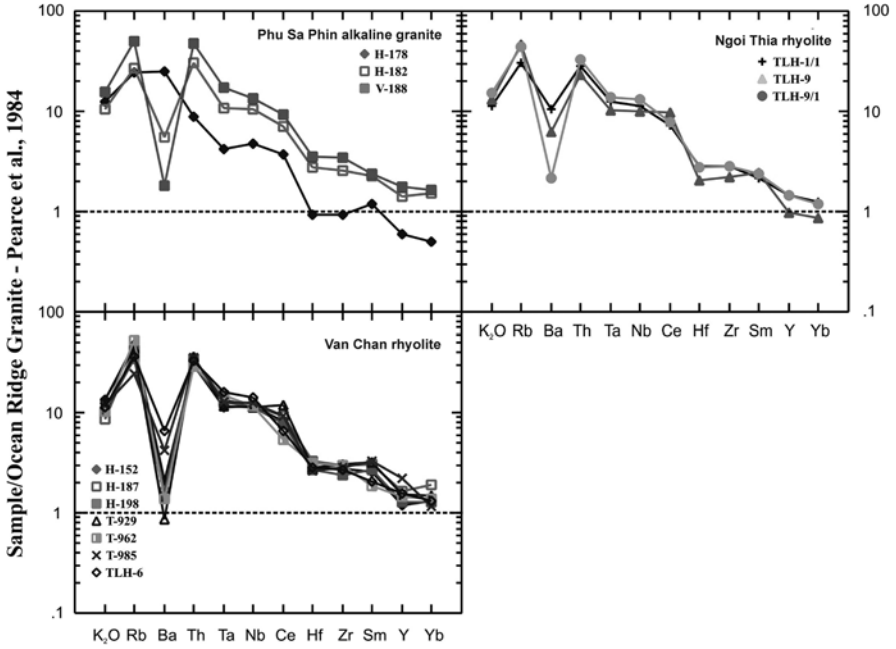

Fig. 3.9 Mid-ocean ridge granite multiple elemental normalized diagram of Tu Le felsic magmas (After Pearce 1984)

ment associated with the ASRR system (Zelazniewicz et al. 2012). However in some localities the granite is less deformed and show clear granular texture. Pyroxenes in alkaline granites, according to EPMA results, are aegirine or aegirine-augite ($Ae_{51–94.17}Jd_{1,78–6.47}WEF_{4.05–30.19}$) (Table 3.4, Fig. 3.13) and amphibole is arfvedsonite showing distinctly high Ti, Fe and Mn. Note that amphibole in granite

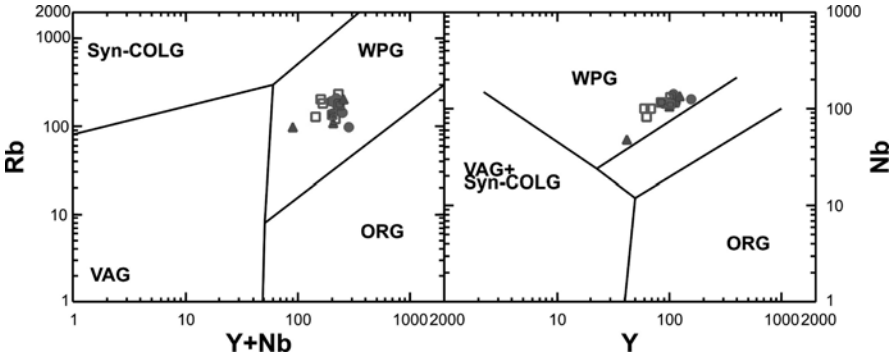

Fig. 3.10 Compositional positions of Tu Le felsic magmas in the Nb vs. Y and Rb vs. (Y + Nb) tectonic setting discrimination diagram of Pearce (1984)

in northwest Muong Hum (Den Sang area) is Mg-arfvedsonite having Mg 10 times higher compared with arfvedsonite in Ban Xeo Pass granites (Table 3.5, Fig. 3.14).

Chemical compositions show that the amphibole is vastly riebeckite showing relatively poor in Ti-Al and Fe. Biotite in the alkaline granite is rich in TiO_2 (4.37 to 5.95 wt%), very rich in FeO* (33.24 to 34.26 wt%), equivalent to annite (Table 3.6). Note that this type of biotite has not been discovered elsewhere in northwest Vietnam. K-feldspar shows a stable chemical composition at $Or_{91.20–97.10}Ab_{2.90–8.8}$ (Table 3.7).

The permian Phan Si Pan granites occur in the south-eastern part of the Phan Si Pan range and forms relatively large body of 70 km long with 10–20 km wide (Fig. 3.1B). They are also excluded from cenozoic Ye Yen Sun complex (massif) in previous works (Dovjikov 1965; Thuc et al. 1995) and named as Phan Si Pan granite in the recent studies (Dung et al. 2012; Hoa et al. 2015). The Cenozoic Ye Yen Sun granite occurs in the northwest part of the Phan Si Pan range (Dung et al. 2012) (Fig. 3.1B). It intrudes Permian Phan Si Pan granites and the intrusive boundary is well observed along National Road 4D near the Hoang Lien Pass (Fig. 3.1B). Zircons in the Phan Si Pan granitic rocks are dated. Usuki et al. (2015) reported zircons ages by LA-ICPMS for the Phan Si Pan granites (261 ± 4.4 and 257 ± 3 Ma). The Phan Si Pan granites are composed of quartz (20–30 %) + K-feldspar (35–60 %) + plagioclase (20–25 %) + biotite (5–10 %) ± hornblende (<1 %). Accessory minerals include apatite and zircon with minor amounts of opaque minerals. The rocks are medium to coarse grained and in some localized cases displays a fabric.

3.3.2 Elemental and Isotopic Geochemistry

The chemical composition of the Phu Sa Phin granitoids mainly correspond to granites (SiO_2 = 74.79–77.0 wt%, Table 3.9). They are poor in Al_2O_3 (11.0–12.1 wt%) and rich in total alkaline oxides ($Na_2O + K_2O$ = 8.2–9.4 wt%, Fig. 3.16) with K_2O/Na_2O values of ~1.3. The ASI (aluminum saturation index) versus (Na + K)/Al diagram shows the rocks are plotted in peralkaline, metaluminous and peraluminous fields (Fig. 3.17). The very high Fe# values (0.98–0.99) correspond to the ferroan

Table 3.3 Representative Sr-Nd isotopic compositions of the Tu Le magmas

Sample	Location	Rb (ppm)	Sr (ppm)	$^{87}Rb/^{86}Sr$	$^{87}Sr/^{86}Sr$	±2σ	Nd (ppm)	Sm (ppm)	$^{147}Sm/^{144}Nd$	$^{143}Nd/^{144}Nd$	±2σ	εNd(0)[f]	εNd(T)[e]	T_{DM} (Ga)
H152	Ngoi Thia	190[a]	9.2[a]	59.76	0.87464	±2	204.24[e]	23[e]	0.0681	0.512529	±23	−2.13	−0.93	0.65
H187	–	168[a]	9.4[a]	51.71	0.82458	±3	159.84[d]	27.32[d]	0.1033	0.512507	±18	−2.56	−1.69	0.89
H198	–	139[a]	14.6[a]	27.55	0.78648	±2	122.38[d]	22.67[d]	0.112	0.512504	±18	−2.61	−1.83	0.97
T929[e]	–	176[a]	15[a]	33.95	0.81556	±2	243.3[e]	28.8[e]	0.0716	0.512562	±33	−1.48	−0.32	0.63
T962[e]	–	209[a]	13[a]	46.52	0.81486	±2	121.8[e]	16.9[e]	0.0839	0.512529	±29	−2.13	−1.08	0.73
T985[e]	–	97[a]	18[a]	15.59	0.74819	±2	209.4[e]	29.7[e]	0.0857	0.512551	±17	−1.7	−0.66	0.71
H178	Phu Sa Phin	98[a]	196[a]	1.45	0.70988	±1	62.34[d]	11.15[d]	0.1081	0.512532	±19	−2.07	−0.76	0.92
H182[e]	–	108[a]	26[a]	12.02	0.73919	±2	134.9[e]	20.4[e]	0.0914	0.512542	±24	−1.87	−0.26	0.76
V188[a]	–	202[a]	7[a]	83.50	0.91009	±4	160.6[e]	21.4[e]	0.0806	0.512494	±36	−2.81	−1.03	0.75
T931331	Suoi Be	45.4[a]	250[a]	0.53	0.71012	±1	58.3[e]	10.58[e]	0.1097	0.512183	±19	−8.88	−7.1	1.42
T931344	–	358[a]	18[a]				18.54[e]	4.13[e]	0.1347	0.51247	±19	−3.28	−2.01	1.31
T931352	–	2.1[a]	97[a]	0.06	0.70735	±1	41.59[e]	9.18[e]	0.1335	0.512455	±23	−3.57	−2.28	1.32
H154	Ban Hat	152[a]	408[a]	1.08	0.7111	±1	71.87[d]	15.04[d]	0.1265	0.512233	±16	−7.9	−6.47	1.60
H155	–	34[a]	276[a]	0.04	0.70618	±2	23.33[e]	4.91[e]	0.1272	0.512541	±16	−1.89	−0.47	1.07
H156	–	21.1[a]	299[a]	0.20	0.70916	±2	34.86[e]	8.03[e]	0.1393	0.512258	±15	−7.41	−6.24	1.82
H158	–	22[a]	401[a]	0.16	0.70881	± 1	29.62[e]	7.26[e]	0.1482	0.512253	±21	−7.51	−6.52	2.08
H161	–	79[a]	387[a]	0.59	0.71065	± 2	69.68[d]	14.74[d]	0.1279	0.512215	±13	−8.25	−6.84	1.66
H167	–	96[a]	169[a]	1.64	0.71546	±2	33.75[e]	7.94[e]	0.1422	0.512206	±22	−8.43	−7.32	2.01
TLH-9	Van Chan	183.4[b]	24.55[b]	21.62	0.76477	±2	138.1[b]	21.8[b]	0.0954	0.512492	±21	−2.85	−2.85	0.85
RR-34A	–	232[a]	16[a]	41.96	0.73985	±2				0.512568	±16			
RR-34B	–	202[a]	9[a]	64.94	0.77814	±2				0.512559	±20			
RR-38	–	135[a]	14[a]	99.83	0.77568	±2				0.512501	±17			
RR-39	–	128[a]	88[a]	4.21	0.71820	±2				0.512495	±18			

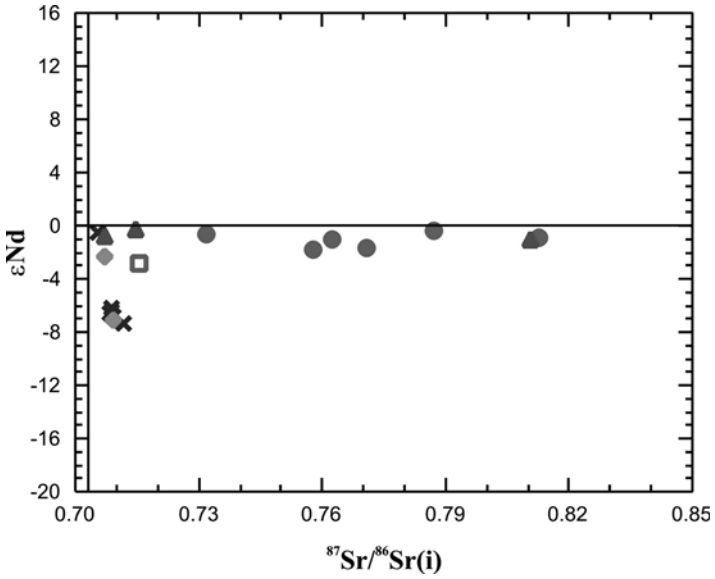

Fig. 3.11 Plots of ε_{Nd} vs. $^{87}Sr/^{86}Sr_{(i)}$ of Tu Le volcanic and sub-volcanic magmas

alkaline granitoids of Frost et al. (2001). They also exhibit low abundance of MgO (<0.1 wt%), CaO (< 0.25 wt%), MnO (< 0.1 wt%) and TiO_2 (0.18–0.30 wt%) (Table 3.9, Fig. 3.18).

The trace elements of the Phu Sa Phin granites are typically enriched in Ga (28–29 ppm), Zr (654–1213 ppm), Nb (122–191 ppm) and Y (71–134 ppm), but depleted in Ba (129–228 ppm) and Sr (16–25 ppm) (Table 3.9, Fig. 3.19). The total rare earth element (REE) of the Phu Sa Phin granites are high (423–836 ppm). The chondrite-normalized REE pattern show an enrichment of light REE [$(La/Yb)_N = 8.4–12.5$] and a relatively flat heavy REE profile [$(Gd/Yb)_N = 1.3–2.0$] with significant negative Eu anomalies ($Eu/Eu^* \approx 0.2$) (Fig. 3.20a). In the primitive normalized spidergrams, they have no negative Nb-Ta anomaly and show significant depletion of Ba, Sr and Ti (Fig. 3.20b). The elevated high field strength elements (HFSE) contents and the high $10000 \times Ga/Al$ ratios (4.5–4.6) indicate that the Phu Sa Phin granites correspond to A-type granites (Whalen et al. 1987). The Phu Sa Phin granites have weakly positive $\varepsilon Nd(t)$ values of +1.6 to +0.3 with $(^{143}Nd/^{144}Nd)_I$ values between 0.512389 and 0.512323 (Table 3.10). Their measured $^{87}Sr/^{86}Sr$ ratios have a very wide range (0.60720 to 0.87066). The variability could be due to a significant fractional crystallization (i.e. highly depleted Sr) or mobility of Rb.

The Muong Hum granitoids generally have high SiO_2 between 71.07 and 75.98 wt% (Table 3.9), although few syenitic rocks also occur (Fig. 3.16). They are poor in Al_2O_3 (10.7–13.7 %) and rich in total alkaline oxides ($Na_2O + K_2O = 8.7–13.0$ %, Fig. 3.16) with K_2O/Na_2O values ranging between 1.13 and 6.23. ASI and (Na + K)/Al indicate that they are peralkaline to metaluminous compositions (Fig. 3.17). The very high Fe# values (0.80–1.00) suggest that they are similar to the ferroan alkali peralkaline granitoids of Frost et al. (2001). They also exhibit low abundance of

Table 3.4 Chemical compositions of pyroxenes in Permian granitoids in the Phan Si Pan Uplift

	Aegirine			Aegirine-Augite			Aegirine-Augite
	Muong Hum			Muong Hum			Phu Sa Phin
Sample	Min	Max	Average n = 16	Min	Max	Average n = 4	PSP 22/2_19
SiO_2	50.5	54.01	52.20	51.09	53.42	52.40	51.74
TiO_2	0.06	0.81	0.32	0.19	0.24	0.22	0.21
Al_2O_3	0.39	2.07	0.92	0.59	0.98	0.77	0.9
FeO	26.95	32.67	29.96	28.12	29.89	28.95	34.27
Cr_2O_3	0	0.02	0.00	0	0.06	0.02	0
MnO	0.04	0.75	0.35	0.15	0.94	0.56	0.47
MgO	0.21	1.47	0.84	0.08	1.42	0.77	1.16
CaO	0.43	3.64	2.18	3.24	5.92	4.53	0.17
Na_2O	10.94	12.94	11.87	9.64	10.69	10.13	8.58
K_2O	0	0.26	0.04	0	0.02	0.01	0.58
F	0.54	0.77	0.62				1.03
Cl	0	0.01	0.00				0.04
Cations on the basic of 6 O							
Si	1.94	2.01	1.98	2.01	2.03	2.02	2.04
Al	0.02	0.1	0.04	0.03	0.04	0.04	0.04
Ti	0.78	0.94	0.86	0.61	0.72	0.67	0.55
Fe^{3+}	0	0.21	0.10	0.21	0.33	0.27	0.59
Fe^{2+}	0	0.02	0.01	0.01	0.01	0.01	0.01
Mg	0.01	0.08	0.05	0.01	0.08	0.05	0.07
Mn	0	0.02	0.01	0.01	0.03	0.02	0.02
Ca	0.02	0.15	0.09	0.14	0.24	0.19	0.01
Na	0.82	0.96	0.87	0.71	0.8	0.76	0.66
K	0	0.01	0.00			0.00	0.03
WEF	4.05	16.59	11.98	21.25	30.21	25.53	34.01
JD	0	6.47	2.33	2.88	4.76	3.73	4.7
AE	78.43	94.17	85.69	66.5	75.87	70.98	61.29

MgO (<0.2 wt%), CaO (0.1–0.9 wt%), MnO (< 0.15 wt%) and TiO_2 (0.39–0.23 wt%) (Table 3.9, Fig. 3.18).

The Muong Hum granites are characterized by high Rb (110–270 ppm), Ga (26–32 ppm), Zr (669–1384 ppm), Nb (83–253 ppm), Y (51–347 ppm), very low Sr (18–265 ppm) (Table 3.9, Fig. 3.19), and high total rare earth element (REE) contents (508–2125 ppm). The chondrite-normalized REE pattern of the Muong Hum granites show an enrichment of light REE [$(La/Yb)_N = 6.2–51.3$] and a relatively flat heavy REE profile [$(Gd/Yb)_N = 1.5–2.8$)] with distinct negative Eu anomalies ($Eu/Eu^* = 0.1–0.5$) (Fig. 3.20a). In the primitive mantle-normalized spidergrams, the Muong Hum granites exhibit significant depletions in Ba, Sr and Ti (Fig. 3.20b). The elevated high-field-strength elements (HFSE) contents and high Ga/Al ratios ($10000 \times Ga/Al = 4.0–5.2$) of the Muong Hum granites have the characteristic of A-type granite (Whalen et al. 1987). The characteristics of the major and trace element compositions are simi-

Table 3.5 Chemical compositions (wt%) of amphiboles in Permian granitoids in the Phan Si Pan Uplift

	Arfvedsonite			Arfvedsonite Mg			Riebeckite		
	Muong Hum			Muong Hum			Phu Sa Phin		
Sample	Min	Max	Average n = 5	Min	Max	Average n = 5	Min	Max	Average n = 10
SiO_2	46.14	49.34	48.01	52.69	53.52	53.17	49.68	51.29	50.72
TiO_2	0.89	1.03	0.99	0.18	0.36	0.27	0	2	0.34
Al_2O_3	2.75	2.9	2.82	0.95	2.35	1.48	0.22	2.38	0.97
FeO	33.98	34.94	34.40	18.06	21.15	19.12	28.72	35.64	32.62
Cr_2O_3	0	0.03	0.01	0	0.01	0.00	0	0.3	0.04
MnO	1.65	1.81	1.73	0.52	2.17	1.50	0.26	0.95	0.45
MgO	0.49	0.64	0.57	10.34	12.32	10.94	0.04	1.97	1.02
CaO	2.05	2.44	2.32	1.74	2.12	1.93	0.03	2.31	0.67
Na_2O	6.18	6.51	6.33	6	7.54	6.58	5.45	11.38	7.64
K_2O	1.43	1.48	1.46	1.38	2.48	2.03	0	0.55	0.19
F	0	0		2.72	2.84	2.77	0.61	1.34	0.94
Cl	0	0		0	0.02	0.01	0	0.02	0.01
Cations on the basic of 23 O									
Si	7.36	7.63	7.50	7.6	7.92	7.80	7.72	8	7.90
Al	0.5	0.55	0.52	0.17	0.4	0.25	0.13	0.43	0.23
Ti	0.11	0.12	0.12	0.02	0.04	0.03	0	0.24	0.04
Fe^{3+}	1	1.53	1.26	1.06	1.5	1.24	1.79	2	1.92
Fe^{2+}	3.09	3.4	3.24	0.8	1.34	1.10	2.32	2.73	2.51
Cr	0	0		0	0	0.00	0	0.01	0.00
Mg	0.12	0.15	0.13	2.24	2.65	2.39	0.05	0.45	0.35
Mn	0.22	0.24	0.23	0.06	0.27	0.19	0.04	0.13	0.06
Ca	0.34	0.41	0.39	0.27	0.34	0.30	0.01	0.05	0.03
Na	1.88	1.96	1.92	1.72	2.12	1.87	1.65	1.98	1.89
K	0.28	0.3	0.29	0.25	0.47	0.38	0.02	0.11	0.05

lar to those of the Phu Sa Phin granites. The Muong Hum granites have εNd(*t*) values ranging from +0.5 to −2.2 with $(^{143}Nd/^{144}Nd)_I$ values between 0.512199 and 0.512337 (Table 3.10). The Sr values are highly variable (0.68914 and 0.81155) probably due to a significant fractionation. The Phan Si Pan granitoids show high to moderate SiO_2 compositions (65.5–78.2 wt%, Table 3.9). They correspond to metaluminous to peraluminous based on ASI (0.87–1.18) versus Na + K/Al (0.8–1.1) diagram, which is different from the peralkaline to metaluminous Phu Sa Phin and Muong Hum granites (Fig. 3.17). The Fe# (0.9–1.0) indicates ferroan alkali peralkaline granitoids of Frost et al. (2001). The total alkaline concentration is high ($Na_2O + K_2O = 7.7$ to 10.9 wt%, Fig. 3.16) and K_2O/Na_2O ratios are also high (1.3 to 2.6). In the SiO_2 versus $Na_2O + K_2O$ diagram, they are plotted in the alkaline granite field (Fig. 3.16). Compared to the Phu Sa Phin and Muong Hum granites, the Phan Si Pan granites are higher in MgO, TiO_2, Al_2O_3 and P_2O_5 (Table 3.9, Fig. 3.18).

Table 3.6 Chemical compositions of biotites in Permian granitoids in the Phan Si Pan Uplift

	H17-92/10	H17-92/11	PSP 11_1	PSP 11_2	PSP 11_4	PSP 11_5	PSP 11_6	PSP 11_7	PSP 18/1_11	PSP 18/1_12	PSP 18/1_13	PSP 18/1_14	PSP 18/1_15	PSP 18/1_16	V-9263
Sample	Ban Xeo pass								Hoang Lien pass						
SiO_2	36.64	32.98	39.82	40.15	40.24	40.08	39.93	40.03	38.56	37.96	38.49	39.25	39.65	38.52	42.04
TiO_2	5.95	4.37	1.25	1.18	1.33	1.31	1.75	1.48	0.79	0.62	0.79	0.51	0.78	0.56	2.41
Al_2O_3	10.01	10	9.04	11.60	9.03	8.73	9.75	8.48	15.29	14.92	13.32	13.60	13.52	15.90	9.27
Cr_2O_3	0.03	0	0.02	0.02	0.00	0.00	0.01	0.10	0.00	0.00	0.00	0.00	0.00	0.05	
FeO	34.66	34.24	18.51	18.64	18.38	17.96	18.98	17.85	18.87	18.47	18.23	18.12	17.35	18.19	15.91
MnO	1.06	0.99	0.40	0.33	0.49	0.52	0.26	0.36	1.21	1.38	1.61	1.55	1.62	1.57	0.93
MgO	0	0.03	14.13	12.29	13.91	13.97	13.55	12.67	10.46	10.99	12.25	12.99	12.28	11.11	13.10
CaO			0.03	0.08	0.00	0.02	0.07	0.14	0.01	0.00	0.02	0.03	0.04	0.10	0.02
Na_2O	0.06	0.05	0.20	0.24	0.20	0.21	0.26	0.23	0.16	0.15	0.13	0.11	0.14	0.13	0.13
K_2O	8.65	8.02	9.96	9.83	9.97	9.88	9.83	10.00	9.44	9.72	9.70	9.72	9.83	9.70	10.40
F			2.13	2.15	2.00	2.15	2.06	2.18	1.20	1.32	1.27	1.23	1.32	1.27	
Cl			0.05	0.05	0.07	0.06	0.06	0.05	0.02	0.02	0.03	0.03	0.02	0.02	
H_2O	1.77	1.63													1.88
Total	98.83	92.31	95.54	96.56	95.62	94.89	96.51	93.57	96.01	95.55	95.84	97.14	96.55	97.12	
Cations on the basic of 24 O															
Si	6.2	5.95	6.50	6.44	6.54	6.57	6.44	6.66	6.16	6.12	6.19	6.21	6.29	6.09	6.66
AlIV	1.81	2.05	1.50	1.56	1.46	1.43	1.56	1.34	1.84	1.88	1.81	1.80	1.71	1.91	1.34
AlVI	0.19	0.08	0.23	0.63	0.27	0.25	0.29	0.32	1.04	0.96	0.72	0.74	0.81	1.04	0.39
Ti	0.76	0.59	0.15	0.14	0.16	0.16	0.21	0.19	0.10	0.08	0.10	0.06	0.09	0.07	0.29
Fe^{2+}	4.9	5.17	2.53	2.50	2.50	2.46	2.56	2.48	2.52	2.49	2.45	2.40	2.30	2.40	2.11
Cr	0.01	0	0.00	0.00	0.00	0.00	0.00	0.01	0.00	0.00	0.00	0.00	0.00	0.01	0.00

(continued)

Table 3.6 (continued)

	H17-92/10	H17-92/11	PSP 11_1	PSP 11_2	PSP 11_4	PSP 11_5	PSP 11_6	PSP 11_7	PSP 18/1_11	PSP 18/1_12	PSP 18/1_13	PSP 18/1_14	PSP 18/1_15	PSP 18/1_16	V-9263
Sample	Ban Xeo pass								Hoang Lien pass						
Mn	0.15	0.15	0.06	0.05	0.07	0.07	0.04	0.05	0.16	0.19	0.22	0.21	0.22	0.21	0.13
Mg	0	0.01	3.44	2.94	3.37	3.41	3.26	3.14	2.49	2.64	2.94	3.06	2.90	2.62	3.09
Ca			0.01	0.01	0.00	0.00	0.01	0.03	0.00	0.00	0.00	0.01	0.01	0.02	0.00
Na	0.02	0.02	0.06	0.08	0.06	0.07	0.08	0.07	0.05	0.05	0.04	0.03	0.04	0.04	0.04
K	1.87	1.85	2.07	2.01	2.07	2.07	2.02	2.12	1.92	2.00	1.99	1.96	1.99	1.96	2.10

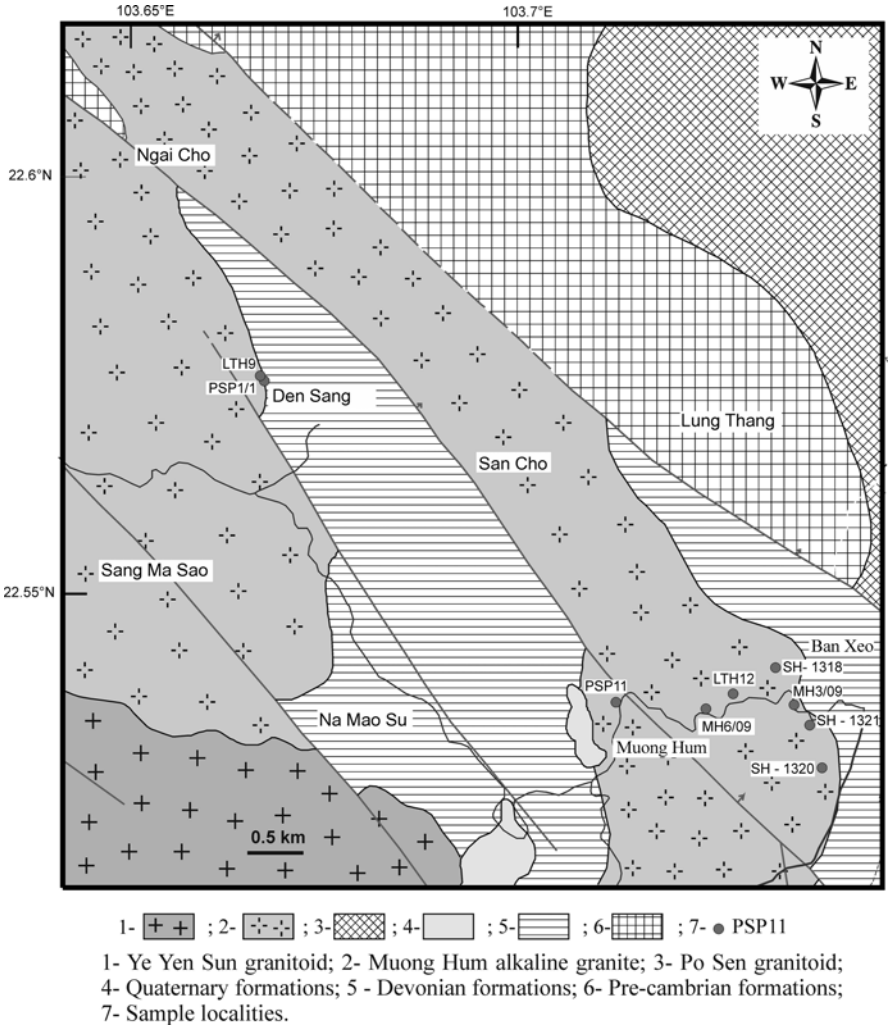

Fig. 3.12 Muong Hum alkaline granite massif in geological scheme, northwestern part of Phan Si Pan Uplift

The chemical composition of Phan Si Pan granite is characterized by low titanium (TiO_2 = 0.56–1.14 %), relatively high aluminia (Al_2O_3 = 13.71–15.35 %) and magnesia (MgO = 10.61–13.10 %) (Table 3.9).

The Phan Si Pan granites show enrichment of light REE [(La/Yb)N = 3.6–13.0] and a relatively flat heavy REE profile [(Gd/Yb)N = 1.2–1.6)] with distinct negative Eu anomalies (Eu/Eu* = 0.1–0.7) (Fig. 3.20a) as well as the Phu Sa Phin and Muong Hum granites. In the primitive mantle-normalized spidergrams, they are also rich in HFSE (Zr, Nb, Ta, and Hf) and exhibit significant depletions in Ba, Sr and Ti (Fig. 3.20b). High Ga/Al ratio (10000 × Ga/Al = 4.1) of the Phan Si Pan granites have the characteristic of A-type granite (Whalen et al. 1987). Although the Phan Si Pan

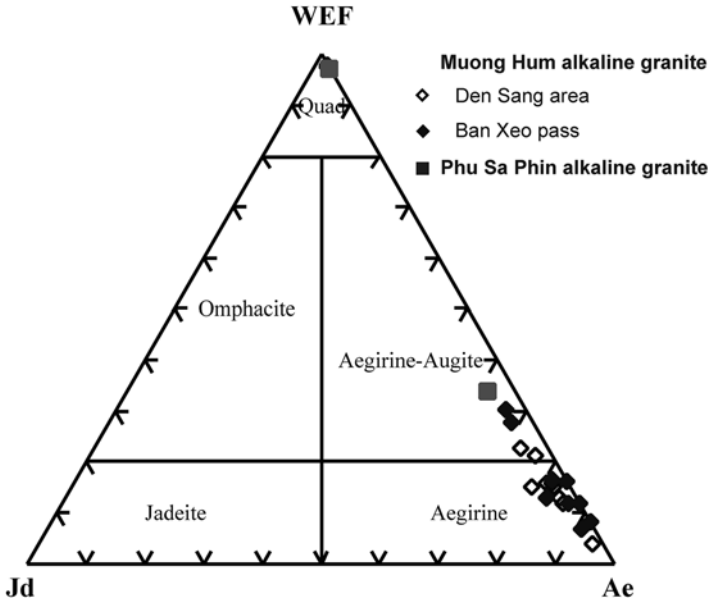

Fig. 3.13 Chemical compositions of pyroxenes in Permian granitoids in the Phan Si Pan Uplift in plots of Jd-WEF-Ae

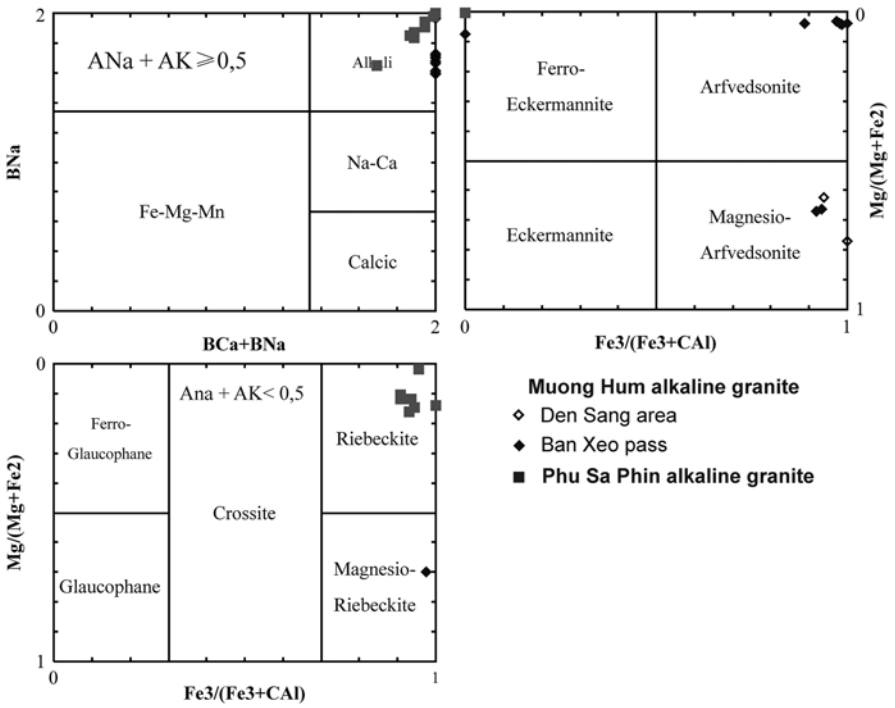

Fig. 3.14 Chemical compositions of amphiboles in Permian granitoids in the Phan Si Pan Uplift

Table 3.7 Chemical compositions of K-feldspar in Permian granitoids in the Phan Si Pan Uplift

	Muong Hum			Phan Si Pan			Phu Sa Phin		
Sample	Min	Max	Average (n = 16)	Min	Max	Average (n = 5)	Min	Max	Average (n = 6)
SiO_2	62.28	66.53	64.88	64.44	64.90	64.70	64.33	65.37	64.92
TiO_2	0.00	0.07	0.01	0.00	0.01	0.00	0.00	0.03	0.01
Al_2O_3	16.46	18.36	17.76	17.73	18.04	17.93	17.30	18.15	17.85
FeO	0.10	0.54	0.30	0.02	0.10	0.05	0.00	0.35	0.09
MnO	0.00	0.05	0.01	0.00	0.02	0.01	0.00	0.04	0.01
MgO	0.00	0.02	0.00	0.00	0.05	0.02	0.00	0.03	0.01
CaO	0.00	0.02	0.00	0.01	0.03	0.02	0.00	0.07	0.02
Na_2O	0.32	0.97	0.53	0.34	0.74	0.53	0.16	0.61	0.31
K_2O	15.08	16.49	15.97	15.79	16.49	16.10	15.60	16.55	16.07
Cations on the basic of 32 O									
Si	6.01	6.13	6.05	6.02	6.05	6.03	6.01	6.10	6.04
Al	1.87	1.99	1.95	1.95	1.98	1.97	1.90	2.00	1.96
Ti	0.00	0.01	0.00	0.00		0.00	0.00	0.08	0.01
Fe	0.01	0.04	0.02	0.00	0.01	0.00	0.00	0.03	0.01
Mn	0.00	0.00	0.00	0.00		0.00	0.00	0.00	0.00
Mg	0.00	0.00	0.00	0.00	0.01	0.00	0.00	0.00	0.00
Ca	0.00	0.00	0.00			0.00	0.00	0.01	0.00
Na	0.06	0.18	0.10	0.06	0.13	0.09	0.03	0.11	0.06
K	1.83	2.00	1.90	1.88	1.97	1.92	1.86	1.97	1.91

Table 3.8 Chemical compositions of plagioclase in Permian granitoids in the Phan Si Pan Uplift

	Muong Hum			Phan Si Pan			Phu Sa Phin		
Sample	Min	Max	Average (n = 18)	Min	Max	Average (n = 5)	Min	Max	Average (n = 6)
SiO_2	67.31	69.76	68.69	65.80	67.39	66.41	68.02	69.69	68.91
TiO_2	0.00	0.02	0.00	0.00	0.01	0.01	0.00	0.02	0.01
Al_2O_3	18.39	20.53	18.93	19.97	20.81	20.52	18.19	20.23	19.22
FeO	0.18	0.54	0.33	0.09	0.15	0.12	0.00	0.93	0.14
MnO	0.00	0.06	0.01	0.00	0.02	0.01	0.00	0.04	0.01
MgO	0.00	0.02	0.01	0.00	0.02	0.01	0.00	0.01	0.00
CaO	0.00	0.04	0.01	1.29	1.95	1.75	0.00	0.12	0.03
Na_2O	10.16	11.94	11.26	10.15	10.76	10.40	9.41	11.64	10.70
K_2O	0.09	0.24	0.15	0.11	0.32	0.22	0.01	0.95	0.15
Cations on the basic of 32 O									
Si	11.84	12.21	12.07	11.65	11.88	11.73	11.98	12.28	12.09
Al	3.80	4.25	3.92	4.15	4.32	4.26	3.79	4.17	3.97
Ti	0.00		0.00			0.00	0.00	0.00	0.00
Fe	0.03	0.08	0.05	0.01	0.02	0.02	0.00	0.14	0.02
Mn	0.00	0.01	0.00			0.00	0.00	0.01	0.00
Mg	0.00	0.01	0.00	0.00	0.01	0.00	0.00	0.00	0.00
Ca	0.00	0.01	0.00	0.24	0.37	0.33	0.00	0.02	0.00
Na	3.45	4.07	3.84	3.47	3.69	3.56	3.21	3.96	3.64
K	0.02	0.05	0.04	0.03	0.07	0.05	0.00	0.21	0.03

Table 3.9 Chemical compositions of Permian granitoids in the Phan Si Pan Uplift

Sample	PSP22/2	PSP26	PSP37	SH-1320	PSP11	PSP13	MH3/09	MH6/09	LTH12
Rock	Aeg-Rieb granite			Aeg-Arfve granite		Grano-syenite	Aeg-Arfve granite		
Area	Phu Sa Phin			Ban Xeo pass					
SiO_2	77	74.79	75.63	72.91	75.98	66.34	71.48	71.96	75.27
TiO_2	0.18	0.3	0.27	0.28	0.23	0.53	0.33	0.38	0.23
Al_2O_3	11.43	12.12	11.03	12.46	10.81	14.13	12.34	12.02	11.18
Fe_2O_3T	2.32	3.16	3.76	3.09	3.37	3.88	3.79	3.12	3.24
Fe_2O_3	1.41	1.77			2.1	1.81	3.5	2.83	
FeO	0.82	1.25			1.14	1.86	0.26	0.26	
MnO	0.07	0.06	0.02	0.05	0.06	0.28	0.07	0.04	0.02
MgO	0.05	0.06	0.04	0	0.05	0.99	0.08	0.12	0.09
CaO	0.21	0.28	0.02	0.22	0.17	0.43	0.2	0.47	0.1
Na_2O	3.87	4.13	3.11	1.85	3.7	1.8	2.74	2.52	4.22
K_2O	4.92	5.27	5.07	8.37	4.85	11.22	8.82	8.55	4.9
P_2O_5	0.01	0.02	0.01	0.03	0.01	0.12	0.03	0.07	0.01
LOI	0.37	0.44	0.51	0.73	0.84	0.86	0.22	0.29	0.44
Total	100.43	100.63	99.47	99.99	100.07	100.58	100.1	99.54	99.7
Ba	129	228	152.46	1940	721	856	1705	5655	301.29
Rb	175.7	165.9	239.4	210.4	191.9	271	210.9	216.5	177.6
Sr	24	25	16.4	121.9	51	142	84	265	18.2
Cs			0.29	0.65					0.47
Ta	9.04	11.8	39.3	9.37	14.6	6.57	9.48	12.6	13.17
Nb	122	179	191.1	91.41	230	105	139	155	159.81
Hf	17.8	30.2	22.25	20.69	32.8	13.9	22.3	21.5	20.72
Zr	654	1213	1051	734.3	1275	591	912	881	874

Y	70.6	134	87.58	50.95	194	66.4	57.4	92.2	84
Th	17.5	30.8	21.26	13.81	37.5	13.3	33.5	30.6	23.32
U	4.75	6.08	4.75	3.26	11.6	3.97	4.71	4.75	4.07
Ga	27.9	29.3			30	31.6	27.9	25.6	
Cr	0.88	0.31	3.83	1.1	15.4	0.67	0.42	0.53	4.08
Ni	0.65	0.65	2.78		0.73	1.09	0.59	0.49	3.05
Co	–	–	0.37	0.51		2.02	0.22	0.18	0.53
Sc	1	2	0.94	20.64	<1	6	2	3	1.47
V	3	9	10.1	10.86	8	12	15	24	10.9
Cu	<1	2		14.86	1	9	26	113	
Pb	10	6		39.76	4	130	2	4	
Zn	121	183	82.3	89.1	114	1034	45	30	108.1
La	88.2	194	127.24	234.2	155	121	189	589	355.91
Ce	179	323	257.37	366.2	263	237	358	934	245.57
Pr	20.2	43.1	29.65	39.43	34.4	27.8	40	94.3	60.83
Nd	74	159	103.73	124.1	134	107	143	303	197.87
Sm	13.9	28.7	18.36	16.51	28.5	18.8	23.3	36	28.66
Eu	0.79	1.48	1.04	1.96	1.68	3.3	2.23	5.13	2.31
Gd	12.2	25.1	17.72	13.78	30.5	15.2	17.4	24.3	24.47
Tb	2.06	3.98	2.79	1.85	5.05	2.19	2.5	3.47	3.05
Dy	12.8	23.5	15.66	9.53	31.5	11.7	12.6	16.8	14.84
Ho	2.72	4.85	3.17	1.78	6.58	2.32	2.3	3.31	2.86
Er	7.86	13.5	9.26	5.28	18	6.42	6.04	9.28	8.47
Tm	1.18	1.98	1.26	0.83	2.59	0.91	0.88	1.31	1.14
Yb	7.58	12.4	7.33	5.1	15.8	5.77	6.11	8.23	7.23
Lu	1.11	1.79	0.9	0.84	2.27	0.91	1.03	1.22	1.03

(continued)

Table 3.9 (continued)

Sample	H-902	H-903	H10/92	H12/92	PSP 1/1	H17/92	SH-1317	SH-1318	SH-1319
Rock	Aeg-Arfve granite in Den Sang area					Aeg-Arfve granite in Ban Xeo pass			
Type	Muong Hum								
SiO_2	71.52	71.07	75.21	76.14	74.13	73.67	71.51	75.54	75.35
TiO_2	0.33	0.3	0.29	0.39	0.31	0.26	0.35	0.25	0.24
Al_2O_3	11.66	11.06	10.74	12.35	12.01	10.72	13.65	11.97	11.96
Fe_2O_3T	3.15	4.18	3.4	4.04	3.57	3.05	3.64	3.39	2.56
Fe_2O_3					2.11				
FeO					1.31				
MnO	0.05	0.05	0.03	0.13	0.12	0.07	0.12	0.07	0.03
MgO	0.06	0.19	0.15	0.04	0.03	0.05	0	0	0
CaO	0.38	0.91	0.18	0.52	0.48	0.36	0.59	0.39	0.29
Na_2O	2.65	3.67	3.05	4.59	4.1	4.29	4.3	4.29	3.89
K_2O	7.34	5.45	6.01	4.81	4.86	4.84	5.63	4.38	4.95
P_2O_5	0.03	0.02	0.02	0.03	0.02	0.02	0.03	0.01	0.01
LOI	1.41	1.56	0.13	0.07	0.31	0.34	0.57	0.18	0.65
Total	98.58	98.46	99.21	103.11	99.94	97.67	100.39	100.47	99.93
Ba	1880	3854	285.6	1325	168	420.4	409.4	327.2	1127
Rb	205.1	194.4	110.4	158.6	149.3	187.5	115.4	220.1	184.8
Sr	171	180	76.97	85.3	30	70.34	22.34	25.33	19.06
Cs	1.29	0.63	0.51	0.36		1.09	0.49	0.73	0.74
Ta	21.28	9.78	12.08	14.96	9.42	14.14	5.58	15.64	9.13
Nb	252.6	125.8	154.2	169.6	133	168.3	83.44	185.3	124.9
Hf	41.16	22.91	29.87	30.16	19.2	30.24	16.01	35.93	19.96
Zr	1384	874.3	1008	911.4	737	890.5	668.9	1167	759
Y	346.8	72.18	108.9	108.4	80	117.6	58.15	172	93.14

Th	60.57	24.6	30.35	29.19	20.1	32.02	17.61	31.49	27.57
U	10.8	6.91	5.74	8.98	4.36	6.83	3.05	7.71	5.95
Ga									
Cr	0.87	1.68	2.18	4.18	2.87	1.2		1.65	
Ni	0.76		0.59	0.27	0.56			1.08	
Co	1.99	2.06	1.46	3.19		2.1		0.24	
Sc	14.49	4.91	22.36	7.62	1	12.55	11.89	20.46	10.33
V	9.11		3.05	8.82	10	9.03		2.24	
Cu	15.65	10.61	4.91	4.65	1	6	0.88	7.93	4.97
Pb	38.32	22.95	6.54	5.73	9	19.76	6.33	20.08	25.73
Zn	267.5	218.4	195	47.32	115	152.6	112.4	250.9	188.6
La	503.6	205.1	239.9	212.3	149	126.3	113.6	121.7	111.4
Ce	891.9	374.5	361.4	364.8	288	262	220.4	258.6	209.5
Pr	98.31	42.51	49.2	40.13	32.1	28.85	26.38	28.06	26.42
Nd	379.3	141.8	178.7	147.1	115	108	92.07	111.1	94.06
Sm	64.03	20.7	28.83	24.63	19.4	21.41	15.26	23.72	17.83
Eu	4.35	2.25	1.27	1.9	1.3	1.01	1.18	1.15	1
Gd	55.91	16.84	23.47	20.98	15.8	18.4	12.11	20.61	15.08
Tb	8.9	2.39	3.55	3.27	2.46	3.29	1.82	3.99	2.62
Dy	50.41	12.6	20.05	18.63	14.2	20.13	9.87	25.73	15.3
Ho	9.82	2.37	3.93	3.74	2.9	4.1	1.88	5.36	2.98
Er	26.54	6.87	11.34	10.62	8.1	11.8	5.57	15.24	8.51
Tm	4.12	1.09	1.9	1.75	1.21	1.98	0.92	2.43	1.36
Yb	23.93	6.81	12.07	10.57	7.8	12.09	5.98	14.13	8.3
Lu	3.58	1.14	1.89	1.58	1.18	1.75	1.02	2.04	1.31

(continued)

Table 3.9 (continued)

Sample	SH-1331	SH-1332	OQH8	LTH 21A	H-03/1	H-03-2/1	H-03/3	YB 24	YB 27	YB 29
	Biotite granite						Grano-syenite	Biotite granite		Grano-syenite
Rock	Hoang Lien pass							Khau Co pass		
Type	Phan Si Pan									
SiO_2	78.15	71.9	71.02	76.68	70.69	70.51	66.4	73.99	70.27	65.54
TiO_2	0.27	0.36	0.39	0.16	0.31	0.64	0.82	0.29	0.56	0.81
Al_2O_3	11.48	14.25	13.81	10.92	12.77	12.38	15.62	12.42	12.24	13.93
Fe_2O_3T	2.66	2.92	3.3	2.78	4.64	6.38	5.15	2.89	4.47	5.94
Fe_2O_3			1.63					1.77	1.27	3.71
FeO			1.5					1.01	2.88	2.01
MnO	0.01	0.05	0.07	0.05	0.04	0.06	0.05	0.08	0.15	0.08
MgO	0	0.22	0.51	0.41	0.76	0.53	0.31	0.18	0.64	1.15
CaO	0.11	0.17	0.22	0.04	0.9	0.29	0.38	0.13	1.56	1.3
Na_2O	2.16	3.73	3.95	2.8	3.81	3.86	4.55	3.71	3.48	5.89
K_2O	5.55	6.13	6.3	5.37	5.58	5.05	6.32	5.17	5.24	3.5
P_2O_5	0.02	0.04	0.05	0.01	0.03	0.09	0.13	0.02	0.12	0.17
LOI	0.17	0.54	0.53	0.28	0.53	0.18	0.16	1.21	1.9	2.06
Total	100.58	100.31	100.15	99.5	100.07	99.97	99.9	100.09	100.63	100.37
Ba	109.2	349.3	385	291.43	343.8	788.5	1071.42	281	460	653
Rb	201.4	219.3	266.6	237.8	196.07	141.98	178.5	125.3	143.6	91.5
Sr	46.7	26.02	46	23.9	35.32	56.64	87.7	31	54	124
Cs	2.87	1.68		1.96						
Ta	12.98	6.86	10.1	14.96	13.18	7.41	7.53	9.35	9.34	8.85
Nb	167.7	94.12	135	139.93	238.06	133.51	128.34	134	130	128
Hf	28.06	20.32	20.8	21.24	36.95	23.23	22.66	18.8	23.5	19.5
Zr	1013	728.8	795	755.1	1051.52	884.95	840.06	772	966	828

Y	97.52	64.37	98.4	79.11	135.18	60.49	71.09	83.9	99.7	81
Th	27.52	22.1	22.7	26.82	40.46	20.76	17.85	23.8	23.4	17.6
U	6.86	4.21	6.01	5.31	12.79	5.09	4.42	4.49	5.54	3.92
Ga			29.6							
Cr	−0.68	−1.12	3.32	4.38	80.45	28.55	96.08	1.2	1.42	0.93
Ni	−8.95	−9.31	0.57	2.96	3.5	3.5	7.3	0.76	0.94	0.93
Co	−0.51	−0.27	0.33	0.24	0.94	2.7	2.79	0.27	1.32	1.39
Sc			2	1				1	5	5
V	−4.3	−18.33	13	10.1	9.36	8.1	31.2	6	21	28
Cu	4.83	4.52	9		4	3.8	6.52	1	6	4
Pb	16.74	11.13	12					3	135	3
Zn			107	96				29	244	29
La	124.5	121.5	152	42.87	123.88	111.19	123.09	142	125	96.7
Ce	259.2	238.4	293	97.33	265.06	226.62	254.8	283	253	195
Pr	31.92	28.27	32	12.21	37.11	29.32	34.23	33.5	31.2	24
Nd	112.1	97.27	114	46.5	133.08	101.62	123.94	118	113	88.7
Sm	21.78	16.7	19.8	11.77	25.8	16.2	20.26	20.6	20.7	16.7
Eu	0.71	1.64	2.28	0.54	2.49	2.78	4.27	1.31	2.4	3.3
Gd	18.1	13.41	17	12.07	26.12	14.2	16.53	16.6	17.1	14.7
Tb	3.06	2.08	2.71	2.19	4.29	2.08	2.33	2.58	2.68	2.33
Dy	17.84	11.54	15.7	13.21	26.58	12.73	14.05	14.8	16	14.1
Ho	3.45	2.22	3.27	2.79	5.46	2.55	2.79	3.11	3.42	2.98
Er	10.18	6.51	9.24	8.63	16.37	7.64	8.38	8.65	9.67	8.25
Tm	1.66	1.06	1.36	1.33	2.65	1.23	1.4	1.3	1.47	1.22
Yb	10.19	6.69	8.76	8.64	17.54	7.87	9.08	8.34	9.12	7.61
Lu	1.56	1.08	1.28	1.13	2.57	1.16	1.32	1.26	1.34	1.12

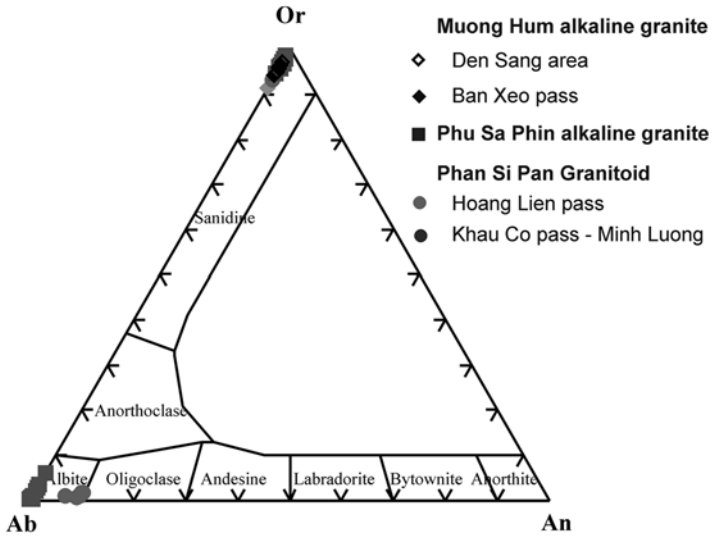

Fig. 3.15 Chemical compositions of feldspar in Permian granitoids in the Phan Si Pan Uplift

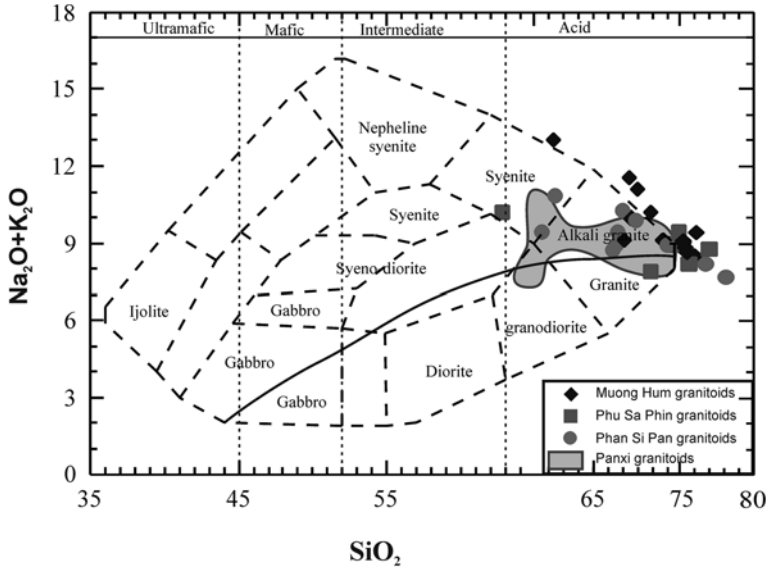

Fig. 3.16 Na_2O+K_2O vs SiO_2 plots of the Permian granites (After Cox et al 1979 and Wilson 1989). The *bold solid line* separates subalkaline and alkaline compositions. *Grey* field indicates granitoids of the Panxi area (Shellnutt et al. 2009b)

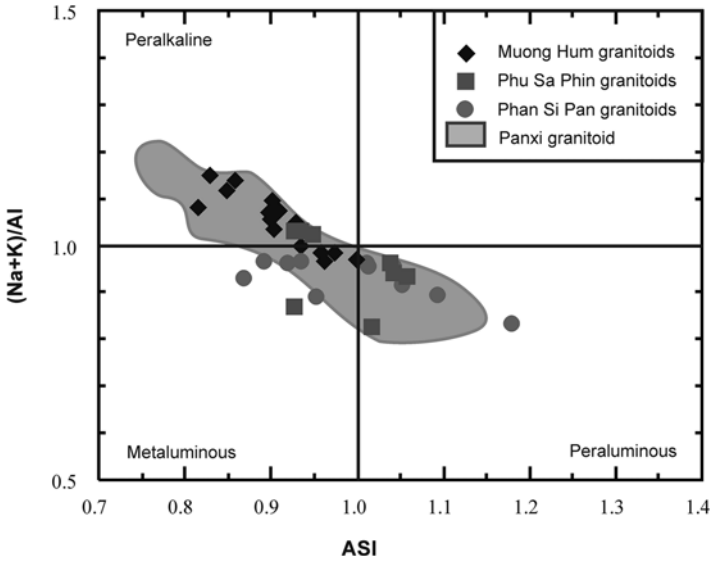

Fig. 3.17 Molecular (Na + K)/Al vs ASI (alumina saturation index, Frost et al. 2001) for the Muong Hum, Phu Sa Phin, and Phan Si Pan granite. *Grey* field indicates granitoids of the Panxi area (Shellnutt et al. 2009b)

granites show some difference in major element compositions, the characteristics of trace element compositions are similar to the Phu Sa Phin and Muong Hum granites.

The Phan Si Pan granites have εNd(t) values ranging from +1.7 to −0.6 with (143Nd/144Nd)I values between 0.51240 and 0.51228 (Table 3.10). This range overlaps with those the Phu Sa Phin and Muong Hum granites. The ISr values are between 0.74900 and 0.70277, probably due to a significant fractionation.

3.4 Magmatic Formation and Tectonic Settings

The argument mentioned above suggests that pluton-volcanic associations in the Tu Le basin and Phan Si Pan Uplift are products of Permian – Triassic magmatic activities in northwest Vietnam. This statement is meaningful in clarifying the nature of Song Da tectonics and its formation and evolution history. The information will shed light on history of geological evolution of the Tu Le basin, in particular, and northwest Vietnam, in general.

Petrologic-chemical (high Ti, alkalis and P) and geochemical and isotopic characteristics (rich in Nb, Ta, Zr, Hf, REE and high $^{87}Sr/^{86}Sr$) of the basalts in Suoi Be area and monzogabbroids in Ban Hat area are quite similar to those of Permian basalts and high-Ti mafic intrusive magmas in the Song Da structure. The spatial proximity and chemical similarity among those magmas suggest that they are all related to Song Da ultramafic – mafic magmatic activity, thus may be derived from

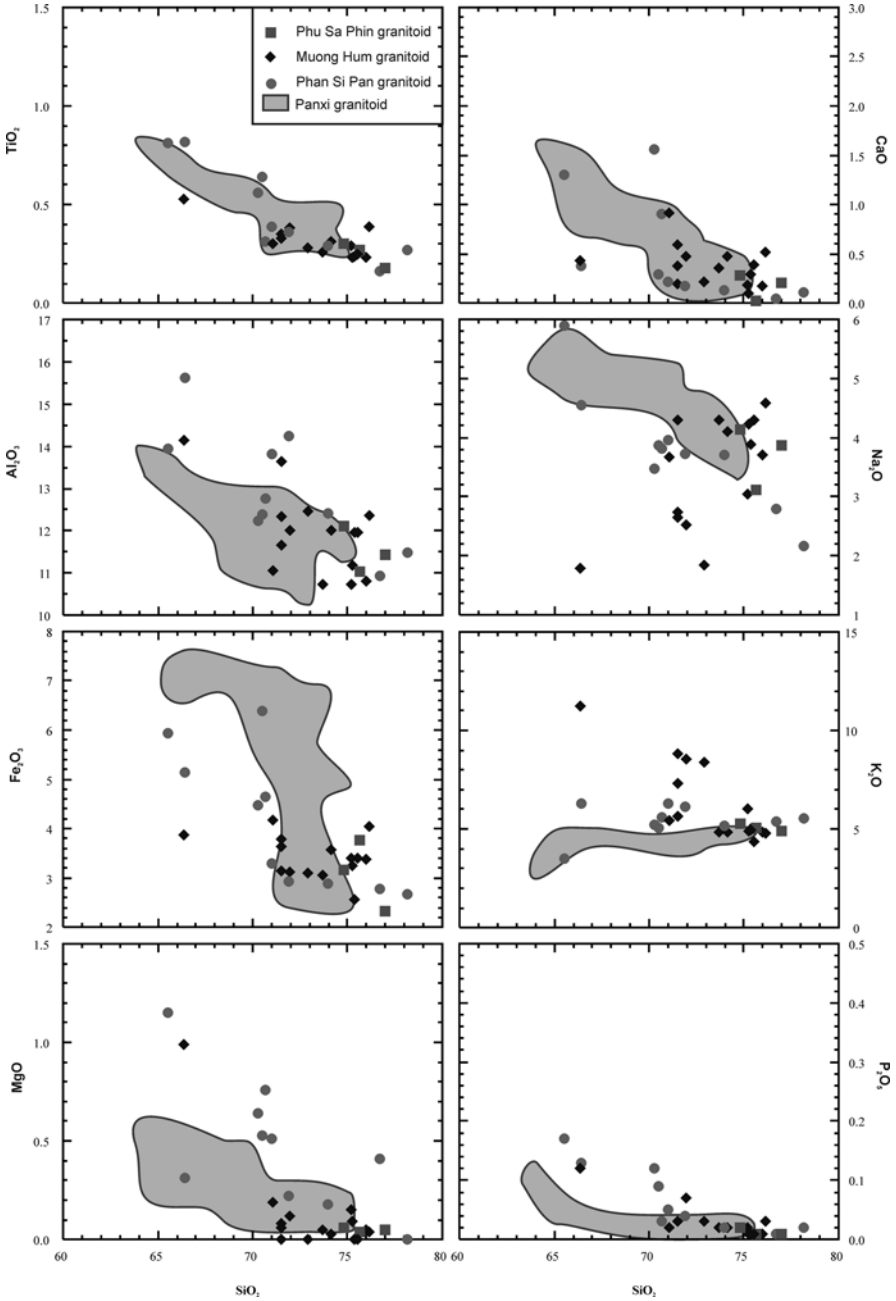

Fig. 3.18 Concentration of selected major elements versus SiO_2 for the Phu Sa Phin, Muong Hum and Phan Si Pan granites. *Grey* field indicates granitoids of the Panxi area (Shellnutt et al. 2009b)

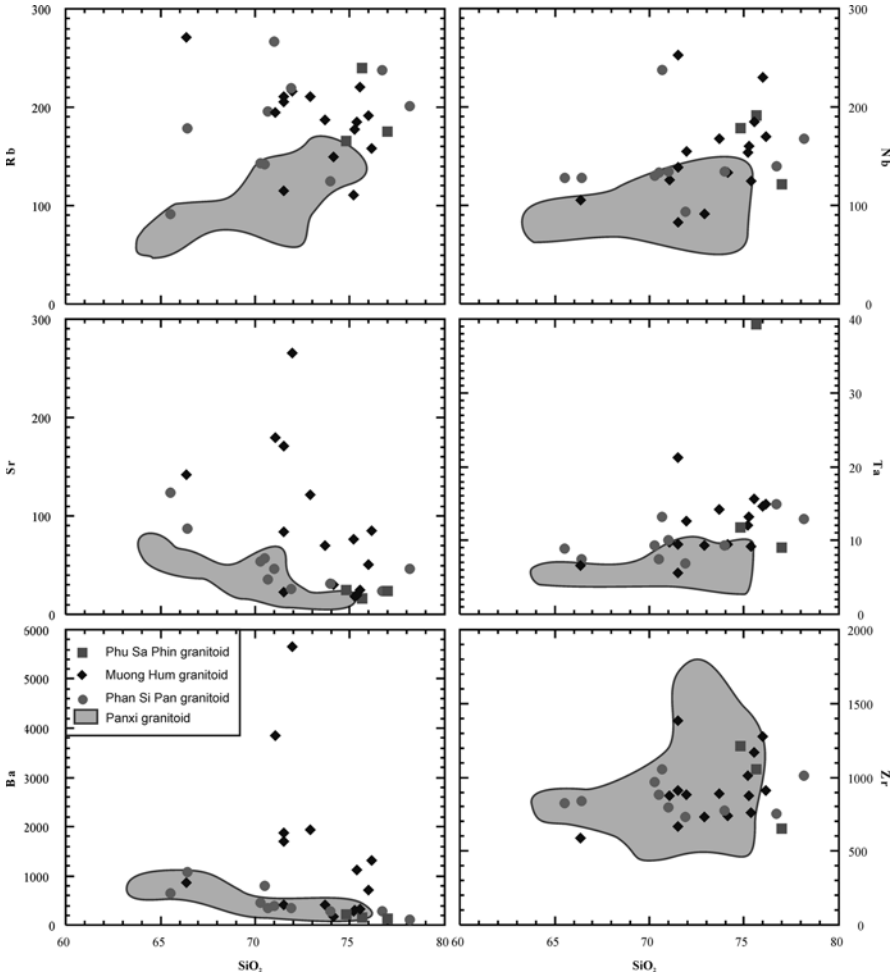

Fig. 3.19 Concentration of selected trace elements versus SiO_2 for the Tu Le rhyolite and the Phu Sa Phin, Muong Hum, and Phan Si Pan granites. *Grey* field indicates granitoids of the Panxi area (Shellnutt et al. 2009b)

the same high-Ti Song Da sub-continental lithospheric mantle source. As presented in Chap. 1 this type of mantle may present under marginal regions of the Yangtze craton since late Paleozoic. Similar to high-Ti Song Da basalts, characteristically high 87Sr/86Sr ratios and low $\varepsilon_{Nd(T)}$ in the Tu Le mafic magmas may be explained by mantle contamination of crustal material evidenced by having relatively low Nb, Ta, and Sr in their derived magmas.

The origin of sub-alkaline and alkaline felsic pluton-volcanic and plutonic associations in the Tu Le basin and Phan Si Pan Uplift are complicated for their inconsistent Nd and Sr isotopic data. For example, while their initial strontium isotopes show a crust-related origin, the Nd isotopic compositions indicate an enriched

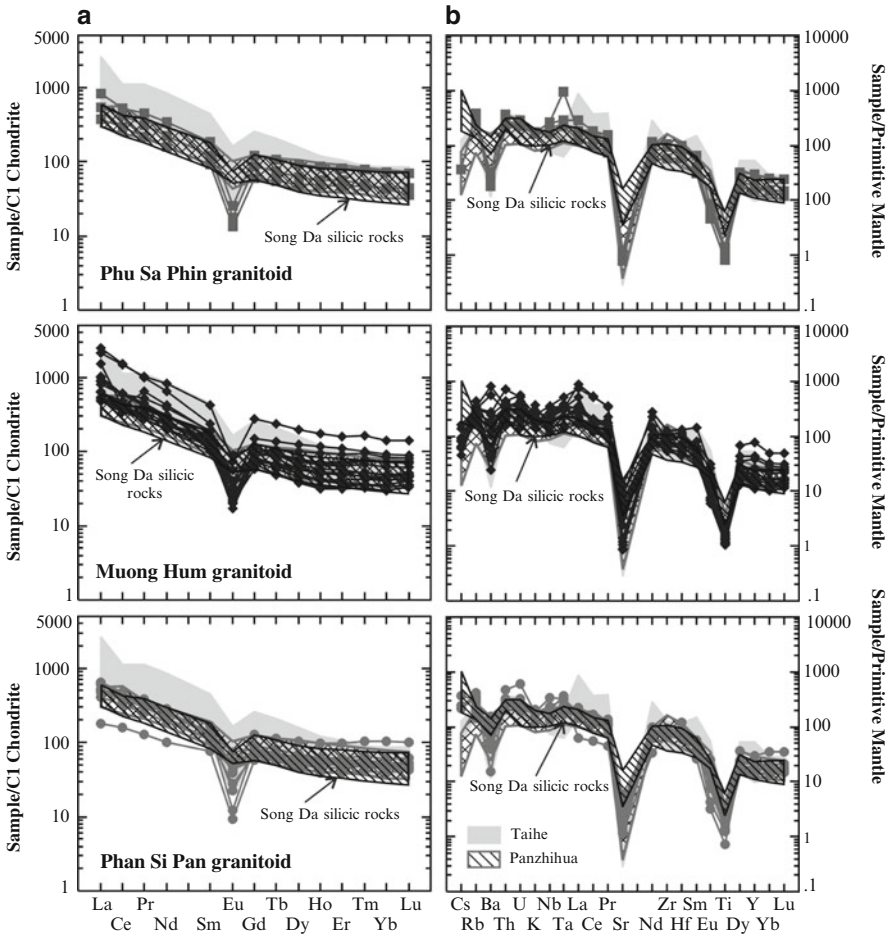

Fig. 3.20 (**a**) Chondrite (Sun and McDonough 1989) normalized REE and (**b**) Primitive-mantle (Sun and McDonough 1989) normalized trace element diagrams for the Phu Sa Phin, Muong Hum and Phan Si Pan granites. For comparison data from the Song Da silicic rocks (Tran Viet Anh et al. 2011) and those from the Taihe and Panzhihua granites (Shellnutt and Zhou 2007) are also shown

mantle source. Based on elemental and Nd isotope geochemistry, Lan et al. (2000)'s model suggested that pluton-volcanic magmas in the Tu Le Basin were produced by fractional crystallization of mantle-derived melts most similar Emeishan basalt and picrite enriched mantle parental melts. Tran Tuan Anh et al. (2004) shows that the mantle source of high-Ti basalt/gabbro from the Tu Le basin is similar to high-Ti basalt from the Song Da belt.

The geochemical and Sr-Nd isotopic characteristics of Permian silisic magmatic rocks in Tu Le basin and Phan Si Pan uplift allow to suggest: (i) they are cogenetic; (ii) in comparing with Permian Song Da silisic-mafic magma and, they could be

Table 3.10 Rb-Sr and Sm-Nd isotopic data for the Permian silicic magmatic rocks from Phan Si Pan Uplift (After Hoa et al. (2015))

Sample	Rb[a] (ppm)	Sr[a] (ppm)	$^{87}Rb/^{86}Sr$	$^{87}Sr/^{86}Sr$	2σ	Sm[b] (ppm)	Nd[b] (ppm)	$^{147}Sm/^{144}Nd$	$^{143}Nd/^{144}Nd$	2σ	$(^{87}Sr/^{86}Sr)_i$[c]	$\varepsilon_{Sr}(t)$[c]	$(^{143}Nd/^{144}Nd)_i$[c]	$\varepsilon_{Nd}(t)$[cd]	T_{DM} (Ma)[d]
Phu Sa Phin															
PSP22/2	175.7	24	21.1828	0.9475	10	13.9	74	0.1136	0.512528	6	0.87066	2359.2	0.512338	0.56	947
PSP26	165.9	25	19.2013	0.8918	8	28.7	159	0.1091	0.512505	6	0.82215	1670.6	0.512323	0.26	940
Muong Hum															
PSP1/1	149.3	30	14.4	0.86378	8	19.4	115	0.102	0.512507	4	0.81155	1520.1	0.512337	0.53	878
PSP11	191.9	51	10.8875	0.73038	10	28.5	134	0.1286	0.512505	6	0.69088	−192.8	0.51229	−0.38	1154
PSP13	271	142	5.5221	0.71385	9	18.8	170	0.0669	0.512434	8	0.69382	−151.1	0.512322	0.25	744
MH3/09	210.9	84	7.2648	0.71549	9	23.3	143	0.0985	0.512457	6	0.68914	−217.6	0.512293	−0.33	917
MH6/09	216.5	265	2.3639	0.71218	8	36	303	0.0718	0.512319	6	0.70361	−12.1	0.512199	−2.16	893
Phan Si Pan															
OQH-8	266.6	46	16.7697	0.80983	9	19.8	114	0.105	0.512489	6	0.749	632.1	0.512314	0.08	927
YB24	125.3	31	11.6953	0.76877	7	20.6	118	0.1055	0.512504	6	0.72634	310.6	0.512328	0.35	911
YB27	143.6	54	7.6946	0.73669	7	20.7	113	0.1108	0.512462	6	0.70878	61.2	0.512277	−0.64	1019
YB29	91.5	124	2.1351	0.71359	10	16.7	88.7	0.1138	0.512502	6	0.70584	19.5	0.512312	0.05	989
RR30[e]	123	123	2.8935	0.71575	4	15.7	131.3	0.0723	0.512518	28	0.70525	11.2	0.512397	1.71	682
RR31A[e]	164	200	2.3727	0.71138	4	20.6	135.4	0.092	0.512504	28	0.70277	−24	0.51235	0.8	809

[a]Concentration obtained by XRF
[b]Concentration obtained by ICP-MS
[c]t = 255 Ma
[d]The $^{143}Nd/^{144}Nd$ and $^{147}Sm/^{144}Nd$ value of chondrite and depleted mantle at present day are 0.512638 and 0.1967, 0.51315 and 0.2137, respectively
[e]Data taken from Lan et al. (2000), recalculated initial isotopic value to t = 255 Ma

derived from the same mantle source with the Song Da high-Ti basalt (Hoa et al. 2015). The mantle source of the silisic magmas is supported by Usuki et al., (2015) study on zircon εHf(t) from rhyolite and granite (+14 to +3) (Usuki et al. 2015). The highly variable of Sr values (0.68914 and 0.81155) in rhyolite and granite of Tu Le basin and Phan Si Pan uplift were interpreted probably due to a significant fractionation (Hoa et al. 2015).

Temporal and spatial closeness and geochemical and isotopic of silisic magmas (in the Tu Le basin and Phan Si Pan uplift) similarity with the Permian Panxi A-type granitoids (Shellnutt et al. 2011) suggest that Phan Si Pan-Tu Le silicic magmatic rocks were formed in relation to the Emeishan mantle plume (Hoa et al. 2013, 2015). The original location of the Phan Si Pan-Tu Le region was very close to the inner zone of ELIP (Usuki et al. 2015).

References

Andrzey Z, Hoa Trong Tran, Larionov AN (2012) The significance of geological and zircon age data derived from the wall rocks of the Ailao Shan–Red River Shear Zone, NW Vietnam. J Geodyn 69:122–139

Cox KG, Bell JD, Pankhurst RJ (1979) The interpretation of igneous rocks. George Allen & Unwin, London, 445 pp

Đao Đinh Thuc, Huynh Trung (eds) (1995) Geology of Viet Nam, P II: magmatic formations. Department of Geology and Minerals of Viet Nam publication, Hanoi

Dovjikov (ed) (1965) Geology of northern Viet Nam. Science and Technology Publication, Hanoi, 668 p

Fromaget J (1932) Sur les plissements calédoniens du massif du Fansipan (Tonkin). Comptes Rendus de l'Académie des Sciences de France Paris 195:552–554

Frost CD, Bell JM, Frost BR, Chamberiain KR (2001) Crustal growth by magmatic underplating: isotopic evidence from the northern Sherman batholith. Geology 29:515–518

Hieu PT, Chen FK, Nguyen Thi Bich Thuy, Nguyen Quoc Cuong, Li SQ (2013) Geochemistry and zircon U-Pb and Hf isotopic composition of Permian alkali granitoids of the Phan Si Pan zone in northwestern Vietnam. J Geodyn 69:106–121

Hutchison CS (1989) Geological evolution of southeast Asia. Calendron, Oxford, 368 pp

Nguyen Vinh (1977) Upper Silurian – Devonian sediment in northwest Vietnam. In: The geological problems of northwest Vietnam. Science and Technics Publishing House, Hanoi, pp 82–108 (in Vietnamese)

Nguyen Vinh (1978) Geology of Yen Bai map sheet of 1:200,000 (in Vietnamese)

Nguyen Đac Đong (ed) (2000) Explanations attached to geological and mineral exploration mapping of Tram Tau serial sheet of 1:50,000 scale. Center for Geological Archives, HaNoi (in Vietnamese)

Nguyen Trung Chi (ed) (2003) Petrology and mineralization of alkaline magma formations in northern Viet Nam. Final Report of ministerial project (Ministry of Natural Resources and Environment), Center for Information and Literature Archives, Department of Geology and Minerals, Hanoi (in Vietnamese)

Nguyen Van Nhan, Hoang Minh Thao (2002) Geochemical – mineralogical characteristics of Pb-Zn ore in the Tu Le area. J Geol A271:7–8 (in Vietnamese with English abstract)

Nguyen Hoang, Nguyen Đac Lu, Nguyen Van Can (2004) Paleozoic volcanics in the Song Da structure: Rb-Sr age of Doi Bu volcanics. J Geol A 281:11–17 (in Vietnamese with English abstract)

Pearce JA, Harris NBW, Tindle AG (1984) Trace element discrimination diagrams for the tectonic interpretation of granitic rocks. J Petrol 25:956–983

Pham Thi Dung, Tran Trong Hoa, Tran Tuan Anh, Tran Van Hieu, Vu Hoang Ly, Lan CY, Usuki T (2012) The new date on Ye Yen Sun granitoid complex in the Phan Si Pan. J Earth Sci 34(3):193–204 (in Vietnamese with English abstract)

Shellnutt JG, Zhou MF (2007) Permian peralkaline, peraluminous and metaluminous A-type granites in the Panxi district, SW China: their relationship to the Emeishan mantle plume. Chem Geol 243:286–316

Shellnutt JG, Zhou M-F, Zellmer G (2009a) The role of Fe–Ti oxide crystallization in the formation of A-type granitoids with implications for the Daly gap: an example from the Permian Baima igneous complex, SW China. Chem Geol 259:204–217

Shellnutt JG, Wang CY, Zhou M-F, Yang Y-H (2009b) Zircon Lu-Hf isotopic compositions of metaluminous and peralkaline A-type granitic plutons of the Emeishan large igneous province (SW China): constraints on the mantle source. J Asian Earth Sci 35:45–55

Shellnutt JG, Jahn BM, Zhou MF (2011) Crustally-derived granites in the Panzhihua region, SW China: implications for felsic magmatism in the Emeishan large igneous province. Lithos 123:145–157

Sun SF, McDonough WF (1989) Chemical and isotopic systematics of oceanic basalts: implication for mantle composition and processes. In: Saunders AD, Norry NJ (eds) Magmatism in ocean basins. Geol. Soc. Spec. Publ, Boston, pp 313–345

Tong Duy Thanh, Vu Khuc (eds) (2005) Stratigraphic divisions of Viet Nam. National University Publ, Hanoi, 504 p (in Vietnamese)

Tran Trong Hoa (ed) (1995) Study of Mesozoic – Cenozoic magmatism and its mineralization potential. Final report for national project KT- 01-04 (1992-1995), Archives of the National Center for Science and Technology Information, Hanoi (in Vietnamese)

Tran Van Tri (ed) (1977) Geology of Vietnam, northern part. Science and Technics Publishing House, Hanoi (in Vietnamese)

Tran Trong Hoa, Tran Tuan Anh, Ngo Thi Phuong, Tran Viet Anh (2003) Genetic characteristics of Muong Hum granitoids based on geochemical and isotopic studies. J Earth Sci 25(4):389–400 (in Vietnamese with English abstract)

Tran Tuan Anh, Tran Trong Hoa, Lan CY, Chung SL, Lo CH, Wang PL, Mertzman SA (2004) Mesozoic bimodal alkaline magmatism in Tu Le basin, North Vietnam: constraints from geochemical and isotopic significances. J Geol Ser B 24:1–9

Tran Trong Hoa, Tran Tuan Anh, Ngo Thi Phuong, Pham Thi Dung, Tran Viet Anh (2005) Permian – Triassic magmatic activities in Viet Nam and prospect of associated rare and precious metal (Pt, Au) mineralization. In: Proceedings of 60-Anniversary of geology of Viet Nam, pp 63–79 (in Vietnamese)

Tran Viet Anh, Pang KN, Chung SL, Lin HM, Tran Trong Hoa, Tran Tuan Anh, Yang HJ (2011) The Song Da magmatic suite revisited: a petrologic, geochemical and Sr–Nd isotopic study on picrites, flood basalts and silicic volcanic rocks. J Asian Earth Sci 42:1341–1355

Tran Trong Hoa, Tran Tuan Anh, Pham Thi Dung, Lan Ching-Ying, Usuki Tadashi, Polyakov GV, Izokh AE (2013) Permian plume-related magmatic associations in the Song Da – Tu Le rift system and Phan Si Pan uplift, northwest Vietnam. Extend. Abstract volume of international symposium Large igneous provinces of Asia: mantle plume and metallogeny, LIPs, Hanoi 7 Nov 2013, pp 57–61

Tran Trong Hoa, Ching–Ying Lan, Tadashi Usukib, Gregory Shellnutt J, Pham Thi Dung, Tran Tuan Anh, Pham Ngoc Can, Ngo Thi Phuong, Izokh AE, Borisenko AS (2015) Petrogenesis of late Permian silicic rocks of Tu Le Basin and Phan Si Pan Uplift (NW Vietnam) and their association with the Emeishan large igneous province. J Earth Sci 109:1–19

Usuki T, Lan CY, Tran Trong Hoa, Pham Thi Dung, Wang KL, Shellnutt JG, Chung SL (2015) Zircon U-Pb ages and Hf isotopic compositions of alkaline silicic magmatic rocks in the Phan Si Pan-Tu Le region, northern Vietnam: identification of a displaced western extension of the Emeishan large igneous province. J Asian Earth Sci 97:102–124

Whalen JB, Currie KL, Chappell BW (1987) A-type granites: geochemical characteristics, discrimination and petrogenesis. Contrib Mineral Petrol 95:407–419

Wilson M (1989) Igneous petrogenesis: a global tectonic approach. Springer, Berlin, 466 pp

Chapter 4
Permian – Triassic Pluton – Volcanic Magmatic Associations in the Song Hien Structure, Northeast Vietnam

Abstract The Song Hien Basin in northeast Vietnam is linear- shaped, running in the northwest – southeast direction from Vietnam-China border to the easternmost of Lang Son province; with a total length about 200 km the structure divides the Ha Lang belt to the northeast and Phu Ngu belt in the south and southwest. Permian – Triassic magmatism comprises pluton-volcanic felsic and mafic bimodal magmatic associations, including basalt, gabbrodolerite – dolerite (and lherzolite-gabbronorite); rhyodacite – rhyolite and granite. These magmatic associations are spatially, temporally and genetically related. Detailed mineralogical, geochemical and chemically mineralized studies have been conducted intensively on the Song Hien magmatism; among these, the mafic and ultramafic magmas have been described separately while gabbrodolerites were grouped to pluton-volcanic basaltoidic associations. Formation ages of lhrzolite and gabbro-dolerite are 260–262 Ma, while rhyolite – 246 Ma. Geochemical and isotopic data show genetic relationship between basalts and gabbro-dolerite and rhyolite and porphyric granite.

Geochemical features of the Permian Song Hien magmas indicate a uniform evolutional trend for the Permian – Triassic magmas. The Nb, Ta, Sr and Ti depletion is a geochemically streamline character for ultramafic, mafic and felsic rock types, suggesting that their common mantle source may have been contaminated by subduction-derived materialsand are produced by mantle melting following continental collapse that occurred around craton marginal regions under the impact of super-mantle plumes developed under Asian continent.

The Song Hien Belt in northeast Vietnam is linear- shaped, running in the northwest – southeast direction from Vietnam-China border to the easternmost of Lang Son province; with a total length about 200 km the structure divides the Ha Lang belt to the northeast and Phu Ngu belt in the south and southwest. Serving as boundaries among the above structures are Cao Bang – Lang Son (Tien Yen) and Yen Minh – National Route 13 deep faults (Fig. 4.1). In the modern tectonic framework Song Hien belt exposes in an irregular shape, containing a number of enlarged and contracted sections being filled with terrigenous sediments and Permian – Triassic volcanic rocks. Permian – Triassic magmatism comprises pluton-volcanic felsic and mafic bimodal magmatic associations, including (1) andesite – basalt, gabbrodolerite – dolerite (and granophyre); rhyodacite – rhyolite and granite. These

T.-H. Tran et al., *Intraplate Magmatism and Metallogeny of North Vietnam*,
Modern Approaches in Solid Earth Sciences 11,
DOI 10.1007/978-3-319-25235-3_4

Fig. 4.1 Schematic distribution of basalt, rhyolite, gabbrodolerite and lherzolite magmas in the Song Hien structure

magmatic associations are spatially, temporally and genetically related. Besides, as observed in the Cao Bang area basaltoids and doleritic gabbro are associated with mafic – ultramafic intrusive magmas such as lherzolite, picrite and olivine gabbronorite. In previous studies these associations and the mafic gabbrodolerite intrusions were viewed as part of the Cao Bang intrusive complex (Dovjikov 1965; Tri 1977; Thuc and Trung 1995; Polyakov et al. 1996). In the recent years detailed mineralogical, geochemical and chemically mineralized studies have been conducted intensively on the Song Hien magmatism; among these, the mafic and ultramafic magmas have been described separately while gabbrodolerites were grouped to pluton-volcanic basaltoidic associations (Hoa et al. 2005). The division seems to be convenient for reflecting closely the practical evolution process of the Song Hien Permian – Triassic magmatic evolution as well as their relation to the regional mineralization. Note that aside from basalts outcropped in the Song Hien structure and

being described in this monograph there are other geochemically distinct basalts, for example, those outcrop in the Nguom Chang iron mine area, northwest of Ma Phuc Pass, northeast of Cao Bang town. Also, in the Lang Son area aside from Permian – Triassic basalts, a constituent of the Song Hien complex, there are Late-Mesozoic (Jurassic – Cretaceous) basalts in the Tam Danh complex. However, for lacking of details these Cenozoic basalts are not included in this study. In terms of tectonic nature Song Hien basin (belt, structure) is considered as an aulacogeny (Bach 2001), or pre-rift structure (Tung and Tri 1992).

4.1 Basalt – Rhyolite Associations

4.1.1 Geology, Age and Petrologic and Mineralogical Characteristics

Permian – Triassic basalt and rhyolite magmas are popular in the Song Hien basin. They are found mostly in Cao Bang and Lang Son areas, some volcanic felsic magmas of Song Hien complex are also found in the Meo Vac area (Ha Giang province), northwestern extreme of the basin. Distribution limit of the mafic and felsic magmas is controlled by northwest – southeast direction Cao Bang – Tien Yen fault. Rhyolite and sub-volcanic granitoid (granodiorite, granite with granophyric texture as of Nui Dieng complex) are outcropped in the Tam Dao area, a large distance toward south-eastern wing of the structure. Rhyolite and granite-granophyre are also widely spread in the areas of Binh Lieu and Mong Cai, along the border between Triassic An Chau and Quang Ninh structures. These formations have not been well studied, age of their magmatic activity is not determined, therefore, the authors will describe only Permian – Triassic magmatic associations exposed in the central and south-eastern regions of Song Hien belt. The two regions most representing are Cao Bang and Lang Son. Volcanic rocks in these areas, especially the mafic type, aside showing many similar features they also obtain a number of geochemical properties.

Detailed geological survey along cross-sections perpendicular to the continuation trend of terrigenous – volcanic layers reveal that mafic and felsic magmas are closely associated, somewhere basalts are clearly overlain by rhyolites. Mafic inclusions are found in sub-volcanic rhyolites along a Ky Cung riverbank near Van Quan and Dong Dang intersection. Geological surveys also show that basaltoids are dominant over rhyolites in the Cao Bang area while rhyolite and rhyodacite are more voluminous in the Lang Son area.

Ar-Ar age dating on doleritic basalts in the Cao Bang area yielded values between 263 and 244 Ma (Fig. 4.2) (Hoa 2007). The older age is closely matched with U/Pb age dating (by SHRIMP) on zircon in gabbrodolerite and lherzolite collected in the Suoi Cun massif, yielded 262–266 Ma (Hoa et al. 2008).

However, result of a U-Pb age dating on zircon in rhyolite (sample AH 8003) in the Suoi Cun area (Cao Bang) showed 248 ± 4.5 Ma, corresponding to Permian – Triassic. There are melt inclusions in prismatic zircons which are characterized by having various cores surrounded by zoned layers (Photo. 4.1).

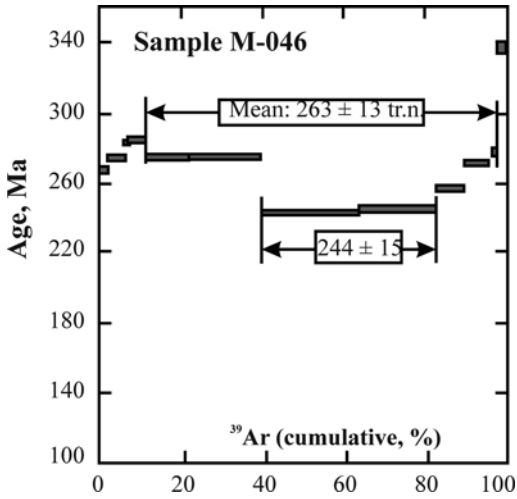

Fig. 4.2 Ar-Ar age of Cao Bang basalts (Hoa 2007)

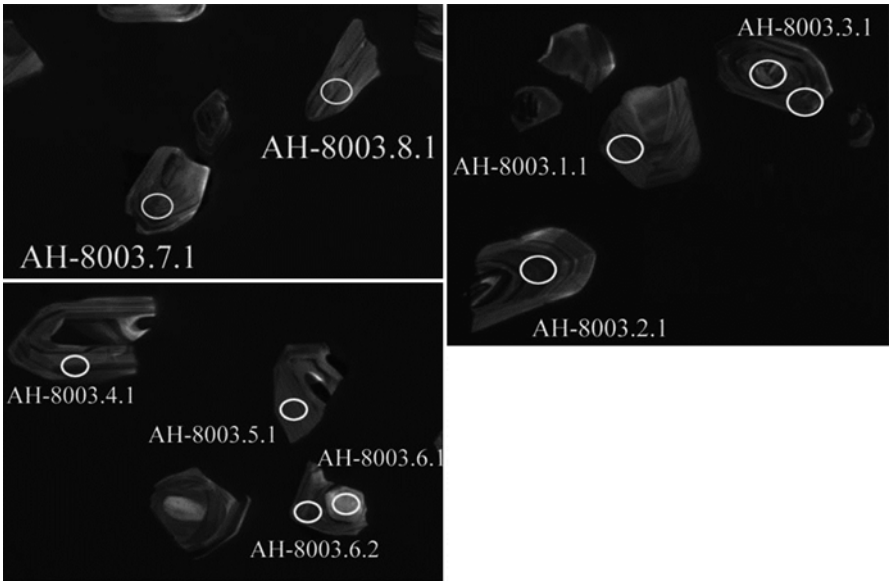

Photo 4.1 Back-scattered image of zircons in rhyolites in the Suoi Cun area (Cao Bang, sample AH-8003). Point labels are corresponding to samples in Table 4.1

The U and Pb contents (Table 4.1) in the margins of zircons are 200–500 ppm and 50–130 ppm, respectively. $^{232}Th/^{238}U$ ratios vary between 0.2 and 0.3. The concordant ages calculated for all the analyzed zircon grains show 248 ± 4.5 Ma (MSWD = 0.054) (Fig. 4.3), corresponding to early Triassic (Hoa et al. 2008). This age is in complete agreement with field survey (Hoa et al. 2005), and shows that the basalt and rhyolite are parts of Song Hien bimodal basalt – rhyolite magmatic associations. Note that among the zircons chosen for analysis there are several grain-cores

Table 4.1 Chemical and isotopic compositions of U and Pb of zircons in rhyolites from the Suoi Cun stream area. Data were acquired from VSEGEI, Russia

Points	% $^{206}Pb_c$	ppm U	ppm Th	$^{232}Th/^{238}U$	ppm $^{206}Pb^*$	(1) $^{206}Pb/^{238}U$ Age		(1) $^{207}Pb/^{206}Pb$ Age		(1) $^{238}U/^{206}Pb^*$	±%	(1) $^{207}Pb^*/^{206}Pb^*$	±%	(1) $^{207}Pb^*/^{235}U$	±%	(1) $^{206}Pb^*/^{238}U$	±%	err corr
AH-8003.5.1	1.08	248	50	0.21	8.3	244.7	±6.4	233	±180	25.85	2.7	0.0508	7.6	0.271	8	0.0387	2.7	.331
AH-8003.6.2	0.50	384	99	0.27	12.9	245.1	±6.3	282	±130	25.8	2.6	0.0519	5.5	0.277	6.1	0.0388	2.6	.427
AH-8003.7.1	0.68	332	93	0.29	11.2	246.0	±6.3	210	±130	25.71	2.6	0.0503	5.5	0.27	6.1	0.0389	2.6	.430
AH-8003.4.1	1.54	324	79	0.25	11.0	246.8	±6.4	362	±170	25.62	2.6	0.0538	7.7	0.289	8.1	0.039	2.6	.325
AH-8003.3.2	0.56	419	105	0.26	14.1	247.1	±6.3	261	±100	25.59	2.6	0.0515	4.5	0.277	5.2	0.0391	2.6	.497
AH-8003.1.1	0.59	359	85	0.24	12.2	247.9	±6.4	211	±170	25.5	2.6	0.0504	7.2	0.272	7.7	0.0392	2.6	.344
AH-8003.8.1	0.50	316	84	0.28	10.7	248.2	±6.5	228	±190	25.48	2.7	0.0507	8.2	0.274	8.6	0.0392	2.7	.307
AH-8003.2.1	0.57	553	131	0.24	19.1	252.8	±6.4	268	±79	25	2.6	0.0516	3.4	0.285	4.3	0.04	2.6	.598
AH-8003.6.1	0.45	204	153	0.78	24.9	854.0	±21	856	±60	7.06	2.6	0.0676	2.9	1.32	3.9	0.1417	2.6	.669
AH-8003.3.1	0.25	436	160	0.38	60.3	960.0	±23	1485	±21	6.23	2.6	0.0929	1.1	2.055	2.8	0.1605	2.6	.916

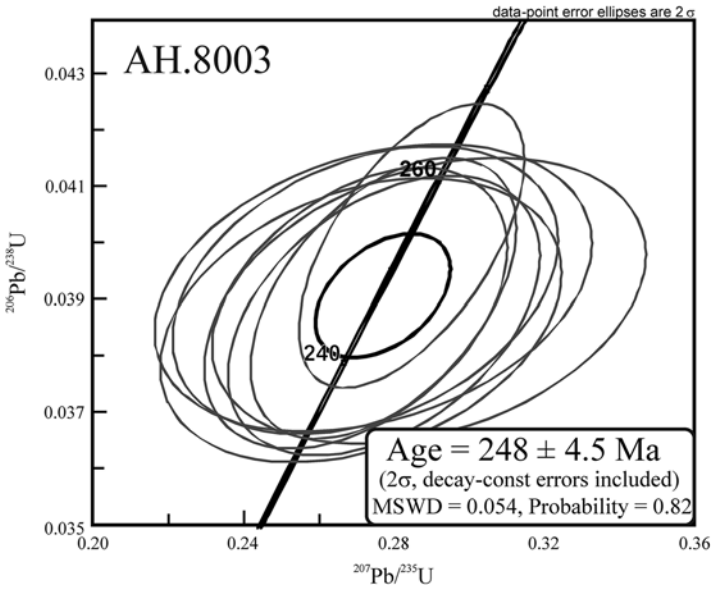

Fig. 4.3 Concordant age of zircons in rhyolite in the Suoi Cun area (Cao Bang). Analyzed in Institute of Geology and Mineralogy, Siberian Branch, Russian Academy of Science

yielding ages between 850 and 960 Ma (sample AH 8003 3.1., 6.1.), indicating strong crustal assimilation during the magma generation.

The mafic volcanic type is mainly basalt. Based on mineralogical, geochemical compositions and textural characteristics the basalts are divided into various rock types. Afanitic basalts show 'spinifex' texture for having needle-shape clinopyroxene and plagioclase microlites, lying parallel or crossing each other, or having skeleton-shaped distribution in the brownish green volcanic glass groundmass (Photo 4.2a, b). The popularity of frozen clinopyroxene spinifex texture indicates that the magma was quickly crystallized from an enriched iron melt (Magmatic rocks 1985). Basalts with microdoleritic and doleritic textures are also widely spread (Photo 4.2c). They are found in central parts of lava flows, sometimes show highly crystallized similar to sub-volcanic magmas. Andesitic basalt (leucobasalt) and andesitic dacite are also encountered elsewhere. Basaltic and andesite-basaltic tuff-lava and tuff-breccia are rare. Fragments in the tuff-lava and tuff-breccia, being cemented by volcanic glass, volcanic ash or products of altered basic volcanic glass, are majorly basaltic or andesite-basaltic. Basalts in the Lang Son area show higher rate of crystallization.

Clinopyroxenes in Cao Bang basalts are compositionally stable within Mg-, Ca-rich augite or augite – diopside. They are characterized by relatively high TiO_2 (0.53–1.11 wt%), average to high Al_2O_3 (2.26–3.53 wt%) and high Cr_2O_3 (0.22–0.70 wt%) as compared to the accompanying sub-volcanic types (Table 4.2). In general, the chemical compositions of clinopyroxene in basalt are mostly matched with the mineral in gabbro-dolerite which shows closely spatial relation to the

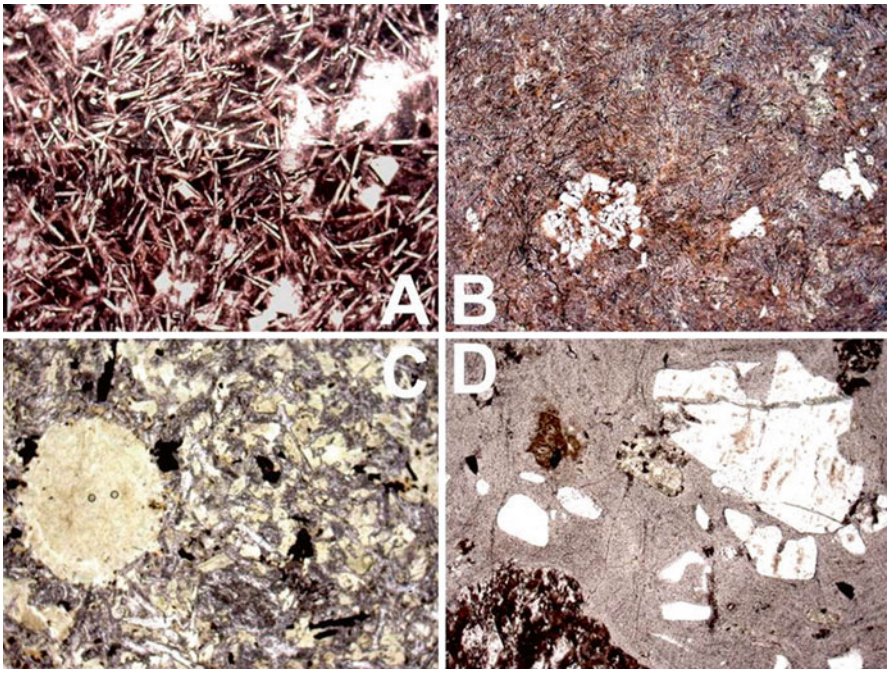

Photo 4.2 Microphotographs of basalt (**a, b**), dolerite (**c**) and rhyolite (**d**) in the Cao Bang area

basalt, indicating their synchronously magmatic nature. Plagioclases in basalt and andesitic basalt are usually FeO-rich (1.76 wt%) andesine – labrador ($Ab_{50.2}An_{46.6}Or_{3.2}$).

Felsic members in the basalt-rhyolite bimodal associations are rhyodacite and rhyolite. Silicic tuffs of explosive eruption origin are dominant in the Cao Bang area, while in Lang Son area rhyodacite and rhyolite lavas are overwhelming. They are porphyritic with idiomorphic microcline and plagioclase; whereas, remnant-shaped pyroxene and amphibole, and plagioclase phenocrysts forming separate aggregates are sometimes observed in dacite (Photo 4.2d). In sub-volcanic magmas in the Lang Son area garnet phenocrysts are also found. Fragments in rhyodacitic and rhyolitic tuffs are commonly quartz, K-feldspar, rhyolite, basalt and sediment. The rhyodacite and rhyolite are porphyritic with K-feldspar ($Or_{90.7}Ab_{7.9}An_{1.4}$) and quartz being most common phenocrysts. Their groundmasses are felsic, sometimes microgranitic or granophyritic. The felsic texture is constructed by feldspar, quartz and volcanic glass.

4.1.2 Geochemistry and Isotope

Chemical compositions of rock-forming oxides, trace elements and rare earths of representative basalt-rhyolite associations in the Cao Bang and Lang Son areas are given in Table 4.3. Plots of SiO_2 vs. $Na_2O + K_2O$ show the Song Hien magmas fall

Table 4.2 Chemical compositions (wt%) of clinopyroxene in Cao Bang mafic – ultramafic, Song Hien structure (Hoa et al. 1999)

Sample	SiO_2	TiO_2	Al_2O_3	Cr_2O_3	FeO	MnO	MgO	CaO	Na_2O	K_2O	Sum
Olivine gabbro-norite, Khuoi Giang Block											
M- 204/1	51.47	0.52	2.75	0.88	6.92	0.26	16.81	18.94	0.32	0.01	98.88
M- 204/2	52.83	0.35	1.92	0.66	5.83	0.15	18.36	18.4	0.18	0.01	98.68
M- 204/3	50.99	0.88	2.54	0.81	7.54	0.2	16.65	18.52	0.24	0	98.37
M- 204/4	53.13	0.33	1.68	0.65	5.87	0.2	18.23	18.45	0.17	0.02	98.73
M-204-5	51.2	0.44	2.78	0.21	7.39	0.21	18.96	16.03	0.17	0.09	98.07
M-204-6	52.68	0.46	1.8	0.21	6.11	0.21	18.12	18.79	0.16	0.04	99.1
Ophitic gabbro, Khuoi Luong Block											
M- 221-1	52.18	0.44	1.97	0.41	7.35	0.22	18.17	17.3	0.22	0.02	98.29
M-221-2	51.98	0.56	2.75	0.63	6.38	0.2	17.06	19.08	0.26	0	98.88
M-221-3	51.62	0.59	2.34	0.43	6.67	0.22	16.9	19.56	0.22	0.01	98.65
Gabbro-dolerite, Lung Bat Block											
CD-204/1-	51.38	0.46	1.81	0.01	9.33	0.26	15.67	18.34	0.32	0.02	97.6
CD-204/1-	51.71	0.68	2.46	0.17	8.24	0.18	16.37	18.56	0.17	0.01	98.56
Aphanitic basalt											
M- 046	50.01	1.11	3.53	0.22	9.23	0.19	15.43	18.17	0.2	0.01	98.09
M- 201	52.05	0.53	2.26	0.7	7.51	0.2	17.87	17.43	0.2	0.02	98.77

Table 4.3 Chemical compositions (wt%), trace and rare earth element abundances of Song Hien volcanics (Hoa et al. 2005)

Sample	M001	M046	M600	CB-6	CB-7	CB-1	CB-5	M609	M611/1	CD-1387/1
	1	2	3	4	5	6	7	8	9	10
SiO_2	46.90	49.96	48.50	49.48	50.40	62.44	67.38	70.69	70.59	70.59
TiO_2	1.08	1.36	1.11	1.13	1.18	1.28	0.55	0.45	0.48	0.47
Al_2O_3	14.76	14.40	13.75	14.77	14.52	14.39	13.10	13.90	14.25	14.38
Fe_2O_3	11.28	11.02	10.40	10.73	10.40	8.11	3.23	3.29	3.47	2.53
MnO	0.19	0.19	0.17	0.18	0.18	0.11	0.04	0.05	0.04	0.03
MgO	8.27	7.44	7.66	7.36	7.08	2.16	0.53	0.52	0.81	0.26
CaO	10.18	9.95	11.16	9.03	10.77	3.26	4.53	2.02	2.51	2.54
Na_2O	2.01	1.89	2.22	2.73	1.82	4.92	3.14	1.88	1.67	2.64
K_2O	1.38	1.30	0.59	1.38	0.92	1.81	3.06	4.85	4.68	5.20
P_2O_5	0.12	0.15	0.13	0.13	0.15	0.20	0.13	0.11	0.13	0.13
L.O.I	3.98	2.76	4.03	2.88	2.29	1.72	4.61	1.94	1.05	1.43
Total	100.15	100.42	99.72	99.80	99.70	100.40	100.30	99.70	99.68	100.19
Cu	47.00	62.00	47.00	54.00	60.00	23.00		18.00	11.00	
Ni	100.00	105.00	138.00	92.00	83.00	28.00		10.00	13.00	
Co	32.00	46.00	41.00	34.00	45.00	19.00		7.00	9.00	
Cr	266.00	267.00	280.00	375.00	429.00	40.00		19.00	16.00	
V	139.00	208.00	166.00	218.00	253.00	126.00		36.00	22.00	
Rb	74.00	65.50	25.60	70.00	36.00	72.00	173.00	260.00	232.00	316.00
Sr	91.00	109.00	165.00	83.60	144.00	96.70	144.00	109.00	126.00	200.00
Y	32.10	32.80	31.00	24.50	21.70	50.90	40.00	45.00	44.50	50.60
Zr	112.00	143.00	134.00	89.70	95.70	252.00	168.00	340.00	222.00	264.00
Nb	8.70	5.70	4.10	4.00	5.40	10.40	5.90	9.70	7.60	9.90
Sc	42.00	41.00	37.00	44.00	45.00	27.00	8.80	8.60	8.30	7.10

(continued)

Table 4.3 (continued)

Sample	M001	M046	M600	CB-6	CB-7	CB-1	CB-5	M609	M611/1	CD-1387/1
	1	2	3	4	5	6	7	8	9	10
Cs	1.80	3.00	2.70	4.50	3.70	3.00	12.00	4.00	6.40	5.40
La	16.00	16.00	13.50	12.00	11.50	37.00	47.00	52.00	51.00	50.00
Ce	31.00	34.00	28.00	25.00	26.00	69.00	87.00	92.00	90.00	91.00
Nd	17.00	21.00	17.00	15.00	16.00	36.00	44.00	46.00	45.00	46.00
Sm	4.30	5.90	4.60	4.20	4.70	9.20	10.80	10.80	10.60	11.00
Eu	0.98	1.44	1.14	1.20	1.10	1.45	1.23	1.35	1.30	1.40
Gd	5.80	6.90	5.90	5.00	5.50	11.00	10.00	10.00	11.30	11.00
Tb	1.00	1.20	1.00	0.92	0.95	1.90	1.60	1.70	2.00	1.80
Yb	3.30	4.00	3.20	3.10	3.30	4.80	3.30	4.20	4.10	4.30
Lu	0.48	0.59	0.46	0.45	0.48	0.67	0.45	0.58	0.56	0.60
Hf	3.00	4.50	3.20	3.00	2.60	6.50	5.60	5.40	6.30	6.00
Ta	0.65	0.60	0.50	0.50	0.25	1.20	1.00	1.10	1.20	1.20
Th	4.00	5.60	5.50	4.00	4.00	17.00	25.00	26.00	29.00	28.00
U	1.30	1.60	1.50	1.10	1.00	3.50	4.50	5.00	5.60	5.50
Zr/Y	3.49	4.36	4.32	3.66	4.41	4.95	4.20	7.56	4.99	5.22
Nb/Y	0.27	0.17	0.13	0.16	0.25	0.20	0.15	0.22	0.17	0.20
Nb/La	0.54	0.36	0.30	0.33	0.47	0.28	0.13	0.19	0.15	0.20
$(La/Yb)_N$	3.48	2.87	3.03	2.78	2.50	5.53	10.22	8.88	8.92	8.34
$(La/Sm)_N$	2.40	1.75	1.89	1.84	1.58	2.60	2.81	3.11	3.11	2.93
$(Ce/Yb)_N$	2.61	2.36	2.43	2.24	2.19	3.99	7.32	6.08	6.10	5.88
Eu/Eu*	0.60	0.69	0.67	0.80	0.66	0.44	0.36	0.39	0.36	0.38
Remarks: Cao Bang: 1–5- basalt; 6–7- andesitic basalt, 8–10- rhyodacite and rhyolite; Lang Son: 11–13- basalt, 17–23- dacite and rhyolite										

Sample	LS-1	LS-1/1	LS-9	LS-10	LS-13	LS-2	LS-8
	11	12	13	14	15	16	17
SiO_2	46.93	48.53	53.60	70.29	66.67	71.08	74.54
TiO_2	2.47	2.22	3.39	0.38	0.96	0.43	0.48
Al_2O_3	13.34	14.77	12.71	15.49	13.83	15.51	12.76
Fe_2O_3	13.53	13.23	14.72	2.41	7.45	1.75	3.67
MnO	0.20	0.21	0.21	0.04	0.08	0.05	0.03
MgO	3.90	6.25	2.62	0.35	0.95	0.25	0.28
CaO	9.74	9.92	5.69	2.17	2.24	1.91	0.22
Na_2O	4.25	1.92	4.14	1.88	2.01	1.67	1.65
K_2O	0.74	0.70	0.12	5.21	3.85	5.11	5.21
P_2O_5	0.51	0.29	0.28	0.12	0.20	0.12	0.09
L.O.I							
Total	95.61	98.04	97.47	98.35	98.25	97.88	98.92
TiO_2/P_2O_5	4.81	7.60	12.31	3.11	4.81	3.49	5.10
Cu	81.27	56.61	19.04	20.85	23.43	12.58	61.35
Ni	30.04	18.56	3.90	6.86	11.37	6.49	7.93
Co	32.74	38.20	30.21	2.83	10.53	3.37	4.23
Cr	21.88	117.40	6.26	6.70	19.26	9.81	11.86
V	254.50	264.50	207.90	13.03	63.70	11.94	12.76
Rb	13.50	37.71	8.00	214.00	194.30	203.90	231.80
Sr	447.00	199.90	142.20	140.20	199.60	116.90	91.13
Y	30.78	49.28	58.36	39.24	62.15	41.16	59.68
Zr	150.50	186.90	256.20	196.20	301.90	223.00	375.20
Nb	23.17	6.45	13.82	9.60	14.46	10.38	15.52
Sc	18.97	42.85	42.72	21.66	21.99	10.66	26.06

(continued)

Table 4.3 (continued)

Sample	LS-1	LS-1/1	LS-9	LS-10	LS-13	LS-2	LS-8
	11	12	13	14	15	16	17
Cs	0.33	3.17	2.02	5.94	2.26	12.42	2.41
La	39.00	12.76	31.61	38.87	52.71	43.44	47.20
Ce	81.08	29.38	64.43	75.69	104.20	84.64	96.36
Nd	43.66	20.67	33.33	33.51	47.53	37.37	44.14
Sm	8.51	6.10	7.87	6.98	10.12	7.75	9.40
Eu	3.28	1.74	1.55	1.10	1.65	1.13	1.39
Gd	7.14	6.54	7.88	6.24	9.16	6.91	8.43
Tb	1.11	1.28	1.50	1.07	1.73	1.16	1.56
Yb	2.47	4.53	5.73	3.30	6.14	3.49	6.05
Lu	0.36	0.73	0.89	0.52	0.93	0.54	0.92
Hf	3.86	4.91	7.04	5.52	8.36	6.27	10.44
Ta	1.76	0.50	1.30	0.97	1.42	1.05	1.48
Th	3.47	2.90	12.64	24.84	21.14	28.31	26.73
U	0.81	0.73	2.68	5.62	4.80	5.77	5.73
Zr/Y	4.89	3.79	4.39	5.00	4.86	5.42	6.29
Nb/Y	0.75	0.13	0.24	0.24	0.23	0.25	0.26
Nb/La	0.59	0.51	0.44	0.25	0.27	0.24	0.33
$(La/Sm)_N$	2.96	1.35	2.59	3.59	3.36	3.62	3.24
$(Ce/Yb)_N$	9.14	1.80	3.12	6.36	4.72	6.73	4.42
Eu/Eu*	1.25	0.84	0.60	0.50	0.51	0.46	0.47

Sample	H1452	H1454	H1454/1	H1455	H1457	H1457/1
	18	19	20	21	22	23
SiO_2	66.67	65.78	58.26	64.73	69.39	66.68
TiO_2	0.715	0.946	1.255	0.947	0.913	1.022
Al_2O_3	14.21	13.46	14.78	12.52	12.52	11.84
Fe_2O_3	4.68	7.79	11.16	7.93	6.93	9.63
MnO	0.068	0.079	0.133	0.126	0.071	0.093
MgO	1.29	1.3	1.95	1.04	0.86	1.18
CaO	2.56	1.86	3.44	4.36	1.04	2.28
Na_2O	1.7	2.5	1.76	2.97	4.01	1.75
K_2O	4.23	3.84	3.87	3.43	2.4	2.61
P_2O_5	0.159	0.217	0.285	0.215	0.21	0.227
L.O.I	3.16	1.99	2.9	1.48	1.45	2.14
Total	99.55	99.84	99.87	99.81	99.84	99.49
TiO_2/P_2O_5	4.50	4.36	4.40	4.40	4.35	4.50
Co	9	13	10	7.9	12	16
Rb	139	173	182	160	128	130
Sr	104	180	145	150	66	45
Y	35	55	61	51	45	55
Zr	258	292	318	294	305	333
Nb	16	15	17	15	15	17
La	47	50	56	47	47	49
Ce	93	95	104	93	92	96
Nd	42	47	50	46	45	47
Sm	7.6	9.4	9.9	9.3	8.3	9.4

(continued)

Table 4.3 (continued)

Sample	H1452	H1454	H1454/1	H1455	H1457	H1457/1
	18	19	20	21	22	23
Eu	1.1	1.7	2.1	1.7	1	1.3
Gd	7.6	11	12	11	9.2	10
Tb	1.1	1.7	1.8	1.6	1.5	1.5
Yb	4	6.1	6.7	5.9	5.7	6.4
Lu	0.59	0.91	1	0.85	0.87	0.92
Hf	7.2	8.6	9.1	8.4	8.8	10
Ta	1.2	1.7	1.8	1.6	1.7	2
Th	23	23	22	22	23	25
U	4	5.3	5.3	5.1	5.3	6
Zr/Y	7.37	5.31	5.21	5.76	6.78	6.05
Nb/Y	0.46	0.27	0.28	0.29	0.33	0.31
Nb/La	0.34	0.30	0.30	0.32	0.32	0.35
$(La/Sm)_N$	3.99	3.43	3.65	3.26	3.66	3.37
$(Ce/Yb)_N$	6.46	4.33	4.31	4.38	4.48	4.17
Eu/Eu*	0.44	0.51	0.59	0.51	0.35	0.41

Eu/Eu* is a measure of the size of the Eu anomaly: $Eu/Eu^* = Eu_N/^{1/2}(Sm_N*Gd_N)$
The subscript N indicates chondrite value normalized

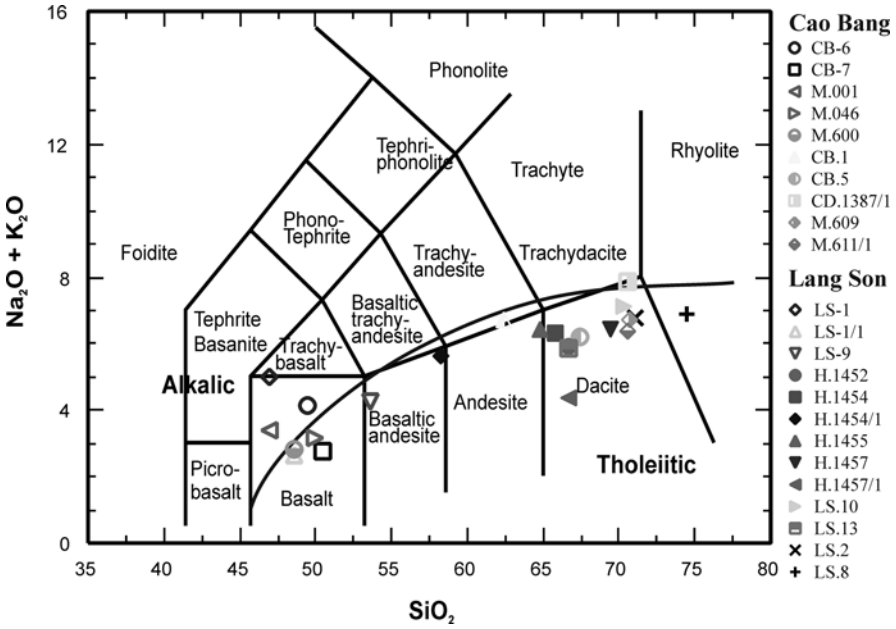

Fig. 4.4 Song Hien volcanic magmas in the classification diagram $NaO_2 + K_2O$ versus SiO_2

in two major groups, basalt and rhyodacite, with some transitional types including andesitic basalt and rare andesite (Fig. 4.4). The basalts are divided into two rock types based on their TiO_2 concentrations, low- and high-Ti basalt. Low-Ti basalts are typical in the Cao Bang area, showing $SiO_2 = 46.9–50.4$ wt%, $MgO = 3.9–8.27$ wt%, $TiO_2 = 1.08–1.36$ wt% ($TiO_2/P_2O_5 = 8.08–9.07$), low alkalis ($Na_2O + K_2O = 2.74–4.11$ wt%) but high K_2O (0.59–1.38 wt%), may be considered as tholeiitic. Whereas, high-Ti basalts are common in the Lang Son area, showing $TiO_2 = 2.22 – 3.39$ wt%, $TiO_2/P_2O_5 = 4.8–12.3$, relatively low $MgO = 2.62–6.25$ wt%, and low alkalis ($Na_2O + K_2O = 2.62–4.79$ wt%, $K_2O = 0.12–0.74$ wt%. Na_2O/K_2O ratios in the two basalt types are highly variable, from 1.4 to 8.5, where the high ratios are characterized by those in the Lang Son area which were undergone strong albitization. The two basaltic types are characteristically high FeO (FeO*/MgO = 0.7–1.0) and low Al_2O_3 (=12.72–14.76 wt%).

The difference in chemical indexes seen in Fig. 4.5 is again expressed in Harker diagrams of MgO vs. SiO_2, TiO_2, Al_2O_3, Fe_2O_3, CaO, Na_2O, K_2O and P_2O_5 (Fig. 4.5). Note the similarity among the majority of Song Hien, high-Ti Song Da rift, low-Ti Emeishan and Siberian trap basalts in terms of TiO_2, K_2O, Na_2O, P_2O_5, Fe_2O_3, Al_2O_3 concentrations, as well as comparison of other geochemical indexes to the high-Ti basalts in Emeishan and Siberian trap.

Basalts in the Cao Bang and Lang Son areas are characteristically enriched in the rare earths, especially the light ones, where Lang Son basalts are slightly more enriched than the Cao Bang (Table 4.3, Fig. 4.6); however, their $(La/Sm)_N = 1.58–$

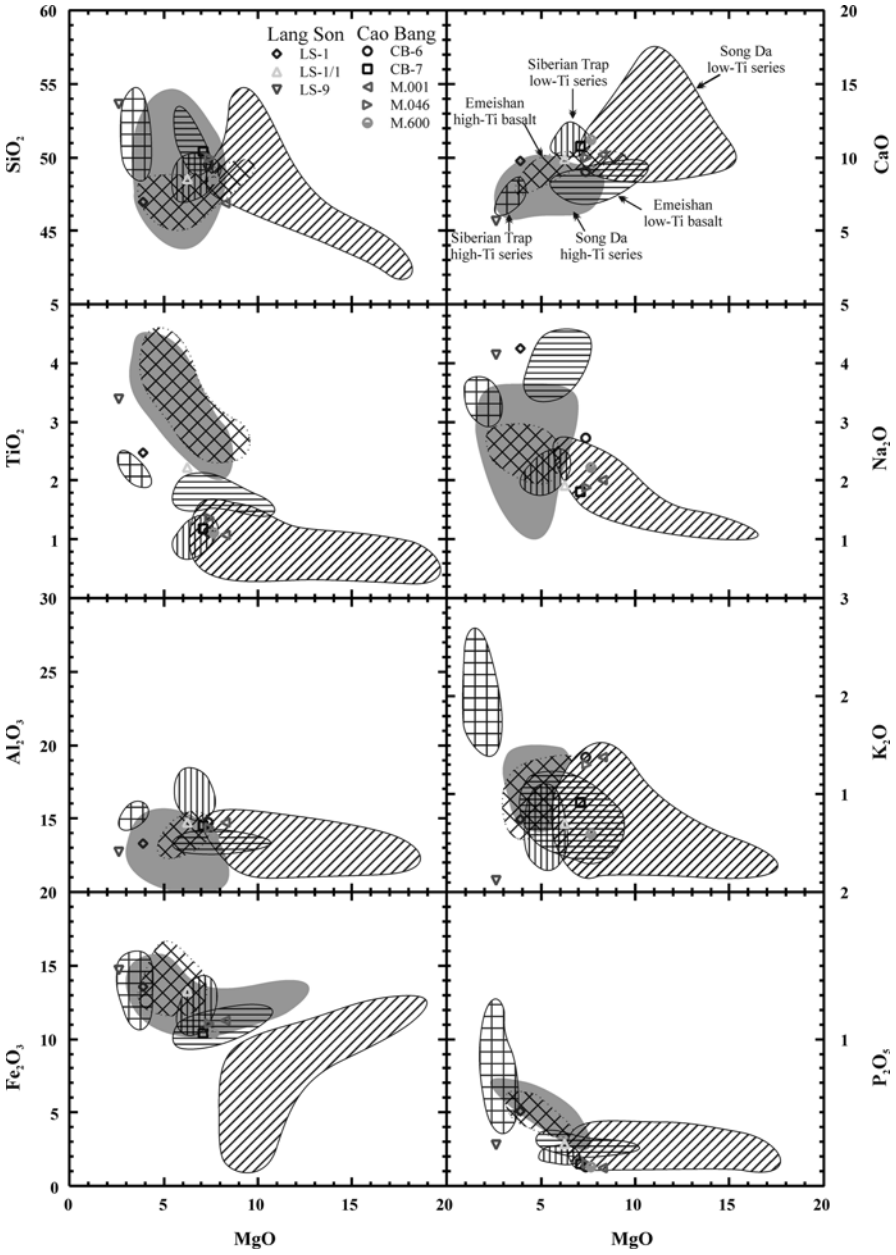

Fig. 4.5 Harker variation diagrams for Song Hien basalt and rhyolite magmas. Emeishan basalts are plotted for comparison (After Chung et al. 1998); Siberian trap basalts provided by P.A. Balykin

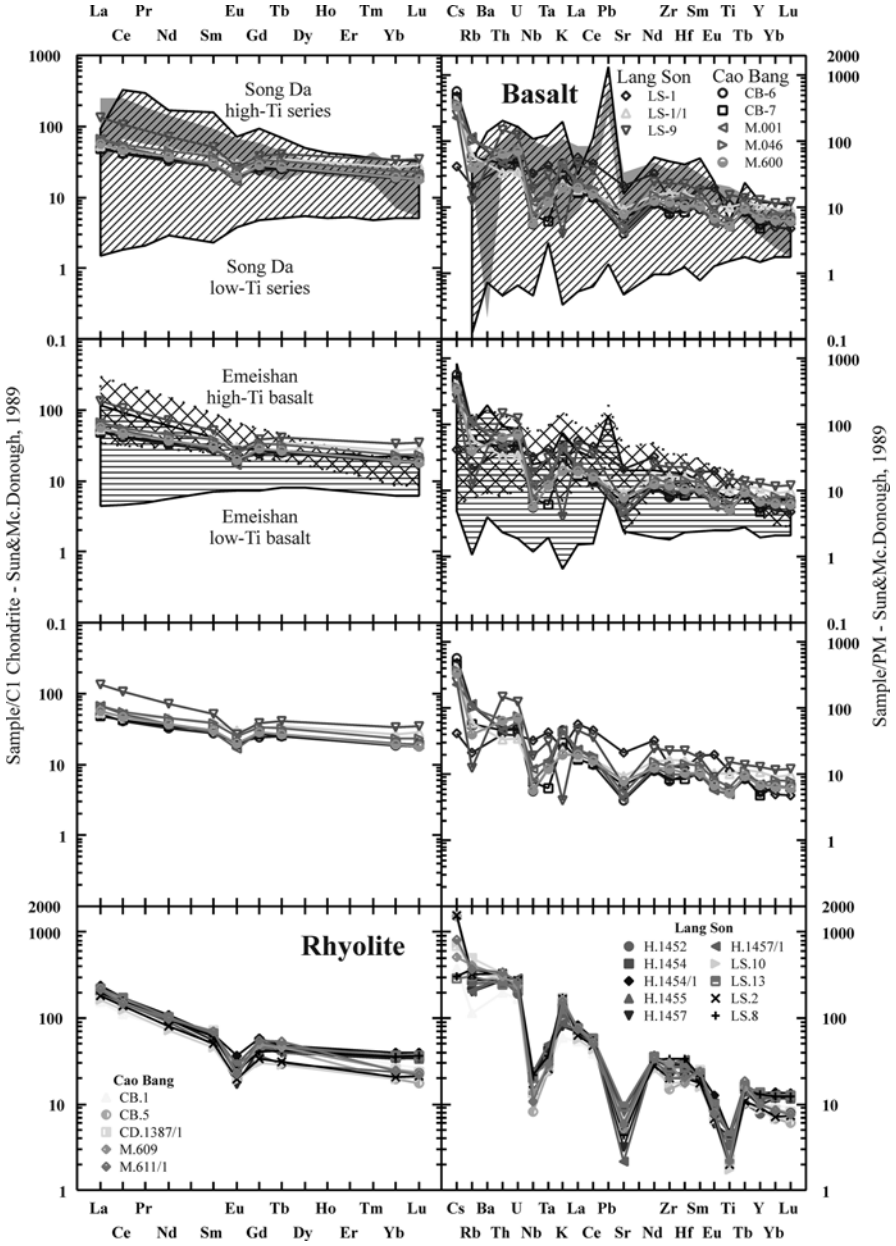

Fig. 4.6 Chondrite (*right*) rare earth element and primitive mantle (*left*) trace element normalized distribution patterns for Song Hien basalt and rhyolite magmas (Data for Emeishan basalt are from Chung et al. (1998); Siberian trap basalts were provided by P.A. Balykin)

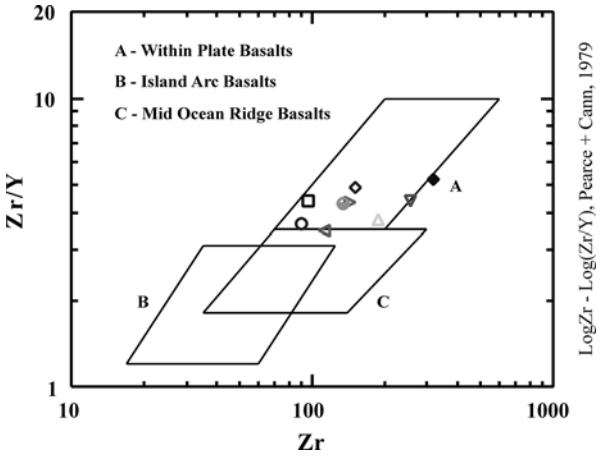

Fig. 4.7 Song Hien basalts in tectonic discrimination diagram of Zr/Y vs. Zr

2.45 and $(Ce/Yb)_N = 1.8–3.12$ are nearly close. They both show characteristically low Eu (Eu/Eu* = 0.6–0.8), indicating strong separation of plagioclase during fractional crystallization or involvement of crustal material during the magma generation. Involvement of crustal rocks in the magmatic melt is indicated by the presence of inherited zircons in Suoi Cun rhyolites showing inconsistent ages of 850–960 Ma. These ages will be discussed later in chapter devoting the origin and formation conditions of lherzolite and their co-existing gabbrodolerite. Crustal involvement may also be expressed by high initial $^{87}Sr/^{86}Sr$ isotopic ratios in Cao Bang basalts (0.70649 after Hoa et al. 1999) and in Lang Son lavas (0.70766–0.71277, after Hoa 2005b). In general, according to the REE distribution characteristics Cao Bang basalts are similar to those of low-Ti Emeishan and low-Ti Siberian trap, while the Lang Son basalts are closely matched with high-Ti Emeishan and Siberian basalts (Fig. 4.7).

Primitive mantle trace element normalized patterns for the basalts show high enrichment of Rb, Th, U, K, La, Ce, Nd, Zr and Hf and depletion of Nb, Ta and Sr, and Ti being more depleted in Cao Bang basalts. The depletion of Nb, Ta and Sr in these basalts is comparable to the low-Ti Song Da rift, Emeishan and Siberian trap basalts. Lang Son basalts are more enriched in Nb, Ta and Zr than the Cao Bang types. Trace element distribution configuration of Lang Son basalt is closely similar to that of high-Ti Song Da, Emeishan and Siberian trap basalts; besides ratios of Zr/Y (3.49–4.41), Th/Ta (5.75–16.0), Nb/La (0.30–0.54) and Nb/Y (0.13–0.27) among the high-Ti basalts are quite similar. Compositional position of the basalt in plots of Zr/Y vs. Zr is in the field of intraplate magmatism (Fig. 4.7).

In general, within the Song Hien basin there are two mafic magmatic fields showing different geochemical properties expressed by various enrichment and depletion of incompatible elements. The depletion in some particular elements indicates relation of the magmas to lithospheric mantle source above a subduction zone. This geochemical character is also observed for other Permian – Triassic magmas in the Song Hien basin.

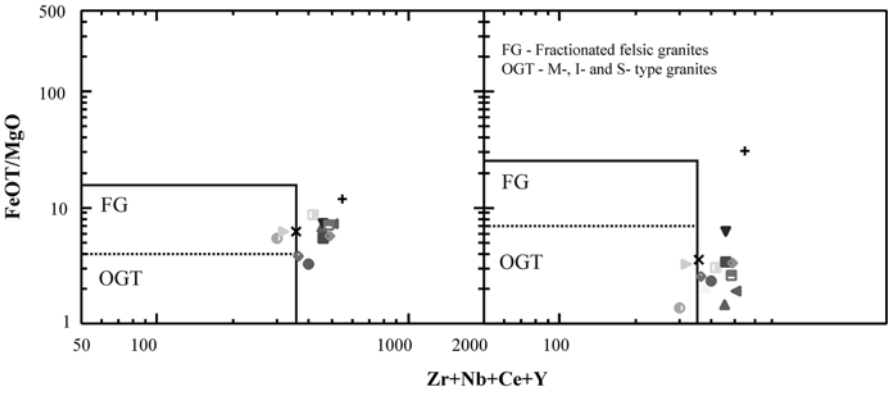

Fig. 4.8 The Cao Bang and Lang Son felsic magmas in plots of Zr + Nb + Ce + Y vs. Fe*/Mg and $(Na_2O + K_2O)/CaO$

Geochemical compositions of the felsic magmas is dacite ($SiO_2 = 62.44–67.38$ wt%) and rhyolite ($SiO_2 = 70.29–74.54$ wt%) (Table 4.3). They show medium- to – low alkalis ($Na_2O + K_2O = 5.21$ wt%), but often have high K_2O (3.06–5.21 wt%). The Na_2O/K_2O ratios vary between 0.3 and 0.5; but the ratios >1 are observed in volcanic tuffs for the presence of large amount of terrigenous sediments and metamorphic rocks. Both Cao Bang and Lang Son dacite and rhyolite magmas are rich in Rb (194–316 ppm), Th (21–28.3 ppm), Zr (196.2–375 ppm), Hf (5.4–10.44 ppm), but relatively poor in Sr (91–200 ppm), Nb (5.9–15.5 ppm) and Ta (1–1.2 ppm), although Nb in the Lang Son dacite and rhyolite is higher than that in the Cao Bang magmas. Ratios of Zr/Y (4.86–7.56), Nb/La (0.13–0.54), Nb/Ta (5.9–10.51), Nb/Y (0.17–0.26) and Th/Ta (14.91–26.94) in the felsic magmas being closely matched with those in the basaltic magmas may indicate source similarity while the geochemical differences may be caused by magmatic differentiation (or fractional crystallization) of the same parental melts. In primitive mantle and mid-ocean ridge granite trace element normalized distribution patterns the dacite and rhyolite show minimal at Nb, Ta, P and Sr while having maximal peaks at Rb, Th, Zr. The magmas also show high rare earth elements. Rare earth elemental geochemistry (Fig. 4.6) and ratios of $(La/Sm)_N = 2.81–3.61$ and $(Ce/Yb)_N = 4.42–7.32$ of the dacite and rhyolite magmas are mostly similar to K-rich calc-alkaline felsic magmas. However, the dacite and rhyolite magmas belong to intraplate magmatic field in plots of Zr + Nb + Ce + Y vs. FeO*/MgO and $(Na_2O + K_2O)/CaO$ (Fig. 4.8). Geochemical characteristics of the felsic magmas show contamination in the parental melts because, on the one hand, the magmas show geochemical features similar to subduction-related calc-alkaline, and features that are typical for intraplate magmas, on the other. Note that, although there are differences in petrology between Lang Son and Cao Bang dacite and rhyolite, they share many comparably geochemical characteristics. High initial $^{87}Sr/^{86}Sr$ ratios in Cao Bang and Lang Son rhyodacites at, respectively, 0.7231 and 0.71547–0.7207, and low Eu*/Eu (0.36–0.51) suggest strong contamination of crustal material in the primitive melts.

4.2 Gabbro-Dolerite and Gabbronorite – Lherzolite Associations

Ultramafic, mafic and porphyric granite intrusive magma associations in the Song Hien structure being compositionally heterogeneous were previously grouped into a single magmatic complex (Thuc and Trung 1995; Polyakov et al. 1996). The felsic magma component has been recently re-examined and reconsidered as a sub-volcanic member within the dacite-rhyolite volcanic association (Hoa et al. 1999); whereas the ultramafic and mafic types have been grouped as, respectively, gabbronorite-lherzolite and gabbro-dolerite (Hoa 2005b). The intrusive bodies form separate blocks, different in petrologic, mineralogical, geochemical and mineralization characteristics. Based on chemical compositions and Ni-Cu-(PGE) mineralization features the first intrusive type is closely similar to picrite-dolerite having Ni-Cu-Pt potential comparable to Li Mahe-, Paijunchun- and Jang Baoshan-type in China (Fang Hue et al. 1985; She Chuan Jing 1986). This intrusive type has been first discovered in the Song Hien structure only in Cao Bang, in the southeastern wing relative to the center of the structure. The second group is spatially related to the andesite- basalt volcanic association that is widely developed along the Cao Bang – Tien Yen fault, running from Meo Vac (Ha Giang province) in the north to Lang Son in the south (Fig. 4.1).

4.2.1 Gabbrodolerite (and Congadiabase)

4.2.1.1 Distribution Characteristics and Structural Geology

Among a number of gabbro-dolerite intrusive bodies in the Song Hien structure the most detailed studies have been conducted by the authors of this monograph including the following blocks Ban Giem, Nguyen Binh, Lung Luong, Ta Sa, Khuoi Piong, Ban Nung, Khau Khoang and Lung Bat in the central area of the structure. According to their petrologic and geochemical compositions the mafic magmas are representing sub-volcanic companions of the basalt-andesite volcanic associations. The mafic sub-volcanic bodies are small-sized and elongate or sometimes symmetric in shape. The mafic bodies penetrate overlying terrigenous sediments; gabbro at upper contact zone shows poor-crystalline which is overall similar to a phenocryst-poor basaltic rock (Photo 4.3). Sometimes the gabbro penetrated Carboniferous limestone, forming garnet-pyroxene-epidote skarns along the contact between the two formations (Photo 4.4). The major petrologic compositions of the mafic magmas include ophitic gabbro, dolerite and quartz-bearing diabase, sometimes granophyre (Ban Nung block) and pegmatite-like gabbro (Nguyen Binh block). Elongate crystals of pyroxene and plagioclase (Photo 4.5) are observed in some Ban Giem and Khau Khoang gabbro. The gabbrodolerite magmas at upper contact zone show texture most similar to that in basalt (Photo 4.5). The most dark-colored type among the gabbro magmas is Cpx-rich fine-grained gabbro.

Photo 4.3 Gabbrodolerite lens body in the Song Hien terrigenous formation. Outcrop in the national road from Cao Bang to Dong Khe

Photo 4.4 Dyke-like skarn body at the contact of gabbrodolerite with C-P limestone. Outcrop H-1528, Ban Giem block

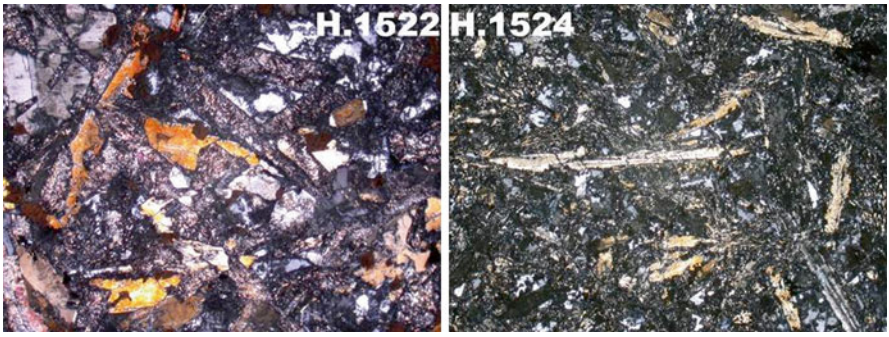

Photo 4.5 Textures of gabbrodolerite (center sample H-1522) and (rim sample H-1524), Ban Giem block

- Ban Giem Block: located about 20 km south of Bao Lac town, outcropped along river Nheo bank on the way from Tinh Tuc to Bao Lac, the magmas in the cross-section are mainly ophitic gabbro with phenocrysts of elongated Cpx and Pl, gabbrodolerite and dolerite (Photo 4.5). The gabbro penetrates Carboniferous-Permian limestone, forming zoned skarnization with garnet at the center and pyroxene (scapolite) at periphery (Photo 4.4). Gabbro at the upper contact zone with the limestone shows fine-grained texture as of aphyric basalt (Photo 4.5). Also in the upper contact layers sometimes found are sulfurized crushed zones. The sulfurized veins are sometimes observed in the surrounding marbleized limestone.
- Nguyen Binh Block: located near Nguyen Binh town outcrops about 3 km^2. Major petrologic compositions are ophitic gabbrodolerite, monzodiorite and congadiabase, sometimes pegmatite-like gabbro. Some outcrops to northeast of Nguyen Binh there are quartzized zones having gold-bearing sulfide mineralization (Nguyen Binh gold mine).
- Ta Sa Block: is outcropped about 0.5 km^2 in the Minh Thanh village area, Nguyen Binh district, next to Ta Sa bridge crossing the Nguyen Binh river on national route 32, and is symmetrically shaped (Hoa 1995). The surrounding rocks are tuff-lavas; lavas are basaltic, andesite- basaltic and andesitic, having chemical composition, textural and structural features similar to basic volcanic rocks in southeastern Cao Bang. The rock compositions are heterogeneous, including fine-grained ophitic gabbrodolerite and congadiabased. Congadiabased and granophyre are outcropped in southern block, showing compositions varying from diorite to granophyre. Occurring in western Ta Sa block and having a volume of about 10 % of total volume, the congadiabase and granophyre show transitionally compositional relationship, e.g., from gabbrodolerite to congadiabase and granophyre, which is also expressed by rock textural characteristics. There are a number of quartzitized, chloritized, actinolitized accompanied by Au-bearing listvenite-type sulfurized veins in Ta Sa gabbro outcrop. There are at least two Au-bearing sulfate ore spots in quartzized zones at roof-top of Ta Sa

block, having concentrations of native gold from 0.8 g to 1.4 g/ton. Above the native sulfate ore zone there are Au-bearing helmet-shaped limonite formations having concentration up to 3.2–3.7 g/ton (Hoa 1995).

- Khuoi Pong Block: located in Ha Tri village, Hoa An district, about 10 km northeast of Cao Bang town, the block obtains an elongated lens shaped, running in the northwest – southeast direction coincided with deposition trend of the surrounding volcanic – sediment rocks. The block is about 4 km long, 0.4 km wide and occupied about 1.5–2 km^2. Surrounding rocks are most shale, rhyodacitic, rhyolitic tuff and some small amount of tuff-like rock. There not much alteration is observed at contacts with the intrusive magmas. The major petrologic compositions are ophitic gabbrodolerite and fine-grained dolerite. The magmas show transitional relationship. A relatively continuous outcrop cross-section is found from Na Lai toward Na My. There is an outcrop of garnet – pyroxene skarn, possibly represented metasomatic products between Khuoi Pong gabbrodolerite and surrounding carbonate to the south of Khuoi Pong block. Hydrothermal alteration zones followed by quartzization are found in northwestern block.
- Khau Khoang Block: is outcropped mainly along National route 4 in the Khau Khoang pass area along upper Ban Lung stream, about 16–18 km from Cao Bang. The full outcrop is not yet known but it is estimated about 2 km^2. The petrologic composition of the magmas, as observed along an auto route, is simple, containing only gabbrodolerite and fine-to-medium-grained dolerite, some showing ophitic texture. Fine-grained, dark-colored gabbrodolerite-type varieties (with MgO being up to 10 wt%) are exposed in southern foot of Khau Khoang Pass. Basalt with doleritic texture and pillow-lava structure (?) are found about 300 meters from the Khau Khoang block. Aside the major block outcropped along the Khau Khoang pass small-sized intrusive bodies are also observed penetrated conformably sand and siltstone layers of Song Hien formation (?) (Photo 4.3).
- Lung Bat Block: the gabbroic magmas are described mainly along a cross-section from Lung Bat (near National route 4) toward Trong Con. The outcrop is about 200 m long. The block is comprised by gabbrodolerite and dolerite having petrologic and textural features vastly similar the Khau Khoang gabbroids.
- Ban Lung Block: Mafic intrusive such as dolerite and congadiabase of Cao Bang complex are found only at separate outcrops in the form of inclusions in granite-granophyres to the east of Ban Lung block. Distribution relations among the granite-granophyres and congadiabase-diabase may be observed at Boong Quang stream branches as well as in iron- ore exploration drill cores in Ban Lung block. These granite-granophyres are petrologically, mineralogically and geochemically similar to the rhyolite and rhyodacite as described above. Ban Lung granophyres show petrologic, mineralogical and geochemical characteristics equivalent to gabbrodiorite and diorite (granodiorite); therefore, basically Ban Lung block may be viewed as a rhyolite – rhyodacite sub-volcanic accompanying formation.

4.2.1.2 Petrologic and Mineralogical Characteristics

Gabbrodolerites are fine-grained some porphyritic with phenocrysts of plagioclase and/or pyroxene. The groundmass is doleritic containing volcanic glass and almonds filled with chlorite and epidote. Mineral composition of the gabbrodolerite is relatively stable with plagioclase (55–60 %), pyroxene (30–35 %) and ore minerals such as ilmenite, magnetite and (rare) sulfur. Amphibole is commonly present and a minor amount of biotite, developed in association with pyroxene. Pyroxene-rich (60–65 %) magmas are found in the Khau Khoang Pass area. Rock textures are poikilitic and doleritic with elongated pyroxene and plagioclase crystals. The dolerite is slightly different from gabbro in that their textural grain sizes are finer, closely comparable with accompanying sub-volcanic dolerite. The congadiabase contains some amount of quartz (up to 7–10 %). The granophyre shows chemical composition varying between diorite and granodiorite and having characterized granophyric texture. Plagioclase in the gabbrodolerite and dolerite is matched with labrador ($An_{64.70–66.5}Ab_{32–35.2}Or_{0.2–9.5}$) (Table 4.4). The pyroxene is high-Mg and -Ca augite ($Wo_{35.7–38.7}En_{47.5–52.1}Fs_{12.2–15.7}$), low Al_2O_3 (1.81–2.75 wt%), high TiO_2 (0.44–0.68 wt%) but rather low chrome (Cr_2O_3 = 0.17–0.63 wt%) (Table 4.4; Fig. 4.9) as compared with pyroxene in accompanying basalt.

4.2.1.3 Petrology and Geochemistry

Geochemically the sub-volcanic gabbrodolerite and dolerite are similar to basaltoids (Table 4.5). They are low in TiO_2 (0.5–1.45 wt%), very low P_2O_5 (0.03–0.2 wt), and high TiO_2/P_2O_5 = 15.6–26. The MgO contents are highly variable from 4.85

Table 4.4 Chemical compositions (wt%) of clinopyroxene and plagioclase in Cao Bang gabbro magmas. The data were analyzed by EPMA (Hoa et al. 1999)

Sample	SiO_2	TiO_2	Al_2O_3	Cr_2O_3	FeO	MnO	MgO	CaO	Na_2O	K_2O	Total
M- 046	55.23	0.06	25.59	0	1.76	0.03	0.86	9.41	5.6	0.54	99.06
Ophitic gabbro in Khuoi Luong Block											
M221-1	52.18	0.44	1.97	0.41	7.35	0.22	18.17	17.3	0.22	0.02	98.28
M222-2	51.98	0.56	2.75	0.63	6.38	0.2	17.06	19.08	0.26	0	98.9
M223-3	51.62	0.59	2.34	0.43	6.76	0.22	16.9	19.56	0.22	0.01	98.65
Ophitic gabbro in Lung Bat Block											
CD-204/1-1	51.38	0.46	1.81	0.01	9.33	0.26	15.67	18.34	0.32	0.02	97.6
CD-204/1-2	51.71	0.68	2.46	0.17	8.24	0.18	16.37	18.56	0.17	0.01	98.55
M-046	50.01	1.11	3.53	0.22	9.23	0.19	15.43	18.17	0.2	0.01	98.1
M-201	52.5	0.53	2.26	0.7	7.51	0.2	17.87	17.43	0.2	0.02	99.22
M-046	55.23	0.06	25.59	0	1.76	0.03	0.86	9.41	5.6	0.54	99.08
B-5142	50.02		30.49		0.11			13.25	3.98	0.03	97.88
B-5146	51.21		31.01		0.07			13.58	3.72	0.1	99.69
B-5158	51.73		29.18		0.94			13.48	3.58	0.26	99.17

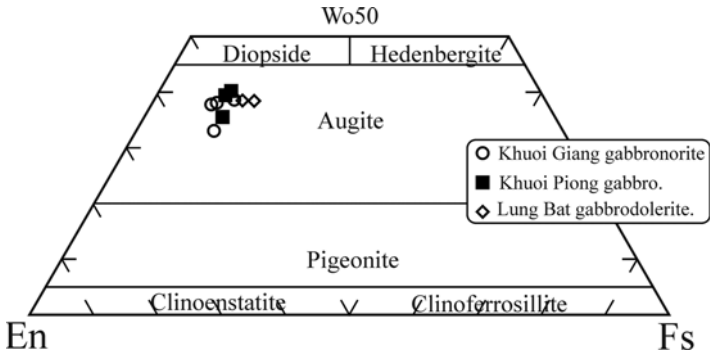

Fig. 4.9 Wo-En-Fs chemical compositions of clinopyroxene from gabbrodolerites

to 8.6 wt%, dark gabbrodolerite in the Khau Khoang Pass area in particular shows MgO at 10.35 wt%. Their alkalis vary from low to medium ($Na_2O + K_2O$ =1.83–2.91 wt%), where K_2O varies from low to medium and mostly lower than Na_2O contents (Na_2O/K_2O =3.9–24.8, average 14.7). In AFM (total alkalis – FeO* – MgO) correlation diagram the gabbro and dolerite fall in tholeiitic field (Fig. 4.10), while in plots of SiO_2 vs. K_2O they fall in mafic calc-alkaline field, two congadiabase samples from Ban Giem block (H-1523-1524) have K_2O contents comparable to high-K calc-alkaline or sub-alkaline type (Fig. 4.11).

The Cu, Ni, Co and Cr in gabbrodolerite and dolerite are generally low, respectively, at 13–72 ppm, 23–273 ppm, 35–63 ppm, and 68–105 ppm (some reaching 911–988 ppm), much lower than those in gabbroids, differentiated products from Khuoi Giang (or Suoi Cun) ultramafic magmas (Table 4.5). Ratios of Ni/(Ni + Cu) vary between 0.46 and 0.76, and Ni/Co between 0.6 and 1.3 (sometimes 3–24.3) in gabbrodolerite much too low compared with those in Khuoi Giang gabbronorite showing 0.83 and 7, respectively. These geochemical features indicate that subvolcanic mafic magmas in gabbrodolerite – congadiabase associations are different from mafic magmas in peridotite – gabbro associations (Suoi Cun or Khuoi Giang type) that have Cu-Ni mineralization potential (Hoa et al. 1999). The V contents in gabbrodolerite and dolerite are relatively high from 138 to 352 ppm, most similar to those in picrite – dolerite associations. In general, the Ni and Cu concentrations in major mafic magmas in the 'Cao Bang magmatic complex' are mostly comparable with those in the Cao Bang basalts, suggesting their genetic relationship.

The gabbrodolerite and dolerite are relatively rich in Rb (16–70 ppm, average at 25 ppm), Th (2.1–10 ppm), Ce (5.8–53 ppm) and Zr (14.8–282 ppm, average at 92 ppm) (Table 4.5) compared with those in depleted mantle-derived mafic magmas. The Zr/Nb ratios varying between 17 and 32, and Zr/Y ratios changing from 1.76 to 4.39 are closely similar to corresponding values of Cao Bang basalts. However, plots of Nb vs. Zr (Fig. 4.12) show that Khuoi Pong, Ban Giem and Nguyen Binh gabbroids have higher Nb and Zr compared with Lung Bat, Khau Khoang and Lung Phai gabbroids.

Table 4.5 Chemical compositions (wt%) and trace element abundances of Cao Bang gabbrodolerites (Hoa et al. 2005)

Sample	H1522	H1523	H1524	P508	P512	T02-14	M226
	1	2	3	4	5	6	7
SiO_2	51.99		51.52	49.61	47.14	53.22	53.26
TiO_2	1.928		1.677	0.807	0.480	1.551	1.95
Al_2O_3	13.10		13.53	14.63	13.05	14.28	13.43
Fe_2O_3	13.59		12.90	7.17	10.44	12.04	11.93
MnO	0.216		0.216	0.123	0.164	0.193	0.18
MgO	4.65		5.10	8.33	12.83	4.62	4.22
CaO	8.77		9.24	12.42	10.26	7.18	8.44
Na_2O	2.03		1.47	2.21	0.98	2.47	2.60
K_2O	0.91		1.14	1.27	0.52	1.89	0.64
P_2O_5	0.270		0.242	0.115	0.061	0.219	0.26
L.O.I	3.07		2.82	3.00	3.00	2.40	2.58
Total	100.52		99.86	99.69	98.93	100.06	99.46
V	344	352	348	232	138	346	238.00
Cr	86	68	127	911	988	105	75.00
Co	39	38	41	35	63	36	41.00
Ni	40	26	53	117	273	23	51.00
Cu	42	30	35	13	32	48	72.00
Rb	40	38	49	57	16	70	26.80
Sr	304	260	200	109	69	122	197.00
Y	55	48	46	22	15.1	44	54.00
Zr	218	282	192	67	14.8	167	227.00
Nb	11.4	10.0	9.4	4.3	2.8	8.8	9.40
Ba	145	221	172	161	66	300	
La	21	17.8	18.8	5.6	4.6	20	26.00
Ce	43	37	40	12.3	9.8	40	53.00
Pr	6.2	5.3	5.6	1.9	1.4	5.8	
Nd	24	21	21	7.7	5.9	22	30.00
Sm	5.3	4.8	4.7	2.0	1.4	5.0	8.00
Eu	1.4	1.2	1.2	0.53	0.42	1.3	1.84
Gd	5.9	5.4	5.0	2.2	1.6	5.4	9.80
Tb	1.2	1.1	1.1	0.51	0.30	1.0	1.70
Dy	7.6	6.6	6.7	3.1	2.1	6.8	
Ho	1.6	1.3	1.4	0.67	0.48	1.4	
Er	4.6	3.9	4.0	1.9	1.3	3.8	
Yb	4.3	4.1	4.0	1.9	1.3	3.9	5.10
Lu	0.60	0.59	0.51	0.28	0.18	0.58	0.75
Hf	1.6	1.9	1.2	0.53	0.15	1.3	4.80
Ta	0.61	0.60	0.48	0.19	0.10	0.39	0.90
Th	9.4	9.3	5.1	3.2	2.1	8.8	10.00
U	1.8	1.4	1.8	0.67	0.42	1.7	2.30

Remarks: 1–3: Ban Giem Block; 4–6: Nguyen Binh Block, 7: Khuoi Luong Block

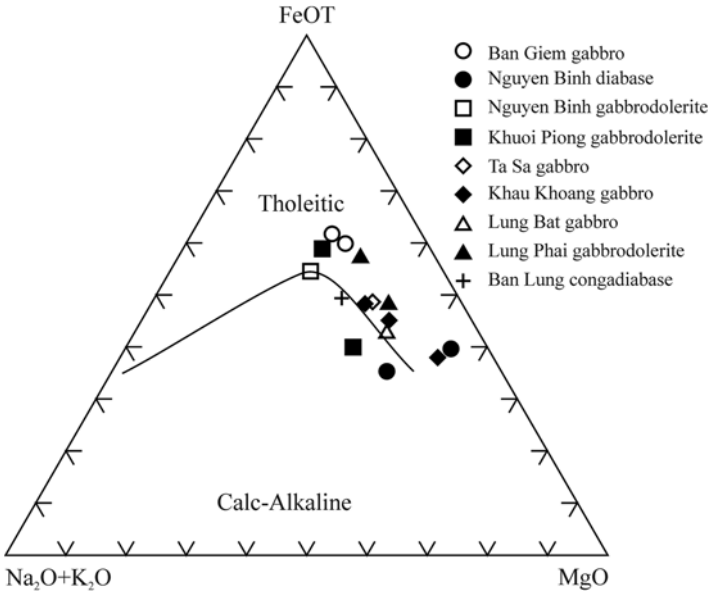

Fig. 4.10 Compositions of gabbrodolerite in AFM diagram

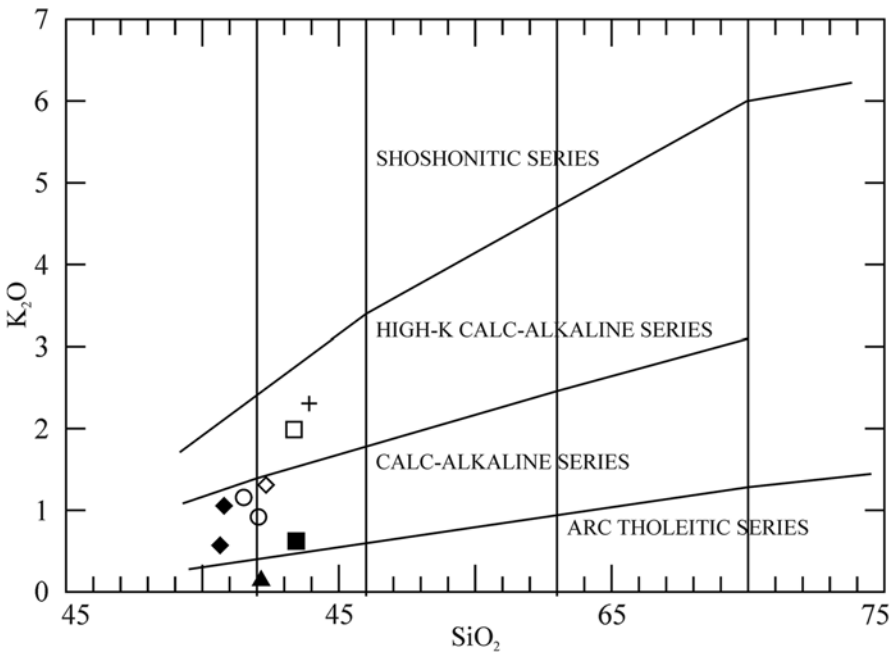

Fig. 4.11 Chemical compositions of Cao Bang gabbrodolerite in plots of SiO_2 vs. K_2O

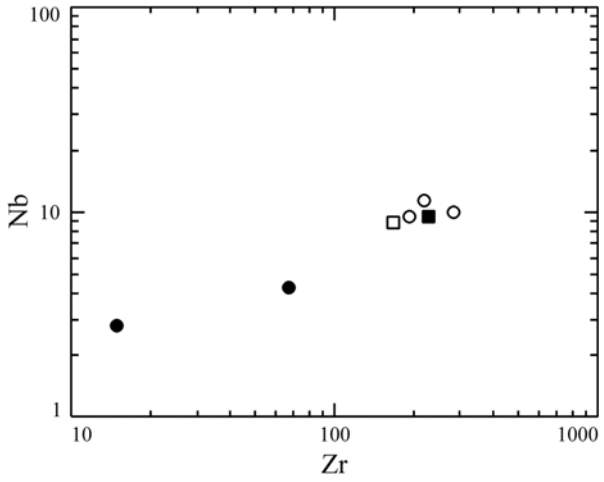

Fig. 4.12 Chemical compositions of Cao Bang gabbrodolerite in Nb and Zr correlation diagram

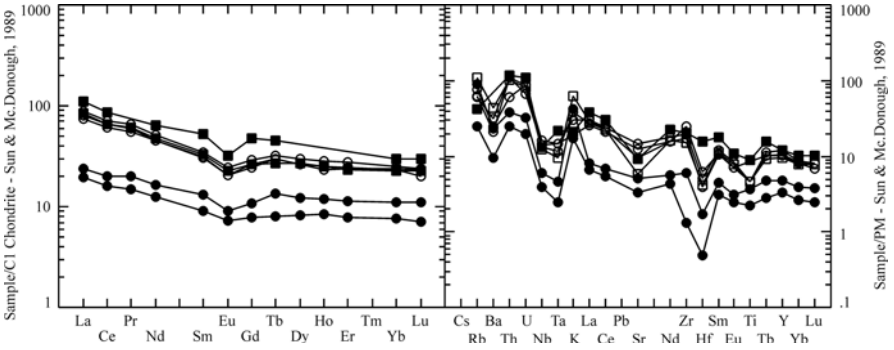

Fig. 4.13 Chondrite rare earth element normalized and primitive mantle trace element normalization patterns for Cao Bang gabbrodolerite

The gabbrodolerite is enriched in the rare earths, especially the light elements; however, they show strong depletion at Eu as seen in chondrite normalized distribution configuration (Fig. 4.13). The light rare earths are 30–70 times higher as compared with a chondrite reference. Note that the ratios of La/Sm (3.25), Th/U (4.35) and Ce/Yb (10.39) in gabbroids are essentially similar to those of the basalts. Also note that some Nguyen Binh dolerites show rare earth element concentrations that are much different from Khuoi Pong gabbrodolerite and Ban Giem gabbro and even from some other Nguyen Binh dolerites which are more depleted (Fig. 4.13). The above inconsistency will need further investigation to clarify.

Primitive mantle trace element normalized distribution configuration patterns for the gabbrodolerite and congadiabase are shown in Fig. 4.13. The configuration is

closely similar to that observed for basalts showing strong depletion at Nb, Ti and Hf.

Note that, the gabbrodolerite and dolerite are characteristically enriched in K, Rb, Th, Ce, and Sm, and that their distribution patterns of Nb, Ta, Zr, Ti and Yb are rather similar to mafic calc-alkaline magmas. The geochemical difference between two magmatic types is the depletion magnitude of Nb, Ta and Ti that is not clear and stable as of the calc-alkaline magmatic series (Fig. 4.13).

Chemical composition of a representative Ban Lung congadiabase (M-53/4) shows $Fe_2O_3 = 10.46$ wt%), MgO = 5.97 wt%, $Na_2O = 1.51$ wt% and $K_2O = 2.2$ wt%. The sample is low in Cu = 10 ppm, Ni = 4 ppm, Co = 9 ppm, Cr = 18 ppm and Nb = 5.8 ppm, much lower than in gabbrodolerite and dolerite, but higher in Zr = 155 ppm, Sr = 123 ppm compared with the latter. Ratios of Zr/Nb and Zr/Y (at 26.72 and 3.54, respectively) in the congadiabase are highly comparable to the above mentioned gabbroids.

In summary, the above petrologic and geochemical indexes of Cao Bang gabbro and dolerite being similar to those of the basalts and their closely spatial relation suggest their commonly genetic relationship.

4.2.2 Gabbronorite – Lherzolite Intrusions

4.2.2.1 Geological Characteristics and Occurrence Ages

Ultramafic – mafic intrusions occur in the central area (Cao Bang) of Song Hien belt as small blocks at Suoi Cun, Khuoi Giang, Khau Mia, Khac Thieu and Bo Ninh; however, detailed studies have been conducted on Suoi Cun and Khuoi Giang ultramafic – mafic magmas (Polyakov et al. 1996; Hoa et al. 1999). Petrologic compositions among these blocks are almost similar, including mainly Pl-peridotite, lherzolite, and small amount of marginal –type picritoid, picrite-dolerite, olivine gabbro, gabbronorite, and gabbrodolerite similar to the above described. Veins of gabbronorite are often found within lherzolite outcrop (Photo 4.6). Among lherzolite and gabbronorite dykes in the Suoi Cun area dense sulfur mineralization was observed elsewhere. Lherzolite outcropped along a newly built road to the north of Suoi Cun contains sulfur-rich zones with drop-shaped sulfur cumulates (Photo 4.7). Multiple hydrothermal mineralization activities forming listvenite zones are often observed in strongly crushed zones. Porphyritic mafic magmas with olivine and pyroxene phenocrysts and glassy groundmass are outcropped in the southeast of Suoi Cun block; the rock texture is closely similar to a volcanic picrite (Photo 4.8). Picrite samples having almond-shaped structure have been collected in the area. This picrite may volcanic accompanier of the Suoi Cun ultramafic intrusive magmas. Lherzolite in the east and southeast of the Khuoi Giang block has tectonic contact with surrounding shale and sand-siltstone, representing lowest layers of Song Hien formation (T_1 *sh*); while in the north and northwest side the lherzolite is overlain by sandstone – tuff-like and rhyolite of 248 ± 4.5 Ma. A drill conducted

Photo 4.6 Cu-Ni sulde-bearing gabbronorite dyke in the lherzolite, Suoi Cun massif. Outcrop H-1506

Photo 4.7 Suoi Cun Lherzolite with drop-shaped sulphide cumulate

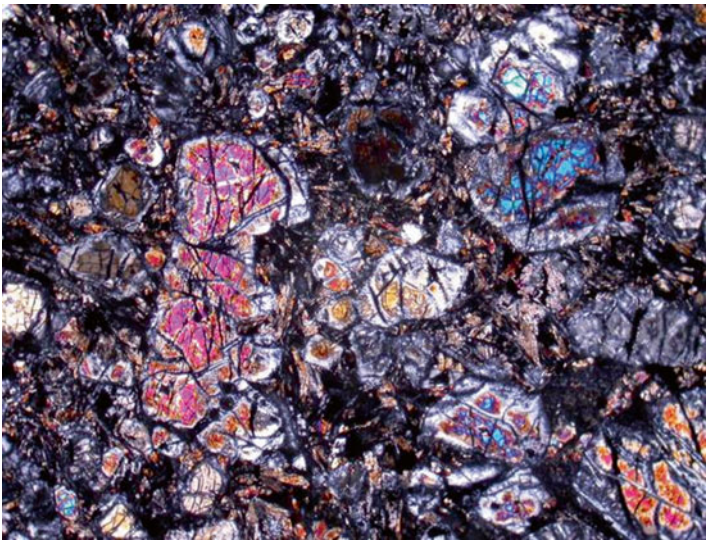

Photo 4.8 Porphyric texture picrite in southeast of Suoi Cun massif. Sample M-009. Nicol (+), 40x

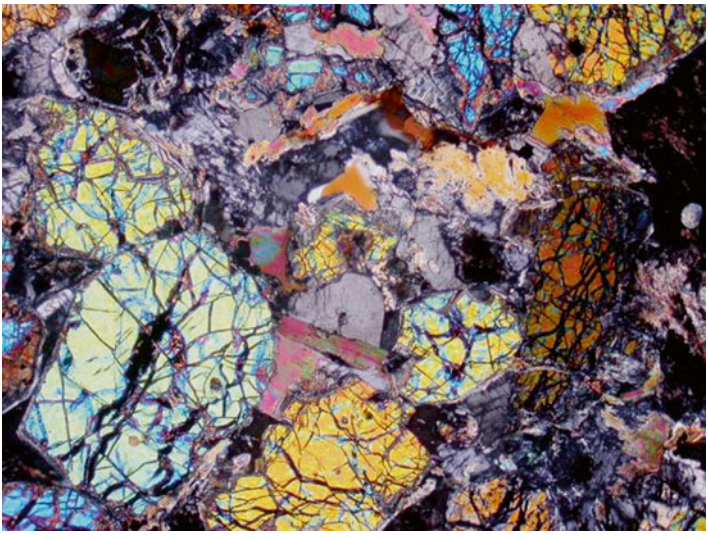

Photo 4.9 Lherzolite with phlogopite in Suoi Cun massif. Sample SC-2A, niclo (+), 40x

within the lherzolite outcrop in the Dong Chang area (Khuoi Giang block) showed some sulfur-rich lherzolite (Ramdin 1960). Phlogopite is often observed in the lherzolite (Photo 4.9).

Age dating for Suoi Cun lherzolite and gabbrodolerite was attempted on zircon U/Pb method using SHRIMP.

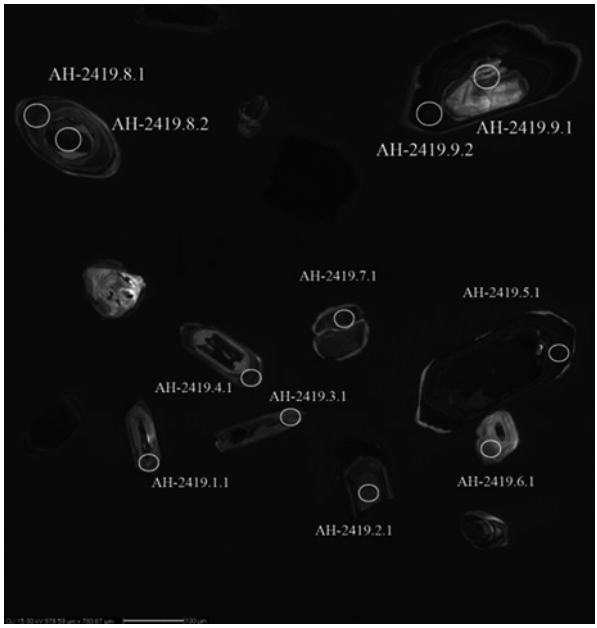

Photo 4.10 Back-scattered images of zircons in Suoi Cun lherzolite; sample H-2419 analyzed points are given in Table 4.6

Pl-lherzolite (sample AH-2419) is med-grained having cumulated idiomorphic olivine, clinopyroxene and orthopyroxene. Co-existing mineral assemblage intercalated with above cumulates includes zone-free basic plagioclase and phlogopite. Dense, diffused sulfur was also observed. Chemical composition of the lherzolite is as follows (in wt%): $SiO_2 = 40.71$; $TiO_2 = 0.50$, $Al_2O_3 = 6.29$, $Fe_2O_3 = 14.42$, $MnO = 0.17$; $MgO = 25.43$, $CaO = 6.67$, $Na_2O = 0.39$, $K_2O = 0.40$, $P_2O_5 = 0.074$.

There are three zircon groups: zircon showing eroded, zoned- crystal (Photo 4.10).

Analytical points at zircons' zone-free cores yielded a concordia for age of 2.9 Ga (Fig. 4.14) while those in zoned cores showed a concordia for age of 1.6 Ga. Unsorted (ungraded) zone-free zircons showed a concordant age about 1 Ga. There are thin, newly formed, marginal layers sur-rounding zircon cores. In summary, the majority of zircons yielded early Paleozoic ages between 480 and 460 Ma (Fig. 4.14).

Among the analyzed crystals there were eroded as well as fragmental grains which yielded rather high U/Th at 0.22 (484 Ma, Table 4.6). Zone-free or weakly zoned zircon rims showed U/Th as low as 0.07 (469 Ma). Although the zircon grains may have different and/or multiple origins but the majority showed concordant values corresponding to internal activities during the Ordovician as recorded in the Song Chay uplift massif (Ponomareva et al. 1997; Maluski et al. 2001). There are several zoned zircons showing a Permian age, e.g. 262 Ma (Fig. 4.14). This value may be viewed as lower age limit of the Suoi Cun ultramafic block. Moreover, the wide presence of zircon xenocrysts having various ages indicates strong contamination of crustal materials.

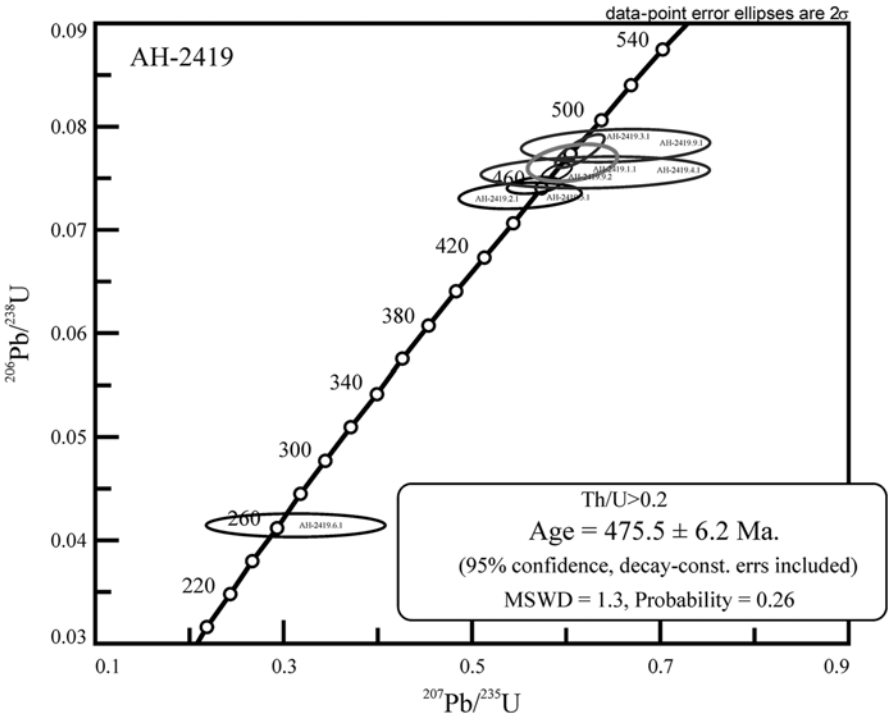

Fig. 4.14 Concordia diagram of Suoi Cun lherzolite zircons. Remnant zircons yielded 475 ± 6.2 Ma while magmatic crystals showed 262 ± 2.7 Ma

The gabbrodolerite is fine-grained, with plagioclase, orthopyroxene and clinopyroxene are major mineral phases. There are three zircon types being recognized in a gabbrodolerite sample (AH 2418). The first group includes tree-branch shaped crystals with zone-free cores and being surrounded by zoned zircons (point 2.3.1: 2200 Ma) and fragmental zone zircons (2.8.1: 938 Ma). The second group, similar to zircons in lherzolite, includes melted short-cubic crystals with both zone-free and clearly zoned cores. Rims contain thin having strong illumination. Concordant ages acquired from these zircons showed Paleozoic (Table 4.6). The third group includes small-sized, elongated cubic, clearly zone crystals (Photo 4.11).

Concordant values calculated on 3 zircon grains (1.1, 2.1, 6.1) are Permian (266 ± 3.7 Ma, Fig. 4.15). This age may be considered as crystallizing time of the Suoi Cun gabbrodolerite (Table 4.7). Therefore, similar to the lherzolite, crustal contamination can be firmly demonstrated. Amount of truly magmatic zircons in gabbrodolerite are higher than in plagioclase-peridotite indicating that the zircons were crystallized from less differentiated basic melts. Crystalline ages of the dolerite and lherzolite are quite close showing values most corresponding to Emeishan formation age, e.g. 260 Ma (Lo et al. 2002; Saunders et al. 1997).

Table 4.6 U-Pb compositions of Suoi Cun lherzolite zircons (Data were acquired in Saint Petersburg, Russia)

Point	% $^{206}Pb_c$	ppm U	ppm Th	$^{232}Th/^{238}U$	ppm $^{206}Pb^*$	(1) $^{206}Pb/^{238}U$ Age		(1) $^{207}Pb/^{206}Pb$ Age		% Discordant	Total $^{238}U/^{206}Pb$	±%
AH-2419.1.1	0.19	594	297	0.52	38.8	471.2	±2.6	459	±65	−3	13.162	0.56
AH-2419.2.1	0.91	489	57	0.12	31.1	455.9	±3	387	±110	−15	13.519	0.61
AH-2419.3.1	0.00	755	147	0.20	50.3	481	±3.9	510	±31	6	12.91	0.85
AH-2419.4.1	3.68	568	93	0.17	38.3	469.4	±3.6	619	±170	32	12.746	0.58
AH-2419.5.1	0.37	1580	63	0.04	101	462.1	±1.9	416	±45	−10	13.405	0.4
AH-2419.6.1	1.58	405	143	0.36	14.7	262.3	±2.7	323	±290	23	23.7	0.83
AH-2419.7.1	–	334	21	0.07	49.7	1031.8	±6.6	1017	±42	−1	5.772	0.69
AH-2419.8.1	–	495	7	0.01	121	1615.1	±7.7	1502	±21	−7	3.518	0.53
AH-2419.8.2	–	795	942	1.22	389	2908.7	±9.9	2706	±6.8	−7	1.7543	0.42
AH-2419.9.1	0.72	360	107	0.31	24.4	484.9	±3.7	611	±130	26	12.706	0.71
AH-2419.9.2	0.02	1946	93	0.05	126	469.7	±2	469	±21	0	13.229	0.44

Point	Total $^{207}Pb/^{206}Pb$	±%	(1) $^{238}U/^{206}Pb^*$	±%	(1) $^{207}Pb^*/^{206}Pb^*$	±%	(1) $^{207}Pb^*/^{235}U$	±%	(1) $^{206}Pb^*/^{238}U$	±%	Err. corr
AH-2419.1.1	0.05773	1.5	13.188	0.58	0.0562	2.9	0.587	3	0.07583	0.58	.195
AH-2419.2.1	0.0618	1.7	13.644	0.68	0.0544	4.7	0.55	4.8	0.07328	0.68	.142
AH-2419.3.1	0.0575	1.4	12.91	0.85	0.05747	1.4	0.6139	1.6	0.07747	0.85	.522
AH-2419.4.1	0.0901	2.1	13.23	0.79	0.0605	7.8	0.629	7.9	0.07553	0.79	.101
AH-2419.5.1	0.05807	1.4	13.454	0.42	0.0551	2	0.565	2	0.07432	0.42	.204
AH-2419.6.1	0.0655	6.5	24.08	1	0.0529	13	0.303	13	0.04153	1	.082
AH-2419.7.1	0.0717	1.7	5.762	0.7	0.0731	2.1	1.749	2.2	0.1736	0.7	.316
AH-2419.8.1	0.09247	0.92	3.513	0.54	0.0937	1.1	3.679	1.2	0.2847	0.54	.432
AH-2419.8.2	0.18564	0.41	1.7539	0.42	0.18588	0.41	14.614	0.59	0.5702	0.42	.717
AH-2419.9.1	0.066	3.7	12.8	0.79	0.0602	6.2	0.649	6.3	0.07813	0.79	.126
AH-2419.9.2	0.0566	0.91	13.232	0.44	0.05642	0.97	0.5879	1.1	0.07558	0.44	.417

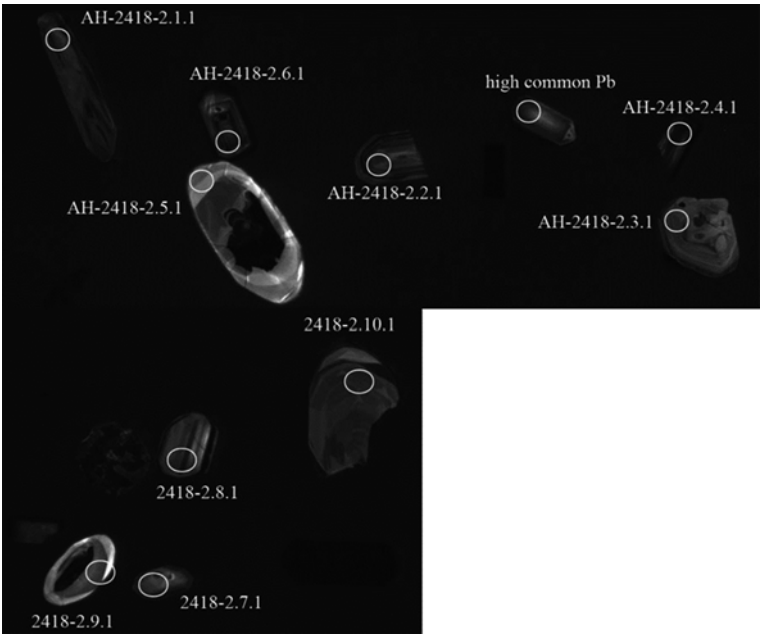

Photo 4.11 Back scattered images of zircons in Suoi Cun gabbrodolerite. Sample H-2418-2, data of analyzed points is given in Table 4.7

4.2.2.2 Mineralogical and Geochemical and Isotopic Characteristics

Chemical compositions of major rock-forming minerals are given in Tables 4.8, 4.9 and 4.10. Major characteristically mineralogical properties in lherzolite and picrite can be summarized as follows: olivine is chrysolite (F_{Ol} = 0.15–0.29) having high Ni (NiO = 0.14–0.24 wt%), CaO = 0.11–0. 27 wt%; clinopyroxene is between augite and diopside ($En_{41.6–54.1}Wo_{34.7–45.2}Fs_{7.8–13.2}$) having low aluminum ($Al_2O_3$ = 1.76–2.89 wt%), low Ti and high Cr (TiO_2 up to 0.89 wt%; Cr_2O_3 between 0.57 and 1.13 wt%) much lower in sodium (Na_2O (0.17–0.32 wt%); orthopyroxene is low-Al type (Al_2O_3 = 1.02–1.75 wt%), low titanium (TiO_2 = 0.36–0.57 wt%), and high chromium (Cr_2O_3 = 0.34–0.57 wt%), showing compositions varying between bronzite and enstatite ($Wo_{3.9–4.5}En_{75.3–81.4}$ $Fs_{14.3–20.8}$) (Fig. 4.16). Pyroxene crystallizing temperatures were calculated after Wood and Banno (1973), Wells (1967), Lindsley (1983) showed 1200 °C for Pl-lherzolite to 900 °C for dolerite. Augite in basalt showed relatively high crystallization temperatures, between 1120 °C and 1200 °C.

Phlogopite in lherzolite is brownish red and high Mg (f_{Bi} = 29–32 %), while that in gabbronorite and dolerite are more enriched in iron (f_{Bi} = 40–45 %), chromium (Cr_2O_3 = 0.3 wt%) and titanium (TiO_2 = 8 wt%) (Oktyabrski et al. 1986).

Common ore minerals found in the lherzolite and picrite are Cr-spinel, pyrotine, pentlandite, chalcopyrite, arsenopyrite, troilite and cubanite. Cr-spinel is normally idiomorphic having compositions between Al-chromite to chrome-

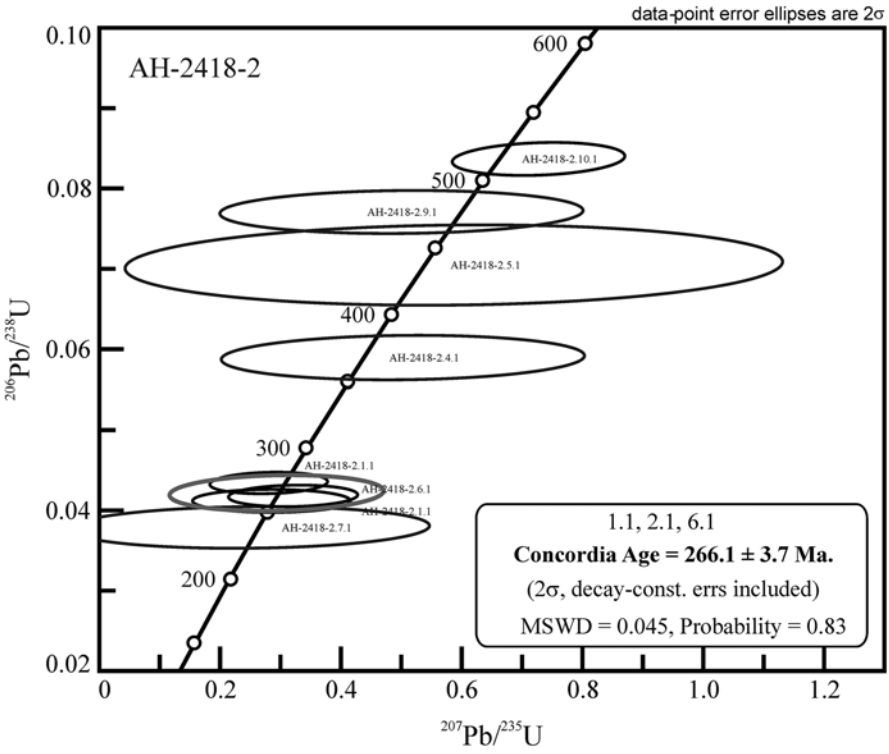

Fig. 4.15 Concordia diagram for zircons in Suoi Cun gabbrodolerite

magnetite (Polyakov et al. 1996). The mineral shows typical evolution trend from picrite to dolerite (Plasenko 1989). Equilibrium temperature of olivine and Cr-spinel calculated after Fabriec (1979) and Roeder et al. (1979) show values varying between 1350 °C and 800 °C, but most concentrating between 1000 °C and 1200 °C.

Ilmenite shows high Cr_2O_3 (up to 1.5 wt%), Al_2O_3 (0.9 wt%) and MnO (up to 2.9 wt%), suggesting high crystallization temperatures (Oktyabrski et al. 1986). The crystals are tablet or needle-shaped up to 0.5–0.8 mm long. Magnetite is found as euhedral crystals, having sizes similar to those of ilmenite.

The most complete sulfur mineralization is observed in Suoi Cun Pl-lherzolites. Their spatial distribution is irregular, most concentrated to the west of eastern Suoi Cun block (up to 15 % of total volume). The sulfur mineralization forms mostly small diffused mineral pockets and a minor amount of drop-shaped cumulates less than 1 mm. Among the sulfur minerals pyrotine is predominant (60–70 %). Pentlandite (15–20 %) forms tablet or fire-shaped within pyrotine, rarely formed as independent units. Ferrous sulfur in ore zones in the Suoi Cun block is normally hexagonal pyrotine, sometimes troilite. Chemical compositions of pentlandite is correspondent to Fe-rich, Cr-poor series. The chalcopyrite is chemically heterogeneous; in association with cubanite the mineral becomes richer in Cu

Table 4.7 U-Pb compositions acquired from zircons in Suoi Cun gabbrodolerite

Point	% $^{206}Pb_c$	ppm U	ppm Th	$^{232}Th/^{238}U$	ppm $^{206}Pb^*$	(1) $^{206}Pb/^{238}U$ Age		(1) $^{207}Pb/^{206}Pb$ Age		% Discordant	Total $^{238}U/^{206}Pb$	±%
AH-2418-2.1.1	1.29	374	95	0.26	14.1	273.9	±3.1	39	±330	−86	22.75	0.87
AH-2418-2.2.1	5.52	530	138	0.27	19.8	260	±3.5	205	±430	−21	22.96	0.75
AH-2418-2.3.1	0.72	293	86	0.30	103	2200	±12	2151	±23	−2	2.436	0.64
AH-2418-2.4.1	2.56	393	240	0.63	20.3	367.9	±6.7	674	±520	83	16.59	0.9
AH-2418-2.5.1	6.37	92	21	0.24	5.91	438	±12	623	±810	42	13.31	1.6
AH-2418-2.6.1	3.45	525	478	0.94	19.5	263.7	±3	436	±300	65	23.12	0.88
AH-2418-2.7.1	7.50	176	71	0.42	6.17	239.3	±6.4	100	±1100	−59	24.47	1.5
AH-2418-2.8.1	0.77	205	177	0.89	27.8	938.2	±8.9	885	±100	−6	6.331	0.98
AH-2418-2.9.1	4.19	171	151	0.91	11.8	476.7	±6.4	64	±580	−87	12.47	0.95
AH-2418-2.10.1	1.11	277	27	0.10	20.1	516.4	±5	717	±170	39	11.85	0.93

Analyzed point	Total $^{207}Pb/^{206}Pb$	±%	(1) $^{238}U/^{206}Pb^*$	±%	(1) $^{207}Pb^*/^{206}Pb^*$	±%	(1) $^{207}Pb^*/^{235}U$	±%	(1) $^{206}Pb^*/^{238}U$	±%	Err. corr
AH-2418-2.1.1	0.0572	2.8	23.04	1.2	0.0468	14	0.28	14	0.0434	1.2	.084
AH-2418-2.2.1	0.0946	1.8	24.31	1.4	0.0502	19	0.285	19	0.04115	1.4	.073
AH-2418-2.3.1	0.1405	0.86	2.454	0.66	0.1341	1.3	7.52	1.5	0.4068	0.66	.448
AH-2418-2.4.1	0.0825	9.1	17.02	1.9	0.062	24	0.5	24	0.0587	1.9	.076
AH-2418-2.5.1	0.112	11	14.22	2.8	0.061	38	0.59	38	0.0703	2.8	.075
AH-2418-2.6.1	0.0832	4.8	23.95	1.2	0.0556	13	0.32	14	0.04176	1.2	.087
AH-2418-2.7.1	0.108	12	26.46	2.7	0.048	48	0.25	48	0.0378	2.7	.057
AH-2418-2.8.1	0.075	3.2	6.38	1	0.0685	5	1.48	5.1	0.1567	1	.201
AH-2418-2.9.1	0.0817	9.5	13.02	1.4	0.047	24	0.5	24	0.0768	1.4	.057
AH-2418-2.10.1	0.0722	5.5	11.99	1	0.0633	7.9	0.728	8	0.0834	1	.125

Table 4.8 Chemical compositions (EPMA, wt%) of olivines in Cao Bang lherzolite and picrite (Hoa et al. 2005)

Sample	SiO_2	FeO	MgO	CaO	NiO	Total
Plagioclase lherzolite. Suoi Cun Block						
342/a	40.4	14.25	44.03	0.16	0.23	99.18
233c	39.94	16.32	42.57	0.2	0.17	99.2
256	40.06	15.83	42.83	0.26	0.17	99.15
333	40.18	15.45	43.08	0.2	0.24	99.07
233/2	40.12	17.54	40.68	0.11	0.14	98.59
249	40.59	15.02	42.51	0.27	0.18	98.56
Lherzolite and picrite. Khuoi Giang Block						
264a	39.99	16.15	42.67	0.18	0.19	99.18
264	36.83	26.94	37.12	0.02	0.08	100.99
265	39.25	17.03	43.34	0.25	0.18	100.05
261b	39.4	18.21	41.46	0.24	0.17	99.48

(>35.8–36.7 %), poorer Fe and S. This case indicates that equilibrium in the sulfur system shifted toward higher Cu at later stages of crystallization. Cubanite contains small amount of Ni = 0.02–0.12 % (Glotov et al. 2004).

Representative chemical compositions and trace element abundance of Cao Bang ultramafic magmas are given in Table 4.11. They are characteristically high Mg, low Ti (TiO_2 = 0.4–0.83 wt%), relatively low Al (Al_2O_3 = 4.76–6.94 wt% for ultramafic and 10.41 wt% for mafic types), and low alkalis ($Na_2O + K_2O$ = 0.6–1.4 wt%). Na_2O/K_2O ratios vary widely from a magma type to another for the presence of a considerable amount of phlogopite. Plots of ($Na_2O + K_2O$) vs. FeO and MgO show Pl-peridotite, lherzolite and picrite belonging to tholeiitic ultramafic series, while based on K_2O vs. SiO_2 correlation the magmas are more calc-alkaline-like. All the magmas are rich in Ni, Cu and Cr, but poor in Co and V. Ni/(Ni + Cu) and Ni/Co of the magmas vary, respectively, 0.74–0.84 and 7.86–18.17, characterizing for ultramafic magmas having the potential of Cu-Ni-PGS sulfur mineralization. In correlation between Cu and Ni, the lherzolite, picrite and gabbronorite form a group that is separated from gabbrodolerite mafic associations. The Cao Bang ultramafic magmas are rich in the REE, but showing negative anomaly at Eu in the chondrite REE normalization curve (Table 4.11, Fig. 4.17). The REE distribution configuration curve of olivine gabbro is comparable to the lherzolite and picrite's, the difference is the REE abundances in the latter are much lower. The ratios of La/Sm (2.7–3.4), Th/U (2.3–3.7) and Ce/Yb (6.8–8.3) are close for all the magmas.

They are characteristically high in Rb, Th and Ce, low in Zr and Nb as compared with low-K magmas. Primitive mantle trace element normalization shows positive anomalies at Rb, Th, U, and Ce, and negative anomalies at Nb, Ta, Sr, P and Ti. These geochemical characteristics observed for the Song Hien ultramafic magmas are vastly distinguished from low-Ti komatiite ultramafic in the Song Da rift zone, northwestern Vietnam and high-Ti picrite in the Emeishan large igneous province (China).

Table 4.9 Chemical compositions (EPMA, wt%) of clinopyroxenes in Cao Bang lherzolite and picrite (After Polyakov et al. 1996; Hoa et al. 1999)

	M-006	PB-62	B5142	B5146	B5147	B5143	P135	M-204/1	PB-86	PB-78	M-211
Sample	1	2	3	4	5	6	7	8	9	10	11
SiO_2	51.94	52.99	52.11	51.72	52.19	52.08	52.72	51.47	51.63	52.52	52.18
TiO_2	0.89	0.60	1.18	1.39	0.7	0.51	0.44	0.52	0.89	0.36	0.44
Al_2O_3	2.00	2.70	2.51	2.57	1.76	2.31	2.51	2.75	3.37	2.89	1.97
FeO	7.84	5.14	4.94	5.99	7.64	4.87	6.31	6.92	7.69	4.95	7.35
Cr_2O_3	0.58	1.13	0.91	0.78	0.52	1.05	1	0.88	0.50	0.57	0.41
MgO	17.09	17.83	18	16.87	19.1	17.65	19.1	16.81	17.72	17.94	18.17
CaO	18.26	20.08	19.99	19.42	17.28	20.12	17.62	18.94	17.06	19.64	17.30
Na_2O	0.26	0.50	0.33	0.35	0.26	0.24	0.23	0.32	0.18	0.21	0.22
Total	98.86	100.97	99.97	99.09	99.45	98.83	99.93	98.61	99.04	99.08	98.04
Wo.%	37.77	41.06	40.9	45.2	34.7	41.5	35.9	39.51	35.75	40.52	35.68
En.%	49.19	50.73	51.2	41.6	53.3	50.7	54.1	48.79	51.67	51.50	52.14
Fs.%	13.04	8.20	7.9	13.2	12	7.8	10	11.70	12.58	7.97	12.19

Remarks: 1–7: Suoi Cun wehrlite, lherzolite and picrite; 8–11: Khuoi Giang gabbronorite

Table 4.10 Chemical compositions of orthopyroxene in Cao Bang ultramafic blocks (After Polyakov et al. 1996)

	PB-61	PB-62	PB-73	PB-78	PB107	282A/83
Sample	1	2	3	4	5	6
SiO_2	55.53	55.73	54.83	54.85	55.32	54.73
TiO_2	0.49	0.44	0.36	0.38	0.39	0.57
Al_2O_3	1.64	1.63	1.51	1.02	1.75	1.14
FeO	9.5	11.01	12.75	10.58	10.62	13.75
Cr_2O_3	0.48	0.54	0.34	0.57	0.5	
MgO	30.38	29.87	28.43	29.94	29.36	28
CaO	2.23	2.37	2.02	2.13	2.37	2.05
Na_2O	0.04	0.02	0.03	0.02	0.05	0.06
Total	0.00	0.00	0.00	0.00	100.26	100.22
Wo.%	4.3	4.51	3.92	4.09	6.5	3.9
En.%	81.42	79.13	76.77	80.04	77.8	75.3
Fs.%	14.28	16.36	19.31	15.87	15.7	20.8

Remarks: 1–3: Suoi Cun wehrlite and lherzolite; 4–6: Khuoi Giang gabbronorite

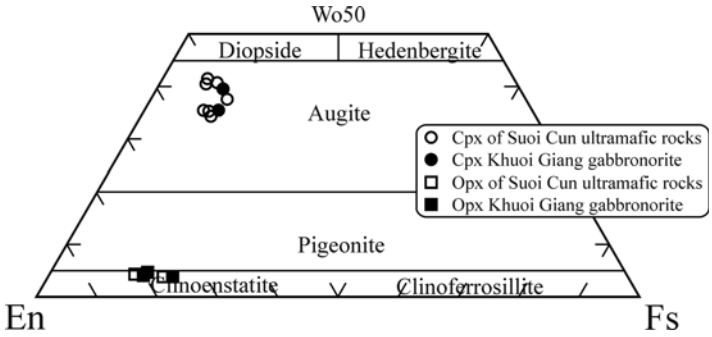

Fig. 4.16 Compositions of clinopyroxenes in Cao Bang lherzolite and picrite in En-Wo-Fs correlation

4.2.2.3 Formation Modeling and Estimation of Chemical Composition of Primitive Melts

Study of formation modeling and chemical composition of primitive melts was conducted on the Suoi Cun magmas. Suoi Cun magmas show clearly phase differentiation feature, as a result the chemical composition of magmas changes vertically in a given cross-section. This feature facilitates for choosing Suoi Cun block as study target (Balykin et al. 2001). The thermo-dynamic model of Suoi Cun block formation was constructed based on concept of accumulation – convection after Frenkel et al. (1988) using software 'Pluton' (Balykin et al. 2001; Lavrenchuc et al. 2002).

Estimation of porous rate in (melt) segregation (?) (essential parameter) was conducted based on geochemical thermal method of Frenkel et al. (1988). According to

Table 4.11 Chemical compositions and rare earth and trace element abundances of Cao Bang ultramafic magmas (Hoa et al. 2005)

Sample	M006	M009	H1500	H1606	B5143	P108	SC-2A	M206	M204
	1	2	3	4	5	6	7	8	9
SiO_2	44.87	44.72	43.89	42.94	42.68	41.69	43.92	43.12	48.24
TiO_2	0.55	0.54	0.46	0.52	0.33	0.35	0.44	0.38	0.87
Al_2O_3	8.16	7.38	6.26	7.76	9.12	6.38	6.06	5.11	10.97
FeO*	13.51	13.76	12.86	14.95	11.65	14.56	13.91	15.4	12.75
MnO	0.21	0.2	0.2	0.21	0.17	0.18	0.21	0.19	0.19
MgO	25.76	26.31	30.94	26.79	29.66	31.09	30.27	31.48	17.49
CaO	5.97	5.79	4.13	5	5.52	4.72	4.49	3.67	7.91
Na_2O	0.51	1	0.83	1.36	0.34	0.67	0.38	0.32	1.01
K_2O	0.4	0.23	0.38	0.36	0.44	0.27	0.25	0.28	0.46
P_2O_5	0.06	0.06	0.06	0.1	0.11	0.1	0.05	0.04	0.11
Cu	328	447	524	901	430	490	233	1088	104
Ni	1189	1450	2337	2502	2240	2020	956	2726	500
Co	105	108	143	146	102	120	106	150	75
Cr	512	696	3941	4619	1300	1600	812	1237	1160
V	114	96			120	70	63	70	138
Rb	18	13	10.8	13.6			16.5	15.3	14.2
Sr	54.3	43	32	43			43.5	22.7	148
Y	13.7	12.8	11.2	14.1			12.3	8.7	25.4
Zr	49.9	49.3	79	46			44	32.6	86.5
Ta	0.2	0.2	0.11	0.11		0.14	0.16		
Nb	1.5	1.9	2	2.3			2.4	1.3	3
Ba			48	64					
La	5.4	5.1	3.6	4.4	2.7	3.5	4.3	3.9	7.8
Ce	11	10.6	7.5	9.1	5.6	7.7	9.3	8.4	16.4
Pr	1.1	1.6	1.1	1.4					
Nd	6.1	6	4.4	5.5	5	4.8	6	5	10
Sm	1.56	1.64	1.1	1.3	0.9	1.4	1.59	1.44	2.8
Eu	0.5	0.4	0.3	0.38	0.3	0.3	0.4	0.36	0.8
Gd	2.1	1.9	1.2	1.5	1.5	1.6	1.9	1.8	3.5
Tb	0.38	0.35	0.25	0.32	0.3	0.3	0.34	0.31	0.64
Dy	1.8	2	1.6	1.9					
Ho	0.38	0.42	0.31	0.38					
Er	1.13	1.3	0.96	1.3					
Yb	1.46	1.31	1	1.2	0.8	0.9	1.12	1.05	2.4
Lu	0.22	0.2	0.13	0.19	0.12	0.13	0.16	0.16	0.36
Hf	1.2	1.1	0.5	0.25		0.83	0.9		
Th	1.6	1.2	1.6	1.9			1.5		
U	0.6	0.4	0.31	0.38			0.4		
La/Sm	3.46	3.11	3.27	3.38	3	2.5	2.7	2.71	2.79
Th/U	2.67	3	5.16	5			3.75		
Ce/Yb	7.53	8.09	7.5	7.58	7	8.56	8.3	8	6.83

Remarks: 1–2: Suoi Cun picrite; 3–7: Khuoi Giang lherzolite; 8: lherzolite; 9: olivine gabbro

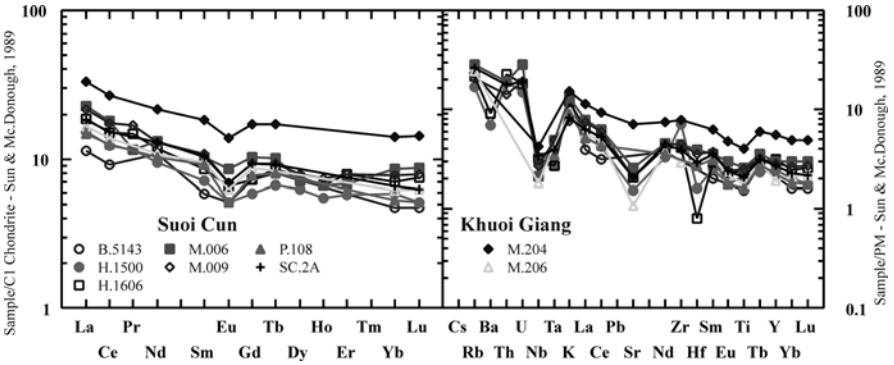

Fig. 4.17 Chondrite normalized rare earth distribution (**a**) and primitive mantle trace element normalized patterns (**b**) of Cao Bang ultramafic magmas

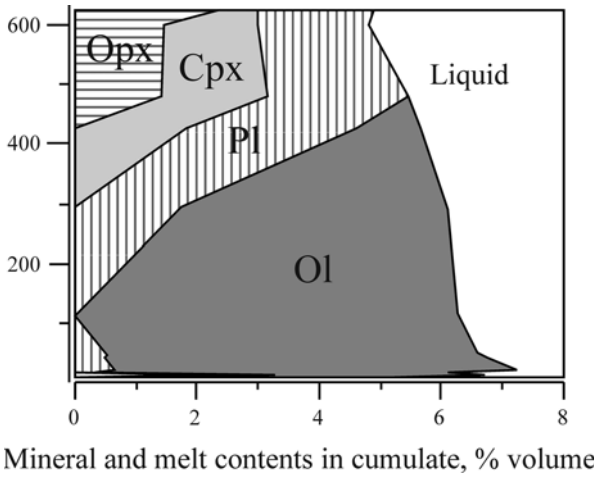

Fig. 4.18 Changes of magmatic compositional phases in Suoi Cun cross-section based on thermal-geochemical analysis

the calculation, the change in co-existing cumulate mineral assemblages during magmatic evolution occurred as follows: Ol → Ol + Pl → Ol + Pl + Cpx → Pl + Cpx + Opx, most coincided with petrographic observation. However, there is reasonable doubt on the late occurrence of large, anhedral orthopyroxene in Pl-peridotite in lower layers of the Suoi Cun cross-section. A possible explanation may be orthopyroxene formed by interaction between olivine and melt. Figure 4.18 shows porous rate in cumulate increase from ca. 35 % in lower portion to ca. 50 % at upper portion of the cross-section.

The above explanation may be related to the increase of viscosity in melts at late stages of block formation, which affects the density of particles (or particle compaction, after Naslund and McBirbey 1996) as result of gravitational load from upper layers. The increase of cumulate minerals at the lowermost layer from 50 to 60 % is due to mechanism of oriented crystallization (frozen mechanism, after Frenkel et al. 1988), that leads to increasing sedimentation of scattered crystals in the magma chamber. Change from oriented crystallization mechanism to cumulate mechanism in the Suoi Cun block occurred at porous level ca. 35%vol when the cumulate surface separated from solidus boundary. An average chemical composition of Suoi Cun magma is equivalent to picritic basalt, showing SiO_2 = 48.75 %, TiO_2 = 0.92 %, Al_2O_3 = 12.16 %, FeO* = 10.69 %, MgO = 15.43 %, CaO = 9.66 %, Na_2O = 1.71 %, K_2O = 0.52 %, P_2O_5 = 0.16 % (FeO* is total iron oxides). The chemical composition was calculated based on generalized cross-section using linear interpolation of elemental concentrations in magmas as well as coordination as gypsometric function in the cross-section. In order to construct the generalized cross-section, an additional large number of samples were analyzed by XRF adding to the available database (e.g. Polyakov et al. 1996). According to thermogeochemical modeling constructed for the Suoi Cun magmatic block, the magma crystallization started between 1260 °C and 1090 °C at pressures 1–3 kb with oxygen fugacity close to wustite – magnetite buffer. Figure 4.19 compares geochemi-

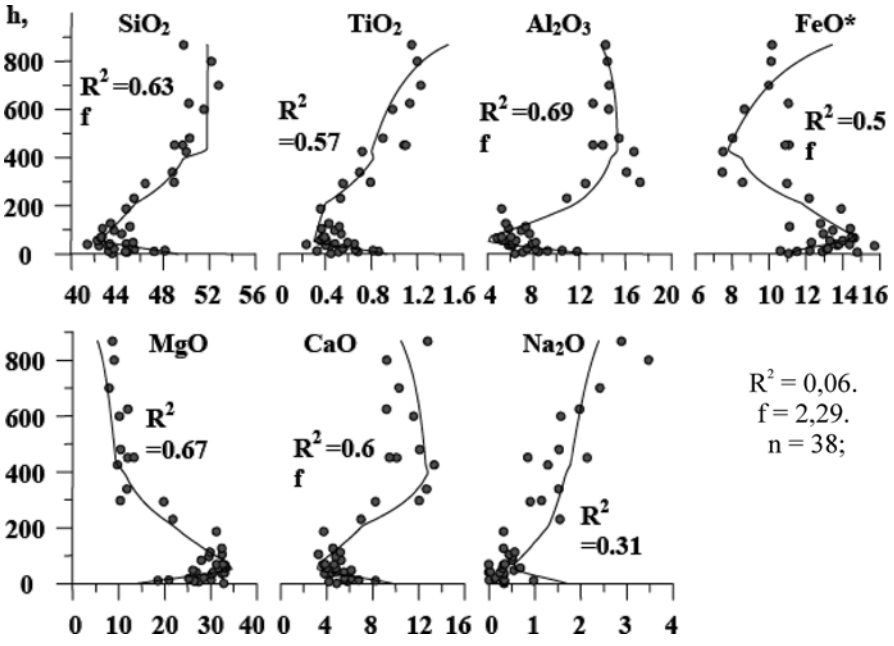

Fig. 4.19 Compositional changes in magmas from Suoi Cun cross-section (*points*) compared with those of cumulate model (*thick lines*). Critical values of R2 and diffusion indexes are given, amount n = 38. Compositions are in wt%

cal characteristics of the magmas in Suoi Cun cross-section with the corresponding indexes used in block formation modeling. It is obvious that geochemical variation characteristics of the magmas are closely reconstructed by the modeling calculation. This suggested that the modeling is applicable with error less than 0.1 %, and that the Suoi Cun block was formed by a magmatic intrusion, and that the magmatic composition is equivalent to picritic basalt.

In explaining the presence of orthopyroxene in Pl-peridotite at the lowermost layers of the block cross-section, note that the pyroxene grains are large, anhedral and containing rounded fragments of olivine. Such the relation shows that orthopyroxene was formed after olivine. According to the thermo-geochemical model, melt compositional interaction point during crystallization equilibrium of melts correspondent to harzburgite and an average of the upper layer magmas is at 1190 °C, most likely being the formation temperature of the magma. Composition of the magma at this temperature contains 65 %vol olivine and 35 %vol of melt. Orthopyroxene is observed to occur in magma having about 80 %vol crystallized melt, whereas, at 90 %vol crystallization, appearance of orthopyroxene must less than 10 %vol, much smaller than actual observation in the magma. However, the cumulate density not only contradicts to the thermo-geochemical modeling, but is also inconsistent with estimated block differentiation (Sarapov and Cherepanov 1986). This argument proposes that orthopyroxene in the lower layers of the Suoi Cun block is not cumulate in nature but rather being formed by cumulate olivine with magmatic melt at the late stages of the magmatic formation.

Chemical composition of the parental melts may be justified using compositions of primary melt inclusions in olivine and Cr.spinel in Suoi Cun picrite. These melt inclusions briefly studied (by Glotov and Kovyazin) were glass containing micro air-liquid bubbles, euhedral Cr-spinel (in olivine's inclusions), in some cases, pyroxene microspinifex. Micro-sulfur relics were observed in Mg-bearing inclusions; however, the sizes were too small to analyze using a conventional EPMA. A Mg-rich inclusion shows a chemical composition as follows: SiO_2 = 42.6–44.1 %; Al_2O_3 = 10.2–10.4 %; MgO = 25.4–26.5 %; CaO = 0.9–1.3 % và K_2O = 3.9–5.9 %, correspondent to an alkaline ultramafic magma. Other glassy inclusions show higher silicic composition but much lesser potassium content, such as SiO_2 = 61.2–64.2 %; Al_2O_3 = 20.7–22.8 %; CaO = 7.8–9.3 %; K_2O = 0.2–1.6 %. The presence of high-Si and -Al inclusions may indicate involvement of crustal material. Supporting to this phenomenon is high initial $^{87}Sr/^{86}Sr$ = 0.7079 in lherzolite as well as non-magmatic ages found in zircons as mentioned above. It is noteworthy that mostly compositionally homogenous glass-bearing inclusions in sub-liquidus minerals indicate that crustal contamination occurred at very early stage even before the initial stage of mantle melt crystallization. Based on the presence of air-liquid inclusions in glass and the lack of total analytical components in EPMA analyses on glass inclusions it may suggest that the glass inclusions themselves are fluid-saturated.

4.3 Geodynamics

The above descriptions have demonstrated that formation and evolution of the Song Hien structure were closely related to the formation of bimodal pluton – volcanic associations namely, basalt – andesite, gabbro – dolerite and lherzolite – gabbronorite, dacite – rhyolite and granite granophyre. Geological correlation between the magmatism and sedimentary formations as well as radiometric age data (within acceptable errors) show that the magmas are Permian – Triassic, where mafic – ultramafic intrusive magmas were determined to be 266–262 Ma, and bimodal felsic – basic volcanic magmas were dated at 250–248 Ma.

Paleomagnetic and paleogeographic studies have shown that the major volume of Emeishan trap basalts was formed within a short duration from 1 to 2 million years during the Permian (260 Ma) (Zhong et al. 2007). Intrusive mafic and ultramafic magmas in the Panzhihua area, the central part of Emeishan trap, were believed to form at the same time interval, for example, Baima at 262 Ma (Zhou et al. 2005), Honghe block at 259 Ma (Zhong and Zhu 2006) and also type A-granite intrusive formations at 261 ± 4 Ma (Zhong et al. 2007). Besides, field survey reveals that Triassic sediments and volcaniclastic sediments overlie the basalt unconformedly as results of lithosphere uplift in the central region of Emeishan large igneous province and trap erosion (Saunders et al. 1997). Meanwhile, syenite and I-type granite in the central region of the LIP are correspondent to an age of 251 Ma (Lo et al. 2002; Zhong et al. 2007).

In general, review of published research papers on mantle plume-induced Emeishan LIP and isotopic age data of the authors of current monograph on Permian – Triassic in the Song Hien, the Song Da and the Lo Gam belts (see the next chapter) it may divide the magmatic activity into two stages of internal reactivation related to mantle plumes: Permian (260 Ma) and Permian – Triassic (250 Ma). The early magmatic stage in the Song Hien rift zone is coincident to the time of pluton – volcanic formations in the Song Da rift, whereas the Song Hien later stage characterized by bimodal basalt – rhyolite pluton – volcanic associations is correspondent to the formation time of plutonic gabbro – granite and gabbro – syenite in the nearby Lo Gam belt (see the below chapter). The common presence of picritic magmatism showing Cu-Ni-PGE potential is typical character of mantle plume-related magmas such as Emeishan.

Ultramafic – mafic volcanic (and corresponding intrusive counterparts) magmas show a common geochemical evolution as seen in summarized diagram for elemental distribution (Fig. 4.20a, b). Note the similarity in distribution configuration of the lithophile, high field strength and rare earth elements among the rock types from various magmatic associations, suggesting that they may share a common source that was enriched in incompatible elements. This is evidenced by their high commonly initial $^{87}Sr/^{86}Sr$ ratios, for example, the value vary between 0.706–0.712 in basalts, 0.709 in lherzolite and 0.715–0.723 in rhyolite (Hoa 2007). The high strontium isotopic ratios in felsic magmas indicate strong wall-rock assimilation in transitional magma chambers in the crust during magmatic evolution. Increasing crustal

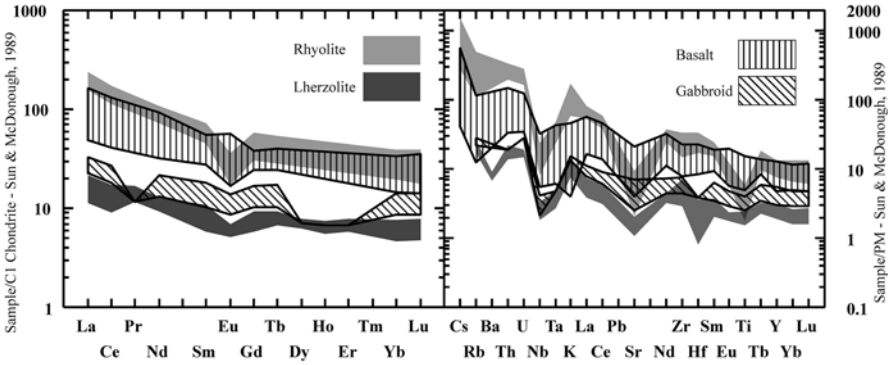

Fig. 4.20 Summarized chondrite (*left*) and primitive mantle (*right*) trace element normalization distribution diagrams for Song Hien magmas magma

contamination with differentiation trend from ultramafic to mafic and felsic magmas is obvious, which is expressed by their geochemical and isotopic characteristics also by the presence of 'foreign' zircons in lherzolite, gabbrodolerite and rhyolite as mentioned earlier.

There are two geochemically distinct magmatic associations in the Song Hien rift zone, Cao Bang low-Ti basalt – andesite association and the other, high-Ti basalt – andesite association in the Lang Son area. The two associations, however, do not show clear geochemical differences as compared to those low- and high-Ti magma types in the Song Da rift or in Emeishan and Siberian large igneous provinces. The clear differences, however, in Nb, Ta and Zr between Cao Bang and Lang Son magmas indicate geochemical heterogeneity in the lithospheric mantle along the Song Hien structural trend.

The occurrence of pluton – sub-volcanic lherzolite – gabbronorite and mafic volcanic magmas in the Song Hien rift zone presents an opportunity for researchers to understand the geochemical compositions and the nature of regional geodynamics of the lithospheric mantle in Permian – Triassic period under this region, and Cu-Ni-PGE potential in relation to the magmatism (Polyakov et al. 1996; 1999; Glotov et al. 2004; Izokh et al. 2005). The above described geochemical features of the pluton – volcanic magmas indicate a uniform evolutional trend for the Permian – Triassic magmas. The Nb, Ta, Sr and Ti depletion is a geochemically streamline character for ultramafic, mafic and felsic rock types, suggesting that their common mantle source may have been contaminated by subduction-derived materials. Subduction-related geochemical signatures are also recognized in granite and gabbro-syenite magmas elsewhere in northwest Vietnam (Hoa et al. 2004) and in picrite in the Shijong Mai belt, southeast South China craton (Izokh et al. 2005). Geochemical differences observed in picritic magmas in northeast and northwest Vietnam, in Emeishan trap indicate geochemical heterogeneity in the regional lithospheric mantle, on the one hand, and point to the presence of sub-oceanic- type mantle to the west and continental-type mantle above a subduction zone to the southeast of South China craton.

In summary, Permian – Triassic pluton-volcanic magmatic associations in the Song Hien structure basically are produced by mantle melting following continental collapse that occurred around craton marginal regions under the impact of super-mantle plumes developed under Asian continent.

References

Balykin PA, Polyakov GV, Petrova TE, Shelepaev PA, Tran Trong Hoa, Ngo Thi Phuong, Hoang Huu Thanh (2001) Composition of initial melts for Permo-Triassic and Triassic-Jurassic ultramafic-mafic complexes in North Vietnam. Rep RAS 378(2):225–229 (in Russian)

Bogatikov OA, Sharkov EV (1985) Magmatic rocks: vol 3 – Mafic rocks. 552.2, Nauka, Moscow, 488 pp

Chung SL, Jahn BM, Genyao W, Lo CH, Bolin C (1998) The Emeishan flood basalt in SW China: A mantle plume initiation model and its connection with continental breakup and mass extinction at the Permian-Triassic boundary. In: Flower MFJ, Chung SL, Lo CH, Lee TY (eds) Mantle dynamics and plate tectonics in East Asia, vol 27. AGU Geodynamics Series, Washington, DC, pp 47–58

Đao Đinh Thuc, Huynh Trung (eds) (1995) Geology of Viet Nam, P. II: Magmatic formations. Department of Geology and Minerals of Viet Nam publication, Vietnam

Dovjikov AE (ed) (1965) Geology of Northern Viet Nam. Science and Technology Publ, Hanoi, 668 p

Fabriec J (1979) Spinel-olivine geothermometry in the peridotites from ultramafic complexes. Contrib Mineral Petrol 69:329–336

Fang Hua, Yao Jiadong, He Daqui, Jiang Qinsheng (1985) The significance of deep-seated magmatic differentiation in the rock- and ore-forming processes of copper-nickel sulfide deposits – examplited by the Limahe copper-nickel sulfide deposit of Sichuan Province. Acta Geol Sin 2:141–154

Frenkel' MY, Yaroshevsky AA, Ariskin AA, Barmina GS, Koptev-Dvornikov EV, Kireev BS (1988) Dynamics of in situ differentiation of mafic magmas. Nauka, Moscow, p 216 (in Russian)

Glotov AI, Polyakov GV, Tran Trong Hoa, Ngo Thi Phuong, Izokh AE, Kovyazin SV, Balykin PA, Hoang Huu Thanh, Bui An Nien, Pham Thi Dung (2004) The Late Permian Cao Bang PGE-Cu-Ni-bearing complex og the Song Hien structure, Northeastern Viet Nam. J Geol B 23:89–98

Izokh, Polyakov GV, Tran Trong Hoa, Balykin PA, Ngo Thi Phuong (2005) Permian-Triassic ultramafic-mafic magmatism of Northern Vietnam and Southern China as expression of plume magmatism. Russ Geol Geophys 46(9):942–951

Lavrenchuc AV, Balykin PA, Borodina EV (2002) Composition of the initial melt and mantle substrate of dunite-troctolite-gabbro's block in Stanovoi fold system. Petrology of magmatic and metamorphic complexes. In: Proceedings of Russian science conference, Tomsk, vol 1, pp 114–119 (in Russian)

Le Duy Bach (2001) Composite terrane: theory and reality. J Earth Sci 23(1):1–15 (in Vietnamese with English abstract)

Lindsley DH (1983) Pyroxene thermometry. Am Mineral 68:477–493

Lo CH, Chung SL, Lee TY, Wu G (2002) Age of the Emeishan flood magmatism and relations to Permian-Triassic boundary events. J Earth Planet Sci Lett 198:449–458

Maluski H, Lepvrier C, Jolivet L, Carter A, Roques D, Beyssac O, Ta Trong Thang, Nguyen Duc T, Avigad D (2001a) Ar-Ar and fission track ages in the Song Chay massif: early Triassic and Cenozoic tectonics in northern Vietnam. J Asia Earth Sci 19(1):233–248

Naslund HR, McBirbey AR (1996) Mechanism of formation of igneous layering. Layered intrusions, Elsevier. Scienc B.V. 5:1–43

Nguyen Xuan Tung, Tran Van Tri (eds) (1992) Geological and geodynamic formations of Viet Nam. Science and Technology Publication, Hanoi

Oktyabrski RA, Hoang Huu Thanh, Sapin VI, Natarova ZS (1986) Study of sub-volcanic hyperbazite in Song Hien Zone (Vietnam). In: Ophiolite in the Asian's east margin". Far-East Center of Sciences, Khabarovsk, pp 66–68 (in Russian)

Plasenko AN (1989) Typomorphic secondary chromspinels in the ultramafic-mafic magmatic formations. VGU, Voronej, 88 pp

Polyakov GV, Nguyen Trong Yem, Balykin PA, Tran Trong Hoa, Hoang Huu Thanh, Tran Quoc Hung, Ngo Thi Phuong, Petrova TE, Vu Van Van (1996) Permian – Triassic mafic and ultramafic formations in northern Viet Nam. Science and Technology Publ, Hanoi, 172 p (in Vietnamese)

Polyakov GV, Tran Trong Hoa, Akimsev VA, Balykin PA, Ngo Thi Phuong, Hoang Huu Thanh, Tran Quoc Hung, Bui An Nien, Tolstyk AI, Glotov TEP, Vu Van Van (1999) Ore-geochemical specialization of the permo-triassic ultramafic-mafic complexes in north Vietnam. Geol Geophys 10(40):1474–1497 (in Russian)

Ponomareva AP, Vladimirov AG, Phan Luu Anh, Kruk NN, Rudnev SN, Ponomarchuk VA, Bibikova EV, Juravlov DJ (1997) High-aluminous granites of Song Chay massif (North Vietnam): Ordovician age, petrogenes, tectonic position. Geol Geophys 38(11):1792–1806 (in Russian)

Ramdin (ed) (1960) Final report to Nickel exploration in Cao Bang province. Center for Geological Informations

Roeder PL, Campbell IH, Jamieson HE (1979) Are-evaluation of the olivine-spinel geothermometer. Contrib Mineral Petrol 68:325–334

Sarapov VN, Cherepanov AN (1986) Dynamics of magma differentiation. Assemblage of publications of the IGG, SB RAS, No 642, 188 pp

Saunders AD, Fitton JG, Kerr AC, Norry MJ, Kent RW (1997) The North Atlantic Igneous Province. In: Mahoney JJ, Coffin MF (eds) Large igneous provinces: continental, oceanic and planetary flood volcanism. American Geophysical Union, Washington, DC, pp 45–93

She Chuan-jing (1986) A preliminary study on the metallogenic model of magmatic copper nickel sulfide ores in China. Metallogeny of basic and ultrabasic rocks. Regional presentafims. pp 325–358

Tran Trong Hoa (ed) (1995) Study of Mesozoic – Cenozoic magmatism and its mineralization potential. Final report for National project KT- 01–04 (1992–1995). Archives of the National Center for Science and Technology Information, Hanoi (in Vietnamese)

Tran Trong Hoa (2007) Intraplate magmatism in North Vietnam and related metallogeny. Dissertation of Dr. of Science. Institute of Geology and Mineralogy, Siberian Branch, RAS, Novosibirsk, 382 p

Tran Van Tri, Truong Cam Bao (eds) (1977) Geology of Vietnam, northern part. The explanation to geological map of north Vietnam, scale 1: 1,000,000. Institute of Geology and Mineral Resources (in Vietnamese)

Tran Trong Hoa, Ngo Thi Phuong, Hoang Huu Thanh, Vu Van Van, Bui An Nien, Tran Tuan Anh, Hoang Viet Hang (1999) Magmatic complexes in the Cao Bang – Dong Khe area, Geological map of Cao Bang – Dong Khe sheet of 1:50,000. Archives of the Center for Geological Information and Literature, Dept. of Geology and Minerals of Viet Nam, Vietnam (in Vietnamese)

Tran Trong Hoa, Tran Tuan Anh, Ngo Thi Phuong, Izokh AE, Polyakov GV, Balykin PA, Ching-Ying Lan, Hoang Huu Thanh, Bui An Nien, Pham Thi Dung (2004) Gabbro-syenite associations of East Bac Bo structures: evidences of intra- plate magmatism? J Geol series B 23:12–25, Hanoi

Tran Trong Hoa, Tran Tuan Anh, Ngo Thi Phuong, Pham Thi Dung Tran Viet Anh (2005) Permian – Triassic magmatic activities in Viet Nam and prospect of associated rare and precious metal (Pt, Au) mineralization. In: Proceedings of 60-Anniversary of Geology of Viet Nam, pp 63–79 (in Vietnamese)

Tran Trong Hoa, Tran Tuan Anh, Ngo Thi Phuong, Pham Thi Dung, Tran Viet Anh, Izokh AE, Borisenko AS, Lan CY, Chung SL, Lo CH (2008) Permo-Triassic intermediate-felsic magmatism of the Truong Son belt, eastern margin of Indochina. Compt Rendus Geosci 340:112–126

Wells PR (1967) Pyroxene thermometry in simple and complex systems. Contrib Petrol 62:129–139

Wood J, Banno S (1973) Garnet-ortopyroxene and ortopyroxene-clinopyroxene. Relationships in simple and complex systems. Contrib Mineral Petrol 42(2):109–124

Zhong H, Zhu WG (2006) Geochronology of layered mafic intrusions from the Pan Xi area in the Emeishan large igneous province, SW China. Mineral Deposits 41:599–606

Zhong H, Zhu WG, Chu ZH, He DF, Song XY (2007) Shrimp U-Pb geochronology, geochemistry, and Nd-Sr isotopic study of contrasting granites in the Emeishan large igneous province, SW China. Chem Geol 236:112–133

Zhou MF, Robinson PT, Lesher CM, Keays RR, Zhang CJ, Malpas J (2005) Geochemistry, petrogenesis and metallogenesis of the Panzhihua gabbroic layered intrusion and associated Fe-Ti-V oxide deposits, Sichuan province, SW China. J Petrol 46:2253–2280

Chapter 5
Gabbro and Syenite Intrusions in the Lo Gam Structure, Northeast Vietnam

Abstract Lo Gam structure (including Phu Ngu) in northeast Vietnam comprises Permian – Triassic gabbro-peridotite, monzogabbro, high-Al granite and syenite intrusive blocks. The studies have also revealed that gabbro – syenite magmas in folded structures around southeastern margin of the Song Chay anticlinoria form three association types distinguished by their co-existing mineral assemblages, mineralogical compositions and geochemical indexes (titanium content and alkalinity): layered peridotite- gabbro (Nui Chua complex), biotite granite (Phia Bioc complex) and compositionally heterogeneous gabbro-syenite. The uniformity of their geochemical and isotopic compositions indicates, on the one hand, generic relationship of the gabbro and syenite, and geochemically common source origin of the magmas, on the other. Being enriched in large ionic lithophile elements (LILE), rare earth elements (REE) and strongly depleted in Nb, Ta and Zr the gabbroid and syenite magmas reflect typical geochemistry of an above-subduction-zone affiliation. This is the basic feature of Permian – Triassic pluton – volcanic and plutonic magmatic associations in various geological structures in northeastern Vietnam. The formation ages of lherzolite and monzogabbro (Nui Chua complex), gabbro, syenite and biotite granite (Cho Don area) are 251–246 Ma (U-Pb, zircon, SHRIMP, Ar-Ar).

Lo Gam structure (including Phu Ngu) in northeast Vietnam comprises Permian – Triassic gabbro-peridotite, monzogabbro, high-Al granite and syenite intrusive blocks. In previous studies these blocks were listed to separate magmatic complexes, having even different occurrence ages. For instance, the peridotite-gabbro, monzogabbro and high-Al granite were viewed as contrast bimodal gabbro – granite series, whereas the gabbro blocks were grouped with Nui Chua complex, the high-Al granites belonged to Phia Bioc complex and had a late Triassic age. The other alkaline felsic intrusions (syenite and nepheline syenite) either listed to early Phia Ma Paleozoic complex, or Cho Don Paleogene complex (Dovjikov 1965; Tri 1977; Thuc and Trung 1995). Distribution scheme of Lo Gam – Phu Ngu gabbro, granite and syenite intrusive outcrops is shown in Fig. 5.1.

Recent mineralogical, geochemical – isotopic and geochronological studies suggest that the above mentioned intrusive magmas belong to Permian – Triassic magmatic activities (Hoa et al. 2004, 2008; Hoa 2007). The studies have also revealed that Lo Gam Permian – Triassic magmas are compositionally and petrologically heterogeneous, including three types of intrusion: layered peridotite- gabbro

T.-H. Tran et al., *Intraplate Magmatism and Metallogeny of North Vietnam*,
Modern Approaches in Solid Earth Sciences 11,
DOI 10.1007/978-3-319-25235-3_5

(Nui Chua complex), biotite granite (Phia Bioc complex) and compositionally heterogeneous gabbro-syenite. According to spatial and age relation the first two magmatic types clearly form a typical gabbro – syenite series (Hoa et al. 2008). Magmas with the gabbro-syenite associations show not only spatial-temporal but also genetic relationship (Hoa et al. 2004; Hoa 2007).

5.1 Gabbro-Granite Series

5.1.1 Layered Gabbro-Peridotite Intrusions

5.1.1.1 Distribution Features and Formation Ages

In northern Vietnam Permian – Triassic layered gabbro-peridotite intrusive magmas are mainly found in the two following structures: Lo Gam zone, including the Song Chay anticlinoria in the Northern fold zone, southern rim of the North Vietnam – South China geo-composite terrain (Cathaysian fold zone), and Sam Nua zone in the Sam Nua – Hoanh Son volcanic belt to the east of the Dong Duong (Indochina) Geoblock (Truong Son fold belt). Representatives of layered intrusive magmas in northeastern Vietnam are Nui Chua and Khao Que, while in the Sam Nua zone are Tri Nang and Nui Yen Chu (Polyakov et al. 1984, 1996); Thanh 1994, 2004; Balykin 2002). For this monograph detailed descriptions will be given only to the Nui Chua and Khao Que blocks within Lo Gam structure (Fig. 5.1). These blocks were previously grouped with Phia Bioc granites to form Ban Xang – Phia Bioc, having a complicated composition such as hyperbasic – gabbro – granite (Dovjikov 1965) or late Triassic Nui Chua – Phia Bioc gabbro – granite (Thuc and Trung 1995). To support the above claim a Rb-Sr age showed 195 Ma for a Tri Nang gabbro in the Nui Chua complex (e.g. Luan 1985). However, the accuracy of Rb-Sr age was suspicious but no verification had been done for a long time at least till 2007 a proper answer on the position of large gabbro-peridotite intrusive blocks in the history of geological evolution in northern Vietnam had not yet been given. Particularly, observing the intrusions distributed in Paleozoic sediment-metamorphic rocks, spatial relation with Ban Rin-type serpentinized dunite and their geochemical characteristics some researchers suggested that the layered gabbro-peridotite in northern Vietnam may be products of early-middle Paleozoic arc-like volcanic activities (Thanh et al. 2004).

In order to solve the problem of formation age and related tectonic setting of the Lo Gam layered gabbro – peridotite intrusions authors of the monograph collected a fine-grained gabbronorite weighed about 15 kg (AH 2437) nearly the eastern margin of Nui Chua intrusive block to process for U-Pb isotopic dating using SHRIMP (Hoa et al. 2008). Mineral compositions of the gabbronorite include zone-free basic plagioclase, clino- and orthopyroxene. Chemical composition (wt%) of the magma is SiO_2=47.26; TiO_2=0.35; Al_2O_3=15.31; Fe_2O_3=7.31; MnO=0.24; MgO=6.67; CaO=17.37; Na_2O=1.25; K_2O=0.77; P_2O_5=0.04. Zircon collected were fragments from short highly euhedral, cubic-shaped crystal and up to 0.2 mm sized. The crystal is thinly zoned (Photo 5.1). In some grains zone-free cores were also observed. The U

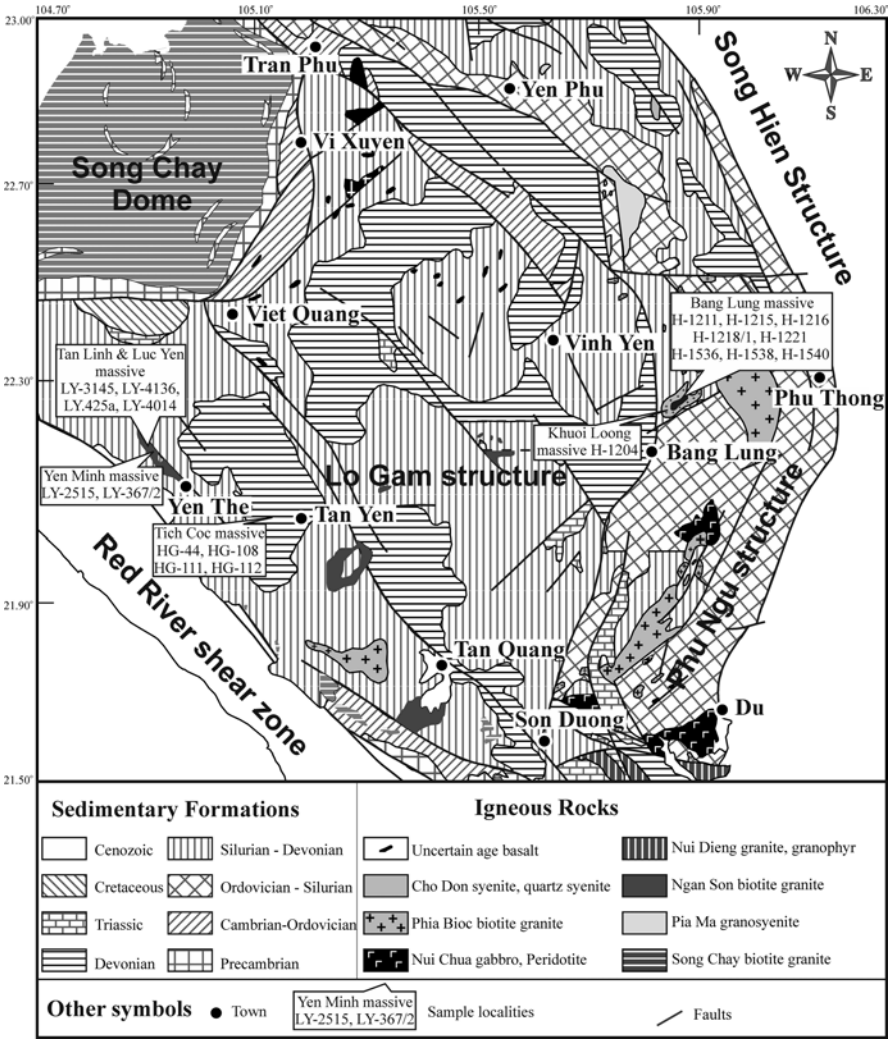

Fig. 5.1 Distribution scheme of gabbro – syenite associations in Lo Gam – Phu Ngu structure

and Th concentrations are high (U = 1300–4800 ppm, Th = 1200–11,200 ppm) and the U/Th ratios are relatively, between 0.6 and 2.6 (Table 5.1). The values indicate that zircons were crystallized from evolved mafic melts. All the acquired $^{206}Pb/^{238}U$ isotopic ratios were concordant (Fig. 5.2; Table 5.1). A concordant age calculated for all the analyzed zircons was 251 ± 3.4 Ma (MSWD = 0.36). Based on the isotopic compositions and morphology of zircon crystals it is highly possible that the calculated age was correspond to the gabbronorite crystallization and that Nui Chua intrusive block was formed by Permian – Triassic magmatic activities (Hoa et al. 2008).

The age is believed to fit the geological relation between Nui Chua-type gabbro and Phia Bioc-type granite and its age, 251–242 Ma, determined using Ar-Ar and U-Pb methods (see below). This allows for taking the Nui Chua and Phia Bioc

Table 5.1 U-Pb isotopic ratios of zircon separates from a Nui Chua gabbronorite. Sample AH-2437-1

Points analyzed	% $comm^{206}$	ppm U	ppm Th	$^{232}Th/^{238}U$	ppm $Rad^{206}Pb$	$^{204}corr$ $^{206}Pb/^{238}U$ Age	1 s err	$^{238}/^{206}r$	% err	$^{207}r/^{206}r$	% err	$^{207}r/^{235}$	% err	$^{206}r/^{238}$	% err	err corr
AH-2437-1.1.1	3.05	2120	4102	2.00	76.8	258.2	5.5	24.47	2.2	.0522	6.5	0.29	6.8	.0409	2.2	.319
AH-2437-1.2.1	0.34	2085	1278	0.63	67.3	237.0	5.0	26.71	2.2	.0523	2.8	0.27	3.5	.0374	2.2	.612
AH-2437-1.3.1	0.30	3174	3436	1.12	111.8	258.2	5.4	24.47	2.1	.0519	2.2	0.29	3.1	.0409	2.1	.694
AH-2437-1.4.1	2.63	1459	1749	1.24	51.2	251.3	5.5	25.16	2.2	.0509	8.5	0.28	8.8	.0397	2.2	.253
AH-2437-1.5.1	0.57	1784	1586	0.92	58.9	241.8	5.1	26.16	2.2	.0528	5.0	0.28	5.4	.0382	2.2	.400
AH-2437-1.6.1	0.70	2446	5239	2.21	88.0	262.7	5.5	24.04	2.1	.0500	3.0	0.29	3.7	.0416	2.1	.578
AH-2437-1.7.1	0.45	4523	11,239	2.57	156.8	253.9	5.3	24.90	2.1	.0514	2.1	0.28	3.0	.0402	2.1	.719
AH-2437-1.8.1	2.58	3905	2923	0.77	135.7	249.1	5.3	25.38	2.2	.0569	7.2	0.31	7.5	.0394	2.2	.289
AH-2437-1.9.1	0.87	1399	1884	1.39	48.0	250.5	5.5	25.24	2.2	.0512	6.0	0.28	6.4	.0396	2.2	.349
AH-2437-1.10.1	1.01	4804	6766	1.46	167.1	253.3	5.3	24.95	2.1	.0502	3.9	0.28	4.4	.0401	2.1	.480

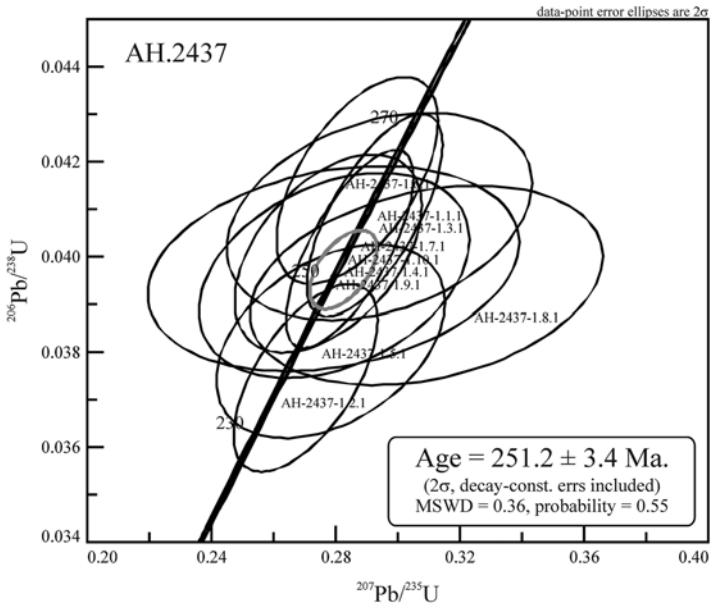

Fig. 5.2 Concordant diagram of zircons from a Nui Chua gabbronorite

magmatic complexes as well as other Permian – Triassic magmatic activities in northern Vietnam, as mantle plume-induced magmatism developed in the south of Yangtze craton (Izokh et al. 2005; Hoa et al. 2004, 2008; Zhou et al. 2005; Zhong et al. 2007).

5.1.1.2 Geological Structure and Magmatic Compositions

The geological features and magma compositions of Nui Chua layered gabbro – peridotite intrusions were given in detail in Polyakov et al. (1996). In this chapter we will summarize some pronounced characteristics and add new research results achieved recently for Nui Chua magmatic block.

Nui Chua pluton, occupying about 55 km^2, is a gabbro body that includes the most representative layered gabbro-peridotite intrusions in northern Vietnam. The pluton is located to the south of Lo Gam Paleozoic folding structure (Fig. 5.1) in Ordovician – Silurian terrigenous sediments comprised mainly of quartzite, silicic – sericite shale, sand- and siltstone of Phu Ngu complex (O-S*pn*); formed a tectonic contact with Devonian shale, limestone and sandstone to the northwest, and being overlain by Triassic molasse-type sediments in the west (Fig. 5.3).

The pluton is tectonically separated forming a number of micro-blocks having characteristically heterogeneous differentiation (Thanh 1994; Polyakov et al. 1996). Magmatic compositions of the micro-blocks include strongly evolved rock series such as olivine gabbro, gabbronorite and troctolite intercalated by thin layers of Pl-wehrlite, lherzolite, olivinite, dark-colored gabbronorite, leucogabbro and anorthosite (Fig. 5.4).

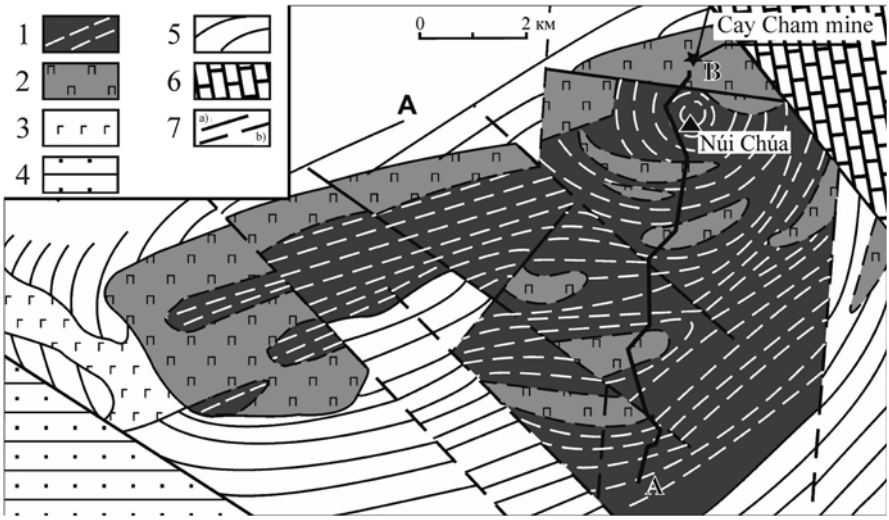

Fig. 5.3 Geological and petrologic scheme of the Nui Chua pluton, showing simplified tectonic map of Northern Vietnam: *1*- differentiated series, *2*- pegmatoidic series, *3*- fine-grained biotite-gabbro and monzodiorite, *4–6* surrounding sediments: *4*- Triassic, *5*- Devonian carbonate sediments, *6*- Ordovician-Silurian sandstone and shale, *7*- geological boundaries: *a*- confirmed, *b*- hypothetical; A-B cross-section (see Fig. 5.4)

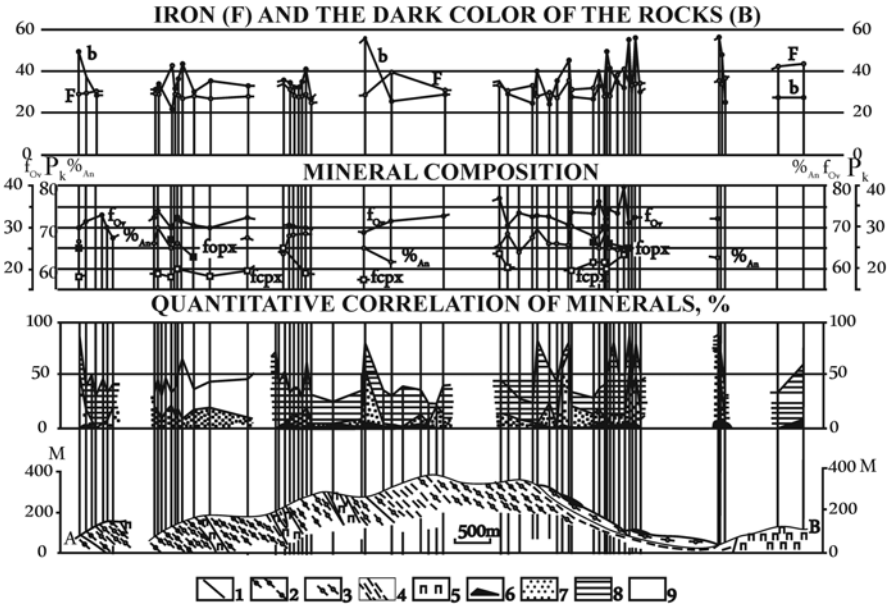

Fig. 5.4 Cross-section A-B (see Fig. 5.3) showing *1*: peridotite and pyroxenite; *2*: evolved series with dominance of dark-colored olivine-bearing gabbro; *3*: differentiated meso- and leucogabbroidic series; *4*: gabbro and gabbronorite; *5*: pyroxenite pegmatoid and gabbro pegmatoid. Chemical compositions of rock-forming mineral: *6*: ore minerals (sulfide, magnetite and ilmenite); *7*: olivine; *8*: pyroxene; *9*: plagioclase

Cu-Ni-PGE minerals were discovered in thin layers of these magmatic series (Thanh 1994; Polyakov et al. 1996, 1999). The magmatic layering and parallel-oriented texture (trachyte-type) in northeast direction trend is corresponding to the direction of block elongation and dip angle seen at central and southwest micro blocks. While at the micro-block, defined as center of the structure, dip angle of the layers has opposite direction as compared with that in the southwest, also there as less dark-colored magma series as compared with those in upper sections of the block. Among the outcrops of differentiated magma series encountered are lenses or dykes of coarse-grained pegmatoid having compositions ranging from olivine-free gabbronorite, light-colored gabbro and gabbronorite to melanogabbronorite and Pl-pyroxenite. To the southwest of Nui Chua block pegmatoid magmas are predominant while in the east there are also taxitic coarse-grained gabbro and pyroxenite of inner contact phase having Ti-magnetite – ilmenite mineralization (Cay Tram mine). Ti-Fe mineralization accompanying coarse-grained gabbro and pyroxenite is also found in northwest margin of the Nui Chua block (Na Hoe area).

5.1.1.3 Mineralogical and Geochemical Characteristics

Typical differentiated and pegmatoid magmas show relatively invariable compositions. Most significant character for the differentiated magmas is olivine character showing ferrous component varying from chrysolite (f_{ol} = 27.8 %) in ultramafic magma to hyalosiderite (f_{ol} = 40.3 %) in gabbroid and high concentrations of Ni (230–1100 ppm) and CaO (0.2 wt%) (Balykin 2002; Polyakov et al. 1996). Olivine is absent in pegmatite series while pyroxene is commonly present showing eroded, pine-branched texture with thin films of high-Ca diopside. Ophitic bronzite and single pigeonite crystals are observed in taxitic gabbronorite and pyroxenite. Pigeonite in evolved olivine gabbronorite series forms complicated, intercalated texture in incorporation with diopside, or in some rare cases forming independent euhedral crystals. Pigeonite in pegmatoidic series develops compositionally contrast type, once degraded to form high-Ca diopside (f_{Cpx} = 23–31 %) and hypersthene (f_{Opx} = 38–65 %). Chemically major rock-forming clinopyroxene and orthopyroxene (Tables 5.2, 5.3, 5.4 and 5.5) of pegmatoidic gabbronorite and pyroxenite are high in Fe and low in Mg and Al compared with pyroxene in evolved series.

Orthoclase component in the plagioclase is high which is comparable to a higher potassic type (Table 5.5). Chemical variation of the major rock-forming minerals (plagioclase, olivine and clinopyroxene) is shown in Fig. 5.5.

Distinct features and compositional differences of evolved and pegmatoidic series are significant when taken petro-chemical characteristics into comparison. The comparison of petro-chemical characteristics was based on 200 chemical analyses by the authors; among these 170 analyses were conducted on evolved magmatic series and 30 from pegmatoidic series. Average chemical compositions of the layered and pegmatoidic series are shown in Table 5.6. The petro-chemical indexes for the evolved and pegmatoidic series are illustrated using 'VADIC' classification program by V.V. Khlestov (Institute of Geology and Mineralogy, Siberian Branch, Russian Academy of Sciences) showing errors about 2 % (Fig. 5.6).

Table 5.2 Average chemical compositions (wt%) of olivine in Nui Chua in layered series

Group	Average	FeO*	MgO	CaO	NiO	Ni, ppm	F_{Ol}
1	X	28.65	34.23	0.04	0.09	707	31.3
	S	2.26	2.49	0.04	0.02	170	2.5
2	X	26.7	35.17	0.02	0.07	509	30
	S	0.91	1.26	0.01	0.01	84	1.18
3	X	27.8	33.56	0.02	0.06	462	31.6
4	X	28.4	34.19	0.02	0.06	453	31.8
	S	2.19	0.84	0	0.03	195	2.02
5	X	27.99	35.39	0.02	0.08	597	30.6
	S	1.32	1.54	0.01	0.02	165	1.69
6	X	29.19	33.96	0.02	0.08	593	32.5
	S	1.56	1.49	0.01	0.03	211	1.71
7	X	30.36	31.8	0.03	0.09	686	34.9
	S	1.88	1.88	0.02	0.02	164	2.65
8	X	29.21	34.44	0.02	0.08	629	32.3
	S	1.81	1.5	0.01	0.03	200	2.04
9	X	30.19	33.38	0.02	0.07	516	33.6
	S	2.28	1.18	0.01	0.02	139	2.32
10	X	30	31.99	0.04	0.1	786	34.4
	S	0.71	1.09	0.03	0.05	360	1.29

Remarks: 1- lherzolite and olivinite (n=6); 2- melanotroctolite, olivine melanogabbro and melanogabbronorite (n=5); 3- ore-bearing melanogabbronorite (n=2); 4- ore-bearing melanogabbro (n=4); troctolite, mesogabbro and gabbronorite (n=36); 6- olivine-bearing (n=30); 7- ore-bearing gabbronorite (n=14); 8- bright-colored troctolite, leucogabbro and leucogabbronorite (n=14); 9- olivine-bearing leucogabbronorite (n=5); 10- ore-bearing leucogabbro (n=3). FeO* total of FeO and Fe_2O_3

Table 5.3 Average chemical compositions (wt%) of Nui Chua clinopyroxene

Group	1	2		3		4		5		6
Oxides	Kp6378	X	S	X	S	X	S	X	S	X
SiO_2	52.39	52.31	0.61	52.18	0.85	52.27	0.52	52.34	0.95	52.08
TiO_2	0.85	0.82	0.13	0.82	0.1	0.78	0.17	0.76	0.11	0.65
Al_2O_3	2.6	2.48	0.08	2.55	0.4	2.34	0.3	2.08	0.44	1.78
Cr_2O_3	0.29	0.3	0.04	0.25	0.12	0.27	0.07	0.08	0.1	0.11
FeO*	6.86	6.51	0.86	7.48	1.32	7.38	0.97	9.28	0.93	9.6
MgO	15.7	15.59	0.53	15.74	0.87	15.06	0.56	14.42	0.65	14.21
CaO	21.13	21.02	1.11	20.2	1.99	21.37	0.81	20.04	2.17	20.54
Na_2O	0.46	0.31	0.06	0.35	0.06	0.31	0.07	0.23	0.07	0.28
Wo, %	45.5	42	3.42	40.7	5.96	43.7	3.23	38.8	5.67	43
En, %	44.4	46.9	2.05	46.3	3.7	44	2.07	43.8	2.61	41.3
Fs, %	10.1	11.1	1.58	13	2.72	12.3	2.08	17.4	3.55	15.7
F	18.4	19.9	1.64	20.2	1.99	21.9	3.08	28.3	3.45	27.6

Remarks: 1–4: Layered series: 1- Pl-lherzolite; 2- olivine gabbro and dark gabbronorite (n=6); 3- olivine gabbro and gabbronorite (n=16); 4- olivine leucogabbro and gabbronorite (n=7); 5-6- pegmatoidic series: Pl-websterite (n=4); 6- gabbronorite (n=2)

Table 5.4 Average chemical compositions (wt%) of orthopyroxene from various rock types in Nui Chua pluton

Group	1	2		3		4		5	6
Oxides	X	X	S	X	S	X	S	X	X
SiO_2	53.7	54.58	0.47	53.91	0.84	54.11	0.63	53.94	52.83
TiO_2	0.37	0.32	0.05	0.35	0.12	0.35	0.16	0.2	0.32
Al_2O_3	1.16	1.38	0.11	1.38	0.13	1.2	0.38	1.12	0.98
Cr_2O_3	0.12	0.07	0.05	0.14	0.11	0.15	0.11	0.08	0.1
FeO	16.58	16.44	1	17.83	1.72	16.53	1.29	20.17	22.15
MgO	27.17	26.16	1.13	25.54	1.3	25.91	2.42	23.11	23.12
CaO	1.05	1.72	0.61	1.34	0.58	1.91	2.03	2	0.94
Na_2O	0.01	0.02	0.03	0.04	0.05	0.06	0.08	0.01	0.02
Wo, %	2.1	5.1	1.91	3.4	2.18	4.2	1.57	4.7	1.9
En, %	73	70.2	3.31	69.5	3.32	70.4	3.92	63.6	63.8
Fs, %	24.9	24.7	1.99	27.1	3.29	25.4	1.59	31.7	34.3
F	25.6	26.7	1.88	28.41	2.78	26.6	1.57	33.2	35.1

Remarks: 1–4 layered series: 1- Pl-lherzolite (n = 2); 2- olivine melanogabbronorite (n = 7); 3- olivine mesogabbronorite (n = 9); 4- olivine leucogabbronorite (n = 5); 5-6- pegmatoidic series: 5- Pl-websterite (n = 2); 6- mesogabbronorite (n = 3)

Table 5.5 Average chemical compositions (wt%) of plagioclase from different rock types in Nui Chua pluton

Group	1		2		3		4	
Oxides	X	S	X	S	X	S	X	S
CaO	13.82	0.45	13.59	0.35	13.51	0.57	13.45	0.72
Na_2O	3.52	0.3	3.61	3.19	3.74	0.32	3.79	0.21
K_2O	0.05	0.03	0.1	0.01	0.06	0.04	0.12	0.02
FeO	0.1	0.08	0.05	0.05	0.05	0.05	0.06	0.05
An, %	68.6	2.11	67.5	2	66.6	2.5	66.5	2.7
Ab, %	31.1	2.3	32	2.8	33	2.6	32.8	2.6
Or, %	0.3	0.2	0.5	0.2	0.4	0.2	0.7	0.1

Remarks: 1-3- Layered series; 1- olivine melanogabbronorite (n = 4); 2- olivine mesogabbronorite (n = 10); olivine leucogabbro (n = 5); pegmatoidic series: 4- melanogabbronorite (n = 3)

Distinct features between two magma series are clearly expressed on binary scattered diagrams such as MgO vs. Al_2O_3, TiO_2 and V_2O_5 (Fig. 5.7).

Note that petro-chemical fields of the two magma series are either close to or parallel each other such as along division lines of Ol-Pl, Cpx-Pl, and Opx-Pl (Fig. 5.8).

As seen in Fig. 5.8 the chemical compositions of evolved magma series move closer to Ol-Pl line (troctolite line) while pegmatoidic magma series tend toward Opx-Pl and Cpx-Pl. The pegmatoidic magma series show higher iron, titanium and vanadium oxides as compared to the evolved magma series (Figs. 5.9, 5.10, and 5.11). Representative major and trace element concentrations of the gabbro and peridotite magma series in various plutons are given in the Table 5.7. The magma series are characteristically low Ti, alkalis (relatively high Na and low K), variable

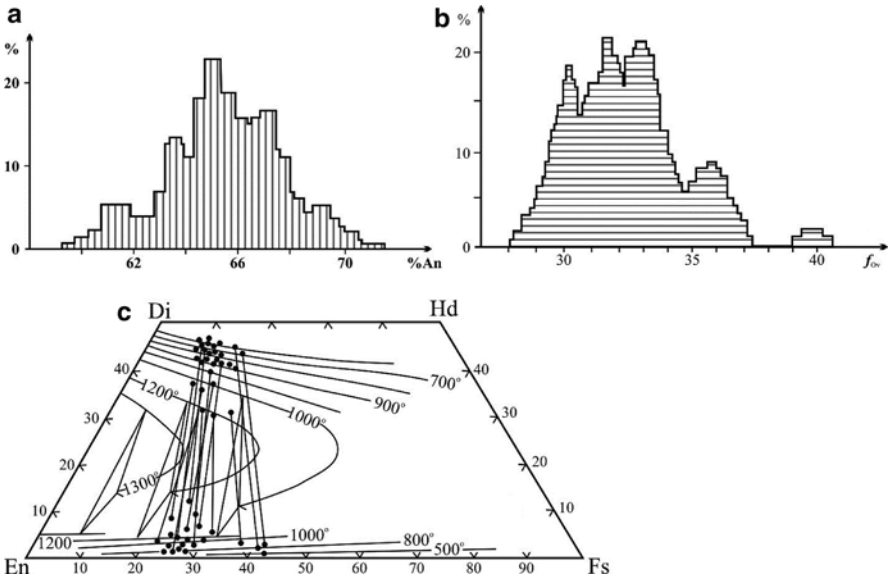

Fig. 5.5 Chemical variation of plagioclase (**a**), $n = 131$), olivine (**b**), $n = 123$), clinopyroxene ($n = 35$) and orthopyroxene (n = 30) (**c**) from Nui Chua block

Table 5.6 Average chemical compositions (wt%) of Nui Chua magma groups

Rock group	SiO_2	TiO_2	Al_2O_3	FeO*	MnO	MgO	CaO	Na_2O	K_2O	P_2O_5
1	41.29	0.22	5.06	22.67	0.27	24.66	5.22	0.37	0.16	0.06
	1.10	0.11	0.83	1.47	0.06	0.47	1.98	0.32	0.11	0.04
2	38.92	0.20	3.82	26.26	0.27	26.84	3.34	0.25	0.07	0.04
	3.21	0.12	1.47	1.89	0.06	1.38	1.46	0.21	0.09	0.03
3	40.50	0.21	3.94	23.74	0.27	27.03	3.88	0.28	0.10	0.05
	2.01	0.11	1.47	2.55	0.06	2.23	1.69	0.03	0.03	0.03
4	45.11	0.22	13.41	13.32	0.20	17.23	9.01	1.08	0.30	0.12
	1.52	0.07	1.02	1.98	0.02	1.27	1.34	0.34	0.33	0.11
5	48.03	0.42	10.30	12.69	0.21	15.88	11.28	0.98	0.13	0.06
	1.10	0.09	1.69	0.69	0.03	0.61	1.24	0.21	0.07	0.08
6	42.70	0.23	10.72	19.73	0.23	18.26	7.13	0.88	0.08	0.06
	2.71	0.14	2.97	3.26	0.04	5.41	2.42	0.33	0.09	0.07
7	45.28	0.28	11.45	15.16	0.22	17.65	8.76	0.97	0.15	0.08
	2.80	0.14	2.62	3.82	0.04	5.99	2.59	0.31	0.19	0.08
8	44.41	0.21	16.19	14.76	0.17	12.50	10.05	1.50	0.13	0.09
	8.03	0.09	4.23	4.04	0.05	4.10	2.44	0.57	0.09	0.08
9	48.63	0.34	16.36	9.99	0.17	10.60	12.07	1.59	0.16	0.09
	1.43	0.09	1.74	1.78	0.03	2.01	1.88	0.41	0.08	0.07
10	47.55	0.32	16.95	11.63	0.16	9.47	12.06	1.57	0.16	0.12
	1.31	0.06	1.77	1.26	0.02	1.85	1.05	0.47	0.15	0.08

(continued)

Table 5.6 (continued)

Rock group	SiO_2	TiO_2	Al_2O_3	FeO*	MnO	MgO	CaO	Na_2O	K_2O	P_2O_5
11	48.37	0.30	17.15	9.59	0.17	10.63	11.90	1.63	0.16	0.10
	1.64	0.10	1.85	1.82	0.02	2.04	1.58	0.43	0.10	0.08
12	47.77	0.18	22.39	7.42	0.11	7.98	11.73	2.09	0.25	0.06
	1.17	0.07	1.17	0.86	0.02	1.07	0.82	0.29	0.08	0.07
13	49.28	0.35	20.38	8.06	0.14	7.31	11.76	2.30	0.30	0.12
	1.40	0.32	0.76	1.31	0.02	0.85	1.31	0.56	0.34	0.12
14	48.95	0.45	24.30	7.49	0.12	3.33	11.94	2.63	0.69	0.10
	1.50	0.42	3.16	1.68	0.05	2.55	1.20	0.15	0.48	0.09
15	48.19	0.24	20.20	10.58	0.13	6.70	11.60	2.00	0.29	0.07
	1.17	0.06	1.12	2.29	0.03	0.71	1.32	0.24	0.20	0.07
16	47.71	0.25	27.08	7.49	0.08	1.53	12.31	2.62	0.84	0.09
	0.64	0.14	1.30	0.71	0.05	0.61	1.43	0.25	0.45	0.09
17	48.91	0.30	22.22	7.11	0.13	6.70	11.94	2.25	0.35	0.09
	1.41	0.28	2.33	1.60	0.03	2.27	1.06	0.42	0.31	0.09
18	49.85	0.49	10.27	13.15	0.25	15.04	9.83	0.96	0.10	0.07
	2.01	0.15	1.02	2.14	0.06	1.06	0.87	0.29	0.08	0.06
19	47.63	0.71	6.79	17.89	0.26	15.53	10.19	0.70	0.14	0.16
	2.33	0.33	3.59	3.14	0.04	3.37	4.22	0.35	0.12	0.22
20	49.37	0.64	8.19	14.57	0.26	15.64	10.26	0.81	0.13	0.13
	2.10	0.31	3.34	3.04	0.05	2.75	3.41	0.34	0.10	0.18
21	49.99	0.48	14.91	11.62	0.18	9.70	11.44	1.39	0.14	0.15
	0.90	0.15	2.80	2.58	0.02	2.09	1.20	0.58	0.07	0.03
22	47.96	0.41	15.15	18.05	0.20	8.25	8.51	1.24	0.14	0.10
	2.05	0.08	3.13	2.26	0.05	3.53	4.06	0.72	0.10	0.08
23	50.56	0.47	15.36	11.90	0.20	9.36	10.53	1.35	0.14	0.13
	1.60	0.14	2.60	2.94	0.05	2.52	2.67	0.60	0.08	0.06
24	48.56	0.98	15.41	12.91	0.20	7.46	12.24	1.62	0.37	0.24
	1.75	1.03	1.93	3.79	0.05	2.43	2.52	0.35	0.37	0.26

Remarks: Layered series: 1 – Pl-lherzolit and olivinite (n = 3); 2 – Pl-lherzolite, olivinite and ore-bearing wehrlite chứa quặng (n = 9); 3 – an average of 1 and 2; 4 – melanotroctolite and olivine melanogabbronorite (n = 5); 5 – melanogabbronorite (n = 5); 6 – melanotroctolite and olivine-ore bearing- melanogabbronorite (n = 10); 7- an average of 4, 5 and 6 (n = 20); 8 – mesotroctolite, gabbronorite and olivine gabbro (n = 24); 9 – mesogabbronorite and gabbro (n = 45); ore-bearing mesogabbroid (n = 25); 11 – an average of 8, 9 and 10 (n = 94); 12 – leucotroctolite and olivine leucogabbronorite (n = 15); 13 – olivine-free gabbronorite (n = 11); 14 – anorthosite (n = 8); 15 – ore-bearing leucogabbro (n = 6); 16 – ore-bearing anorthosite (n = 3); 17 – an average of 12, 13, 14, 15 and 16 (n = 47). P*egmatoidic series*: 18 – websterite and pegmatite-type melanogabbronorite (n =4); 19 – ore-bearing melanograbbronorite (n =7); 20 – an average of 18 and 19 (n = 11); 21 – mesogabbronorite pegmatite-type gabbro (n = 7); 22 – ore-bearing mesogabbronorite pegmatite-type gabbro (n = 4); 23 –an average of 21 and 22 (n = 11); 24 – inner contact gabbroid (n = 9)

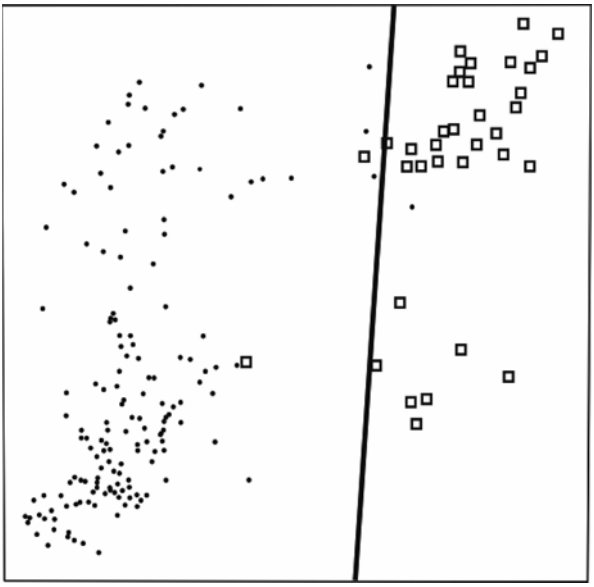

Fig. 5.6 Non-linear correlation of evolved magma (*small black dots*) and pegmatoidic series (*squares*)

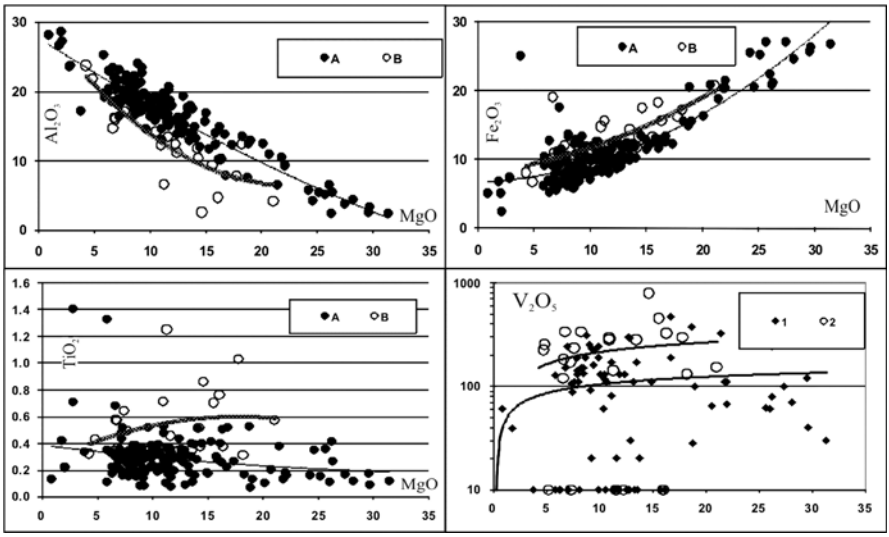

Fig. 5.7 Correlation between major and trace elements in evolved (*A, 1*) and pegmatoid (*B, 2*) magma series

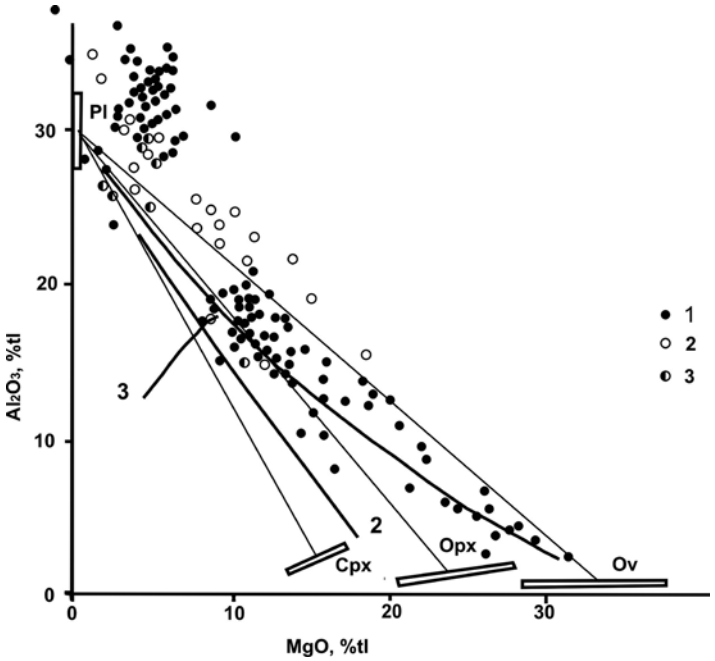

Fig. 5.8 *1*- Layered series; *2*- pegmatoid series; *3*- gabbroid of inner contact zone; direction of mineralogical variation: *Ol* – olivine, *Pl* – plagioclase, *Cpx* – clinopyroxene, *Opx* – orthopyroxene; *thick, dark lines*: evolutional trend of evolved magma series (*1*), pegmatoid (*2*) and inner contact zone (*3*); *thin lines*: division lines of Ol-Pl, Opx-Pl, and Cpx-Pl

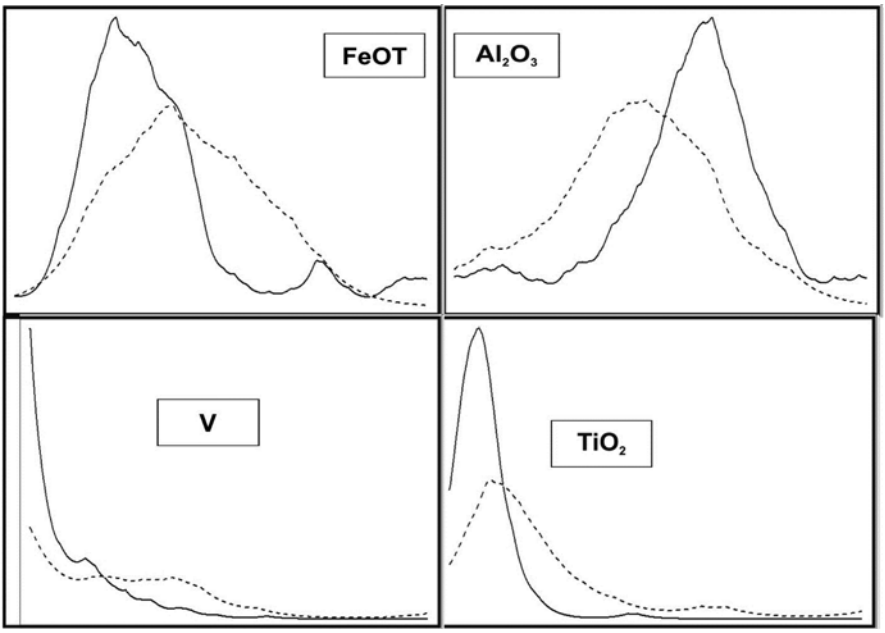

Fig. 5.9 Elemental distribution scheme of layered series (*continuous line*) and pegmatoidic series (*dashed line*)

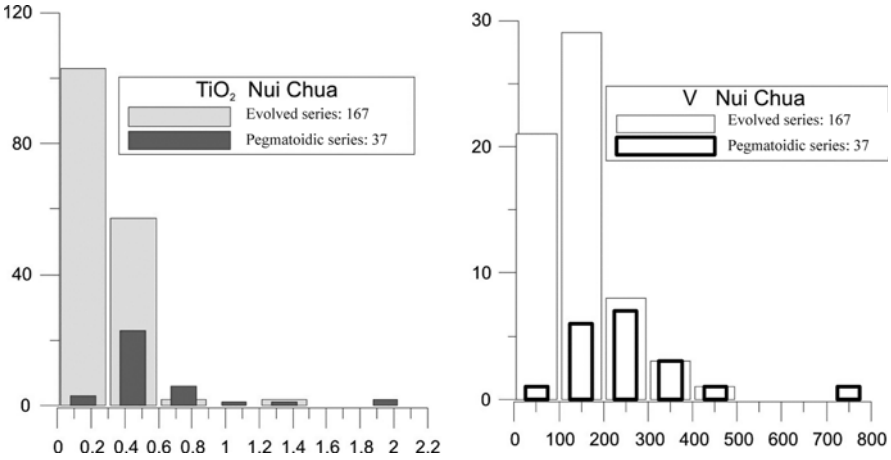

Fig. 5.10 TiO_2 and V_2O_5 histograms for evolved series (*empty*) and pegmatoidic series (*filled*)

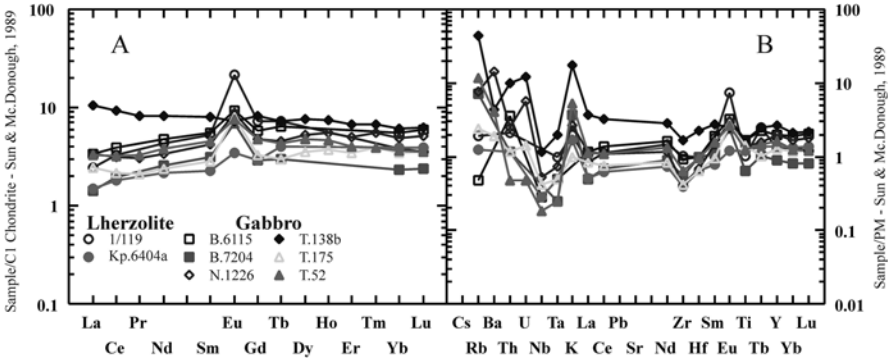

Fig. 5.11 Chondrite normalized rare earth (**a**) and primitive mantle (**b**) normalized trace element distribution patterns for Permian – Triassic layered mafic – ultramafic magmas

Al from low to mid- and high, and high Mg. The magmas have high concentrations of Cu, Ni, Co, occasionally high Cr and V, while having low Rb, Sr, Nb, Zr, Y, Ta, Th, U and the rare earths.

Chondrite normalized rare earth element distribution patterns shown in Fig. 5.11a reveal a similarity in distribution configuration among plutons in different structures especially the homogeneous depletion of light relatively to heavy rare earths and a slightly positive anomaly at Eu. Primitive mantle normalized trace element configuration (Fig. 5.11b) shows extreme depletion of Nb, Ta, La, Ce and Zr and relative enrichment at K, Sr and Eu. The trace element distribution features suggest that the layered intrusive rocks reflect both tholeiitic-type mafic-ultramafic magmas and subduction-related calc-alkaline type.

Table 5.7 Chemical compositions (wt% by XRF) and trace element abundances (ppm, by ICP-MS) for gabbro – peridotite plutons in Northwestern Vietnam (After Thanh et al. 2004)

Sample	T175	B6115	Kp6404a	T138b	T52	N1266	1/119	B7204
Rock type	Gabbro	Gabbro	Lherzolite	Gabbro	Gabbro	Gabbro	Lherzolite	Gabbro
Pluton	Núi Chúa	Núi Chúa	Núi Chúa	Khao Quế	Tri Năng	Yên Chu	Yên Chu	Yên Chu
SiO_2	48.15	48.02	41.82	48.61	49.06	49.54	39.12	44.47
TiO_2	0.31	0.36	0.26	0.36	0.27	0.30	0.22	0.14
Al_2O_3	15.48	16.56	5.27	14.92	17.97	15.79	7.15	25.73
Fe_2O_3*	9.30	8.49	21.09	11.16	4.62	14.06	10.27	4.55
MnO	0.17	0.17	0.25	0.11	0.09	0.22	0.16	0.13
MgO	12.19	11.23	25.98	10.34	9.06	9.55	30.65	6.72
CaO	11.25	12.89	5.45	15.19	13.35	14.26	5.53	15.15
Na_2O	1.45	1.94	0.46	1.34	2.50	1.42	0.56	1.29
K_2O	0.03	0.00	0.05	0.53	0.16	0.08	0.06	0.11
P_2O_5	0.03	0.16	0.02	0.03	0.02	0.01	0.07	0.20
LOI		0.12	0.66	2.21		1.46	6.01	1.54
Total	98.36	99.94	101.31	104.80	97.10	106.69	99.80	100.03
Cu	52.95	57.00	1038.00	945.20	153.80	59.98	107.00	65.00
Ni	149.40	190.00	1021.00	284.00	74.97	85.20	1160.00	80.00
Co	45.04	46.00	118.00	53.87	26.07	26.87	88.00	20.00
V	199.00		78.00	190.00	142.20	418.70	55.00	50.00
Cr	555.50	630.00	616.00	300.00	1182.00	157.10	294.00	75.00
Rb	1.50	0.30	0.80	27.44	7.33	4.90	1.20	4.50
Y	5.89	9.10	6.20	12.01	7.29	8.82	5.90	4.00
Zr	4.70	10.50	4.40	18.62	7.24	4.61	11.50	6.00
Nb	0.30	0.20	0.20	0.83	0.13	0.38	0.00	0.00
Ba	13.18			30.81	28.68	100.30		
La	0.58	0.80	0.35	2.51	0.77	0.80	0.58	0.34
Ce	1.33	2.40	1.10	5.69	1.95	1.91	2.00	1.20
Pr	0.20			0.78	0.31	0.29		
Nd	1.12	2.20	1.00	3.79	1.79	1.59	2.00	1.20
Sm	0.43	0.84	0.35	1.23	0.70	0.64	0.80	0.48
Eu	0.46	0.54	0.20	0.42	0.44	0.51	1.24	0.40
Gd	0.68	1.20	0.60	1.68	0.99	0.99	1.50	0.60
Tb	0.11	0.24	0.15	0.27	0.16	0.17	0.27	0.11
Dy	0.91			1.93	1.22	1.35		
Ho	0.21			0.42	0.26	0.31		
Er	0.57			1.11	0.67	0.83		
Tm	0.10			0.17	0.10	0.14		
Yb	0.58	0.95	0.66	1.03	0.62	0.83	0.65	0.40
Lu	0.09	0.15	0.10	0.16	0.09	0.13	0.09	0.06
Hf	0.20	0.30	0.20	0.69	0.29	0.21	0.30	0.30
Ta	0.02	0.02	0.02	0.08	0.01	0.03	0.04	0.01
Th	0.10	0.30	0.10	0.83	0.04	0.21	0.18	0.10
U	0.03			0.25	0.01	0.12		

5.1.1.4 Composition of Primitive Melt and Modeling of Magma Generation

Determination of chemical composition of the primitive melts of mafic and ultramafic plutonic magmas having undergone complicated differentiation and modeling the magma generation are the most complex petrologic tasks. For the case of Lo Gam layered intrusive magmas with Nui Chua block being a representative example the complexity is, within a plutonic body aside from evolved magma series there are mafic – ultramafic pegmatoidic series, which also play important roles in the pluton formation. Determination of primitive melts was conducted separately for both evolved and pegmatoidic series while taking common source sharing and phase relationship between the two magma types.

To estimate the composition of primitive melt of an evolved magma series an average chemical composition of the whole magma series or average of each separate magmatic phase were taken for calculation. In some case chemical composition of melt inclusions within a given plutonic body was taken as representative. A representative composition, that is most corresponding to actual observation, determined using one of the above methods may be evaluated by software 'pluton' created at the Institute of Geology and Mineral resources, Siberian branch, Russian Academy of Sciences (Lavrenchuc et al. 2002). Input data for the modeling calculation includes appearance order of liquidus minerals and their compositions, depth of pluton formation and water contents of the melt. For the Nui Chua evolved series liquidus minerals appeared following order: olivine, plagioclase and pyroxene. The most significant feature of this magma series is the presence of eroded-texture orthopyroxene (pigeonite). It is estimated that formation depth of evolved magma series may not exceed 2 Kbar for hornfels are observed in the inner contact zone while surrounding rocks are low grade metamorphic types. There may be an amount of water present in the primitive melt for there is a small amount of hornblende and phlogopite in the accessory mineral assemblage. If averages of chemical composition of the evolved and pegmatoidic magma series are viewed as corresponding primitive melts, model composition of the magmas may be illustrated in Fig. 5.12. In this case there is a large difference in both major and trace element concentrations between the model and actual compositions. The similar difference is also noticed should modeling calculation be taken an average composition of evolved magmas as primitive melt.

The modeling calculation showed better results should a Permian, relatively low Ti-basalt (sample M-001) occurred in the Song Hien structure be presented as primitive melt. The basalt may be viewed as co-magma of the evolved series of the Nui Chua pluton because age of basaltic magmas in the Cao Bang area is (about) Permian and having similar geochemical characteristics to those in the Song Hien structure. The similarity may be illustrated by comparing trace element configuration patterns of Song Hien basalts and Nui Chua evolved magma series (Fig. 5.13), with Nb and Ta having large negative anomalies.

The calculation results show that, generally Song Hien Permian basalts and Nui Chua evolved magma series belong to a similar mafic type having arc-related geo-

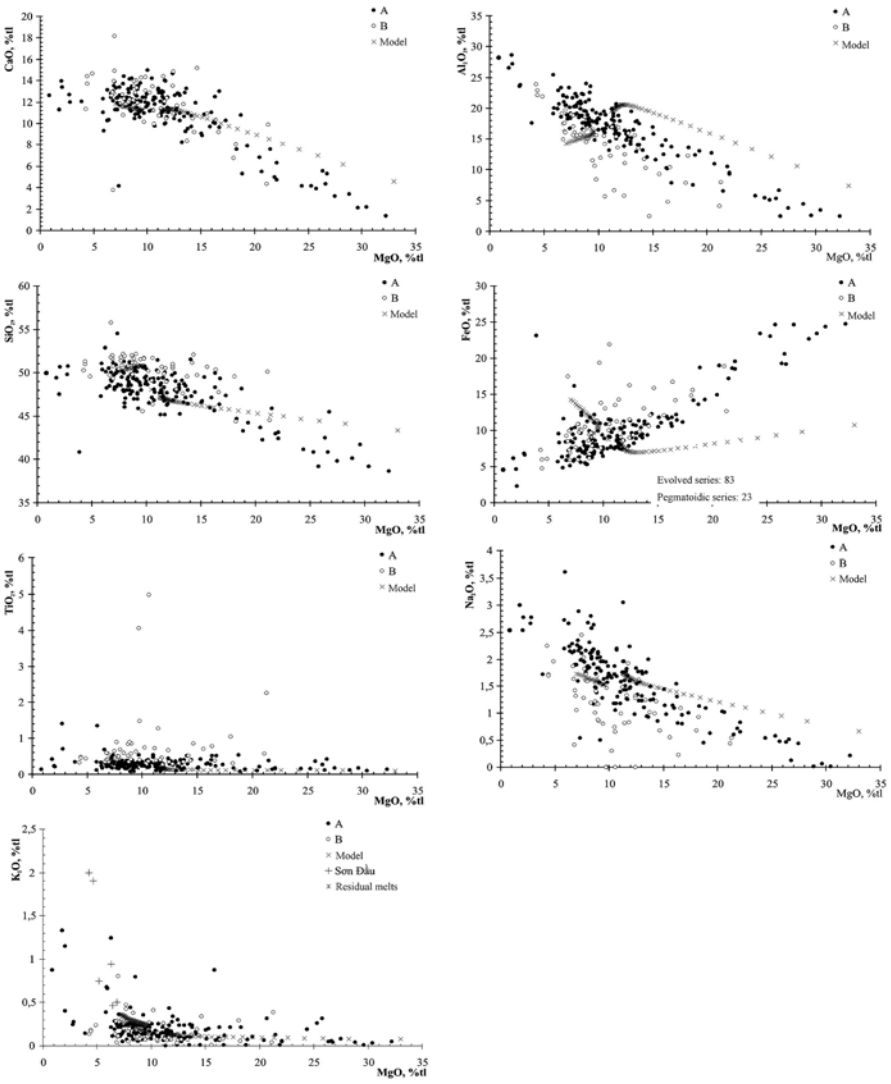

Fig. 5.12 Chemical compositions of Nui Chua evolved (*A*) and pegmatoidic (*B*) magma series and model composition calculated as average of *A* and *B*

chemical signatures. However, while the Song Hien basalts are characterized by Sr and Eu negative anomaly the Nui Chua gabbroids in contrast show positive anomalies at these elements. The difference may be explained by plagioclase fractionation at transitional magma chambers. In this case, Nui Chua block may be viewed as a transitional magma chamber where gabbroids being enriched in Sr and Eu by plagioclase cumulates while Song Hien basalts may be viewed as residual melts erupted from the (Nui Chua) transitional magma chamber. The primitive melt in the transi-

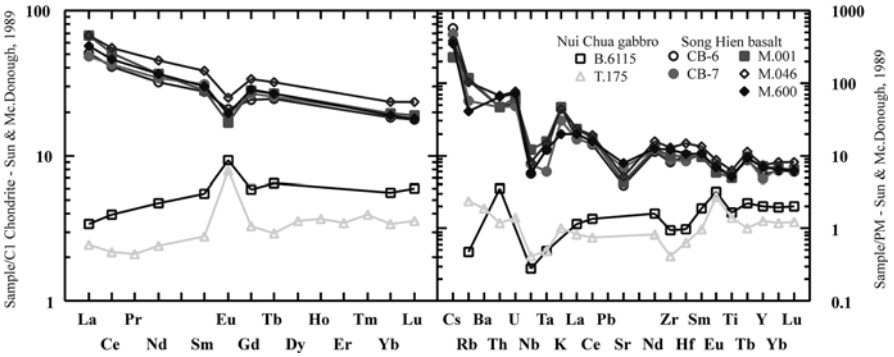

Fig. 5.13 Comparison of rare earth (*left*) and trace element (*right*) configuration patterns between Nui Chua gabbroids and Song Hien basalts

tional chamber (as hypothesized) may be a chemical composition lying between Song Hien basalt and early cumulates of Nui Chua evolved magma series.

Results of the modeling calculation basing fractional crystallization process of a melt having chemical composition similar to the basalt M-001 (primitive melt calculated basing on the chemical composition is given in Table 5.8) showing liquid phase crystallization in the following order olivine + plagioclase → plagioclase + clinopyroxene. This crystallization order is in fact being commonly observed for the middle and upper sections in the Nui Chua block. For this chemical composition to apply for the whole Nui Chua evolved magma series it needs to add 10 % of olivine (viewed as the first crystallized mineral) of $Fo_{70–75}$. This concept is closely coincided with actual observation if the possibility of increasing ultramafic magma components with depths under yet exposed Nui Chua block. It has been determined using the similar chemical composition for modeling calculation would produce a magma having petrologic and geochemical properties mostly coincident with actual magmas of the Nui Chua evolved series (Fig. 5.12).

The modeling calculated compositions of the minerals are in fact coincident with the actual observation (Table 5.9). The calculation shows that the fractionation process occurred in a transitional magma chamber having the preferred composition would form an alkali-rich residual melt, and minerals crystallized from this melt and corresponding late cumulates would have a chemical composition closely similar to monzodiorite magma series.

In fact, magmas having a similar chemical composition were found in small intrusive, satellite bodies in western wing of the Nui Chua block, most representative example is at the Son Dau pluton. Magmas having comparable chemical composition with monzodiorite in pegmatoidic series in other plutons (such as Khao Que and Yen Chu) within the Nui Chua block are expressed as an average composition of pegmatoidic series of this block (Table 5.10). The calculation results show that during fractional crystallization process residual melt and late cumulate crystals are enriched in titanium, this explains the formation of titanomagnetite – ilmenite mineralization related to taxitic gabbroids and pegmatoids in the northeast and northwest of Nui Chua block such as Cay Tram mine and Na Hoe ore-site.

Table 5.8 Chemical composition of Song Hien basalts and modeling calculated composition based on basalt sample M-001 viewed as primitive melt composition of Nui Chua evolved and pegmatoidic magma series

	SiO_2	TiO_2	Al_2O_3	FeO*	MnO	MgO	CaO	Na_2O	K_2O	P_2O_5
M001	49.35	1.14	15.53	10.68	0.20	8.70	10.71	2.11	1.45	0.13
Olivine	38.38	0.00	0.00	25.37	0.00	36.25	0.00	0.00	0.00	0.00
M001 + 10 % Olivine	48.25	1.02	13.98	12.15	0.18	11.46	9.64	1.90	1.31	0.11
M001 + 10 % Olivine, f = 0,3	49.08	1.40	14.22	13.89	0.00	6.59	10.74	2.18	1.73	0.15

Remarks: M001- Song Hien belt relatively low-Ti basalt; olivine- composition of early olivine cumulate; M001 + 10 % olivine – hypothesized primitive melt of the Nui Chua evolved series; M001 + 10 % olivine, f = 0.3- hypothesized primitive melt of the Nui Chua pegmatoidic series (composition of the basalt M001 + 10 % olivine having been fractionated 30 %)

Table 5.9 Modeling calculated actual composition of minerals in Nui Chua evolved magma series

Mineral composition	Ol, Mg#	Px, Mg#	Pl, An%
Actual	60–80		65–75
Calculated	76–85	48–68	70–77

Table 5.10 Average chemical composition of evolved (A) and pegmatoidic (B) series of North Vietnam gabbro-peridotite plutons

Pluton			SiO_2	TiO_2	Al_2O_3	FeO*	MnO	MgO	CaO	Na_2O	K_2O	P_2O_5	n
Nui Chua	A	X	47.89	0.29	17.11	10.01	0.17	11.50	11.07	1.65	0.22	0.09	165
		S	7.71	0.03	26.92	20.92	0.00	34.99	7.51	0.45	0.06	0.01	
	B	X	50.59	0.73	14.22	10.75	0.21	10.19	11.76	1.16	0.24	0.16	24
		S	5.69	0.63	21.56	13.20	0.00	16.09	6.39	0.32	0.14	0.01	
Khao Que	A	X	47.62	0.28	16.35	5.67	0.15	12.52	15.98	1.01	0.22	0.20	98
		S	2.55	0.05	23.07	9.68	0.00	33.79	8.09	0.31	0.04	0.00	
	B	X	46.77	1.28	14.41		0.17	5.50	16.66	1.73	0.91	0.35	18
		S	5.29	0.56	14.53		0.00	6.17	17.77	0.96	0.54	0.03	
Tri Nang	A	X	48.43	0.23	18.13	5.80	0.15	11.50	13.76	1.60	0.24	0.16	118
		S	5.76	0.02	25.64	9.17	0.00	41.93	9.74	0.68	0.06	0.00	
	B	X	49.16	0.53	13.11		0.15	10.07	16.00	1.39	0.20	0.21	16
		S	3.56	0.08	28.98		0.00	5.81	11.57	0.57	0.02	0.01	
Yen Chu	A	X	45.40	0.24	17.40	6.69	0.15	15.98	12.86	0.84	0.25	0.19	47
		S	7.58	0.04	43.77	6.11	0.00	124.01	22.95	0.26	0.07	0.01	
	B	X	50.72	0.38	11.40		0.18	11.45	12.48	1.41	0.59	0.20	9
		S	5.21	0.01	10.59		0.00	11.08	14.76	0.59	0.16	0.01	

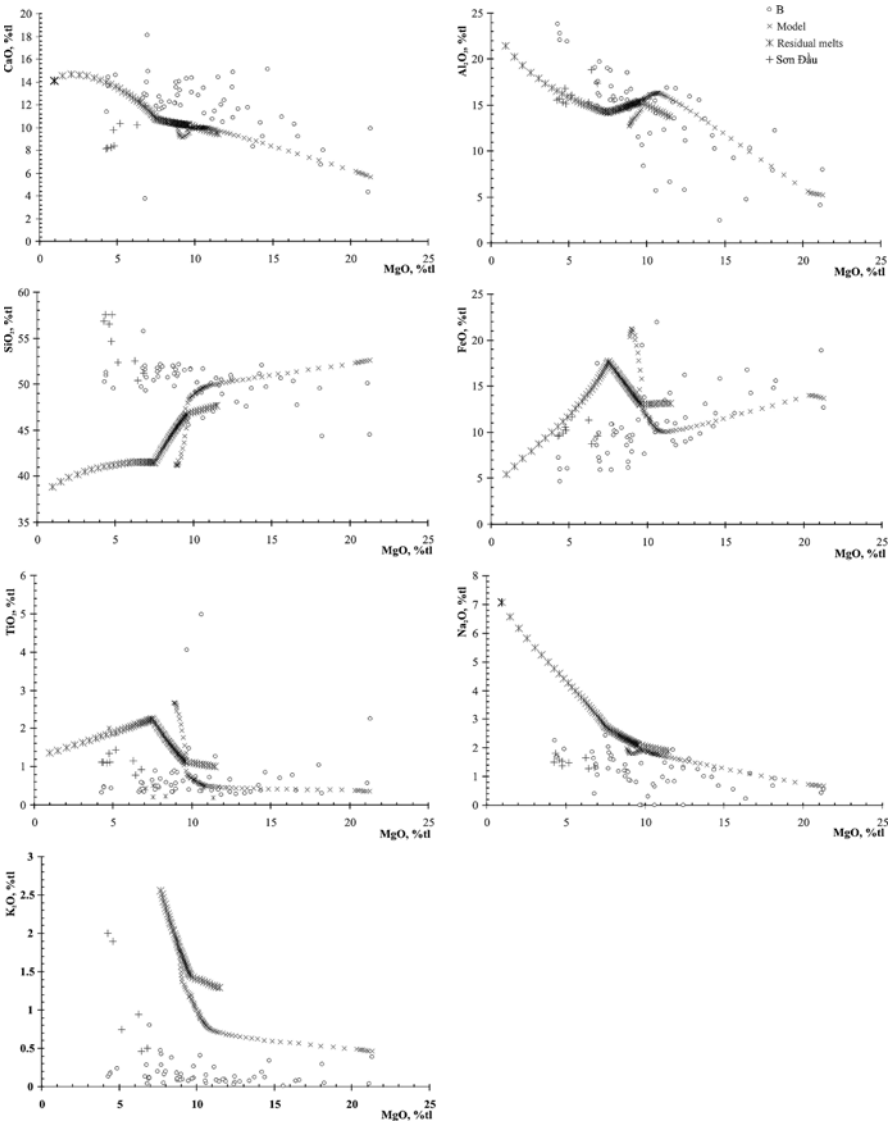

Fig. 5.14 Chemical compositions of Nui Chua pegmatoidic series (*B*) and modeling composition calculated based on basalt M001 + 10 % olivine having been fractionated 30 %

We have modeled for Nui Chua pegmatoidic formation. As mentioned above the Nui Chua evolved magma series are olivine-free. The modeling shows that olivine disappears as the fractional crystallization (differentiation) process of the primitive melts reaching 30 %. Therefore, to model the pegmatoidic series it is essential that residual melt after 30 % differentiation be considered as parental melt of the pegmatoidic magma series. Although the achieved compositions of magma types are slightly different as compared with the actual compositions with regard to SiO_2, FeO, K_2O contents, however, the CaO, MgO, Na_2O and TiO_2 are closely matched (Fig. 5.14).

Therefore, the modeling suggests that the formation of Nui Chua pegmatoidic series was genetically related to the evolved magma series in that the pegmatoidic magma series may be viewed as residual melts that evolved toward higher alkalis and Ti. This is evidenced by the presence of monzodiorites along with other pegmatoids in several plutons (Khao Que and Yen Chu) within the Nui Chua complex. On the other hand, increase of alkaline metals may be evidenced by the increase of orthoclase components in plagioclase in Nui Chua pegmatoidic-type gabbronorite. Moreover, biotite-gabbro and monzodiorite occurred as small intrusive satellites such as Son Dau body in western Nui Chua may be genetically related to the pegmatoidic series.

5.1.2 Phia Bioc-Type High-Al Granites

5.1.2.1 Distribution, Geological Structure and Formation Age

Outcrops of Permian – Triassic high-Al granites, previously grouped to Triassic Phia Bioc complex, are common in folded structures in marginal regions of Song Chay anticlinoria. The most representative of high-Al granite bodies are Phia Bioc and Tam Tao located in the boundary between Phu Ngu and Lo Gam structures (Fig. 5.1). Also, there are a number of smaller bodies outcropped in the west of Lo Gam belt; these bodies are being described in The (1999). High-Al granites are also found in the southeast of Song Da structure where Kim Boi massif is representative.

Basically high-Al granite massifs in northeast Vietnam have similar geological structure and petrologic composition showing mostly porphyry biotite-granite with color varying in a range of brightness and a minor amount of two-mica granite. Granite magmas having chemical composition comparable with quartz-diorite and biotite-granite are also common. Dyke phase containing aplite-granite, sometimes pegmatite, are commonly found. Northeastern Vietnam granite massifs show clear cut-crossing Ordovician – Silurian or Devonian terrigenous sediments (in northeastern region) and Permian mafic (basalt and andesite) volcanics in the Song Da structure (by Kim Boi massif) causing hornfels metamorphism the surrounding rocks forming contact metamorphic zones containing pyroxene and cordierite hornfels having up to thousands of meters wide (Dovjikov 1965; Tri 1977).

Age determination of Phia Bioc- type granite is essential for the magma is widely spread in many geological structures in northeastern Vietnam, which was previously believed to be orogeny-induced magmatism and grouped with Nui Chua-type gabbro-peridotite complex that was viewed as late Triassic gabbro-granite series (Dovjikov 1965; Thuc and Trung 1995). As mentioned above, if the Nui Chua gabbro complex belonged to a Permian – Triassic magmatic period, which magmatic stage that the Phia Bioc-type high-Al granite belonged to?

Radiometric age dating for the high-Al granites were conducted on two samples collected at Tam Tao massif in the Lo Gam structure (sample H-1531/1) and at Kim Boi massif in the Song Da structure (sample HB-0601). A biotite granite from Tam

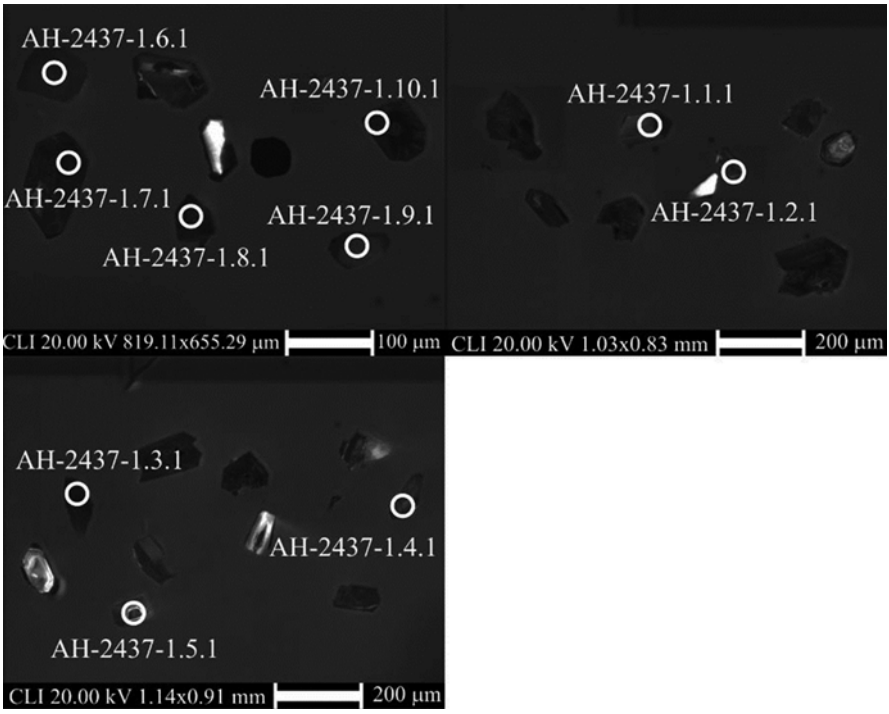

Photo 5.1 Back-scattered images of zirons separated from a gabbronorite from Nui Chua block. Sample AH-2437-1. See Table 5.1 for corresponding isotopic compositions

Tao massif in the Cho Don area was dated by Ar/Ar that yielded 250 ± 0.5 Ma (Hoa et al. 2005; Anh and Hang 2005), suggesting that high-Al granites were formed slightly later relative to the Nui Chua gabbroids. Second sample is medium –grained, weakly porphyry biotite- granite, having phenocrysts of K-feldspar and plagioclase, collected from Kim Boi massif that was dated by U-Pb isotopic method on zircons using a SHRIMP. The typical high-Al metallic phase is cordierite, sometimes garnet. The chemical composition of granite (sample HB-06-01) is (wt.%): $SiO_2 = 73.72$, $TiO_2 = 0.11$, $Al_2O_3 = 13.91$, $Fe_2O_3 = 1.79$; $MnO = 0.023$, $MgO = 0.16$, $CaO = 0.60$, $Na_2O = 3.55$, $K_2O = 5.75$, $P_2O_5 = 0.024$. The analyzed zircon grains separated from the Kim Boi granite are large-sized, short-cubic, rhythm-zoned crystals or their fragments (Photo 5.1). The U concentrations vary between 160 and 1700 ppm, Th varies between 70 and 1000 ppm, and $^{232}Th/^{238}U$ ratios vary within a narrow range of 0.45–0.7 (Table 5.11).

A concordant age calculated for all the analyzed zircons yielded an early Triassic age (242.4 ± 2.2 Ma, MSWD = 0.035) (Fig. 5.15). In summary, analyzed ages suggest Phia Bioc high-Al granite is corresponding to the early Triassic. The age, with an acceptable error, is contemporaneous with Nui Chua –type gabbroids in the Phu Ngu belt and gabbro-syenite intrusive magmas in the Lo Gam belt (see below). However, geological literature has shown that the gabbroids in two intrusive belts occurred much earlier than the high-Al granite.

Table 5.11 U-Pb compositions of zircons from Kim Boi granite HB-06-01

Analyzed points	% $^{206}Pb_c$	ppmU	ppmTh	$^{232}Th/^{238}U$	ppm $^{206}Pb^*$	(1) $^{206}Pb/^{238}U$ Age		(1) $^{207}Pb/^{206}Pb$ Age		% Discordant	Total $^{238}U/^{206}Pb$	±%
HB-06-01.1.1	2.70	330	144	0.45	11.2	243.1	±4.1	−271	±670	−211	25.32	1.2
HB-06-01.2.1	3.21	343	152	0.46	11.7	242.5	±3.3	−24	±550	−110	25.25	1.1
HB-06-01.3.1	1.46	544	368	0.70	18.2	242.9	±2.7	297	±290	22	25.67	0.92
HB-06-01.4.1	6.42	1701	1018	0.62	55	223.4	±1.9	192	±270	−14	26.55	0.57
HB-06-01.5.1	5.08	272	156	0.59	9.38	241.3	±4.5	−330	±1000	−236	24.89	1.3
HB-06-01.6.1	2.62	349	182	0.54	12	246.6	±3.8	−17	±470	−107	24.98	1.1
HB-06-01.7.1	2.37	744	404	0.56	24.9	240.8	±2.4	275	±290	14	25.65	0.8
HB-06-01.8.1	5.24	162	71	0.45	5.56	239	±7.1	5	±1100	−98	25.1	1.6
HB-06-01.9.1	1.10	530	572	1.11	17.6	241.2	±2.4	512	±220	112	25.94	0.94
HB-06-01.10.1	2.76	349	237	0.70	11.9	244.4	±3.4	4	±450	−99	25.17	1.1

Analyzed points	Total $^{207}Pb/^{206}Pb$	±%	(1) $^{238}U/^{206}Pb^*$	±%	(1) $^{207}Pb^*/^{206}Pb^*$	±%	(1) $^{207}Pb^*/^{235}U$	±%	(1) $^{206}Pb^*/^{238}U$	±%	Err. corr
HB-06-01.1.1	0.0631	6.1	26.03	1.7	0.041	26	0.219	26	0.03843	1.7	.064
HB-06-01.2.1	0.0715	11	26.09	1.4	0.046	23	0.241	23	0.03833	1.4	.061
HB-06-01.3.1	0.0639	5.5	26.05	1.1	0.0523	13	0.277	13	0.0384	1.1	.091
HB-06-01.4.1	0.1014	2.6	28.37	0.85	0.05	12	0.243	12	0.03526	0.85	.072
HB-06-01.5.1	0.082	13	26.23	1.9	0.04	40	0.212	40	0.03814	1.9	.048
HB-06-01.6.1	0.0668	3.5	25.65	1.6	0.0457	19	0.246	20	0.03899	1.6	.080
HB-06-01.7.1	0.0707	5.8	26.28	1	0.0518	13	0.272	13	0.03806	1	.080
HB-06-01.8.1	0.0883	6.2	26.49	3	0.046	47	0.24	47	0.0378	3	.065
HB-06-01.9.1	0.0662	6.7	26.23	1	0.0575	9.9	0.302	10	0.03813	1	.104
HB-06-01.10.1	0.0684	7.2	25.88	1.4	0.0461	19	0.246	19	0.03864	1.4	.077

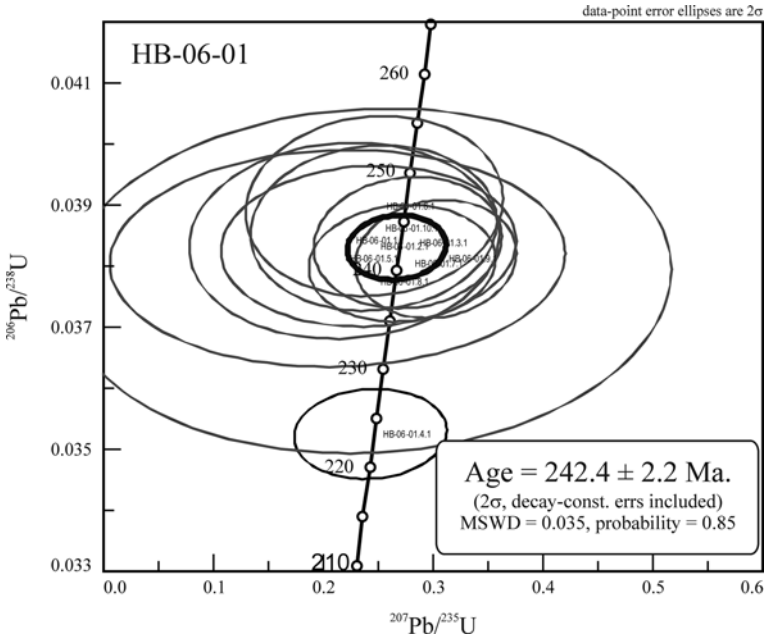

Fig. 5.15 Concordia age diagram of zircons from Kim Boi granite sample HB-06-01

5.1.2.2 Mineralogical, Geochemical and Isotopic Characteristics

Mineralogical compositions of the high-Al granites are rather monotonous and closely similar with each other even from different intrusive bodies, including mostly the following mineral assemblage: quartz + K-feldspar + plagioclase + biotite ± muscovite. High-Al minerals include garnet and cordierite, where garnet is characterized by intrusive magmas in northeastern Vietnam; cordierite is present in Kim Boi massif in the Song Da structure. Popular accessory minerals include zircon and tourmaline (in dyke phases). Biotite in Phia Bioc-type high-Al granite is characteristically brownish-red, chemically high titanium (TiO_2 = 3.02–4.05 wt%), high iron (FeO = 23.7–26.92 wt%) and relatively high aluminum (Al_2O_3 = 16.29–18.11 wt%), most similar to biotite in high-Al granitoids (Hoa et al. 1996). Garnet is common in Phia Bioc-type granite, especially in the bright-colored type, having composition corresponding to almandine (The 1999). Cordierite is found in Kim Boi granite, being recognized only under polarized microscope.

Representative chemical compositions and trace element abundances of Kim Boi and Phia Bioc granitoids are shown in Table 5.12 Basically the chemical compositions are correspondent to granite (SiO_2 = 68–71 wt%), although there are some higher silicic contents comparable to quartz diorite and granodiorite (SiO_2 = 62–65 wt%). As a results Mg and Ca in the granitoids are relatively high (Table 5.12). The total alkalis vary within a wide range, from low alkaline series via medium to high alkaline series ($Na_2O + K_2O$ = 5.47–9.16 wt%). All the magmas show K higher than Na.

Chondrite rare earth and primitive mantle normalized trace element patterns of the granitoids showing similar configuration among magmas from different blocks that they are highly enriched in light rare earths relative to the heavy elements and clearly depleted in Eu (Fig. 5.16a) (after Sun and McDonough 1989).

Table 5.12 Chemical compositions (by XRF, wt%) and trace element abundances (by ICP-MS, ppm) of Phia Bioc, Tam Tao and Kim Boi high-Al granites (Hoa 2008)

Samples	H 1531/1	PB 4	218/76	213/76	228A/76
Massif	Tam Tao	Tam Tao	Phia Bioc	Phia Bioc	Phia Bioc
SiO_2	62.68	68.32	68.72	63.83	71.45
TiO_2	1.1	0.3	0.39	1.26	0.12
Al_2O_3	14.74	14.05	14.79	15.42	15.14
Fe_2O_3*	8.11	6.47	3	6.7	1.42
MnO	0.1	0.07	0.04	0.08	0.05
MgO	2.08	1.04	0.77	1.82	0.26
CaO	3.59	2.17	1.48	3.27	0.63
Na_2O	2.85	2.46	2.37	2.89	2.44
K_2O	3.69	4	6.58	2.58	6.72
P_2O_5	0.2	0.22	0.16	0.33	0.13
LOI	0.9	1.14	1.37	1.73	1.87
Total	100.04	99.6	99.67	99.91	100.23
Rb	110	227	292	217	254
Sr	180	100	132	126	58
Y	65	49	33.5	30.3	38.7
Zr	378	263	228	242	109
Nb	21	25	13.7	23.8	7.8
Ba	628	516	824	289	169
La	54	62	38.97	43.38	19.74
Ce	99	110	75.27	89.38	40.03
Pr			8.71	11.81	4.68
Nd	43	43	30.69	45.2	18.76
Sm	7.3	10.5	5.82	11.14	4.05
Eu	1.3	1.3	1.1	1.21	0.44
Gd	6.9	6.4	5.14	10.11	4.11
Tb	1.2	1.9	0.82	1.52	0.83
Dy	7.7	10	4.63	7.84	5.89
Ho			0.93	1.46	1.42
Er			2.46	3.82	4.34
Tm		0.8	0.35	0.54	0.75
Yb	5.6	4.5	2.26	3.27	4.67
Lu	0.79	0.7	0.33	0.49	0.69
Hf	9.9	8.5	4.41	9.02	4.08
Ta	1.4	1.45	1.18	2.14	1.31
Th	31	36	23.4	10.8	10.4
U			3.5	3.1	4.3

(continued)

Table 5.12 (continued)

Samples	210/76	HB-H-41	HB-H-42	HB-H-43	HB-H-44
Massif	Phia Bioc	Kim Bôi	Kim Bôi	Kim Bôi	Kim Bôi
SiO_2	65.26	67.59	70.13	70.69	73.56
TiO_2	0.71	0.56	0.33	0.34	0.14
Al_2O_3	14.63	15.11	15.05	14.73	13.57
Fe_2O_3*	5.24	3.65	1.92	1.95	1.49
MnO	0.07	0.05	0.03	0.03	0.03
MgO	1.12	1.8	0.95	0.98	0.14
CaO	2.55	2.32	1.67	1.57	0.71
Na_2O	2.29	2.49	3.13	2.82	2.87
K_2O	5.38	3.83	4.67	4.91	5.97
P_2O_5	0.38	0.16	0.17	0.17	0.08
LOI	2.08	2.1	1.52	1.52	0.08
Total	99.71	99.66	99.57	99.71	98.64
Rb	211	183	237	249	288
Sr	132	168	143	127	45
Y	70	27	22.5	20.2	46
Zr	603	179	142	136	183
Nb	24.5	12.3	12.7	12.9	14.7
Ba	665	444	402	356	285
La	57.1	38.39	35.34	30.91	47.31
Ce	124.07	78.01	73.34	65.98	106.08
Pr	14.95	9.24	8.61	7.59	12.77
Nd	55.58	34.81	32.35	29.06	45.71
Sm	12.91	6.64	6.62	6.28	10.42
Eu	1.29	1.07	0.78	0.64	0.31
Gd	11.93	5.76	6.02	5.16	9.35
Tb	2.14	0.86	0.85	0.79	1.58
Dy	13.99	4.79	4.46	4.23	9.25
Ho	2.84	0.97	0.86	0.83	2.05
Er	8.09	2.26	2.33	2.01	5.57
Tm	1.22	0.38	0.34	0.3	0.83
Yb	8.09	2.47	1.98	1.77	5.54
Lu	1.22	0.37	0.31	0.28	0.78
Hf	21.68	5.39	4.74	4.45	6.59
Ta	2.08	1.15	1.72	1.61	1.46
Th	47	15.9	16.1	14.8	23.8
U	6.8	2.8	3.5	3.5	5.5

Remarks: Tam Tao biotite-granite: H 1531/1, PB 4 (Anh 2005); Phia Bioc granite: 218/76, 213/76, 228A/76, 210/76; Kim Boi massif: HB-H-41, HB-H-42, HB-H-443, HB-H-44 (Analyzed at the Academia Sinica, Taiwan, analyst: Tran Tuan Anh)

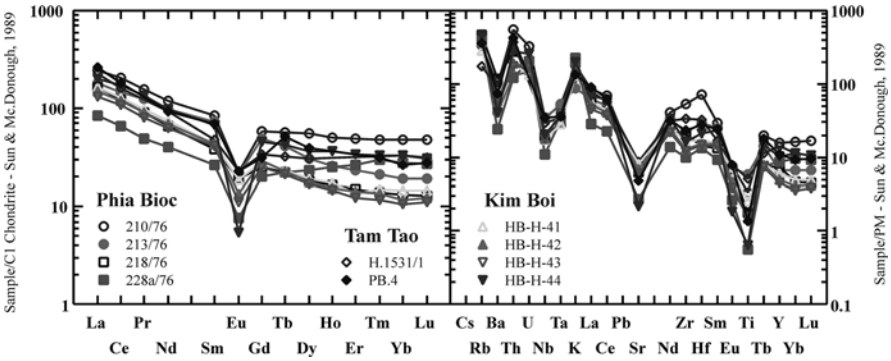

Fig. 5.16 Chondrite normalized rare earths (**a**) and primitive mantle normalized trace elements (**b**) of Phia Bioc, Tam Tao and Kim Boi granites

The granitoids are high in Rb (110–420 ppm), Ba (285–824 ppm), Y (22–70 ppm), Zr (135–595 ppm), Th (10.8–36 ppm), U (2.3–12 ppm), relatively low Nb (7.15–25 ppm, sometimes 36 ppm), Ta (0.89–2.14 ppm). Primitive mantle normalized trace element configuration shows peaks at K, Rb, Zr, Th, La, Ce and troughs at Sr, Nb and Ta, mostly similar to subduction-related calc-alkaline magmas (Fig. 5.16b).

The initial $^{87}Sr/^{86}Sr$ ratios of Permian – Triassic Phia Bioc biotite-granite vary between 0.7308 and 0.7388 and for Kim Boi type being between 0.7339 and 0.7427, accompanied by $^{143}Nd/^{144}Nd$, respectively, at 0.5119 and 0.5120, with corresponding $\varepsilon_{Nd(T)}$ at −11.11 and −13.64, respectively. These highly enriched isotopic compositions suggest that the Permian – Triassic high-Al granites are crust-origin, in agreement with above mentioned mineralogical and geochemical characteristics.

5.1.2.3 Geodynamic Setting of the Phia Bioc-Type High-Al Granite Generation

The above descriptions on block structure, petrologic- mineralogical compositions and geochemical – isotopic characteristics of granitoids in the Lo Gam and Song Da structures suggest that aside from slight differences in compositions among granitoidic magmas from various intrusive bodies most of the granites mentioned in this monograph belong to high-Al magma series characterized by a mineral phase such as garnet (Lo Gam structure) or cordierite (Song Da structure). Geochemical and isotopic characteristics show that the Permian – Triassic magmas were produced by melting of ancient (grown) crust. Occurring in folded and rifted structures in marginal regions of the Song Chay anticlinoria and Song Da rift, the chemically homogenous high-Al granitoids dated between 250 and 242 Ma is mostly coincident with the Indosinian orogeny time thus complicating the nature of tectonic setting of the magma occurrence. Generally, high-Al granites are viewed as magmatic indicator

of collision tectonic setting which, in the old time when geosyncline concept was popular, was also termed as co-orogeny granites. Therefore, for a long time (even at the present) Phia Bioc-type high-Al granites have been considered as late Triassic co-orogeny magmas (Dovjikov 1965; Tri 1977; Thuc and Trung 1995). However, reviewing evolutional history of the Northern Vietnam geology from northwestern Song Ma suture zone during the Permian – Triassic (between 250 and 240 million years) it is difficult for a subduction-related orogeny to occur in this region; although subduction-induced features were recognized in a number of magmatic formations in northern Vietnam such as the Permian – Triassic Song Hien rift. Subduction-related features will be again mentioned in the below sub-section on Lo Gam gabbro – syenite magmatic associations. The subduction-related geochemical features in the Permian – Triassic magmatic associations in northeastern Vietnam, according to the authors, are inherited from regional subduction-influenced lithospheric mantle domain believed to reside under southeastern margin of the Yangtze craton. Melting to form high-Al granitic felsic melts occurred in the crust, in difference to melting process to form mafic melts of Nui Chua-type layered gabbroids about 251 Ma that occurred at the top layer of a mantle plume. Mantle plume signatures in Permian and Permian – Triassic pluton –volcanic formations are recognizable. On the other hand, the spatio-temporal relationship between the Permian – Triassic high-Al granitoids and the Nui Chua layered gabbroids suggests that the granitoids were produced under mantle plume impact at the base of lithosphere in the southern rim of Yangtze craton. Back in the early 60s of the twentieth century E.P. Izokh presented a model to illustrate the passage of mantle melts forming Nui Chua gabbroids and Phia Bioc granitoids (in Dovjikov 1965). Although at the time mantle plume concept was not yet present; however, the idea is up-to-date valid for consideration, in that, in a narrow folding structure such as that surrounding Song Chay anticlinoria both intraplate gabbro and granite are present, the magmas are believed to occurred in cratonic marginal structures under impact of mantle plumes.

5.2 Gabbro-Syenite Intrusive Formations in the Lo Gam Structure

5.2.1 Geology and Formation Age of the Gabbro and Syenite

Diversified mafic intrusive gabbro, monzogabbro, syenite-diorite (monzodiorite) and syenite are widely occurred in the Lo Gam structure, a unit within the folding system in northeastern Vietnam. In previous studies the gabbroids were classified as late Triassic Nui Chua gabbro-peridotite complex, whereas the syenitoids were grouped as Paleozoic Pia Ma alkaline complex or Paleogene Cho Don complex (Dovjikov 1965; Tri 1977; Thuc and Trung 1995). According to the latest

geochemical and isotopic studies by authors of this monograph the gabbro and syenite magmas have been viewed as a unified Permian – Triassic gabbro – syenite association (Hoa et al. 1999b, 2004). The authors concluded that geochemistry of this gabbro – syenite association is subduction-related in nature. Similar conclusions were also found elsewhere (e.g. Chi 2003; Duong 2007).

Studies of mineralogy, geochemistry and isotope of the Lo Gam gabbro and syenite magmas show that there are three gabbro-syenite association-types within the structure: (1) low-Ti gabbro – syenite; (2) high-Ti monzogabbro – syenite; and (3) alkaline gabbro – nepheline- syenite. The first two types are distributed in the Luc Yen and Tich Coc areas, the structures surrounding the Song Chay – Lo Gam anticlinoria while the third type is outcropped in the Cho Don area, on the boundary between Phu Ngu and Lo Gam structures, as a constituent of the Bang Phuc block (Fig. 5.1). A compositionally complex gabbro block including gabbroids of the first and third types termed as Khuoi Loong block is found to locate about 1.5–2 km west of Bang Phuc. Along with alkaline gabbro and nepheline-syenite magmas low-Ti, relatively low- alkaline gabbro mostly similar to that in the gabbro-syenite association (first type), and nepheline- and alkaline, colored mineral-free syenite are also found in the Bang Phuc block.

The magmatic associations form separate, small-sized (ca. several square kilometers) intrusive bodies. The first association type located in the Luc Yen area (including Tan Linh, Luc Yen and other small bodies in Luc Yen district, Yen Bai province (e.g. Hoa 1999c) contains low-Ti pyroxene and amphibole gabbro, and smaller amount of gabbro-diorite monzodiorite and syenite. No clear contact among these bodies was observed. The most representative of second magmatic association type is occurred in the Tich Coc area (Tich Coc block), Ham Yen district, Tuyen Quang province. The block is comprised of monzogabbro, monzodiorite and syenite, showing high-Ti and high alkalinity geochemistry and having a typical co-existing mineral assemblage being pyroxene, amphibole and biotite. The gabbro associations penetrated Devonian terrigenous sediments forming outer contact zone filled with veins of metamorphic hornfels.

The geological structure of Khuoi Loong gabbro block is interesting. The block is about 2.5 km to the northeast of Bang Lung town (center of Cho Don district), with a symmetric-shaped outcrop of about 1 km^2, and having penetrating contact with two-mica shale and cordierite-bearing (?) silimanite. The main composition of the block is gabbro and pyroxenite, which are crisscrossed to form a number of separate fragments separated by veins of granosyenite and syenite, making the block to look like a breccia (Photo 5.3). The fragments are mostly gabbro and pyroxenite being partly amphibolized to various degrees, and porphyric syenite and granosyenite. The latter, except for containing a minor amount of biotite, are colored mineral-free. Among the alkaline intrusive magmas in the Cho Don area, nepheline-biotite (myaskite) syenite is dominant although K-felspar-, amphibole-, calcite-, sphene-, nepheline-, and garnet-gabbro and pyroxenite are also found (Bang Phuc block). The gabbro and pyroxenite are med- to coarse-grained having

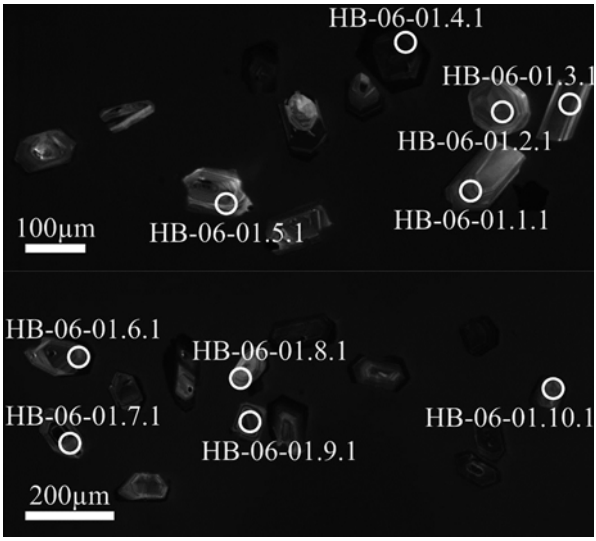

Photo 5.2 Back-scattered images of zirons separated from Kim Boi granite (sample HB-06-01). Analyzed points are shown in Table 5.11

Photo 5.3 Breccia – like of a Khuoi Loong magma fragment. *Dark*-colored material is gabbro, *bright*-colored is syenite

Ti-augites up to 1–2 cm long. In Thuc and Trung (1995) these magmas were described as metasomatic products under reaction between the syenite and gabbro. However, typical textures of the gabbro and pyroxenite together with lacking of evidence of inter-mineral replacement and gradual transition from the magmas to syenite do not support the metasomatic explanation rather suggest that the gabbro and syenite were differentiated magmas from a single parental melt.

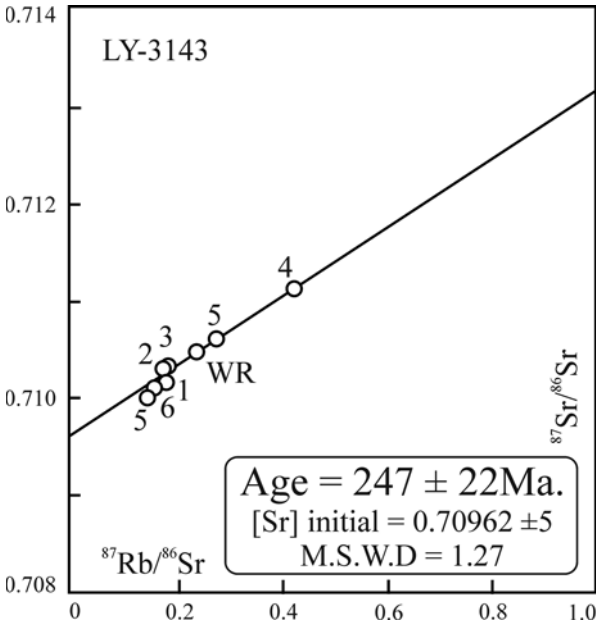

Fig. 5.17 Rb-Sr of a Luc Yen low-Ti gabbro (Hoa 2007)

The Permian – Triassic age of the gabbro-syenite magmas were determined based on geological correlation and radiometric dating. In many cases, the gabbro –syenite penetrate Ordovician – Silurian (Phu Ngu complex) and Devonian sediment-metamorphic strata (sandstone, clayish shale, sericite shale) (Tri 1977; Thuc and Trung 1995). Alkaline gabbro in the Cho Don area is penetrated by Permian – Triassic (250 Ma by Ar-Ar age dating) high-Al Tam Tao granite. Radiometric age dating on low-Ti gabbro in the Luc Yen area yielded 247 ± 22 Ma (Rb-Sr; Fig. 5.17) and 243 Ma (Ar-Ar) (Hoa 2007), and on nepheline-syenite yielded 233 Ma (Rb-Sr) (Chi 2003). Meanwhile Rb-Sr age dating on an alkaline syenite from Phia Ma block (having composition similar to Bang Lung syenite) showed a early Paleozoic result (540 Ma; Chi 2003). This needs a further detailed investigation to clarify.

In summary, in the southeastern rim of Song Chay anticlinoria identified are gabbro – syenite associations differentiated by alkalinity varying from normal to highly alkaline and mineralogical and geochemical features (will be described in detail below); however, all the magmas are Permian – Triassic. It is noteworthy that the re-determination of Permian – Triassic age for the regional mafic intrusive magmas has basically changed chronology of the regional magmatic activities and the explanation of geological evolution in northeastern Vietnam (Hoa et al. 2005), which will be described in the following chapter.

5.2.2 Mineralogy

The gabbroids in Tan Linh, Yen Minh blocks in the Luc Yen area (the first type), Khuoi Loong and southeast Bang Phuc block in the Cho Don area contain common gabbro (comprising plagioclase and clinopyroxene), amphibole gabbro (plagioclase, residual clinopyroxene and amphibole) or gabbro-diorite. Somewhere dark-colored varieties such as pyroxenite and gabbro-pyroxenite (containing mainly clinopyroxene, small amount of plagioclase and amphibole) are also occurred. The clinopyroxene is correspondent to diopside or augite in composition having characteristically low Al_2O_3 (=0.23–1.30 wt%), low Cr2O3 (=0–0.05 wt%), relatively high Mg and Ca ($En_{34.8–40.2}Wo_{48.6–49.0}Fs_{10.7–16.7}$) (Table 5.13).

However, compared with clinopyroxene in layered intrusive magma (Nui Chua type) magnesium contents in the studied clinopyroxene are much lower. Amphibole in these magmas are hornblende and Mg-hornblende which commonly replace pyroxene. In many cases together with amphilization is accompanied by biotitization and epidotization. The gabbro-diorite and gabbro-pyroxenite are distinguished from common gabbro by quantitative proportions between dark-(Cpx) and bright-colored (plagioclase) minerals (Phuong 2003; Hoa et al. 2004).

Monzonitic monzogabbro and monzodiorite (second type) are popular in the Tich Coc block. They have a stable co-existing mineral assemblage of Opx + Cpx ± Amp + Bi + Fsp + Pl. The orthopyroxene is correspondent to hypersthene ($Wo_{1.9–4.5}En_{37.3–39.3}Fs_{58.7–60.2}$), and is characteristically low Ti, Al and Mg and high Fe (Table 5.14). The clinopyroxene in Tich Coc block is correspondent to augite, compared with those in Luc Yen gabbro the mineral is much higher in Fe ($Wo_{42.6–45.3}En_{28.1–29.3}Fs_{25.7–29.5}$) (Phuong 2004). The amphibole in Tich Coc gabbro is compositionally correspondent to normal hornblende, sometimes relatively high alkalis (Table 5.15)

The biotite in monzogabbro and monzodiorite (Table 5.16) is characteristically high iron (Fe = 0.6–0.62), very low magnesium (Mg# = 0.38–0.40) and relatively low aluminum (Al_2O_3 = 13.35–13.89 wt%). Perhaps in the current Vietnamese geological literature there has not yet reported on a similar biotite. Popular accessory minerals are ilmenite and apatite.

There are two magmatic associations in the Bang Phuc block: normal (feldspathoid-free)- gabbro – syenite and feldspathoid-bearing alkaline gabbro – alkaline syenite association. The first association is characterized by mineral assemblage containing Pl + Cpx + Amp + Bi ± Fsp, which suggests the similarity of this gabbro with other gabbro in the Lo Gam structure. The first association's syenite has the following co-existing mineral assemblage Fsp + Cpx + Bi. Mineralogical compositions of the gabbro and pyroxenite of the second magmatic association is rather complex such as Cpx + Amp + Pl + Fsp ± Ne ± Bi + Ca ± Gr while the accompanying syenite contains Fsp + Pl + Ne + Bi. Chemical compositions of the minerals are given in Tables 5.13, 5.14, 5.15 and 5.16. Below are brief descriptions of the minerals.

Table 5.13 Chemical composition (wt%) of clinopyroxenes from Lo Gam gabbro-syenite associations

Sample	LY-10507	LY-10763	LY-10765	LY-10505/1	LY-10505/2	LY-10505/3
	1	2	3	4	5	6
SiO_2	52.38	53.18	52.23	52.23	52.75	51.58
TiO_2	0.05	0.14	0.01	0.03	0.02	0.03
Al_2O_3	0.62	0.75	0.23	0.42	0.45	1.32
FeO	9.63	6.33	10.44	10.18	9.55	10.1
Cr_2O_3	0.01	0	0.01	0.02	0.05	0.05
MnO	0.38	0.35	0.46	0.46	0.46	0.42
MgO	11.93	14.04	11.73	12.2	12.36	12.68
CaO	23.28	23.79	23.54	22.69	22.64	21.2
Na_2O	0.36	0.28	0.17	0.24	0.22	0.23
K_2O	0.02	0.02	0	0.02	0.06	0.13
Si^{4+}	1.996	1.993	1.996	1.996	20.11	1.98
Ti^{4+}	0.001	0.004	0	0.001	0.001	0.001
Al^{3+}	0.028	0.033	0.01	0.019	0.02	0.059
Fe^{3+}	0.005	0	0	0.005	0	0.001
Fe^{2+}	0.302	0.198	0.334	0.32	0.304	0.323
Cr^{3+}	0	0	0	0.001	0.02	0.002
Mn^{2+}	0.012	0.011	0.015	0.015	0.015	0.014
Mg^{2+}	0.678	0.784	0.668	0.695	0.703	0.725
Ca^{2+}	0.95	0.955	0.964	0.929	0.925	0.872
Na^{+}	0.027	0.02	0.013	0.018	0.016	0.017
K^{+}	0.001	0.001	0	0.001	0.003	0.006
WO	48.81	49.01	48.66	47.30	47.58	45.05
EN	34.80	40.24	33.74	35.38	36.09	37.49
FS	16.39	10.75	17.60	17.32	16.41	17.46

(continued)

Table 5.13 (continued)

Sample	H4/28	H4/30	H4/31	H4/32	H4/35	H4/49	H4/50	H4-51	H4/52	H4/42	H1/5
	7	8	9	10	11	12	13	14	15	16	17
SiO_2	50.7	50.42	50.53	50.71	50.71	51.23	51.11	50.81	51.1	50.5	51.2
TiO_2	0.22	0.22	0.22	0.2	0.2	0.13	0.08	0.17	0.13	0.13	0.15
Al_2O_3	1.23	1.31	1.45	1.32	1.3	1.15	1.11	1.23	1.09	1.24	1.32
FeO	15.47	15.44	15.14	17.17	16.11	14.84	14.87	15.37	14.98	15.63	15.43
Cr_2O_3	0	0	0	0.01	0	0.03	0	0	0.01	0.02	0
MnO	0.42	0.42	0.39	0.46	0.44	0.41	0.46	0.48	0.46	0.37	0.57
MgO	9.63	9.65	9.41	9.83	9.67	9.81	9.87	9.74	9.74	9.62	9.71
CaO	20.92	20.67	21.35	19.27	19.96	21.16	20.94	20.72	21.18	20.88	20.77
Na_2O	0.26	0.28	0.28	0.3	0.32	0.25	0.27	0.27	0.24	0.26	0.32
K_2O	0	0.01	0	0	0	0.02	0.01	0.01	0.02	0	0
Si^{4+}	1.971	1.968	1.965	1.968	1.976	1.984	1.985	1.975	1.982	1.967	1.977
Ti^{4+}	0.006	0.006	0.006	0.006	0.006	0.004	0.002	0.005	0.004	0.004	0.004
Al^{3+}	0.057	0.06	0.067	0.061	0.06	0.053	0.051	0.056	0.05	0.057	0.06
Fe^{3+}	0	0	0	0	0	0	0	0	0	0	0
Fe^{2+}	0.503	0.504	0.492	0.557	0.525	0.481	0.483	0.499	0.486	0.51	0.498
Cr^{3+}	0	0	0	0	0	0.001	0	0	0	0.001	0
Mn^{2+}	0.014	0.014	0.013	0.015	0.015	0.013	0.015	0.016	0.015	0.012	0.019
Mg^{2+}	0.558	0.561	0.546	0.569	0.562	0.566	0.571	0.564	0.563	0.559	0.559
Ca^{2+}	0.871	0.864	0.89	0.801	0.833	0.878	0.871	0.863	0.88	0.872	0.859
Na^{+}	0.02	0.021	0.021	0.023	0.024	0.019	0.02	0.02	0.018	0.02	0.024
K^{+}	0	0	0	0	0	0.001	0	0	0.001	0	0
WO	44.77	44.47	45.85	41.25	43.08	45.29	44.89	44.42	45.27	44.66	44.40
EN	28.68	28.89	28.12	29.28	29.04	29.22	29.44	29.05	28.97	28.63	28.88
FS	26.55	26.64	26.04	29.47	27.89	25.49	25.66	26.53	25.77	26.72	26.71

SiO_2	47.54	45.39	49.75	50.45	44.84	45.69	51.56	52.10	51.87	49.94
TiO_2	1.37	1.90	0.09	0.08	1.80	1.91	0.14	0.12	0.05	0.56
Al_2O_3	6.67	6.83	0.60	0.51	9.81	8.77	0.86	0.72	0.50	3.37
FeO	12.65	15.85	21.77	19.74	9.89	9.76	14.42	12.78	14.98	12.59
Cr_2O_3	0.00	0.00	0.00	0.01	0.02	0.00	0.06	0.02	0.01	0.01
MnO	0.24	0.32	0.54	0.56	0.15	0.17	0.53	0.48	0.38	0.35
MgO	8.55	6.41	4.72	5.91	8.96	9.30	10.68	11.32	10.25	8.62
CaO	22.98	22.61	21.90	21.81	24.27	23.73	21.43	21.89	21.11	22.97
Na_2O	0.72	0.82	0.29	0.27	0.47	0.51	0.30	0.23	0.28	0.87
K_2O	0.00	0.00			0.00	0.01	0.01	0.00		
Total	100.72	100.14	99.65	99.34	100.22	99.85	100.00	99.66	99.43	99.27
TSi	1.79	1.75	1.99	2.00	1.69	1.72	1.97	1.99	2.00	1.92
TAl	0.21	0.25	0.02	0.00	0.32	0.28	0.03	0.01	0.00	0.09
M1Al	0.09	0.06	0.01	0.02	0.12	0.11	0.01	0.02	0.02	0.07
M1Ti	0.04	0.06	0.00	0.00	0.05	0.05	0.00	0.00	0.00	0.02
M1Fe^{2+}	0.39	0.51	0.70	0.62	0.31	0.31	0.38	0.33	0.39	0.40
M1Mg	0.48	0.37	0.28	0.35	0.50	0.52	0.61	0.64	0.59	0.49
M2 Fe^{2+}	0.01	0.00	0.02	0.03	0.00	0.00	0.08	0.07	0.10	0.00
M2Mn	0.01	0.01	0.02	0.02	0.01	0.01	0.02	0.02	0.01	0.01
M2Ca	0.93	0.93	0.94	0.93	0.98	0.96	0.88	0.89	0.87	0.94
M2Na	0.05	0.06	0.02	0.02	0.03	0.04	0.02	0.02	0.02	0.07
Wo	51.14	51.21	47.73	47.53	54.45	53.42	44.68	45.61	44.57	50.97
En	26.47	20.20	14.31	17.92	27.97	29.13	30.98	32.82	30.11	26.61
Fs	22.39	28.60	37.96	34.55	17.59	17.45	24.33	21.57	25.32	22.42

(continued)

Table 5.13 (continued)

	P536/1	P537	P543	P543/1	H1545	H1546	H1548	P545	P550
Sample	28	29	30	31	32	33	34	35	36
SiO_2	52.92	52.30	51.89	47.98	52.12	52.94	51.51	52.47	53.62
TiO_2	0.06	0.29	0.04	1.38	0.26	0.02	0.57	0.08	0.07
Al_2O_3	0.49	1.35	0.59	5.20	2.22	0.54	2.71	1.26	0.99
FeO	10.03	11.02	14.10	13.56	8.07	10.97	8.28	9.11	7.05
Cr_2O_3	0.00	0.00	0.00		0.05	0.00	0.02	0.04	0.03
MnO	0.39	0.33	0.39		0.20	0.22	0.21	0.19	0.20
MgO	11.77	12.28	8.78	7.78	12.41	11.06	11.94	12.15	13.51
CaO	24.10	21.61	23.24	22.72	23.88	24.19	24.23	24.22	24.40
Na_2O	0.20	0.31	0.67	0.59	0.60	0.36	0.33	0.45	0.40
K_2O									
Total	99.97	99.49	99.70	99.21	99.80	100.29	99.81	99.97	100.28
TSi	2.00	1.98	2.00	1.85	1.95	2.00	1.93	1.97	1.99
TAl	0.00	0.02	0.01	0.15	0.05	0.00	0.07	0.03	0.01
M1Al	0.02	0.04	0.02	0.09	0.04	0.02	0.05	0.02	0.03
M1Ti	0.00	0.01	0.00	0.04	0.01	0.00	0.02	0.00	0.00
M1Fe^{2+}	0.32	0.26	0.45	0.42	0.25	0.35	0.26	0.29	0.22
M1Mg	0.66	0.69	0.50	0.45	0.69	0.62	0.67	0.68	0.75
M2 Fe^{2+}	0.00	0.09	0.00	0.02	0.00	0.00	0.00	0.00	0.00
M2Mn	0.01	0.01	0.01	0.00	0.01	0.01	0.01	0.01	0.01
M2Ca	0.97	0.88	0.96	0.94	0.96	0.98	0.97	0.97	0.97
M2Na	0.02	0.02	0.05	0.04	0.04	0.03	0.02	0.03	0.03
Wo	49.57	45.44	49.69	51.49	50.17	50.07	51.04	50.06	49.94
En	33.69	35.93	26.12	24.53	36.27	31.85	35.00	34.94	38.47
Fs	16.74	18.63	24.19	26.96	13.56	18.08	13.96	15.00	11.59

Remarks: Clinopyroxene: Tan Linh block: LY-1057- syenite; LY-1063 – gabbro and amphibole monzogabbro; Yen Minh block: LY-10505: syenite (The 1999; Hoa et al. 1999b); Tich Coc block: H-4 – H-1: monzogabbro; Bang Phuc block: alkaline gabbro: H-1215; H-1538; H-1616; P-543; monzonitoid: H-1535, H = 1536, P-536; alkaline pyroxenite: H-1539, H-1614; Khuoi Loong block: gabbroid: H-1545, H-1546, H-1548, P-545, P-550 (Phuong 2004; Hoa et al. 2004)

Table 5.14 Chemical compositions (wt.%) of orthopyroxene in Tich Coc monzogabbro (Hoa et al. 2004)

Sample	H 4/33	H 4/34	H 4/36	H 4/39	H 4/40	H 4/41	H1/6	H 1/11	H 1/15
SiO_2	49.21	49.41	49.12	49.25	49.35	49.24	49.51	49.29	49.61
TiO_2	0.1	0.1	0.1	0.1	0.15	0.1	0.15	0.1	0.1
Al_2O_3	0.58	0.63	0.65	0.64	0.54	0.61	0.48	0.63	0.68
FeO	33.15	33.28	33.13	33.28	33.47	33.18	32.41	32.81	32.21
Cr_2O_3	0	0	0.03	0.02	0	0	0	0	0
MnO	0.95	0.9	0.87	0.9	0.87	0.89	1.11	1.1	1.15
MgO	12.21	12.36	12.13	12.16	12.11	12.46	12.6	12.25	11.98
CaO	0.93	0.92	0.93	0.9	0.9	0.88	0.91	1.08	2.0
Na_2O	0.02	0	0.01	0.01	0.01	0	0	0	0
K_2O	0	0	0.01	0	0.01	0	0	0	0
Si^{4+}	2.01	2.01	2.01	2.01	2.01	2.01	2.01	2.01	2.01
Ti^{4+}	0.003	0.003	0.003	0.003	0.003	0.003	0.003	0.003	0.003
Al^{3+}	0.028	0.03	0.03	0.03	0.02	0.03	0.02	0.03	0.03
Fe^{3+}									
Fe^{2+}	1.135	1.135	1.136	1.138	1.144	1.132	1.107	1.121	1.094
Cr^{3+}									
Mn^{2+}	0.033	0.031	0.03	0.031	0.03	0.031	0.038	0.038	0.04
Mg^{2+}	0.745	0.75	0.742	0.741	0.738	0.758	0.767	0.746	0.726
Ca^{2+}	0.041	0.04	0.041	0.039	0.039	0.038	0.04	0.047	0.087
Na^{+}	0.002	0	0.001	0.001	0.001	0	0	0.002	0.002
K^{+}									
WO	2.09	2.05	2.10	2.02	2.02	1.96	2.04	2.42	4.47
EN	38.14	38.38	38.05	38.02	37.81	38.68	39.29	38.21	37.27
FS	59.77	59.56	59.85	59.96	60.17	59.36	58.67	59.37	58.25

Pyroxene is present in all rock types except for miyaskite in the Ban Phuc block. Chemical compositions of the clinopyroxene is variable from association to association but basically ranging within the diopside – hedenbergite group (Table 5.13, Fig. 5.18), the mineral in alkaline gabbro and pyroxenite is usually more enriched in wollastonite component. Two clinopyroxene types may be identified based on Ti- and Al- concentrations. Low-Ti and low-alkali gabbro in the Luc Yen area (Tan Linh, Luc Yen and Yen Minh blocks), monzogabbro in the Tich Coc area and Khuoi Loong pyroxenite as well as Bang Phuc monzogabbro in the Cho Don area are characterized by low-Ti (TiO_2 = 0.02–0.26 wt%), low-Al (Al_2O_3 = 0.5–0.86 wt%) diopside ($Wo_{44.57–51.04}En_{29.13–38.47}Fs_{11.59–25.32}$) whereas diopside in the Khuoi Loong gabbro is enriched in enstantite component and diopside in monzonite from Bang Phuc block is poor in MgO, compositionally close to hedenbergite (Figs. 5.18 and 5.19; Table 5.13).

Table 5.15 Chemical compositions (wt%) of amphibole in Cho Don gabbro – syenite (Hoa et al. 2004)

	H1532/2	H1536/2	H1538/2	H1538_03	H1538_12	H1538_13	H1538_19
Sample	1	2	3	4	5	6	7
SiO_2	40.62	42.39	39.11	38.32	38.10	38.24	38.35
TiO_2	1.96	1.26	1.57	1.23	1.06	1.08	1.22
Al_2O_3	9.48	8.84	16.47	17.14	16.70	16.72	16.84
FeO	27.54	23.92	18.55	15.11	15.09	14.97	15.02
Cr_2O_3				0.01	0.01	0.00	0.01
MnO				0.22	0.21	0.20	0.22
MgO	3.27	5.98	3.57	9.18	9.30	9.40	9.31
CaO	10.94	11.37	14.69	11.70	11.78	11.79	11.61
Na_2O	1.71	1.50	1.50	1.82	1.91	1.90	1.90
K_2O	1.64	1.75	1.95	2.93	2.95	2.93	2.90
Total	97.16	97.01	97.41	97.68	97.13	97.25	97.40
Si	6.51	6.67	6.31	5.80	5.81	5.82	5.82
Ti	0.24	0.15	0.19	0.14	0.12	0.12	0.14
Al	1.79	1.64	3.13	3.05	3.00	3.00	3.01
Fe^{3+}	0.11	0.09	0.00	0.18	0.15	0.15	0.19
Fe^{2+}	3.58	3.05	2.51	1.73	1.78	1.76	1.71
Mn	0.00	0.00	0.00	0.03	0.03	0.03	0.03
Mg	0.78	1.40	0.86	2.07	2.12	2.13	2.10
Ca	1.88	1.92	2.54	1.90	1.93	1.92	1.89
Na	0.53	0.46	0.47	0.53	0.57	0.56	0.56
K	0.34	0.35	0.40	0.57	0.57	0.57	0.56

	P536/2	P537/1	P540/2	H1215_10	H1215_11	P537/3
Sample	8	9	10	11	12	14
SiO_2	39.31	40.92	37.59	38.27	37.91	46.34
TiO_2	3.05	3.10	1.87	1.90	1.86	1.19
Al_2O_3	12.56	11.51	14.58	15.69	15.64	7.16
FeO	20.64	19.30	22.82	20.15	20.13	19.97
Cr_2O_3				0.00	0.01	
MnO				0.30	0.30	
MgO	6.20	7.26	4.74	6.52	6.49	9.75
CaO	11.69	11.25	11.29	11.46	11.29	10.67
Na_2O	1.40	1.72	1.86	2.04	1.97	1.24
K_2O	2.24	1.36	2.61	2.56	2.55	0.72
Total	97.09	96.42	97.36	98.89	98.15	97.04
Si	6.16	6.35	5.94	5.85	5.83	6.93
Ti	0.36	0.36	0.22	0.22	0.22	0.13
Al	2.32	2.10	2.71	2.83	2.83	1.26
Fe^{3+}	0.00	0.00	0.06	0.17	0.26	0.69
Fe^{2+}	2.71	2.51	2.96	2.41	2.33	1.81

(continued)

Table 5.15 (continued)

	P536/2	P537/1	P540/2	H1215_10	H1215_11	P537/3
Sample	8	9	10	11	12	14
Mn	0.00	0.00	0.00	0.04	0.04	0.00
Mg	1.45	1.68	1.12	1.49	1.49	2.17
Ca	1.96	1.87	1.91	1.88	1.86	1.71
Na	0.43	0.52	0.57	0.61	0.59	0.36
K	0.45	0.27	0.53	0.50	0.50	0.14

Remarks: Bang Phuc block: H-1532- syenite, H-1536 – monzonite, H-1538, H-1614 – alkaline gabbro, P-540, H-1215- alkaline pyroxenite; Khuoi Loong block: P-536-537 – gabbro

Table 5.16 Chemical compositions (wt%) of biotite in Lo Gam gabbro and syenite (Hoa et al. 2004)

Sample	LY-10505/1	LY-10505/2	H4/1	H4/2	H1539a	H1539b	H1539c	H1540	H1541
SiO_2	37.23	38.24	34.97	34.86	34.22	34.22	34.45	33.43	33.14
TiO_2	2.93	3.00	5.48	5.44	1.62	1.97	1.75	4.67	3.22
Al_2O_3	13.83	14.39	13.73	13.79	18.21	18.05	18.07	18.76	20.34
FeO	17.41	16.89	22.87	22.42	17.20	16.67	17.39	26.04	25.69
MnO	0.19	0.17	0.12	0.08	0.17	0.17	0.18	0.68	0.80
MgO	13.66	12.91	7.89	8.06	12.35	12.42	12.10	2.82	3.10
Na_2O	0.11	0.12	0.10	0.19	0.23	0.22	0.20	0.21	0.21
K_2O	9.36	9.66	9.19	9.15	9.25	9.28	9.28	9.31	9.27
H_2O	4.50	4.50	4.50	4.50	4.50	4.50	4.50	4.50	4.50
Si^{4+}	5.73	5.88	5.67	5.67	5.33	5.35	5.37	5.47	5.38
Al^{4+}	2.27	2.12	2.32	2.32	2.67	2.65	2.63	2.53	2.62
Al^{6+}	0.24	0.49	0.29	0.31	0.68	0.67	0.69	1.08	1.26
Ti^{4+}	0.34	0.35	0.67	0.66	0.19	0.23	0.21	0.58	0.39
Fe^{2+}	2.24	2.17	3.10	3.01	2.24	2.18	2.27	3.56	3.49
Mn^{2+}	0.02	0.02	0.01	0.01	0.02	0.02	0.02	0.09	0.11
Mg^{2+}	3.13	2.96	1.91	1.95	2.87	2.89	2.81	0.69	0.75
Na^{+}	0.03	0.03	0.03	0.06	0.07	0.07	0.06	0.07	0.07
K^{+}	1.84	1.89	1.90	1.93	1.84	1.85	1.85	1.94	1.92
Mg#	0.58	0.56	0.38	0.39	0.56	0.57	0.55	0.16	0.18

Remarks: LY-10505: Luc Yen syenite (Tan Linh block); H-4: monzogabbro, Tich Coc block; H-1539: alkaline gabbro and H-1540 – 1541: nepheline syenite (miyaskite), Bang Phuc block

Alkaline gabbro and pyroxenite in the Bang Phuc block contain the two pyroxene types, low-Ti and –Al and high-Ti and –Al. The low-Ti, −Al pyroxene is chemically similar to the above described, while the high-Ti, −Al pyroxene is more enriched in wollastonite component ($Wo_{49.69–54.43}En_{20.20–29.13}Fs_{17.45–28.60}$) and TiO_2

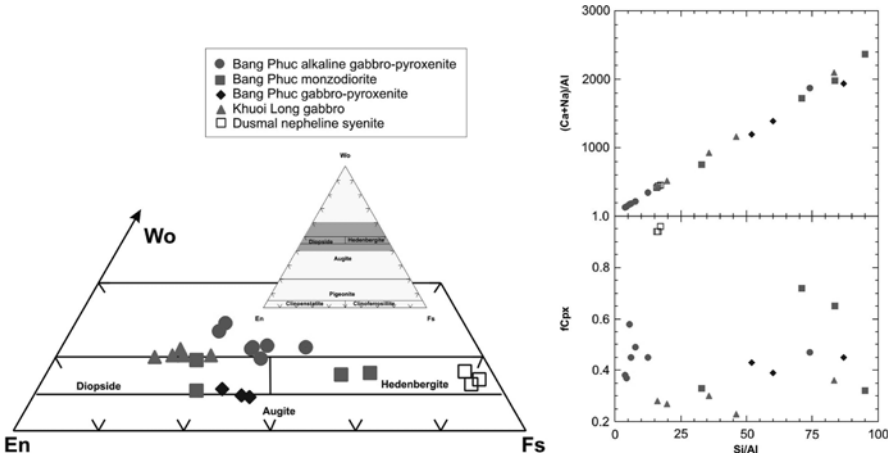

Fig. 5.18 Chemical compositions of clinopyroxene in Cho Don gabbro expressed in En-Wo-Fs (*left*), and fCpx versus Si/Al and (Ca + Na)/Al (*right*) relationship

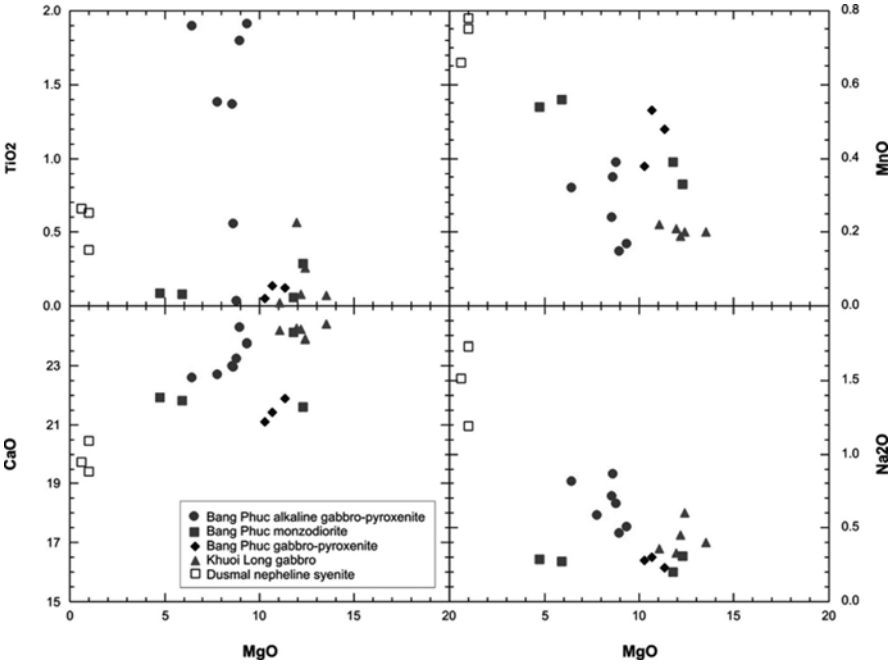

Fig. 5.19 Plots of Mg vs. TiO_2, MnO, CaO and Na_2O showing chemical variation of the clinopyroxene

(1.37–1.91 wt%), the content is equivalent to that of Ti-augite. The pyroxene is also rich in aluminum (Al_2O_3 = 5.20–9.8 wt%), sodium (Na_2O = 0.47–0.82 wt%) and MgO lying between gabbroic and monzonite diopside (Table 5.13 numbers 18–19, 22–23). In plots of f_{Cpx} versus (Ca + Na) and Si/Al (Fig. 5.18) the clinopyroxene compositional points concentrate near the axial cross-section.

According to the mineralogical compositions mentioned above clinopyroxene in the low-Ti, low-alkaline gabbro and monzonite is closely similar to clinopyroxene in tholeiitic or sub-alkaline mafic – ultramafic associations; while clinopyroxene in the alkaline gabbroids and alkaline pyroxenites (Bang Phuc block) is similar to clinopyroxene in the alkaline mafic – ultramafic, especially in the Dismal nepheline gabbro and syenite, South Victory, Antarctica (e.g. Worley and Cooper 1995). In the Tich Coc monzogabbro and monzodiorite also found is orthopyroxene having a composition similar to hypersthene ($Wo_{1.9–4.4}En_{37.8–39.3}Fs_{58.6–60.1}$) (Table 5.14).

Chemical compositions of amphibole are heterogeneous among the magma types although basically they are correspondent to magnesian hornblende and pargasite where the hornblende is characterized for low-Ti gabbro and pargasite is found only in Ban Phuc alkaline gabbroid. The hornblende commonly develops among the diopside – hedenbergite minerals. Chemical composition of the gabbroic hornblende (Table 5.15, sample P-549/2) is characteristically low SiO_2, very high Al_2O_3 (14.56 wt%), FeO (22.82 wt%) and K_2O (up to 14.56 wt%). In contrast, hornblende in monzodiorite is higher TiO_2 (1.28–3.05 wt%), Al_2O_3 (7.16–12.56 wt%), FeO (19.97–23.92 wt%) and relatively higher K_2O (0.72–1.75 wt%) compared with that in the gabbro (Table 5.15, Fig. 5.20). Pargasite in the Bang Phuc alkaline gabbroids is characteristically low titanium (TiO_2 = 1.02–1.9 wt%), very high aluminum (Al_2O_3 = 15.64–17.14 wt%), and high alkalis, especially potassium (K_2O = 2.55–2.95 wt%).

The biotite is classified to three types according to the chemical compositions (Table 5.16). The first type is characterized by high titanium (TiO_2 = 2.93–5.48 wt%), iron (FeO = 17.41–22.42 wt%), low aluminum (Al_2O_3 = 13.73–14.39 wt%) and variable magnesium (MgO = 7.78 = 13.66 wt%). This biotite type is present in Luc Yen syenite and Tich Coc monzogabbro. The second type is characterized by having relatively low TiO_2 (1.05–2.02 wt%), high Al_2O_3 (17.77–17.92 wt%), and high MgO (13.07 = 14.92 wt%). This type is found in Bang Phuc alkaline gabbroids in the Cho Don area. The third biotite type is typical in nepheline syenite (miyaskite). Its chemical composition is rather distinct, such as, very high TiO_2 (3.62–4.67 wt%), Al_2O_3 (20.34–21.81 wt%), FeO (25.59–26 wt%) but very poor MgO (2.98–3.32 wt%) (Table 5.16). With these chemical properties the biotite in Bang Phuc nepheline syenite (miyaskite) is chemically comparable with biotite in Dismal nepheline syenite (South Victory, Antarctica); however, the first is higher in titanium, aluminum and magnesium (Fig. 5.21).

Nepheline is commonly found in the alkaline gabbro and nepheline-biotite syenite. The chemical compositions of nepheline are relatively less variable (Table 5.17) with Al_2O_3 ranging between 33.60 and 34.10 wt%, Na_2O between 15.42 and 15.82 wt% and K_2O between 5.75 and 6.10 wt%, the compositions are within the mineral worldwide observed ranges, but especially similar to Dismal nepheline (South Victory, Antarctica).

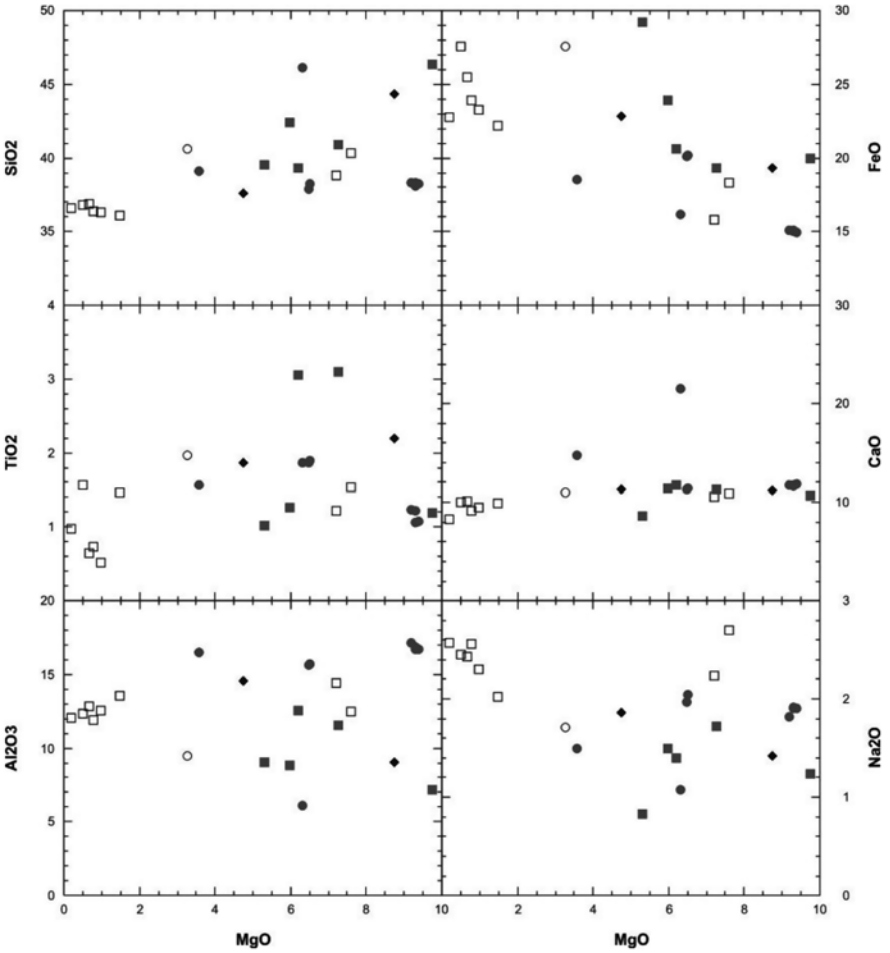

Fig. 5.20 The Harker diagram for amphiboles from Cho Don gabbroids. *Symbols* are as of in Fig. 5.19

Garnet is present only in alkaline pyroxenite and monzonite. The chemical composition is correspondent to the grossular – andradite series showing grossular component between 81.13 and 98.97 % (Table 5.18). The composition is commonly found in feldspathoid-bearing magmatic associations.

Chemical compositions of plagioclase in the gabbroids vary between andesine and labrador ($Ab_{45.9–65.1}An_{33–53.4}Or_{0.5–2.1}$) while in the nepheline syenite the composition is mostly albite ($Ab_{97.8}$). K-feldspar in the nepheline syenite is characteristically more enriched in albite component ($Or_{82.70}Ab_{16.90}$) compared with other rock types (Hoa 2007).

Trace elements such as Rb, Sr, Ba, Y, Zr, Nb, Hf, Ta, Th, U and the rare earths in the pyroxene, garnet, calcite and apatite in gabbroids and pyroxenites being ana-

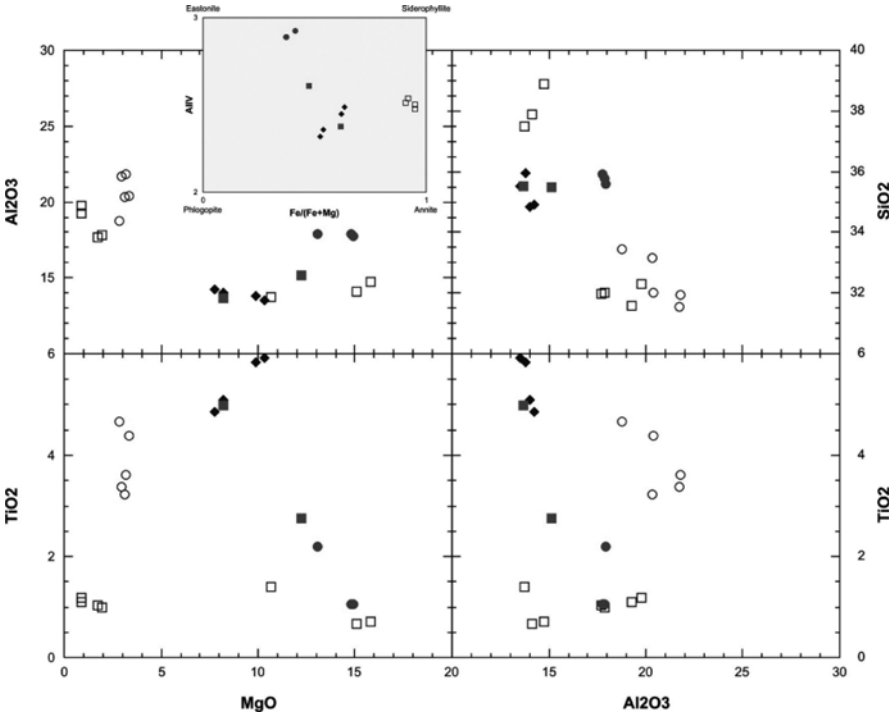

Fig. 5.21 Plots of MgO vs. TiO_2 and Al_2O_3, and Al_2O_3 vs. SiO_2 and TiO_2 for biotite in syenite from the Cho Don area

Table 5.17 Chemical compositions of nepheline in Bang Phuc syenite (Hoa et al. 2004)

Sample	H1221_13	H1221_15	H1221_7
SiO_2	44.38	43.28	43.35
Al_2O_3	33.97	33.66	34.10
CaO	0.96	1.16	1.03
Na_2O	15.82	15.42	15.73
K_2O	5.75	6.08	6.10
Total	100.88	99.60	100.31
Si	8.41	8.33	8.29
Al	7.58	7.63	7.68
Na	5.81	5.76	5.84
Ca	0.20	0.24	0.21
K	1.39	1.49	1.49

lyzed by ICP-MS are given in Table 5.19. Chondrite normalized rare earth and primitive mantle normalized trace element configurations show the similarity between high-Ti, −Al (sample H-1538) and low-Ti, −Al pyroxene (sample H-1539)

Table 5.18 Chemical compositions of garnet in Bang Phuc alkaline gabbro in the Cho Don area (Phuong 2004)

Sample	H1538_1	H1538_2	H1538_3	P536_1	P536_2	P536_3	P540_1	P540_2
SiO_2	40.61	40.61	40.55	40.61	40.64	40.60	39.61	39.51
Al_2O_3	29.51	29.25	29.02	29.12	29.43	29.19	20.62	19.46
FeO	0.84	0.49	0.97	0.35	0.30	0.54	4.44	4.54
MnO	0.08	0.07	0.06	0.11	0.09	0.09	0.11	0.12
MgO	0.02	0.00	0.01	0.02	0.01	0.02	1.13	1.26
CaO	29.97	30.58	30.34	30.77	30.54	30.54	33.82	34.66
Total	101.03	100.99	100.96	100.98	101.01	100.98	99.73	99.55
Al_{VI}	2.57	2.55	2.53	2.53	2.56	2.54	1.84	1.74
Fe^{3+}	0.00	0.00	0.00	0.00	0.00	0.00	0.16	0.25
Fe^{2+}	0.05	0.03	0.06	0.02	0.02	0.03	0.13	0.04
Mg	0.00	0.00	0.00	0.00	0.00	0.00	0.13	0.14
Mn	0.01	0.00	0.00	0.01	0.01	0.01	0.01	0.01
Ca	2.37	2.42	2.41	2.44	2.42	2.42	2.75	2.82
Alm	2.14	1.22	2.42	0.87	0.75	1.35	4.22	1.17
And	0.00	0.00	0.00	0.00	0.00	0.00	7.75	12.70
Gross	97.59	98.61	97.35	98.77	98.97	98.33	83.56	81.13
Pyrope	0.07	0.01	0.06	0.09	0.05	0.10	4.25	4.75
Spess	0.20	0.17	0.16	0.27	0.23	0.23	0.23	0.26

showing weak differentiation of the rare earth, except for slight depletion at Eu, Ba and Sr, and enrichment at Hf. However, the absolute values of the rare earth (Table 5.19), the Sm/Nd, Ce/Yb and Nb/Ta ratios of the high-Ti, −Al pyroxene, respectively, at 2.46, 7.5 and 30.5, are higher than those in the low-Ti, −Al type at 1.4, 1.05 and 4.6, respectively.

High-Ti, −Al pyroxene is also higher in Nb, Zr and Rb compared with the low-Ti, −Al pyroxene; therefore, the concentrations of REE, Nb, Zr and Rb in high-Ti, −Al pyroxene show a clear relationship with Ti and Al in the pyroxene. It is noteworthy that the REE concentrations in gabbroid pyroxenes are much lower compared with those in mantle-derived alkaline basalts (sample DL-026), being given in Table 5.19 and shown in Fig. 5.22 for comparison. Compared with the gabbroid pyroxene the alkaline basalt pyroxene is more enriched in middle rare earth elements. Chondrite normalized rare earth configuration for calcite is mostly similar to that in pyroxene although the calcite that in association with high-Ti, −Al pyroxene is normally more enriched in the rare earths than in the calcite associated with the low-Ti, −Al pyroxene. Both the calcite types are low in Nb, Ta, Zr and Hf (Fig. 5.22). In difference from pyroxene and calcite, garnet and apatite in association with high-Ti, −Al pyroxene are characteristically enriched in the REE, especially the light elements; they are also high in Th, U but low in Nb, Ta, Sr, Zr and Hf (Fig. 5.22).

The above described chemistry and elemental geochemistry of minerals from the Cho Don gabbroids indicate the complexity in source and magma generation; however, they also reflect the uniformity of the studied magmas. The enrichment of

Table 5.19 Trace element abundances (ppm) in minerals from Bang Phuc alkaline gabbroids (Phuong 2004)

Sample	H1538Ap	H1538Gr	H1538Carb	H1538Px	H1539Px	H1539Carb	DL026Px
Rb	2.3	0.41	<0.1 ppM	15.7	1.67	<0.1 ppM	1.11
Sr	1101	57.1	670	40.5	48.4	303	108
Y	1260	357	18.5	13.4	7.43	2.82	36.0
Zr	9.4	347	0.035	61	58	0.43	81
Nb	0.46	415	0.12	12.5	0.84	0.07	1.32
Ba	24	1.08	1.51	11.3	1.102	2.32	1.42
La	2236	148	16.9	6.4	2.0	3.4	16.4
Ce	4200	371	20.9	12.9	5.2	3.8	39.0
Pr	486	65	2.28	2.2	0.9	0.39	6.9
Nd	1660	330	8.4	10.6	5.3	1.7	39.9
Sm	294	88	1.50	2.6	1.45	0.22	11.7
Eu	67.2	16.2	0.35	0.48	0.35	0.08	3.161
Gd	277	85	1.62	2.9	1.56	0.42	12.4
Tb	34.8	12.8	0.26	0.42	0.232	0.045	1.68
Dy	196	77	1.77	2.6	1.45	0.31	9.0
Ho	38.8	14.5	0.49	0.55	0.30	0.067	1.53
Er	114	37.7	1.69	1.6	0.90	0.22	3.5
Tm	13.2	4.05	0.26	0.22	0.13	0.028	0.38
Yb	78	21.4	2.05	1.7	1.05	0.21	2.1
Lu	8.9	2.02	0.29	0.28	0.19	0.067	0.26
Hf	0.152	19.5	0.0066	3.0	3.4	0.009	6.6
Ta	0.015	84	0.0070	0.41	0.18	0.0012	0.21
Th	247	75	0.013	0.65	0.14	0.011	0.31
U	43.4	10.0	0.0093	0.14	0.027	0.0056	0.047

Remarks: Ap: apatite; Gr: garnet; Carb: calcite, Px: pyroxene. DL-026 pyroxene in Cenozoic alkaline basalt from Tay Nguyen (S. Vietnam)

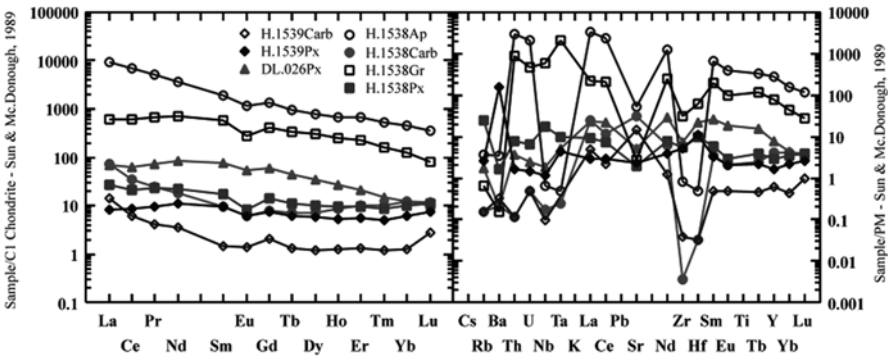

Fig. 5.22 Chondrite normalized rare earth (*left*) and primitive mantle normalized trace element (*right*) characteristics of minerals from the Bang Phuc alkaline gabbro in the Cho Don area

wollastonite component in high-Ti, –Al pyroxene, the presence of carbonate magma as well as the popularity of sphene in a series of dark-colored magmas (melteigite and malinite) may be a result of contamination of the nepheline syenite magma by carbonate sediments in transitional magma chambers for carbonate rocks (marble) are common wall-rocks in the outer contact zones of the alkaline gabbro and nepheline syenite magmas.

5.2.3 Geochemical and Isotopic Characteristics

Luc Yen –type gabbro – syenite association (first type): chemically the Luc Yen gabbroids are low-Ti type (TiO_2 = 0.49–1.0 wt%), having relatively low MgO (=5.74–8.41 wt%), high Al_2O_3 (=16.97–17.94 wt%) and low alkalinity ($Na_2O + K_2O$ = 0.72–2.71 wt%) (Table 5.20). Judged by titanium and alkali contents the magma association is chemically close to tholeiitic mafic series, in contrast, the magma is calc-alkaline if judged by its aluminum contents. The concentrations of Cu, Ni Co, Cr and V in the gabbroid are relatively low Nb and Ta, while Rb, Sr, Th and U concentrations are high (Table 5.20). These features are distinctly illustrated in a primitive normalized trace element diagram (Fig. 5.23b). The gabbroids are also enriched in the rare earths, especially the light elements; and their primitive mantle trace element normalized patterns are typical for calc-alkaline-like magma (Fig. 5.23a). Ratios of Nb/Ta, Nb/La, Ce/Yb and Th/U of the gabbroid are essentially mantle-derived mafic magmas. Syenite in the Luc Yen area (SiO_2 = 54.23–66.31 wt%; Na_2O = 1.5–4.26 wt%; K_2O = 6.72–11.36 wt%) is characteristically enriched in Rb, K, Th, U and the rare earths but are relative poor in Nb, Ta and Zr showing primitive mantle trace element normalized distribution pattern similar to calc-alkaline magma (Fig. 5.23b). Note the unusually high concentrations of the REE, Zr, Ba in sample LY-367/2 which needs further investigation for clarification. Ratios of Nb/Ta, Nb/La, Ce/Yb and Th/U in the syenite vary widely, suggesting strongly crustal contamination. Crustal contamination may be evidenced by high initial $^{87}Sr/^{86}Sr$ isotopic ratios, e.g. 0.71014–0.71055 for gabbroid and 0.71023–0.71913 for syenite. Besides, the closeness of initial $^{143}Nd/^{144}Nd_{250}$ isotopic ratios between the gabbroid and syenite, respectively, 0.51198–0.51213 and 0.51188–0.51205 (ε_{Nd} = −3.58 – −6.45 and −5.19 – −8.51, respectively) suggests they may be generated from a common source.

Monzogabbro and syenite in the Tich Coc area (the second type) show distinct composition features. The monzogabbro (SiO_2 = 50.42–51.27 wt%) is high-Ti type (TiO_2 = 1.66–3.34 wt%), low- Mg (MgO = 3.73–4.31 wt%) and high-alkali ($Na_2O + K_2O$ = 5.53–6/79 wt%), especially potassic (K_2O = 2.91–4.16 wt%). Their P_2O_5 contents are also high. In Harker plots (e.g. SiO_2 vs. TiO_2, CaO, MgO, Fe_2O_3, K_2O, Na_2O, Al_2O_3) (Fig. 5.24) field of the second-type Tich Coc monzogabbro is clearly separated from the first- and third-type gabbroids. The second- type gabbroid is poor in Cu, Ni, Co and Cr but relatively rich in V, Rb, Sr, Zr, Ba, Y and

Table 5.20 Chemical compositions (wt.%) and trace element abundances (ppm) of the Lo Gam gabbroid and syenite magmas (Hoa et al. 2004)

Location	Luc Yen						Tich Coc			
Sample	LY3145	LY2515	LY4136	LY425/A	LY4014	LY367/2	HG-108	LY-H1	HG-112	HG-111
Block	Tan Linh	Yen Minh	Tan Linh	Luc Yen	Luc Yen	Yen Minh	Tich Coc			
Rock-type	Gabbro		Syenite				Monzogabbro			syenite
SiO_2	43.57	49.18	54.23	62.92	66.31	63.73	50.42	50.59	51.27	54.63
TiO_2	1	0.49	0.67	0.28	0.02	0.2	2.51	3.34	1.66	1.36
Al_2O_3	17.94	16.97	15.57	17.03	17.17	17.56	15.82	15.09	15.36	19.64
Fe_2O_3	5.62	0.74	1.29	1.26	0.36	1.5	13.11	14.57	11.87	9.09
FeO	3.98	5.82	4.14	1.77	0.19	1.93				
MnO	0.14	0.12	0.09	0.06	0.01	0.05	0.18	0.19	0.18	0.12
MgO	5.74	8.41	6.53	1.9	0.4	0.28	3.73	4.17	4.31	0.59
CaO	18.67	12.82	12.52	1.77	1.13	1.94	6.68	6.86	7.06	4.13
Na_2O	0.5	2.08	1.5	3.97	1.94	4.26	2.76	2.62	2.63	3.10
K_2O	0.22	0.63	1.38	7.12	11.36	6.72	3.66	2.91	4.16	5.43
P_2O_5	0.19	0.05	0.15	0.12	0.03	0.06	0.61	0.53	0.70	0.33
LOI	2.08	2.61	1.6	0.93	0.37	1.19	0.65	0.54	0.89	
Sc	29	31	31	7	3	3	74.75	30.89	26.1	11.08
V	171	193	167	28	6	6	252.1	386.1	235.5	
Cr	20	216	60	91	8	4	12.95	6.204	19.48	
Co	37	34	24	6	6	2	21.5	24.97	21.29	10.84
Ni	70	62	66	49	6	5	4.926	4.938	12.66	
Cu	76	43	44	2	19	13	14.99	32.54	17.36	41.03
Zn	62	56	45	77	8	49	133.5	175.2	127.3	121.8
Ga	25.5	13.8	16	16.3	9.3	20.3	21.68	22.85	20.94	23.23
Cs							4.018	3.223	3.893	1.26
Rb	9	22.8	45.1	241	272	253	115.4	106.3	133.7	137.5
Sr	231	268	389	127	309	180	333.9	306.1	308.7	721.4
Y	27.4	14.6	20.7	14.5	2.5	49	28.3	28.1	32.86	22.28
Zr	79	45	38	323	19	569	116.3	115.5	113.2	65.13
Nb	14.1	4.1	9	8.7	1.6	24.9	13.26	24.54	9.976	8.53
Ba	46	110	380	538	2395	667	1396.	1005.	1332.	1919
La	22.86	6.4	17.84	32.76	10.08	493.56	31.41	27.66	33.94	24.85
Ce	52.93	14.53	38.97	56.39	16.67	679.33	63.33	60.28	71.54	52.16
Pr	6.85	1.89	5.3	6.59	1.63	71.7	7.394	7.785	8.779	7.395
Nd	28.56	9.35	22.21	23.62	7	197.39	31.04	35.98	37.5	31.2
Sm	6.19	2.3	4.6	4.11	1.11	25.62	6.493	9.223	8.046	7.183
Eu	1.45	0.68	1.03	0.66	0.81	1.61	2.599	2.271	2.41	1.637
Gd	5.73	2.52	4.19	3.68	1.22	21.88	5.603	7.345	6.722	5.811
Tb	0.88	0.47	0.71	0.49	0.19	2.25	0.892	1.134	1.071	0.868
Dy	5.05	2.85	4.04	2.43	0.82	9.88	5.093	5.766	5.942	4.386

(continued)

Table 5.20 (continued)

Location	Luc Yen						Tich Coc			
Sample	LY3145	LY2515	LY4136	LY425/A	LY4014	LY367/2	HG-108	LY-H1	HG-112	HG-111
Block	Tan Linh	Yen Minh	Tan Linh	Luc Yen	Luc Yen	Yen Minh	Tich Coc			
Rock-type	Gabbro		Syenite				Monzogabbro			syenite
Ho	1.05	0.61	0.81	0.48	0.15	1.91	1.014	1.013	1.149	0.738
Er	2.75	1.65	2.14	1.3	0.35	5.64	2.766	2.589	3.087	1.978
Tm	0.38	0.27	0.32	0.22	0.08	0.7	0.432	0.392	0.48	0.27
Yb	2.42	1.59	1.88	1.33	0.32	4.51	2.646	2.419	2.888	1.618
Lu	0.35	0.25	0.29	0.25	0.07	0.66	0.402	0.357	0.433	0.243
Hf	2.86	1.84	2.26	6.75	1.51	12.31	2.931	2.868	2.924	1.583
Ta	0.86	0.28	0.67	0.64	0.24	2.22	1.166	2.718	0.835	0.718
Pb	14	10	15	20	32	40	14.41	12.49	17.38	17.43
Th	1.8	1.8	4	49	4.4	65	4.934	1.986	4.901	2.546
U	0.5	0.7	1.1	6	3.8	9.2	0.996	0.958	1.275	0.717

Location	Cho Don								
Sample	H-1204	H-1218/1	H 1538	H-1215	H-1211	H-1221	H-1540	H-1536	H-1216
Block	Khuoi Loong	Bang Phuc							
Rock-type	Gabbro and alkaline-gabbro				Syenite and miaskite				
SiO_2	47.78	42.08	43.23	44.95	53.03	55.95	56.83	57.43	60.47
TiO_2	0.63	0.76	0.902	0.98	0.40	0.14	0.080	0.712	0.17
Al_2O_3	16.98	18.78	16.68	12.33	19.40	26.57	24.31	15.86	22.63
Fe_2O_3	6.13	7.14	9.19	10.13	3.58	1.40	1.08	7.43	1.63
MnO	0.08	0.12	0.164	0.16	0.06	0.04	0.030	0.138	0.04
MgO	7.10	2.84	4.87	4.42	1.31	0.00	0.23	2.33	0.00
CaO	19.35	21.41	17.04	19.92	9.83	1.24	1.02	7.47	1.27
Na_2O	0.96	1.68	1.77	1.63	2.81	7.05	7.43	2.76	5.36
K_2O	0.22	0.96	1.92	2.04	6.00	7.29	8.08	4.75	7.56
P_2O_5	0.03	0.76	0.616	0.64	0.48	0.01	0.030	0.229	0.02
LOI			3.91				0.99	0.26	
Sc	26.03	9.56		21.72	5.98	0.72			1.86
V	151.3	68.14	59	109.90	38.65		3.4	39	5.79
Cr	47.84	12.78	29	19.60	–0.33		35	38	–0.07
Co	32.47	21.75	20	36.05	9.38	0.50	34	11	0.77
Ni	55.6	17.29	23	24.39	4.43		325	29	
Cu	43.6	23.17	115	56.08	55.31	9.34	8661	2.07	7.57
Zn	40.29	45.6		84.8	62.8	21.9			54.3
Ga	14.17	14.09		16.04	14.89	27.46			23.45
Cs	2.6	2.28		3.437	4.698	20.43			16.71
Rb	12.03	38.0	51	85.5	242.8	451.1	266	126	436.7

(continued)

Table 5.20 (continued)

Location	Cho Don								
Sample	H-1204	H-1218/1	H 1538	H-1215	H-1211	H-1221	H-1540	H-1536	H-1216
Block	Khuoi Loong	Bang Phuc							
Rock-type	Gabbro and alkaline-gabbro				Syenite and miaskite				
Sr	292.1	604.5	441	334.5	562.4	90.4	41	263	126.3
Y	14.48	23.74	23	29.32	23.89	18.81	15	47	30.30
Zr	53.59	78.14	183	143.90	67.90	216.00	239	444	338.70
Nb	1.546	2.893	8	6.635	6.41	30.77			35.22
Ba	77.03	169	167	109	416	82	20	850	156
La	5.399	28.38	20	35.08	30.74	9.10	3.7	45	9.20
Ce	12.08	54.8	40	66.1	57.0	18.2	8.5	8.1	20.3
Pr	1.575	6.85	5.3	8.13	6.73	2.18	1.2	10	2.73
Nd	7.784	25.62	19	30.09	23.63	7.44	4.3	34	10.29
Sm	2.016	4.94	3.5	5.93	4.37	1.58	1	6	2.46
Eu	0.604	1.136	0.87	1.146	1.064	0.397	0.31	1.12	0.599
Gd	2.019	4.18	3.2	5.03	3.82	1.51	1.04	5.4	2.38
Tb	0.377	0.698	0.56	0.852	0.646	0.315	0.25	0.99	0.533
Dy	2.423	3.91	3.3	4.83	3.74	2.12	1.7	5.9	3.64
Ho	0.491	0.759	0.62	0.964	0.753	0.466	0.37	1.18	0.838
Er	1.357	2.14	1.8	2.77	2.13	1.52	1.2	3.5	2.63
Tm	0.206	0.314		0.420	0.315	0.261			0.445
Yb	1.352	2.09	1.7	2.82	1.95	1.75	1.2	3.2	2.76
Lu	0.204	0.325	0.25	0.45	0.273	0.229	0.12	0.43	0.351
Hf	1.794	1.85	4	3.52	1.58	4.52	4.5	9.7	5.78
Ta	0.111	0.277	0.42	0.362	0.298	2.260	2.2	1.7	2.869
Pb	8.892	6.46		12.45	20.00	88.05			89.99
Th	2.48	7.48	12	15.81	12.49	27.71	38	65	37.97
U	0.984	2.143	1.5	4.527	3.270	9.709	8	8.4	16.770

REE, and very poor in Nb and Ta (Table 5.20; Fig. 5.23b). Compared with the first rock type the second gabbroid type shows lower Nb/La (0.29–0.88), Nb/Ta (9.02–12.0) and much higher Ce/Yb (23.9–32.2). Its REE contents are high, where HREEs being about 20 folds and LREEs being about 160 folds higher compared with Chondrite values. Primitive mantle normalized trace element configuration patterns show slight negative anomalies at Nb, Ta, Zr, Hf, La and Ce. There is no trough being observed at Eu as commonly present in other gabbroid types in the area. These chemical features of Tich Coc monzogabbro are closely similar to those in mafic lamprophyre-type magmas in central Vietnam. The monzodiorite chemistry, except for having higher alkalis ($Na_2O = 3.1$ wt%; $K_2O = 5.43$ wt%) and showing clear troughs at Nb, Ta, Zr and Hf (Fig. 5.23b), is completely similar to the monzogabbro. Initial strontium isotopic ratios $^{87}Sr/^{86}Sr_i$ are 0.71296–0.71502 and 0.71193 for the monzogabbro and syenite, respectively. The isotopic ratios are high suggesting involvement of crustal material in the magmas.

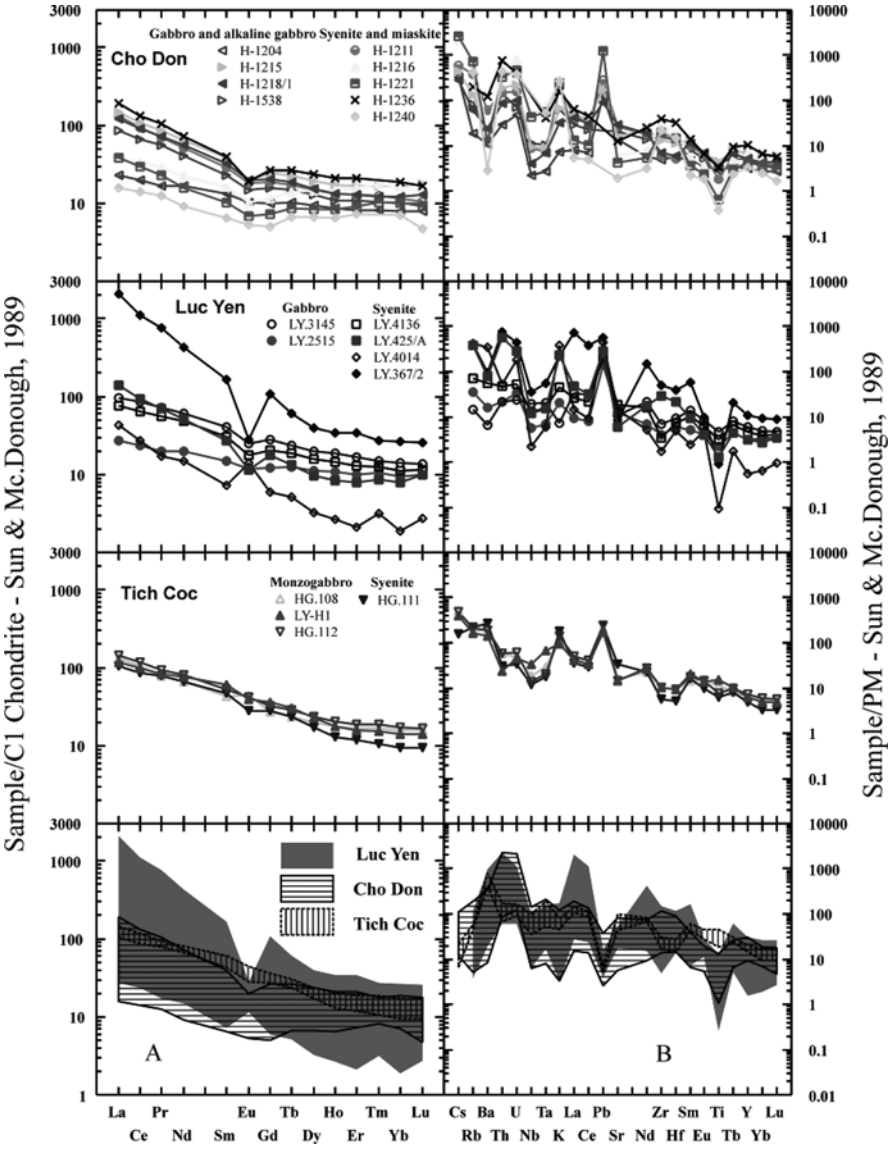

Fig. 5.23 Chondrite normalized rare earth (**a**) and primitive mantle (**b**) normalized trace element patterns of gabbroid and syenite magmas in the Lo Gam structure

Gabbro in the Khuoi Loong block and in southeastern margin of the Bang Phuc block in the Cho Don area (sample H-1204) is characterized by low Ti, alkalis, relatively high Al and high Ca; the magma is low in Cu, Ni, Cr, Co and the REEs but rather high in Sr (Table 5.20). Ratios of Nb/Ta (14), Nb/La (0.3), Ce/Yb (8.9) and Th/U (2.5) in the gabbro are lower compared with those in Luc Yen and Tich Coc gabbroids. Basically, enrichment and depletion configuration of the trace and rare

earth elemental concentrations of the magmas is closely comparable (Fig. 5.25). An initial strontium isotopic ratio ($^{87}Sr/^{86}Sr_i$) of a Khuoi Loong gabbro being 0.70937 is close to isotopic values for Luc Yen and Tich Coc gabbroids. A Bang Phuc pyroxene syenite (sample H-1536) has relatively low Al_2O_3 (15.86 wt%), high Fe_2O_3 (7.43 wt%), and medium alkalis ($Na_2O + K_2O = 7.51$ %, $K_2O/Na_2O > 1$). This syenite type is rich in Rb (126 ppm), Sr (263 ppm), Zr (444 ppm), Ba (850 ppm), Th (65 ppm) and REEs (Table 5.20). The trace and rare earth distribution configuration of the pyroxene syenite (Fig. 5.23a–b) is similar to that of Luc Yen and Tich Coc syenite, except for the low Ce feature, which needs to be further studied to clarify.

Alkaline intrusions in the Bang Phuc block, based on ($Na_2O + K_2O$) and SiO_2 relationship and Ti, Al, Mg, Na and K concentrations, may be divided into three groups: gabbro – pyroxenite ($SiO_2 = 42.08$–44.95 %; $Na_2O + K_2O = 2.64$–3.69 %), monzogabbro ($SiO_2 = 53.03$ %; $Na_2O + K_2O = 8.81$ %) and syenite ($SiO_2 = 55.95$–60.47 %; $Na_2O + K_2O = 12.92$–15.41 %, $K_2O/Na_2O > 1$) (Table 5.20).

The pyroxenite and gabbro are rich in K, Rb, Sr, Th, Pb and REE and low in Nb, Ta and Ba. The Nb, Ta and Ba concentrations are much too low compared with other alkaline mafic magmas such as ijolite, urtite, melteigite (after Sorensen 1979). The primitive mantle normalized trace element and Chondrite normalized rare earth element configuration lines (Fig. 5.23a–b) show enrichment of K, Rb, Sr, Th and Pb and depletion of Nb, Ta, Ba and Ti; on the other hand, enrichment of light rare earths (LREEs) and slight depletion of Eu. Ratios of Ce/Yb (23.5–26.2), Nb/La (0.1–0.4) and Nb/Ta (10.4–19.0) of the gabbroids are different compared with other gabbroids and monzogabbro in the Luc Yen and Tich Coc areas. Initial Sr isotopic ratios of the pyroxenite are similar to those in gabbroids mentioned above. Rare earth concentrations of gabbro and pyroxenite are much lower compared with common alkaline mafic – ultramafic magmas (e.g. Sorensen 1979). A monzogabbro (sample H-1211/1) shows a trace element pattern similar to the above mentioned gabbro, the only difference is the sample has higher concentrations and higher Ce/Yb ratio (30). The studied magmas are relatively enriched in Rb (243 ppm), Sr (562 ppm), Th (12 ppm), very depleted in Nb (6 ppm) and Ta (0.3 ppm). Ratios of Nb/Ta (21.4), Nb/La (0.2) and Th/U (3.8) are mostly similar to those in the accompanying pyroxenite.

Nepheline-biotite- syenites (samples H-1216, H-1521, H-1540) is geochemically different from the pyroxene syenite in that they are relatively richer in Rb, Nb, Ta, Zr, Hf, Th and U but rather poorer in Ba, Sr and REEs (Table 5.20). Their ratios of Nb/La (3.4–3.8), Nb/Ta (12.3–23.6), Ce/Yb (7.1–10.4) and Zr/Hf (53–58) are better illustrating the difference between the magmas. Compared with nepheline syenite in Ilimaussaq (SW Greenland), Lovozero and Khibina-Kola Peninsula, Vishnevogorsk-Urals (Nb = 152–696 ppm, Ta = 14–60 ppm) (after Sorensen 1979) the Cho Don magmas are much poorer in Nb, Ta and REEs, that is expressed in the primitive mantle normalized configuration shown in Fig. 5.23b, where negative anomalies at Zr, Hf, Th, and U and stronger negative anomalies being at Nb and Ta are recognized. These anomalies are much clearer compared with those in the pyroxenite and monzogabbro as mentioned above. Initial $^{87}Sr/^{86}Sr$ isotopic ratios in nepheline-biotite syenite at 0.71913 are much higher compared with those in the

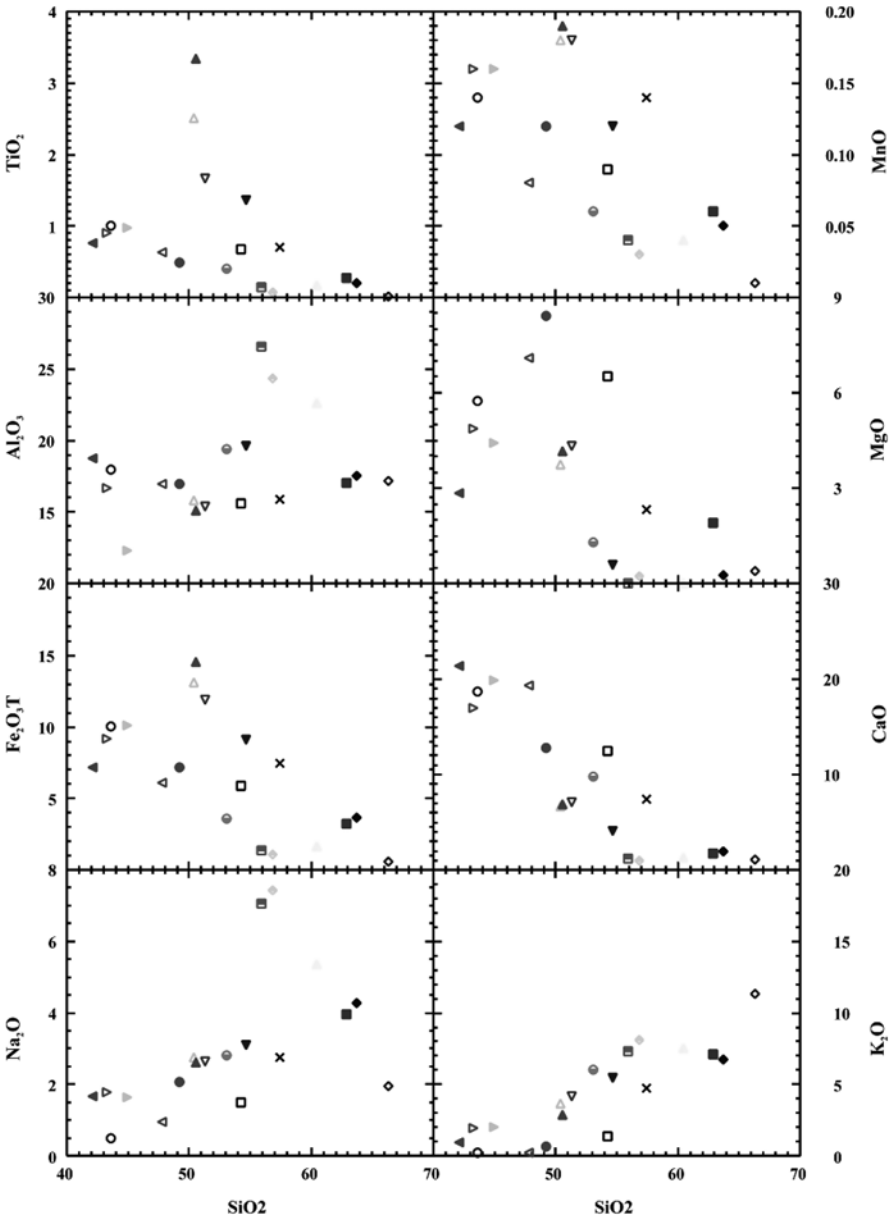

Fig. 5.24 Harker diagrams for gabbro and syenite in the Lo Gam structure

pyroxenite; however, are not exceeding the values recorded for regional monzogabbro and syenite.

5.2.4 Formation Condition and Geodynamic Setting

Detailed mineralogical and geochemical-isotopic studies of gabbro – syenite associations in structures surrounding the Song Chay anticlinoria within folded systems in northeastern Vietnam, whose geological development history is associated with the evolution of southeastern margin of the South China craton (Cathaysian Folded belt), allow for establish three types of association (massif): gabbro – syenite (Luc Yen type), monzogabbro – syenite (Tich Coc type) and alkaline gabbro – nepheline syenite (Bang Phuc type). The first and second types are sub-alkaline series, while the third is alkaline, miyaskite series.

Gabbro in the first association type, according to its geochemical indexes, is similar to mafic magma in calc-alkaline formations. The accompanying syenite is sub-alkaline (K-type), although having wide variation in trace elements (including the rare earths) but in general the magma shows geochemical characteristics suggesting involvement of subduction-related components. The similarity in geochemical and isotopic indexes between gabbro and syenite in the first magmatic association suggests that they both were mantle-derived melts having been contaminated strongly by crustal materials.

Monzogabbro and syenite in the second-type association (Tich Coc type) compared with the first are vastly different in co-existing mineral assemblage (such as the presence of hypersthene, high-Ti, low-Al biotite, apatite…), their geochemistry (higher Ti, alkalis, K, Cs, Pb and REE) although they also show subduction-related signatures (highly depleted Nb, Ta, Zr and Hf). The uniformity in geochemical compositions in monzogabbro and syenite indicate their common mantle source-derived melts having been interacted with crustal materials. This magma generation process would explain the geochemistry of this magmatic association. Crustal involvement may also be evidenced by high Ba, Ce/Yb and $^{87}Sr/^{86}Sr$ in the magmas.

Alkaline gabbro and nepheline syenite in the second-type association although having distinct mineral assemblage and geochemical indexes relative to the first and second magmatic associations there are similar geochemical characteristics worthmentioned such as trace and rare earth elemental distribution configuration and strontium and neodymium isotopic compositions.

In general, based on the isotopic compositions, gabbro – syenite associations in Paleozoic folded structures in marginal areas of the Song Chay anticlinoria were formed by melting of a geochemically common mantle source but having been contaminated by crustal materials. The difference in geochemical mineralogical compositions among the gabbro and syenite magmas may be explained by different wall-rock involvement. In other words, the difference among the magmas is a result of mantle melts contaminated with crustal rocks having taken part either in transi-

tional magma chambers or at contacts of the magma bodies with the crustal wall-rocks. Example of carbonate assimilation in the Bang Phuc magmatic block may be illustrated by metasomatically replacement of Ti-augite by pargasite, the presence of REE-poor calcite and grossular – andradite garnet in gabbroids (Phuong et al., 2004). Besides, strong depletion of Zr, Nb, Sr, Ta and REEs does not lend support to the (near-craton) gabbro being crystallized at deep mantle levels as proposed by Chi (2003) and Duong (2007). There are two explanations on the origin of Zr-Nb-Sr-REE-poor alkaline magmas in the Cho Don area: (1) the parental melts were depleted in the elements; and (2) the more enriched magmas were assimilated by carbonate wall-rock; but the combined effect to the two processes should not be eliminated.

Based on the geochemical and isotopic characteristics of the gabbro – syenite magmatic associations in structures surrounding the Song Chay anticlinoria, although having some difference in details, the magmas in general are produced by melting of lithospheric mantle above a subducted slab to the southeast of Emeishan large igneous province, south of the Yangtze craton. It is noteworthy that the subduction-related geochemistry of gabbro and syenite as well as high- Al granite (all Permian – Triassic) in the studied area is not in conflict with the given geodynamic setting where they were occurred for bimodal basalt – rhyolite volcanism in the nearby Song Hien basin also shows subduction-related geochemical characteristics. The presence of an ancient (early Paleozoic?) subduction zone in northeast Vietnam may be explained by the occurrence of ophiolite-type mafic – ultramafic (serpentinized dunite, amphibolized pyroxenite) bodies along southern and southeastern rims of the Song Chay anticlinoria (Tung and Tri 1992; Nien et al. 2005).

In summary, gabbro – syenite magmas in folded structures around southeastern margin of the Song Chay anticlinoria form three association types distinguished by their co-existing mineral assemblages, mineralogical compositions and geochemical indexes (titanium content and alkalinity). The uniformity of their geochemical and isotopic compositions indicates, on the one hand, generic relationship of the gabbro and syenite, and geochemically common source origin of the magmas, on the other. Being enriched in large ionic lithophile elements (LILE), rare earth elements (REE) and strongly depleted in Nb, Ta and Zr the gabbroid and syenite magmas reflect typical geochemistry of an above-subduction-zone affiliation. This is the basic feature of Permian – Triassic pluton – volcanic and plutonic magmatic associations in various geological structures in northeastern Vietnam.

References

Balykin PA (2002) Formation types of peridotite – gabbro massifs and their primary melts. Autograph of Dr. of Sci. thesis. SB RAS, Novosibirsk, p 44

Bui An Nien, Tran Trong Hoa, Ngo Thi Phuong, Hoang Huu Thanh, Tran Tuan Anh, Pham Thi Dung (2005) Mafic and ultramafic magmatic formations in the Ha Giang and North Pho Rang areas. J Earth Sci 27(2):103–114 (in Vietnamese with English abstract)

Bui Quang Luan, Nguyen Xuan Han, Tran Quoc Hung, Hoang Huu Thanh (1985) Isotopic age and origin of gabbroids in North Vietnam. J Earth Sci 7(1):19–22

Dao Đinh Thuc, Huynh Trung (eds) (1995) Geology of Viet Nam, part. II: magmatic formations. Department of Geology and Minerals of Viet Nam publication, Hanoi VietNam

Dovjikov AE (1965) Geology of Northern Viet Nam. Science and Technology Publ, Hanoi, p 668

Hoang HuuThanh (1994) Mesozoic peridotite-gabbro massifs in the North Vietnam. PhD thesis. United Institute of Geology, Geophysics and Mineralogy. SB RAS, Novosibirsk, p 48

Hoang Huu Thanh, Polyakov GV, Balykin PA, Tran Quoc Hung, Ngo Thi Phuong, Bui An Nien (2004) Island arc nature of the layered intrusions in the Nui Chua magma formation in folded belts in Northern Viet Nam. J Earth Sci 26(4):532–543 (in Vietnamese with English abstract)

Izokh AE, Polyakov GV, Tran Trong Hoa, Balykin PA, Ngo Thi Phuong (2005) Permian-Triassic ultramafic-mafic magmatism of Northern Vietnam and Southern China as expression of plume magmatism. Russ Geol Geophys 46(9):942–951

Lavrenchuc AV, Balykin PA, Borodina EV (2002) Composition of the initial melt and mantle substrate of dunite-troctolite-gabbro's block in Stanovoi fold system. Petrology of magmatic and metamorphic complexes. In: Proceedings of the Russian science conference, vol 1. Tomsk, pp 114–119(in Russian)

Ngo Thi Phuong, Tran Trong Hoa, Tran Tuan Anh, Tran Viet Anh, Pham Thi Dung, Nguyen Viet Y (2003) Chemical composition of olivine, pyroxene, amphibol, spinel and the forming conditions of high grade mafic-ultramafic metamorphosed rock of the Red River shear zone. J Sci Earth 25(4):453–463

Ngo Thi Phuong, Tran Trong Hoa, Tran Tuan Anh, Tran Viet Anh, Pham Thi Dung (2004) Mineralogy of rock-forming minerals in gabbro-syenite intrusions of Cho Don area, Northeast Vietnam. J Geol 23:65–78

Nguyen Van The (ed) (1999) Geology and mineral resources of the Luc Yen map sheet of 1:50,000. Archives of the Center of Geology Information and Literature, Hanoi

Nguyen Xuan Tung, Tran Van Tri (eds) (1992) Geological formations and geodynamics of Vietnam. Science and Technics Publishing House, Hanoi (in Vietnames)

Nguyen Trung Chi (ed) (2003) Petrology and mineralization of alkaline magma formations in Northern Viet Nam. Final report of ministerial project (Ministry of Natural Resources and Environment), Center for Information and Literature Archives, Dept. Geology and Minerals, Hanoi (in Vietnamese)

Nguyen Thuy Dương (2007) Geochemical and mineralogical characteristics of alkaline magma associations in Northeastern Viet Nam. Summary of PhD thesis. Univ. Science & Tech., Viet Nam National University

Phan Luu Anh and Hoang Viet Hang (2005) Crust-origin of the Tam Tao granite block: evidence of late Permian age. J Earth Sci, 27(2):115–124 (in Vietnamese with English abstract)

Polyakov GV, Tran Quoc Hung, Hoang Huu Thanh (1984) New date on ore-productivity of Nui Chua complex. Geol Geophys 11:14–22, in Russian

Polyakov GV, Nguyen Trong Yem, Balykin PA, Tran Trong Hoa, Hoang Huu Thanh, Tran Quoc Hung, Ngo Thi Phuong, Petrova TE, Vu Van Van (1996) Permian – Triassic mafic and ultramafic formations in northern Viet Nam. Science and Technology Publishing, Hanoi, p 172 (in Vietnamese)

Polyakov GV, Tran Trong Hoa, Akimsev VA, Balykin PA, Ngo Thi Phuong, Hoang Huu Thanh, Tran Quoc Hung, Bui An Nien, Tolstykh ND, Glotov AI, Petrova TE, Vu Van Van (1999) Ore-geochemical specialization of permo-triassic ultramafic-mafic complexes in North Vietnam. Russ Geol Geophys 40(10):1474–1487 (in Russian)

Sorensen H (ed) (1979) The alkaline rocks. A Wiley – Interscience Publication, Chichester

Sun SF, McDonough WF (1989) Chemical and isotopic systematics of oceanic basalts: implication for mantle composition and processes. In: Saunders AD, Norry NJ (eds) Magmatism in ocean basins. Geol. Soc. Spec. Publ 42, London, pp 313–345

Tran Trong Hoa (2007) Intraplate magmatism in North Vietnam and related metallogeny. Dissertation of Dr. of Science. Institute of Geology and Mineralogy, Siberian Branch, RAS, Novosibirsk, 382 p

Tran Van Tri and Truong Cam Bao (eds) (1977) Geology of Vietnam, northern part. The explanation to geological map of North Vietnam, scale 1:1,000,000. Institute of Geology and Mineral Resources (in Vietnamese)

Tran Trong Hoa, Nguyen Trong Yem, Hoang Huu Thanh, Ngo Thi Phuong, Vu Van Van, Tran Quoc Hung, Bui An Nien, Hoang Viet Hang, Polyakov GV, Balykin PA, Panina LI, Tran Tuan Anh (1996) New results of high magnesium – alkaline magmas in Northwest Viet Nam. J Earth Sci 18(3):159–170 (in Vietnamese with English abstract)

Tran Trong Hoa, Ngo Thi Phuong, Hoang Huu Thanh, Vu Van Van, Bui An Nien, Tran Tuan Anh, Hoang Viet HangVu Van Van, Bui An Nien, Tran Tuan Anh, Hoang Viet Hang (1999a) Magmatic complexes in the Cao Bang – Dong Khe area. Geological map of Cao Bang – Dong Khe sheet of 1:50,000. Archives of the Center for Geological Information and Literature, Dept. of Geology and Minerals of Viet Nam (in Vietnamese)

Tran Trong Hoa, Ngo Thi Phuong, Tran Tuan Anh, Nguyen Van The, Nguyen Đuc Thang (1999b) New findings of Proterozoic ultramafic intrusive magmas in the Phan Si Pang belt. J Earth Sci 21(2):159–170 (in Vietnamese with English abstract)

Tran Trong Hoa, Tran Tuan Anh, Ngo Thi Phuong, Nguyen Van The, Nguyen Duc Thang (1999c) Classification and correlation of mafic-ultramafic intrusives of Luc Yen Chau. Geol Miner Resour III:103–116

Tran Trong Hoa, Tran Tuan Anh, Ngo Thi Phuong, Izokh AE, Polyakov GV, Balykin PA, Ching-Ying Lan, Hoang Huu Thanh, Bui An Nien, Pham Thi Dung (2004) Gabbro-syenite associations of East Bac Bo structures: evidences of intra- plate magmatism? J Geol 23:12–25, Hanoi

Tran Trong Hoa, Tran Tuan Anh, Ngo Thi Phuong, Pham Thi Dung Tran Viet Anh, Pham Thi Dung Tran Viet Anh (2005) Permian – Triassic magmatic activities in Viet Nam and prospect of associated rare and precious metal (Pt, Au) mineralization. In: Proceedings of 60-Anniversary of Geology of Viet Nam, pp 63–79 (in Vietnamese)

Tran Trong Hoa, Tran Tuan Anh, Ngo Thi Phuong, Pham Thi Dung, Tran Viet Anh, Izokh AE, Borisenko AS, Lan CY, Chung SL, Lo CH (2008) Permo-Triassic intermediate-felsic magmatism of the Truong Son belt, Eastern margin of Indochina. Compt Rendus Geosci 340:112–126

Worley BA, Cooper AF (1995) Mineralogy of the Dismal Nepheline Syenite, Southern Victoria Land, Antarctica. Lithos 35:109–128

Zhong H, Zhu WG, Chu ZH, He DF, Song XY (2007) Shrimp U-Pb geochronology, geochemistry, and Nd-Sr isotopic study of contrasting granites in the Emeishan large igneous province, SW China. Chem Geol 236:112–133

Zhou MF, Robinson PT, Lesher CM, Keays RR, Zhang CJ, Malpas J (2005) Geochemistry, petrogenesis and metallogenesis of the Panzhihua gabbroic layered intrusion and associated Fe-Ti-V oxide deposits, Sichuan province, SW China. J Petrol 46:2253–2280

Chapter 6
Permian – Triassic Metallogeny

Abstract Three mineralization complexes were formed during the Permian – Triassic period in the following order: PGE-Cu-Ni and V-Ti – Fe of magmatic origin; Au – sulfide and Sn – sulfide. The first ore complex including magma-origin Cu-Ni-(Pt) mineralization is related to ultramafic - mafic magmatic differentiation in structures of Song Da, Song Hien rifts (such as Ban Phuc, Ban Khoa, Suoi Cun blocks, etc.) as well as being connected to layered gabbro – peridotite intrusions in folded structures surrounding the Song Chay anticlinoria (such as Nui Chua and Khao Que blocks). Cu-Ni-(PGE)-type mineralization is found in Ta Khoa – and Suoi Cun-type mafic – ultramafic, while Ti-Fe-(V) (mainly) ore type and Cu-Ni-(PGE) are characterized for Nui Chua-type ultramafic intrusion. Radiometric age determined for Ta Khoa ultramafic magmas is 257–270 Ma, for Suoi Cun is 260 Ma and for Nui Chua mafic magmas is 251 Ma; the ages are also applied for the related ore formation, implying that the mineralization of Cu-Ni-(PGE) and Ti-Fe-(V) in geological structures in northern Vietnam was associated with Permian – Triassic tectono-magmatic period. Besides, associated with Cu-Ni-(PGE) ore type is highly potential Ni-Co-As hydrothermal mineralization (discovered in inner contact zones in Ban Phuc block within the Song Da structure). Au-sulfur-type ore complex is widely developed in various structures in northern Vietnam; Representatives of Sn-sulfur-type ore complex are located to the southern margin of Song Hien rift and Lo Gam belt.

Three mineralization complexes were formed during the Permian – Triassic period in the following order: PGE-Cu-Ni and V-Ti – Fe of magmatic origin; Au – sulfide and Sn – sulfide (Table 6.1) (Hoa 2007). The first ore complex including magma-origin Cu-Ni-(Pt) mineralization is related to ultramafic – mafic magmatic differentiation in structures of Song Da, Song Hien rifts (such as Ban Phuc, Ban Khoa, Suoi Cun blocks, etc.) as well as being connected to layered gabbro – peridotite intrusions in folded structures surrounding the Song Chay anticlinoria (such as Nui Chua and Khao Que blocks). Cu-Ni-(PGE)-type mineralization is found in Ta Khoa – and Suoi Cun-type mafic – ultramafic, while Ti-Fe-(V) (mainly) ore type and Cu-Ni-(PGE) are characterized for Nui Chua-type ultramafic intrusion. Radiometric age determined for Ta Khoa ultramafic magmas is 257–270 Ma, for Suoi Cun is 260 Ma and for Nui Chua mafic magmas is 251 Ma; the ages are also applied for the related ore formation, implying that the mineralization of Cu-Ni-(PGE) and Ti-Fe-(V) in

T.-H. Tran et al., *Intraplate Magmatism and Metallogeny of North Vietnam*,
Modern Approaches in Solid Earth Sciences 11,
DOI 10.1007/978-3-319-25235-3_6

Table 6.1 Ore complexes related to intraplate magmas in northern Vietnam (Hoa 2007)

Period	Ore complex	Mineralization type	Representative ore occurrences	Magma association
Permian – Triassic	Cu-Ni and Ti-Fe (magnetite)	Cu-Ni- (PGM)	Ban Phuc, Ban Mong (Song Đa), Suoi Cun (Song Hien), Nui Chua (Phu Ngu)	Komatiite – basalt (257–270 Ma, Song Da), lherzolite-gabbronorite (255–263 Ma, Song Hien), gabbro-peridotite (251 Ma, Phu Ngu)
		Ti – magnetite (Ti-Fe) and Fe-skarn magnetite	Cay Cham and other deposits (Phu Ngu), Na Lung and others (Song Hien)	Pyroxenite and gabbroid series pegmatoid (Permian-Triassic, Nui Chua); gabbro-dolerite (266 Ma., Song Hien)
	Gold – sulfur (Au-As-Sb)	Gold – sulfur (Au-As)	Ban Nung, Na Pai (Song Hien); Neo Village (Song Đa) and others	Rhyolite – basalt (256 Ma., Song Đa); rhyolite-basalt and granite-granophyre (248 Ma; Song Hien), monzogabbro-syenite (247–233 Ma; Lo Gam)
		Antimony – Gold (Au-Sb)	Vai Village-Khuon Puc (Lo Gam), Ban Chang Village (228 Ma, Song Hien); Đong Mo, Khe Chim, Đong Quang (254 Ma, Quang Ninh), Na Bac (Song Đa)	
		Anntimony-Mercury-Gold (Au-Sb-Hg)	Ban Cam Village (Lo Gam), An Bình (230 Ma, Song Đa)	
		Antimony – Mercury (Sb-Hg)	Than Sa (Phu Ngu), An Binh (Song Đa), Vang Pouc (Song Hien)	
	Tin – sulfur (Sn, Pb, Zn, Ag)	Cassiterite – silicate-sulfide (Sn)	Khuon Phay, Tam Đao and others (Song Hien)	Rhyodacite – rhyolite, granite – granophyre (Triassic) Song Hien structure; biotite-granite (250 Ma) and gabbro-syenite intrusions (247–233 Ma) Lo Gam – Phu Ngu structure; Permian rhyolite and granite (Tu Le)
		Tin – Zinc – Silver (Pb, Zn, Ag)	Pb-Zn deposits in the Cho Đon, Cho Đien, Lang Hich (Phú Ngữ structure); in the Tu Le basin and Song Hien structure	
		Barit – đa kim	Lang Cao, Cai Sen (Song Hien structure)	

(continued)

Table 6.1 (continued)

Period	Ore complex	Mineralization type	Representative ore occurrences	Magma association
Cenozoic	Rare Earth-Fluorite-Barite (F-Ba-)	Rare Earth-fluorit-barit (F-Ba-U-TR); Rare Earth-uran-lead – zinc (Pb-Zn-U-TR)	Deposits in Đong Pao and Nam Xe areas, Song Đa structure	K-alkaline and ultrapotassic plutonic mafic – felsic magmas (lamproite, absarokite, minet, trachyte, syenite; 42–35 Ma) Song Đa structure
	Gold – Copper – sulfur (Cu-Au)	Gold – Coper – sulfur (Cu-Au)	Chinh Sang in Song Đa structure	
	Molibdenum-rare metals (Mo-W-Cu-Au)	Molibdenum – rare metals (Mo-W-Cu-Au)	Ban Khoang, O Quy Ho and others in Phan Si Pan uplift	Sub-alkaline granite (35 Ma.) (Phan Si Pan uplift)
	Ruby – sapphire		Tan Huong (27–24 Ma), Truc Lau (Red River shear zone); Luc Yen (Lo Gam belt)	Lherzolite-websterite-gabbro (35–25 Ma), leucogranite (24–22 Ma) Red River sheare zone

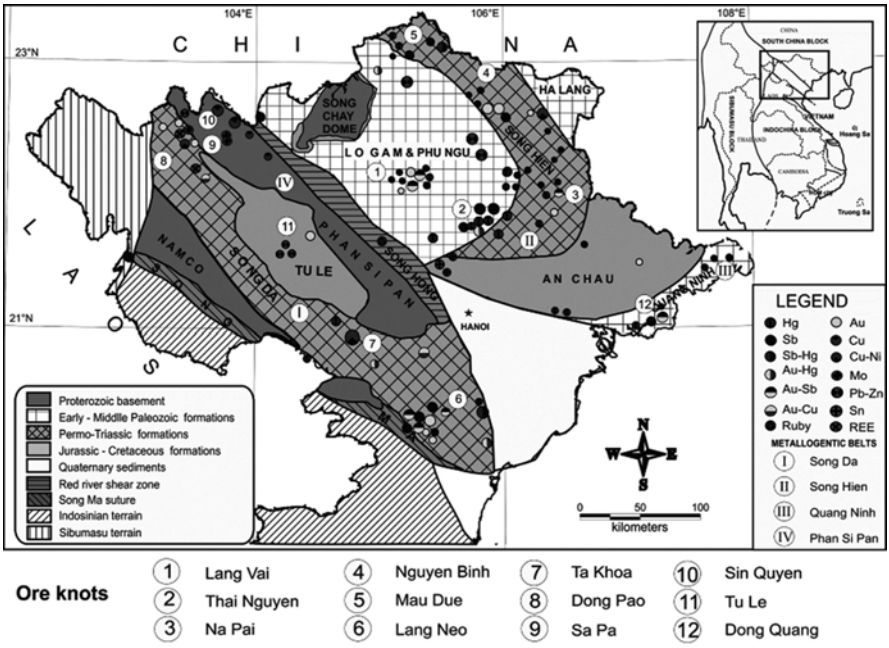

Fig. 6.1 Metallogenic scheme of northern Vietnam (Hoa 2007)

geological structures in northern Vietnam was associated with Permian – Triassic tectono-magmatic period. Besides, associated with Cu-Ni-(PGE) ore type is highly potential Ni-Co-As hydrothermal mineralization (discovered in inner contact zones in Ban Phuc block within the Song Da structure). Au-sulfur-type ore complex is widely developed in various structures in northern Vietnam; these include a number of mines and ore spots. Representatives of Sn-sulfur-type ore complex are located to the southern margin of Song Hien rift and Lo Gam belt (Fig. 6.1). Descriptions of the typical ore types (ore formations) listed above are given below.

6.1 PGE-Cu-Ni and V-Ti-Fe Mineralization Complexes

6.1.1 Komatiite-Basalt Related PGE-Cu-Ni Mineralization Complex in Song Da Rift

It is well known that sulfide nickel and copper and natural nickel deposits are commonly associated with basalt – komatiite magmatic formations, sometimes minerals of platinum group are also found as companions. The majority of this deposit type is normally sided with Precambrian rock complexes (Arndt and Nisbet 1982). Similar examples are rare to find in Phanerozoic structures; the Ni-Cu sulfide Ban Phuc mine and other deposits such as Ban Mong, Nam Chim and others in the Song Da zone are among these rare cases. The popularity of Ni-Cu mineralization indicates its formation is associated with Permian – Triassic Song Da mafic – ultramafic magmatic activities (Phuong 1994, 2001; Hoa 1995; Polyakov et al. 1996; Glotov et al. 2001).

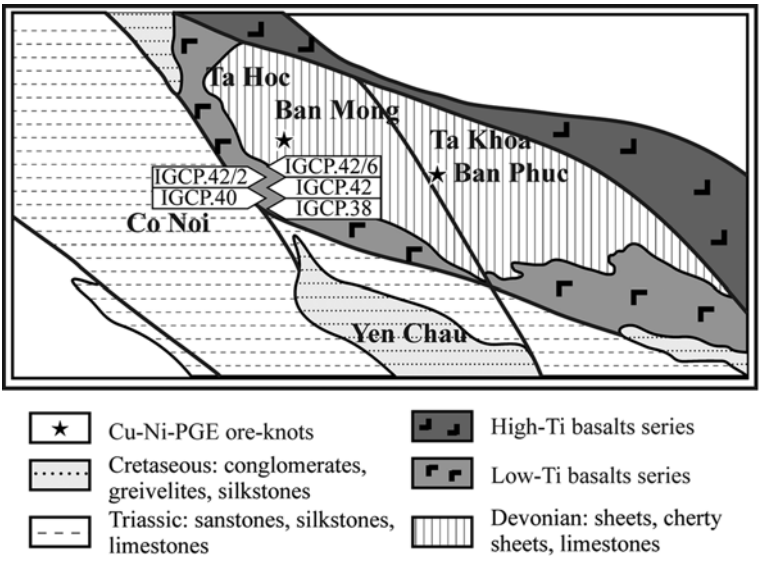

Fig. 6.2 Distribution scheme of the Ban Phuc deposit and ore occurrence at Ban Mong

The Ban Phuc Ni-Cu mine is located in the central region of the Song Da rift, on northeastern wing of the Ta Khoa anticlinoria (Fig. 6.2). The anticlinoria are elongate-shaped running in northwest – southeast direction for more than 50 km and about 20 km wide. The central part of the structure having been deeply eroded is comprised by crystalline shale, quartzite, gneiss, marble, siliceous limestone and amphibolite. In the southeastern, southwestern and northwestern wings of the anticlinoria being less eroded are consisted of volcanic magmas of basalt – komatiite formations (Fig. 6.2). To the northeast the volcanic rocks show tectonic relation to mafic volcanics that belong to high-Ti magmatic associations. Ore-bearing ultramafic (peridotite) massif (e.g. Ban Phuc mine) has an outcrop about 1 km^2, oval-shaped with northwest – southeast elongation and hopper-like cross-section (Minh 2003). The Ban Phuc massif contains mainly dunite and serpentinized lherzolite, somewhere changed into tremolitite. The mineralogical composition of the major rock type contains 45–65 vol.% olivine (serpentinized), 30–35 vol.% clinopyroxene (amphibolized), and 10–15 vol.% tremolite, chlorite, greenish biotite. The accessory minerals include sulfide, sulfo-arsenide and Ni-Co arsenide, tsumoite, Cr-spinel, magnetite, ilmenite and platinum group minerals (PGM). These ultramafic bodies are commonly cut and intruded by dykes and veins having heterogeneous compositions such as pyroxenite – pegmatite, dolerite and ophitic gabbro, and even tourmaline-, biotite- and muscovite-bearing granophyre. Other small-sized intrusive bodies outcropped in the area such as Ban Khoa and Ban Xang also show similar geological structure and structural position as of the Ban Phuc.

After Tri (2000) there are two major ore bodies in the Ban Phuc mine: (1) vein-shaped ore in the outer contact zone having about 640 m long located at (vertical) depth of 450 m. The center of the ore body is filled with dense chalcopyrite – (violarite) – pentlandite – pyrotine minerals having thickness about 1.25 m. The ore occurs as disseminated in surrounding rocks, enriched in copper (Ni/Ni + Cu = 0.4), having up to 7.15 m thick. The ore is characterized by tablet (plate) structure having between-tremolite-crystal pores filled by chalcopyrite. Lenses of hydrothermal pyrite mineralization having low Ni (about 0.006–0.02 wt.%), Cu (ca. 0.03–0.102 wt.%) and low Co (ca. 0.001–0.055 wt.%) are commonly occurred in the peripheral zones of vein-shaped ore body and in surrounding rocks. Second ore body is seam-shaped up to 2–40 m thick, formed by diffusion from disseminated ore bodies that are distributed at the base of Ban Phuc block. The ore appears as aggregates and veins, having average Ni concentration about 0.56 wt.%. By estimate of Tri (2000) the Ban Phuc mine reserves about 119,400, 40,500, 3400, 161,000, 14 and 67 t, respectively of, Ni, Cu, Co, S, Te and Se.

According to the monograph's authors (Table 6.2) the maximal Ni content of ore veins in outer contact zones is higher than 7 wt.%; other metals such as Cu, Co, Pt and Pd are, respectively, about 5.5 wt.%, 0.24 wt.%, 3.5 wt.% and 1.3 wt.%, whereas Au and Ag are rather low. High PGE concentrations are found in Fe-Ni ore varieties where Pt being higher relative to Pd, probably due to the dominance of sperrylite ($PtAs_2$) (Glotov et al. 2001).

The major ore type in the Ban Phuc mine is chalcopyrite (violarite) – pentlandite – pyrrhotite; also present are small-sized Ni-Co-hexatextibiopanikelite, parkerite, suomite, breithauptite, sperrylite and michenerite. Followings are average concentrations (wt.%) of metals in the ore: Ni = 6.42, Cu = 1.63, Co = 0.11, Se = 0.046; and (g/T)

Table 6.2 Concentrations of ore-forming elements (wt.%) and rare metals (g/t) in ores and sulfide-bearing magmas in the Ban Phuc Cu-Ni mine and Ban Mong dyke-phase magmas (Song Da structure) (Hoa 2007)

No	Sample	Ni	Co	Cu	Ni/Co	S	Pt	Pd	Au	Ag	Ni/S	$\delta^{34}S$
Ban Phuc mine												
1	B5185	7.07	0.17	0.81	41.59	34.88			0.01	2.40	0.20	
2	B5186	4.40	0.10	1.05	44.00	34.33	0.01	0.03	0.01	1.90	0.13	
3	567c/84	3.40	0.16	0.45	21.25	30.95	1.60	0.19	0.02	2.50	0.11	
4	G1429	5.60	0.20	0.16	28.00	35.07	0.91	0.35	0.03		0.16	
5	G1431	6.60	0.16	0.88	41.25	33.80	0.21	0.05	0.02	3.11	0.20	
6	M-673	3.19	0.18	0.80	17.72	23.00	0.27	0.16	0.09	2.51	0.14	
7	201E	5.15	0.24	1.89	21.46	34.20	2.45	0.22	0.02	2.94	0.15	
8	Kr6506	2.67	0.08	0.35	33.38	12.48	0.01	0.14	0.02	0.98	0.21	
9	567d/84	1.17	0.05	0.45	23.40	9.82	0.04	0.15	0.02	1.10	0.12	
10	567 k84	0.90	0.03	3.59	30.00	5.41	0.03	0.04	0.02	1.00	0.17	
11	G1422	0.26	0.02	0.18	13.00	4.40	0.03	0.03	0.05	1.42	0.06	
12	G1431/1	2.40	0.06	1.65	40.00	16.30		0.02	0.69		0.15	
13	Kr6507	3.38	0.19	3.75	17.79	20.62	3.55	0.57	0.07	3.60	0.16	
14	B5-94	0.30	0.49	2.03	0.61	30.00	0.09	0.09	0.18	1.00	0.01	
15	B1-94	0.93		1.53		7.45	0.66	1.33	0.05	1.49	0.12	
16	B2-94	0.56		1.92		7.29	0.14	0.44	0.2	2.99	0.08	
17	B3-94	0.41		4.29		8.23	0.05	0.61	0.20	6.21	0.05	

18	423	2.14	0.11	0.10	19.45	28.86		0.03				–2.0
19	PV197	4.96	0.29	0.78	17.10	34.09	0.02	0.12				–3.1
20	PV198	3.09	0.13	0.50	23.77	32.47		0.015				–2.4
21	PV200	0.11	0.11	0.48	1.00	31.16	0.004	0.046				–2.2
22	2-123	3.42	0.13	1.73	26.31	35.77	0.005	0.072				–3.1
23	2-125	1.51	0.06	3.21	25.17	24.46	0.004	0.017				–2.6
24	2-133	1.07	0.05	5.50	21.40	15.33	0.012	0.011				–2.4
25	2-132	3.08	0.13	1.26	23.69	30.43	0.005	0.03				–3.1
26	B-1	4.84	0.12	1.32	40.33	30.37	0.042	0.105				
Ban Mong dykes												
27	Sl100AP	0.19	0.02	0.21	9.50	1.26	0.21	0.20	0.04	1.20	0.15	
28	SL101P	0.04	0.01	0.29	4.00	0.28	0.35	0.19	0.04	1.12	0.14	
29	SL01AP	0.12	0.01	0.27	12.00	5.54	0.21	0.20	0.04	1.20	0.02	
30	M-665	0.27	0.02	0.26	13.50	1.88	0.23	0.22	0.04	1.12	0.14	
31	M-666	0.94	0.04	1.66	23.50	22.80	1.08	0.84	0.07	30.00	0.04	

Remarks: Ore in Ban Phuc mine and Ban Mong dykes: 1–7, 18–26: massive ore; 8–17: disseminated ore; 27, 30, 31: disseminated dyke-like bodies; 28, 29: massif and disseminated ores in contact zones

Au = 0.07–0.27, Ag = 3, and Pt = 0.12. In Cu-rich diffused ore samples the average concentrations of metals are as follows: Ni = 0.49 wt.%, Cu = 0.75 wt.%, Co = 0.02 wt.%, Se = 0.05 wt.%, Au = 0.08–0.14 g/T, Ag = 3 g/T and Pt = 0.05 g/T (Table 6.2).

The sulfur isotopic compositions in the ore are relatively stable that vary in a narrow range of −2.0 to −3.1 ‰, with an average of −2.6 ‰ (Glotov et al. 2001). The isotopes do not depend on S contents and composition of the ore but show similarity to isotopic values in Cu-rich ore. This feature indicates that general ore formation processes are different for different Cu-Ni- ores. The S isotopic composition of mineralized pyrite in surrounding rocks is close to a chondrite value, between −0.3 and −0.8 ‰, having an average at −0.45 ‰ (Table 6.2). The clear difference between S isotopes in Ban Phuc Cu-Ni ore deposit and surrounding rocks and the lack of dependence between S contents and its isotopes indicate that role of S assimilation from surrounding rocks in the Cu-Ni mineralization process is minor, rather suggests that the major S was derived from the komatiic magma (Glotov et al. 2001).

Major minerals in ore bodies in inner contact zones of the Ban Phuc block include pyrrhotite, pentlandite, chalcopyrite and pyrite. Other minor minerals include violarite, heazlewoodite, polydimite, Ni-Co sulfoarsenide, Ni-arsenide, Bi-Ni- Ag-telluride, galenite, sphalerite, antimonite, sperrylite, mechenerite, and complexes of sulfo-Pb-Cu-Ni and Au, Ag and Cu. Pyrrhotite is dominant mineral, forming tablet crystals distributed in spaces between plagioclase crystals. Concentration of pyrrhotite in massive, diffused ore may reach up to 10–20 wt.%. Rims of pyrrhotite grains or aggregate of pyrrhotite crystals contain 10–15 % of crystal-like pentlandite and chalcopyrite developed intercalated with each other. The chemical compositions of pyrrhotite and chalcopyrite disseminated ore are characterized by low Ni (<0.2 wt.%). Sulfide veins having various thicknesses are often observed in diffused ore bodies. Mineral compositions of the sulfide veins are also pyrrhotite, heazlewoodite, pentlandite and chalcopyrite, co-existed at various proportions. In small-sized ore veins pyrrhotite may contain Pd up to 0.11 wt.% (Table 6.3); whereas, pyrrhotite in massive ore contains high Ni (up to 2.84 wt.%),

Table 6.3 Chemical compositions (wt.%) of sulfides in the Ban Phuc ore deposit

No	Fe	Co	Ni	Cu	Pd	S	Total
1	58.88	0.00	0.00	0.07	0.00	38.88	97.83
2	59.72	0.08	0.08	0.00	0.00	39.28	99.16
3	56.39	0.18	2.45	0.00	0.00	39.03	98.05
4	59.03	0.35	0.65	0.00	0.00	39.23	99.26
5	61.16	0.07	0.2	0.00	0.00	37.03	98.46
6	56.67	0.51	2.84	0.00	0.11	39.73	99.86
7	31.61	0.98	33.7	0.00	0.00	22.11	88.4
8	31.27	2.81	33.62	0.12	0.00	32.17	99.99
9	30.32			34.52	0.00	34.8	99.64
10	30.49			34.27	0.00	35.3	100.06
11	29.55	0.34	0.15	34.96	0.00	33.75	98.75
12	29.57	0.07	0.1	34.04	0.00	33.88	97.66

Remarks: 1–6: pyrrhotite; 7–8: pentlandite; 9–12: chalcopyrite (after Glotov et al. 2001)

higher compared with those in diffused ore (Table 6.3). In massive ore having sulfide concentrations up to 90 wt.% pentlandite can reach up to 20–30 wt.% while Cu being a few percent. Sometimes chalcopyrite is higher in pyrrhotite – pentlandite ore for the presence of vein-type mineralization. Modifying process of primary ore is expressed by replacement of pyrrhotite by pyrite; and pentlandite by heazlewoodite and violarite. The silicate component in the ore is replaced by chlorite – amphibole mineral association (Glotov et al. 2001).

Ni- Co- sulfoarsenide and arsenide are normally found as crystals plated in major sulfide minerals as well as distributed in spaces between the crystals. Although rare but the above minerals are also found among chalcopyrite, suomite, and michenerite. The significant feature of Co- Ni- sulfoarsenide is that it contains a number of plated crystals of poikititic sulfide and telluride, sperrylite and mechenerite. The Ni- Co- and Fe-sulfoarsenide in association with PGE minerals is found as solid liquid varying from cobaltite (CoAsS) to gersdorffite (NiAsS), where arsenopyrite (FeAsS) not exceeding 25 mol.% (Fig. 6.3). Co-rich solid liquid may contain sperrylite inclusions.

Ni concentration is high in cobaltite while Pd-bearing (michenerite) occurs in sperrylite. Co concentration is minimal in gersdorffite, while PGE bearing inclusions are not observed in gersdorffite Pd is comparably high 0.26–0.45 wt.% (Table 6.4), showing positive correlation with Ni and negative relationship with Co (Fig. 6.4). In consistence with sulfoarsenide solid liquid dissolution, compositional points of the cobaltite field reflect being formed at temperature about 500 °C while many of gersdorffite compositional points fall in field between 400 and 500 °C. At this temperature interval Pt and Pd from liquid sulfoarsenide will be settled as independent phases as sperrylite and michenerite. There is no Pd-bearing component observed in sulfide and sulfoarsenide association because PGE and Au having simi-

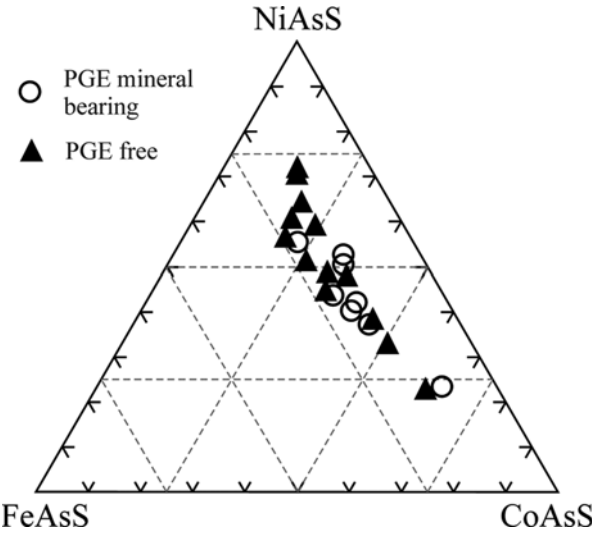

Fig. 6.3 Compositions of Fe- Ni- and Co-sulfoarse-nide in Ban Phuc mine and Ban Mong mineral sites

Table 6.4 Chemical compositions (wt.%) of Ni- Co- Fe- sulfoarsenide in ore and ore-bearing rocks of Ban Phuc mine and Ban Mong ore-dykes; analyzed by EPMA

No	Sample ID	Fe	Co	Ni	Cu	Pd	As	Sb	S	Total
Ban Phuc mine										
1	B3-94	3.17	24.67	7.53	0.08	0.05	46.34	0.02	18.67	100.53
2	B3-94	7.37	10.95	15.73	0.02	0.04	505.56	–	16.22	100.88
3	BP-7/1	4.50	21.13	7.66		0.45	44.74	0.01	18.44	96.93
4	BP-7/1	7.45	8.82	17.81		0.26	46.78	0.08	18.40	99.60
5	BP-10	7.72	6.46	19.37		–	47.64	–	17.85	99.04
6	LO-201/1	7.17	12.02	15.36		0.02	46.81	0.02	18.37	100.24
7	B3-94	4.91	16.82	13.70	0.06	0.01	46.89	0.01	18.33	100.80
8	BP-10	5.43	15.54	13.17		–	46.31	–	18.40	98.92
9	LO-201/1	5.83	15.49	12.90		0.05	46.27	0.05	18.54	99.18
10	LO-201/1	6.70	6.16	20.34		0.16	47.75	0.16	17.75	99.09
Ban Mong dykes and veins										
11	SL-100A	3.66	23.69	8.26		0.08	45.73	0.08	18.90	100.39
12	SL-100A	5.46	17.70	11.59		0.04	46.42	0.04	18.05	99.34
13	SL-100/4	6.76	11.17	16.17		0.05	47.26	0.05	17.73	99.28
14	SL-101	5.35	11.84	18.00		0.04	48.00	0.04	17.60	100.92
15	SL-101	6.00	14.27	14.86		0.07	46.81	0.07	18.47	100.63
16	SL-101A	6.22	13.42	13.65		0.03	46.35	0.03	17.98	98.28
17	SL-101A	5.66	8.20	20.55		0.10	47.84	0.10	17.54	100.05
18	SL-101A	4.63	4.67	24.63		0.24	51.33	0.24	15.14	100.98

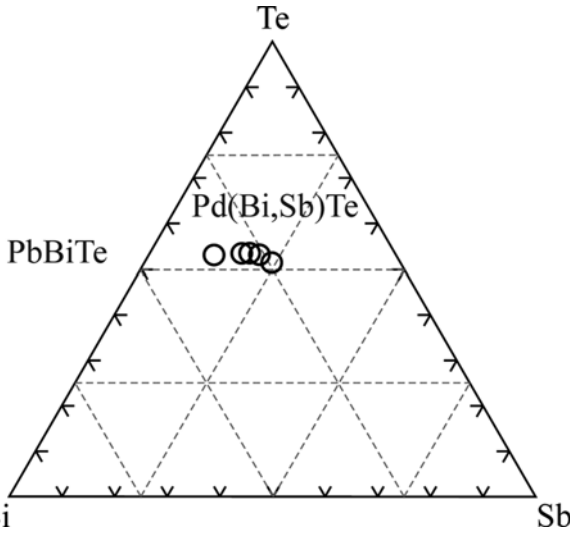

Fig. 6.4 Chemical compositions of michenerite Pd(BiSb)Te and sudberite PdSb in the Ban Phuc and Ban Mong Bi – Te – Sb system

lar properties with arsenide liquid relative to sulfide liquid during separation of these liquids (Gervilla et al. 1996). Ni-arsenide contains up to 0.18 wt.% Sb, while Pb present in the composition of maucherite as isomorphic replacement not niccolite (nickline: NiAs) (Table 6.4).

Bi-telluride (suomite) in association with Ni- and Co- sulfoarsenide form intercalated crystals within or surrounding the host crystals. Sometimes allomorph suomite form crystals developed among chalcopyrite, parkerite, Bi-sulfosalt and michenerite. Pb is found up to a few percent within the minerals (Table 6.5).

Sperrylite is the only mineral containing Pt being discovered in the ore. This mineral is closely associated with sulfoarsenide and Ni- and Co- arsenide forming relatively idiomorphic crystals. Pyrrhorite and pyroxene inclusions are being found in sperrylite crystals. The most significance of the sperrylite composition is that it contains high Sb contents, up to 3.59 wt.%; sometimes Rh, Ni, S and Pd are also found (Table 6.6). Some experimental studies (e.g. Furuseth et al. 1967) determined amount of Sb in the sperrylite structural network depending on the formation temperature. The contents of Rh, Sb and Ni in sperrylite normally decrease in the direction from center to periphery of the crystal. Among the Pd-bearing minerals, michenerite either is formed as inclusions in sulfoarsenide or as crystals intercalated with sulfoarsenide and chalcopyrite. High Sb content in michenerite (Table 6.6) indicates its isomorphic replacement by testibiopaladite (PdSbTe), taking up to 51 mol.% from the total of PdBiTe and PdSbTe (Fig. 6.4).

To the northwest of the Ni-, Cu-, and PGE –ore bearing Ban Phuc ultramafic block there are basalt – komatiite dykes, having tens centimeters to tens of meters, distributed in crystalline shale, amphibolite and quartzite (Ban Mong, Nam Chim, etc.) The outer contact zones of these dykes are rich in sulfide ore. The quartzite in the contact zones contains vein-shaped bodies of sulfide mineralization, while disseminated ores are observed within the dyke rocks. Ni concentration in sulfidized ore reaches 2.53 wt.%, Cu is up to 0.66 wt.% and Ni/Co and Ni/S ratios are similar to those in the Ban Phuc disseminated ore (Table 6.2, number 27–31).

Sulfide ore in the Ban Mong dykes is characterized by high concentration of PGE, where Pt, Pd, Rh and Ag concentrations are, respectively, 0.8–1.5 ppm, 0.2–0.84 ppm, 0.33 ppm, and 17–30 ppm (Phuong et al. 2000). The sulfide in Ban Mong dykes includes mainly pyrrhotite and chalcopyrite of equal quantity, and a minor amount of pentlandite. Chalcopyrite is dominant in inner contact zone followed by pyrrhotite and pentlandite. Besides, as in Ban Phuc mine, sulfide-bearing dykes in Ban Mong the following minerals have been identified violarite, heazlewoodite, sphalerite, galenite, antimonite, Ni-arsenide, Co- and Ni- sulfoarsenide, Bi-telluride, PGE-minerals, gold and natural copper. Pentlandite is characterized by containing high content of Co; while the metal is low in nickeline, in contrast to Sb that is high up to 0.53 wt.%. Ni- and Co-sulfoarsenide are found as relatively idiomorphic crystals including crystals and inclusions of other minerals. The significance of this mineral is that it contain stably high concentration of Pd (0.07–0.63 wt.%) (Table 6.4). Bi-telluride shows a composition mostly similar to that of tsumoite, observed microscopically as crystals intercalated with chalcopyrite, pyrrhotite and pentlandite; such type of tsumoite contains rather high content of Pb. Crystalline tsumoite appeared as inclusion in sulfoarsenide has lower Pb while showing higher Co and Ni (Table 6.5).

Table 6.5 Chemical compositions of telluride and antimonite in ore and ore-bearing rocks in Ban Phuc mine and Ban Mong dykes

No	Sample	Bi	Pb	Ni	Co	Fe	Pd	Te	As	Sb	S	Total
					Ban Phuc mine							
1	LO-201/1	7.19		17.54	1.74	0.09	3.03	50.56	2.93	13.82	1.21	98.11
2	LO-201/1	7.22		18.62	0.55	0.19	2.66	52.99		14.69	0.10	97.02
3	LO-201/1	50.24	4.51	0.22				44.13	0.05			99.15
4	LO-201/1	50.77	4.51	0.05	0.05	0.05		43.00			0.01	98.44
5	BP-10	59.66		26.61		0.04	0.04	0.02		2.05	9.32	97.74
					Ban Mong dykes							
6	SL-100/1	58.04	2.83	0.04			–	37.35	0.04	–	–	98.30
7	SL-100/1	58.49	2.83	0.05	0.02	0.46	0.62	37.23	–	–	0.01	99.71
8	SL-101	54.41	2.17	0.09			–	44.89	0.03	–	–	101.59
9	SL-101	56.55	0.30	1.29	1.94	0.74	0.04	35.52	1.58	–	0.74	98.70
10	SL-101A	58.96	0.68	0.64	0.26	0.15	–	39.20	–	–	0.01	99.90
11	SL-101A	58.85	0.62	0.74	0.34	0.19	0.03	40.07	–	–	0.02	100.86

Remarks: 1–2: hexatestionickeline; 5: parkerite; 3, 4, 6–11: suomite

Table 6.6 Chemical compositions (wt.%) of PGE minerals in ore and ore-bearing rocks in Ban Phuc mine and Ban Mong ore-bearing dykes

No	Sample	Pt	Pd	Rh	Ni	As	Sb	Bi	Te	Sn	S	Total
Ban Phuc mine												
1	B3-94	56.52	–		0.01	43.50	0.22	0.03	–	–	–	100.28
2	B3-94	56.07	0.03		0.37	44.29	0.07	0.05	–	–	–	100.88
3	B1-94	0.05	23.65		0.91	0.05	2.31	42.42	27.69	–	–	97.08
4	BP-7/1	53.77	–	0.57	0.77	42.73	1.92	–	0.06		0.07	99.89
5	BP-7/1	54.29	–	0.13	0.01	40.71	3.44	–	–		0.26	98.84
6	BP-10	54.63	–	0.11	0.14	44.25	0.11	–	–		н.о.	99.24
7	BP-10	54.64	–	0.10	0.09	44.27	0.15	–	–		н.о.	99.25
8	BP-10	54.20	–	0.12	–	43.05	1.37	–	–		0.13	98.87
9	BP-10	54.63	–	0.15	–	43.59	0.89	–	–		0.04	99.30
10	LO-201/1	52.54	–	1.72	0.23	41.97	2.50	–	0.17		0.50	99.63
11	LO-201/1	53.91	–	0.13	0.13	42.09	2.18	–	0.06		0.62	99.12
12	LO-201/1	–	25.07	0.01	1.06	0.01	12.13	28.03	34.03		–	100.34
13	LO-201/1	0.17	26.65	0.03	–	0.01	15.33	25.59	32.96		–	100.74
14	LO-201/1	0.01	25.32	–	1.02	–	10.54	29.68	33.26		–	99.83
15	SL-111	53.81	–	1.56	0.23	41.46	1.72	–	0.09		0.63	99.50
16	SL-111	54.28		0.40	0.08	41.80	0.70	–	0.04		0.00	97.30
17	SL-111	52.91	0.01	2.20	0.17	40.69	2.56	–	0.15		0.72	99.41
Bản Mong dykes												
18	SL-100	50.94	0.88	0.73	0.18	43.23		0.13	н.о.		0.77	96.86
19	SL-100		25.53		0.60	н.о.	7.53	32.10	32.61		0.01	98.38
20	SL-100		25.67		0.77		9.11	31.54	32.99			100.08
21	SL-100		25.07				4.66	38.28	32.99			101.00
22	SL-100		43.97				46.33	9.58	0.20			100.08
23	SL-100		44.33				51.51	3.33	0.09			99.26

(continued)

Table 6.6 (continued)

No	Sample	Pt	Pd	Rh	Ni	As	Sb	Bi	Te	Sn	S	Total
24	SL-100A	53.52	н.о.	0.65	0.02	39.50	5.85		0.12		0.35	100.01
25	SL-100A	54.13	н.о.	0.22	0.12	42.50	2.44		0.22		0.34	99.97
26	SL-100A	н.о.	25.39	0.01	0.63	0.01	7.22	35.74	32.27		н.о.	101.27
27	SL-100A	н.о.	25.19	н.о.	0.73	0.01	5.29	37.91	32.21		н.о.	101.34
28	SL-100/1	54.02	–	0.75	0.06	41.29	3.77	н.о.	0.06		0.30	100.25
29	SL-100/1	53.05	0.08	0.92	0.08	43.28	1.01	н.о.	0.08		0.30	98.80
30	SL-100/1	–	24.59	–	0.99	0.02	6.16	35.15	34.07		–	100.98
31	SL-100/1	0.03	25.56	–	0.85	0.03	10.41	31.55	33.55		–	101.98
32	SL-100/1	0.01	43.25	н.о.	1.65	0.07	52.58	1.91	0.17		–	99.64
33	SL-100/4	53.86	0.01	1.11	0.40	44.07	1.10	–	0.06		0.36	100.97
34	SL-100/4	53.97	0.02	1.18	0.17	43.38	0.91	–	0.03		0.53	100.19
35	SL-101	54.77	–	0.66	0.27	43.57	0.66	0.01	0.01		0.12	100.07
36	SL-101	52.30		2.02	–	39.56	3.74		0.08		0.89	98.59
37	SL-101A	53.21	–	0.91	–	39.74	4.96	–	0.19		0.48	99.49
38	SL-101A	53.70	–	0.75	0.06	43.49	0.94	–	0.09		0.18	99.21
39	SL-101		25.8		0.87		16.05	24.74	33.47		–	100.93
40	SL-101		24.93		0.45		4.91	39.44	31.25		–	100.98
41	SL-101	2.41	1.86		2.41	47.67	0.04				0.88	55.27
42	T1646	–	63.92		–	0.02	0.60	0.02	0.12	34.37	–	99.05

Remarks: in analysis #41 the content of Ir is 20.54 wt.% and Os is 24.08 wt.%; 1–11, 15–18, 24, 25, 28, 29, 33–38, 3, 12–14, 19–21, 26, 27, 30, 31, 39, 40: michenerite; 22, 23, 32: sudberite; 42: paolovite

In Ban Mong sulfide-bearing dykes Pd-bearing minerals are dominant, while ore in the outer contact zone sperrylite is high. PGE mineral association in both rock-ore bearing types is similar. The composition of sperrylite in the outer contact zone and in dyke phase is identical. Minor metals such as Rh, Sb and Ni are commonly present in the sperrylite where Sb decreases from center toward periphery of crystals (Table 6.5). Some sperrylite contains Pd up to 0.88 wt.%. Among the Pd-bearing minerals, michenerite is overwhelming, which is commonly found together with tsumoite as inclusions in sulfoarsenide. Sb is determined to present in the inclusions. Sudberite (?) is also determined to develop alongside with michenerite and tsumoite. The most characteristic feature of sudberite is its containing high content of Bi (Table 6.6). Paolovite has been identified in ultramafic dykes in the Nam Chim area (Table 6.6). Ore in the outer contact zone contains cobalt that includes Os- and Ir-bearing arsenide having high content of Pt, Rh and Ni (Table 6.6). Gold found in this area has higher rate of purity, varying between 760 and 910, and lower Hg content compared with that in the Ban Phuc ore deposit (Phuong et al. 2001).

Therefore, in Ban Phuc, Ban Mong and Nam Chim Ni- and Co-sulfide ores high concentrations of precious metals (such as PGE, Au and Ag) have been determined, the compositions, aside from being viewed as recognizing indicators for chemical compositions and nature of primary magmatic melts, are helpful in ore refining and collecting the metals during Ban Phuc Ni- and Cu-ore processing. The average ratio of Ni/(Ni+Cu) of the Ban Phuc ore deposit is 0.79; average concentration of Pt is 0.35–0.38 ppm abd Pb is 0.21–0.28 ppm in Ban Phuc and Ban Mong Ni-Cu sulfide ores (Hoa 1999; Phuong et al. 2000), the values are closely similar to average Ni-Co sulfide ore mines in Yunnan, China, showing Pt=0.13–1.01 ppm, Pd=0.12–0.9 ppm (average at 0.4 ppm). Refining process using centrifuging separator SKI-01 shows refined Pt and Pd increase by 10 tens of folds, and the discovery of hundreds of grains of Pt- and Pd bearing minerals for study purpose becomes much simpler compared with the investigation of the metals in ore thin sections (Phuong et al. 2000). The new tool emphasizes the efficiency in Pt and Pd separating and collecting for effective use of mineral resources. Therefore, PGE metals in the Ni- Cu- Ta Khoa ore deposit should be accounted as economic values. For example, if the reserve of Ni-Cu ore in the Ban Phuc mine is about 1 million tons (Tri 2000) there are about 300–500 k of Pt should be added to the mine's natural resource balance.

Mantle normalized rare and precious, Ni and Cu metal diagram are used to explain for origin of the PGM. In Fig. 6.5 the configuration curve shows unclear differentiation of the metals in the ore; the feature is typical for komatiite-related mineralization. Sample B-1 has a closely similar elemental distribution configuration to komatiite showing negative anomaly at Ir and enrichment of Pd over Pt. In general, geochemical characteristics of the Ban Phuc, Ban Mong and Nam Chin Ni- Co- ore deposits located in the center of Song Da rift again emphasize the role of komatiite in the regional mafic – ultramafic pluton – volcanic associations. Also the relatively high concentration of Cu, suggesting the potential of the metal in magma – ore system in the area, is a characteristic signature of Phanerozoic komatiite. Sulfur isotope composition, as mentioned above, is typical between ($\sigma^{34}S$ =) (−2.0) and (−3.1) ‰.

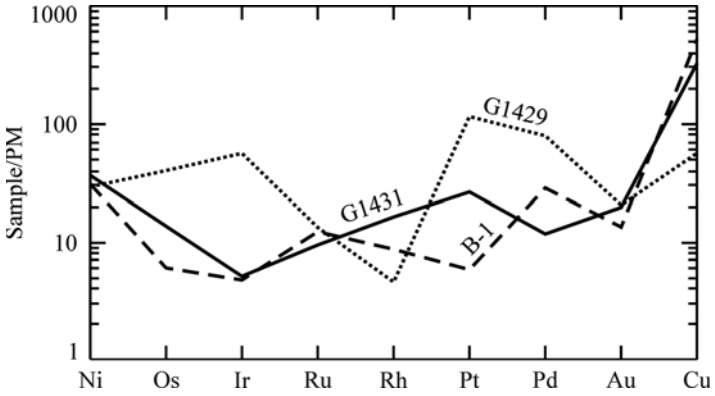

Fig. 6.5 Primitive mantle normalized precious metals in the Ban Phuc sulfide ore deposit (After Glotov et al. 2001)

The intrusion of disseminated sulfide ore-bearing basalt – komatiite dykes into quartzite formations in the Ta Khoa area had led to the interaction between the melt and wall-rock, as a result, to form sulfide ore veins containing Pt-rich minerals in the outer contact zones. The mineralogical compositions of this mineralization type suggest the melt is highly enriched in fluid component, therefore strongly interacts with the surrounding rock leading to the settlement of sulfide and PGE mineralization.

The most significant feature of the above PGE minerals is that their enrichment of Sb. The metal not only participates in isomorphic replacement in some minerals but also forms its own minerals such as breithauptite and antimonite. Experiments on Pt-As-Sb system (Furuseth et al. 1967) show that Sb in isomorphic replacement in sperrylite increases with increasing temperature: in mineral of Pt (As2-xSbx) $0 \leq x \leq 0.2$ at temperature lower than 1000 °C and $0 \leq x \leq 0.3$ with temperature higher than 1200 °C. Concentration of Sb in sperrylite in analyzed ore samples is not higher than 0.2 in an atomic formula unit; for example, Sb has 0.19 atoms in Ban Mong dyke sperrylite (while in outer contact zone is 0.16), and 0.1 in massive Ban Phuc ore. Therefore, the study sperrylite was crystallized at temperatures not higher than 1000 °C. Sperrylite having such high Sb contents was reported for Drikop block in Transvaal (Tarkian and Stumpfl 1975).

Although michenerite is relatively popular in various global Pt-bearing ore deposits but specific Sb-rich minerals are rare, some being described at Witwatersrand (Africa) and Kambalda (Australia) (Hudson et al. 1978). In Bi-Te-Sb triangular relationship (Fig. 6.4) it is clear that Bi in michenerite being from these mines as well as from the Ban phuc ore deposit replaced isomorphically by Sb while the amount of Te remains unchanged in the crystal structure. There is a solid liquid compositionally varies between michenerite (PdBiTe) and Bi-bearing textibiopal-ladinite (Pd(Sb,Bi)Te with Bi varying from 16 to 51 mol.%. It is noteworthy that Kambalda and Ban Phuc mines show similarity not only in their ore compositions but also in geological characteristics such as komatiite-related origin.

Co-, Ni- and Fe-sulfoarsenide, co-existing with PGE-minerals, in the Ta Khoa Ni-Cu- ore deposit represents a member within cobaltite – gersdorffite solid liquid range where arsenopyrite component is not exceeding 25 %. It has been reported that Co-rich solid liquid normally contains sperrylite inclusions. With the increase of cobaltite concentration, among the inclusions and aside from $PtAs_2$, palladium-bearing PdBiTe phase is also present. While Pt metal phase is not observed in Ni-rich solid liquid, Pd, in contrast, takes part in isomorphic replacement in gersdorffite component in a number of solid liquid phases, which is evidenced by the negative correlation between Pd and Co. Mixtures of Pd proved to be absent in sulfide minerals co-existing with sulfoarsenide; this is explained by the fact that PGE- and Au-minerals tend to bond to sulfoarsenide than sulfide liquid during their separation process (Gervilla et al. 1996). As seen on the temperature-dependent solid liquid exsolution curve of sulfoarsendite components lying in the cobaltite field are formed at 500 °C (Klemm 1965) while the majority of components equivalent to gersdorffite are formed at temperatures between 400 and 500 °C. At the temperature of 500 °C, Pt from sulfoarsenide liquid starts to settle as an independent phase. This phenomenon also happens to Pd in gersdorffite at high temperature (ca. 500 °C) in the form of michenerite. As solvus temperature decreases Pd in gersdorffite isomorphism increases. Similar principle is experimentally determined for Ni-arsenide (nickeline and maucherite) (Gervilla et al. 1996). The genetic relation between PGE-minerals and Ni- Co- arsenide and sulfoarsenide in the Ta Khoa area has also been established; where aside from being as independent minerals, Pd also isomorphically participate in other minerals co-existing with sulfoarsenide at concentrations up to a few percent. The fact that Pb-tsumoite being surrounding Ni-Co-sulfoarsenide crystals and their co-existing with low temperature ($\leq$300 °C) Pb- Cu- Ag- and Bi- sulfosalts in the Ban Phuc mine indicate that ore formation process may have been continued even after the crystallization of the ultramafic intrusive block and the sulfide was in hydrothermal liquid phase.

Basically, the distribution characteristics of Ta Khoa Ni-Cu ores, their mineralogical compositions and geochemical properties indicate that their magma – liquid interaction – based mineralization process was clearly episodic. The co-existing mineral assemblages suggest their temperature decreased in the following periods: (1) magmatic stage, including liquid sulfide – silicate separation when Mg-rich melt being S–saturated (may be from a transitional magma chamber) and fractional crystallization of sulfide melt leading to ore differentiation into Fe-Ni and Cu-ore types; (2) magma – fluid stage; and (3) post-magma hydrothermal stage.

Sulfur-saturation process, liquid separation and sulfide melt cumulation; and possibility of sulfide liquid separation into sulfide and arsenide all occurred in the magmatic stage. Crystallization of Ni Co- (and partly) Cu- bearing troilite and pyrrhotite also occurred in this stage. Additional saturation and enrichment of residual melts by ore components and fluids extracted following magma crystallization in transitional chambers could also occur at the magma – fluid stage. At this stage, Cu-Ni-Co sulfide minerals were crystallized as well as the major PGE-bearing minerals, arsenide and Co-Ni- sulfoarsenide, and part of telluride and antimonite. During the hydrothermal – magma, residual hydrothermal liquid ores were active in

early formed ore cumulates and subsequently changed the ore as well as the outer contact zone of the intrusive body. At this stage early formed ore minerals may be partially recrystallized, telluride continued to settle, so did even some Pd-bearing minerals; also occurred was exsolution of unstable solid liquid at this (low) temperature to form sulfosalts of Bi, Sb, Pb, and Cu as well as natural copper, silver, gold and other ore minerals.

6.1.2 (PGE)-Cu-Ni Sulfide Ore Mineralization in Song Hien Pl-Peridotite

(PGE)-Cu-Ni ore mineralization related to ultramafic intrusions in the Song Hien structure has been recently discovered at a number of blocks such as Suoi Cun, Khuoi Giang and Bo Ninh, among these sulfide-ore mineralization in the Suoi Cun block is most studied in detail, especially its eastern margin where sulfide ore is reported to develop in the plagioclase-(Pl) peridotite. The ore mineralization occurs as primarily disseminated form, characterized for the whole cross-section, having concentrations varying between 3 and 7 %, somewhere even reaching 10–15 % of total rock volume. Among the sulfide ore minerals, dominant are pyrrhotite, pentlandite and chalcopyrite while troilite and cubanite are minor phases. Associated with sulfide minerals are Cr-spinel, ilmenite and magnetite. Typical ore contains Ni (up to 0.1 wt.%) higher than Cu where Ni/(Ni + Cu) ratios vary between 0.7 and 0.88, and Co varies from 0.021 to 0.016 wt.% (Table 6.7). The high concentration of the Ni and Co metals is mostly characterized for picritic melt (Magmatic massifs contain Cu, 1990). Sulfide ore-bearing lherzolites characterized by having high PGE are specially high in Pb and Pt (Table 6.7). High concentrations of Pd and Pt are recorded in lherzolite (H-1500, H-1505, H-1607) and dyke-phase gabbronorite (H-1506) while picrite in southeastern side of the Suoi Cun block contains depleted sulfide ore minerals (M-009).

Among the sulfide minerals pyrrhotite and pentlandite are dominant while chalcopyrite is minor (Table 6.8). Most characteristic feature of sulfide phenocrysts in the plagio-peridotite is the presence of pentlandite and chalcopyrite grains, distribute nearly parallel in pyrrhotite; sometimes pentlandite is found in pyrrhotite in the exsolution form of 'thin flame'-shaped. Specifically, sulfide zoning is found in some lherzolites where central part is filled with pyrrhotite, inner rim is with pyrrhotite and outer rim is filled by pentlandite. In magmas having pyroxene spinifex texture between pyroxene crystals commonly found are elongated chalcopyrite and pentlandite grains. Sometimes drop-shaped sulfide cumulates are found in lherzolites, viewed as indicator of liquid separation of magmatic melts in transitional chambers.

Fe-sulfide contains mostly pyrrhotite having Me/S = 0.88–0.92, sometimes troilite is also found, having Me/S = 1–1.01. Pyrrhotite in lherzolites contains 0.08–0.23 wt% of Ni and small amount of Co and Cu (0.0 × wt.%). Pyrrhotite in picrite has

Table 6.7 Chemical compositions (wt.%) and trace element abundances (g/T) of representative Suoi Cun sulfide-bearing magmas

	H1500	H1500/2	H1505	H1514	H1515	H1603	H1604	H1605
Sample	1	2	3	4	5	6	7	8
SiO_2	41.67	41.49		41.89	41.53		42.17	
TiO_2	0.43	0.41		0.40	0.38		0.53	
Al_2O_3	5.94	6.03		6.76	6.96		7.86	
Fe_2O_3	12.21	12.73		13.33	13.74		13.49	
MnO	0.19	0.20		0.20	0.19		0.19	
MgO	29.38	29.92		28.69	28.52		25.08	
CaO	3.92	3.82		4.16	4.18		5.18	
Na_2O	0.79	0.52		0.53	0.54		1.33	
K_2O	0.36	0.33		0.34	0.32		0.48	
LOI	4.39	4.04		3.40	2.57		3.22	
P_2O_5	0.06	0.05		0.06	0.05		0.08	
Total	99.33	99.54		99.77	99.00		99.60	
S	0.37	0.35	1.17	0.22	0.54	0.58	0.24	0.56
	(35.96)	(35.76)	(36.02)	(35.37)	(35.95)	(35.91)	(35.78)	(35.91)
Ni	2058	2265	4042	1950	2280.00	2528	1467	2609
	(20.41)	(23.5)	(12.31)	(32.15)	(15.81)	(15.48)	(22.37)	(16.67)
Co	127	133	163	130	140	135	112	142
	(1.26)	(1.33)	(0.49)	(2.1)	(.93)	(0.87)	(1.64)	(0.90)
Cu	299	608	1716	663	776	1012	372	917
	(2.92)	(6.13)	(5.23)	(11.25)	(5.33)	(6.19)	(5.96)	(5.77)
Cr	979	958	1125	1450	1167	1167	1583	1292
V	60	70	76	77	66	84	97	76
Pd	0.158	0.1	0.19	0.06	0.084	0.08	0.048	0.1
	(15.36)	(10.22)	(5.85)	(9.65)	(5.59)	(4.96)	(7.16)	(6.41)
Pt	0.074	0.08	0.14	0.019	0.029	0.059	0.029	0.04
	(7.19)	(8.17)	(4.31)	(3.05)	(1.93)	(3.65)	(4.32)	(2.56)
Rh	0.005	0.03	0.035	0.005	0.005	0.006	0.005	0.005
		(3.07)	(1.08)			(0.37)		
Au	0.016	0.022	0.12	0.038	0.03	0.04	0.03	0.02
	(1.56)	(2.25)	(3.69)	(6.11)	(2)	(2.48)	(4.47)	(1.28)
Ag	0.1	0.12	0.25	0.19	0.14	0.17	0.08	0.14
	(9.72)	(12.26)	(7.7)	(30.55)	(9.32)	(10.53)	(11.93)	(8.98)
(Fe)	(39.45)	(33.23)	(45.94)	(19.13)	(42.48)	(41.55)	(34.25)	(40.75)

	H1606	H1607	H1608	H1608/2	M006	M009	H1506
Sample	9	10	11	12	13	14	15
SiO_2	41.90		42.39		41.00	40.80	42.07
TiO_2	0.51		0.44		0.49	0.51	1.39
Al_2O_3	7.57		6.22		7.13	7.51	13.45
Fe_2O_3	14.59		13.83		12.75	13.34	9.17

Table 6.7 (continued)

	H1606	H1607	H1608	H1608/2	M006	M009	H1506
Sample	9	10	11	12	13	14	15
MnO	0.21		0.19		0.18	0.19	0.11
MgO	26.14		28.01		34.68	24.28	10.67
CaO	4.88		4.42		4.65	5.05	18.94
Na_2O	1.33		0.54		0.53	0.53	0.54
K_2O	0.35		0.36		0.43	0.49	0.12
LOI	2.20		2.55		7.37	7.27	3.33
P_2O_5	0.10		0.08		0.09	0.09	0.21
Total	99.80		99.03		99.29	100.07	100.01
S	0.47	0.67	0.16	0.32	0.21	0.12	0.45
	(35.89)	(35.98)	(35.62)	(35.78)	(35.71)	(35.40)	(35.84)
Ni	2243	2632	1327	1877	1404	1156	1721
	(16.8)	(13.96)	(28.94)	(21.24)	(23.81)	(35.40)	(13.54)
Co	125	138	116	121	116	112	57
	(0.99)	(0.75)	(2.67)	(1.34)	(2.04)	(3.24)	(0.48)
Cu	776	1034	292	588	360	270	1055
	(6.11)	(5.37)	(6.68)	(6.71)	(6.80)	(8.85)	(8.76)
Cr	1311	1083	1375	1292	541	625	183
V	89	64	66	84	110	96	230
Pd	0.087	0.112	0.028	0.051	0.079	0.063	0.13
	(6.64)	(6.01)	(6.23)	(5.70)	(13.44)	(18.58)	(10.35)
Pt	0.055	0.088	0.01	0.03	0.024	0.026	0.087
	(4.2)	(4.73)		(3.35)	(4.08)	(7.67)	(6.93)
Rh	0.005	0.005	0.005	0.005	0.005	0.005	0.005
							(0.40)
Au	0.03	0.036	0.021	0.02	0.034	0.09	0.016
	(2.29)	(1.93)	(4.45)	(2.24)	(5.78)	(26.55)	(1.27)
Ag	0.12	0.09	0.07	0.08	0.08	0.11	0.16
	(9.16)	(4.83)	(15.58)	(8.94)	(13.61)	(32.44)	(12.74)
(Fe)	(40.21)	(43.94)	(26.10)	(34.93)	(31.63)	(17.12)	(41.38)

Remarks: 1–5: lherzolites; 6–12: plagio-peridotite; 13–14: picrite; 15: melanogabbronorite

higher Ni contents, varying between 0.42 and 0.66 wt.% (Table 6.8). Pentlandite in lherzolites is a high-Fe type while in hardened picrite and lherzolite at contact zones in the Suoi Cun block the mineral is equivalent to actual pentlandite that has Ni/Fe = 0.95–1.11. In general, pentlandite has low Co, but the metal is higher in picrite – (0.83–1.32 wt.%) compared with that in lherzolite-host pentlandite. Microscopic analytical results show pentlandite containing low Pb and Ag concentration. Chemical composition of the chalcopyrite is closely comparable with the phenocryst in the central part of the block, but the mineral becomes higher – Cu (35.8–36.7 wt.%), low-Fe and – S in mineral association with cubanite occurred to the southeast of Suoi Cun, indicating the shift in the sulfide system equilibrium toward higher Cu chemical potential. Highest concentrations of Pd, Pt and Au are

Table 6.8 Chemical compositions (wt.%) of sulfides in Ni-Cu-PGE ore in Suoi Cun magmas

Sample	Fe	Ni	Co	Cu	Ag	Pd	S	Total
Troilite and pyrrhotite								
H-1604-1	63.11	0.06	0.03	0.02			36.3	99.52
H-1605-1	62.8	0.08	0.04	0.02			35.81	98.75
H-1500-1	63.01	0.04	0.04			0.02	35.81	98.91
H-1603-5	60.7	0.29	0.04	0.05		0.01	38.57	99.65
M-006-2	60.32	0.66	0.03	0.05			39.02	100.08
M-006-8	59.94	0.57	0.04		0.01	0.01	38.99	99.56
M-009-1	60.44	0.42	0.04	0.09	0.03		38.8	99.81
Pentlandite								
H-1603-3	32.05	33.7	0.96	0.06	0.02	0.01	32.75	99.55
H-1603-6	32.83	32.75	0.69	0.16		0.02	32.25	98.7
H-1604-2	37.86	28.2	0.58	0.08			32.85	99.57
H-1604-4	37.84	28.07	0.52	0.15		0.01	32.86	99.44
H-1605-2	38.82	27.22	0.62	0.06		0.01	32.26	98.98
H-1500-2	39.21	26.46	0.61	0.14		0.01	32.1	98.53
H-1500/2-3	39.74	25.81	0.6	0.5		0.02	32.69	99.35
H-1505-1	37.03	28.44	0.58	0.06			32.31	98.42
M-006-4	30.04	34.68	1.32	0.06			32.56	98.66
M-006-9	30.29	35.07	1.22	0.03		0.02	31.4	98.03
M-009-3	31.47	34.03	0.83	0.08		0.01	32.19	98.61
Chalcopyrite								
H-1603-4	30.78	0.01	0.03	34.43			34.44	99.69
H-1603-7	30.63	0.11	0.02	33.93	0.04	0.01	33.88	98.61
H-1604-3	30.67	0.05	0.01	33.87		0.01	34.62	99.23
H-1605-3	30.48	0.08	0.02	34.12			34.24	98.94
H-1500-3	30.64	0.15	0.02	33.47			33.61	97.89
H-1500/2-2	30.26	0.49	0.01	35.84			32.66	99.26
H-1500/2-4	29.95	0.57	0.01	36.56			33.29	100.38
H-1500/2-6	29.73	0.5	0.02	36.49			32.74	99.48
M-006-1	31.38	0.13	0.02	33.47			34.07	99.08
M-009-2	30.48	0.14	0.02	34.02	0.01		34.07	98.74
Cubanite								
H-1500/2-1	41.27	0.01	0.03	23.48		0.03	35.36	100.18
H-1500/2-5	40.71	0.02	0.02	23.73			35.54	100.02
H-1500/2-7	40.78	0.02	0.03	23.65		0.01	35.23	99.71
H-1505-2	41.16	0.07	0.03	23			35.12	99.37
H-1505-3	41.17	0.12	0.04	23.11		0.02	34.54	99

Remarks: sulfide minerals: 3, 13–15, 23–26, 29–33: southeast Suoi Cun; 1, 2, 4, 8–12, 20–22: plagio-lherzolite cross-section; 5–7, 16–18, 27, 28: in hardened picrite zone

found at this location (Table 6.8). Ni concentration in chalcopyrite associated with cubanite is relatively high (0.47–0.57 wt.%) because of its partially isomorphic replacement of Fe. Cubanite in this association normally distributes at margins of the sulfide cumulates while the central parts are filled with pyrrhotite and small amount of pentlandite. Chalcopyrite is found in phenocrysts of cubanite, which is the major mineral in the phenocryst phase. The chemical composition of cubanite is correspondent to the theoretical notion having a small amount of Ni of 0.02–0.12 wt.% (Table 6.8). The only PGE-bearing mineral being found is michenerite (PdBiAs).

The distribution characteristics of major ore minerals and PGE- and Au-bearing minerals in the lherzolites are related to compositional variation of the sulfide components in magma – ore system and their contents in the magma. In order to analyze the continuation of compositional evolution of the sulfide phase, results of Cu-tender element (chalcophile) are converted to 100 % sulfide and shown in Fig. 6.6. It is seen that the Suoi Cun Ni-Cu-PGE ore minerals are characterized by tending toward Fe-Ni and not showing any systematic relationship between Cu and other major as well as PGM metals. The PGM ore mineralization is chemically Pd-tending; in addition, Pd in the sulfide system is settled along with Ni at stages of sulfide crystallization, Pt and Rh likewise are also enriched. The distribution of Au and Ag is less dependent on PGE and Pb distribution behavior; in a sulfide phase in picrite (sample M-009) concentration of these precious metals are all anomalously high. The distribution feature of major PGE and Au ore minerals of a sulfide ore mineralization vein in a gabbronorite dyke (H-1506) in plagio-lherzolite is completely similar to that of main host rock, e.g. peridotite.

There may be able to analyze the behavior of Ni in the crystallization processes in silicate and sulfide – silicate systems using the correlation of Ni in Ol – Fa system

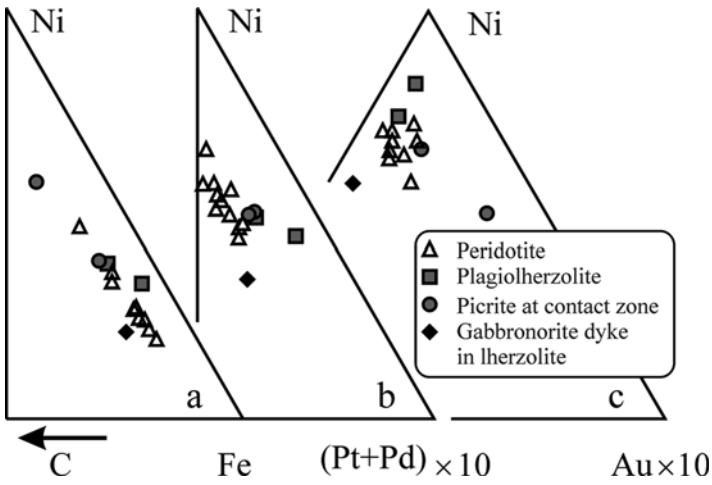

Fig. 6.6 Relationship between Ni-Cu-Fe, Ni-Cu-(Pt + Pd)104 of sulfide phases in Pl-lherzolite in the southeast of Suoi Cun

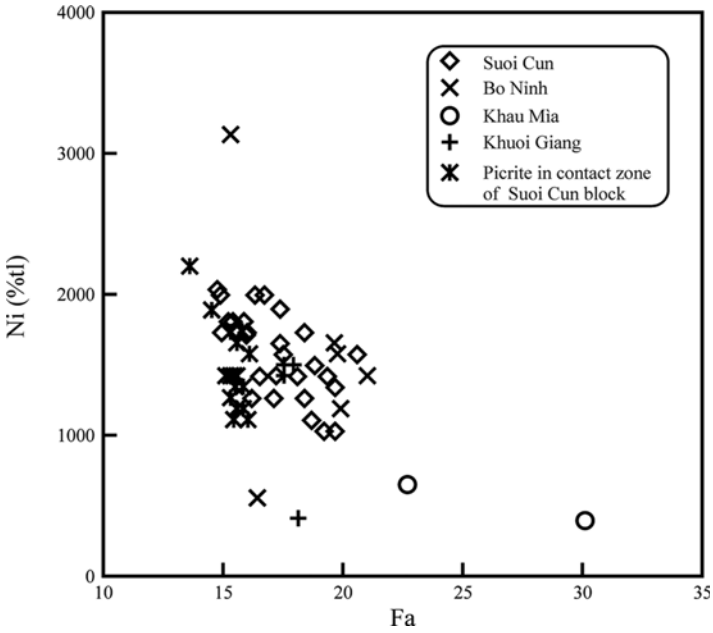

Fig. 6.7 Correlation between Ni in olivines and Cao Bang ultramafic magmas

(Fig. 6.7). In the diagram, olivine of the study block concentrates mostly in a single field corresponding to Ni depletion trend in the silicate system as crystallization of olivine proceeds and F_{Ol}, as a rule, increases. The silicate melt in many cases may retain equilibrium with a small amount of early-formed sulfide while not forming significantly surplus cumulates. Compositional points of hardening phase – picrite in the marginal area fall in a separate field, forming a rather steep trending slope, suggesting input of Ni in the form of early sulfide phase from marginal zones into the center of the block by redistributing phases that were formed by differentiation processes occurred during melt transportation. For magmatic complexes this diagram indicates that olivine is not indicative for Ni concentrations in intrusive bodies.

The above data show that, Ni-Cu-PGE- bearing magma association characterized for developing stage of sulfide ore – magma silicate when the silicate component being weakly differentiated and the temperature of sulfide component being high, such that having high iron and stable Fe-Ni trend in the ore compositional distribution. The high temperature conditions for sulfide ore formation being characterized for ore deposits having genetic relation to komatiitic and picritic magmas have been proven by experimental studies on sulfide systems in recent decades (Barnes et al. 1993). The studies show that the distribution coefficients (D) between singular sulfide solid liquid and residual melt are from 0.07 to 1.90, which have negative correlation with temperatures. At temperatures higher than 1000 °C, Ni remains in the residual phase, this is illustrated by compositional distribution in the

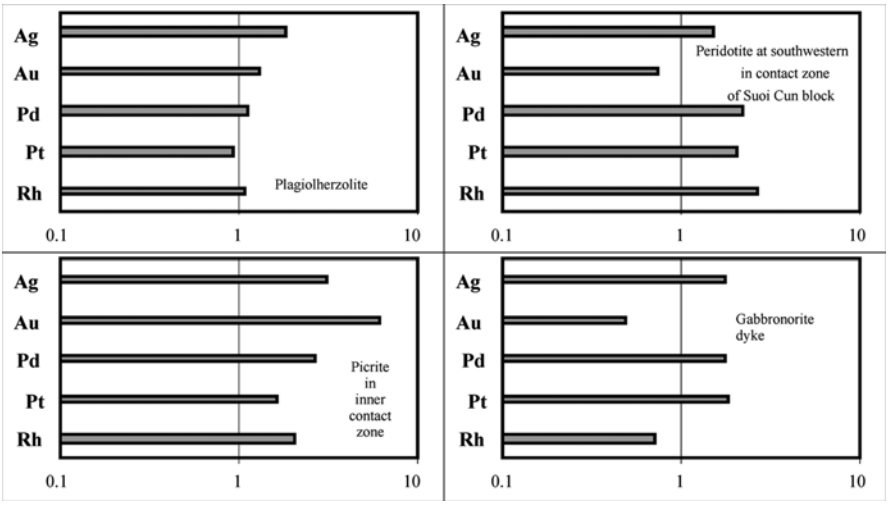

Fig. 6.8 Concentrations of Ag, Au, Pt, Pd and Rh in Suối Củn ore normalized by Fe-rich ore type

form of Fe-Ni trend as recorded in the Suoi Cun block expressed by the presence of troilite sulfide association and Fe-rich pentlandite.

The sulfide component of magma – ore system in the Suoi Cun ultramafic magma association is characterized by sulfur of relatively low chemical potential. Evaluation of the chemical potential of sulfur basing on pentlandite concentration being conducted using study of Kosyakov et al. (2003) shows lgf(S2) for sulfide system in the Suoi Cun block is not exceeding (−11.1) to (−12.4), and that only at the marginal zone and in hardened picrite the value may reach (−9.4) – (−8.7) (Glotov et al. 2004). In principle this reflects, in the one hand, the concentration of S along the contact between the intrusive body and surrounding rock, and on the other, shows the crystallization of pentlandite at the low temperature condition on the background of high S potential, which is appropriate with heat field distribution during formation process of the intrusive body and physic-chemical rules of the differentiation process of sulfide systems.

Because sulfide ore mineralization in Suoi Cun peridotite has complex composition, together with Ni and Cu, precious metals (such as PGM, Au and Ag) play important roles, therefore in analyzing compositional distribution we used method presented by Glotov et al. (2002). While analyzing the distribution of precious metals among various ore types at a given ore mine average concentrations of the metals in ore types are commonly used. The ore types are normally normalized to a high-Fe component as done for Suoi Cun sulfide ore mineralization (Fig. 6.8). Small deflection of the normalized values for all precious metals compared with a unit (e.g. 1) indicates weak fractionation of the sulfide liquid (melt). Pd and Pt in many ore occurrences concentrate mostly in late phases of a sulfide system and corresponding ore mineralization types, in this sense, Suoi Cun block is viewed as Ni-rich ore mineralization. Relatively rich in Pt in Fe-rich sulfide ore illustrated in Fig. 6.8

having normalized value smaller than the unit (1) may reflect the occurrence of feroplatinum metallic alloy co-existing with singular sulfide solid liquid. For all sulfide occurrences in peridotite the ore generation process normally happens in low S condition, expressed by Rh normalized value higher than 1, fitting experimental results on PGE-bearing sulfide ore at various S-saturation levels (Li et al. 1996). Basing on this feature, S-saturation levels of Suoi Cun sulfide liquid may have increased, which is shown by the compositions of sulfide phases in gabbronorite dykes (Fig. 6.8).

From the above descriptions one may come to a conclusion that Suoi Cun sulfide cumulates in the Song Hien structure occurred in transitional magma chambers. The presence of olivine phenoscrysts in hardened magmas as well as in gabbronorite and gabbrodiorite dyke and vein phases suggests the role of transitional magma chambers in the formation process of the intrusive massif (block). Role of transitional chambers may be shown by high concentrations of PGE in sulfide phases in Suoi Cun-type ultramafic block in the Song Hien structure, also by the fact that S-saturation in picrite melts and the separation of sulfide liquid occurred prior to the crystallization of the silicate melts. This is evidenced by the presence of high-PGE, drop-shaped sulfide in gabbronorite dykes penetrating the lherzolite as described earlier. The Ni-Cu-PGE potential in picrite intrusions in the Song Hien structure is not based only on the above descriptions but also on analogy of Ni-Cu-PGE- bearing ultramafic intrusions having similar chemical composition and occurrence age in several geological structures in nearby Chinese southern regions (Limakhe, Yang Baoshan, etc.) (Fang et al. 1985; She Chuan-Jing 1986).

6.1.3 Cu-Ni-PGE and Ti-Fe-V Mineralization Related to Nui Chua- Type Layered Gabbro – Peridotite in Phu Ngu – Lo Gam Structures

Cu-Ni- sulfide ores are popular in Nui Chua and Khao Que layered gabbro-peridotite intrusions. Cu-Ni-and accompanying PGE-sulfide ores are characterized for differentiated magmas, for which the Nui Chua block is well studied (Thanh 1994; Polyakov et al. 1996). Ore minerals in the differentiated magma series are mostly sulfides (such as pyrrhotite, pentlandite and chalcopyrite) and sulfoarsenides (Table 6.9). Magnetite, titanomagnetite and ilmenite are less popular. Occasionally found are linnaeite, polidimite, heazlewoodite, arsenide and Co-Ni- sulfoarsenide. Disseminated sulfide ore minerals are dominant. At drill site LK-2 in the eastern side of Nui Chua block (within differentiated magma series) 9 sulfide-rich magma, mostly ultramafic, layers are reported. Commonly occurred are equal- dissemination sulfide ore types including pyrrhotite (50–79 wt.%), Ni-rich ore (up to 1 wt.%), pentlandite (10–30 wt.%), high-Co ore (up to 4 wt.%) and chalcopyrite (ca. 10–30 wt.%). Complex ore oxide and sulfide mineral associations are found as syn-genetic diffused forms, containing pyrrhotite, pentlandite and chalcopyrite on which oxide minerals such as magnetite, titanomagnetite and ilmenite occurred in later stages.

Table 6.9 Chemical compositions (wt.%) of sulfide and sulfoarsenide in Nui Chua ores and ore-hosting magmas

No	Sample	Fe	Ni	Co	Cu	As	Sb	Se	S	Total
1	LK2-167	59.12	0.55	0.08	0.01	0	0	–	39.02	98.78
2	LK2-439	60.02	0.27	0.07	0	0	0	–	38.23	98.59
3	P9	61.94	0.21	0.05	0.01	0.1	–	0.01	37.52	99.84
4	P12	61.07	0.34	0.12	0	0.09	–	0.03	38.07	99.72
5	P14	60.66	0.68	0.03	0.06	0.1	–	0.06	38.84	100.43
6	P25B	61.18	0.04	0.06	0.01	0.08	–	0.03	37.62	99.02
7	B5036	59.24	1.01	0.08	0.01	0.12	–	0	38.77	99.23
8	G1141	59.68	0.74	0.02	0.05	0.05	–	0.02	38.86	99.42
9	G1444	59.29	0.57	0.21	0	0	–	0	39.37	99.44
10	G1153	60.07	1.08	0.08	0.02	0	–	0	38.93	100.18
11	G1154	59.08	0.57	0.08	0.02	0.02	–	0	39.35	99.13
12	LK2-167	31.83	28.51	4.79	0.04	0	0	–	33.55	98.72
13	P9	31.7	32.23	2.46	0.07	0.01	–	0.1	32.72	99.29
14	P12	32.33	31.36	2.21	0.07	0.03	–	0.01	32.42	98.43
15	P14	30.33	33.32	2.13	0	0.15	–	0.06	32.45	98.44
16	P25B	31.19	30.48	4.03	0.05	0.09	–	0.04	32.64	98.52
17	Kp6404A	34.42	29.51	1.96	0.13	0.07	–	0.04	32.65	98.78
18	G1141	29.96	33.95	2.34	0	0.02	–	0.05	33.06	99.38
19	G1144	28.74	22.65	13.4	0.16	0	–	0	34.89	99.84
20	G1153	29.01	34.28	2.92	0.03	0.03	–	0	33.01	99.28
21	P1154	27.71	34.25	3.49	0.05	0.02	–	0.06	33.14	98.72
22	P9	30.79	0.03	0.06	34.49	0.07	–	0.07	34.89	100.4
23	P12	30.58	0.64	0.1	33.18	0.07	–	0	34.42	98.99
24	B5036	30.94	0.01	0.03	34.35	0.06	–	0.06	34.62	100.07
25	Kp6404A	40.94	0.1	0.06	22.6	0.12	–	0.03	35.06	98.91
26	LK2-438	30.43	0.15	0.08	33.64	0	0	–	34.47	98.77
27	LK2-439	30.27	0.03	0.02	34.41	0	0	–	34.05	98.78
28	LK2-167	4.99	11.37	19.67	0	47.53	0.01	–	17.94	101.51
29	LK2-438	4.95	12.55	18.11	0	46.14	0.62	–	18.43	100.8
30	P25B	3.43	2.49	30.88	0.01	44.57	–	0.2	19.46	101.04
31	LK2-167	0.51	42.5	0.87	0.07	54.44	0.36	–	0.24	98.99
32	LK2-438	1.16	50.77	0.4	0.06	48.39	0.06	–	0.04	100.88
33	LK2-439	40.54	0.01	0.05	23.27	0	0	–	34.66	98.53

Remarks: 1–11: pyrrhotite, 12–21: pentlandite, 22–27: chalcopyrite, 28–30: cobalnite, 31–32: nickeline, 33: cubanite. Pd was analyzed for 28 and 32 samples showing 0.12–0.14 wt.%

Study of Ni in olivine and whole rock of differentiated series shows the same concentration level indicating that Ni concentrates in Ni-rich sulfide-bearing rock in the form of sulfide ore, implying an advantage of the differentiated magmas to contain high Ni contents. Among coarse-grained gabbroid and websterite in pegmatoid series found are fine-grained disseminated ore minerals associated by cumulate aggregate or fractionated cumulates of chalcopyrite, magnetite, titanomagnetite and

Table 6.10 Chemical compositions (wt.%) of PGE minerals in Nui Chua sulfide ores

No	Sample	Pt	Pd	Ni	As	Sn	Sb	Te	Bi	Total
1	LK2418	51.45	0.54	2.4	43.86	–	0.56	–	–	98.81
2	LK2-418	52.56	0.67	1.14	43.34	–	0.69	–	0.04	98.44
3	LK2-418	–	64.25	–	–	36.74	0.59	–	–	101.58
4	LK2-418	–	63.9	–	–	36.77	0.84	–	–	101.51
5	LK2-418	0.08	25.37	0.1	–	0.03	1.87	30.77	44.04	102.26
6	LK2-418	–	25.32	0.1	–	0.04	2.13	31.35	43.55	102.49
7	LK2-438	51.89	1.1	1.59	43.68	0.02	0.41	–	0.12	98.81
8	LK2-438	–	65.11	–	–	35.28	2.41	–	–	102.8
9	LK2-438	–	3.09	29.3	0.32	0.03	65.2	0.35	0.04	98.33
10	LK2-438	0.03	3.15	29.29	0.31	0.02	66.4	0.4	–	99.6
11	LK2-439	–	64.12	–	–	37.02	0.65	–	–	101.79
12	LK2-439	–	64.64	–	–	37.19	0.6	–	–	102.43
13	LK2-439	0.08	38.3	–	–	0.1	7.11	14.72	41.76	102.07
14	LK2-439	0.06	38.55	–	–	0.09	7.18	14.69	41.72	102.29

Remarks: 1, 2, 7 – sperrylite; 5, 6 – michenerite; 3, 4, 8, 11, 12 – paolovite; 13, 14 – sobolevskite; 9, 10 – breithauptite

ilmenite, sometimes having industrial values (for example, Cay Cham mine and other ore occurrences). Ilmenite contents (titan-magnetite) in an ore body may reach 30–70 wt.% showing a characteristic chemical composition (wt.%) of $TiO_2 = 15.36$, $FeO = 23.35$, $Fe2O_3 = 2.89$, $V_2O_5 = 0.12 - 0.25$. Industrial estimate shows that original ilmenite in Nui Chua gabbro – peridotite magmas about 15 million tons (Tri 2000). Aside from the above described titan-magnetite ore occurrences, other potential Ti rich-ore hosts include Nui Chua monzogabbro and monzodiorite as well as Tich Coc high- alkalis, –Ti and $–P_2O_5$ magmas (see Chap. 3 for detail) (Hoa 1999).

PGE-mineralization was discovered in magmas of differentiated series (Thanh 1994; Polyakov et al. 1996, 1999) mainly containing sperrylite, paolovite, sobolevskite and michenerite (Table 6.10), as well as others hosting Pt and Pd. PGM- ore was determined to associate with sulfide-rich gabbroid and lherzolite in lower sections of the differentiated series in the east of Nui Chua block (drill site LK-2, at depths 418 and 438–440 m). Sperrylite forms cubic crystals up to 0.15 mm in association with niccolite, Co-sulfoarsenide and michenerite (Polyakov et al. 1996). Pd-bearing minerals are found in form of crystals inosculated among sulfoarsenide and Co- Ni-arsenide, and as small-sized inclusions in the latter minerals. High Pb and Sb concentrations are reported for maucherite, Co- Ni-sulfoarsenide and pentlandite, while in breihauptite the Pd may reach 3.15 wt.% (Table 6.10).

According to the above documentation one may conclude that in the geological structures in northern Vietnam there are at least three magma – Cu-Ni-PGE-bearing ore complexes as follows: (1) ultramafic intrusive and dyke magmas in low-Ti, high-Mg volcano- plutonic basalt – komatiite associations of the Song Da rift, (2) ultramafic intrusive magmas associated with gabbro – dolerite and basalt – andesite formations in the Song Hien rift, and (3) layered gabbro – peridotite in contrast

gabbro – granite series in the Lo Gam folded structure. The genetic relation between the Cu-Ni-PGE sulfide and the magmas is undeniable. The occurrence timing of the magma – ore complexes is completely coincident with those complexes in China, in the marginal terrains of the Emeishan large igneous province. Based on the spatio – temporal relationship while taking paleo- and recent geodynamical models (late Paleozoic – early Mesozoic and Cenozoic, respectively) into consideration, it is clear that Cu-Ni-PGE and Ti-Fe-V mineralization in northern Vietnam is closely related to Permian – Triassic magmatic activities, an expression of mantle plume.

6.1.4 Fe-Skarn Ore Complexes

Fe-skarn ore mineralization is rather popular in the Song Hien structure. They appear in a number of small-sized deposits and ore sites, having a total natural reserve about 70 million tons (Tri 2000). Occurrence of the ore type spreads along the Cao Bang – Tien Yen fault belt, that can be observed from the northwest extreme (Meo Vac – Ha Giang) to the southeast (Lang Son); they show the close spatio – temporal relationship with lens-shaped small-size intrusive bodies comprising Permian – Triassic gabbro-dolerite and gabbro-diorite magmas. In many cases the ore bodies lie coincidently with contact area between intrusive blocks and carbonate formations. Along with predominant magnetite mineralization, in the ore mineralization belt diffused sulfide ores are relatively popular (such as pyrite, pyrrhotite and chalcopyrite). Gold concentrations in sulfidized belt sometimes reach up to 5–7 g/t (Hoa 1998). It is highly regrettable that this ore type is not yet studied as required.

6.2 Au-Sulfide and Sn-Sulfide Complexes

6.2.1 Au-Cu Mineralization

Au-Cu mineralization related to intraplate magmatism has only been recognized, with some confidence, in the Song Da rift. This type of ore mineralization normally distribute coincidently in Permian – Triassic high-Ti mafic magmatic areas. Most characteristic Au-Cu occurrence in the Song Da structure is Suoi Trat mine and Lung Cua, Cao Ram and Bai Dao ore occurrences (Fig. 6.1). Ore mineralization is crushed belt, hydrothermal metamorphism to various sulfidization levels in high-Ti basaltoid fields. In many cases, basaltoids are strongly foliated, metamorphically altered to albite-chlorite-actinolite rock type. Chloritization and carbonatization are highly developed, accompanied by ore sulfidization. Ore sulfidization is normally controlled crashed zones in basaltoid fields.

Ore bodies in the Suoi Trat mine are tightly controlled by metamorphic foliated belts in Permian high-Ti basaltoids being equivalent to greenschist facies, which were subsequently complicated by later vein-dyke and hydrothermal activities. The Lung Cu ore site locates alongside with a tectonically smashed belt in a volcanic mafic formation. According to the authors of this monograph the Suoi Trat mine, being genetically of a chalcedony-type, was subsequently overlain by a hydrothermal-borne formation. The ore bodies are commonly concurring with rock beds, that are foliated, pressed into thin sheets, containing diffused sulfide of pyrite and a minor amount of chalcopyrite sometimes galenite and sphalerite, distributed unevenly and occupied from 15 to 20 vol.%. The sulfide minerals normally form thin belts oriented following the foliation planes forming strap-shaped ore bodies. Massive sulfide ore veins are common, developed alongside with foliation plane and calcite veins cutting penetrating foliated strap-shaped structures. A sulfide ore body at the Lung Cua ore field is elongated lens-shaped spreading in the crushed, breccia-formed zone in high-Ti basaltoids.

The ore mineral compositions include pyrite, chalcopyrite, with a lesser amount of pyrrhotite, galenite, arsenopyite and sphalerite at various proportions. Mineralogical and geochemical studies suggest complicated origins of the ores, where chalcedony – copper-related was at early stages followed by controlled by medium-temperature hydrothermal processes. Metal concentrations determined using atomic absorption spectrometry (AAS) method show (g/T) Cu: 0.1–8.7, Au: 0.1–33.45, Ag: 0.4–182, Zn: 257–1457, Pb: 33.5–1314, Sn: 1.0–10.7, Mo: 7.97–51.2, and Bi: 5.05–9.94. Other low content metals include Ga: 11.9–15.9, Ge: 0.33–2.83 and Sb: 1.57–2.59 (Hoa et al. 2005). High concentrations of Pb, Zn, Bi, Sn and Mo and variable $\delta^{18}O$ (between +8 to and + 14) and $\delta^{34}S$ (between + 1.28 to + 10.96) suggest that the ore mineralization may have been related to acidic intrusive magmatic activity (Lu et al. 2005). This is consistent with field observation in the Suoi Trat mine area as well as in Cao Ram and Lung Cua ore sites where trachyte, a magma believed to derive by magma differentiation from Permian – Triassic mafic and ultramafic magmatic activities, is well spread. This type of ore deposit is highly potential for Au, Cu and other precious metals to be exploited. The Suoi Trat mine has been mined since 1992 but mostly for gold while other valuable metals being wastefully ignored thus causing loss of natural resources. Other ore sites such as Lung Cua, Cao Ram and Suoi Reo show economic values only available metals are mutually exploited and refined.

6.2.2 Au-As Mineralization Type

This ore type is common in the Song Da and Song Hien belts. Representative Au-As ore type is distributed in Song Da high-Ti mafic volcanic magmas in Lang Neo mine in the Cam Thuy area and Then Sin ore site in the Nam So area, to the southwest and northeast, respectively, of Song Da structure. In the Song Hien structure this ore type is found in Ban Nung and Loc Soa mines in the Cao Bang area (center of the

Table 6.11 Chemical compositions (wt.%) of main ore minerals in Ban Nung (1–7) and Loc Soa (8–15) ore sites in the Song Hien structure

No	Sample	Fe	Co	As	S	Sb	Ni	Total	Mineral
1	AH-7006	2.07	31.52	43.98	19.89	0.04	1.34	98.84	Asenopyrite
2	Ditto	1.91	32.61	44.66	19.83	0.00	0.58	99.60	Asenopyrite
3	Ditto	3.52	29.68	44.47	19.80	0.00	2.19	99.65	Asenopyrite
4	Ditto	46.85	0.00	1.32	51.83	0.00	0.00	100.01	Pyrite
5	Ditto	46.71	0.00	1.04	51.84	0.00	0.00	99.60	Pyrite
6	Ditto	46.96	0.00	0.00	52.37	0.00	0.00	99.34	Pyrite
7	Ditto	22.55	0.00	32.04	0.06	0.00	0.00	54.65	Scorodite
8	AH-3233	34.89	0.00	43.28	21.51	0.00	0.00	99.68	Asenopyrite
9	Ditto	35.10	0.00	43.06	21.87	0.00	0.01	100.03	Asenopyrite
10	Ditto	34.97	0.00	42.93	21.97	0.00	0.00	99.86	Asenopyrite
11	Ditto	35.11	0.00	42.65	22.25	0.00	0.00	100.02	Asenopyrite
12	Ditto	47.22	0.00	0.00	52.61	0.00	0.00	99.83	Pyrite
13	Ditto	47.39	0.00	0.19	52.49	0.00	0.00	100.07	Pyrite
14	Ditto	47.38	0.00	0.00	52.56	0.00	0.01	99.95	Pyrite
15	Ditto	47.31	0.00	0.13	52.70	0.00	0.00	100.14	Pyrite

Song Hien belt) and Na Pai mine in the Lang Son area (southeast of Song Hien belt) (Fig. 6.1).

Ban Nung gold mine is the largest example of this mine type being found in mafic gabbroid intrusions in Vietnam (Hoa et al. 1996). The ore body is distributed in crushed zone accompanied by propylitization and listvenitization developed in rooftop areas of the gabbrodolerite intrusion having spatio-temporal and genetic relationship with andesite – basalt volcanics described as early Triassic in the lower section of the Song Hien formation (currently considered as Late-Permian Bang Giang complex). Recent exploiting trench digging has exposed two ore zones up to 300–700 m long. They are composed of ore veins and vein networks. Mineral compositions in the Ban Nung and Loc Soa mines include mainly pyrite, arsenopyrite and minor amounts of chalcopyrite, galenite, sphalerite, pyrhotitte and native gold. Chemical compositions of arsenopyrite and pyrite in the Ban Nung mine are shown in Table 6.11, that are closely consistent with theoretical estimation. In some cases, As in pyrite is up to 1.5 wt.%; Co-, Fe- and Ni-bearing arsenopyrites are, respectively, 32 wt.%, 3.5 wt.% and 2 wt.%. Microscopic analysis shows Au in pyrite varying between 11.5 and 74.4 g/T and Ag being between 0.8 and 14 g/T; while in arsenopyrite, Au = 6.2 g/t and Ag = 1.9–2.3 g/T (Hoa et al. 2006). Gold concentrations in primary ores are variable, from a few milligrams to 10–15 g/T; while in secondary ores (oxidized zones) Au is higher, particularly some nuclei contain kilograms. Chemical compositions of native gold in ores mainly about 910–940‰ but Ag is lower, between 40 and 80‰, and almost no Cu and Hg.

According to the mineralogical, geochemical and P-T parameter characteristics the Ban Nung ore mineralization is of Au-sulfide type (gold – arsenopyrite). Their genetic relation to the Permian – Triassic magmatism, especially for Au-As miner-

alization in the Song Hien belt, is certainly confirmed by Ar/Ar ages acquired from ore minerals in the Loc Shoa mine, northwest of Nguyen Binh mine, which vary between 224 and 215 Ma (Hoa 2007).

The Na Pai primary gold mine (Binh Gia district, Lang Son province) in the Song Hien structure, based on available data, may be classified as mild-to-low temperature hydrothermal type. Aside from the Na Pai mine there are other deposits having similar characteristic data in the area such as Khuon Pouc, Cao Phu, etc. They all form a gold ore belt up to 50 km long and 15–20 km wide (Tri 2000). Geologically the Na Pai mine is comprised mainly of rhyo-dacite, rhyolite and porphyry granite. Ore minerals include pyrite, arsenopyrite, chalcopyrite, sphalerite, galenite, scorodite, covellite and natural gold. Non-ore minerals, taking up to 90–95 vol.%, include quartz, sericite, cholorite and kaolinite. The gold is not exceeding 0.07–0.01 mm in size. Natural gold and cinnabar flakes are commonly found in alluvial beds near Na Pai mine. Chemical compositions of the natural gold show Hg concentrations varying between 0.1 and 0.3 wt.% (Hoa et al. 2006), characterized for low-temperature ore mineralization.

Early investigations of gold-mineralization in the Suoi Cun area (Song Hien structure) suggest Au-As ore type. The ore body is located in a crushed zone within a Suoi Cun rhyolite formation, a member of Permian – Triassic bimodal mafic – felsic magmatism in the Song Hien structure (see Chap. 3).

6.2.3 Antimony – Gold (Sb – Au), Antimony – Mercury (Sb – Hg) and Mercury – Gold (Hg – Au) Ore Types

These ore types are relatively well-spread in northern Vietnam. They are found in late Paleozoic – early Mesozoic Song Da and Song Hien rift structures as well as in Lo Gam and Quang Ninh Paleozoic folded structures (Fig. 6.1). Their distribution in each structure is characterized by a clear zoning from Sb-Au type to Sb-Hg-Au and then Hg-Au (Tri 2000). Representative of the Sb-Au ore type is found at the Lang Vai, Khuon Puc and Nam Chay ore cumulates in the Lo Gam structure, and Mau Due, Ban Chang, and Son Vi (Ha Giang province), Khau Hai (Cao Bang province), La Son (Lang Son province) in the Song Hien structure; Na Bac and other ore sites in Lang Neo area (Thanh Hoa province) in the Song Da structure, as well as at several ore sites in Quang Ninh Paleozoic folded structure such as Dong Quang and Khe Chim (Fig. 6.1). Among the above listed ore cumulates, based on their gold concentration two sub-types are divided: Sb – Au (with Lang Vai – Khuon Puc viewed as representative) and Au-bearing antimony (including most of the rest of the ore sites). In the work by Tran Van Tri (2000) the second sub- type is grouped as actual antimony type. However, in most of mines of this sub-type there is the presence of other sulfide ores where gold concentrations being considerably high (see below); therefore, the definition of 'actual antimony' has only relative meaning. The occurrence of various Au-ore minerals in these ore types is not viewed as indicative

category for mine classification, because the geological conditions and mineralogical and geochemical – isotopic features of the ores in the mines are closely similar. The ore mineralization of these mines commonly occurs at top sections of anticlinorium structures comprised of terrigenous – carbonate sediments or terrigenous sediments of Ordovician – Silurian (Lang Vai), Cambrian (Nam Chay, Dong Quang) or Triassic ages (Na Bac). In most of the mine cases gabbrodolerite and dolerite are present having similar petrologic and geochemical characteristics with those of Permian – Triassic gabbrodolerite – granite granophyre associations as described in Chap. 2. Ore mineral main assemblage contains pyrite, arsenopyrite, antimonite or pyrite – antimonite. The ores are massive and disseminated or breccia structures. Au in Lang Vai antimony ore deposit varies between 0.5 and 8.0 g/T, sometimes even higher (Tri 2000) while for Nam Chay and Dong Quang ore sites the Au concentration varies from 0.1 to 2.3 g/T (Hoa et al. 2006). The mineralogical compositions of these mines are relatively complex, but mainly contain pyrite, arsenopyrite, antimonite and their Fe-bearing variety group including bertierite, jamesonite, sulfosalts and natural gold, etc. The chemical compositions of the minerals are given in Table 6.12. It is clear that the composition of antimonite is mostly consistent with its theoretical data containing no mixtures; bertierite has Fe = 11.79 to 12.09 wt.% and Pb being up to 0.3 wt%; Fe contents in jamesonite vary between 0.72 and 2.83 wt.%, constantly containing Bi (between 0.17 and 0.37 wt.%) and sometimes Ag up to 0.32 wt.%; sphalerite is high-Fe type showing Fe varying from 4.03 to 6.78 wt.% (Table 6.12).

Ar-Ar age acquired on sericite in antimonite ore from Nam Chay and Ban Chang mines show, respectively, 228 Ma and 254 Ma (Fig. 6.9).

Age of Dong Quang mine is 252 Ma (Fig. 6.10), suggesting that it was related to a Permian – Triassic tectonic – magmatic stage (Hoa et al. 2006). The $\delta^{34}S$ varying in a narrow range of 1.8–2.6‰ for Nam Chay antimonite and 3.3–3.4‰ for Na Bac antimonite (Table 6.13) indicate their genetic relation to pluton – hydrothermal activities.

Sb-Hg-Au ore type has recently been established in northern Vietnam (Hoa et al. 2006), in the An Binh area, southeastern wing of Song Da rift, and south of a Permian – Triassic high-Ti basalt and high-Al granite field (see Chap. 2). The location is a antimony – mercury mine according to some mineral resources geologists. However, the geological, mineralogical and geochemical-isotopic investigation of the ores shows characteristics of Sb-Hg-Au-type mine (Hoa et al. 2006). Mineral exploration activity conducted in the region has discovered a number of ore zones, among these there is an ore belt about 2 km long, running in sub- longitude direction containing an elongated ore body having up to several meters thick, which is being considered as most valuable. Ore mineralization is commonly limited within deformed and strongly smashed carbonate, clay-intercalation carbonate and thin layers of black shale belonged to Middle Triassic terrigenous sediment – carbonate Nam Tham complex. The ore body is coincidently distributed in coal-rich carbonate strata. The ore body is characterized by zoning structure, for example, the major antimony ore is concentrated in the center of the ore body while pyrite ore is distributed to the periphery. Sometimes the pyrite ore may also be located in some distance

Table 6.12 Chemical compositions (wt.%, analyzed by EPMA) of arsenopyrite, jamesonite and bertierite in the Lang Vai ore deposit

No	Sample	Fe	Cu	Zn	As	S	Pb	Bi	Ag	Sb	Te	Total	Mineral
1	AH-3250/1	6.78	3.11	55.04	0.00	34.10	0.10	0.00	0.01	0.04	0.00	99.18	Sphalerite
2	AH-3250/1	2.61	0.00	0.04	0.00	21.18	39.87	0.24	0.00	34.42	0.00	98.36	Jamesonite
3	AH-3250/1	2.46	0.00	0.08	0.00	21.85	39.59	0.19	0.00	36.30	0.00	100.37	Jamesonite
4	AH-3250/1	2.80	0.00	0.08	0.00	21.55	40.17	0.15	0.00	35.83	0.00	100.58	Jamesonite
5	AH-3250/1	2.63	0.00	0.07	0.00	22.01	40.12	0.18	0.00	35.83	0.00	100.85	Jamesonite
6	AH-3250/1	2.64	0.00	0.11	0.00	21.82	40.07	0.23	0.00	35.93	0.00	100.80	Jamesonite
7	AH-3250/2	2.56	0.00	0.13	0.00	22.11	39.76	0.29	0.05	35.98	0.00	100.88	Jamesonite
8	AH-3250/3	0.01	0.00	0.06	0.00	28.15	0.00	0.00	0.00	72.23	0.00	100.45	Atimonite
9	AH-3250/3	0.03	0.00	0.05	0.00	27.93	0.04	0.00	0.00	72.01	0.00	100.06	Atimonite
10	AH-3250/3	0.02	0.01	0.06	0.00	28.03	0.05	0.00	0.00	71.25	0.00	99.92	Atimonite
11	AH-3250/3	11.79	0.00	0.11	0.00	30.62	0.38	0.00	0.00	58.20	0.00	101.10	Berterite
12	AH-3250/3	12.01	0.00	0.03	0.00	30.64	0.71	0.00	0.00	56.55	0.00	99.94	Berterite
13	AH-3250/3	12.09	0.00	0.07	0.00	30.84	0.61	0.00	0.00	58.36	0.00	101.97	Berterite
14	AH-3250/3	4.03	0.02	61.08	0.00	35.61	0.09	0.00	0.00	0.04	0.02	100.87	Sphalerite

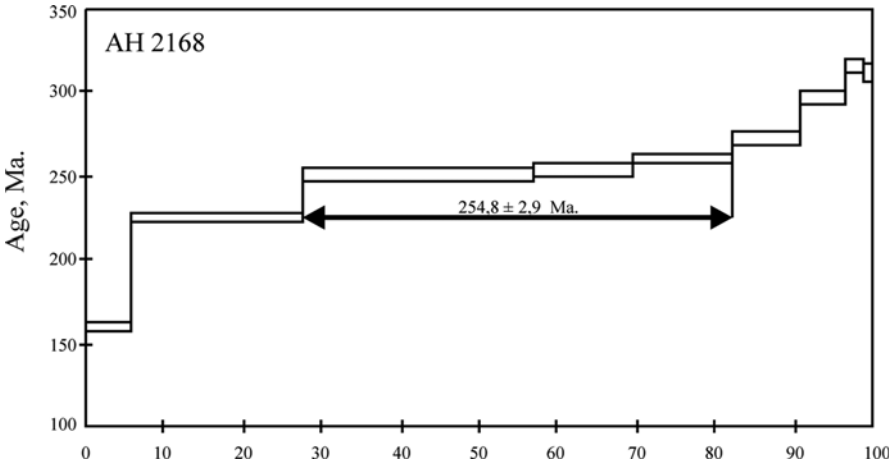

Fig. 6.9 Ar-Ar ages of Au-bearing Sb ore in the Ban Chang area (Song Hien structure). Analyzed at the Analytical Center of Institute of Geology and Mineralogy, Siberian Branch, Russian Academy of Sciences (analyst A.V. Travin)

from the main ore body. Antimony and mercury in turn are divided into separate ore bodies within the ore zone. This may be a reason why these were considered as accordingly dependent mines. Carbonate rocks in the proximity of ore bodies are strongly silicized, dolomitized and sericitized accompanied by pyritized of disseminated or massive form. The antimony ore is composed of antimonite, pyrite, arsenopyrite, galenite, sphalerite, realgar và cinnabar. In some ground and sorted ore samples collected from Kem Hill found are fined and very fined grains of natural gold. Mercury ore contains cinnabar, realgar, auripigment and a minor amount of sulfide minerals. Representative Sb and Hg ore type is seen at An Binh mine as shown in photos 17 and 18. Gold contents in antimony, mercury and in near-ore body metamorphosed carbonate are high, varying between 0.8 and 1.1 g/T (Hoa et al. 2006). In addition, EPMA analysis of shows Hg is high in the native gold (up to 0.7 wt.%). Sulfur isotopic values acquired for the antimony, cinnabar and pyrite at An Binh mine vary from 2.3 to 7.2‰, suggesting a plutonic origin.

Therefore, basing on the following characteristics such as distribution in terrigenous carbonate sediments, ore geochemistry, presence of fined and very fined natural gold grains, high Hg concentrations in natural gold, the An Binh ore deposit may be classified as Sb-Hg-Au type (Au low temperature type), closely similar to Carlin type. Ar-Ar age dating on sericite in antimony ore at An Binh mine yields 233 Ma (Fig. 6.11), implying that the ore mineralization has temporal relation with Permian – Triassic magmatic activity that was widely developed in the Song Da rift zone and nearby structures, most noticeable is the presence of Kim Boi massif, a small mafic gabbrodolerite, Phia Bioc-type intrusive bodies and dykes, in the Song Da rift. Age of the Kim Boi high-Al granite block is 242 Ma (see above). This granite show cutting contact with Permian high-Ti basalts and its occurrence is viewed as an indication of ending of the Song Da rifting in early Triassic.

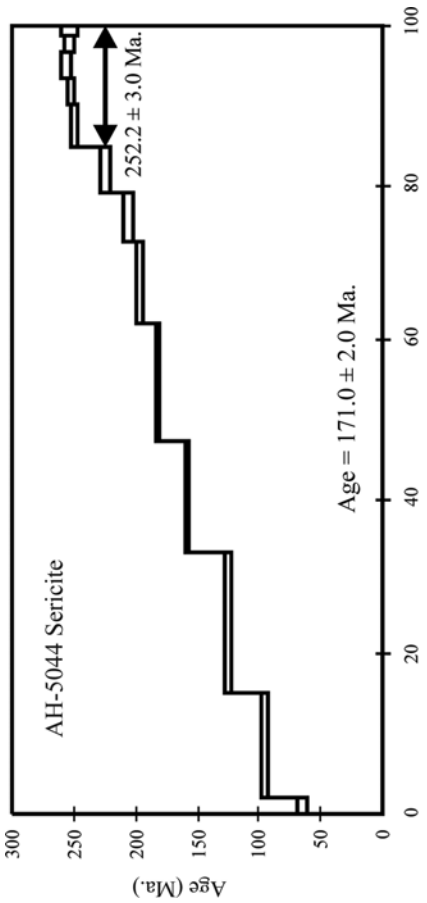

Fig. 6.10 Ar-Ar age of Au-bearing Sb-ore in the Dong Quang area (Quang Ninh structure). Analyzed at the Analytical Center of Institute of Geology and Mineralogy, Siberian Branch, Russian Academy of Sciences (analyst A.V. Travin)

Table 6.13 Sulfur isotopic compositions of Sb-Hg, Au-Sb and Au ores in northern Vietnam (‰ CDT; ±0.1‰) (Hoa et al. 2006)

No	Sample ID	Ore cumulate	Ore type	Mineral	$\delta^{34}S$
1	NB-1	Na Bac	Au – Sb	Antimonite	3.4
2	NB-4	Na Bac	Au – Sb	As above	3.3
3	NB-3	Na Bac	Au – Sb	As above	3.3
4	AH-3166-a	An Binh	Sb – Hg – (Au)	As above	2.3
5	AH-3166-б	An Binh	Sb – Hg – (Au)	As above	4.3
6	AH-3166-в	An Binh	Sb – Hg – (Au)	As above	2.7
7	AH-3167	An Binh	Sb – Hg – (Au)	As above	4.1
8	AH-3168	An Binh	Sb – Hg – (Au)	Pyrite	4.5
9	AH-3174	An Binh	Sb – Hg – (Au)	Antimonite	5.8
10	AH-3178	An Binh	Sb – Hg – (Au)	As above	6.2
11	AH-3182	An Binh	Sb – Hg – (Au)	As above	6.6
12	AH-3/1	An Binh	Sb – Hg – (Au)	Cinnabar	6.4
13	AH-5/1	An Binh	Sb – Hg – (Au)	As above	6.0
14	AH-3182	An Binh	Sb – Hg – (Au)	As above	7.2
15	AH-2016-a	Na Pai	Au	Pyrite	2.2
16	AH-2021	Than Sa	Hg	Cinnabar	4.7
17	AH-2023	Than Sa	Hg	As above	9.5
18	AH-2028	Nam Chay	Au – Sb	Antimonite	1.8
19	AH-2029-a	Nam Chay	Au – Sb	As above	2.6
20	AH-2030	Nam Chay	Au – Sb	As above	3.0
21	H-2000R	Sa Pa	Mo-(Cu-Au)	Pyrite	2.1
22	H-2000 M	Sa Pa	Mo-(Cu-Au)	As above	3.7

To the west of An Binh mine in the southeastern wing of Song Da structure more ore types having been discovered include Sb, Sb-Hg, Au (and Au – As) forming a field of gold –sulfide ore which is termed as Lang Neo ore field (Hoa 2007), among these Lang Neo ore site (Thanh Hoa province) is considered as the most valuable ore body.

Hg-Au ore type is less popular which up to date has only been reported in the areas of Vang Pouc and Than Sa within geological structures in north Vietnam. The Hg-Au Khuon Pouc ore deposit is located a short distance for the above described Na Pai mine. The ore body is spreading coincidently with a Triassic terrigenous sediment bed comprised by sandstone, gravel-stone and siltstone in a crushed and strongly brecciated. The mineral composition of ore is cinnabar, realgar, antimonite and auripigment. In heavy sand samples collected in a nearby stream show a number of cinnabar and natural gold grains of various sizes. The gold purity is variable and its chemical composition always includes some Hg varying from 0.1 to 0.6 wt.% (Table 6.14). The Than Sa ore site in the southeast of Song Hien structure is the largest among those rich-Hg-bearing ores discovered in northern Vietnam. The ore site is distributed in terrigenous carbonate – sediment strata including clay schist, clayish carbonate schist metamorphosed sandstone and deformed, strongly folded

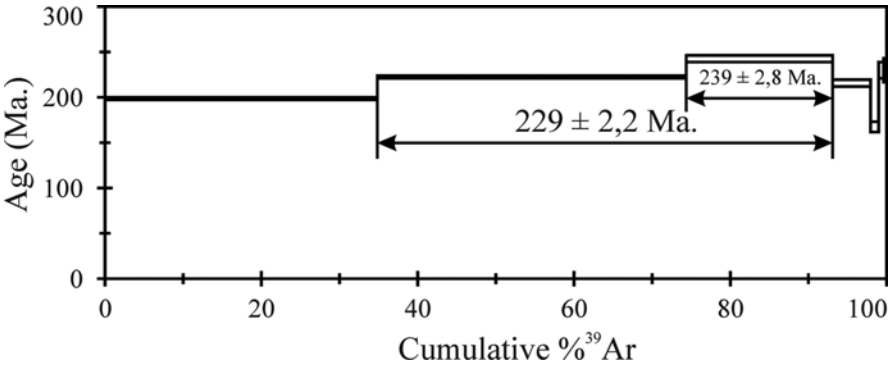

Fig. 6.11 Ar-Ar age of antimony ore of Sb-Hg-(Au) An Binh mine, Song Da structure

limestone belonging to Cambrian Than Sa complex. Mercury concentration in the ore is about 0.12 wt.%. The ore mineral composition contains cinnabar, antimonite, dikite, realgar, auripigment, barite, fluorite, and sometimes sulfide chalcopyrite. Gold in ore-tainted limestone nearly the ore body reaches up to 0.87 g/T (Hoa et al. 2006); while Hg in the native gold (gold ore) varies between 0.06 and 0.19 wt.% (Table 6.14), characterized for all the described ore-types. The sulfur isotopic values $\delta^{34}S$ acquired on cinnabar vary between 4.7 and 9.5‰ (Table 6.13), higher compared with other ore-type minerals.

6.2.4 Sn-Sulfide Mineralization

There are two sub-types are recognized within this mineralization type, e.g., cassiterite – sulfide – silicate and Pb-Zn-Ag developed in the Song Hien and Lo Gam structures.

The cassiterite – sulfide – silicate sub-type is distributed in the southeastern wing of Song Hien structure (Fig. 6.1), there are several ore sites in the Tam Dao area including Khuon Phay, Bac Lung (Tuyen Quang province), Ngoi Lem and Truc Khe (Thai Nguyen province). Geologically the ore bodies in the Khuon Phay mine are located mostly in the Nui Dieng granite porphyry, which is a sub-volcanic type accompanying Triassic rhyolite in the Tam Dao area. The latter is viewed as a component in lower section of the Song Hien structure, which based on the compositional features is completely similar to felsic magma occurred in the Cao Bang and Lang Son regions (Luong and Bao 1989). According to the regional mineral exploration documentation, the upper part of the ore bodies is consisted of cassiterite, tourmaline and quartz, while the lower part is comprised of cassiterite, pyrrhotite, arsenopyrite and chalcopyrite. Ore complex of Sn-Cu-Bi contents Sn = 1.84 wt.%, Cu = 1.39 wt.% and Bi = 0.1 wt.%. Silver in the chalcopyrite is up to 200 g/T (Tri 2000).

Table 6.14 Chemical compositions (wt.%) of the native gold analyzed by EPMA (Hoa et al. 2005)

Sample ID	Au	Hg	Ag	Total	Sample ID	Au	Hg	Ag	Total
AHS2001a_1	87.05	0.135	12.98	100.17	AHS2002_18	77.25	0.455	21.66	99.37
AHS2001a_2	88.68	0.049	11.12	99.85	AHS2002_19	99.58	0.204	0	99.78
AHS2001a_3	86.79	0.24	12.95	99.98	AHS2002_20	87.37	0.199	11.98	99.55
AHS2001a_5	87.17	0.273	12.99	100.45	AHS2002_22	53.41	45.64	0.091	99.14
AHS2002_4	84.93	0.15	15.16	100.24	AHS2002_31	76.85	0.302	23.38	100.53
AHS2002_7	87.61	0.205	11.88	99.70	AHS2002_34	98.97	0.238	0.336	99.54
AHS2002_8	99.85	0.244	0	100.09	AHS2002_35	55.48	34.11	11.43	101.02
AHS2002_9	84.56	0.694	14.61	99.86	AHS2002_36	80.49	3.12	17.21	100.82
AHS2002_10	100.51	0.053	0	100.56	AHS2002_37	101.45	0.184	0.708	102.34
AHS2011_1	100.86	0	0	100.86	AHS2002_38	63.18	0.318	36.22	99.72
AHS2011_2	100.88	0.048	0	100.93	AHS2002_39	61.47	0.59	37.95	100.01
AHS2011_3	100.82	0.124	0	100.94	AHS2002_40	66.19	0.3	31.96	98.45
AHS2011_4	92.74	0.053	7.93	100.73	AHS2002_41	98.13	0.139	1.59	99.86
AHS2011_5	99.97	0.191	0.385	100.55	AHS2002_42	86.27	0.117	13.53	99.92
AHS2011_6	84.67	0.035	15.33	100.04	AHS2002_43	99.32	0.18	0.059	99.56
AHS2011_7	99.31	0.118	0.963	100.39	AHS2002_44	86.01	0.183	13.44	99.63
AHS2011_8	99.88	0.038	0.266	100.18	AHS2009_1	97.81	0.141	0.173	98.12
AHS2011_9	100.4	0.057	0.068	100.53	AHS2009_2	97.06	0.062	1.18	98.30
AHS2011_10	90.71	0.121	9.86	100.69	AHS2009_3	98.76	0.116	0.313	99.19
AHS2011_11	89.54	0.125	10.02	99.69	AHS2009_4	81.5	0.093	16.97	98.57
AHS2002_17	78.02	0.433	21.3	99.75	AHS2001b_2	85.03	0.335	13.63	99.00

Remarks: AHS-2001: Na Pai area; AHS-2002: Vang Pouc (Lang Son province); AHS-2009–2011: Than Sa area (Thai Nguyen province)

Pb – Zn – Pb sub-type is discovered in about 50 mines and ore sites having different sizes in northern Vietnam, but mostly developed in the twin Phu Ngu – Lo Gam structure, containing more than 80 % of total Pb-Zn metal reserve of Vietnam. Besides, Pb-Zn mineralization is also observed in the Song Hien structure at a number of mines and ore sites in the Lang Son and Cao Bang areas. Based on geological characteristics Pb-Zn minerals may be divided into two ore types, e.g., Pb-Zn ore distributed in terrigenous carbonate sediment strata and the other, developed mainly in Devonian (or Silurian – Devonian) volcanic – terrigenous sediment formations (Tri 2000). In the limit of Lo Gam structure Pb – Zn mines and ore sites are normally developed among contrast, bimodal gabbro – granite or complex gabbro – syenite formations of Permian – Triassic age (see Chap. 4). Locations where Pb-Zn mines are highly concentrated are Lang Hich (Thai Nguyen), Cho Don and Cho Dien (Bac Kan province), and Tung Ba (Ha Giang province), among the mines and ore sites those in Thai Nguyen and Bac Kan are most typical representatives of Pb-Zn ore mineralization occurred in terrigenous carbonate sediments; whereas those in Ha Giang province is in terrigenous carbonate-volcanic formations. Origin of these Pb-Zn ore types is controversial, either pseudo-stratification or actually hydrothermal. The mineralogical compositions in many ore occurrences are heterogeneous. For example, mineral compositions in ore deposits and ore sites in the Cho Don ore field normally contain galenite, pyrite, pyrrhotite, arsenopyrite, chalcopyrite, bismuthite and others. Cassiterite and natural gold are also encountered. The galenite is characteristically high (wt.%) Ag (0.05–0.06), Bi (0.06), Cd (0.1) and Sn (0.05), while sphalerite shows (wt.%) Fe = 6–10, Cd = 0.14 = 0.22, Bi = 0.06–0.09 and Sn being up to 0.02 (Tables 6.15 and 6.16). Accompanying metals in Pb-Zn ore show (g/T) Cd = 2500, Cu about 2900, Sn = 680, Ag = 40 – 680, Au = 0.1 to 1.3 and Bi about 3300 (Tables 6.15, 6.16, and 6.17).

Along with Ag-Pb-Zn mineralization Ba-Pb-Zn ore type is also found to associated with carbonate beds in terrigenous carbonate sediment formations in the Song Hien and Lo Gam structures. The zoning of ore bodies is illustrated by having barite mainly in the upper section and galenite and sphalerite filling the lower section. In general, the ore cumulates of this ore type is smaller in scale compared with the above ore types.

6.3 Summary on the Permian – Triassic Mineralization Stage

During the Permian – Triassic period there were three ore complexes successively formed as follows: magma-borne Ni-Cu –(PGE) and Ti-Fe-V ore complex, gold – sulfide and tin – sulfide complexes. The first complex, including Cu-Ni-PGE-ore type minerSalization, is related to mafic – ultramafic intrusions with ranges of differentiated magmas. The latter include various pluton- volcanic magma associations having been crystallized from melts of different parental sources in the Song Da and Song Hien rift zones and folded belts surrounding the Song Chay anticlinoria.

The gold-sulfide ore complex includes the following ore types Au-As, Au-Sb, Sb-Hg-Au and Hg-Sb-(Au), that are widely developed in the Song Da and Song

Table 6.15 Average chemical compositions (wt.%) of galenite in Na Bop, Na Tum, Ba Bo and Coi Ky mines (Hoa et al. 2005)

Element	NB 02-1	NB 02-7	NT 28/30	NT 28/35	NT 28/100	BB 02-1a	CK 02-4
As	0.007	0.013	0	0	0	0.010	0.002
Ge	0.065	0.043	–	–	–	0.057	0.056
S	49.57	49.82	13.32	13.17	13.28	49.43	49.58
Pb	49.99	49.82	87.10	87.11	86.64	50.22	49.91
Bi	0.064	0.066	0	0.004	0.005	0.066	0.057
Ag	0.030	0.022	0	0	0.012	0.002	0.066
Cd	0.094	0.109	–	–	–	0.104	0.106
Sn	0.048	0.019	–	–	–	0.007	0.00
Cu	0.027	0.021	–	–	–	0.022	0.110
Zn	0.063	0.034	–	–	–	0.060	0.051
Te	–	–	0.023	0.007	0.014	–	–
n	10	12	4	2	3	11	12

Remarks: Name of mines: *NB* Na Bop, *NT* Na Tum, *BB* Ba Bo, *CK* Coi Ky, *n* number of analyses

Table 6.16 Average chemical compositions (wt.%) of sphalerite in Na Bop and Na Tum mines (Hoa et al. 2005)

Element	NB02-1	NB02-6	NB02-8	NT28/30	NT28/35	NT28/100	NT 28/105
Zn	54.53	54.59	54.32	59.14	56.54	56.08	56.64
Fe	10.32	10.42	10.47	6.66	9.22	9.46	9.07
Mn	0.51	0.57	0.482	0.024	0.026	0.020	0.040
As	0.04	0.045	0.049	0	0	0	0
Ge	0.002	0.005	0.003	–	–	–	–
S	33.10	33.20	33.04	33.30	33.62	33.55	33.56
Pb	0.05	0.009	0.027	–	–	–	–
Bi	0.093	0.059	0.073	0	0	0	0
Ag	0.08	0.026	0.003	–	–	–	–
Cd	0.22	0.185	0.140	0.178	0.181	0.180	0.190
Sn	0.021	0.008	0.00	–	–	–	–
Cu	–	–	–	0.260	0.400	0.39	0.23
Hg	–	–	–	0.035	0.011	0.040	0.040
In	–	–	–	0.042	0.042	0	0.120
n	12	10	11	3	4	3	4

Remarks: Name of the mines: *NB* Na Bop, *NT* Na Tum, *n* number of analyses

Hien rift zones as well as in the Paleozoic Lo Gam and Quang Ninh folded structures, where they are distributed at Lang Vai, Lang Neo, Loc Shoa and Khe Chim ore fields. The most significant character of these ore fields is the common geochemical characteristics of the (Au, Sb, As, Hg) ore mineralization, their zoning in the following order Au-As → Au-Sb → Au-Sb-Hg → Hg and their transitional relation between different ore types, for example, Au – As and Au – Sb, Au – Sb and Sb – Hg (at the Lang Vai and Lang Neo ore fields). Formation ages of the ore com-

Table 6.17 Abundances of accompanied metals in Pb-Zn ore cumulates in northern Vietnam (Hoa et al. 2005)

Element	NB02-1	NB02-6	NB02-8	NT02-3	BB02-1a	CK02-4	LV02-7	LV02-6
Cu	1160	19592	2044	65	2912	2301	2882	1915
Sn	304	188	84	36.5	683	68.8	117	208
Au	0.16*	0.061*	0.013*	0.53*	0.23*	1.3*	0.005*	0.009*
Ag	843 681*	346 341*	150 101*	50.2 40.7*	1941 657*	165 119*	86 56*	359 307*
Cd	432	290	337	37.8	365	1478	2584	1055
In	325	382	142	5.25	5.32	1.87	16.8	11
Ga	–	–	16.1	–	–	–	3137	640
Sb	186	95	28.9	8.96	1884	360	304	584
Se	1186	996	–	59	12395	315	–	1334
Bi	2793	2218	189	152	19417	718	–	3357

Remarks: Name of mines: *NB* Na Bop, *NT* Na Tum, *BB* Ba Bo, *CK* Coi Ky, *LV* Lung Vang. Analysis was conducted at Analytical Center, Institute of Geology and Mineralogy, Siberian Branch, Russian Academy of Sciences.
* – AAA method

plexes vary between 252 and 228 Ma (by Ar-Ar age dating method). Spatially the complexes are closely related to 251-233 Ma bimodal pluton – volcanic magmatic (basalt – rhyolite, rhyolite – basalt, granite – porphyry) associations as well as to granite and small-scaled gabbro – syenite intrusions.

Younger ore complexes include Sn-sulfide, containing the following ore associations cassiterite – silicate – sulfide, silver – lead – zinc, and barite – multiple metals. Exposition of the ore sequence is different at different ore sites; but general ore zoning may be observed in the following order (Thai Nguyen ore field example) Sn – W (±Bi) → Pb – Zn – (Ag) → Ba – (Pb, Zn) → Ba. This internal zonation is characterized for ore fields having Sn – Ag geochemistry that is observed in many world tin-ore provinces such as Bolivia, Verkhoyan and Primoria (Russia) (Rodionov 2005). This type of zonation is clearly exposed at Khuon Phay – Tam Dao ore fields in Tuyen Quang and Thai Nguyen provinces, northern Vietnam. The ore formations are closely associated with the regional rhyodacite – rhyolite volcanic and granodiorite – granite porphyry sub-volcanic activities, as well as with 251 Ma high-Al granite and 247-233 Ma gabbro – syenite intrusions. Relatively younger age of the Sn-sulfide complex compared with Au-sulfide ore is determined by the development of sulfide minerals such as high-Sn –galenite, –sphalerite and – Ag-bearing minerals overlying Au-Sb ore at the Lang Vai deposit (Hoa 2007). Tin contents are recorded high up to 600 g/T (average at 220 g/T) in Pb-Zn ore at Na Bop mine in the Cho Don area (Table 6.17).

The difference in distribution different Permian – Triassic ore types is controlled by structures generated within the Song Da and Song Hien rift zones, accordingly two ore mineralization belts are being divided (Fig. 6.1). The two ore belts include the following ore types Sn-sulfide (Khuon Phay), Au-sulfide at Lang Neo and Ban Nung and others, and Cu-Ni-PGE, Ti-Fe-V at Ta Khoa, Nui Chua and Suoi Cun

(Fig. 6.1). The Song Hien ore belt starts from the boundary between China and Vietnam in the northwest to Lang Son province in the southeast and is overlain by Jurassic – Cretaceous sediments. There are a number of ore mineralization zones being discovered in the Song Hien ore belt including Thai Nguyen, Na Pai, Nguyen Binh and Mau Due containing ore complexes composed of multiple mineralization types. Whereas in the Song Da ore belt, along with Cu-Ni-PGE and Au-Sb-Hg ore types well-developed are Au-Cu types associated with basalt – andesite and basalt – rhyolite formations, which genetic relationship with the regional Permian – Triassic magmatic activities has yet been established.

In summary, study of ore mineralization during the Permian – Triassic stage allows to:

- Differentiate the ore complexes and determine their formation ages
- Divide terrains of ore mineralization in this stage and define Song Da and Song Hien ore belts as well as Au- and Sn-sulfide ore fields within the two ore belts.
- Relate formation ages among magmatic and ore complexes.
- Establish high concentrations of different mineralization types and the presence of special ore associations (such as Au-Ag, Au-Sb-Hg, Au-Cu) having specific potentials, formed in relation to regional Permian – Triassic magmatic activities, while considering the possibility of Cu-Au porphyry mineralization being associated with widely-spread Permian – Triassic sub-alkaline felsic pluton – volcanic formations in Tu Le and Phan Si Pang uplift areas.

References

Arndt NT, Nisbet EG (1982) Komatiites. George Allen & Unwin, London, 526 p

Barnes S-J, Couture J-F, Sawyer EW, Bouchaib C (1993) Nickelcopper sulfide occurrences in Belleterre-Angliers belt of the Pontiac subprovince and the use of Cu/Pd ratios in interpreting platinum group element distributions. Econ Geol 88:1402–1418

Dinh Huu Minh (2003) Geological structure and mineralization characteristics of Cu-Ni Ban Phuc Mine, Son La. Ph.D thesis, National Library of Vietnam, HaNoi

Fang Hua, Yao Jiadong, He Daqui, Jiang Qinsheng (1985) The significance of deep-seated magmatic differentiation in the rock– and ore-forming processes of copper-nickel sulfide deposits – examplited by the Limahe copper-nickel sulfide deposit of Sichuan Province. Acta Geol Sin 2:141–154

Furuseth S, Selte K, Kyekshus A (1967) The solid solubility and structural properties of PdAs2-xSbx, PtP2-xAsx, PtP2-xSbx, PtP2-xBix, PtAs2-xSbx, Pd1-mPtmAs2, Pd1-mPtmSb2, Pd1-mAumSb2 and Pt1-mAumSb2. Acta Chem Scand 21:527–536

Gervilla F, Jeblanc M, Torres-Ruiz J, Hach-Ali PF (1996) Immiscibility between arsenide and sulfide melts: a mechanism for the concentration of noble metals. Canad Miner 34:485–502

Glotov AI, Polyakov GV, Tran Trong Hoa et al (2001) The Ban Phuc Ni-Cu-PGE deposit related to the phanerozoic komatiite-basalt association in the Song Da rift Northwestern Vietnam. Can Mineral 39:573–589

Glotov AI, Krivenko AP, Polyakov GV et al (2002) Petrology of the Kuolotong sulfide copper-nickel deposit in northwestern China. Russ Geol Geophys 41(11):936–948

Glotov AI, Polyakov GV, Tran Trong Hoa (2004) The late Permian Cao Bang PGE-Cu-Ni-bearing complex og the Song Hien structure, Northeastern Viet Nam. J Geol Ser B 23:89–98

Hoang HuuThanh (1994) Mesozoic peridotite-gabbro massifs in the North Vietnam. PhD thesis, United Institute of Geology, Geophysics and Mineralogy, SB RAS, Novosibirsk, 48 pp

Hudson DR, Robinson BW, Vigers BW (1978) Zoned michenerite-testibiopalladite from Kambalda, Western Australia. Canad Miner 16:121–126

Klemm DD (1965) Synthesen and Analysen in den Dreieckdiagrammen FeAsS-CoAsS-NiAsS und $FeS_{20}CoS_2$-NiS_2. Neues Jb Mineral Abh 103:205–255

Kosyakov VI, Sinyakova EF, Shestakov VA (2003) Depend of sulphur-fugacity on composition of phase associations of the Fe-FeS-NiS-Ni system in 873 K. Geochemistry 7:730–740 (in Russian)

Li C, Barnes SJ, Makovicky M (1996) Partition of Ni, Cu, Ir, Rh, Pt and Pd between monosulfide solid solution and sulfide liquid: effects of composition and temperature. Geochim Cosmochim Acta 60:1231–1238

Ngo Thi Phuong (1994) Permo-Triassic high-magnesium volcano-plutonic associations in the Song Da structure. PhD dissertation, Thesis, Institute of Geology and Mineralogy, SB RAS, Novosibirsk, 24 pp

Ngo Thi Phuong, Tran Trong Hoa, Hoang Huu Thanh, Tran Quoc Hung, Vu Van Van, Bui An Nien, Tran Tuan Anh, Hoang Viet Hang, Phan Luu Anh, Tran Viet Anh (2000) Platinum mineral group in mafic – ultramafic mafic in the Song Da belt. J Geol 260:10–19 (in Vietnamese with English abstract)

Ngo Thi Phuong, Tran Trong Hoa, Tran Tuan Anh (2001) Petro-minerallogical characteristics of the P2-T1 basalts-komatiite association in the Ta Khoa anticline, Song Da Zone (NW Vietnam). J Geol Ser B 17–18:10–19

Nguyen Dac Lu, Iu PV, Rokov AN (2005) Research of gas – liquid inclusions in Cu-Au ore in the Viet Nam area, Song Da structure. J Geol 289(7–8):36–42 (in Vietnamese with English abstract)

Polyakov GV, Nguyen Trong Yem, Balykin PA, Tran Trong Hoa, Hoang Huu Thanh, Tran Quoc Hung, Ngo Thi Phuong, Petrova TE, Vu Van Van (1996) Permian – Triassic mafic and ultramafic formations in northern Viet Nam. Science and Technology Publ, Hanoi, p 172 (in Vietnamese)

Polyakov GV, Tran Trong Hoa, Akimsev VA, Balykin PA, Ngo Thi Phuong, Hoang Huu Thanh, Tran Quoc Hung, Bui An Nien, Tolstyk ND, Glotov AI, Petrova TE, Vu Van Van (1999) Ore-geochemical specialization of the permo-triassic ultramafic-mafic complexes in North Vietnam. Geol Geophys 10(40):1474–1497 (in Russian)

She Chuan-jing (1986) A preliminary study on the metallogenic model of magmatic copper nickel sulfide ores in China. Metallogeny of basic and ultrabasic rocks. Regional presentafims, pp 325–358

Tarkian M, Stumpfl EF (1975) Platinum mineralogy of the Driekop mine South Africa. Miner Deposita 10:71–85

Tran Trong Hoa (ed) (1995) Study of Mesozoic – Cenozoic magmatism and its mineralization potential. Final report for National project KT- 01–04 (1992–1995). Archives of the National Agency for Science and Technology Information, Hanoi (in Vietnamese)

Tran Van Tri (ed) (2000) Mineral resources of Viet Nam. Dept. of Geology and Minerals of Viet Nam Publication, 214 p. Hanoi (in Vietnamese)

Tran Trong Hoa (2007) Intraplate magmatism in North Vietnam and related metallogeny. Dissertation of Dr. of Science. Institute of Geology and Mineralogy, Siberian Branch, RAS, Novosibirsk, 382 p

Tran Duc Luong, Nguyen Xuan Bao (eds) (1989) Geological map of Vietnam, at scale 1: 500,000. General Department of Geology and Minerals of Vietnam, Hanoi

Tran Trong Hoa, Petrov VG, Hoang Huu Thanh, Ngo Thi Phuong, Vu Van Van, Tran Quoc Hung, Bui An Nien, Tran Tuan Anh, Hoang Viet Hang, Le Thi Nghinh, Phan Đong Pha (1996) Investigation and evaluation of gold resource of Cao Bang province. Report of basic study of natural resources and environment. Archives of the Institute of Geological Sciences, Hanoi (in Vietnamese)

Tran Trong Hoa, Hoang Huu Thanh, Tran Tuan Anh, Ngo Thi Phuong, Hoang Viet Hang (1998) High-Ti basaltoidic formations in the Song Da rift zone: chemical compositions and geodynamic conditions of magma genesis. J Geol Ser A 244:7–15 (in Vietnamese)

Tran Trong Hoa, Hoang Huu Thanh, Ngo Thi Phuong, Tran Tuan Anh, Hoang Viet Hang (1999) Potassic alkaline magmas in northwestern Viet Nam: indications of late Paleogene intraplate extension. J Geol Ser A 250(1–2):7–14 (in Vietnamese with English abstract)

Tran Trong Hoa, Tran Tuan Anh, Ngo Thi Phuong, Pham Thi Dung, Tran Viet Anh (2005) Permian – Triassic magmatic activities in Viet Nam and prospect of associated rare and precious metal (Pt, Au) mineralization. In: Proceedings of the 60-anniversary of geology of Viet Nam, Publication by Department of Geology and Minerals of Vietnam, Hanoi, pp 63–79 (in Vietnamese)

Tran Trong Hoa, Borisenko AS, Ngo Thi Phuong, Izokh AE, Tran Tuan Anh, Hoang Huu Thanh, Vu Van Van, Bui An Nien, Hoang Viet Hang, Tran Hong Lam (2006) Study and definition of new Au – mine type (Au-Sb-Hg) related to magmatic activities in northern Viet Nam. Final report to International collaboration sponsored by Viet Nam Academy of Science and Technology (2005–2006). Archives of the Institute of Geological Sciences, 51 p Hanoi (in Vietnamese)

Part III
India – Eurasian Collision-Related Cenozoic Magmatic Activities

Study of Cenozoic magmatic activities and mineralization processes related to India – Eurasian collision tectonics was actively carried out during the 90s of the previous century. Review of recently published studies shows mineralization-types such as Cu, Cu-Au, Cu-Mo-Au porphyry, TR-Ba-F, Pb-Zn-Ag and others that were formed temporally coincident with India- Eurasian collision-induced Cenozoic mafic and alkaline magmatism. The magma associations in collision belts, large-scale shear zones (for example, the Ailao Shan – Red River) as well as in the collision-influenced structures show heterogeneous in compositions and complex in occurrences. Contemporaneous alkaline -mafic and -granitoidic magmatism is reported to found in similar collision-induced geological structures in Pamir, Tibet and southeast margins of the Yangtze craton (e.g. Scharer et al. 1994; Vladimirov et al. 2000; Dimitriev et al. 1976; Hacker et al. 2005). Two granitoidic activity stages are being divided along the collision-induced belt, early stage at 60 – 34 Ma and the other at 21 – 19 Ma; the alkaline mafic magmas occurred mainly in the interval of 45 – 25 Ma, while the alkaline granitoidic magmas appeared between 18 and 11 Ma.

Associated with the alkaline mafic magmatic activities was mineralization of Ag-Sb and Cu-Ag aged about 45 Ma in Pamir (Pavlova and Borisenko 2009) and at 50 – 45 Ma in Tibet (Lanping ore belt) (e.g. Hou et al. 2003); whereas associated with a latite complex in the Yulong belt east of Tibet were Cu- and Cu-Mo-Au porphyry mines aged about 40 – 35 Ma (c). According to Dimitriev (1976) the formation of Cu-Au and Gandeze Au-porphyry ore belt west of Tibet was related to 18 – 11 Ma granitoidic and latite magmatism, while in Pamir (and Tibet) F-TR mineralization in carbonatite was associated with alkaline magmatic associations aged 16 – 11 Ma.

In general, the structures in the current Himalayan collision zone are recorded as mineralized zones having a number of industrial-value ore deposits such as Cu, Mo, Au, Ag, Sb and other precious metals. One of the most important India – Eurasian collision-induced structures is the Ailao Shan – Red River shear zone (Tapponnier et al. 1982; Leloup et al. 1995). Extrusion magnitude of the Indochina block relative to the Yangtze craton along this shear zone in the Cenozoic (35–22 Ma) is about

700 km (Chung et al. 1997). The Ailao Shan – Red River Shear zone starts from east Tibet running along western margin of the Yangtze to the Viet Nam East Sea. Magmatism and ore mineralization in the shear zone is basically analogous to those in structures in the above described Pamir and Tibet. A segment of the Ailao Shan fault zone within China shows a number of Cenozoic magmatic activities including granitoid, alkaline mafic and felsic and their accompanying ore mineralization of Cu-Au- porphyry, Au, Au-Sb and Ag (Hu et al. 1995; Zhang et al. 1998 Zhang et al. 2005; Wang et al. 2001; Hou et al. 2005; Li et al. 2008). Industrial-value ore zone containing Cu- and Cu-Au – porphyry type aged 40 – 36 Ma and 16 – 11 Ma in this segment along with the Au-mineralized Ailao Shan belt (Au-As and Au-Sb mineralization of 30 Ma) as well as other Ag and precious ore deposits are identified.

In Viet Nam, India – Eurasian collision-related magmatic activities are closely associated with the formation of Red River fault zone and nearby structures (such as Phan Si Pan, Song Da) (Hoa 1995, 1997, 1999, 2000, 2003, 2005, 2007; Anh et al. 2001, 2002; Polyakov et al. 1997; Izokh et al. 2004). The Paleogene – Neogene ultrapotassic mafic magmatic activities occurred between Song Da and Phan Si Pan structures in northwestern Viet Nam show characteristics analogous with those magmatic activities in Pamir (e.g. Bargan, Kyzylrabat, Dunkeldyk complexes, etc.) (after Pavlova and Borisenko 2009) and Tibet (Chung et al. 1997; Li 1997). This similarity allows for identifying a collision-related Cenozoic ultrapotassic magmatic belt whereby Viet Nam (especially the northwestern) becomes an important joint of this specific magmatic series. According to the latest studies, Cenozoic magmatic activities in the Red River high-temperature –pressure metamorphic belt as well as in the nearby Phan Si Pan and Song Da structures are divided into three stages based on strong extrusion (motion) rate of the Red River fault zone during 35 – 22 Ma interval. The three stages include pre-extrusion (42-35 Ma), syn-extrusion (35-25 Ma) and post-extrusion (22-19 Ma). The pre-extrusion magmatic formations contain pluton-volcanic bimodal alkaline mafic and ultrapotassic associations including (lamproite, absarokite, minette, etc.) and alkaline felsic, such as trachyte, granosyenite, syenite, etc (Hoa 1995; Hoa 2005, 2007; Chi 2003, Polyakov et al. 1997; Anh et al. 2001). The formation age of this magmatic association may lie between 42 – 35 Ma. The syn-extrusion magmatic associations (35 – 25 Ma) in the Red River zone consist mainly of mafic and ultramafic intrusion bodies of lherzolite, websterite and amphibole gabbro; while magmatic associations in the Phan Si Pan uplift contain 35 Ma Ye Yen Sun granite (Shaerer et al. 1994; Dung 2012). The post-extrusion magmatism is observed in the Red River fault zone as undeformed mafic (dolerite) veins and dykes and small bodies of leuco-granite or granitic aplite, pegmatite having formation ages varying between 24 and 19 Ma (Hoa 2007).

Following the above descriptions it is clear that India – Eurasian collision-related magma – mineralization period in the Cenozoic is one of the appealing tasks in the current geosciences. The authors would like to dedicate this chapter to presenting the latest achievements in research of Cenozoic magmatic activities and associated mineralization in north Viet Nam, and of the specific geological structures which are directly or indirectly influenced by the formation and evolution of Ailao Shan – Red River Shear zone following India – Eurasian collision.

References

Chung SL, Lee TY, Lo CH, Wang PL, Chen CY, Nguyen TY, Tran TH, Wu GY (1997) Intraplate extension prior to continental extrusion along the Ailao Shan – Red river shear zone. Geology 25:311–314

Dmitriev EA (1976) Cenozoic potassic rocks of East Pamir. Donish Publishing, 125 pp (in Russian)

Hacker B, Luffi P, Lutkov V, Minaev V, Ratschbacher L, Plank T, Dugea M, Patino-Douce A, McWilliams M, Metcalf J (2005) Near-ultrahigh pressure processing of continental crust: Miocene crustal xenoliths from the Pamir. J Petrol 46(8):1661–1687

Hou ZQ, Mo XX, Gao YF, Qu XM, Meng XJ (2003) Adakite: a significant Cu-bearing porphyry—a case study on porphyry Cu deposits in Tibet and northern Chile. Miner Deposits 22:1–12 (in Chinese with English abstract)

Hou Z-Q, Xie Y-L, Li Y-Q, Xu W-Y, Rui Z-Y (2005) Yulong: a high-sulfidation Cu–Au porphyry copper deposit in the eastern Indo–Asian collision zone, East Tibet. Int Geol Rev

Hu Xiangzhao (1995) The origin of alkali-rich granite porphyry in Western Yunan Province. J Chin Nonferrous Metal 4(1):1 (in Chinese)

Izokh AE, Tran Trong Hoa, Polyakov GV, Ngo Thi Phuong, Tran Tuan Anh, Travin AV (2004) Syn-kinematic ultramafic-mafic magmatism in the Red river shear zone. J Geol Ser B 23:26–41

Leloup PH, Lacassin R, Tapponnier P, Scharer U, Zhong Dalai, Liu Xaohan, Zhang Shan, Ji Shaocheng, Phan Trong Trinh (1995) The Ailao Shan – Red river shear zone (Yunnan, China), Tertiary transform boundary of Indochina. Tectonophysics 251:3–84

Li P (1997) The significance of late paleogene magmatism on the Ailao Shan – Red river shear zone in Yunan-Sichuan, South China. Ph.D. thesis, University of Illinois at Chicago, Chicago

Li JW, Zhao XF, Zhou MF, Vasconcelos P, Ma CQ, Deng XD, Souza ZS, Zhao YX, Wu G (2008) Origin of the Tongshankou porphyry–skarn Cu–Mo deposit, Eastern Yangtze craton, Eastern China: geochronological, geochemical and Sr–Nd–Hf isotopic constraints. Miner Deposita 43:315–336

Nguyen Trung Chi (ed) (2003) Petrology and mineralization of alkaline magma formations in Northern Viet Nam. Final report of ministerial project (ministry of natural resources and environment), Center for Information and Literature Archives, Department Geology and Minerals, Hanoi (in Vietnamese)

Pavlova GG, Borisenko AS (2009) The age of Ag-Sb deposits of Central Asia and their correlation with other types of ore systems and magmatism. Ore Geol Rev 43:1–2

Polyakov GV, Nguyen Trong Yem, Balykin PA, Tran Trong Hoa, Panina LI, Ngo Thi Phuong, Hoang Huu Thanh, Tran Quoc Hung, Sarygin VV, Bui An Nien, Hoang Viet Hang (1997) The new data from ultrapotassic basic rocks in Northern Vietnam – Cocite. Russ Geol Geophys 38(1):148–158 (in Russian)

Pham Thi Dung, Tran Trong Hoa, Tran Tuan Anh, Tran Van Hieu, Vu Hoang Ly, Lan CY, Usuki T (2012) The new date on Ye Yen Sun granitoid complex in the Phan Si Pan. J Earth Sci 34(3):193–204 (in Vietnames with English abstract)

Schaerer U, Zhang LS (1994) Duration of strike-slip movements in large shear zones: the Red river belt, China. Earth Planet Sci Lett 126:379–397

Tapponnier P, Peltzer G, Le Dain AY, Armijio R, Cobbold P (1982) Propagating extrusion tectonics in Asia: new insights from simple experiment with platicine. Geology 7:611–616

Tran Trong Hoa (ed) (1995) Study of Mesozoic – Cenozoic magmatism and its mineralization potential. Final report for National project KT- 01–04 (1992–1995). Archives of the National Center for Science and Technology Information, Hanoi (in Vietnamese)

Tran Trong Hoa (2007) Intraplate magmatism in North Vietnam and related metallogeny. Dissertation of Doctor of Science. Institute of Geology and Mineralogy, Siberian Branch, RAS, Novosibirsk, 382 p

Tran Trong Hoa, Hoang Huu Thanh, Ngo Thi Phuong, Tran Tuan Anh, Hoang Viet Hang (1997) Mineralization, characteristics and forming conditions of lamproite of Vietnam. J Geol – Ser B 9–10:63–68

Tran Trong Hoa, Hoang Huu Thanh, Ngo Thi Phuong, Tran Tuan Anh, Hoang Viet Hang (1999) Potassic alkaline magmas in Northwestern Viet Nam: indications of late paleogene intraplate extension. J Geol A250(1–2):7–14 (in Vietnamese with English abstract)

Tran Trong Hoa, Phan Luu Anh, Ngo Thi Phuong, Nguyen Van The (2000) Cenozoic granitoids in the Red river fault zone. J Earth Sci 22(4):306–318 (in Vietnamese with English abstract)

Tran Trong Hoa, Tran Tuan Anh, Ngo Thi Phuong, Tran Viet Anh (2003) Genetic characteristics of Muong Hum granitoids based on geochemical and isotopic studies. J Earth Sci 25(4):389–400 (in Vietnamese with English abstract)

Tran Trong Hoa, Hoang Huu Thanh, Ngo Thi Phuong, Vu Van Van, Bui An Nien, Hoang Viet Hang, Tran Tuan Anh, Pham Thi Dung, Tran Hong Lam, Tran Viet Anh, Phan Luu Anh (2005) Survey and evaluation of accompanying minerals in Pb – Zn and Cu mines in Viet Nam. Final report of national project on mineral resources (2002–2004). Archives of the Center for Information and Literature, Viet Nam Academy of Science and Technology (in Vietnamese)

Tran Tuan Anh (2001) Ultrapotassic rocks in the Noth West Vietnam. Ph.D thesis, Vienna University, Austria

Tran Tuan Anh, Tran Trong Hoa, Pham Thi Dung (2002) Granites of the Ye Yensun complex and their significances in tectonic interpretation of the early Cenozoic stage in West Bac Bo. J Geol Ser B 19–20:43–53

Vladimirov AG, Borisenko AS, Rudnev SN, Chupin VP, Kruk NN, Titov AV, Borovikov AA, Pavlova GG, Averkin YA, Turkina OM, Vladimirov VG, Mortsev NK (2000) Ore-bearing granite plutons of the Southern Pamir, Tajikistan. In: Kremenetsky A, Lehmann B, Seltmann R (eds) Ore-bearing granites of Russia and adjacent countries. Publishing House of Institute of Mineralogy and Geochemistry of Rare Elements, Moscow, pp 331–348

Wang FT, Feng J, Hu JW (2001) The characteristics and significance of Tuwu large-type porphyry copper deposit in Xinjiang. Chin Geol 28:36–39 (in Chinese with English abstract)

Zhang YQ, Xie YW, Liang HY, Qiu HN, Li XH, Zhong SL (1998) Petrogenesis series and the ore-bearing porphyries of the Yulong copper metallogenic zone in Eastern Tibet. Geochimica 23(4):236–243 (in Chinese with English abstract)

Zhang LC, Xiao WJ, Qin KZ, Qu WJ, Du AD (2005) Re-Os isotopic dating of molybdenite and pyrite in the Baishan Mo-Re deposit, Eastern Tianshan, NW China, and its geological significance. Miner Deposits 39:960–969

Chapter 7
Paleogene Potassic and Ultra-potassic Volcano-Plutonic Associations in the Song Da Rift

Abstract Paleogene potassic and ultra-potassic alkaline volcano-plutonic magmas in the northwestern Song Da structure and in the boundary between this structure and the Phan Si Pan uplift are compositionally diversified, ranging from alkaline mafic (lamproite, absarokite, minette) to alkaline felsic (trachyte and syenite). Geological, mineralogical, geochemical and isotpe characteristics of Ol-Cpx, Cpx-Phl lamproites, absarokite, minette and trachyte and syenite are presented. Lamproite in the northwest Vietnam are compared with low-Ti Mediterranean-type lamproite. Study on the inclusions in clinopyroxene from lamproite showed formation of the potassic and ultra-potassic magmas in the Song Da rift zone is a result of fractional crystallization of melts whose compositions were equivalent to lamproitic magmas, which were subsequently evolved by magma differentiation would lead to form diversified magmas. Mineralogical and geochemical studies of trachyte and syenite showed their genetic relationship. The formation ages of lamproite, trachyte and syenite (42–30 Ma; Ar-Ar and Rb-Sr methods) suggest they are late Paleogene intraplate extension activities in the northwest Vietnam.

Paleogene potassic and ultra-potassic alkaline volcano-plutonic magmas in the northwestern Song Da structure and in the boundary between this structure and the Phan Si Pan uplift are compositionally diversified, ranging from alkaline mafic to alkaline felsic. These magmatic compositions are also reported for magmas in the Dali Eihai area, northwest of Yunnan, China (Li 1997). Study of potassic and ultra-potassic alkaline mafic was started many years ago, and one of the rock names was introduced to world geological literature as ‘cocite’ (standing for Sin Cao and Coc Pia villages) (Lacroix 1933); later in showing interest to the presence of lamproite in Viet Nam, Wagner (1986) re-analyzed the cocite from samples exposed at the Paris natural museum (Wagner and Velde 1986). Later studies of cocite as well as other potassic alkaline mafic rocks in the Tam Duong and Dong Pao areas showed that the cocite contains basic characteristics similar to those of low-Ti Mediterranean-type lamproite (Hoa 1995, 1997b, 1999; Polyakov et al. 1997; Anh et al. 2001; Chi 2003). Besides, other magmas such as absarokite, minette, trachyte and syenite in the Tam Duong and Dong Pao areas have been studied in detail and will be reported in this chapter.

T.-H. Tran et al., *Intraplate Magmatism and Metallogeny of North Vietnam*,
Modern Approaches in Solid Earth Sciences 11,
DOI 10.1007/978-3-319-25235-3_7

7.1 Geological Features

The Paleogene potassic and ultra-potassic magmas are well-developed and widely distributed in the Tam Duong – Dong Pao area (Lai Chau province) in northwest Vietnam. Geologically the area is located between the Song Da structure and Phan Si Pang uplift, in the vicinity of the Red River Shear zone to the east. Major outcrops of the potassic and ultra-potassic alkaline magmas are defined in two volcanic fields Sin Cao – Pin Ho and Dong Pao (Fig. 7.1). The volcanic magmas and associated dyke and vein types along with small-sized intrusion are distributed mainly only within the area; although there are small-sized syenite intrusions and comparable vein and dyke type magmas are scattered outside the area of two fields, along a regional fault running from Tam Duong to Phong Tho. Based on the compositions the Paleogene potassic and ultra-potassic alkaline magmas are grouped accordingly to the following associations:

- Potassic and ultra-potassic alkaline mafic lamproite, absarokite (and trachyte, trachyandesite), minette and shonkinite.
- Potassic and ultra-potassic alkaline felsic trachyte – trachyrhyolite, syenite – granosyenite.

In previous studies the first magmatic association was grouped to Pu Sam Cap complex, and some of the syenite and granosyenite bodies from the second association were viewed as the major component of a alkaline intrusive complex termed as Nam Xe – Tam Duong according to its geographic distribution (Tri et al. 1977). Recently the alkaline felsic volcanic and dyke magmas were classified as Paleogene Pu Tra complex, the rest including alkaline intermediate and acidic sub-volcanic magmas, along with shonkinite and minette dykes are grouped to Pu Sam Cap complex (Thuc and Trung 1995). Note that syenites in the Nam Xe and Tam Duong areas are not compositionally similar with those in the Dong Pao and Pu Sam Cap areas. However, because of their limited distribution area and geological relationship between individual intrusive bodies and surrounding host rocks has not yet been established; moreover, in areas where syenites of Nam Xe – Tam Duong-type outcropped also found are shonkinite, lamproite and minette having compositions closely comparable to those in Pu Sam Cap intrusive bodies, the syenites, therefore, are remained as a constituent in the Pu Sam Cap complex (Hoa 1995). Recent age dating (U-Pb, zircon, LA-ICP-MS) of syenite and alkaline granite from Nam Xe – Tam Duong complex shows Permian age (253–251 Ma; Hieu et al. 2012).

The potassic and ultra-potassic alkaline mafic and felsic magma associations are widely spread in the northwest of Song Da structure, from Tam Duong – Dong Pao to Phong Tho – Nam Xe (Fig. 7.1). However, they outcrop mostly in the Sin Cao and Dong Pao areas, former Tam Duong district, where their petrologic and occurring types are fully and clearly exposed.

The potassic and ultra-potassic alkaline magmas include the following petrological compositions absarokite, minette, shonkinite and lamproite. Aside from the minette and shonkinite being found in dyke phases, absarokite and lamproite are met in both volcanic and dyke outcrops. The lamproite magma is also found in form of small-sized intrusive necks. Distribution position and geological spreading form

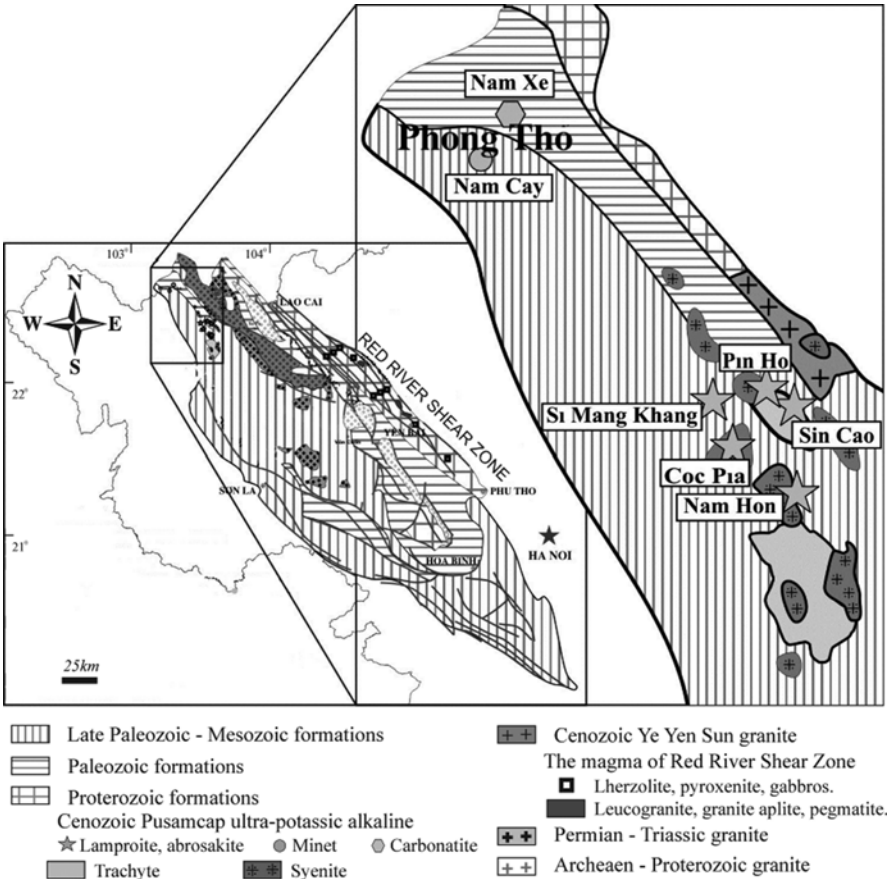

Fig. 7.1 Distribution scheme of potassic and ultra-potassic alkaline magmas in the northwestern wing of Song Da rift, northwest Viet Nam

of the absarokite, minette and lamproite are shown in Fig. 7.1 and described in detail in Hoa (1997b, 1999), thus only major points are briefly given here. Intrusive and dyke necks normally show petrologically homogenous compositions; the difference between intrusive dyke and block magma types is reflected only by their textures; since their compositions are poorly distinctive, suggesting weak magma differentiation at corresponding transitional magma chambers. Meanwhile petrologic compositions of the volcanic magma types are normally complicated. Detail mapping of volcanic structures in the Pin Ho area defined several explosion neck- type eruption forming tuff, tuff-agglomerate, tuff-breccia, tuff-lava and tuff-lapilli of lamproite and absarokite composition (Fig. 7.2). Fined-grained tuff and tuff-breccia overlie trachyte and trachytic tuff. Whereas fragments of trachyte, sometimes syenite, sediments and metamorphic rocks are occasionally observed in lamproite and absarokite tuffs. Note that mantle xenoliths such as pyroxenite, peridotite and glimmerite are commonly found in lamproite tuff. Lamproite dykes of neck facies are outcropped around the Pin Ho volcanic explosion pipe-like structure.

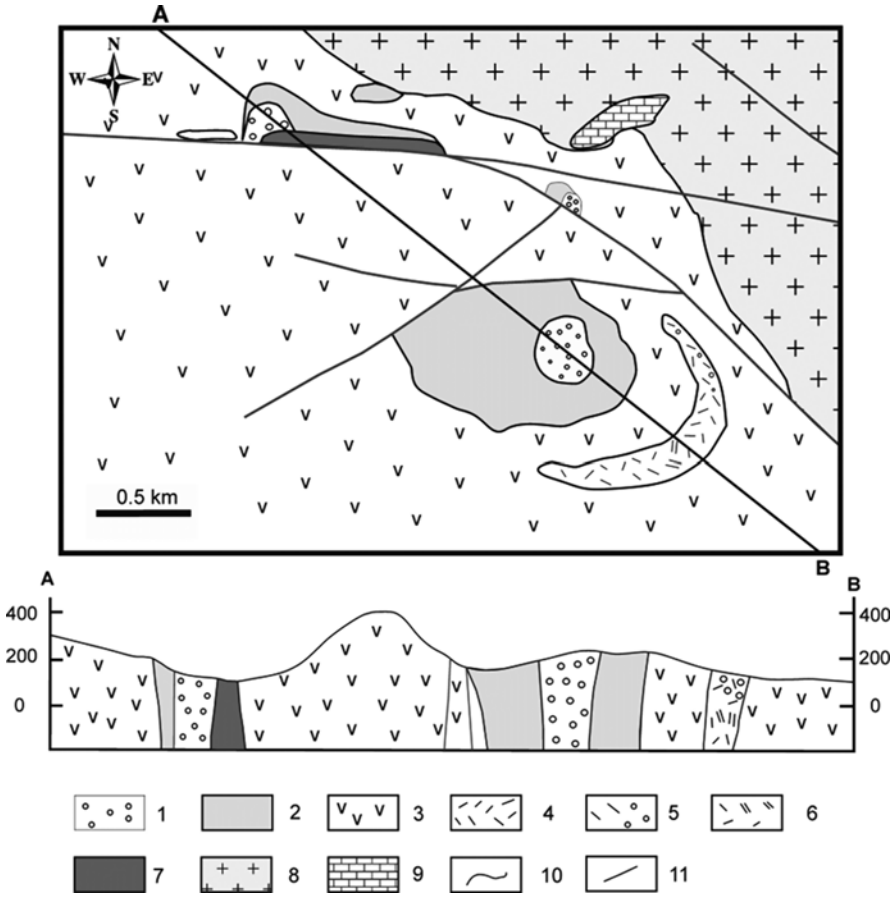

Fig. 7.2 Scheme of Pin Ho pipe-like structure (in Sin Cao, Tam Duong district, Lai Chau province). Remarks: *1* Tuff-breccia and tuff-lapilli of absarokite and lamproite compositions; *2* absarokite and lamproite tuff-lavas; *3* Trachyte and trachy-andesite; *4* Cpx-Phl lamproite; *5* Ol-Cpx lamproite; *6* phlogopite-rich lamproite; *7* monchiquite dyke and sill; *8* granosyenite and syenite; *9* Triassic limestone; *10* boundary between petrologic types; *11* faults (After Hoa et al. 1997b)

Lamproite dyke – sill and neck-type intrusion are normally found to outcrop outside the area of volcanic field in Triassic carbonate sediments. Most representative outcrops include Coc Pia, Si Mang Khang (Hoa 1999) and Phan Si Hoa (Chi 2003). Phan Si Hoa lamproite block also appears crosscutting Pu Sam Cap-type alkaline syenite (Chi 2003). Typical petrologic compositions of the above intrusive blocks contain Ol-Cpx and Cpx- phlogopite (Phl)-lamproite. Serpentinized peridotite xenoliths are discovered in Coc Pia magmas. Recently more lamproite explosion pipes have been found in the Tua Chua area (Dien Bien province), and sites in the boundary between Song Da structure and Nam Co belt (Nguyen et al. 2005). Petrologic compositions of those exposed in the Tua Chua area are lamproites, comparable to those in the Sin Cao area (Lai Chau province).

Dyke and sill bodies of minette,, monchiquite and camptonite are frequently found in late Triassic – Cretaceous terrigenous sediments. One of the most representative dykes is Nam Cay minette crosscutting Cretaceous terrigenous sediments in northwest Tam Duong and in the Phong Tho district. The dyke – sill bodies reach up to 7.5 m thick and are composed mainly of minette showing a co-existing mineral assemblage of Cpx, Phl and San (sanidine).

Shonkinite is found only in dykes in dark-colored syenite in the Cuon Ha block, southeast of the Dong Pao volcanic field.

Trachyte volcanics outcropped in Sin Cao and Dong Pao volcanic fields are compositionally comparable. Coarse-grained, block-sized tuff, tuff-agglomerate, tuff-gravelstone are also common.

7.2 Petrography and Mineralogy

Among the lamproites (cocite) two common petrographic types are Ol-Cpx and Cpx-Phl lamproite; while less common is phlogopite – (Phl) lamproite. The rock types show a rather stable mineral assemblage including Ol + Cpx + Phl + San and ± Leucite. Olivine, clinopyroxene and phlogopite appear both in phenocryst and groundmass, while sanidine and leucite occur only in groundmass. Typical accessory minerals include Cr-spinel, ilmenite, apatite, zircon and rutile. In a sieved lamproite tuff sample from the Pin Ho pipe also found are garnet (grossular), sphene, ultrahigh ore mineralized moissanite (SiC), native iron and gold. The magma is porphyric or porphyric-like having aphanitic or dolerite-like microlitic groundmass. Lamproite in intrusive blocks shows well-crystallized groundmass; however, the magma has yet been found as actually intrusive texture with fully and idiomorphically crystallized minerals. Textural features of lamproite variety are shown in Photos 7.1, 7.2, 7.3, 7.4.

The absarokite has a co-existing mineral assemblage mostly similar to that of the Cpx-Phl lamproite. The difference in textures is used to differentiate the absarokite,

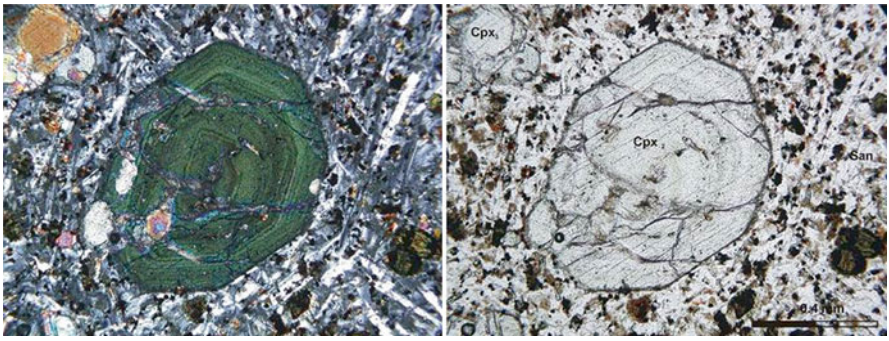

Photo 7.1 Zoned pyroxene in Ol-Cpx lamproite in the Sin Cao area. Sample T-1775; crossed nicols (*left*) and one nicol (*right*)

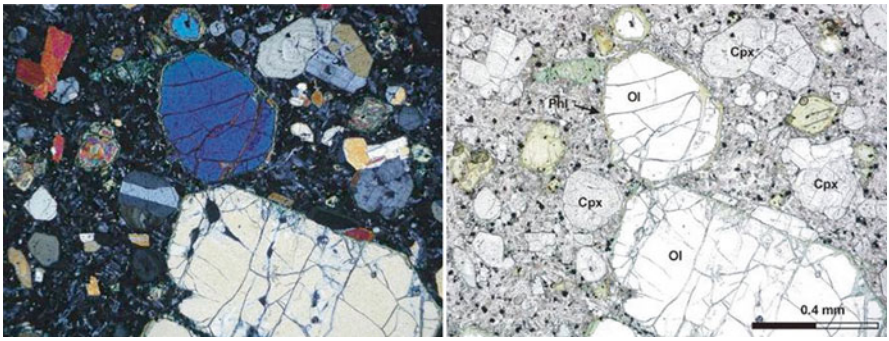

Photo 7.2 Ol-Cpx – lamproite in the Pìn Hồ area. Sample H-737; crossed nicols (*left*) and one nicol (*right*)

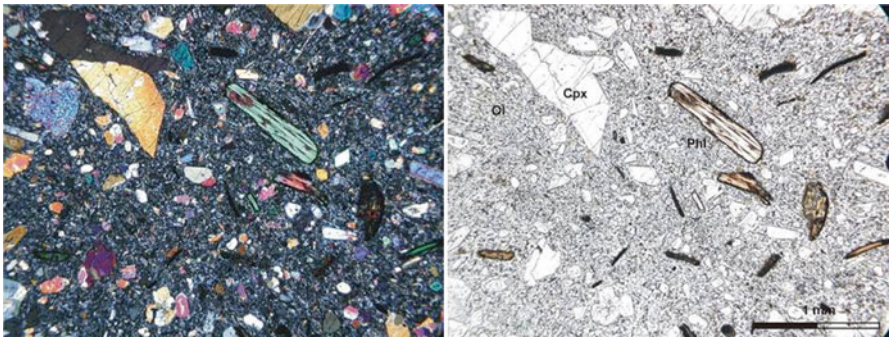

Photo 7.3 Olivine-diopside-phlogopite – lamproite in the Si Mang Khang area. Sample P-236; crossed nicols (*left*) and one nicol (*right*)

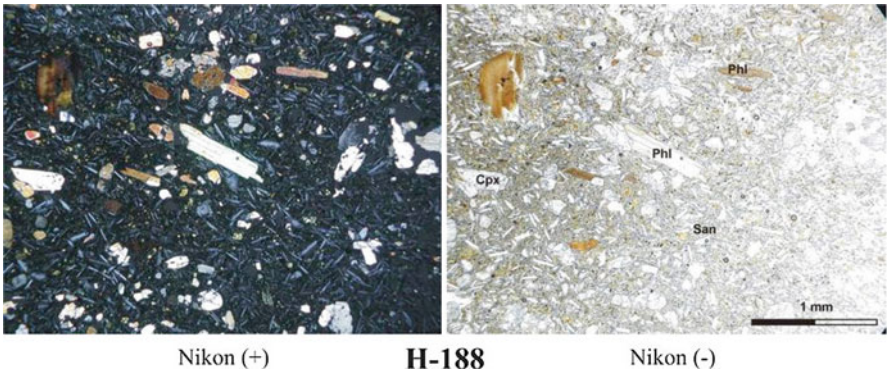

Photo 7.4 Diopside-phlogopite-leucite lamproite in the Pìn Hồ area. Sample H-188: crossed nicols (*left*) and one nicol (*right*)

including absarokite lava, tuff-lava and volcanic bomb types. Olivine is rarely found in absarokite, however, if there is any that would be serpentinized completely. Some olivine grains found in absarokite are viewed as xenocrysts; plagioclase is sometimes seen in the groundmass.

The lamprophyre group includes mainly minette and a minor amount of monchiquite and camptonite; the minette belongs to potassic alkaline series while monchiquite and camptonite are of sodic – potasstic alkaline series. Typical minette is reported in Nam Chay dykes (Phong Tho area); the monchiquite is encountered in Coc Pia neck-type intrusive bodies and in the Pin Ho explosion pipe area; camptonite, on the other hand, is found in dyke-sill bodies in late Triassic terrigenous sediments in the Dong Pao area. Crystallinity of the minette is relatively high. The magma is gabbrodolerite-like texture, having a mineral assemblage containing Cpx + Phl + San, with Cpx being main phenocryst mineral and phlogopite as minor. Sanidine is elongated tablet, arranged parallel with contacts between the dykes and country rocks (Photos 7.5 and 7.6). Monchiquite is clinopyroxene – rich, compositionally analogous to K-clinopyroxenite. The magma is clearly porphyric with Cpx being major phenocryst phase, sometimes formed large aggregates on

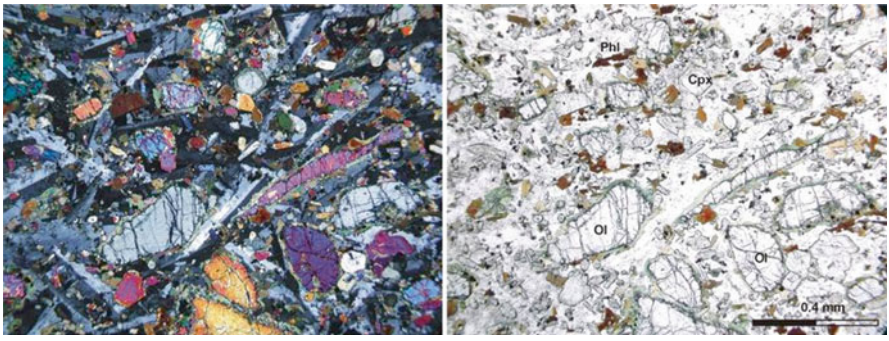

Photo 7.5 Minette in the Nậm Cảy area. Sample P9471: crossed nicols (*left*) and one nicol (*right*)

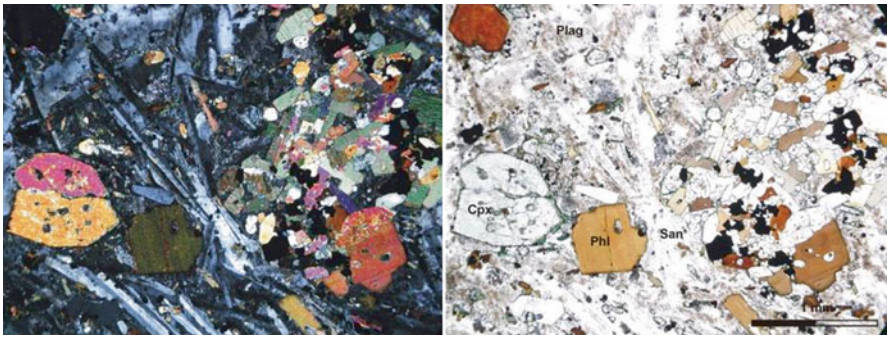

Photo 7.6 Minetet in the Nậm Cậy area. Sample T-1738: crossed nicols (*left*) and one nicol (*right*)

fine-grained groundmass containing mainly Cpx and a minor amount of phologopite and sanidine. The Camptonite shows a co-existing mineral assemblage of Phl + Cpx + San + Pl, with Phl being the major phenocryst phase while the groundmass consisted of Phl + San + Pl + Cpx.

The trachyte group normally has tuff texture comprising compositionally complex fragments, including trachyte, silicic and sandstone. The groundmass is trachyte lava or fine-grained trachyte tuff intercalated by a minor amount volcanic glass. Trachyte contains K-feldspar, albite, clinopyroxene and biotite. The accessory minerals are apatite, zircon, fluorite and sometimes garnet.

The syenite group is compositionally diversified, ranging from dark-colored syenite most similar to gabbro-syenite, Cpx-Amp-biotite- syenite to garnet-bearing syenite and bright-colored syenite containing some biotite. Dark-colored shonkinite-like is found in Cuon Ha block. Rock-forming mineral assemblage of the syenite is Fsp + Pl + Cpx ± Amp + Bi ± Gr. Olivine sometimes is found in gabbro-syenite.

Olivine is normally characterized by the lamproite. Olivine phenocrysts in lamproite are highly magnesian (Mg# = 95–83), equivalent to forsterite – chrysolite; olivines in the groundmass are varying between chrysolite and hyalosiderite. Olivine in the absarokite is normally equivalent to hyalosiderite (Mg# = 80–75) (Table 7.1,

Table 7.1 Chemical compositions (wt.%) of representative olivines in lamproite (After Hoa et al. 1997; Anh 2001)

No	Sample ID	SiO_2	FeO	MgO	CaO	NiO	Total
1	H-101-B	41.26	9.10	48.62	0.09	0.28	99.35
2	H-101 M	39.96	15.51	43.83	0.20	0.12	99.62
3	V-108-B	39.39	16.49	44.81	0.17	-	99.89
4	P-58-B	40.68	9.94	48.91	0.08	0.29	99.89
5	P-63-B	40.17	13.13	46.55	0.08	0.26	100.20
6	P-69-B	40.23	14.87	44.99	0.15	0.16	100.40
7	P-71-B	40.21	13.13	46.23	0.12	0.21	99.90
8	P-73-B	40.94	10.23	47.77	0.09	0.37	99.40
9	G-941-B	40.77	7.49	51.64	0.08	0.43	100.41
10	P-235/1-M	41.09	9.81	47.94	0.11	0.34	99.29
11	P-235/2-B	40.86	7.93	50.92	0.09	0.32	100.17
12	P-245-B	40.78	8.58	50.39	0.08	0.30	100.13
13	P-247-B	40.66	8.28	51.09	0.09	0.29	100.41
14	H-724-B	41.54	7.53	50.33	0.06	0.48	100.12
15	T-1764-B	40.89	10.80	47.22	0.07	0.34	99.32
16	T-1588-T	39.39	14.66	45.98	0.12	0.19	100.34
17	T-1588-R	37.28	21.45	40.83	0.20	0.12	99.88
18	P-119-B	40.12	13.58	45.68	0.12	0.25	100.08
19	P-120-B	40.15	13.18	41.60	0.12	0.26	100.08
20	T-1726-B	40.73	9.94	48.76	0.02	0.36	99.81
21	H-768-B	41.17	7.72	50.43	0.06	0.43	99.81

Remarks: Areas: 1–4: Nam Hon, 5–9: Coc Pia, 10–13: Mang Khang, 14–17: Sin Cao; B: phenocryst, M: groundmass microlite; T: center; R: rim

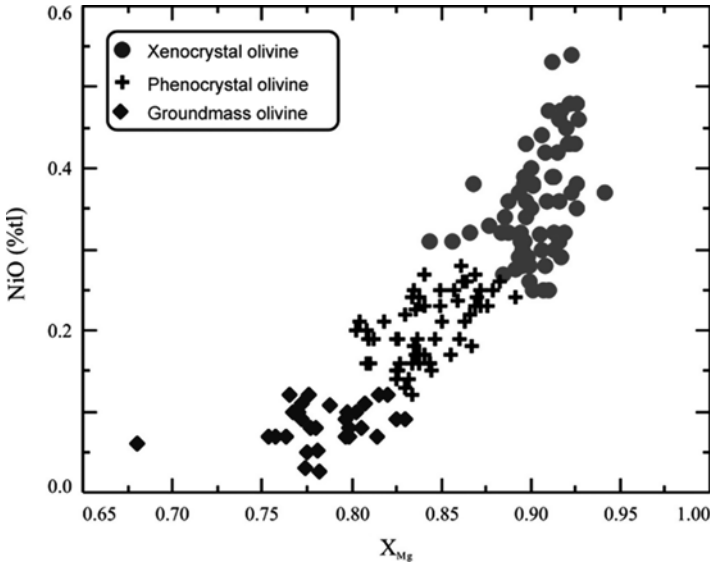

Fig. 7.3 Chemical compositions of olivines in lamproite shown in correlation plots of NiO vs. XMg (Anh 2001)

Fig. 7.3). In general, the Ni contents in olivines are high, 0.10–0.48 wt.%. The olivines are mostly structurally homogeneous although sometimes zoning is also present in some crystals, where Mg# decreasing from 85 to 77 and NiO from 0.19 to 0.12 wt.%, respectively, from center to periphery of crystals, indicating magmatic fractional crystallization process. Olivines as xenocrysts are sometimes found in absarokite tuff, having unusually high Mg# (90–92) and NiO (0.43 wt.%) but very low CaO (0.06 wt.%).

Clinopyroxene (Cpx) is a common mineral in potassic and ultra-potassic alkaline mafic as well as felsic magmas, except for bright-colored trachyte and syenite. Cpx is present in both phenocryst and groundmass phases. In lamproite and absarokite Cpx is normally magnesian diopside or diopside – augite. According to Fe, Mg, Al, Ti, Cr interrelationship clinopyroxenes in the mafic magma types (lamproite, absarokite, minette and monchiquite) is divided into two groups. The first group is high in Cr and Al, relatively low Ti, characterized for lamproite and absarokite; their Cr_2O_3 varying between 0.2 and 0.7 wt.%, exceptionally reaching 1.3 wt.%; the TiO_2 being between 0.15 and 0.3 wt.%, and Al_2O_3 between 0.6 and 1.2 wt.%. The second group has low $Cr_2O_3 < 0.1$ wt.%, while TiO_2 and Al_2O_3 are high, respectively, 0.4–1.2 wt.% and 2.3–5.4 wt.% (Table 7.2). These Cpx normally concentrate in minette and monchiquite. Microscopic analysis shows Cpx phenocrysts, especially those in tablet olivines, having MgO, Cr_2O_3 much higher compared with those in the groundmass. In Cpx zoned crystals concentrations of Ti, Al, Fe, Na increase from center toward rim section, whereas Mg, Cr and Ca decrease, reflecting process of fractional crystallization.

Clinopyroxenes are different in different syenites; in Dong Pao syenite (Cuon Ha block) the Cpx shows chemical features comparable to those in potassic and

Table 7.2 Chemical compositions (wt.%) of representative clinopyroxenes in the Paleogene potassic and ultra-potassic magmas (After Hoa et al. 1997b)

Sample ID	**H-101-B**	**H-101-M**	**H-101-K**	**P-55-B**	**P-55-M**	**P-55-K**
SiO_2	53.75	53.59	51.81	53.39	51.43	52.02
TiO_2	0.15	0.16	0.83	0.20	0.23	0.23
Al_2O_3	1.10	0.91	2.18	1.11	2.52	1.19
FeO	3.36	4.87	6.07	4.57	7.88	5.44
MnO	–	–	–	0.15	0.25	0.18
MgO	17.23	16.81	15.64	16.79	13.43	16.34
CaO	23.70	23.99	23.14	23.39	23.74	23.65
Na_2O	0.30	0.40	0.62	0.37	0.69	0.44
Cr_2O_3	0.42	0.15	0.18	0.15	0.01	0.22
Total	100.00	100.90	100.50	100.10	100.20	99.70
Sample ID	**V-108-B**	**P-63-B**	**P-73a-B**	**P-237-B**	**P-245-B**	**T-1588-B**
SiO_2	53.59	52.72	52.85	53.54	52.78	53.30
TiO_2	0.20	0.28	0.43	0.13	0.09	0.22
Al_2O_3	0.94	1.42	1.47	0.84	1.72	1.14
FeO	4.12	3.94	5.67	4.11	6.93	5.34
MnO	–	0.10	0.17	0.12	0.26	0.13
MgO	17.29	16.84	16.55	17.17	14.22	15.59
CaO	23.05	22.41	21.96	22.54	22.42	23.42
Na_2O	0.29	0.37	0.31	0.29	0.86	0.45
Cr_2O_3	0.03	0.63	0.29	0.02	0.04	0.12
Total	99.50	98.71	99.71	98.77	99.34	100.00
Sample ID	**T-1588-M**	**T-1588-K**	**T-1588-T**	**T-1588-R**	**P-184-B**	**P-195-B**
SiO_2	53.33	52.46	55.15	53.39	53.74	51.33
TiO_2	0.20	0.35	0.12	0.41	0.17	0.27
Al_2O_3	1.31	1.09	0.79	1.92	0.72	3.96
FeO	3.77	3.63	3.64	6.30	4.32	7.13
MnO	–	–	0.11	0.11	0.16	0.22
MgO	17.50	18.02	17.80	15.30	17.61	13.49
CaO	23.34	23.26	21.61	22.18	21.78	21.57
Na_2O	0.44	0.47	0.33	0.53	0.32	1.11
Cr_2O_3	0.70	0.61	0.33	0.06	0.38	0.03
Total	100.60	99.89	99.88	100.02	99.20	99.12
Sample ID	**P-188-B**	**T-1589-B**	**T-1589-B**	**P-215-B**	**T-1724-B**	**T-1592-B**
SiO_2	54.25	53.51	53.18	52.80	53.19	52.18
TiO_2	0.11	0.20	1.24	0.25	0.26	0.18
Al_2O_3	0.64	1.09	1.21	1.32	0.88	1.30
FeO	3.85	2.86	4.66	4.86	4.83	5.82
MnO	0.14	–	–	0.15	0.15	0.17
MgO	18.74	17.45	16.23	16.67	16.91	16.22
CaO	20.89	23.25	23.21	22.39	22.28	23.39
Na_2O	0.30	0.34	0.30	0.38	0.37	0.56

(continued)

Table 7.2 (continued)

Cr_2O_3	0.21	0.98	0.19	0.26	0.25	0.09
Total	99.15	99.68	99.22	99.08	99.13	99.91
Sample ID	**T-1592-M**	**T1735-B**	**P-66B**	**P-179-B**	**P-193-B**	
SiO_2	52.88	50.64	46.98	52.44	52.79	
TiO_2	0.27	0.72	1.22	0.25	0.18	
Al_2O_3	1.38	4.05	5.35	1.40	2.34	
FeO	6.17	5.38	10.84	5.11	3.32	
MnO	–	0.11	0.10	0.15	0.09	
MgO	15.87	15.76	10.68	16.15	17.35	
CaO	23.18	21.01	22.55	22.94	22.47	
Na_2O	0.50	0.98	0.74	0.34	0.31	
Cr_2O_3	0.05	0.57	0.07	0.08	0.14	
Total	99.80	99.23	98.53	98.87	98.98	

Remarks: Ol-Cpx- and Cpx-Phl- lamproite: 1–7: Nam Hon; 8–9: Coc Pia; 10–11: Si Mang Khang; 12–16: Sin Cao; 17–19: Pin Ho; absarokite tuff-lava: 20–21: Sin Cao; 22–23: Pin Ho; mixed tuff: 24–25: Sin Cao; lamprophyre: 26: Nam Cay minette; 27: monchiquite Coc Pia; trachyte: 28–29: Pin Ho. B: phenocryst; M: microlite in groundmass; K: inclusive crystals: 3–6: phlogopite, 14: olivine; T: center; R: rim

ultra-potassic mafic magmas, except for having lower Mg# and higher Na ($Na_2O = 0.8–1$ wt%); in Tam Duong syenite the Cpx is even higher Na (Na2O = 0.8–5.6 wt.%), comparable to augite-aegirine (Hoa 1995).

Phlogopite is popular in all magma groups, especially in Cpx-Phl – lamproite, absarokite minette and camptonite, present both in phenocryst and groundmass. Note that phlogopite in lamproite and absarokite is greenish-brownish red, while in minette, camptonite, trachyte and syenite the mineral is brownish green. Cr-spinel and magnetite are commonly found embedded in lamproite phlogopite, sometimes the latter is replaced by magnetite; the process is analogous to opacitization commonly observed in volcanic rocks. Sometimes phlogopite is replaced by sky-blue fuchsite, an unusual appearance characterized for high-Cr – phlogopite in kimberlite and lamproite. Zoned structure is characteristic for the phlogopite. Another characteristic feature of phlogopite in the mafic magmas is low Al_2O_3, between 12.5 and 14.0 wt.%, while TiO_2 and MgO contents are high, respectively, 2.4–6.9 wt.% and 16–24 wt.% (Fig. 7.4, Table 7.3). In plots of Al_{IV} versus Fe/(Fe + Mg) most of the compositional points of the lamproite phlogopite show higher phlogopite component compared with minette and absarokite phlogopites, which are higher in annite and siderophyllite. Phlogopite in the syenite is characteristically high TiO_2 (2.46–4.46 wt.%), relatively high Al_2O_3 (13.2–14.6 wt.%) and low MgO (14.3–17.7 wt.%) (Anh 2001). Biotite in syenite is high in TiO_2 up to 3 wt.%, low Al_2O_3 (11.5 wt.%) and MgO (7 wt.%), but high FeO* (28 wt.%) (Hoa 1995). Comparison of Mg, Fe, Ti and Cr contents in lamproite and lamprophyre phlogopite reveals two contrast trends: Ti-rich phlogopite is usually poor in Cr and vice versa. The minette and camptonite phlogopites are also high in TiO_2 (3–6 wt.%) and low Cr ($Cr_2O_3 = 0.06–0.19$ wt.%), although compared with the lamproite phlogopite they

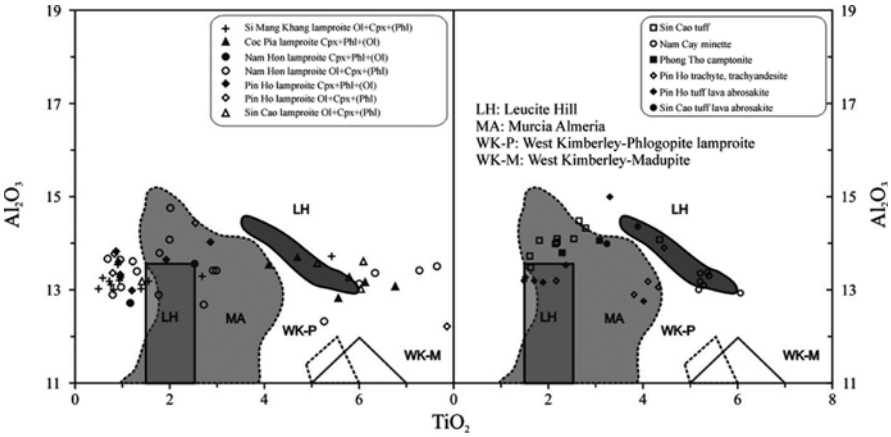

Fig. 7.4 Chemical compositions of phlogopite in Paleogene Su Sam Cap lamproite shown in relation between Al_2O_3 and TiO_2; plotted for comparison including *LH*: Leucite Hill, *MA*: Murcia Almeria; *WK-P*: Phl-lamproite in West Kimberley; *WK-P*: madupitic lamproite West Kimberley (after Mitchell and Bergman 1991)

Table 7.3 Chemical compositions (wt.%) of representative phlogopite in the Paleogene potassic and ultra-potassic mafic and felsic magmas (After Hoa et al. 1997)

Sample ID	**V108-B**	**V101-B**	**H101-M**	**P55-B**	**H81-B**	**H81-B**
SiO_2	38.13	36.00	39.41	38.82	40.14	36.42
TiO_2	5.87	7.46	4.31	0.97	0.80	2.72
Al_2O_3	12.94	13.46	12.71	13.06	12.90	12.68
FeO	9.56	9.90	8.36	9.73	4.43	12.89
MgO	18.71	16.87	20.93	20.46	24.88	18.29
CaO	0.02	0.01	0.00	0.00	0.04	0.06
Na_2O	0.28	0.36	0.31	0.36	0.30	0.58
K_2O	10.18	8.72	9.86	9.50	10.17	9.67
Cr_2O_3	0.10	0.16	0.09	1.23	0.89	0.05
BaO	0.51	2.57	0.03	0.11	0.11	0.49
Sample ID	**P73a-B**	**P63-B**	**P263-B**	**P245-B**	**H763-B**	**T1588-B**
SiO_2	37.46	37.44	40.67	38.63	38.87	38.13
TiO_2	4.09	6.77	0.93	1.55	1.42	4.76
Al_2O_3	13.54	13.07	13.21	13.18	13.19	13.28
FeO	10.23	8.39	4.81	8.33	9.75	10.24
MgO	18.56	18.57	23.68	21.16	20.63	18.67
CaO	0.00	0.08	0.00	0.00	0.05	0.04
Na_2O	0.41	0.58	0.62	0.40	0.46	0.51
K_2O	9.55	9.50	9.39	9.47	9.13	9.88
Cr_2O_3	0.05	0.04	0.90	0.05	0.07	0.07
BaO	0.57	–	0.16	0.25	–	0.19
Sample ID	**T1588-M**	**T1588-K**	**P184-B**	**P195-B**	**P188-B**	**T1589-B**
SiO_2	37.05	35.20	40.45	38.98	38.04	37.53
TiO_2	6.07	5.33	0.92	1.93	2.86	3.44

(continued)

Table 7.3 (continued)

Al_2O_3	13.32	13.55	13.60	13.65	14.02	14.23
FeO	10.35	11.23	4.34	8.82	11.87	8.48
MgO	16.59	18.99	23.96	21.28	18.15	19.99
CaO	0.73	0.01	0.00	0.00	0.00	0.03
Na_2O	0.56	0.50	0.53	0.31	0.59	0.42
K_2O	9.08	9.43	9.31	8.69	9.18	9.30
Cr_2O_3	–	0.66	1.63	0.14	0.16	0.30
BaO	0.22	0.04	0.19	0.19	0.62	0.51
Sample ID	**T1589-M**	**P215-B**	**T1722-B**	**T1724-B**	**T1592-B**	**T1592-B**
SiO_2	37.55	38.14	40.47	40.20	38.05	39.23
TiO_2	3.55	2.36	7.73	0.82	2.18	2.14
Al_2O_3	14.18	13.54	11.98	13.45	14.34	14.00
FeO	8.33	8.94	5.37	4.14	8.86	8.18
MgO	20.37	21.04	20.70	23.90	19.88	21.57
CaO	0.02	0.00	0.00	0.00	0.00	0.03
Na_2O	0.44	0.47	0.99	0.41	0.57	0.61
K_2O	9.37	9.57	8.69	9.67	9.25	9.40
Cr_2O_3	0.24	0.19	0.02	2.14	0.02	0.26
BaO	0.51	0.31	0.36	0.05	–	–
Sample ID	**T1735-B**	**V124-B**	**P66-B**	**P179-B**	**P193-B**	
SiO_2	37.36	36.36	37.30	39.64	37.46	
TiO_2	6.06	3.07	6.13	0.75	3.81	
Al_2O_3	12.94	14.07	13.16	12.78	12.90	
FeO	12.66	15.39	14.09	8.98	14.28	
MgO	16.06	15.32	14.25	20.89	15.34	
CaO	0.00	0.02	0.08	0.00	0.00	
Na_2O	0.57	0.11	0.45	0.52	0.55	
K_2O	8.83	9.97	9.35	9.29	8.35	
Cr_2O_3	0.06	0.19	0.07	0.70	0.01	
BaO	0.51	–	–	0.08	0.65	

Remarks: Ol-Cpx- and Cpx-Phl- lamproite: 1–6 Nam Hon; 7–8: Coc Pia; 9–10: Si Mang Khang; 11–14: Sin Cao; 15: Pin Ho; absarokite tuff-lava: 18–19: Sin Cao; 20–22: Pin Ho; mixed tuff: 23–24: Sin Cao; 25: minette Nam Cay; 26: Phong Tho camptonite; 27: Sin Cao monchiquite; trachyte: 28–29: Pin Ho. B: phenocryst; M: groundmass microlites; K: inclusions in magnetite; T: center; R: rim

have lower MgO and higher FeO*. According to T.T. Anh (2001) phlogopite in glimmerite (inclusions in absarokite tuff-lava) is characteristically high Mg# (89–92) and Cr_2O_3 (1.71–2.4 wt.%), and low TiO_2 (0.72–0.84 wt.%), indicating magma formation at high pressures. The chemical compositions of the regional phlogopites shown in comparison with worldwide phlogopites are given in Fig. 7.4.

Cr-spinel in lamproite is usually found as small-sized crystals in olivine and phlogopite crystals. Chemical compositions of Cr-spinel vary from chromite to Fe-Al-chromite and Cr-magnetite (Table 7.4). Cr-spinel types having higher Cr, Mg

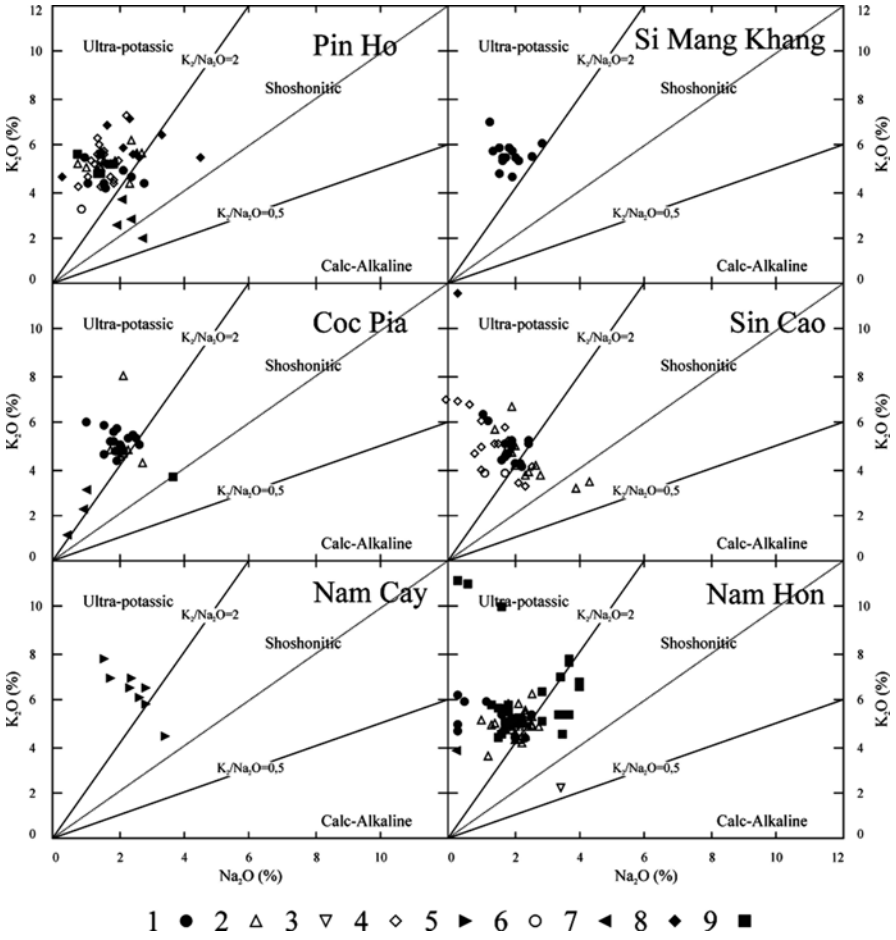

Fig. 7.5 Chemical compositions of potassic and ultra-potassic alkaline magmas in the Pu Sam Cap area shown in relation between K2O and Na2O; *1*: Ol-Cpx-(Phl) lamproite; *2*: Cpx-Phl-(Ol)-lamproite; *3*: mixed tuff; *4*: absarokite tuff-lava; *5*: minette; *6*: camptonite; *7*: monchiquite; *8*: trachyte; *9*: syenite and granosyenite

and Al concentrations are crystals embedded in olivine phenocrysts, compared with those microlites in the groundmass. Basically the chemical compositions of Cr-spinel in lamproite in northern Viet Nam are closely comparable to those reported elsewhere in the world; however, the significant difference between the Cr-spinel in northern Viet Nam and elsewhere is the lack of corroded faces of the crystals, indicating a deep mantle origin.

Magnetite is usually found in lamproite groundmass or embedded in phlogopite and clinopyroxene phenocrysts, showing variable TiO_2 from 2 to 8 wt.% (Table 7.4). The low Ti-magnetite types normally have higher Cr_2O_3 (up to 5 wt.%). Some magnetite may have V_2O_5 up to 0.6 wt.% and MnO about 1 wt.%.

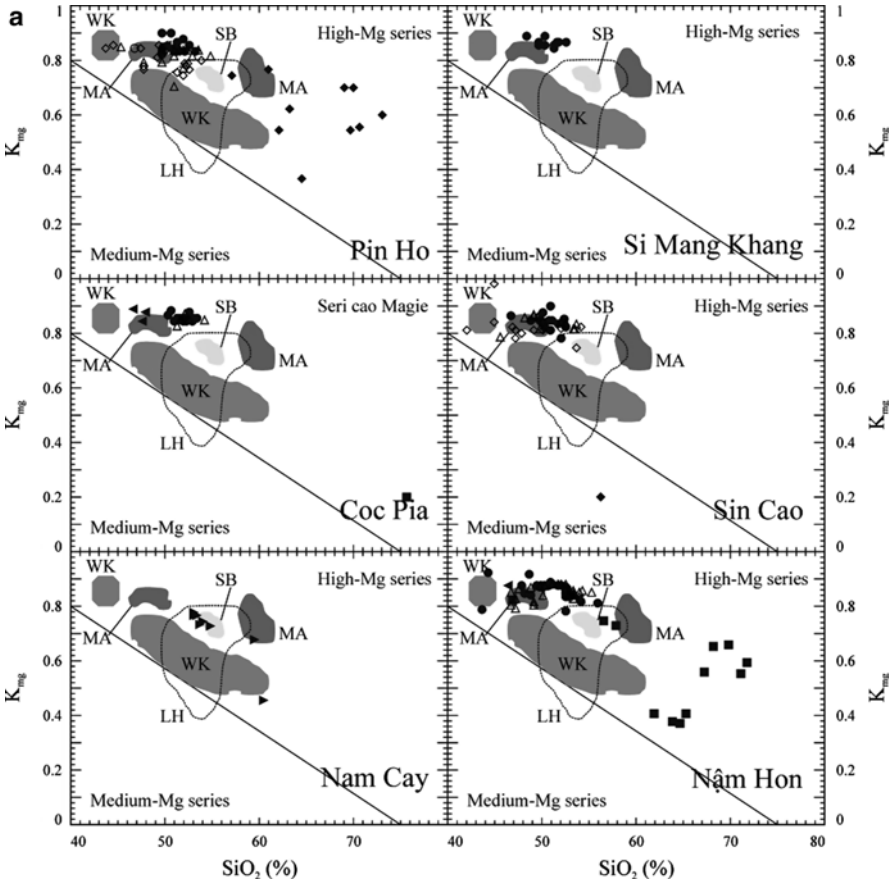

Fig. 7.6 Chemical compositions of the potassic and ultra-potassic magmas shown in relationship between SiO_2 and KMg (**a**), SiO_2 and CaO (**b**), SiO_2 and $(K_2O+Na_2O)/Al_2O_3$ (**c**). *Symbols* are as of in Fig. 7.5

Ilmenite in lamproite shows composition analogous to that in mafic magmas except having higher MnO (up to 1.6 wt.%) and showing no picroilmenite, characterized for lamproite of a deep mantle origin.

In a (ground and) sieved lamproite sample in the Pin Ho pipe area natural iron and gold are also discovered showing Au = 78–84 wt.%, Ag = 16 wt.% and Hg = 0.1–0.38 wt.%.

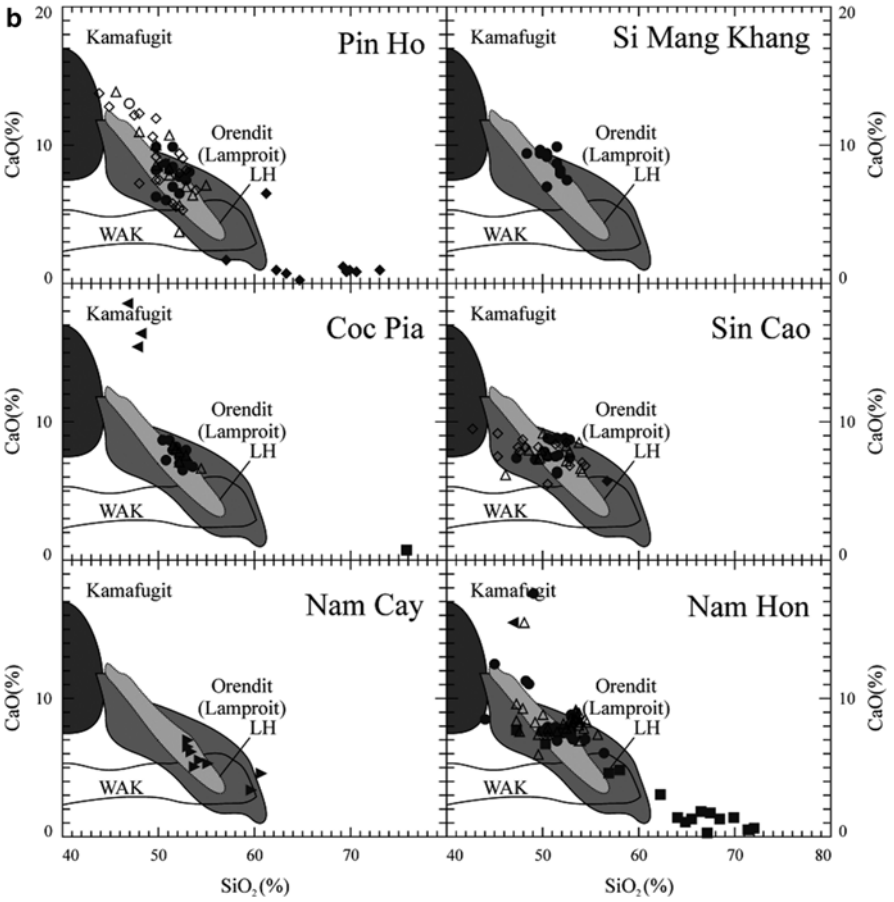

Fig. 7.6 (continued)

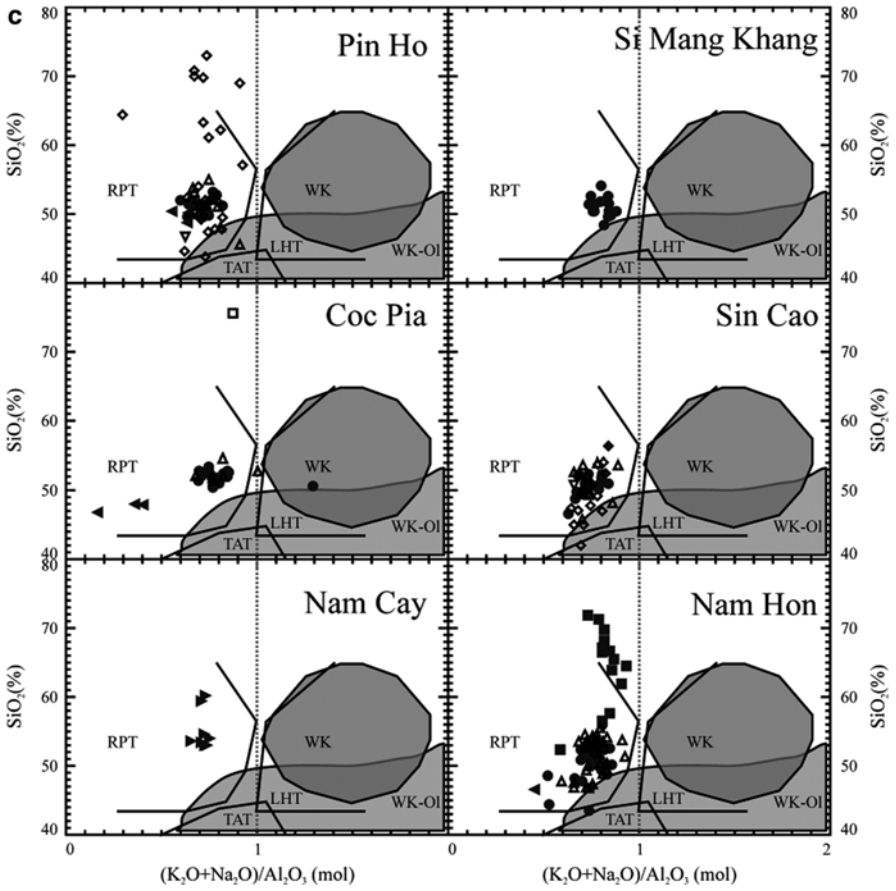

Fig. 7.6 (continued)

Table 7.4 Chemical compositions of representative Cr-spinel and magnetite in the Paleogene lamproite (wt.%, by EPMA analysis) (After Hoa et al. 1997b)

KHM	H101-B	H101-M	B10-B	P69-B	P77-B	T1588-B	T1588-M	T1592-M
TiO_2	0.82	1.91	0.44	0.3	0.34	0.54	6.7	5.94
Al_2O_3	4.05	0.19	8	7.56	8.7	4.92	2.88	0.93
Cr_2O_3	43	5.1	53.86	53.71	54.93	51.08	0.75	0.15
FeO	42.3	84.5	27.05	29.74	24.56	35.97	84.85	81.27
MnO	0.55	0.68	0.25	0.29	0.2	0.65	0.95	0.48
MgO	5.4	0.61	9.2	7.22	9.81	4.8	0.71	2.56
Total	96.12	92.99	98.8	98.82	98.54	97.96	96.84	91.33
Ti	0.02	0.06	0.01	0.01	0.01	0.01	0.18	0.16
Al	0.17	0.01	0.32	0.3	0.34	0.2	0.12	0.04
Cr	1.22	0.15	1.44	1.47	1.46	1.44	0.02	0
Fe^{3+}	0.56	1.72	0.22	0.22	0.18	0.33	1.48	1.52
Fe^{2+}	0.72	1	0.54	0.62	0.51	0.74	1.12	1.11
Mn	0.02	0.02	0.01	0.01	0.01	0.02	0.03	0.02
Mg	0.29	0.04	0.46	0.37	0.49	0.26	0.05	0.15

Remarks: 1–3: Ol-Cpx lamproite, Nam Hoa area; 4: Ol-Cpx lamproite, Coc Pia; 5: Coc Pia monchiquite; 6–7: Ol-Cpx Sin Cao lamproite; 8: mixed tuff. B: crystals included in olivine phenocrysts; M: microlites in groundmass

7.3 Geochemistry and Isotopes

Average chemical compositions of the study magma groups are calibrated and shown in Table 7.5, based on a number of analyses of major, trace and rare earth elements (Hoa 1997b; Anh 2001). Major deductions may be drawn as follows:

The potassic and ultra-potassic alkaline mafic magmas in the Song Da rift zone are high-Mg, -alkali and low-Ti. There are clear differences among the lamproite, absarokite and minette as expressed in the statistic calculation.

The typical lamproite has high MgO contents (with Mg# = 85–95), and usually the highest MgO type among the potassic and ultra-potassic alkaline mafic magmas, besides, the Ol-Cpx lamproite has higher MgO (11–12 wt.%) compared with the Cpx-Phl- analog (MgO = 8–9 wt.%). These two lamproite magma types show similarity in Ti, Al, Fe and Ca contents (Table 7.5). The total alkalis ($K_2O + Na_2O$) in lamproite is usually higher than 7 wt.% where K_2O/Na_2O is higher than 2, and most of the lamproite magmas are ultra-potassic series.

The geochemistry of absarokite is basically different from lamproite by having lower MgO but higher Al_2O_3 and CaO. Average concentrations of MgO in absarokite vary between 6.7 and 8.9 wt.%, Al_2O_3 between 12 and 13 wt.%. Compared with the lamproite, absarokite is higher in the total alkalis (7.5–8.1 wt.%) and is also an ultra-potassic type.

Table 7.5 Average chemical compositions (wt.%) of the Pu Sam Cap potassic and ultra-potassic alkaline magmas (After Hoa et al. 1997b)

No		SiO_2	TiO_2	Al_2O_3	Fe_2O_3	MnO	MgO	CaO	Na_2O	K_2O	P_2O_5	n
1	X	52.67	0.66	11.81	8.01	0.15	11.34	7.48	2.2	5.23	0.45	6
	S	0.99	0.04	0.18	0.12	0.01	0.87	0.63	0.31	1.29	0.02	
2	X	52.81	0.63	11.28	7.9	0.14	11.92	7.56	1.97	5.26	0.52	17
	S	0.71	0.04	1.18	0.39	0.01	1.18	0.68	0.39	0.5	0.07	
3	X	48.46	0.66	11.84	6.78	0.3	11.46	17.14	0.81	2.25	0.3	3
	S	0.97	0.09	0.71	0.32	0.35	1.51	1.56	0.32	0.98	0.18	
4	X	55.07	0.83	16.14	6.75	0.15	5.17	6.08	2.52	6.72	0.58	6
	S	0.69	0.03	0.4	0.24	0.01	0.5	0.76	0.41	0.42	0.03	
5	X	54.76	0.86	13.89	7.45	0.17	7.8	7.79	3.06	3.74	0.47	2
	S	2.73	0.3	1.72	0.81	0.04	2.11	0.95	0.94	1.71	0.07	
6	X	67.2	0.36	15.56	3.44	0.08	1.1	1.75	3.01	7.37	0.15	13
	S	4.2	0.13	0.89	1.28	0.04	1.17	1.54	1.27	2.26	0.1	
7	X	53.6	0.69	12.2	7.24	0.14	9.73	8.4	2.22	5.14	0.66	33
	S	1.37	0.06	0.71	0.39	0.02	1.49	1.61	0.39	0.59	0.73	
8	X	52.02	0.65	11.67	7.27	0.15	1.84	8.68	1.71	5.5	0.53	30
	S	1.44	0.13	0.7	0.97	0.03	1.97	2.32	0.6	0.49	0.1	
9	X	62.23	0.44	16.23	4.43	0.11	1.24	4.74	1.86	8.49	0.22	3
	S	2.33	0.05	0.24	0.47	0.03	1.22	1.18	1.68	3.68	0.07	
10	X	54.59	0.71	12.38	7.33	0.17	7.66	9	1.86	5.78	0.52	11
	S	2.29	0.06	0.86	0.92	0.02	1.56	3.24	0.4	0.35	0.05	
11	X	53.5	0.66	11.75	7.29	0.16	11.26	7.98	1.89	5.04	0.52	10
	S	1.56	0.04	0.81	0.41	0.02	3.32	1.4	0.47	0.5	0.03	
12	X	53.42	0.62	10.81	7.87	0.2	11	10.3	2.14	3.11	0.53	5
	S	0.33	0.01	0.97	0.51	0.06	1.12	2.58	0.74	0.71	0.06	
13	X	70.78	0.32	14.74	3.11	0.11	1.3	0.89	2.68	5.96	0.13	6
	S	2.87	0.23	0.6	1.81	0.06	0.76	0.22	0.97	0.57	0.04	
14	X	63.69	0.9	16.14	6.59	0.17	2.85	0.94	2.03	6.32	0.39	3
	S	4.24	0.15	3.31	1.7	0.05	2.47	0.86	1.58	1.25	0.17	
15	X	55.31	0.69	12.22	6.74	0.17	7.47	9.67	1.59	5.65	0.49	23
	S	2.33	0.07	1.2	0.62	0.04	1.59	2.98	0.4	0.79	0.06	
16	X	51.38	0.61	11.18	7.82	0.16	12.16	8.79	1.75	5.67	0.47	13
	S	1.25	0.03	0.33	0.4	0.01	1.1	0.98	0.26	0.58	0.03	
17	X	52.95	0.7	12.53	8.03	0.14	10.3	7.78	2.57	4.46	0.52	13
	S	1.77	0.06	0.9	0.73	0.02	2.04	0.81	0.84	0.74	0.06	
18	X	52.66	0.7	12.15	7.82	0.14	10.94	7.9	2.03	5.12	0.53	16
	S	1.21	0.07	0.97	0.44	0.02	2.53	0.88	0.42	0.66	0.05	
19	X	55.74	0.67	12.27	6.79	0.15	7.85	8.64	1.63	5.72	0.53	13
	S	3.49	0.05	0.98	2.06	0.02	1.46	1.29	0.79	1.21	0.1	
20	X	57.46	0.63	10.69	6.26	0.17	7.34	11.05	1.64	4.37	0.39	2
	S	2.3	0.06	0.05	0.22	0.06	0.17	2.05	0.45	0.12	0.08	

Remarks: 1–3: Coc Pia area, (1: Cpx-Phl-(Ol)- lamproite, 2: Ol-Cpx-(Phl)- lamproite, 3: pyroxenite); 4: Nam Cay minette; 5–9: Nam Hon area (5: camptonite, 6: syenite and granosyenite, 7: Cpx-Phl-(Ol)- lamproite, 8: Ol-Cpx-(Phl) lamproite, 9: trachyte); 10–15: Pin Ho area (10: Cpx-Phl-(Ol)- lamproite, 11: Ol-Cpx-(Phl) lamproite, 12: monchiquite, 13: trachyrhyolite, 14: trachyte, 15: absarokite tuff-lava), 16: Ol-Cpx-(Phl)- Si Mang Khang lamproite; 17–20: Sin Cao area: 17: Cpx-Phl-(Ol)- lamproite, 18: Ol-Cpx-(Phl) lamproite, 19: absarokite tuff-lava, 20: mixed tuff; n: number of analysis; X: average value; S: squared deviation

The minette shows rather a homogeneously chemical composition, having high potassium, aluminum, silica, and low magnesium, with a average of K_2O at 6.7 wt.%, Al_2O_3 at 16.14 wt.%, SiO_2 at 55.07 wt.% while MgO being only at 5.17 wt.%, having high K_2O/Na_2O ratios the minette is classified as a ultra-potassic magma (Fig. 7.5). The camptonite is mostly similar with the minette in terms of Si, Al and Ca contents but vastly different in higher Mg and Na while lower in K, comparable to a shoshonite type ($1 < K_2O/Na_2O < 2$). According to the relationships between CaO and SiO_2, Mg# and SiO2 and $(K_2O + Na_2O)/Al_2O_3$ the magma is chemically analogous to a absarokite type. Monchiquite has the chemical composition comparable to lamproite with regard to Mg, Ti and Al contents although being different in having high to very high Ca while showing low alkalis (Fig. 7.6).

Representative chemical compositions and trace element abundances of lamproite from various areas, absarokite, monchiquite, minette, trachyte along with syenite are given in Table 7.6. The primitive mantle and Chondrite normalized trace and rare earth element configurations are shown in Fig. 7.7 (after Sun and McDonough 1989). Studies of trace and rare earth element abundances and their distribution patterns reveal the followings:

The potassic and ultra-potassic alkaline volcano-plutonic mafic magmas are relatively enriched in Ni, Cr, Rb, Sr, Ba, Zr, Th, U and the light rare earths; and are depleted in Nb, Ta and Hf. The ratios of La/Nb, La/Sm_N and Ce/Yb_N are high showing a steep slope from the light toward the heavy rare earth elements, indicating dark-colored minerals having been strongly fractionated from the melt. Highly enrichment of large ionic lithophile elements (LILE) may indicate the melts may be enriched by metasomatism in the lithospheric mantle. However, relative depletion of Eu observed in all magmas may reflect crustal interaction of the rising melts. Low concentrations of Nb, Ta and Ti (high field strength elements: HFSE) are clearly expressed by their negative anomalies in the primitive mantle normalization patterns. These geochemical features of the Paleogene potassic and ultra-potassic magmas are consistent with those occurred following India-Eurasian collision, such as Dali – Shichuan and Tibet (China) potassic magmas, Mediterranean-type low-Ti lamproite and Roman-type volcanics in Italy (Li 1997). The broad depletion of HFSE in the potassic and ultra-potassic mafic magmas suggests subduction-related metasomatism in the lithospheric mantle where melts believed to generate. The uniformity of the Chondrite normalized rare earth element distribution patterns of the potassic magmas in northwest Viet Nam (with magnitude of 200–1000 folds) may indicate their common mantle sources, and their diversity of petrologic and geochemical compositions may due to magmatic differentiation of the parental melts, the process being proven by study of melt inclusions in clinopyroxene in Pin Ho cocite (see below).

The volcano-plutonic potassic alkaline felsic magmas in different areas also show similar geochemical characteristics to those of the mafic, such as enrichment of Ba, Sr, Zr, Th, U and the light rare earths, and depletion of Nb and Ta (Table 7.6). Their chondrite and primitive mantle normalized rare earth and trace element configurations are closely comparable with the mafic magma types, however, showing much clearer Eu negative anomalies. The ratios of La/Nb, Zr/Hf, La/Sm_N and Ce/

Table 7.6 Representative chemical compositions (wt.% by XRF) and trace element abundances of trace and rare earth elements (ppm, analyzed by ICP-MS) of the potassic and ultra-potassic alkaline magmas in the Pu Sam Cap area (After Hoa et al. 1997b; Anh 2001)

Rock type	Ol-Cpx- lamproite						Cpx-Phl-lamproite		
Location	Nam Hon		Coc Pia	Sin Cao	Pin Ho		Nậm Hon	Sin Cao	Pin Ho
Sample	G-916	P-55	P-81	T-1765	P-178	T-1725	T1545	T1597	P168
SiO_2	50.29	48.01	50.33	51.07	52.12	51.23	54.43	49.48	52.93
TiO_2	0.72	0.57	0.57	0.78	0.66	0.63	0.67	0.72	0.81
Al_2O_3	11.09	10.60	11.07	12.28	12.40	10.75	11.49	11.56	12.73
Fe_2O_3	7.71	6.07	7.50	7.10	7.61	6.95	7.17	8.02	7.44
MnO	0.14	0.13	0.13	0.15	0.16	0.14	0.13	0.16	0.14
MgO	12.94	10.84	12.61	9.87	9.27	11.79	10.34	12.85	8.00
CaO	7.60	11.09	7.92	7.34	7.60	6.93	7.96	7.16	6.91
Na_2O	1.79	0.58	0.83	1.98	0.92	2.09	2.17	2.38	1.42
K_2O	5.71	5.96	6.66	5.25	5.48	4.99	4.26	3.78	5.71
P_2O_5	0.62	0.50	0.54	0.58	0.50	0.51	0.40	0.50	0.57
LOI	1.18	4.42	1.42	3.40	2.93	3.83	0.90	2.94	3.14
Total	99.79	98.76	99.58	99.81	99.74	99.84	99.93	99.54	99.82
Cu	56	60	43.51	67	65	59	59	60	58
Ni	217	210	314.10	215	95	187	228	397	68
Co	43	42	42.64	37	26	43	37	36	34
Cr	889	600	1113	478	353	1100	663	725	370
V	30	50	169	131	110	120	128	80	129
Ba	1690	6090	1669	2094	1406	2080	1570	1553	1657
Rb	256.5	104.5	245.6	284	113	176	205	216.6	259
Sr	2138	13,458	1149	1922	1594	1470	1456	1452	1472
Zr	269	299	162.6	290	210	231	191	225	244

(continued)

Table 7.6 (continued)

Rock type	Ol-Cpx- lamproite						Cpx-Phl-lamproite		
Location	Nam Hon		Coc Pia	Sin Cao	Pin Ho		Nậm Hon	Sin Cao	Pin Ho
Sample	G-916	P-55	P-81	T-1765	P-178	T-1725	T1545	T1597	P168
Nb	10.7	8.5	13.5	7.0	3.54	7.00	15.0	4.7	8.9
Y	31.3	21	23.3	30.8	29.8	20.8	25.8	33.4	39.0
Cs	–	–	–	26.0	–	–	–	–	25.0
Sc	21	19	25.3	19.0	23.2	20.4	24.6	21.4	21.8
La	56	142	34.21	75.00	47.00	52.00	57.00	34.60	63.00
Ce	107	189	66.79	129.00	80.00	85.00	96.00	69.00	107.0
Nd	46	52	30.63	62.00	38.00	38.00	46.00	32.00	50.00
Sm	8.1	8.3	6.21	14.30	8.60	8.30	8.60	6.20	11.40
Eu	2.2	2	1.43	3.00	2.04	1.98	2.10	1.70	2.70
Gd	5.9	4.9	5.75	9.80	7.70	6.70	6.30	4.70	9.00
Tb	0.8	0.7	0.77	1.45	1.11	1.00	1.10	0.70	1.30
Yb	1.6	1.5	2.05	2.37	1.68	1.75	1.80	1.60	1.95
Lu	0.2	0.2	0.31	0.31	0.22	0.23	0.30	0.30	0.25
Hf	4.1	4.1	4.06	4.60	3.40	4.00	4.20	4.10	4.60
Ta	0.64	0.41	0.84	0.80	0.60	0.60	0.66	0.43	0.80
Th	15.1	14.2	11.72	2.00	12.20	13.90	14.30	9.70	15.20
U	3.7	5.8	4.24	5.10	5.50	0.40	4.80	3.00	4.70

Rock type	Absarokite		Monchiquite	Minette			Trachyte and trachyrhyolite		Syenite	
Location	Sin cao		Coc Pia	Nam Cay			Pin Ho		Dong Pao	Tam Duong
Sample	T1772	T1589	P66	T1737	T1740	T1735	P193	P210	V111	H43
SiO_2	49.55	49.31	47.89	52.88	53.28	54.66	69.96	63.29	62.15	64.29
TiO_2	0.60	0.74	0.61	0.80	0.78	0.78	0.23	0.76	0.41	0.30
Al_2O_3	11.80	12.01	12.14	15.36	15.62	16.00	14.69	14.04	15.63	16.81
Fe_2O_3	7.74	7.52	6.83	6.73	6.28	6.47	2.10	6.39	4.01	2.84
MnO	0.12	0.18	0.12	0.15	0.15	0.14	0.11	0.21	0.14	0.06
MgO	7.11	8.24	9.49	5.59	4.99	4.35	1.23	2.69	0.49	0.17
CaO	7.57	7.98	15.44	6.52	6.12	5.29	0.90	0.56	2.98	2.52
Na_2O	1.41	1.78	1.03	2.61	2.32	2.37	2.14	1.65	4.20	3.57
K_2O	7.04	5.88	3.08	6.23	6.60	6.93	5.83	6.85	8.27	9.40
P_2O_5	0.64	0.50	0.33	0.55	0.53	0.60	0.11	0.21	0.18	0.08
LOI	6.00	5.85	2.14	2.45	3.24	2.41	2.60	3.08	4.00	1.50
Total	99.57	99.99	99.09	99.88	99.90	100.00	99.89	99.73	99.87	99.97
Cu	28.36	65	–	61	57	78	25	36	13.75	11.54
Ni	71.39	121	–	76	70	68	20	65	7.86	2.14
Co	27.72	57	36	28	27	29	15	37	4.69	2.41
Cr	366.5	420	1000	169	195	180	33	353	1.95	1.33
V	66.23	120	–	118	114	114	26	120	60.66	75.32
Ba	1449	1721	945	3100	3600	3086	1083	1586	7511	6655
Rb	402	298	72	163	250	204	313	409	241.6	280.4
Sr	1017	1628	2634	2555	1776	1465	715	979	2535	1606
Zr	149.6	264	178	469	546	449	261	244	559.1	91.77
Nb	12.05	15.20	1.80	13.10	21.00	15.50	22.70	9.10	32.27	13.03

(continued)

Table 7.6 (continued)

Rock type	Absarokite		Monchiquite	Minette			Trachyte and trachyrhyolite		Syenite	
Location	Sin cao		Coc Pia	Nam Cay			Pin Ho		Dong Pao	Tam Duong
Sample	T1772	T1589	P66	T1737	T1740	T1735	P193	P210	V111	H43
Y	37.86	14.70	1.00	25.00	37.20	30.70	30.30	22.30	43.52	37.91
Sc	28.98	22.00	19.90	15.00	14.40	14.40	3.40	15.80	9.11	5.58
La	32.29	48.80	30.50	117.0	118.0	121.00	58.00	31.00	146.10	31.35
Ce	59.09	89.00	52.70	185.0	188.0	185.00	90.00	72.00	268.20	70.53
Nd	33.59	38.00	24.20	81.00	83.00	78.00	35.00	30.00	91.79	44.09
Sm	7.43	7.80	5.30	17.20	18.00	16.30	7.10	5.80	14.65	9.96
Eu	1.76	2.30	1.12	3.70	3.80	3.71	1.46	1.50	3.27	2.55
Gd	6.88	6.90	4.20	13.60	11.80	12.70	5.60	5.00	10.07	3.28
Tb	1.00	1.00	0.67	1.91	1.70	1.81	0.90	0.75	1.46	1.20
Yb	2.89	1.90	1.53	2.58	2.46	2.61	2.13	1.44	3.38	3.03
Lu	0.41	0.20	0.21	0.33	0.32	0.34	0.30	0.20	0.52	0.46
Hf	3.97	4.30	4.80	9.20	9.60	9.50	5.40	4.20	13.28	3.89
Ta	0.74	0.61	0.70	1.40	1.60	1.60	1.80	0.70	1.49	0.80
Th	11.78	14.70	11.00	4.30	4.50	4.20	28.00	11.70	38.12	10.07
U	2.42	3.10	4.90	1.40	13.40	1.50	12.00	5.60	9.31	2.70

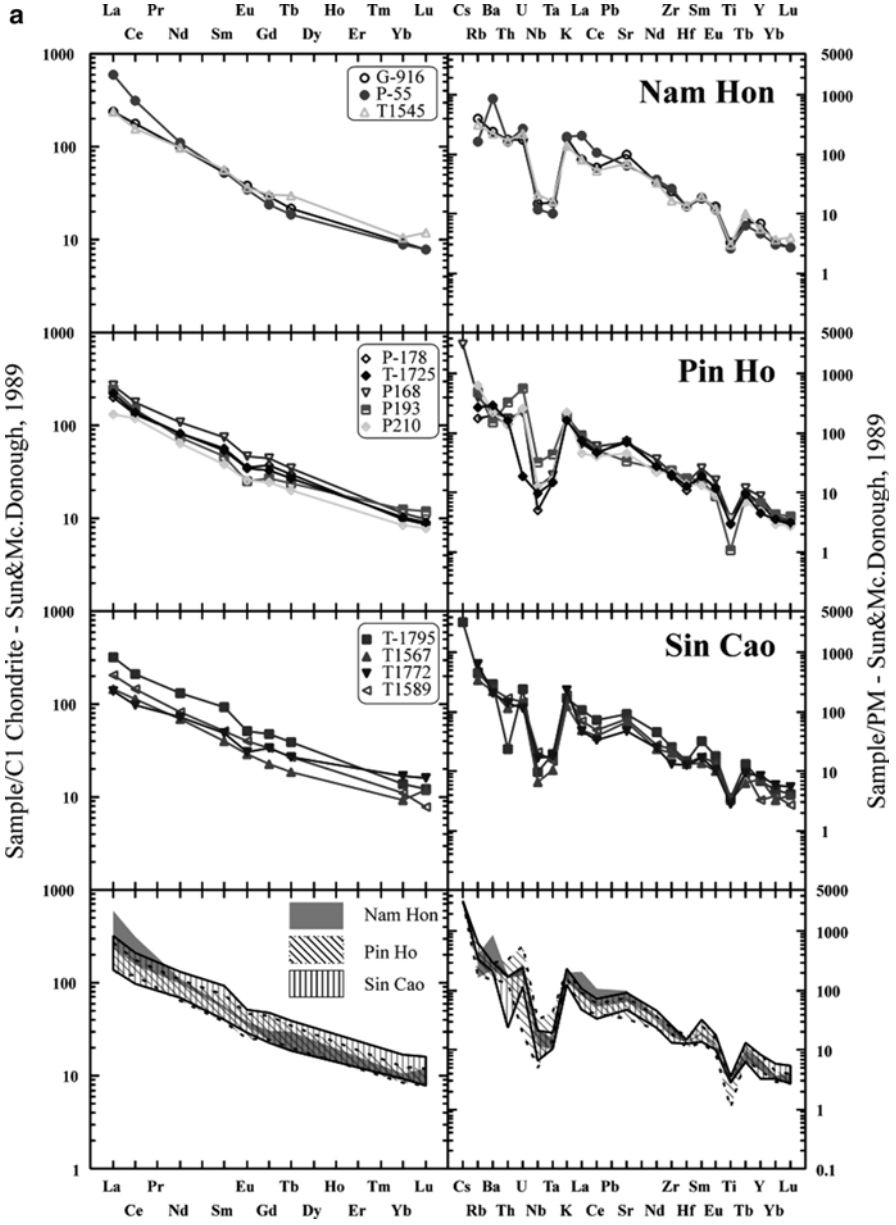

Fig. 7.7 Chondrite (*left*) and primitive mantle (*right*) normalized rare earth and trace element distribution patterns for Ol-Cpx-(Phl)- and Cpx-Phl- lamproite (*top*), lamproite and monchiquite (*middle*) and lamproite and absarokite (*low*)

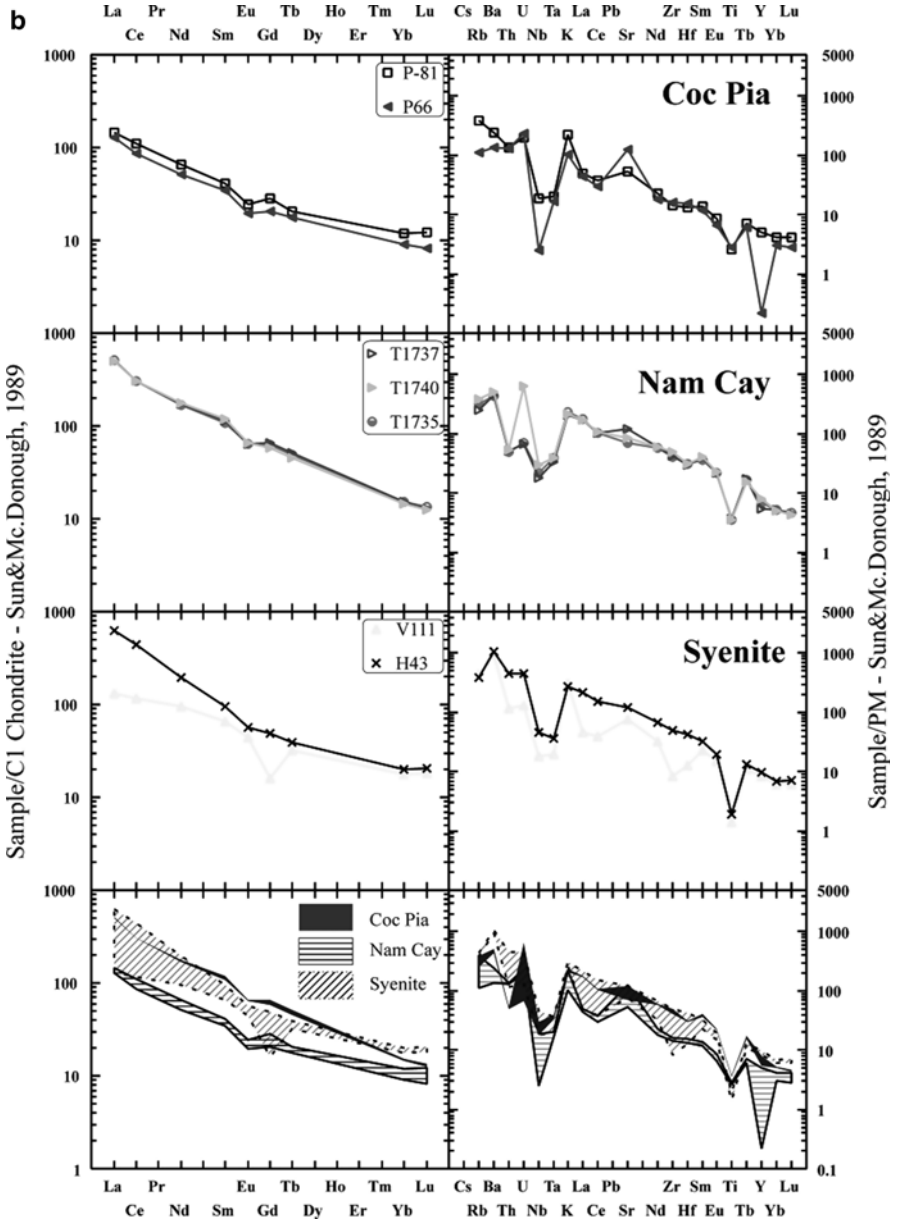

Fig. 7.7 (continued)

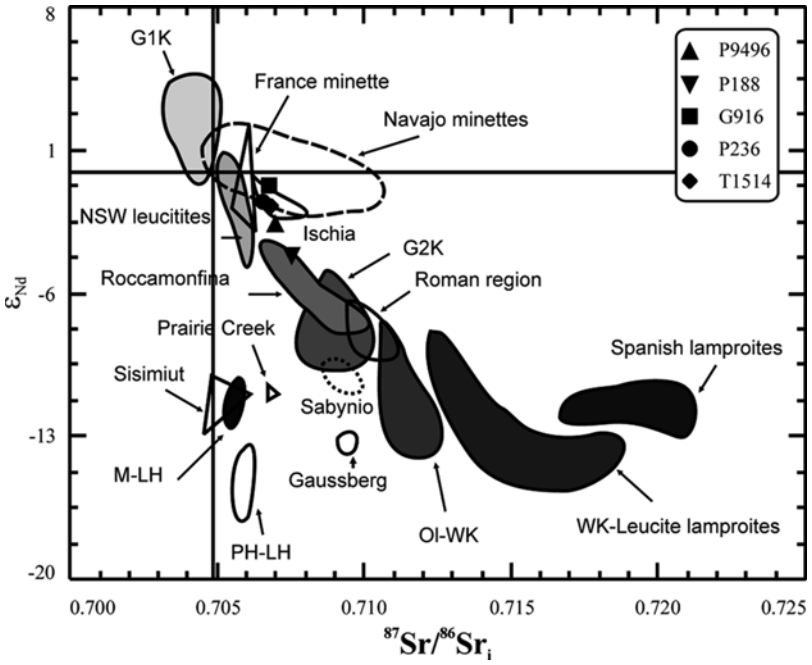

Fig. 7.8 The Pu Sam Cap lamproites in the relation of eNd and 87Sr/86Sr

Yb_N in trachyte and syenite are equivalent to those in the potassic and ultra-potassic alkaline mafic, reflecting their source mantle genetic relationship.

Strontium and neodymium isotopic ratios analyzed for lamproite samples from different areas show $^{87}Sr/^{86}Sr$ varying between 0.7066 and 0.7075 and $^{143}Nd/^{144}Nd$ being between 0.512336 and 0.512450 ($\varepsilon_{Nd} = -0.76 - -4.0$). Rb-Sr radiometric age dating yielded 42 Ma (Dong Pao lamproite) and 40 Ma (Nam Cay minette) and, initial $^{87}Sr/^{86}Sr = 0.7069$ and 0.7056, respectively. The isotopic enrichment is mostly considered as an enriched mantle type 2 source (EM2) (e.g. Zindler and Hart 1986). In plots of ε_{Nd} versus $^{87}Sr/^{86}Sr$ the northwest Viet Nam lamproite samples fall closely to the minette and leucite fields than 'traditional' lamproite (Fig. 7.8). N.T. Chi (2003) showed initial $^{87}Sr/^{86}Sr$ ratios of Pu Sam Cap syenite and trachyte at 0.7072 most comparable to the lamproite values, suggesting their common source of origin (Table 7.7).

Table 7.7 Sr and Nd isotopic ratios of Pu Sam Cap lamproite (Anh et al. 2001)

No	Sample	Rb	Sr	$^{87}Sr/^{86}Sr_i$	±2σ	
1	G916	256.5	2138	0.706735	0.000008	
2	T1545	205	1456	0.706839	0.000005	
3	P188	259	1472	0.707521	0.000006	
4	P236	227	966	0.706585	0.000007	
5	P9496	232	1135	0.706964	0.000004	
No	**Sample**	**Sm**	**Nd**	$^{143}Nd/^{144}Nd$	±2σ	ε_{Nd}
1	G916	8.1	46	0.512450	0.000003	–3.67
2	T1545	8.6	46	0.512411	0.000005	–4.43
3	P188	11.4	50	0.512336	0.000004	–5.89
4	P236	8.2	34	0.512447	0.000004	–3.73
5	P9496	6.8	29.9	0.512402	0.000002	–4.60

Remarks: 1. Ol-Cpx-(Phl) lamproite Nam Hon area; 2. Nam Hon Cpx-Phl-(Ol)- lamproite; 3. Pin Ho Cpx-Phl-(Ol) lamproite; 4. Si Mang Khang Ol-Cpx-(Phl)-lamproite; 5. Coc Pia Ol-Cpx-(Phl) lamproite

7.4 Magma Origin, P-T Parameters and Geodynamic Settings

The similarity of mineralogical, geochemical and isotopic characteristics among the Paleogene potassic and ultra-potassic mafic and felsic in the Song Da rift zone suggest their parental melts have a common Southeast Asian lithospheric mantle source. Three models to explain their enrichment of K, Sr (and $^{87}Sr/^{86}Sr$) and LILE include (1) basaltic magma fractional crystallization (O'Hara and Yoder 1967); (2) crustal assimilation as basaltic melts rise to shallower levels (Rock 1980); (3) mantle enrichment by (subduction-derived) fluid metasomatism prior to partial melting (Menzies 1989). The first two models cannot explain the level of potassic enrichment in the study magmas, e.g., $K_2O = 4.5–6.6$ wt.% and 9–12 wt.%, respectively, in alkaline mafic and felsic magmas, not to mention the K_2O contents and K_2O/Na_2O ratios in the lamproite and absarokite are higher than crust-derived magmas such as high-Al granites.

Magma fractional crystallization or crustal assimilation would not result in having magmas depleted in high field strength elements such as above mentioned Nb and Ti; therefore, the HFSE depletion may be explained by Ti-bearing minerals being retained in the source at low melting temperature and pressure or interaction with depleted lithosphere of the melt as it entered the crust (Kelemen 1990). Magma and crust interaction may also explain Eu negative anomalies in the rare earth relative enrichment curves; the feature is not a result of plagioclase fractionation as commonly seen in the mafic magma fractional crystallization process. However, the HFSE depletion may reflect the geochemical nature of the lithospheric mantle source eventually inherited by the melts. Along with the enrichment of magnesium in the lamproite and absarokite, a reasonable explanation is that the magmatic melts were generated from a metasomatized mantle source. Evidence of a metasomatized

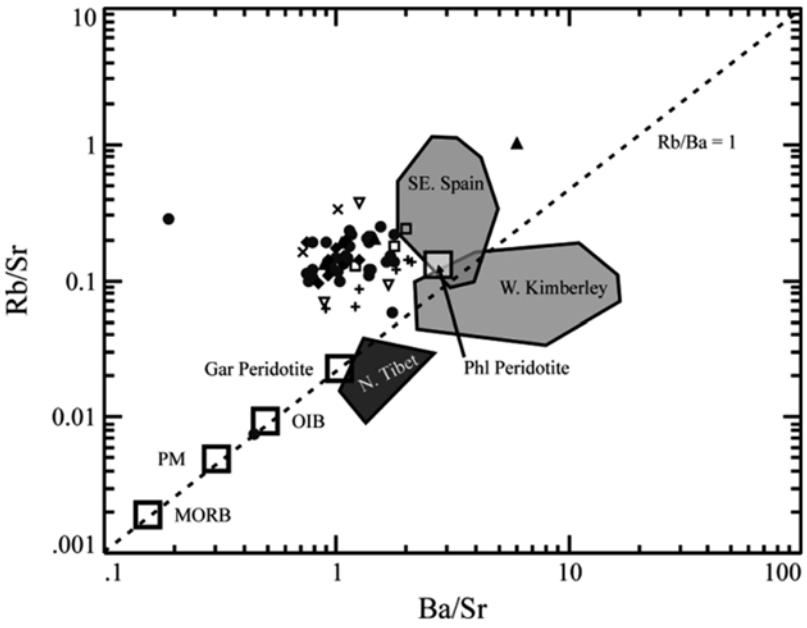

Fig. 7.9 Positions of Paleogene lamproite, absarokite and minette of northwestern Vietnam in the Rb/Sr and Ba/Sr relation; shown for comparison are fields of ultra-potassic magmas from southeast Spain, West Kimberley and North Tibet (After Mitchell 1995). *Symbols* as of in Fig. 7.5; *MORB* mid-ocean ridge basalt, *PM* primitive mantle, *OIB* oceanic island basalt

source includes highly enriched Sr and Nd isotopic compositions and high Rb/Sr while Rb/Ba ratios are low. This model is commonly used to explain the origin of 'traditional' lamproite. Experiments using high-SiO2 phlogopite – lamproite as a starting alkaline magma had found a co-existing mineral assemblage of K-feldspar + amphibole + mica + clinopyroxene crystallized at a temperature lower than 1300 °C and a pressure lower than 5.5 Gpa (Mitchell 1995). A starting source composition believed to form the Italian- or (Chinese) Yunnan-type ultra-potassic alkaline volcanics, according to experiments by Foley and Venturelli (1987) and Li (1997), is metasomatized phlogopite – lherzolites. Based on the geochemical and petrologic comparability among the potassic and ultra-potassic mafic magmas from northwestern Vietnam, Italy and Yunnan, it may suggest that their parental melts were generated partial melting of similarly K and LILE–rich metasomatized, phlogopite–lherzolite mantle sources. High Mg-olivine and the similarity of Rb/Sr and Ba/Sr in northwestern Vietnam lamproites to those in worldwide phlogopite peridotites lend an additional support to this explanation (Fig. 7.9). However, the presence of phlogopite pyroxenite and glimmerite as inclusions in absarokite in the Pin Ho explosion pipe area (e.g. Anh 2001) may suggest alternatively that source mantle of the ultra-potassic magmas in northwestern Viet Nam may be equivalent to phlogopite pyroxenite in composition. Thus, the problem of magma origin needs further investigation to clarify.

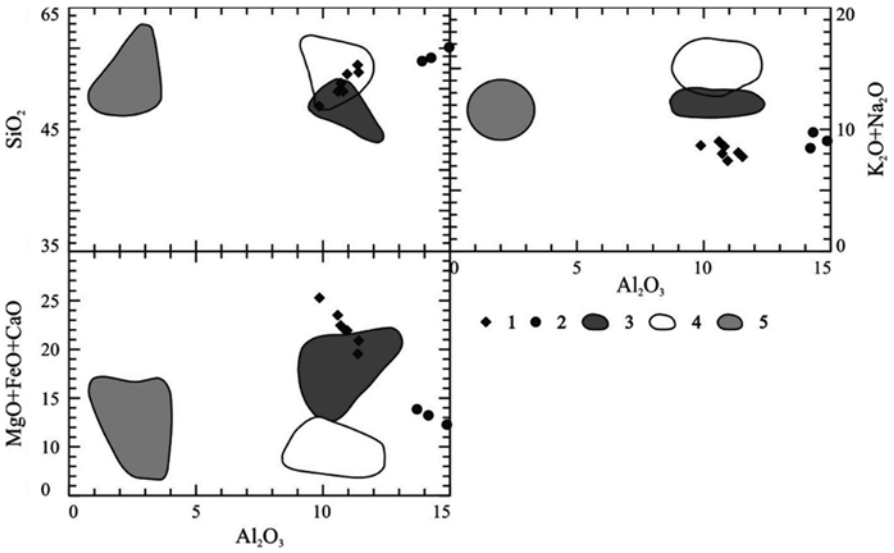

Fig. 7.10 Pu Sam Cap lamproite in the relation between SiO2, K2O + Na2O, MgO + FeO + CaO and Al_2O_3 by data of pyroxene inclusions. *1* uniform inclusion in bright-colored pyroxene; *2* inclusion in greenish pyroxene; *3* wyomingite and orendite field; *4* verite and fortunite field; *5* glass inclusions in wyomingite (Simonov et al. 1997; Hoa et al. 1997a)

Study of homogenization temperature and composition of inclusions in Sin Cao lamproite clinopyroxene (Hoa 1997a; Simonov et al. 1997) suggests melt formation parameters of the ultra-potassic alkaline magmas as follows:

- The clinopyroxene crystallization temperature occurred in the interval of 1210–1250 °C corresponding to crystallizing temperature of wyomingite (Phl- Cpx-leucite lamproite) at 1220–1270 °C or verite and fortunite in southeast Spain at 1200–1240 °C (Sharygin 1997).
- The lamproite magma was produced by fractional crystallization from melts whose compositions were comparable to the parental melts of lamproite and other volcanics at the Leucite Hills (Wyoming, USA). The features of increasing Si and Al and decreasing Mg, Fe and Ca in evolutional trend of clinopyroxene inclusions in the lamproite are closely similar to those observed in lamproite in southeast Spain (Figs. 7.10 and 7.11).
- The formation of the potassic and ultra-potassic magmas in the Song Da rift zone is a result of fractional crystallization of melts whose compositions were equivalent to lamproitic magmas, which were subsequently evolved by magma differentiation would lead to form diversified magmas. This explanation is differed from that of Chi (2003) who suggested that the parental melt was a upper mantle-derived continental basaltic melt-like. Evidence for a parental melt having a composition similar to a lamproitic melt for the ultra-potassic mafic magmas was derived from studies of crystallized inclusions in clinopyroxene in a Nam Hon

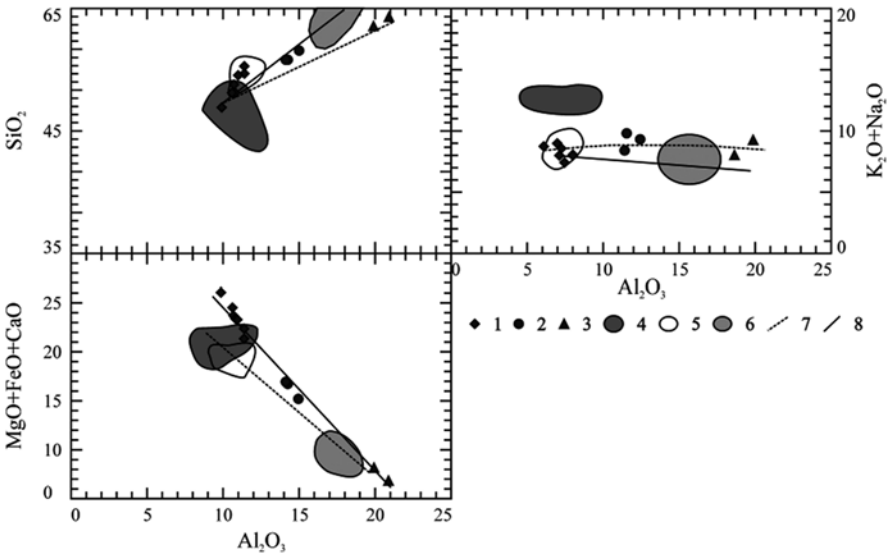

Fig. 7.11 Compositional evolution of melt inclusions in clinopyroxene in Sin Cao lamproite (Simonov et al. 1997; Hoa et al. 1997a). *1*- uniform inclusion in bright-colored pyroxene; *2*- inclusion in greenish pyroxene; *3*- glass in un-heated inclusion in bright pyroxene. Field of: *4*-wyomingite and orendite; *5*- verite, fortunite and lamproite in southeast Spain; *6*- glass in inclusion in verite and fortunite. Evolution trend of inclusions: *7*- lamproite and inclusions in Sin Cao pyroxene; *8* – lamproite and inclusions in pyroxene in southeastern Spain (Data 4-5-6 are after Sharygin 1997)

lamproite having an ultra-potassic ultramafic magma composition of $SiO_2 = 41.61$ %, MgO = 20.41 %, $K_2O = 5.58$ % and $Na_2O = 0.78$ % (Hoa 1997a). In addition, within the study area, ultra-potassic mafic magmas are dominant, while the others, viewed as evolved rock types from alkaline basalts or alkaline basalt-like magmas themselves have not been found. This observation again states that parental melts of the potassic and ultra-potassic mafic magmas should have compositions that were closely similar to lamproitic magmas.

Radiometric dating of cocite, absarokite, minette, trachyte and syenite in the northeastern wing of Song Da rift zone by Rb-Sr and Ar-Ar yielded values ranging from 35 to 42 Ma (Figs. 7.12, 7.13 and 7.14), indicating that temporally these magmas occurred prior the high magnitude – extrusion of the Indochina block along the Red River Fault zone (35–22 Ma).

Many researchers have pointed out that India – Eurasian collision-induced tectonics leading to the building of the Himalayan mountain range and continental rifting expressed by a series of east – southeast direction faults covering a major part of Chinese and southeast Asian territory. Eocene – Oligocene potassic and ultra-potassic mafic and felsic magmatic formations are well-spread in the southwestern margin of Yangtze craton, from Tibet (China) to northwestern Vietnam. The formation age of the potassic magmas in Vietnam were dated to be Eocene or early Oligocene as youngest Meanwhile, in southwest China the youngest age of potassic

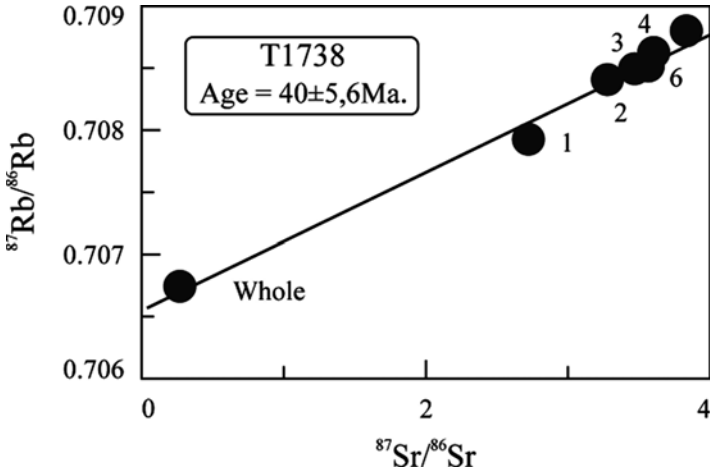

Fig. 7.12 Rb-Sr age of Nam Cay minette (Hoa 1997)

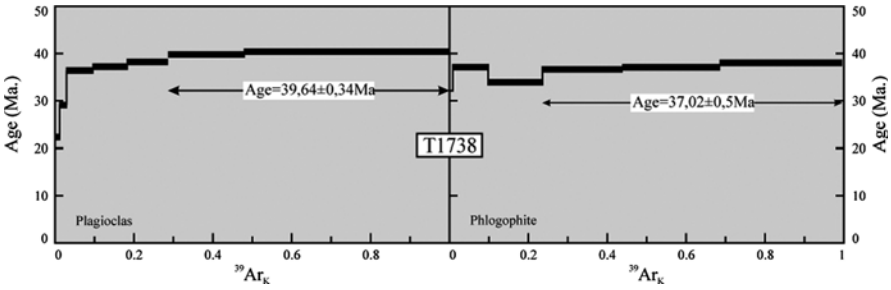

Fig. 7.13 Ar-Ar age of Nam Cay minette (Anh 2001)

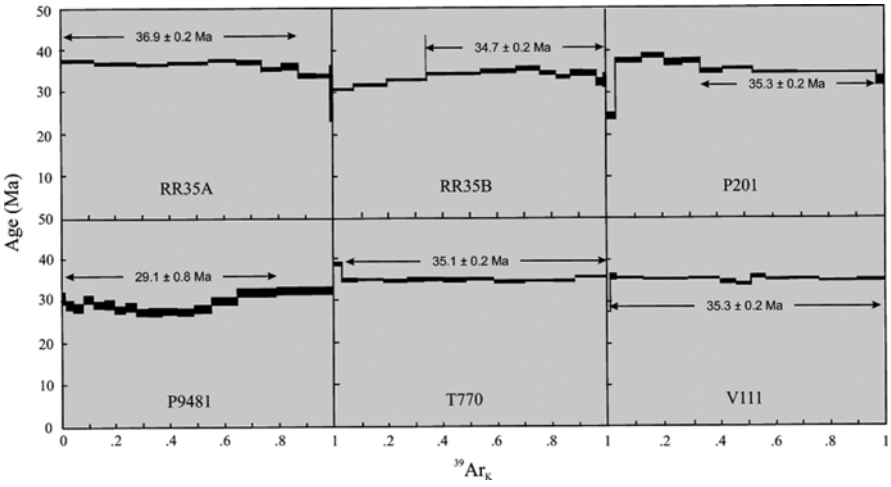

Fig. 7.14 Ar-Ar age of lamproite (RR35A-B; P-9481), absarokite (P-201), trachyte (T-770) and syenite (V-111) in the Coc Pia and Sin Cao areas (Hoa et al. 1997b)

and ultra-potassic magma formation is early Miocene (Li 1997), implying that the early Cenozoic continental extension and the formation of potassic and ultra-potassic magmas had been continuing to occur parallel with lithosphere extrusion along the Red River fault zone. The timing of the formation of potassic and ultra-potassic alkaline magmas in northwestern Vietnam was coincided with the potassic magmatic activity in southern margin of the Yangtze craton. Therefore, the Paleogene potassic and ultra-potassic alkaline magmatism in northwestern Vietnam was closely associated with the India – Eurasian-induced continental extension processes. Correlation between the Paleogene potassic and ultra-potassic magmas (and Permian alkaline picrite) in the Song Da rift zone with similar magma types in the Dali area (China) Chung et al. (1997) estimated the extrusion magnitude along the Red River fault as far as about 600 km.

References

Chung SL, Lee TY, Lo CH, Wang PL, Chen CY, Nguyen TY, Tran TH, Wu GY (1997) Intraplate extension prior to continental extrusion along the Ailao Shan – Red River shear zone. Geology 25:311–314

Đao Đinh Thuc, Huynh Trung (eds) (1995) Geology of Viet Nam, P. II: magmatic formations. Department of Geology and Minerals of Viet Nam Publication, Hanoi

Foley SP, Venturelli GV (1987) The ultrapotassic rocks: characteristics, classification and constraint to petrogenetic models. Earth Sci Rev 24:81–134

Kelemen PB (1990) High field-strength element depletions in arc basalts due to mantle-magma interaction. Nature 345(7):521–524

Lacroix A (1933) Contribution a` la connaissance dela composition chimique et mine'ralogique des roches eruptives de l'Indochine. Bulletin du Service Ge'ologique de l'Indochine, Hanoi, 20: 190 pp

Li P (1997) The significance of Late Paleogene magmatism on the Ailao Shan – Red River Shear Zone in Yunan-Sichuan, South China. Ph.D. thesis, Univ. of Illinois at Chicago

Menzies MA (1989) Cratonic, circum-cratonic and oceanic mantle domain beneath the western U.S.A. J Geophys Res 94:7899–7915

Mittchell RH (1995) Melting experiments on a sanidine-phlogopite lamproite at 4-7 Gpa and their bearing on the sources of lamproite magma. J Petrol 36(5):45–59

Mitchell RH, Bergman SC (1991) Petrology of lamproites. Plenum Press, New York, p 159

Nguyen Trung Chi (ed) (2003) Petrology and mineralization of alkaline magma formations in northern Viet Nam. Final report of ministerial project (Ministry of Natural Resources and Environment), Center for Information and Literature Archives, Dept. Geology and Minerals, Hanoi (in Vietnamese)

Nguyen Van Nguyen, Đao Đinh Thuc, Hoang Quang Chi, Le Duy Nguyen, Tran Thanh Tuyen, Ha Xuan Binh (2005) Exploration of an lamproite volcanic explosion diatreme (pipe) in the Tua Chua area, Dien Bien province. Proceedings of 60-anniversary of geology of Viet Nam, Department of Geology and Minerals of Vietnam, Hanoi, pp 64–170

O'Hara MJ, Yoder HS (1967) Formation and fractionation of basic magma at high pressures. Scottish J Geol 3:67–117

Pham Trung Hieu, Fukun Chen, Thi Bich Thuy Nguyen, Quoc Cuong Nguyen, Shuang-Qing Li (2012) Geochemistry and zircon U-Pb age and Hf isotopic composition of Permian alkali granitoids of the Phan Si Pan zone in northwestern Vietnam. J Geodynam. doi:10.1016/j.jog.2012.03.002

Polyakov GV, Nguyen Trong Yem, Balykin PA, Tran Trong Hoa, Panina LI, Ngo Thi Phuong, Hoang Huu Thanh, Tran Quoc Hung, Sarygin VV, Bui An Nien, Hoang Viet Hang (1997) The new data from ultrapotassic basic rocks in Northern Vietnam – Cocite. Russ Geol Geophys 38(1):148–158 (in Russian)

Rock NMS (1980) Rare Earth and other trace element contents and the origin of minettes. Cosmochim Acta 44

Sharygin VV (1997) Evolution of lamproites according to melt inclusions in minerals. Geol Geophys 38(1):136–147 (in Russian)

Simonov VA, Polyakov GV, Balykin PA, Tran Trong Hoa, Hoang Huu Thanh, Ngo Thi Phuong (1997) Physic-chemical conditions of formation of lamproites (cocite) in North Vietnam. Reports of RAS 357(2):239–242

Sun SF, McDonough WF (1989) Chemical and isotopic systematics of oceanic basalts: implication for mantle composition and processes. In: Saunders AD, Norry NJ (eds) Magmatism in ocean basins. Geol Soc Spec Publ 42:313–345

Tran Tri Van (ed) (1977) Geology of Vietnam, northern part. Science and Technics Publshing House, Hanoi (in Vietnamese)

Tran Trong Hoa (ed) (1995) Study of Mesozoic – Cenozoic magmatism and its mineralization potential. Final report for national project KT-01-04 (1992–1995). Archives of the National Center for Science and Technology Information, Hanoi (in Vietnamese)

Tran Trong Hoa, Hoang Huu Thanh, Ngo Thi Phuong, Tran Tuan Anh, Hoang Viet Hang (1997a) Mineralization, characteristics and forming conditions of lamproite of Vietnam. J Geol Ser B, 9–10:63–68

Tran Trong Hoa, Polyakov GV, Balykin PA, Hoang Huu Thanh, Tran Tuan Anh, Tran Quoc Hung, Ngo Thi Phuong, Vu Van Van, Bui An Nien, Hoang Viet Hang, Phan Luu Anh, Petrova TE (1997b) Investigation and evaluation of diamond prospect in northwest Viet Nam. Report of national fundamental study of natural resources, Archives of the Institute of Geological Sciences, 225 p (in Vietnamese)

Tran Trong Hoa, Hoang Huu Thanh, Ngo Thi Phuong, Tran Tuan Anh, Hoang Viet Hang (1999) Potassic alkaline magmas in northwestern Viet Nam: indications of late Paleogene intraplate extension. J Geol A250(1-2):7–14 (in Vietnamese with English abstract)

Tran Tuan Anh (2001) Ultrapotassic rocks in the North West Vietnam. PhD thesis, Vienna University

Tran Tuan Anh, Hoa TT, Richter W, Koller F (2001) Characteristics of trace elements, rare earth and isotopes of lamproites from Northwest Vietnam. J Geol – Ser B 17–18:20–27

Wagner C, Velde D (1986) Lamproite in North Vietnam? A re-examination of cocites. Geology 94:770–776

Zindler A, Hart S (1986) Chemical geodynamics. Annu Rev of Earth Planet 14:493–571

Chapter 8
Magmatic Activities in the Phan Si Pan Uplift and Red River Zone

Abstract Cezonoic magmatic activities in the Phan Si Pan Uplift and Red River Shear Zone, northwest Viet Nam are related with India – Eurasian collision.

The Cenozoic biotite granite and porphyric granite in the Phan Si Pan Uplift are exposed in the shape of small blocks and dykes. They have geochemical indications analogous to high-K calc-alkaline magmatics series were occurred between 35 and 32 Ma (U-Pb, zircon, LA-ICP-MS), coincident with the timing of an early strong shear motion along the Red River zone. A primarily crustal source of the magmas is supported by high-Al, -alkaline, relatively low Nb, Ta and Zr, and high initial $^{87}Sr/^{86}Sr$ isotopic ratios. On the other hand, the contemporaneous occurrence of the granite magmatism and start of the major shear motion phase suggests that the magmas can be viewed as syn-kinetic.

The syn-kinetic magmatism in the Red River Shear Zone formed an uniform association including small intrusive bodies comprised of lherzolite, websterite and gabbro, which were subsequently turned into shear boudinage in later stages. The magmas occurred in two major stages at 35 and 25 Ma (Ar-Ar). These observations suggest that the formation of mafic – ultramafic magmas in the early stage may be associated with the exhumation process, while the later magmas may be related to post-gneiss exhumation activities along the Red River shear zone. However, the magmas of two stages are geochemically similar, suggesting their common source.

The occurrence of high-Al, –alkaline and high-pressure melting granite during 24–22 Ma (Ar-Ar) is a specific character of the Red River shear zone. The undeformity or weak deformity feature of the granite indicates that magnitude of shear motion in the Red River zone decreased after the peak time between 35 and 22 Ma. Note that the occurrence of granite aplite and pegmatite in gneiss in the Red River zone is not related to the nature of Tan Huong –type granite generation. This is evident by their spatially separated distribution as well as the large difference in their intitial strontium isotopic ratios as mentioned earlier.

T.-H. Tran et al., *Intraplate Magmatism and Metallogeny of North Vietnam*,
Modern Approaches in Solid Earth Sciences 11,
DOI 10.1007/978-3-319-25235-3_8

8.1 Cenozoic Ye Yen Sun Granite Complex in the Phan Si Pan Uplift

According to previous studies Ye Yen Sun granites were grouped to the Ye Yen Sun complex, including a single batholith running in the northwest – southeast direction and being outcropped along China – Vietnam boundary. The batholith is consisted of a complex rock assemblage including granodiorite, biotite-granite, granosyenite, and alkaline feldspar granite, with biotite-granite being the major component (Dovjikov 1965; Tri 1977; Thuc and Trung 1995). There are several concepts on the origin of the Ye Yen Sun granite, including (a) calc-alkaline magmatism and (b) sub-alkaline intraplate magmatism (Thuc and Trung 1995). Besides, some believed that Ye Yen Sun magma was a deep intrusive phase of the Phu Sa Phin granite and had a genetic link with the Tu Le alkaline volcanics (trachydacite and trachyrhyolite) (Thuc and Trung 1995; Chi 2003). According to Anh et al. (2002) study there are two geochemical granite-types being observed in the Ye Yen Sun granite outcrop area: the first is potassic-rich and Nb-Ta-Zr-rich subalkaline; while the second is Na-K-type and Nb-Ta-Zr-poor granite type (Anh et al. 2002). Recent studies have shown that the Nb-Ta-Zr-rich granite is Permian (261–257 Ma), which is termed as Phan Si Pan granite in this monograph (Hoa et al. 2011, 2015). The other Nb-Ta-Zr-poor is Cenozoic, being termed as Ye Yen Sun granite (Hoa et al. 2011; Dung et al. 2013), the name was given by E.P. Izokh (e.g. Dovjikov 1965). The Phan Si Pan Permian granite is being described in Sect. 3.3 of Chap. 3, Part II.

8.1.1 Geological, Petrological and Mineralogical Characteristics

Ye Yen Sun Cenozoic granite outcrops mainly in the northwestern region of Phan Si Pan mountain range, from Hoang Lien Pass, in the center, to Si Lo Lau area (Fig. 8.1). To the southwest of the study area, along the Hoang Lien Pass from O Quy Ho toward Binh Lu (Fig. 8.1) commonly found are penetrating contacts between undeformed Cenozoic granite and Phan Si Pan-type Permian deformed granite (Photos 8.1 and 8.2). Also found are porphyry granite dykes in Neoproterozoic sericite schist (Photo 8.3). Bright-colored, fined-grained granite being found here is also outcropped in the Trung Leng Ho area, about 3 km west of Muong Hum village.

To the northwest of the study area, along the cross-section from Si Lo Lau to Tung Qua Lin (bordered with China) as well as along the Ye Yen Sun stream, and in Nam Xe area mostly found is bright, fined-grained biotite granite. The granite is sometimes porphyric, almost undeformed. Dykes of porphyric granite similar to that in O Quy Ho – Binh Lu cross-section is also popular in this area.

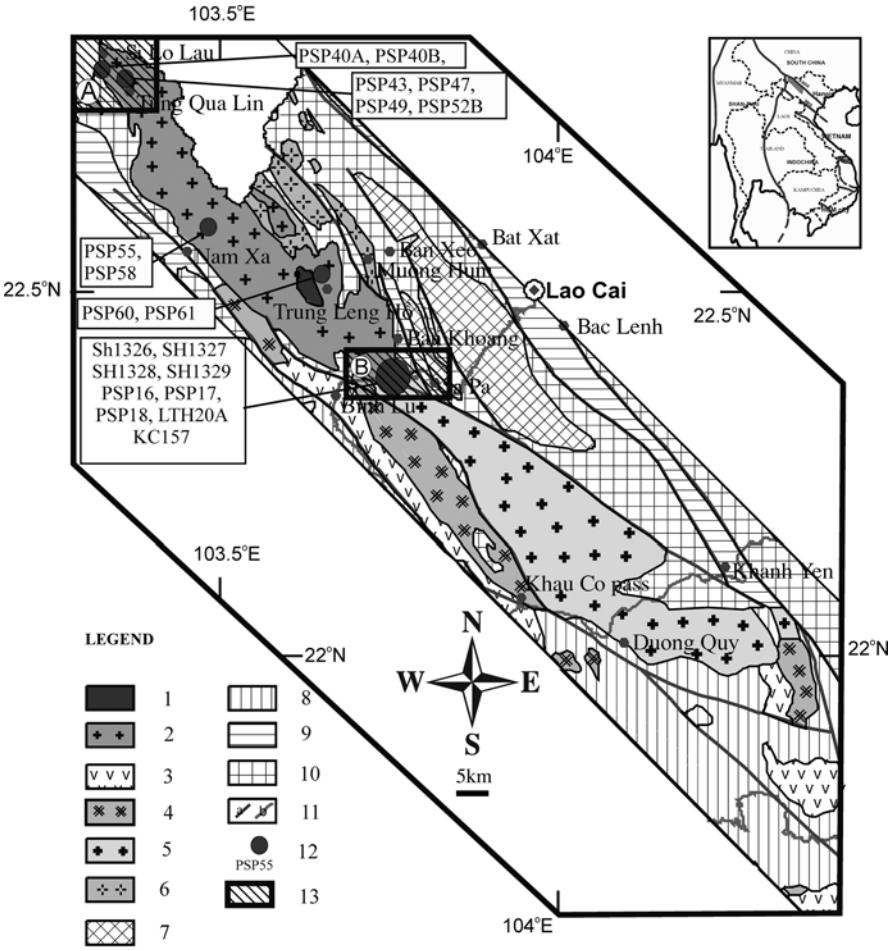

1-Cenozoic Pu Sam Cap syenite and granite; 2- Cenozoic Ye Ye Sun granite; 3- Tu Le rhyolite and trachyrhyolite, 4- Phu Sa Phin riebeckite-aegirine granite; 5- Phan Si Pan biotite (±hornblend) granite; 6- Muong Hum granite; 7- Po Sen granite; 8- Mesozoic formations; 9- Paleozoic formations; 10 Precambrian formations; 11: a- Faults; b- National roads; 12- Sample localities; 13- Study areas.

Fig. 8.1 Schema of distribution of Cenozoic granites in the Phan Si Pan Uplift and sample locations

The Hoang Lien Pass Cenozoic granite is porphyritic, sometimes equigranular, with K-feldspar being the major phenocryst phase and a minor amount of biotite and amphibole (Photo 8.4). Dyke-type granite is clearly porphyritic with phenocrysts of plagioclase, quartz and biotite; the groundmass is composed of quartz, K-feldspar, plagioclase and biotite microlites (Photo 8.5).

Photo 8.1 Contact of Cenozoic (*bright color*) and Permian (*dark color*) granites in the Thac Bac (*Silver*) water fall (Photo by Hoa 2009)

Photo 8.2 Deformated Permian granite is intrudited by Cenozoic granite in the Hoang Lien pass

Photo 8.3 Outcrop of porphyric granite dyke in Cambrian sericite shale. National Road from Sa Pa to Silver Water Fall (LTH-8)

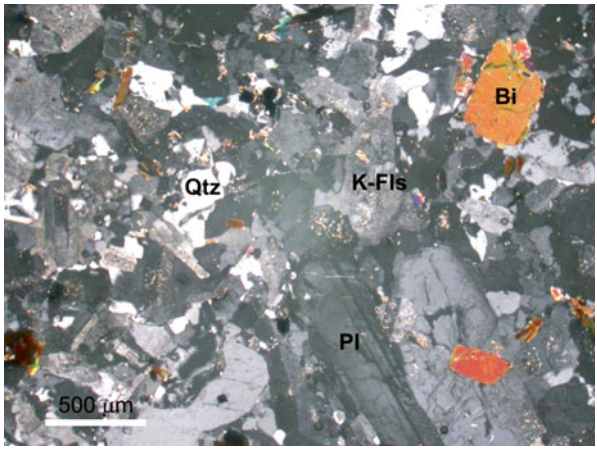

Photo 8.4 Fine-grain (non-deformated) granite in outcropt KC-157. Thin section, Nicol (+). *Qtz* quartz; *Pl* plagioclase, *K-Fls* K-feldspar; *Bi* biotite

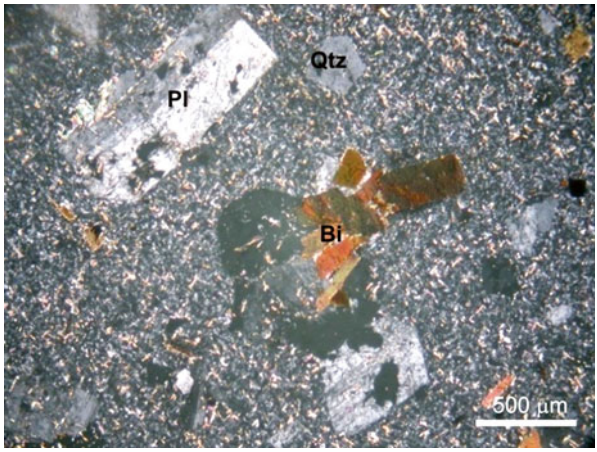

Photo 8.5 Porphyric granite in outcropt LTH-20A. Thin section, Nicol (+). *Pl* – plagioclase; *Bi* – biotite

Common rock-forming mineral assemblage in the studied biotite- (amphibole)-granite is K-feldspar + plagioclase + biotite ± hornblende + sphene + zircon ± fluorite. The K-feldspar has an orthoclase- equivalent composition (K_2O = 16.13–16.96 wt%; Na_2O = 0.32–0.63 wt%; Al_2O_3 = 17.43–17.95 wt%; SiO_2 = 64.78–65.18 %) (Table 8.1). The biotite is brightly greenish brown, being characterized by low-Ti content (TiO_2 = 0.83–1.1 wt/%), relatively low aluminum (Al_2O_3 = 13.71–14.92 %) and high magnesium oxide (MgO = 11.83–13.1 %) (Table 8.2).

Table 8.1 Chemical compositions of K-feldspar in Cenozoic granite in the Sa Pa – Binh Lu cross-section

Sample	PSP-18_6	PSP-18_7	PSP-18_8	PSP-18_9	PSP-18_12	PSP-18_15
SiO_2	64.98	65.18	64.85	65.07	64.78	65.04
TiO_2	0.00	0.02	0.02	0.01	0.01	0.02
Al_2O^3	17.50	17.67	17.43	17.95	17.63	17.58
FeO	0.02	0.06	0.05	0.03	0.02	0.05
MnO	0.00	0.00	0.02	0.00	0.00	0.03
MgO	0.00	0.01	0.01	0.00	0.01	0.01
CaO	0.01	0.01	0.00	0.00	0.01	0.02
Na_2O	0.34	0.43	0.32	0.43	0.46	0.63
K_2O	16.42	16.62	16.96	16.26	16.23	16.13
Sum	99.27	100.00	99.66	99.75	99.15	99.51
Si	6.07	6.06	6.08	6.04	6.06	6.07
Al	1.93	1.94	1.92	1.96	1.94	1.93
Ti	0.00	0.00	0.00	0.00	0.00	0.00
Fe^2	0.00	0.01	0.00	0.00	0.00	0.00
Mg	0.00	0.00	0.00	0.00	0.00	0.00
Ca	0.00	0.00	0.00	0.00	0.00	0.00
Na	0.06	0.08	0.06	0.08	0.08	0.11
K	1.96	1.97	2.03	1.93	1.94	1.92
Ab	3.10	3.80	2.80	3.80	4.10	5.60
An	0.00	0.00	0.00	0.00	0.00	0.10
Or	96.90	96.20	97.20	96.20	95.80	94.30

Table 8.2 Chemical compositions of biotite in granite in Sa Pa – Binh Lu cross-section

Sample	V-9274	V-9272	PSP-18_2	PSP-18_3	PSP-18_4	PSP-18_13	PSP-18_14	PSP-18_17
SiO_2	38.97	39.05	37.32	38.26	37.82	36.92	37.18	37.1
TiO_2	1.1	0.83	0.92	1.19	0.57	1.16	0.91	0.88
Al_2O_3	14.92	13.71	15.42	15.53	14.62	13.81	14.12	15.35
Cr_2O_3			0.01	0.01	0.01	0	0	0
FeO	18.27	19.2	18.14	18.69	18.07	17.31	17.95	18.06
MnO	0.42	0.75	0.59	0.64	0.67	0.63	0.68	0.63
MgO	11.83	13.1	10.95	10.89	11.88	12.45	11.77	10.61
CaO	0	0.01	0.01	0.03	0.02	0.03	0.01	0.05
Na_2O	0.11	0.09	0.12	0.12	0.13	0.13	0.09	0.11
K_2O	10	10.1	9.34	9.26	9.6	9.31	9.39	9.08
F			1.09	1.06	1.3	1.37	1.42	1.16
Cl			0.01	0.01	0.02	0.01	0.01	0.02
H_2O	1.9	1.91						

(continued)

Table 8.2 (continued)

Sample	V-9274	V-9272	PSP-18_2	PSP-18_3	PSP-18_4	PSP-18_13	PSP-18_14	PSP-18_17
Calculated based on 24 oxygen atoms								
Si	6.02	5.94	6.07	6.1	6.13	6.08	6.11	6.09
Al^{IV}	1.98	2.06	1.93	1.9	1.88	1.92	1.89	1.91
Al^{VI}	0.73	0.4	1.03	1.02	0.91	0.76	0.85	1.06
Ti	0.13	0.1	0.11	0.14	0.07	0.14	0.11	0.11
Fe^{2+}	2.36	2.44	2.47	2.49	2.45	2.38	2.47	2.48
Cr	0	0	0	0	0	0	0	0
Mn	0.06	0.1	0.08	0.09	0.09	0.09	0.1	0.09
Mg	2.72	2.97	2.66	2.59	2.87	3.06	2.88	2.6
Ca	0	0	0	0.01	0	0.01	0	0.01
Na	0.03	0.03	0.04	0.04	0.04	0.04	0.03	0.04
K	1.97	1.96	1.94	1.88	1.98	1.96	1.97	1.9

8.1.2 Geochemical Characteristics

Geochemical compositions of the Ye Yen Sun granite are shown in Table 8.3. In the classification diagram (SiO_2 vs. $Na_2O + K_2O$) by Cox et al. (1979) modified by Wilson (1989) (Fig. 8.2) the magma plots in granite and alkaline granite fields, with SiO_2 varying between 68 and 72.59 wt%. The granite is characterized by relatively high $Na_2O + K_2O$ (=8.07–9.88 wt%) with K_2O/Na_2O ratios varying from 0.43 to 0.73 (Table 8.3), (Na + K)/Al and ASI varying in intervals, respectively, 0.70–0.84 and 1.00–1.30, suggesting an Al-saturated character (Table 8.3). The Al-saturated feature is illustrated by the Ye Yen Sun granite plotting in field of peraluminous type as shown in correlation between ASI vs. (Na/K)/Al (Fig. 8.3). The Fe# index (0.70–0.92) in the Ye Yen Sun granite implies that it is different from alkaline type (0.9–1.0, after Frost et al. 2001). Most notably, dyke-type porphyric granite in the O Quy Ho area to the southeast, and Nam Xe to the northwest of the study area, shows indexes of (Na/K)/Al, ASI and Fe# similar to those of massive granite.

Trace element concentrations and their distribution configuration (Table 8.3) suggest Ye Yen Sun Cenozoic granite is depleted in Ta (0.45–3.62 ppm), Nb (6.62–28.1 ppm), Zr (45.6–181 ppm), Y (3.62–26.4 ppm) and Hf (2.63–6.98 ppm); however, relatively rich in large ion lithophile elements such as Sr (216.7–1289 ppm) and Ba (481.1–2513.56 ppm) (Table 8.3). The granite is differentiated from an A-type granite as shown in discrimination diagram of Whalen et al. (1987) expressed by Zr + Nb + Ce + Y vs. FeO^*/MgO and/or $(K_2O + Na_2O)/CaO$ (Fig. 8.4).

Table 8.3 Major (wt%) and trace element (ppm) compositions of Ye Yen Sun granite

Sample	SH-1326	SH-1327	SH-1328	SH-1329	PSP16	PSP16/3	PSP17	KC157	LTH20A
SiO_2	75.74	69.75	70.10	71.99	73.69	69.88	73.06	71.84	70.11
TiO_2	0.08	0.22	0.20	0.17	0.09	0.17	0.11	0.25	0.34
Al_2O_3	14.89	16.27	16.56	16.10	14.81	15.66	15.11	14.88	15.05
$Fe_2O_3^*$	0.35	1.33	1.19	0.80	0.95	2.04	0.77	1.68	2.12
MnO	0.00	0.04	0.02	0.02	0.02	0.04	0.02	0.04	0.03
MgO	0.00	0.13	0.00	0.07	0.10	0.19	0.20	0.41	0.53
CaO	0.81	1.75	1.45	1.60	1.22	0.97	1.26	1.59	0.52
Na_2O	4.04	4.44	4.34	4.12	4.92	5.06	4.20	3.81	3.46
K_2O	4.03	4.56	4.72	4.17	4.07	5.12	4.64	4.70	5.07
P_2O_5	0.01	0.07	0.03	0.04	0.02	0.11	0.03	0.07	0.12
L.O.I					0.24	0.74	0.81	1.08	1.51
Total	99.95	98.54	98.60	99.09	100.13	99.98	100.21	100.35	98.86
Ba	481.1	2890	3319	1229	1775	1524	658	1333	1297.86
Rb	187.6	150.4	135.3	163	133.1	164.8	191.6	203.3	197.60
Sr	216.7	1289	1447	448.6	1064	981	280	303	278.20
Cs	3.348	3.092	1.642	3.319					1.74
Ta	1.594	0.751	0.454	0.762	0.628	1.28	0.497	1.72	5.62
Nb	17.9	11.35	7.148	11.91	9.57	20.4	6.62	17.6	25.91
Hf	3.612	5.382	4.643	3.007	3.31	6.15	2.63	5.34	6.98
Zr	92.89	177.2	178.3	103.6	106	181	76	205	261.80
Y	10.21	11.58	8.1	6.051	8.86	26.4	3.62	6.5	6.69
Th	16.61	20.97	19.67	12	14.7	11.8	17.5	31	29.27
U	8.978	4.524	4.514	4.036	14.2	7.19	6.44	5.54	4.75
Cr	3.821	2.717	3.557	1.041	30.7	13.1	33	5.52	8.78
Ni	16.07	6.793	16.67	8.213	1.11	1.84	1.15	3.48	34.47
Co	1.048	0.995	0.321	0.508	0.335	0.416	0.304	2.2	4.23
Sc	12.5	21.01	3.003	14.99	2	3	4	3	3.46
La	9.57	42.32	37.42	14.62	21.9	56.8	9.6	71.4	76.45
Ce	17.15	71.63	60.06	25.44	34	59.3	16.7	121	132.24
Pr	1.981	7.945	6.364	2.896	3.55	9.58	1.69	11.4	12.58
Nd	6.61	26.89	20.5	9.875	12.4	37.1	6.04	35.5	38.19
Sm	1.278	4.419	3.117	1.796	1.95	6.63	1.12	4.83	5.1
Eu	0.249	1.38	1.057	0.68	0.61	1.65	0.376	0.974	1.1
Gd	1.163	3.462	2.44	1.412	1.66	6.22	0.798	2.74	4.12
Tb	0.19	0.416	0.282	0.167	0.237	0.837	0.109	0.346	0.39
Dy	1.272	1.98	1.329	0.865	1.29	4.43	0.562	1.3	1.45
Ho	0.257	0.339	0.221	0.163	0.267	0.866	0.103	0.202	0.22
Er	0.916	1	0.651	0.525	0.795	2.38	0.298	0.54	0.63
Tm	0.165	0.146	0.09	0.082	0.126	0.355	0.046	0.06	0.069
Yb	1.259	1.002	0.645	0.62	0.845	2.44	0.291	0.361	0.41
Lu	0.236	0.159	0.095	0.1	0.15	0.404	0.049	0.052	0.057

(continued)

Table 8.3 (continued)

Sample	SH-1326	SH-1327	SH-1328	SH-1329	PSP16	PSP16/3	PSP17	KC157	LTH20A
K_2O/Na_2O	0.66	0.68	0.71	0.67	0.54	0.67	0.73	0.81	0.96
Eu/Eu*	0.61	1.04	1.13	1.26	1.01	0.77	1.16	0.75	0.71
ΣREE	42.30	163.09	134.27	59.24	79.78	188.99	37.78	250.71	273.01

Sample	PSP 40A	PSP43	PSP47	PSP52B	PSP 52C	PSP55	PSP 60
SiO_2	72.59	71.31	69.01	69.67	68.00	68.71	71.70
TiO_2	0.14	0.22	0.25	0.23	0.42	0.31	0.15
Al_2O_3	14.91	15.23	15.56	15.81	16.22	15.77	15.67
$Fe_2O_3^*$	1.03	1.63	1.76	1.50	2.47	1.96	1.26
MnO	0.02	0.02	0.03	0.02	0.03	0.02	0.03
MgO	0.30	0.55	0.46	0.32	0.90	0.71	0.31
CaO	1.35	1.78	1.85	1.40	2.05	1.99	1.46
Na_2O	4.05	4.92	4.78	4.79	4.75	4.25	5.06
K_2O	4.40	3.67	4.83	5.09	3.99	4.38	4.06
P_2O_5	0.05	0.08	0.12	0.08	0.18	0.15	0.05
L.O.I	0.38	0.49	0.33	0.27	0.64	0.46	0.74
Total	99.22	99.90	98.98	99.18	99.65	98.71	100.49
Ba	2242.04	1427.42	2972.84	2513.56	2552.78	1800.52	1970.93
Rb	273.90	159.10	159.90	127.90	126.70	172.80	142.00
Sr	252.90	703.30	1408.00	1424.00	949.10	704.70	1103.00
Cs	10.49	4.79	1.72	1.46	1.97	3.88	2.45
Ta	5.16	5.38	4.38	2.82	3.8	3.6	3.77
Nb	19.12	28.1	26.56	15.28	10.59	17.21	18.29
Hf	3.75	6.09	6.64	4.72	6.61	6.68	5.31
Zr	101.40	137.70	121.00	66.60	211.50	171.60	68.50
Y	5.28	9.4	13.1	12.79	5.5	7.27	5.67
Th	16.42	9.97	11.45	6.79	23.60	20.14	10.79
U	10.72	3.46	1.88	1.92	2.89	3.65	6.19
Cr	7.03	7.79	6.32	5.1	15.27	11.65	4.67
Ni	17.49	12.28	16.29	5.33	25.5	27.78	16.2
Co	1.46	3.29	2.41	1.75	4.99	3.9	1.38
Sc	3.23	3.58	4.03	2.61	4.21	3.82	1.93
La	15.77	21.39	43.04	32.08	67.93	44.52	16.46
Ce	28.19	41.37	72.8	62.7	117.02	78.38	29.41
Pr	3.05	4.65	7.58	7.35	11.96	8.19	3.17
Nd	10.51	16.58	25.69	26.97	38.96	27.41	10.94
Sm	2.14	3.1	4.2	4.79	5.56	4.23	1.87
Eu	0.55	0.74	1.42	1.39	1.62	1.19	0.69
Gd	1.85	2.7	3.78	3.98	4.2	3.41	1.56
Tb	0.24	0.36	0.45	0.48	0.39	0.37	0.18

(continued)

Table 8.3 (continued)

Sample	PSP 40A	PSP43	PSP47	PSP52B	PSP 52C	PSP55	PSP 60
Dy	1	1.73	2.18	2.22	1.29	1.46	0.83
Ho	0.17	0.31	0.4	0.4	0.2	0.24	0.16
Er	0.44	0.87	1.17	1.12	0.51	0.63	0.49
Tm	0.059	0.11	0.161	0.15	0.051	0.074	0.071
Yb	0.36	0.66	1.03	0.9	0.3	0.45	0.48
Lu	0.052	0.077	0.14	0.126	0.036	0.056	0.071
K_2O/Na_2O	0.71	0.49	0.66	0.70	0.55	0.68	0.53
Eu/Eu*	0.82	0.76	1.07	0.95	0.98	0.93	1.20
$(La/Yb)_N$	31.42	23.25	29.97	25.57	162.42	70.96	24.60
ΣREE	64.38	94.65	164.04	144.66	250.03	170.61	66.38

Remarks: SH-1327, 1328, 1329, PSP16, PSP16/3, PSP17, KC-157: Granite along Sa Pa-Binh Lu cross-section; LTH-20A: porphyritic granite O Quy Ho area; trace elements were analyzed by an ICP-MS at National Taiwan University. PSP40A, PSP43, PSP47, PSP52B, PSP52C – biotite granite of Tung Qua Lin-Si Lo Lau area; PSP55 – granite, Nam Xe area (Ye Yen Sun stream); PSP60 – granite, Chung Leng Ho; analyzed by ICP-MS at the Institute of Geological Sciences, Vietnam Academy of Science and Technology

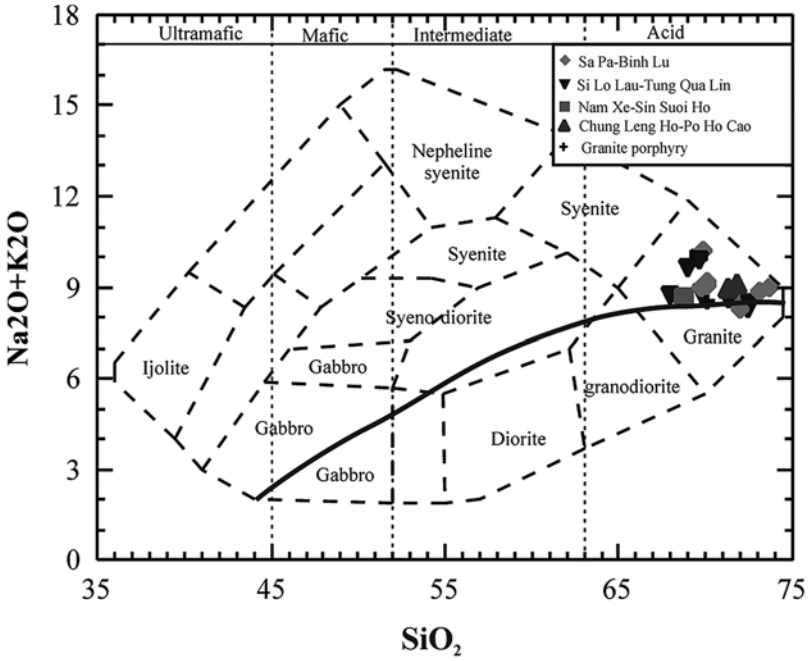

Fig. 8.2 $Na_2O + K_2O$ vs SiO_2 of the Cenozoic granite (After Cox et al., (1979) and Wilson, (1989)). The *bold solid line* separates subalkaline and alkaline compositions

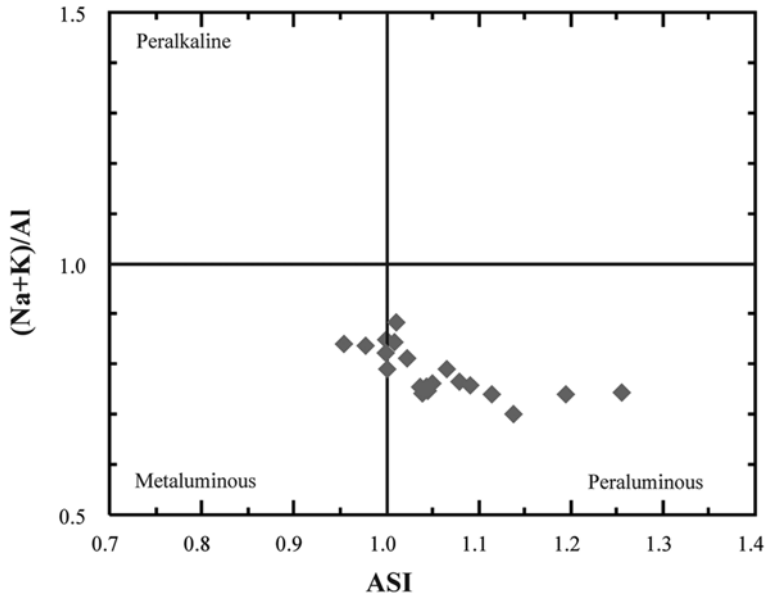

Fig. 8.3 Molecular (Na + K)/Al vs ASI (alumina saturation index), (After Frost et al. 2001) for the Cenozoic granite in the Phan Si Pan uplift

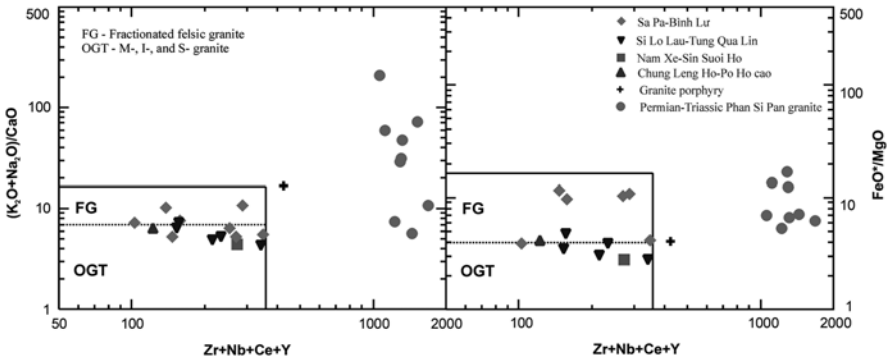

Fig. 8.4 Composition of Cenozoic granite on the plot of $(K_2O + Na_2O)$/Cao and FeO/MgO vs Zr + Nb + Ce + Y (After Whalen et al. 1987)

Chondrite normalized rare earth element configuration patterns (Fig. 8.5a; after Sun and McDonough 1989) show similar distribution characteristics among the studied granites in that they are all enriched in the light rare earths relative to the heavy elements, with $(La/Yb)_N = 5.45–162.42$ while showing no Eu anomaly and Eu/Eu* ratios varying between 0.61 and 1.26 for Sa Pa – Binh Lu cross-section granite, and 1.01–1.28 for the others. Total rare earths ($\sum$REE) in the Ye Yen Sun granite (both dyke- and massive-type) vary from 40 to 250 ppm, equivalent to those

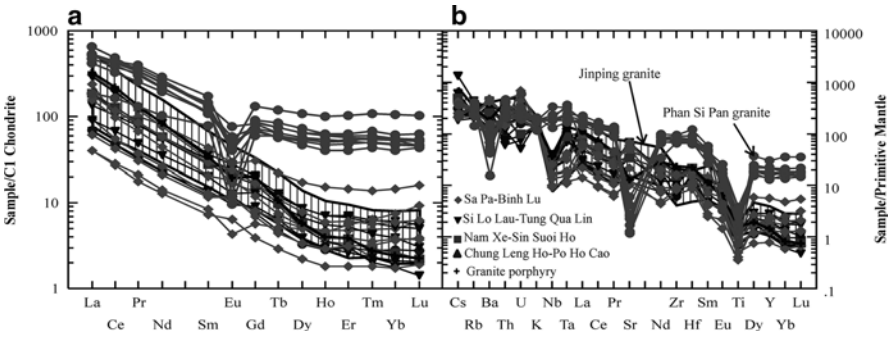

Fig. 8.5 (**a**) Chondrite (Sun&McDonough 1989) normalized REE and (**b**) Primitive-mantle (Sun&McDonough 1989) normalized trace element diagrams for the Cenzoic granite in the Phan Si Pan uplift. For comparison data of Cenozoic Jinping (China) granite from Dung et al., (2010) are also shown

in calc-alkaline or high-aluminum granite type. Primitive mantle normalized incompatible trace element patterns (Fig. 8.5b) show negative anomalies at Nb, Ta and Ti, although the signature is not as clear as observed in calc-alkaline granite.

The trace and rare earth element geochemical characteristics of Ye Yen Sun Cenozoic granite in the Phan Si Pan mountain range and the contemporaneous granite in the Jinping area of China (considered as the Phan Si Pan continuation in China) are vastly comparable (Fig. 8.5). Recent studies have also revealed that the magmas in two areas show closely similar mineral-petrologic and geochemical characteristics, suggesting that the two regional granite magmas may belong to a same association-type and were originated from a same source.

8.1.3 Magma Source and Geodynamic Setting

The Ye Yen Sun granitoids was thought to belong to a Cenozoic magma-tectonic stage (Izokh in Dovjikov 1965; Tri 1977; Thuc and Trung 1995). U-Pb isotopic age dating (using LA-ICP-MS) on zircon separates from weakly deformed or undeformed, biotite- and bright-colored granite from the Ye Yen Sun block (Phan Si Pan Range) yielded values between 35 and 30 Ma (Hoa et al. 2012; Dung et al. 2013).

Having geochemical indexes such as relatively high aluminum oxide (Na + K/Al = 0.70–0.84 and ASI = 1.0–1.3), and being rich in potassium, LILE and (light) LREE the Cenozoic granite in the Phan Si Pan uplift massif is closely comparable to high-potassic calc-alkaline granitoid, a result of mantle – crust interaction. This type of mixing source commonly occurs in crust transforming from compression to extension (Bonin 1990; Ludwig 2003). On the other hand, ratios of $(Yb/Lu)_N$ are nearly unchanged (0.8–1.28), while $(La/Yb)_N$ are highly variable (5.45–162.42), suggesting mantle-crust mixing melts. The depletion of HFSE such as Nb, Ta, Hf… while lacking of Eu anomaly the granite magma source may be similar to that com-

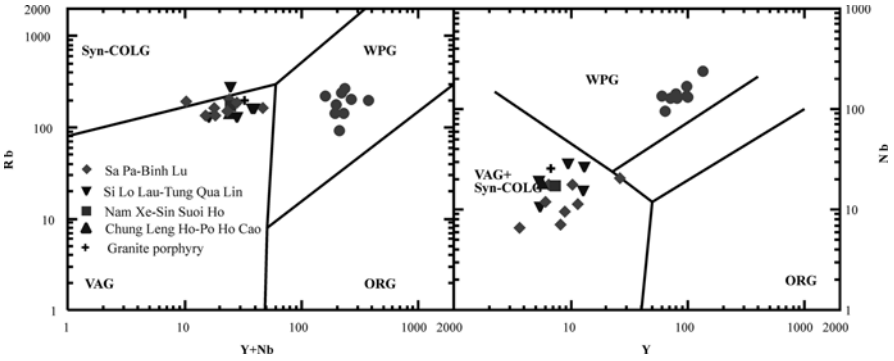

Fig. 8.6 Composition of Cenozoic granite in plots of Rb vs Y + Nb and Nb vs Y (Pearc et al. 1984). For comparison data of Permian granite from Part II, Chap. 4 are also showed (*circles*)

monly presumed for calc-alkaline type granitoids, for example, Dien Bien Permian (272–260 Ma) or Po Sen Neo-Proterozoic (750 Ma) granitoids in northwestern Vietnam (Lan et al. 2000). In tectonic discrimination diagrams, for example, Rb vs. Y + Nb and Nb vs. Y (Fig. 8.6) (after Pearce et al. 1984) Ye Yen Sun granite plots in fields of VAG (volcanic arc granite) or between island arc type and syn-collision granite (VAG + Syn-COLG). Initial $^{87}Sr/^{86}Sr$ isotopic ratios are high, 0.73175, suggesting more crustal origin (Chi (editor) 2003). Further Sr and Nd isotopic study may help clarify the source nature. Hafnium isotopes analyzed from zircon separates showing $\varepsilon_{Hf(t)}$ between −12 and −1.0, strongly suggests a crust-origin (Hoa et al., unpublished data).

The Red River Fault zone (the Ailao Shan – Red River Shear zone) runs more than 1000 km from Tibet to the Bac Bo (Northern) Gulf of Vietnam, embedding four high temperature metamorphic belts. These are Day Nui Con Voi in Vietnam, Ailao Shan, Diancang Shan and Xuelong Shan in Yunnan, China. Recent studies of the metamorphic belts have shown that the Red River Fault zone were undergone three major tectonic stages during the Tertiary: (i) 34–17 Ma: strong amplitude left lateral strike slip coincided with the first period of strong exhumation and fast cooling event; (ii) 17 (20) to 5 Ma (?): slow cooling; and (iii) 5 (?) – present: right lateral, coincided with the second period of strong exhumation, lithosphere extrusion and cooling event (Allen et al. 1984; Tapponnier et al. 1986; Leloup et al. 1995, 2001; Harrison et al. 1996; Gilley et al. 2003; Trinh et al. 2004a).

There have been a number of debates on the relationship between Ye Yen Sun granitoid and Red River Fault (Shear) zone. To date there two major points of view. The first is that, the Ye Yen Sun granitoid (termed as Phan Si Pan granitoid including Cenozoic Ye Yen Sun, Muong Hum alkaline, Phan Si Pan and Phu Sa Phin Permian granites in foreign literature) is not spatial-temporally related to the Red River Shear zone, rather the granite is considered as pre-shear activity (Searle 2006). The second opinion is more popular, suggesting that Ye Yen Sun granitoid is syn-extrusion and is related to the Red River Shear zone (Leloup et al. 2001; Wang et al. 2001; Gilley et al. 2003; Trinh et al. 2004b; Hoa et al. 2009, 2011; Zelazniewicz et al. 2012).

According to Searle (2006), Phan Si Pan (Ye Yen Sun in this book) granite, lying about 10 km to the southwest of Red River Shear zone and having a crystallizing age at about 35 Ma (Zhang and Scharer 1999) is separated from Po Sen, undeformed granitoid block, and Sa Pa marble belt (phlogopite- corundum marble). Most of the Phan Si Pan granitoids are undeformed, showing clear intrusive texture; however, there is no clear evidence of the block being penetrated by left lateral strike slip. All the above evidence had led Searle (2006) come to the conclusion that the Phan Si Pan granitoids are completely not spatial-temporally linked to the Red River Shear zone.

As described above, Ye Yen Sun granite is massive, equigranular or clearly porphyritic, and almost undeformed. However, foliated structure is sometimes observed in granite at a number of outcrops along the Hoang Lien Pass. Trinh et al. (2004b) demonstrated that, although not being strongly deformed, elongate shear plane running in northwest-southeast direction is observed along the left lateral slip that led the granite block to shift with an amplitude about 20 km, as a result. Besides, field survey recorded a series of intrusive dykes penetrate the shear plane while the others were schist-like metamorphosed, suggesting that the intrusive dykes occurred during the displacement of the Ye Yen Sun granite. The occurrence of elastic deformation (foliation structure) and mylonitization in association to Cenozoic Red River Shear activities is also observed in Po Sen Neo-Proterozoic and Permian granites (Chap. 3, Part II). Deformation at various rates (or no deformation) observed for various magmatic bodies (gabbro, pyroxenite and granite) in gneiss in the Red River Shear zone has been described elsewhere (Hoa et al. 2000a; Hoa 2007; Izokh et al. 2005). Therefore, the existence of undeformed Ye Yen Sun granite outcropped at numerous areas suggests the heterogeneity of deformation processes but not negating the relation of the latter to activities of the Red River Shear zone.

Uranium-lead isotopic age dating on zircons from Ye Yen Sun granite yielded 35–30 Ma (Hoa et al. 2012; Dung et al. 2013), coincided, on the one hand, with the timing of strong left lateral strike slip along the Red River Shear zone between 35 and 17 Ma (or up to 20 Ma, after Anczkiewicz et al. 2007) and the first stage of strong exhumation and fast cooling rate, on the other (Leloup et al. 1995, 2001; Harrison et al. 1996; Zhang and Scharer 1999; Gilley et al. 2003; Cuong et al. 2009).

From the above discussion the generation of Ye Yen Sun granitoids may be summarized as follows: about 35–30 Ma, left lateral strike slip Red River Fault zone was formed following the India-Eurasian collision, magma chambers were formed by melting of the lower crust, the source material may be similar to that of Neo-Proterozoic Po Sen and Permian Phan Si Pan Uplift granitoids, occurred in a transtensional terrain between the two slip margins. Following lithospheric exhumation, compression and extrusion along the fault zone the crust becomes thin and ruptured paving ways for (Ye Yen Sun) magmas to intrude. The magmas may have been deformed instantly after formation as well as during their rising (Trinh et al. 2004b).

8.2 Peridotite – Gabbro Associations in the Red River Shear Zone

8.2.1 Summary on the Red River Shear Zone

The zone is also termed as Ailao Shan – Red River Shear zone (ASRR) has appealed for research interest from a large number of geo-scientists (Tapponnier et al. 1982, 1990; Leloup et al. 1995; Harrison et al. 1996). According to Tapponnier et al. (1982, 1990) the ASRR is formed following the India – Eurasian collision that synchronously led to the spreading of Viet Nam East Sea (East Sea). The ASRR is about 1000 km long starting from Tibet to the East Sea. There are 4 narrow-elongated zones composed of metamorphic rocks of different grades up to granulite facies, including Day Nui Con Voi (in Viet Nam), Ailao Shan, Diacang Shan and Xuelong Shan in Yunnan, China (Leloup et al. 1995; Harrison et al. 1996). The importance of ASRR in the regional tectonic evolution and mineralization is undebatable; however there are a number of questions in relation to the evolution of this shear zone needed answers (e.g. Tapponnier et al. 1982, 1986; Briais et al. 1993; Leloup and Kienast 1993; Leloup et al. 1995; Harrison et al. 1996; Dewey et al. 1989; Molnar and Gipson 1996; England and Molnar 1990; Murphy et al. 1997; Rangin et al. 1995; Chung et al. 1997, and others).

In the geological map of Viet Nam (Dovjikov 1965; Tri 1977; Geology of Viet Nam 1989) metamorphic formations are sandwiched between two deep Song Hong (Red River) and Song Chay fault zones. They are viewed as Precambrian high grade metamorphic rocks, up to granulite facies (Thang and Anh 2000). Usual rock types such as granitic hyper-metamorphic gneiss and crystalline schist are commonly found in the Red River fault zone. E.P. Izokh was the first petrologist to describe biotite granite and leucogranite rocks in the Red River fault zone as magmatic but considered dark-colored rocks in gneiss and blastomylonite as amphibolite (Dovjikov 1965).

Recent radiometric age results showed that metamorphic rocks in the Red River fault zone are late Oligocene – early Miocene (Leloup et al. 1995; Harrison et al. 1996; Nam and Itaya 1998; Wang et al. 1998). However, U-Pb isotopic measurements by SHRIMP on zircons in gneiss in the Red River zone yielded a late Proterozoic age (838 Ma; Lan et al. 2001). The timing of the formation of the shear zone, activity periods and heat source that caused high grade metamorphism, are hotly debated. The incompatibility between the cooling age along the shear zone and the timing of the left-lateral strike slip is controversial. Wang et al. (2000) suggested that motion along the ASRR occurred about 27 Ma, 3 million years prior to the East Sea opening (Wang et al. 2000). Leloup and Kienast (1993), in contrast, proposed that shear motion occurred before the extension. The authors believed that there was no relation between the cooling age and distance along the shear zone. Extrusion motion happened earlier and continued during the cooling time and lithosphere denudation in the Red River fault zone (Leloup and Kienast 1993; Leloup et al. 1995, 2001). This statement is supported by deformation age determined by

U-Pb isotopic measurements on a monazite in metamorphosed granite in the Red River zone that showed 31.9 ± 0.3 Ma. This age may be considered as minimal in a progressive metamorphic process. Early magnetic anomaly recorded in the East Sea showed an age of 30 Ma.

Results of Ar-Ar and fission track age dating for metamorphic rocks in the Red River fault zone allow for dividing two tectonic reactivation and exhumation phases (e.g. Maluski et al. 2001). The early Oligocene phase (37–35 Ma) is expressed by Phan Si Pan (Ye Yen Sun) granite intrusions along with potassic mafic and ultramafic (lamproite, minette, absarokite) magmas. The later occurred synchronously with the major motion along the Red River shear zone during 25–21 Ma. An Ar-Ar age dating on a muscovite collected in the Bao Yen area (in the Red River fault zone) shows 24.2 Ma, while fission track age on an apatite is 18–22 Ma, indicating that exhumation rate in the Red River zone was high while the cooling rate was also high. These results are most consistent with previous studies (e.g. Harrison et al. 1996; Leloup et al. 1995; Nam et al. 1998; Wang et al. 1998). Ar-Ar age dating on mica from a gneiss collected on the way from Lao Cai toward Sa Pa yielded a value of 40 Ma, while fission track on an apatite yielded values between 37 and 27 Ma, indicating a fast cooling rate (Leloup et al. 1995). Age of the Ye Yen Sun granite in western Sa Pa is determined to be Oligocene at 34 Ma (Leloup et al. 1995), 35 Ma (Zhang and Scharer 1999) and 35–30 Ma (Hoa et al. 2012; Dung et al. 2013), closely consistent with a fission track, showing 30–32 Ma (Maluski et al. 2001), and formation age of ultra-potassic alkaline mafic lamproite magma in northwestern Song Da rift zone (see Chap. 2).

8.2.2 Mafic and Ultramafic Magmatism in the Red River Fault Zone

Mafic and ultramafic magmas in the Red River fault zone were not a matter of interest in recent studies. Studies by Hoa et al. (2000b) showed that ages of granite in the Red River shear zone determined by Ar-Ar isotopic measurements ranged between 24 and 22 Ma, indicating that the granites were formed after the formation of the shear zone. Inclusions of lherzolite, olivine pyroxenite and amphibole- pyroxenite and gabbro occasionally containing garnet are commonly found in gneiss and mylonite in the Red River shear zone. The rocks are seen in forms of lens and boudinage in garnet- biotite- silimanite gneiss and crystalline schist of the Red River metamorphic complex. Several researchers believed the mafic and ultramafic inclusions were residues or fragments of ophiolite of the Song Ma suture zone that happened to fall in the Red River shear zone (Leloup et al. 1995). Indeed, there are a great number of highly deformed serpentinized (apo-harzburgite) fragments found along the way between Lao Cai and Yen Bai in the Bao Yen district area; whose composition, texture and structure are completely different from those of lherzolite, pyroxenite (websterite) and gabbro in the Red River shear zone. Study of the mafic

and ultramafic inclusions conducted by geoscientists while working on the Doan Hung 1:50,000 geological maps suggested that the lherzolite and pyroxenite belonged to Bao Ai complex while the (garnet-bearing) gabbro was grouped with Cam An complex. The inclusions were determined to be Proterozoic (Son 1997).

The authors of the monograph demonstrated that the lherzolite, olivine-bearing pyroxenite, websterite and amphibole gabbro form a uniform formation along with the small-sized intrusions; they have also identified two formation ages at 35 Ma and 25 Ma (Izokh et al. 2004; Hoa et al. 2004). The ultramafic magmatic activity periods were coincident with the timing of high temperature and pressure metamorphism and strong left-lateral motion along the Red River shear zone (Maluski et al. 2001). Besides, a number of weakly deformed granites aged 24–22 Ma, along with veins comprising aplitic granite, pegmatic granite dated at 21–19 Ma appeared as metamorphosed products, are being found in gneiss and crystalline schist in the Red River zone (Hoa et al. 2000b; Hao 2007), consistent with previous studies (Tapponnier et al. 1990). The presence of these felsic magmas indicate that hyper metamorphism in the Red River gneiss continued even after strong motion in the period between 35 and 22 Ma.

As India – Eurasian collision- induced Red River shear zone tectonics becoming increasingly attracting research topics in geosciences; more supporting evidence for understanding the evolution of the shear zone is much needed. This includes determining the nature and origin of magmas and their periodic activities in high grade metamorphic beds, and their relation to the left-lateral motion of the shear zone in the Cenozoic.

8.2.3 Distribution and Geological Structure Characteristics

Mafic and ultramafic associations in the Red River zone are distributed in almandine- amphibolite and granulite facies (biotite-silimanite-garnet- (±) cordierite- (±) orthopyroxene, amphibolite, crystalline schist, marble and calciphyre) belonging to the Red River metamorphic complex. Their compositions are diversified, including spinel- lherzolite, olivine-spinel-bearing pyroxenite and amphibole-gabbro. Field survey of a cross-section running in the Red River structure direction along the road from Bao Yen – Bao Ha and Mau A – Tan Nguyen and other outcrops in the Yen Bai city and Yen Kien (Viet Tri) areas shows a large number of small-sized lenses distributed unconformity in plagio-gneiss or crisscrossing surrounding gneiss (Fig. 8.7). The magma lenses sometimes are found as aggregates, comprised of several lenses each. The magmatic units, according to their structural and compositional features may be viewed as boudinage, a result of elastic deformation of plagio-gneiss. In the Red River case, the formation of mafic and ultramafic lenses (boudinage) may be related to elastic deformation in the early Cenozoic. Length of the lenses ranges from several meters, sometime reaching tens of meters of hundreds of meters in some cases. The mafic and ultramafic units are widely spread along the Red River high grade metamorphic belt. Field survey also finds that

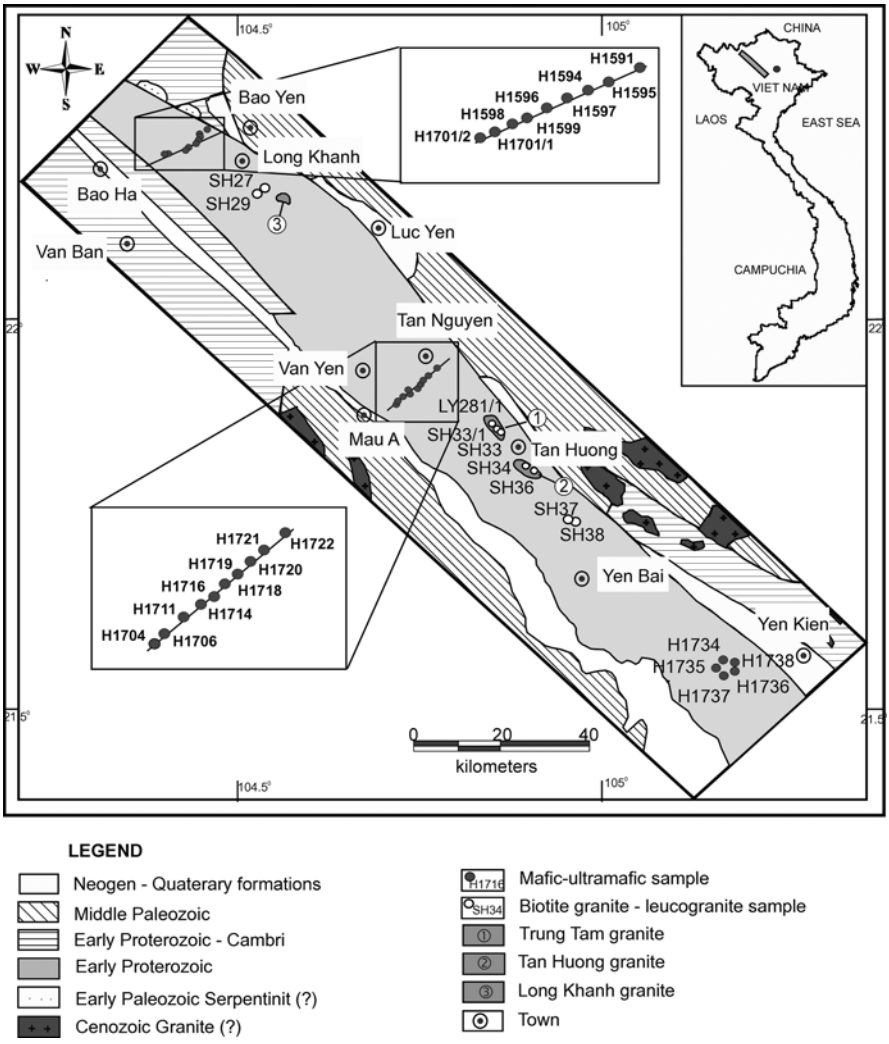

Fig. 8.7 Simplified geological scheme of the Red River shear zone showing survey cross-sections and sampling sites and identification (H-1722… – sample position) (After Hoa 2007)

ultramafic rock types (lherzolite and olivine-spinel websterite) are in the central area (along cross-section Mau A – Tan Nguyen, Lang Chang area, 8th kilometer from Yen Bai), while amphibole gabbro (and hornblendite) or diorite are usually found at southeastern and northwestern margins of the Day Nui Con Voi (metamorphic belt). At the Mau A – Tan Nguyen cross-section magmas of complex compositions including lherzolite, olive-spinel- websterite, dark gabbro and amphibole gabbro are occasionally found.

Bao Yen – Bao Ha cross-section: at a site about 9 km from Bao Yen (Pho Rang) town found are metamorphosed-like layered garnet amphibolites embedded in biotite-silimanite-garnet gneiss along with migmatite entities (Photos 8.6 and 8.7). The amphibolites together with the gneiss form small-scaled complexly foliated units thus being considered as metamorphic rock type (para-amphibolite). Massive gabbro containing fine-grained diffused garnet-pyrrhotite- chalcopyrite and poikilitic biotite is also encountered at this site. Chemically the gabbro is equivalent to a sub-alkaline type such as monzogabbro with characteristically high TiO_2 and K_2O contents. The monzogabbro is crisscrossed by garnet- and cordierite- granite pegmatite, whose age determined by Ar-Ar radiometry yields 20 ± 0.9 Ma (Hoa 2007). The similar biotite-amphibole- metagabbro and biotite-pyroxenite are outcropped to the southwest of the cross-section, closer to Bao Ha, where augen (eyes) biotite-silimanite-garnet gneiss containing graphite and sulfide and boudinage rocks are also found (Photo 8.8 and 8.9). The gneiss is strongly migmatized. Contact between the gneiss and websterite is sharp, along which biotization is usually developed. Thus, the presence of biotite in the pyroxenite may be related to process of repeated metamorphism. However, for pyroxenite and lherzolite magmas in other areas such the biotization development is not observed. Sulfide drop-shaped dissemination with sizes ranging 2–3 cm containing pyrrhotite- chalcopyrite-pentlandite is commonly occurred in websterite. Sulfide-rich diffused entities are also found in gneiss although only at contact with websterite. Also at the cross-section an amphibole- and biotite-gabbro in form of boudinage up to 30 cm thick is found (Photo 8.10). In difference from amphibolite the gabbro is massive, lacking metamorphosed differentiation, a characterized indicator for amphibolite. The gabbro contains garnet, suggesting deep level formation.

From the above observations it may suggest that gabbro and pyroxenite outcropped in the marginal areas of Red River zone having relatively high alkalis and containing garnet may appear during the early formation phase of the shear zone. The timing of these magmatic formations may be comparable to that of potassic mafic magmas of the Red River shear zone in the Song Da rift zone as mentioned earlier.

Amphibole gabbro and hornblendite in dyke – vein phase are found in the northeast of Bao Yen – Bao Ha cross-section, respectively, at outcrop H-1701 and H-1701/2 (Photo 8.10); however, no garnet-gabbro is seen at the sites. Small bodies showing indications of strong elastic deformation and effect of boudinage are found in gneiss. The boudins show various metamorphic modification, ranging from complete, partial or unaffected. The mafic intrusions are crisscrossed by granitoidic injection, which the closer to mafic bodies the more concentrated. The geological appearance at this site is similar to a scenario of syn-plutonic intruding molten granitoids. Unlike amphibolite the magmas show no indications of metamorphic modification or micro-foliation. The gabbro, showing typical microscopically magmatic texture, is defined as amphibole- and hornblende gabbro. Dissemination of pyrrhotite and chalcopyrite is observed in the gabbro. The Ar-Ar isotopic age dating on plagioclase from a granite pegmatite dyke shows 21.2 ± 0.2 Ma (sample H1597) (Hoa 2007). Websterite, lherzolite, garnet- websterite and garnet-bearing amphibole gabbro are found in the central part of Bao Yen – Bao Ha cross-section. It is noted

Photo 8.6 Metamorphic foliation structure of amphibolite in garnet-similanite-biotite gneiss and sign of migmatite at Bao Yen-Bao Ha cross-section, outcrop H-1597

Photo 8.7 Garnet-silimanite-biotite gneiss of Red River complex. Outcrop H-2012b between Bao Yen and Bao Ha

once again that garnet-bearing gabbro is not see in the marginal areas of the cross-section. As described in the following section garnet appearance is an indication of depths of magma formation and timing of intrusion.

Mau A – Tan Nguyen cross-section: occurred along the national route 70 from Mau A, Van Yen district in the southwest (near Red River) toward Tan Nguyen in the northeast (Fig. 8.7). There are a large number of small boudins and separated blocks up to 100 m wide comprised of amphibole gabbro, garnet-bearing amphibole gabbro, amphibole websterite and lherzolite. To the south of the cross-section a large block is identified to consist of amphibole gabbro, gabbro and websterite, where websterite in the center of the block gradually changes to gabbro. Also at the cross-section separate outcrops comprised of coarse-grained lherzolite and orthopyroxene megacrysts are being found. Garnet-bearing amphibole gabbro observed in gneiss and blastomylonite as boudins. Contacts between the gabbro and gneiss and blastomylonite are clearly sharp although there is no hardened zone being observed

Photo 8.8 Boudinage entities of monzogabbro and websterite (*dark*) outcropped in Bao Yen – Bac Ha

Photo 8.9 Boudin of biotite-websterite in gneiss. Contact is sharp; blastomylonite is visible; outcrop H-2012c (Bao Ha)

(Photo 8.11). A large number of lherzolite and websterite units are found at the center of the Mau A – Tan Nguyen cross-section; garnet bearing amphibole gabbro and diorite are also popular. Differentiation trend from lherzolite to olivine-websterite is observed in some places while in the others olivine websterite changing olivine-free websterite and dark amphibole gabbro.

At the cross-section the gneiss somewhere contains fine-grained (no-deformated) amphibole gabbro-dolerite (Photo 8.12) dykes about 2–3 m long. The dyke is boudinage-free, it penetrates gneiss host-rock and being crosscutting by granite pegmatite veins. The above observations suggest that the mafic magmatic intrusion occurred repeatedly and continued even after the cessation of the major extrusion phase.

The lherzolite and websterite in the Lang Chang area and the olivine-spinel websterite in Yen Bai, whose details were given in Hoa et al. (2000a) and Hoa (2004), structurally are also distributed in the central area of the Red River shear zone. It is

Photo 8.10 Boudinage effects of different levels comprised of amphibole-gabbro intruded by aplitic granite; outcrop H-1701/1 and H-1701/2

Photo 8.11 Sharp contact between amphibole gabbro and gneiss; outcrop H-1716, between Mau A and Tan Nguyen

noteworthy that together with pseudo-conformity contact with the host gneiss there some clearly cutting contacts are being reported between the magmas and gneiss.

Metamorphically differentiated amphibolite is outcropped at a quarry in the Yen Kien area, north of Viet Tri province. Plagiomigmatite is found in the amphibolite suggesting that the magma was modified under effect of a high heat source. Aside from amphibolite, massive amphibole gabbro, hornblendite and amphibole-bearing olivine websterite having similar compositions as those occurred in other cross-

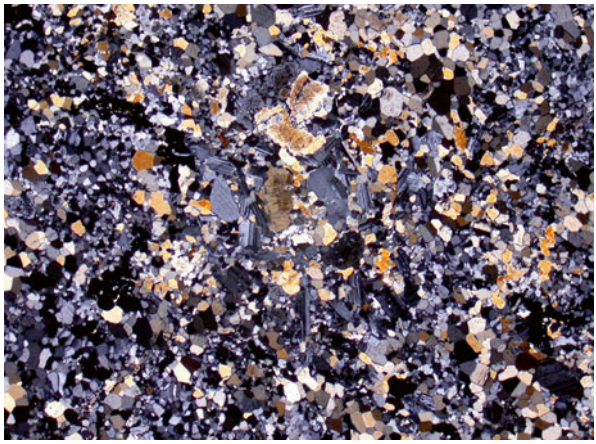

Photo 8.12 Undeformed gabbro-dolerite in dykes cutting gneiss between Mau A and Tan Nguyen; thin section H-1722, Nichol (+)

sections are also found. The findings suggest that the mafic and ultramafic magmatic activities occurred synchronously with shear motion in entire length of the Red River zone. The presence of similar amphibolite and amphibole gabbro rocks in biotite-silimanite-garnet gneiss in the Nui Goi (Goi Mount, Nam Dinh province, southeastern Red River Shear Zone) lends a firm support to this suggestion.

At the Tan Huong ruby mine, amphibolite and garnet-bearing variety are found among graphitized marbles. Also encountered are amphibole gabbro, olivine- websterite and websterite along with a number of poikilitic orthopyroxene megacrysts. Basically this magma association is compositionally comparable to that outcropped in Mau An – Tan Nguyen cross-section in the central area of Red River zone. This observation suggests that mafic and ultramafic magmatic activities may take part in the ruby mineralization process. Similarly, model of ruby formation with participation of dark-colored magma (amphibolite) was once proposed by Trinh et al. (2004a). In order to learn more about this process, the authors have examined and collected samples from Tan Huong exploration drill cores LK-4-T for study. Along with the presence of amphibolite owning metamorphic differentiation characteristics, amphibole gabbro and websterite are also found at contact with the host marble. Regardless of poor observation at the direct contact between the magmas and host rock in the cored samples; however, near-contact zone, toward the host rock, an order of minerals seen as follows: phlogopite- calciphyre, graphite, spinel and Cr-pargasite; followed by fuchsite and sulfide-bearing marble zone. A distance from the contact is gas-saturated marble where hydro sulfuric smell can be felt as long as the marble being physically smashed. In the gabbro, on the other hand, garnet grains are found similar to those in skarn formations in inner contact zones. The above observations indicate the gabbro and websterite were at high temperatures at the time their intruding to the marble host rocks. There is no granitoid being found in the core as hypothesized by Quoc (1995), at the depth of 46.7–50 m there appeared calciphyre, not granite as previously described (Fig. 8.8).

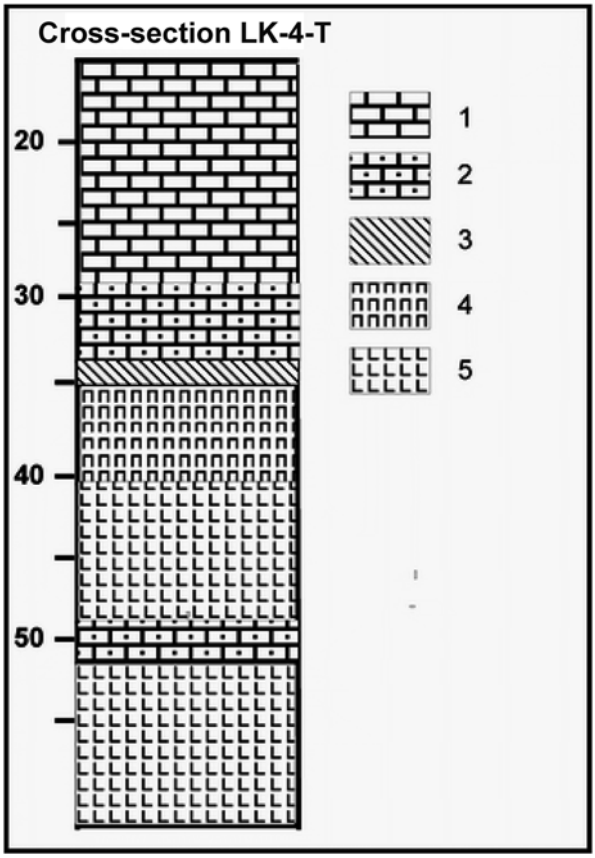

Fig. 8.8 Drill hole cross-section LK-4-T at Tan Huong ruby mine. *1* – sulfur bearing marble; *2* – fuchsite bearing marble; *3* – inner-skarn; *4* – amphibole gabbro and websterite; *5* – amphibolite and garnet-amphibolite

Formation age of ruby at the Tan Huong mine was determined using Ar-Ar isotopic method showed 23.2 ± 0.6 (Garnier et al. 2002), consistent with the timing of the second stage's mafic and ultramafic magmatic activities in the Red River fault zone. Ruby mineralization in regions outside the Red River zone occurred between 30 and 34 Ma, correspondent to the early stage of garnet-bearing amphibole gabbro, pyroxenite and lherzolite. Researchers suggested that a large-magnitude strike slip would eventually lead to exhumation of deep layers usually in the form of (thrusting) obduction as observed in Pribaikal, Russia (e.g. Rozen and Phedorovsky 2001). The obduction effect is especially applied to carbonate formations such as in the Luc Yen and Tan Huong and other ruby mines that are associated with exhumation geodynamics in the Red River fault zone.

In general, geological surveys allow for division of syn-strike slip motion mafic and ultramafic magmas into separate activity stages. Accordingly, high-K metamafic and pyroxenite associations occurred a number of sections in the marginal areas of

Red River zone represent magmas of early development stage of the Red River shear zone (Fig. 8.9). The lherzolite, srisgeimite, olivine websterite, garnet-bearing amphibole gabbro are well developed in the central regions of the fault zone. These magmas believed to generate at very deep levels (e.g. Izokh et al. 2004) may be viewed as representatives for an intermediate stage; followed by small-scaled dyke-sill phased amphibole gabbro and hornblendite showing weak boudinage effect, along with amphibole gabbrodolerite that were generated at shallower levels at the final stage.

8.2.4 Petrological and Mineralogical Characteristics

Basing on petrological-mineralogical and geochemical characteristics the mafic and ultramafic associations in the Red River fault zone may be divided into the following magmatic formations: peridotite and amphibole peridotite (lherzolite and

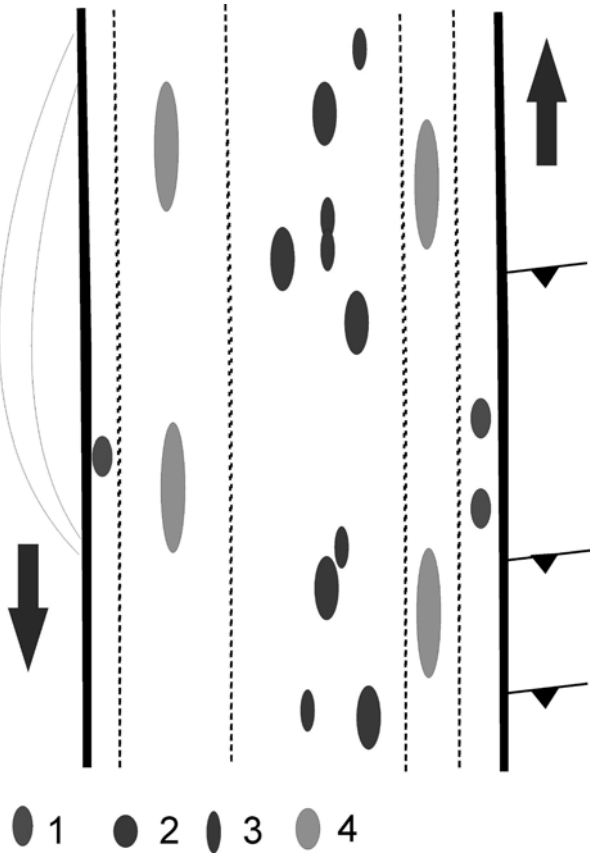

Fig. 8.9 Schematic distribution of mafic and ultramafic magmas in the Red River fault zone. *1* – early stage high-K metagabbroid and pyroxenite; *2*, *3* – high pressure mafic and ultramafic; *4* – final stage amphibole gabbroid. *Arrow* shows direction of left-lateral motion of the Red River fault zone

srisgeimite), pyroxenite (olivine websterite, websterite, garnet- websterite, coarse-grained websterite and poikilitic pyroxenite), amphibole gabbro, amphibole gabbrodolerite and metamonzogabbro.

Ultramafic magmas in the Lang Chang area, the central area of Mau An – Tan Nguyen cross-section, in the Bao Yen – Bao Ha cross-section and Yen Bai show similar mineralogical and geochemical characteristics. Note that those belonged to lherzolite group contain olivine more than 40 vol% (Classification of IUGS); otherwise they should belong to olivine websterite group. To the latter group are olivine-spinel pyroxenite in the Yen Bai area. There are two rock types within the lherzolite group, including lherzolite – amphibole-bearing lherzolite and srisgeimite (cortlandite). These magmas have direct transition relationship with olivine websterite; the difference between the magmas is in the amount of olivine and their petro-geochemical properties. For example, the lherzolite contains MgO higher than 25 wt% while MgO in the pyroxenite ranges from 15 to 22 wt%; besides, olivine in lherzolite is idiomorphic containing some amount of brown poikilitic Cr-spinel grains.

Typical lherzolite includes a mineral assemblage of olivine, orthopyroxene, clinopyroxene, amphibole and spinel; there is no plagioclase in lherzolite, the mineral only presents in pyroxenites. Spinel, instead of garnet, is commonly present in lherzolite. Lherzolite is usually fine to medium-grained texture and massive structure (Photo 8.13).

Pyroxenites in the Red River fault zone are olivine websterite and websterite. They are closely associated with lherzolite, on the one hand, and participating as a member in the differentiation trend from pyroxenite to gabbro, on the other. Sometimes websterite containing large megacrysts of poikilitic orthopyroxene. Rolling garnet-bearing websterite is occasionally seen in Bao Yen – Bao Ha cross-section.

Olivine in the lherzolite has a composition correspondent to chrysolite (f = 17–27) with low TiO_2 and high NiO (0.17–0.20 wt%) typical for plutonic magma (Table 8.4,

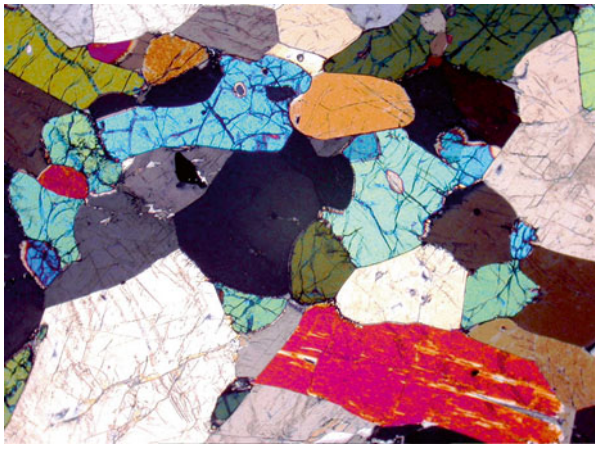

Photo 8.13 Srisgeimite (lherzolite) in Mau A – Tan Nguyen cross-section. Ol – olivine, Am – amphibole, Sp – Cr-spinel; sample H-1722; Nichol (+); magnification 40×

Table 8.4 Chemical compositions (wt% by EPMA) of olivines in lherzolite and olivine-websterite in the Red River fault zone (After Hoa et al. 2004; Izokh et al. 2004)

Sample	SiO_2	FeO	MnO	MgO	CaO	Na_2O	K_2O	Total	f
H1715	39.36	17.41	0.161	42.52	0.000	0.000	0.000	99.45	0.19
H1715_1	39.48	17.20	0.196	42.66	0.028	0.000	0.000	99.56	0.18
H-1718	40.42	16.27	0.260	42.70	0.004	0.039	0.014	99.71	0.18
H-1719/1	39.97	15.82	0.160	42.92	0.000	0.014	0.007	98.89	0.17
H-1719/2	40.65	15.35	0.170	42.92	0.000	0.003	0.004	99.10	0.17
H-1719/2_1	40.01	15.95	0.170	42.46	0.000	0.012	0.009	98.61	0.17
H-1719/2_2	40.32	15.80	0.190	42.92	0.000	0.012	0.008	99.25	0.17
H-1720/1	40.46	14.43	0.150	43.34	0.021	0.018	0.017	98.44	0.16
H-1720/1_1	40.65	14.90	0.170	43.73	0.023	0.012	0.017	99.50	0.16
H-1721/2	40.03	16.32	0.290	42.71	0.008	0.024	0.011	99.39	0.18
H-1722	38.69	23.75	0.390	36.34	0.005	0.028	0.016	99.22	0.27

Remarks: H-1715 – H-1721: lherzolite; H-1722: hornblendite; H-1718: websterite

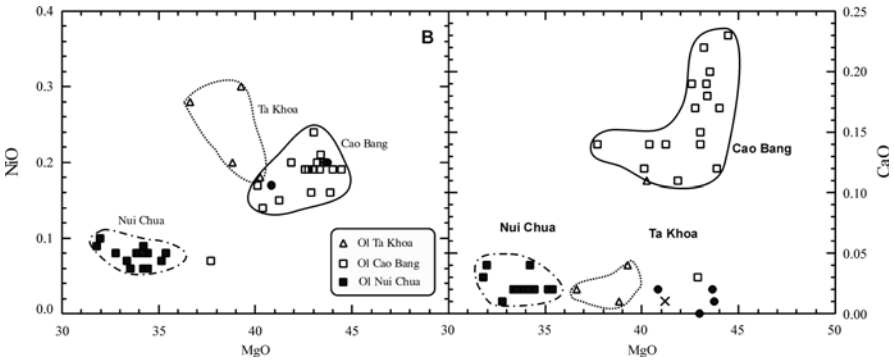

Fig. 8.10 Compositions of olivine in Red River mafic-ultramafic in NiO and CaO versus MgO relationship. Olivines from Cao Bang and Nui Chua ultramafic magmas shown for comparison (See Part II, Chap. 5)

Fig. 8.10). The Ni contents indicate the magmatic nature of olivine as recrystallized olivine is very low in Ni and Fe (Hoa et al. 2000; Izokh et al. 2004). High ferrous nature in the olivine suggests the lherzolite is not an ophiolitic remnant being involved in the Red River shear zone. Also olivine geochemistry in the lherzolite suggests the ultramafic magma is different from that of deep mantle origin (such as intrusive lherzolite in the Ta Khoa area, NW Vietnam) and lherzolite xenoliths in Cenozoic alkaline basalts. A crystallization order was calculated using program 'Pluton' for a dyke-phased gabbrodolerite (sample H-1712), having a composition that was taken as primitive melt. The calculation showed that the primary liquidus phase occurred at 1335 °C was olivine with FeO contents from 12 to 18 wt%, closely consistent with the above analyzed lherzolite olivine. Therefore, the lherzo-

lite magmas may be considered as early cumulates from a primitive melt having the same chemical composition or higher MgO contents (but no lower).

Pyroxene: Chemical compositions of clinopyroxene are shown in Table 8.5 and their compositional positions in En-Wo-Fs diagram are given in Fig. 8.11. Usual high Al_2O_3 concentrations (7–8 wt%) in pyroxenes are recorded in lherzolite and pyroxenite at the Mau A – Tan Nguyen cross-section; the high aluminum contents accompanied by high Cr_2O_3 (=0.25–0.38 wt%) indicate their deeper origin compared with olivine-bearing websterite in the Yen Bai area. Clinopyroxenes in the Yen Bai and Yen Kien (Viet Tri province) areas have compositions corresponding to diopside ($Wo_{45.23–49.14}$ $En_{36.58–38.59}$ $Fs_{14.27–15.93}$), with low Cr_2O_3 (0.04–0.18 wt%) and Al_2O_3 not surpassing 3 wt% (Hoa et al. 2000a). Some lherzolite and websterite clinopyroxene separates show indications of solid liquid reaction texture expressed by systematic orientation of poikilitic Cr-spinel crystals (Photo 8.14). The observations, indicate that, in some cases, the Al- and Cr-rich pyroxenes may appear as primary crystals settled at high pressure condition (deep level) subsequently transported to shallower levels by later magmas. The pyroxene disintegration may be resulted from the change in oxidation level occurred during interaction with the host gneiss. As seen in Sangilen case (Russia), amphibole is highly developed at contact between mafic magmas intruding into metapelite strata, indicating the role of water in later stage magmas. Correlation between Cr_2O_3, Al_2O_3 and MgO in clinopyroxene is shown in Fig. 8.11.

Orthopyroxenes in the lherzolite show compositions correspondent to bronzite (f = 13–20 %) with relatively high Al_2O_3, up to 3.4 wt% (Table 8.6). In addition, the highest Al_2O_3 contents are observed in Opx in areas where lherzolite is associated with garnet-bearing pyroxenite and garnet-amphibole gabbro, meaning the magmas of deep mantle origin. In some Opx, Cr_2O_3 contents were determined to be as high as 0.35 wt%. These characteristics indicate deep mantle source for the orthopyroxene (e.g. Lazko and Sarkov 1988). Relationship between olivine and orthopyroxene ferrous contents may also indicate magmatic sources of the minerals. According to a modeling calculation, Opx crystallization may start earlier than Cpx, and with creasing pressure Opx may be crystallized even before olivine.

Amphibole in the lherzolite occurs in various types (Hoa et al. 2000a). Early generation amphiboles are dark-brown, developed around pyroxene crystals; the later generation types are colorless, developed between olivine and pyroxene crystals. The two types show compositions equivalent to magnesian hornblende having high Al_2O_3 up to 8–11 wt% (Table 8.7). The amphibole is divided into two type according to the TiO_2 contents. Dominant low-TiO_2 type (0.7–0.9 wt%) is bright-colored and characteristically low K_2O (<0.5 wt%); the high-TiO_2 type (up to 2 wt%) is high K_2O, up to 1 wt% (Table 8.6). Besides, amphibole of accessory phase is well developed having composition equivalent to actinolite or hornblende. Because of the development of this accessory mineral the radiometric age dating of lherzolite and websterite in the Yen Bai area has not been successful (Hoa et al. 2000a) (Fig. 8.12).

Table 8.5 Chemical compositions (wt% determined by EPMA) of clinopyroxenes in Red River mafic and ultramafic magmas (After Izokh et al. 2004; Hoa et al. 2005)

Sample	SiO_2	TiO_2	Al_2O_3	FeO	Cr_2O_3	MnO	MgO	CaO	Na_2O	K_2O	Total
H1718_1	52.00	0.73	7.26	3.98	0.31	0.08	19.77	12.40	0.26	0.10	96.89
H1718_2	51.69	0.80	7.61	3.94	0.30	0.08	19.53	12.42	0.30	0.12	96.79
H1718_3	52.85	0.77	7.10	4.01	0.35	0.04	19.65	12.40	0.16	0.09	97.42
H1718_4	52.72	0.76	7.52	4.28	0.38	0.06	19.72	12.18	0.25	0.08	97.95
H1718_5	52.89	0.58	6.95	4.29	0.36	0.04	19.86	12.18	0.22	0.07	97.44
H1719/1_1	52.96	0.63	7.08	4.16	0.25	0.09	19.54	12.40	0.25	0.10	97.46
H1719/1_2	52.61	0.64	7.30	4.53	0.24	0.07	20.09	12.36	0.25	0.04	98.13
H1719/2_1	53.23	0.69	7.08	4.13	0.29	0.07	19.56	12.28	0.22	0.10	97.65
H1719/2_2	53.23	0.64	7.07	4.32	0.33	0.11	19.48	12.55	0.23	0.06	98.02
H1726	52.14	0.31	3.07	14.17	0.01	0.25	14.79	12.20	0.42	0.17	97.53
H1701/1_1	51.11	0.33	2.64	9.12	0.05	0.21	12.64	22.56	0.50	0.00	99.16
H1701/1_2	51.70	0.23	2.42	9.14	0.04	0.28	12.84	22.23	0.52	0.00	99.40
SH-1342/8	51.01	0.35	2.7	9.25	0.18	0.32	13.27	22.44	0.53	0	100.05
SH-1342/9	53.36	0.29	1.98	8.7	0.17	0.3	13.41	22.67	0.49	0	101.37
SH-1342/34	50.28	0.35	3.16	9.27	0.16	0.35	12.83	21.81	0.49	0.03	98.73
SH1300-2/36	52.71	0.11	1.51	8.3	0.01	0.3	12.37	23.12	0.36	0	98.79
SH-38/6	55.25	0.04	1.98	13.33	0.1	0.31	29.55	0.24	0.01	0.01	100.82
SH-38/15	55.74	0.07	1.61	13.18	0.12	0.26	29.66	0.24	0.01	0.01	100.9
SH-38/17	55.34	0.06	1.75	13.28	0.07	0.29	29.48	0.24	0.01	0.01	100.53
SH-38/22	55.4	0.03	1.7	13.38	0.06	0.29	29.8	0.24	0	0.01	100.91

Remarks: H1718, 1719/1: lherzolite; H1726, 1701/1: amphibole gabbro; SH-1342: Bao Ha amphibole gabbro; SH-1300: Yen Kien amphibole gabbro

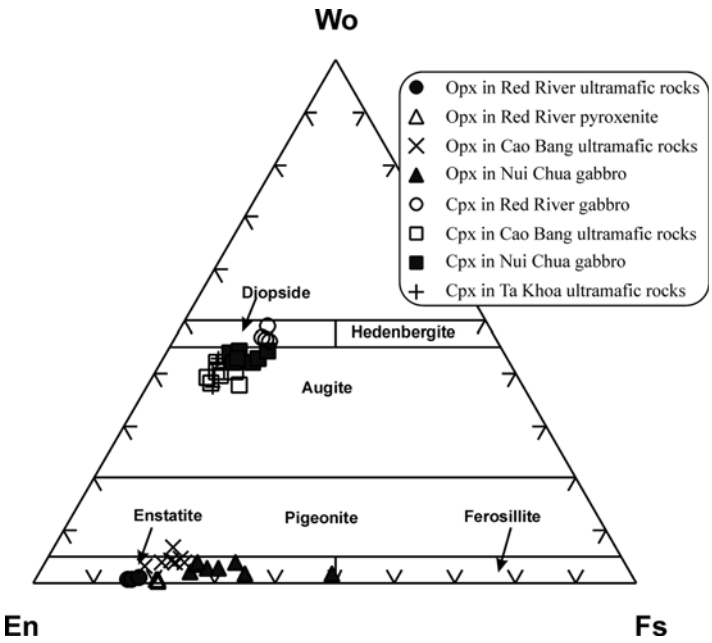

Fig. 8.11 Chemical compositions of pyroxenes in Red River mafic and ultramafic magmas in En – Wo – Fs correlation

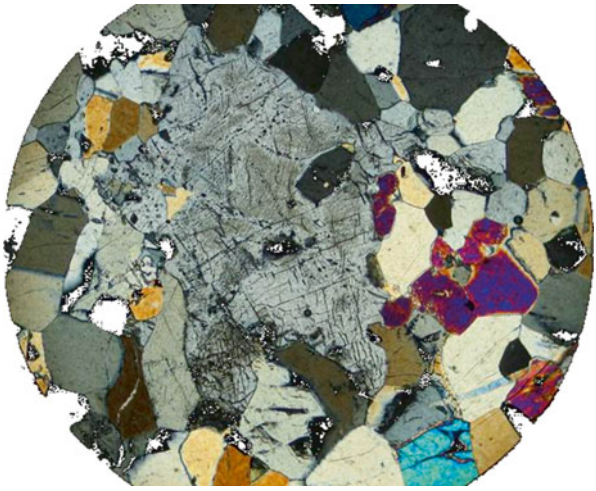

Photo 8.14 Olivine websterite showing megacrysts of clinopyroxene – Cpx (*center*). Disintegration texture in Cpx is seen having brownish red Cr-spinel crystals; sample H-1721, Bao Ha cross-section, Nichol (+), magnification 40×

Table 8.6 Chemical compositions (wt%, by EPMA) of orthopyroxenes in Red River mafic and ultramafic magmas (After Izokh et al. 2004; Hoa et al. 2005)

Sample ID	SiO_2	TiO_2	Al_2O_3	FeO	MnO	MgO	CaO	Cr_2O_3	Total
H1721/2	55.36	0.01	1.63	8.78	0.27	31.69	0.35	0.35	98.45
H1720/1	54.37	0.05	2.91	13.81	0.32	27.56	0.46	0.03	96.07
H1718_1	56.15	0.07	2.38	10	0.23	31.41	0.29	0.13	100.67
H1718_2	54.46	0.1	3.13	13.79	0.27	27.62	0.37	0.02	97.35
H1722/1_1	57.13	0.02	1.57	9.03	0.19	31.35	0.34	0.14	97.49
H1722/1_2	56.33	0.06	2.07	9.97	0.25	30.8	0.27	0.04	97.32
H1722/1_3	54.52	0.02	1.48	14.64	0.30	27.75	0.30	0.04	97.16
H1713	54.71	0.07	3.06	13.72	0.30	27.56	0.44	0.03	98.01
H1738_1	53.35	0.02	2.39	17.77	0.34	26.42	0.15	0.02	100.49
H1738_2	53.37	0	2.64	17.71	0.35	25.95	0.22	0.04	100.29
H1738_3	53.25	0.02	2.69	17.91	0.28	26.07	0.22	0.08	100.54
H1737	54.86	0.01	2.45	14.87	0.23	28.19	0.22	0.08	100.93
SH-38/23	55.2	0.05	1.88	13.41	0.27	29.54	0.26	0.12	100.73
SH-38/24	55.19	0.06	1.71	13.31	0.31	29.65	0.29	0.1	100.62
SH-38/8	55.46	0.07	2.04	13.46	0.3	29.73	0.26	0.11	101.43
SH-38/9	55.44	0.07	1.74	13.28	0.31	29.4	0.22	0.09	100.55
LY-6136/1	55.44	0.06	1.84	10.26	0.31	31.17	0.3	0.1	99.48
LY-6136/2	54.91	0.07	2.25	10.3	0.31	31.22	0.27	0.12	99.45
LY-89	54.49	0.07	2.48	11.04	0.24	30.37	0.42	0.1	99.21
LY-10516	54.85	0.14	2.14	9.99	0.24	30.92	0.28	0.12	98.68

Remarks: H1718, H1721/2: lherzolite in the Mau A – Tan Nguyen cross-section; H1713, H1738: websterite; H1737 amphibole gabbro; SH-38: olivine-websterite in Yen Kien; LY = 6136, LY-89, LY-10516: lherzolite in Lang Chang

Spinel is common in lherzolite and pyroxenite. In many cases, spinel appears in irregular or rounded shapes, plated in orthopyroxene or between Opx and amphibole tablet crystals. The mineral is brownish green, or characteristically greenish yellow. The chemical composition is relative stable, including Al_2O_3 = 56–58.25 %, Cr_2O_3 = 6.02–9.68 %, MgO = 13.05–16.35 % (Table 8.8.). Cr-rich spinel is normally described for high grade metamorphic mafic granulites or in nodules (xenoliths), whose compositions are similar to peridotite or garnet-bearing pyroxenite, found in Cenozoic alkaline basalts in the Kon Tum massif area in Indochina block (Phuong et al. 2001). In other mafic and ultramafic formations (for example, Song Da basalt-komatiite, lherzolite – Cao Bang gabbronorite) spinel usually appears as Cr-picotite, Al-chromite or Cr-magnetite, e.g., Cr- and Al-rich varieties (see Part I).

Amphibole gabbro contains following petrologic compositions basic plagioclase, clinopyroxene – Mg-augite, augite (f = 10–35) and brown amphibole. The

Table 8.7 Chemical compositions (wt%, by EPMA) of amphiboles in mafic and ultramafic in the Red River fault zone (After Izokh et al. 2004; Hoa et al. 2005)

Sample	SiO_2	TiO_2	Al_2O_3	Cr_2O_3	FeO	MnO	MgO	CaO	Na_2O	K_2O	Total
H1591	47.8	0.77	10.9	0.23	6.93	0.13	16.8	11.9	1.5	0.23	97.13
H1704	45.3	1.27	10.8	0.07	15.1	0.27	11.6	11.5	1.26	0.46	97.75
H1706	45.1	1.75	10.8	0.09	14.2	0.33	11.6	11.4	1.39	0.88	97.56
H1712	42.9	2.09	14.5	0.3	7.99	0.05	14.4	11.7	2.46	0.99	97.31
H1713	46.8	1.44	10.5	0.23	10.8	0.15	14.7	10.9	1.86	0.29	97.60
H1714	50.9	0.76	7.55	0.05	12.1	0.28	14.5	11.4	0.42	0.4	98.37
H1715	46	1.62	10.9	0.24	10.9	0.15	14.5	10.7	1.99	0.29	97.18
H1715	46.8	0.48	11.6	0.88	4.17	0.09	17.8	12.4	1.71	0.86	96.84
H1716	46.8	0.93	8.76	0.07	13.8	0.22	13.2	11.4	0.68	0.63	96.53
H1717	48.7	0.52	9.2	0.1	11.2	0.14	15.2	11.6	1	0.66	98.27
H1722	49.4	0.65	9.5	0.67	4.59	0.09	18.5	12.1	1.06	0.41	96.97
H1726	45.8	1.02	9.63	0.01	14.6	0.26	12.3	11.4	1.03	0.81	96.86
H1729	45.9	1.48	9.8	0.18	13.4	0.13	13.5	11.3	1.11	0.52	97.34
H1734	45.5	1.16	11.2	0.13	13.5	0.17	12.6	11.8	1.26	1.04	98.30
H1735	43	2.07	12.2	0.05	17.4	0.27	9.12	11.4	1.32	1.23	98.13
H1736	43.4	0.8	14	0.16	9.58	0.07	15.3	11.4	2.1	0.38	97.16
H1737	45.2	0.67	12.3	0.65	8.07	0.09	16.6	11.5	1.72	0.28	97.06
H1738	44.9	0.73	12.7	0.21	10.4	0.11	15.4	11.1	1.76	0.2	97.47
H1701/1	43.6	2.35	12	0.07	14.2	0.16	11.3	11.8	1.83	1.07	98.27
H1711/1	46.6	0.84	9.69	0.05	12.8	0.27	13.4	11.3	1.06	0.58	96.56
H1720/1	43.1	1.94	14.8	0.31	7.73	0.11	14.2	11.8	2.71	1.16	97.80
H1721/2	43.3	1.98	14.6	0.23	8.21	0.09	14.1	11.7	2.68	1.03	98.00
H1721/2	46	0.69	13	0.25	7.52	0.15	15.8	11.5	1.79	0.54	97.34
H1721/2	45.5	0.69	13.4	0.26	7.64	0.11	15.8	11.5	1.87	0.6	97.32
H1721/2	46.3	1.5	10.9	0.19	11	0.16	14.7	10.9	1.91	0.27	97.78
H1722/1	45.7	0.7	13.4	0.26	7.63	0.13	15.2	11.4	1.65	0.52	96.57

Remarks: H1591- metamonzogabbro; H1701/1, H1704, H1706, H1711/1, H1713, H1716, H1717, H1726, H1737- amphibole gabbro; H1712 – gabbrodolerit; H1713, H1736, H1738 – websterite; H1722 – amphibole-bearing websterite; H1715, H1718, H1719/1, H1720/1, H1721/2 – lherzolite, H1719/2 – gabbrodiorite; H1734, H1735 – amphibolite

clinopyroxene is aluminum-rich, especially that is garnet-bearing amphibole gabbro. Amphibole is correspondent to magnesian hornblende and pargasite, to a lesser extent. Edennite is rare, seen only in dyke phased gabbrodolerite. Ore minerals include titanomagnetite and ilmenite. Dissemination of pyrrhotite and chalcopyrite is commonly found. The magma is gabbro texture, massive, the amphibole being rarely oriented. Micro-foliation is not observed in thin sections under microscope as commonly seen in those surrounded by gneiss. Amphibole in gabbro is more idiomorphic compared with co-existing plagioclase, indicating that water vapor in the melt was high. In summary, the lack of syn-crystallization of olivine and plagioclase, and the early settlement of orthopyroxene relative to clinopyroxene in websterite as well as the presence of garnet in some gabbro types indicates

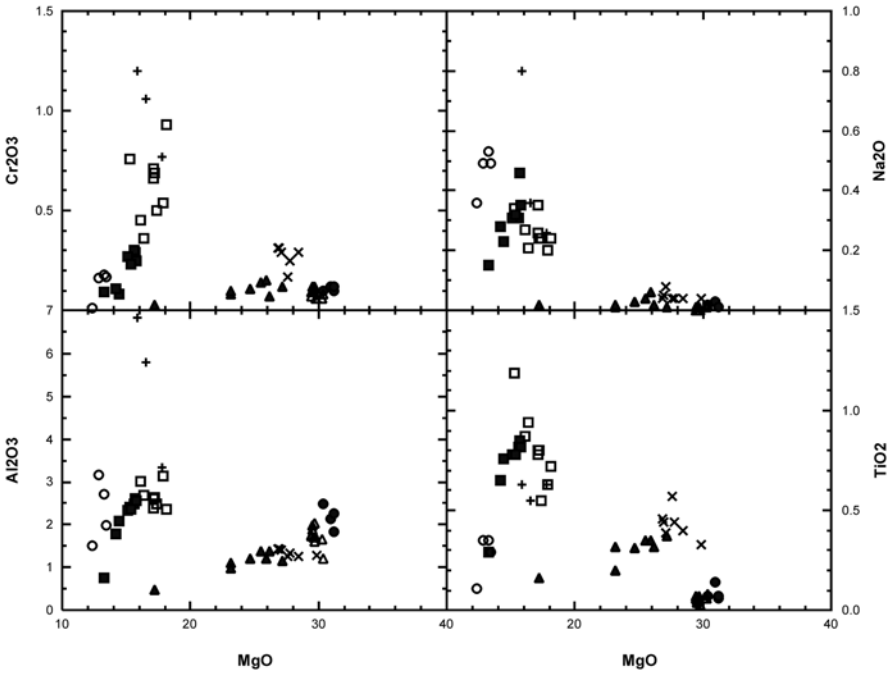

Fig. 8.12 Chemical compositions of pyroxenes in mafic and ultramafic magmas in the Red River fault zone in the correlation of Al_2O_3, Cr_2O_3, Na_2O, TiO_2 versus MgO. *Symbols* as in Fig. 8.11

Table 8.8 Chemical compositions of chrom-spinel in mafic and ultramafic magmas in the Red River zone (After Hoa et al. 2000)

Sample	TiO_2	Al_2O_3	FeO	Cr_2O_3	MnO	MgO	CaO	Total
SH-38/1	0.05	56.21	21.76	7.64	0.14	13.05	0.04	98.89
SH-38/13	0.06	58.25	20.25	6.40	0.13	13.52	0.00	98.61
SH-38/16	0.04	58.21	20.52	6.02	0.12	14.41	0.00	99.32
SH-38/4	0.09	56.00	21.47	7.78	0.14	13.36	0.04	98.88
SH-38/5	0.08	56.08	20.80	7.64	0.17	13.77	0.01	98.55
LY-6136/1	0.04	58.37	17.55	9.21	0.17	16.35	0.13	101.82
LY-6136/2	0.05	57.68	17.67	9.47	0.17	15.80	0.03	100.87
LY-6136/3	0.04	58.09	17.47	8.56	0.15	15.73	0.00	100.04
LY-6136/4	0.03	57.24	17.92	9.68	0.17	15.69	0.00	100.73
LY-89/1	0.06	56.16	20.24	8.99	0.16	14.26	0.01	99.88
LY-89/2	0.05	57.76	19.52	7.97	0.14	14.86	0.00	100.30
LY-89/3	0.07	56.39	20.02	9.04	0.15	14.64	0.00	100.31

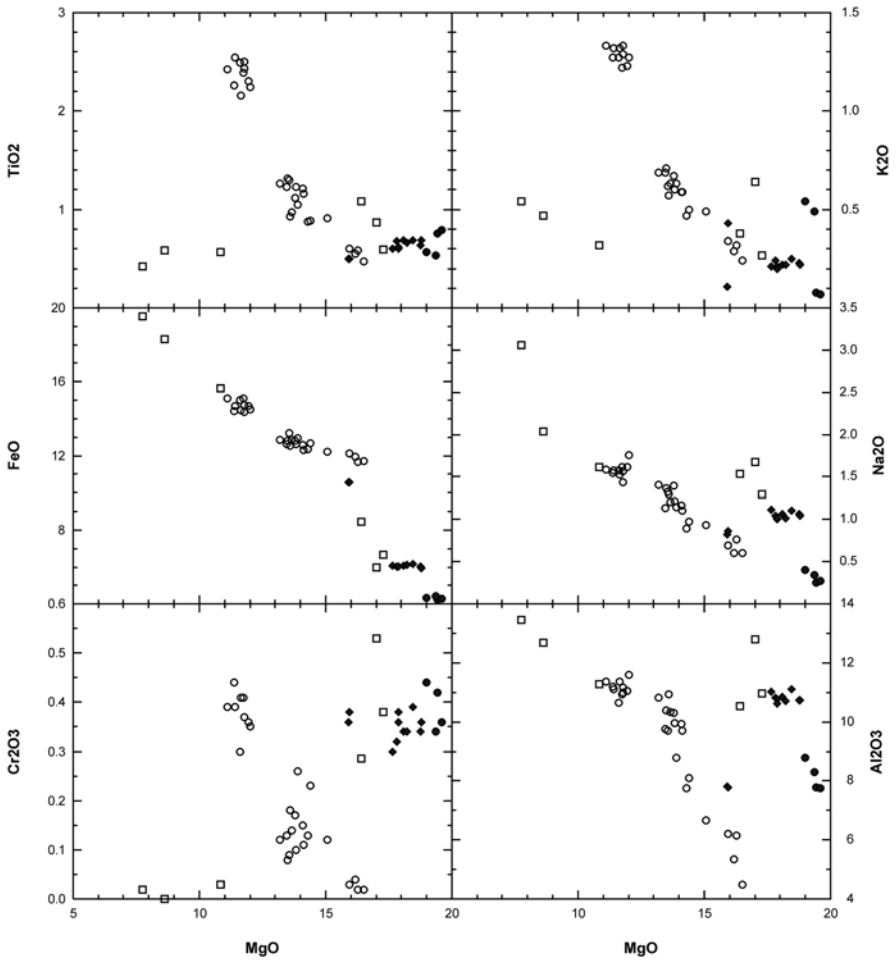

Fig. 8.13 Chemical compositions of amphibole in Red River mafic and ultramafic shown in relation MgO versus Al_2O_3, Cr_2O_3, Na_2O, and TiO_2; *pointed*: amphibole in lherzolite, *diamond*: gabbro amphibole, *circled*: pyroxenite amphibole

that their host magmas were generated at relatively deep levels (more than 5–6 Kbar) (Fig. 8.13).

Based on the aluminum contents in clinopyroxenes (Table 8.5) amphibole gabbro may be divided into two groups. The low-Al clinopyroxene ($Al_2O_3 = 2.5–3$ wt%) in amphibole gabbro in the Bao Yen – Bao Ha cross-section and the high-Al clinopyroxene (up to 8 wt%) in amphibole gabbro and garnet-bearing amphibole gabbro in the Mau A – Tan Nguyen cross-section. The difference in Al-contents indicates that the according magmas were generated at different depths, possibly in association with different magma stages, which will be addressed in a later chapter. The

difference of aluminum concentrations in clinopyroxenes from similar rock types but different outcrops suggests that the high Al_2O_3-clinopyroxene containing magmas (gabbro, pyroxenite and peridotite) were formed at relatively higher pressures (6–8 Kbar), comparable to metamorphic parameters that were determined for the surrounding gneiss and garnet amphibolite (Nam et al. 1998). Thus, it may be assumed that formation and intrusion of the high Al-clinopyroxene- bearing mafic and ultramafic magmas in the Red River shear zone may occurred prior to exhumation of the gneiss. In contrast, the low Al-clinopyroxene gabbro may be formed after the exhumation at shallower depths. As described below, the magmatic episodes have been confirmed by Ar-Ar radiometric age dating.

Biotite- amphibole- metagabbro is also outcropped in the Red River shear zone. The rocks are highly metamorphosed; therefore, their magmatic classification and regional geological position are yet clarified. However, being closely associated with biotite-bearing websterite and garnet-bearing amphibole gabbro in the Bao Yen – Bao Ha cross-section these rocks may be belonged to an early magmatic stage of the Red River shear zone. The significant character of these rocks is a clear orientation observed for their biotite and amphibole crystals. Rounded textures comprised of bright-colored amphibole, orthopyroxene and (sometimes) spinel are observed around garnets. Potassic feldspar sometimes is observed among the coexisting minerals in this gabbro type.

8.2.5 Geochemical Characteristics

The chemical compositions of lherzolite, websterite and amphibole gabbro are shown in Table 8.9. In MgO versus Al_2O_3 and CaO diagrams (Fig. 8.14) the lherzolite, pyroxenite and gabbro plot in separate fields, but in SiO_2 versus total alkalis (TAS) diagram, most of ultramafic compositional points fall in the field of mafic rocks. This is explained by the fact that, in contrast with deep mantle magmas, the study rocks are mostly composed of Fe-rich minerals, especially high in orthopyroxene. Even so, because they have high contents of MgO (>25 wt%), low Al_2O_3 and lack of plagioclase, the magmas, therefore, may be classified as ultramafic. The lherzolite and pyroxenite show MgO varying between 35 and 25 wt%; MgO contents in the lherzolite show negative correlation with Al_2O_3 and CaO (Fig. 8.14), consistent with magmatic differentiation trend although there is no correlation between MgO and SiO_2 indicating olivine, not orthopyroxene, was a fractionated phase. Olivine-bearing websterite and pyroxenite form a separate group although their position in the Harker diagram is consistent with an olivine or olivine and orthopyroxene fractionation trend (Fig. 8.14). The magmas are characteristically rich in Al_2O_3, CaO and FeO*, and poor in TiO_2 and total alkalis. The amphibole gabbro forms a group of compositional points at the end of lherzolite – pyroxenite and gabbro evolutional trend. Geochemically, the garnet-bearing gabbro and garnet-free gabbro are not distinguishable; they both are equally low in Al_2O_3 (<17 wt%), TiO_2 (<1 wt%) and P_2O_5; while based on alkali contents they belong to mafic group

Table 8.9 Chemical compositions (wt%, by XRF) and trace element abundances of Red River mafic and ultramafic magmas (After Izokh et al. 2004; Hoa et al. 2005)

Sample	H1591	H1599	H1701/1	H1701/2	H1704*	H1706	H1711*	H1711/1*	H1714	H1716
	1	2	2	3	4	4	4	4	4	4
SiO_2	44.88	47.81	48.35	47.11	49.64	48.84	50.49	49.57	52.99	52.09
TiO_2	3.85	1.09	1.42	1.49	1.33	0.99	1.01	0.99	0.54	0.63
Al_2O_3	12.81	14.98	11.89	10.58	16.28	14.2	14.49	14.46	16.34	16.04
Fe_2O_3	16.99	11.5	11.18	13.43	10.86	11.38	11.31	11.33	7.7	9.66
MnO	0.25	0.18	0.18	0.21	0.16	0.19	0.21	0.25	0.17	0.19
MgO	6.25	8.31	9.34	13.34	7.68	8.45	8.11	8.24	8.05	7.81
CaO	8.96	12.65	14.45	11.1	12.7	13.21	12.56	12.35	12.36	12.02
Na_2O	2.16	2.06	1.59	1.27	0.49	1.28	0.3	0.41	0.4	0.3
K_2O	1.99	0.42	0.66	0.35	0.42	0.42	0.71	0.55	0.44	0.64
P_2O_5	0.65	0.08	0.13	0.11	0.15	0.09	0.09	0.08	0.05	0.06
LOI	0.52	1.06	0.76	0.79	0.04	0.71	0.91	1.38	0.83	1.2
Total	99.31	100.1	99.95	99.78	99.75	99.76	100.1	99.61	99.87	100.6
Sc	32.19	36.99		33.39	41.12		38.57		36.09	36.79
Rb	91.14	11.73		3.40	5.34		11.57		8.15	18.98
Sr	380.03	201.77		165.98	265.95		106.32		126.30	100.26
Y	44.53	17.06		18.04	28.55		22.10		12.63	14.65
Zr	34.08	25.53		36.90	15.13		18.83		15.39	14.58
Nb	46.49	2.94		4.85	5.48		6.28		4.11	3.84
Cs	1.22	0.37		0.19	0.17		0.63		0.35	0.90
Ba	619.33	51.61		8.22	8.33		152.09		27.85	49.62
La	51.62	3.19		6.32	14.08		8.82		7.90	9.08
Ce	100.00	7.82		13.93	27.29		16.29		13.77	17.02
Pr	13.65	1.08		1.87	3.17		2.04		1.81	1.99

Nd	53.82	5.15		8.13	12.59		7.87		6.58	7.51
Sm	12.42	2.11		2.89	3.96		2.50		1.62	2.26
Eu	3.38	0.76		1.07	1.10		0.75		0.54	0.61
Gd	9.22	2.10		2.53	3.81		2.70		1.79	2.01
Tb	1.60	0.44		0.51	0.75		0.57		0.35	0.40
Dy	8.61	2.83		3.10	4.79		3.66		2.25	2.58
Ho	1.74	0.67		0.65	1.08		0.87		0.49	0.57
Er	4.26	1.68		1.60	2.94		2.24		1.32	1.60
Tm	0.54	0.24		0.21	0.41		0.36		0.19	0.22
Yb	3.84	1.76		1.38	2.99		2.30		1.39	1.49
Lu	0.54	0.25		0.21	0.46		0.36		0.19	0.23
Hf	1.41	0.80		1.05	0.77		0.85		0.61	0.60
Ta	3.16	0.19		0.11	0.44		0.38		0.29	0.22
Pb	5.36	1.10		1.56	14.62		2.86		3.13	5.12
Th	2.00	0.33		0.67	3.64		2.34		2.12	1.95
U	0.47	0.08		0.22	0.72		0.48		0.35	0.37

Sample	H1717	H1708	H1713	H1722	H1722/1	H1720	H1720/1	H1720/2	H1719/1	H1718
	4	5	5	5	5	6	6	6	6	6
SiO_2	50.87	46.06	50.02	45.5	46.59	51.04	50.4	49.42	46.33	46.25
TiO_2	0.38	0.8	0.49	0.88	0.78	0.18	0.17	0.14	0.25	0.23
Al_2O_3	14.92	8.17	9.82	9.55	12.53	5.99	5.54	4.62	5.94	4.88
Fe_2O_3	8.6	14.1	11.55	10.96	10.29	9.73	10.11	9.64	11.38	13.21
MnO	0.13	0.2	0.19	0.19	0.2	0.18	0.19	0.19	0.21	0.21
MgO	9.36	21.34	16.35	20.79	20.19	25.03	27.16	28.71	30.14	30.81

(continued)

Table 8.9 (continued)

Sample	H1717	H1708	H1713	H1722	H1722/1	H1720	H1720/1	H1720/2	H1719/1	H1718
	4	5	5	5	5	6	6	6	6	6
CaO	12.22	8.26	7.63	9.8	6.66	4.78	3.75	3.64	2.55	2.55
Na_2O	1.04	0.3	0.4	1.61	1.04	1.47	1.24	1.24	0.9	0.67
K_2O	0.89	0.19	0.4	0.25	0.19	0.33	0.29	0.27	0.12	0.13
P_2O_5	0.04	0.09	0.04	0.06	0.07	0.03	0.03	0.03	0.03	0.03
LOI	1.52	0.99	1.96	0.52	1.09	1.04	0.52	0.98	1	0.16
Total	99.97	100.5	98.85	100.11	99.63	99.8	99.4	98.88	98.85	99.13
Sc		17.99	20.20	25.40			17.39			11.74
Rb		0.77	5.69	1.67			4.65			0.01
Sr		47.21	6.16	56.60			57.55			34.16
Y		16.40	11.02	10.62			4.33			4.74
Zr		22.90	34.79	29.29			13.35			11.76
Nb		4.66	2.64	0.90			1.08			1.23
Cs		0.08	1.38	0.24			0.07			0.04
Ba		21.98	4.43	30.85			48.50			20.04
La		13.10	5.46	4.43			2.95			2.92
Ce		22.54	10.40	9.20			5.19			5.88
Pr		2.66	1.37	1.33			0.59			0.71
Nd		10.36	5.28	5.92			2.28			2.52
Sm		2.63	1.59	1.90			0.60			0.76
Eu		0.44	0.33	0.66			0.12			0.13
Gd		2.07	1.42	1.72			0.50			0.56
Tb		0.40	0.28	0.32			0.10			0.12
Dy		2.35	1.84	1.95			0.69			0.77
Ho		0.50	0.41	0.44			0.15			0.18
Er		1.32	1.13	1.13			0.45			0.45

Tm		0.17	0.14	0.16			0.07			0.06
Yb		1.19	1.07	1.05			0.47			0.49
Lu		0.17	0.18	0.16			0.08			0.08
Hf		0.91	0.95	0.86			0.28			0.26
Ta		0.14	0.19	0.01			0.07			0.05
Pb		0.94	1.19	0.47			2.23			0.33
Th		3.18	1.49	0.41			0.83			0.74
U		0.53	0.29	0.06			0.20			0.16

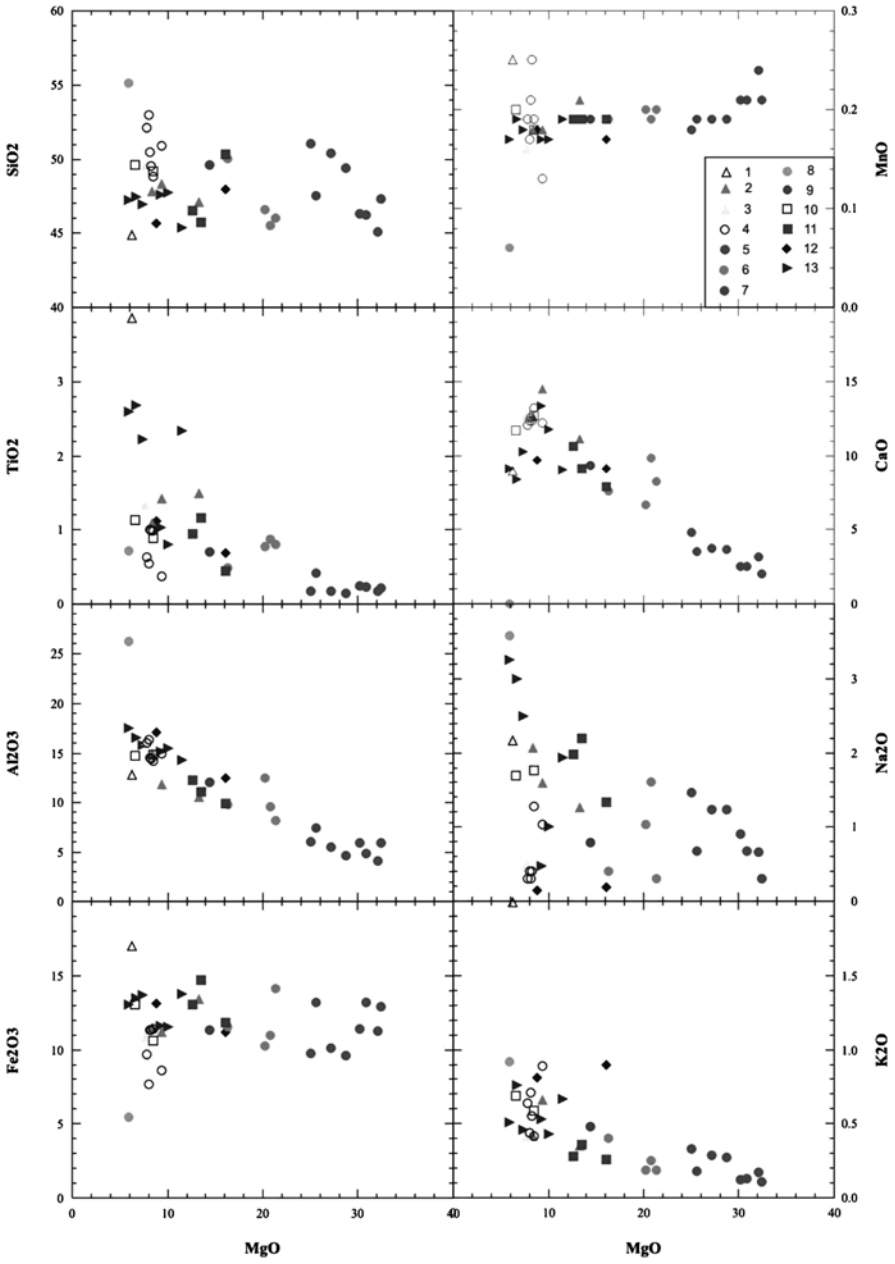

Fig. 8.14 Chemical compositions of the Red River mafic and ultramafic shown in the Harker diagrams. *Symbol* numbers in figure correspond to Table 8.9

of normal alkalinity (Table 8.9). An exceptional case include a metamorphosed gabbro (H-1591), having characteristically high TiO_2 (3.85 wt%), Fe_2O_3 (=16.89 wt%) and K_2O (1.99 wt%). Having high concentrations of TiO_2, K_2O and P_2O_5 and showing distinct rare earth element distribution characteristics the metamorphosed gabbro may be classified as sub-alkaline gabbroid type. The classification poses a question on the presence of the synchronously metamorphic sub-alkaline mafic magma type in the Red River fault zone that should be further investigated for clarification. The topic has yet been studied by the authors. The amphibole gabbro in the Tan Huong ruby mine area falls in a transitional position between amphibole gabbro (for example, the Mau A type) and high-potassium gabbroid. It is highly possible that detailed study of syn-motion magmatic activities may be able to establish particularly regional compositions for various magmatic associations.

Regardless of the similarity in chemical compositions among amphibole gabbro magmas from various areas in the Red River fault zone they are different by having different REE contents and thus different distribution configuration patterns. (Table 8.9; Fig. 8.15a). The REE concentrations in amphibole gabbro in the Bao Yen area are low, about 10 times surpassing that of the Chondrite, showing weak fractionation and slight Eu negative anomaly. The La/Sm and Ce/Yb ratios, respectively, are 0.94–01.1 and 1.11–2.5. On primitive mantle normalized trace element

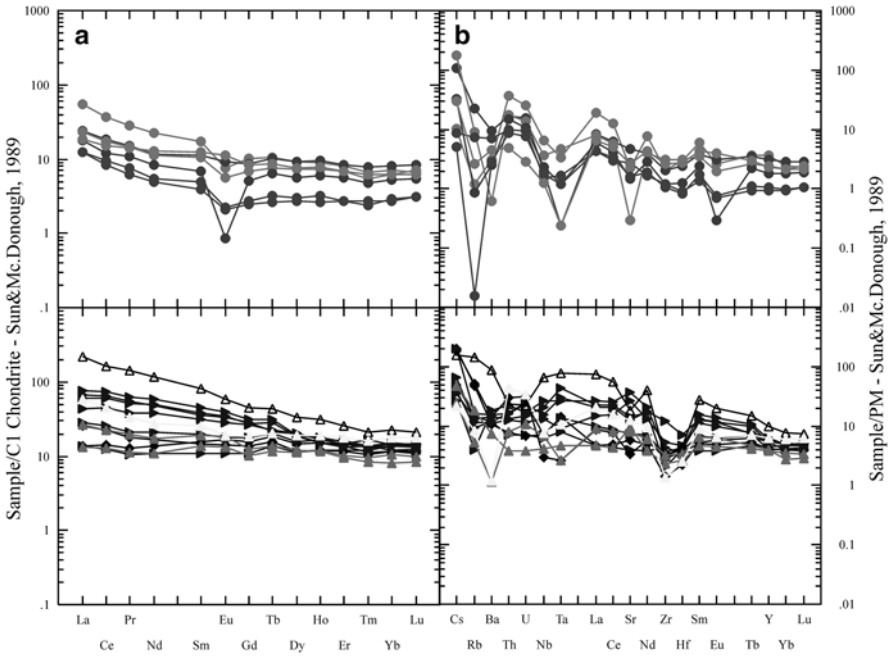

Fig. 8.15 Chondrite (**a**) and primitive (**b**) mantle normalized rare earth and trace element distribution patterns of the Red River mafic and ultramafic magmas. *Symbols* as in Fig. 8.14

curve for a gabbro negative anomalies are observed at Zr and Hf, while positive anomalies being observed at Rb, Th, U and Sr (Fig. 8.15b). A metamorphosed monzogabbronorite (H-1591) show geochemical features mostly different for those of the above amphibole gabbro in that it is comparably richer in REE, showing stronger elemental fractionation; having different La/Sm and Ce/Yb, respectively, at 2.6 and 6.55, and no Eu negative anomaly. The metamorphosed rock has negative anomalies at Zr, Hf and Y, and positive anomalies at Rb, Nb, Ba, Th and U in a primitive mantle normalized trace element distribution curve.

Chondrite normalized rare earth element patterns are similar for lherzolite, pyroxenite and amphibole gabbro in the Mau A – Tan Nguyen cross-section (Fig. 8.15a), their concentrations are 10–50 times higher compared with the chondrite. The relative enrichment in REE among the study mafic and ultramafic magmas is consistent with an expected fractional trend from a parental picrite or picrite-dolerite melt. The lowest REE concentrations are recorded for lherzolite and olivine-bearing websterite; although the values are still higher compared with those in typical mantle-derived peridotites. Weak but clear trough is observed for Eu of the magmas. Amphibole gabbro and garnet-bearing gabbro show similar normalized REE distribution patterns suggesting that genetically belonging to a same magma series. The presence or absence of garnet in the gabbroids may be related to the ferrousity in their corresponding melts or depths of melt generation. Basically, the REE fractionation characteristics are much clearer for magmas in the Mau A area as compared to those in Bao Yen. The ratios of La/Sm and Ce/Yb in lherzolite, pyroxenite and amphibole gabbro, respectively, are 2.4 and 3.0, 2.15 and 2.4; and 2.2 and 2.3, closely comparable. The primitive mantle and chondrite normalized trace and rare earth element patterns of the mafic and ultramafic magmas at the Mau A cross-section are mostly similar to those in the Bao Yen area. A dyke-phased amphibole- gabbrodolerite shows geochemical features that are matched with the above mentioned mafic magmas, suggesting that the geochemical composition may appear to be that of primary picrite-dolerite for MgO content in this gabbrodolerite surpassing 14 wt%.

The preliminary initial $^{87}Sr/^{86}Sr$ isotopic ratios of the lherzolite are very high, at 0.7306, accompanied by very low $\varepsilon_{Nd(0)}$), at −8.04 (Hoa 2007), most certainly reflect crust-origin or strongly contaminated by crustal materials. However, this should be further studied to clarify.

8.2.6 Formation Age and Geodynamic Settings

Mafic and ultramafic magma samples in the Red River zone were collected for radiometric age dating including six amphibole gabbro from different areas, such as sample H-1701/2, a high-Mg- plagioclase hornblendite from a homogenous magma block in Bao Yen; other samples H-1706, H-1711, H-1716 and H-1722 collected at the Mau A – Tan Nguyen cross-section. H-1706 is an amphibole gabbro from a large boudin in gneiss. H-1711 is a garnet bearing- amphibole gabbro;

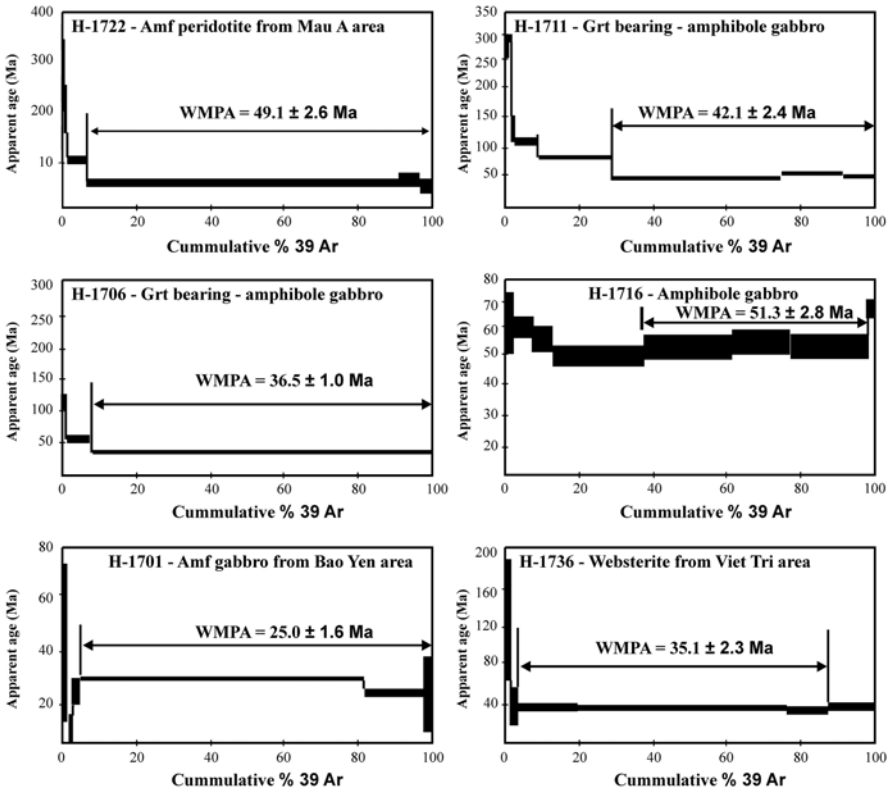

Fig. 8.16 Ar-Ar ages of gabbroids in the Red River zone. See explanations in the text

H-1716 is an amphibole gabbro from a differentiated body in contact with blastomylonite; H-1722 is equivalent to a srisgeimite in lherzolite; and H-1736 is an olivine- amphibole- bearing websterite collected at a quarry in Yen Kien (Viet Tri). The results revealed that, the garnet bearing-amphibole gabbro samples are the oldest, showing H-1711 at 42.1 ± 2.4 Ma, H-1716 at 51.3 ± 2 Ma and H-1722 (a srisgeimite in lherzolite) at 49.1 ± 2.6 Ma. The samples showed indication of Ar-surplus thus it is difficult to estimate the validity of the age results. Sample H-1706 south of Mau A and H-1736 from Viet Tri show ages, respectively, at 35.5 ± 1 Ma and 35.1 ± 2.3 Ma, whereas H-1701/2 (hornblendite) from Bao Yen (northeast margin of the Bao Yen – Bao Ha cross-section) is youngest, at 25 ± 1.6 Ma (Fig. 8.16). There was no Ar-surplus observed in the latter samples thus the age data are meaningful. The ages indicate that the magma formation was occurred synchronously with the Red River shear motion-induced metamorphism. The age data also indicate that the mafic and ultramafic associations are not fragments of older layered mafic and ultramafic massifs. In summary, there are two mafic and ultramafic magmatic stages occurred during the formation and evolution of the Red River fault zone. An early, pre-exhumation, stage produced lherzolite, pyroxenite

and garnet-bearing amphibole gabbro; while the later (post-exhumation) produced amphibole gabbro and hornblendite.

Geological and geochemical characteristics of the peridotite, pyroxenite and amphibole gabbro in the Red River high grade gneiss metamorphic formations suggest that these magmas subsequently formed a uniform mafic – ultramafic lherzolite-websterite-gabbro association via fractional crystallization process. The latter occurred as veins, dykes and sills, being crosscut or deformed into boudinage by regional geodynamic processes. Although some undeformed gabbrodolerite dykes are occasionally found elsewhere (such as at the Mau A – Tan Nguyen cross-section). The (differentiated) magmas may be divided into two pressure-dependent types. The amphibole gabbro, websterite and high-Al pyroxene bearing- lherzolite may be crystallized at pressures on lower than 6–8 Kbar. The other, amphibole gabbro in the Bao Yen (Yen Bai), according to field survey and its fine-grained doleritic texture, may be crystallized after the major phase of gneiss exhumation and shear motion-induced deformation. The geochemical characteristics suggest that primary melts from different areas may be different although there may be some similar features shared among the melts as mentioned above. However, when larger-scaled, regional mantle source domain is taken into account, geochemical characteristics of the primary melts must be homogeneously uniform; therefore the differentiated magmas may be viewed as syn-magmatism.

Preliminary radiometric chronology study indicates two stages of mafic – ultramafic magmatic activities in the Red River shear zone: an early stage at about 35 Ma and a later at about 25 Ma. The early stage was coincided with the timing of intraplate extension-induced magmatism, happened prior to gneiss exhumation in the Red River zone following the India – Eurasian collision. The later stage occurred at about 25 Ma with the formation of hornblendite and amphibole gabbro at lower pressures, after the major exhumation phase thus lacking Ar-surplus.

From the above descriptions following suggestions may be present: within the Red Rive zone it is needed to establish new geological divisions of mafic and ultramafic magmatic associations according to pre-, syn- and post-shear motion magmatism. The presence of high temperature mantle-derived magmas at different formation and evolution stages of the Red River fault zone provides new perceptions of the most important geological structure in current southeast Asian tectonics.

8.3 Granite Formations in the Red River Shear Zone

Biotite granite and garnet-bearing granite are popular in the Red River fault zone. The magmas are near-euhedral texture, relatively uniform structure, indicating melts of common source before reaching shallower levels. Their formation ages have been determined to occur between 24 and 22 Ma (see below). The presence of undeformed or weakly deformed is believed to mark the end of a major phase of strong motion, in terms of both amplitude magnitude, along the Red River fault

zone from the Oligocene. Besides, among paragneiss and high-Al crystalline schist outcrops in the Red River zone a large number of bright-colored granite aplite and granite pegmatite rocks are also found. The latter appear as dykes or sills, similar occurrence for leucosomes in migmatized formations. Thus, the cause of on-site, anatexis melting of these magmas was apparently related to the motion along the Red River Shear zone (Tapponnier et al. 1986). Ar-Ar age dating for the magmas showed values between 21.1 ± 0.9 and 21.2 ± 0.2 Ma (see below), suggesting the granites may be the youngest occurred in the Red River gneiss. Also, the presence of syn-deformed felsic formations may suggest that the shear motion in the Red River zone may continue after a short quiescence between 24 and 21 Ma. However, the felsic magma is an in-situ type, occurred in Red River gneiss after the metamorphic rock being exhumed to relatively shallow, near surface, level.

8.3.1 Biotite Granite and Leucogranite Associations

Garnet granite – leucogranite bodies are massive structured, undeformed or weakly deformed, distributed widely in gneiss and crystalline Bi + Gr + Sil ± Cor schist in the Red River zone. The granite magmas spread from Lao Cai via Bao Yen and Long Khanh to Yen Binh, Tan Huong and possibly elsewhere (Fig. 8.4). The granite bodies appear as small outcrops, from several hundreds of squared meters running up to thousands meters long and hundreds of meters wide. Representing the magmas are three blocks, including Long Khanh, Trung Tam and Tan Huong, occurred along National Route 70 (QL-70) fault (Fig. 8.17). They show pseudo-conformity contacts with surrounding crystalline schist; the contacts are sharp, along which zones of feldsparization and biotization are sometimes developed. The magma is fine- medium- grained biotite granite, occasionally porphyric and bright-colored granite, containing a small amount of garnet and tourmaline and less than 5 %.vol of biotite. Therefore, basing on the geological characteristics and rock-forming mineral assemblage these granites are different from dyke-sill phased granite aplite and pegmatite of anatexis-origin as mentioned above. Instead, the biotite granite and leucogranite are termed as Tan Huong granite-type (Hoa 2000).

8.3.2 Petrologic, Mineralogical and Geochemical Characteristics

The Tan Huong-type granitoid is divided into two varieties based on their mineralogical compositions: biotite granite (with biotite >5–7 %.vol) and leucogranite (biotite <5 %.vol). The granites are usually porphyric and fine- to medium-grained intergranular texture. The phenocrysts include potassic feldspar showing sizes from 1–2 mm to 3–4 mm, highly euhedral. The amount of feldspar always surpass

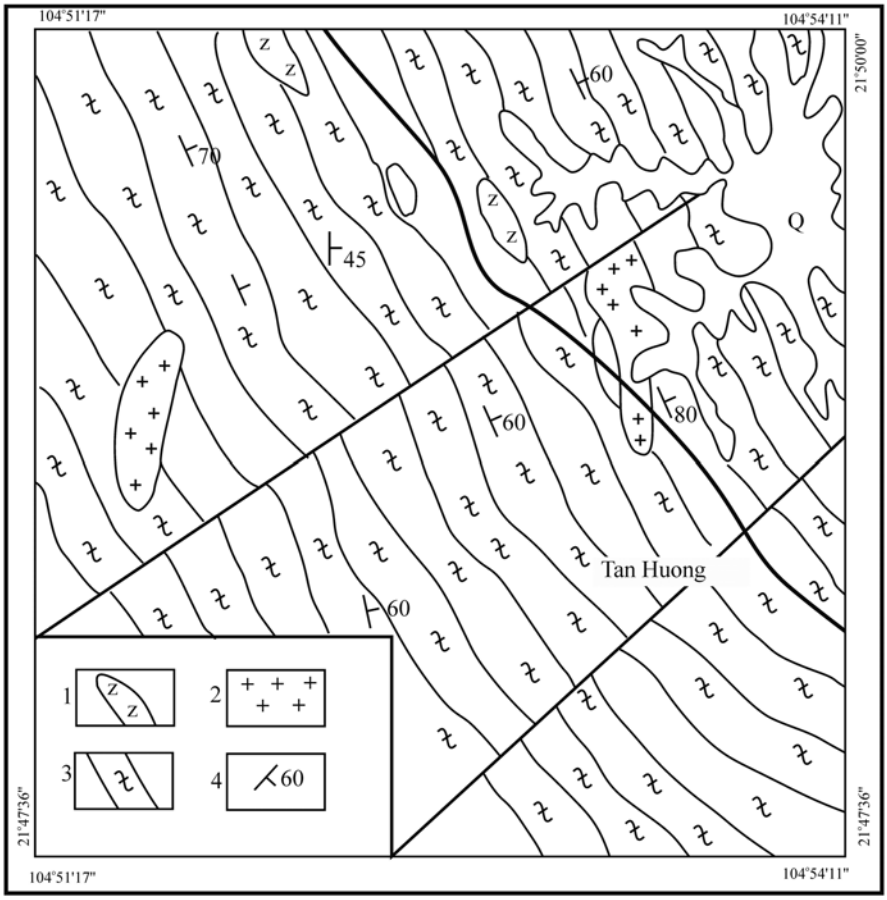

Fig. 8.17 Scheme of geological distribution of Tan Huong –type leucogranite in the Long Khanh and Dong Tam areas (Hoa et al. 2000); *1*. Amphibolite, *2*. Granite, leucogranite, *3*. Biotite-silimanite-garnet gneiss, *4*. Schist-applying plane

accompanying plagioclase. The granite is uniformly structured. Unmodified minerals show idiomorphic degree decreasing in the following order Bi, Pl, Gr, Fsp and Q. Sometimes the magmas show weak orientation structure. Microscopic observation reveals micro-quartz fragments served as cementing feldspar, plagioclase, biotite, etc., suggesting that the rock may have been slightly crashed. Compared with the surrounding gneiss and crystalline schist deformation in the granitoids is weak that occurs only in the vicinity to faulting sites. Minerals that are easily affected by external impact, such as quartz, are seen to be clearly deformed in the crashed magmas.

The rock-forming mineral assemblage is identical for both granite and leucogranite, including Q + Ksp ($Or_{83–86}$ $Ab_{14–12}$) + Pl (An_{45} Ab_{55}) + Bi ± Gr ± Mus. Biotite in granite at the Long Khanh and Trung Tam blocks is brown or brownish red, while the

biotite in Tan Huong is greenish brown. Their chemical compositions are equivalent to siderophyllite – annite (?), showing relatively high TiO_2 (=2–4 wt%), FeO (=23.5–26.9 wt%, f = 68–78), very high Al_2O_3 (=16–20 wt%) and low MgO (=1.77–4.1 wt%), which are typical for biotites in high-Al granites (S-type granite) (Table 8.10). The biotite is sometimes partially chloritized or muscovitized. The biotite also contains some amount of F, up to 0.68–0.7 wt%.

Accessory minerals in the granites include garnet and zircon where garnet is present in both biotite granite and leucogranite. The garnet is cubic, relatively idiomorphic, almost undeformed by external effect, except for broken grains being filled up by quartz fragments. Garnet may be the only high-Al phase mineral in the Tan Huong granitoids.

Chemical compositions of biotite granite and leucogranite show SiO_2 contents, respectively, of 73 wt% and >74 wt%; their total alkalis vary from low, medium to high at 7.3, 8.67 wt% and 9.3 wt%, respectively. The granitoids are more potassic with $K_2O/Na_2O = 1.16–2.87$, with K_2O concentrations being higher than 5 wt%, sometimes even reaching to 6 wt%, equivalent to those of sub-alkaline and alkaline types. Correlations between K_2O and SiO_2 contents (not shown) reveal that most of

Table 8.10 Chemical compositions (wt%) of biotite (Bi), plagioclase (Pl) and K-feldspar (Ksp) in the Red River zone

Sample	LY-5092	SH-36	SH-34	SH-34-1	SH-33	SH-34-1	SH-34-2
Mineral	Bi	Bi	Bi	Bi	Pl	Ksp	Ksp
SiO_2	33.37	34.74	36.63	33.15	56.28	65.26	65.26
TiO_2	4.05	1.96	2.22	2.05			
Al_2O_3	16.29	20.1	17.72	17.79	26.98	18.8	18.41
Cr_2O_3	0.02						
FeO	26.9	26.07	23.54	26.34	0.59	0	0.01
MnO	0.54	0.44	0.29	0.26			
MgO	4.1	20.6	1.77	2.02			
CaO	0.01	0.1	0.04	0.25	9.22	0.05	0.05
Na_2O	0.21	0.17	0.14	0.28	6.27	1.59	1.34
K_2O	9	8.64	8.09	8.35	0.11	4.2	4.64
Cl		0.03	0.05	0.05			
F		0.78	0.78	0.68			
Si	2.53	2.749	2.966	2.756	2.545	2.992	3.004
Ti	0.23	0.117	0.135	0.128			
Al	1.45	1.875	1.691	1.761	1.438	1.016	0.999
Fe	1.705	1.726	1.594	1.832	0.022		
Mg	0.465	0.243	0.213	0.251			
K	0.87	0.873	0.836	0.886		0.83	0.86
F		0.196	0.199	0.179			
Na					0.55	0.141	0.119
Ca					0.447		

Remarks: LY-5092: biotite granite, Long Khanh block; SH-33: leucogranite, Trung Tam block; SH-34, SH-36: biotite granite and leucogranite, Tan Huong block (After Hoa et al. 2000)

the granitoids fall in potassic calc-alkaline field; where the Tan Huong granite is especially rich in K-feldspar having K_2O contents equivalent to a sub-alkaline magma type (such as shoshonite). This is the basic difference between Tan Huong type granite and granite aplite and pegmatite, termed as stress-granite mentioned earlier (after Tapponnier et al. 1990).

Most of the study granitoids show high Al_2O_3 contents, especially the leucogranite, showing a content that is equivalent to a S-type granite. However, generally high K_2O and total alkalis, low Al_2O_3 as compared to typical Sr-type granites are specific characteristics of the Tan Huong –type biotite granite and garnet-bearing leucogranite.

The granitoids are high in Rb (263–609 ppm), very low in Sr (51–93 ppm) and Zr (63–154 ppm) as compared to Permian – Triassic high-Al biotite granite elsewhere in northeastern Viet Nam (Table 8.11). The Nb and Y in most of the granitoids are high, especially in Tan Huong and Trung Tam granites. Correlations between $(Na_2O+K_2O)/CaO$ vs. $(Zr+Nd+Ce+Y)$ and Rb vs. $(Nb+Y)$ show the granitoids having geochemical features similar to post-collision granite-types (Fig. 8.18).

Ratios of Rb/Sr in the granitoids are variable (3–11) but many samples show Rb/Sr ratios high between 9.4 and 11. The Zr/Y ratios are also variable, from 0.8 to 14.5 (Table 8.11). The highly variable ratios may be related to the variability of rock-forming minerals, especially the K-feldspar and garnet in granitoids from different magma blocks as described above.

The granitoids are rich in light rare earths with La/Sm = 4.2–7.97 and Ce/Yb = 9.38–71.3, showing steep curve from the light to heavy rare earths and relatively large negative anomaly at Eu. (Fig. 8.19). The dark-colored magma (biotite granite) is usually richer in the rare earths as compared with the light colored (leucogranite). Absolute concentrations of the rare earths in the biotite granite are as enriched as those in syn-collision Himalaya-type granite; besides the garnet-bearing granitoids are normally more enriched in heavy rare earth (Yb, Lu) relative to the garnet-free type (Table 8.11). The Th, U and Ta in the study magmas are also high, respectively, at 35–80 ppm, 3–30 ppm and 3.1–6.1 ppm; their Th/U ratios are 1.93–8.17 vastly equivalent to those in metapelite rocks (Nojzkin 1997).

8.3.3 Isotopic Characteristics

The $^{87}Sr/^{86}Sr$ and $^{143}Nd/^{144}Nd$ isotopic ratios of biotite granite in the Trung Tam block yielded values, respectively, of 0.7277 and 0.512136 ($\varepsilon_{Nd(0)} = -9.79$ and $T_{DM} = 1.57$Ga), suggesting a crust-origin. These values are vastly different from those of typical crust-origin Permian – Triassic melagranite and high-Al biotite granite in northeastern Vietnam at (unpublished data) $^{87}Sr/^{86}Sr = 0.73285–0.7358$; $^{143}Nd/^{144}Nd = 0.511965–0.512033$, $\varepsilon_{Nd(0)} = (-11.8)–(-13.3)$, $T_{DM} = 1.79–2.19$ Ga. It is regrettable that isotopic studies of granitoids in northeastern Viet Nam in general and in the Red River zone in particular, are scarce; therefore, the above isotopic

Table 8.11 Major (wt%) and trace element compositions in granitoids in the Red River (1–6), Phu Ngu (7) and Lo Gam (8–9) belts

Sample ID	LY5092	LY281/1	SH-33	SH-33/1	SH-34	SH-36	228A/76	LY10502	LY10601
Rock type	GB	GB	LG	LG	GB	LG	GB	GB	GB
	1	2	3	4	5	6	7	8	9
SiO_2	73.15	73.47	75.42	74.21	73.85	74.16	71.75	70.91	71.53
TiO_2	0.18	0.09	0.09	0.12	0.08	0.09	0.12	0.43	0.46
Al_2O_3	13.75	14.33	13.44	13.83	13.39	13.39	15.14	14.14	13.89
Fe_2O_3	2.04	0.87	1.19	2.14	1.68	2.08	1.41	3.64	3.43
MnO	0.04	0.02	0.03	0.05	0.04	0.05	0.05	0.05	0.03
MgO	0.97	0.17	<0.10	0.5	0.21	0.2	0.26	0.9	0.6
CaO	0.83	1.26	0.87	0.68	1.02	1.05	0.63	1.5	1.88
Na_2O	2.57	3.39	2.34	1.89	4.3	3.78	2.44	2.31	1.73
K_2O	6.05	5.28	4.91	5.43	5.01	5.08	6.72	5.18	5.48
Na_2O+K_2O	8.62	8.67	7.25	7.32	9.31	8.86	9.16	7.49	7.21
K_2O/Na_2O	2.35	1.55	2.09	2.87	1.16	1.34	2.75	2.24	3.17
Rb	372	263	524	480	534	609	254.00	420	205
Sr	93	84	55.3	51	56	54.8	58.00	128	239
Zr	118	154	62.9	63.8	95.9	105	109.00	175	595
Nb	26.8	21.5	46.9	94.6	23.1	33.3	7.80	7.15	23.7
Y	10.4	10.6	45	73.3	52.4	34.8	38.70	57	26.4
Rb/Sr	4.00	3.13	9.48	9.41	9.54	11.11	4.38	3.28	0.86
Zr/Y	11.35	14.53	1.40	0.87	1.83	3.02	2.82	3.07	22.54
La	57	32.76	18		24		19.74	45	49
Ce	92	56.39	30		45		40.03	86	101
Nd	36	23.62	12		23		18.76	33	42
Sm	7.5	4.11	3.1		5.7		4.05	7	8.2
Eu	0.7	0.66	0.36		0.54		0.44	0.73	2.6
Gd	5.4	3.68	3.5		6.1		4.11	6.4	6
Tb	0.81	0.49	0.65		1.06		0.83	1	0.85
Yb	1.29	1.33	3.2		4		4.67	3	1.25
Lu	0.17	0.25	0.52		0.62		0.69	0.42	0.17
La/Sm	7.60	7.97	5.81		4.21		4.87	6.43	5.98
Ce/Yb	71.32	42.40	9.38		11.25		8.57	28.67	80.80
Th	80	49	35		58		10.40	38	21
U	17	6	12		30		4.30	12	2.3
Ta	3.4	0.64	6.1		3.1		1.31	1.2	0.89
Hf	4.4	6.75	2.8		3.3		4.08	5.4	11
Th/U	4.71	8.17	2.92		1.93		2.42	3.17	9.13

Explanations: Red River Paleogene granitoids: 1- Long Khanh block; 2,3,4- Trung Tam block; 5,6- Tan Huong block; shown for comparison are Permian – Triassic high-Al granites in northeastern Viet Nam: 7- Phia Bioc massif; 8- Nac Con block; 9-Tich Coc; GB- biotite granite; LG-leucogranite. The major elements and Rb, Sr, Zr, Nd and Y were analyzed by XRF; rare earth and Th, U, Ta and Hf by instrumental neutron activation analysis (INAA) at Institute of Geology and Geophysics, Novosibirsk. Samples Y-281/1 and 228A/76 were analyzed by ICP-MS at Institute of Earth Sciences, Academia Sinica, Taiwan

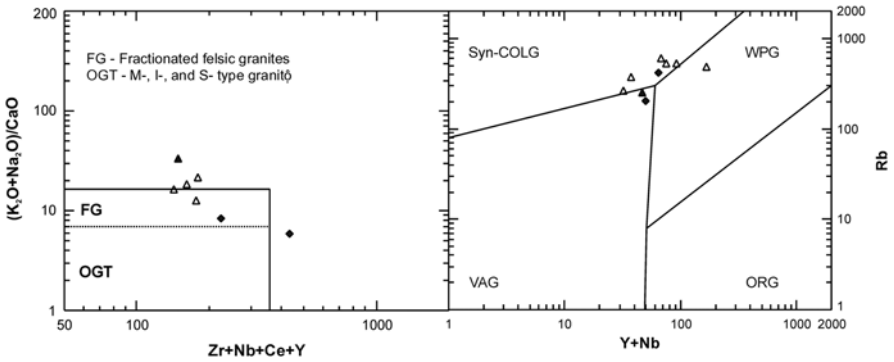

Fig. 8.18 ($K_2O + Na_2O$)/Ca versus (Zr + Nb + Ce + Y) (Whalen et al. 1987) and Rb versus Y + Nb (Pearce et al. 1984) discrimination diagrams for Cenozoic granites in the Red River fault zone

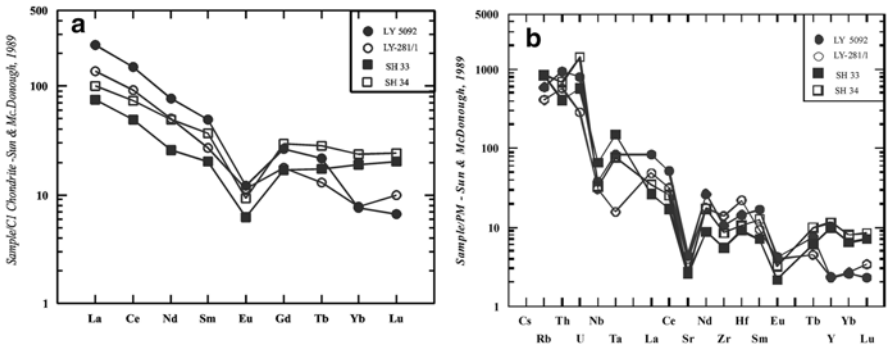

Fig. 8.19 Chondrite (**a**) and primitive mantle (**b**) normalized rare earth and trace element distribution patterns of Red River Cenozoic granites. Normalizing data from Sun and McDonough. 1989. *Symbols* are as in Fig. 8.3

features are preliminary. Nevertheless, the data have suggested that melts of Cenozoic granites in the Red River zone as well the Mesozoic types elsewhere in northeastern Viet Nam were generated from Precambrian sources.

8.3.4 Formation Ages

Ar-Ar radiometric dating method has been applied on biotite and plagioclase from Tan Huong and Trung Tam biotite granite and leucogranite. Results given in Table 8.12 and Fig. 8.20 show formation ages of Tan Huong –type biotite granite and leucogranite lie between 24 and 22 Ma, correspondent to late Oligocene – early Miocene.

Table 8.12 $^{40}Ar/^{39}Ar$ isotopic ratios determined for leucogranite (SH-33) and garnet-bearing biotite granite (SH-34)

Level	Age (mil. yr)	$^{40}Ar/^{39}Ar$	$^{38}Ar/^{39}Ar$	$^{37}Ar/^{39}Ar$	$^{36}Ar/^{39}Ar$	Cumulate ^{39}Ar. %
SH-33 (Biotite)						
1	19.1 ± 4.8	9.43 ± 0.133	0.155 ± 0.0024	0.004 ± 0.0044	0.026 ± 0.0015	1.8
2	22.7 ± 0.4	2.75 ± 0.011	0.152 ± 0.0012	0.002 ± 0.0004	0.002 ± 0.0001	25.5
3	22.6 ± 0.3	2.75 ± 0.016	0.151 ± 0.0010	0.005 ± 0.0001	0.002 ± 0.0000	48.6
4	23.6 ± 0.4	3.50 ± 0.010	0.151 ± 0.0011	0.019 ± 0.0005	0.005 ± 0.0001	59.9
5	24.7 ± 0.5	3.40 ± 0.013	0.162 ± 0.0012	0.017 ± 0.0004	0.004 ± 0.0001	77.7
6	24.3 ± 0.5	3.43 ± 0.052	0.154 ± 0.0035	0.017 ± 0.0003	0.004 ± 0.0001	93.4
7	31.1 ± 0.6	6.13 ± 0.030	0.154 ± 0.0012	0.074 ± 0.0009	0.011 ± 0.0002	100
J = 0.00642 ± 0.000062. Σ : 23.98 ± 0.17 tr.n						
SH-33 (Plagioclase)						
1	20.7 ± 0.4	3.80 ± 0.021	0.022 ± 0.0003	0.047 ± 0.0012	0.007 ± 0.0001	7.6
2	22.7 ± 0.5	3.40 ± 0.009	0.022 ± 0.0002	0.176 ± 0.0007	0.005 ± 0.0001	17.4
3	25.1 ± 0.6	4.38 ± 0.016	0.031 ± 0.0002	0.292 ± 0.0012	0.007 ± 0.0002	24.2
4	24.3 ± 0.7	4.28 ± 0.106	0.020 ± 0.0010	0.083 ± 0.0022	0.007 ± 0.0002	34.6
5	24.5 ± 0.3	2.92 ± 0.008	0.015 ± 0.0001	0.044 ± 0.0002	0.003 ± 0.0000	84.1
6	27.0 ± 0.4	3.91 ± 0.024	0.018 ± 0.0002	0.074 ± 0.0004	0.005 ± 0.0001	97.2
7	50.1 ± 1.5	19.0 ± 0.1	0.051 ± 0.0004	0.342 ± 0.0022	0.049 ± 0.0004	100
J = 0.0064 ± 6.30E-05						
SH-34 (Plagioclase)						
1	16.7 ± 0.5	4.62 ± 0.034	0.017 ± 0.0002	0.028 ± 0.0003	0.011 ± 0.0001	3.1
2	20.4 ± 0.8	2.68 ± 0.017	0.015 ± 0.0001	0.034 ± 0.0003	0.003 ± 0.0002	11.3
3	22.0 ± 0.3	2.58 ± 0.008	0.014 ± 0.0001	0.081 ± 0.0004	0.003 ± 0.0000	19.4
4	21.7 ± 0.5	3.18 ± 0.010	0.015 ± 0.0001	0.082 ± 0.0003	0.005 ± 0.0001	29.9
5	22.7 ± 0.4	3.27 ± 0.020	0.015 ± 0.0001	0.045 ± 0.0005	0.005 ± 0.0001	41.3
6	23.3 ± 0.3	3.59 ± 0.025	0.015 ± 0.0002	0.040 ± 0.0003	0.006 ± 0.0001	52.3
7	23.1 ± 0.3	2.96 ± 0.015	0.015 ± 0.0001	0.032 ± 0.0001	0.004 ± 0.0000	82.1
8	23.7 ± 0.5	4.88 ± 0.060	0.017 ± 0.0002	0.158 ± 0.0019	0.010 ± 0.0001	98.5
9	32.5 ± 2.2	30.6 ± 0.2	0.040 ± 0.0004	2.22 ± 0.017	0.094 ± 0.0007	100
J = 0.00687 ± 6.80E-05. Σ : 22.68 ± 0.26 million years						

Therefore timing of intrusive granitoid formation was later relative to the timing of hyper-metamorphic activity in gneiss and crystalline schist in the Red River fault zone between 35 and 22 Ma; but earlier compared to the appearance of dyke phased granite aplite and pegmatite in the Bao Yen area, determined to occur within 20–19 Ma interval. The latter age data may reflect a short period of elastic deformation related to broad formation and evolution processes of the Red River shear zone.

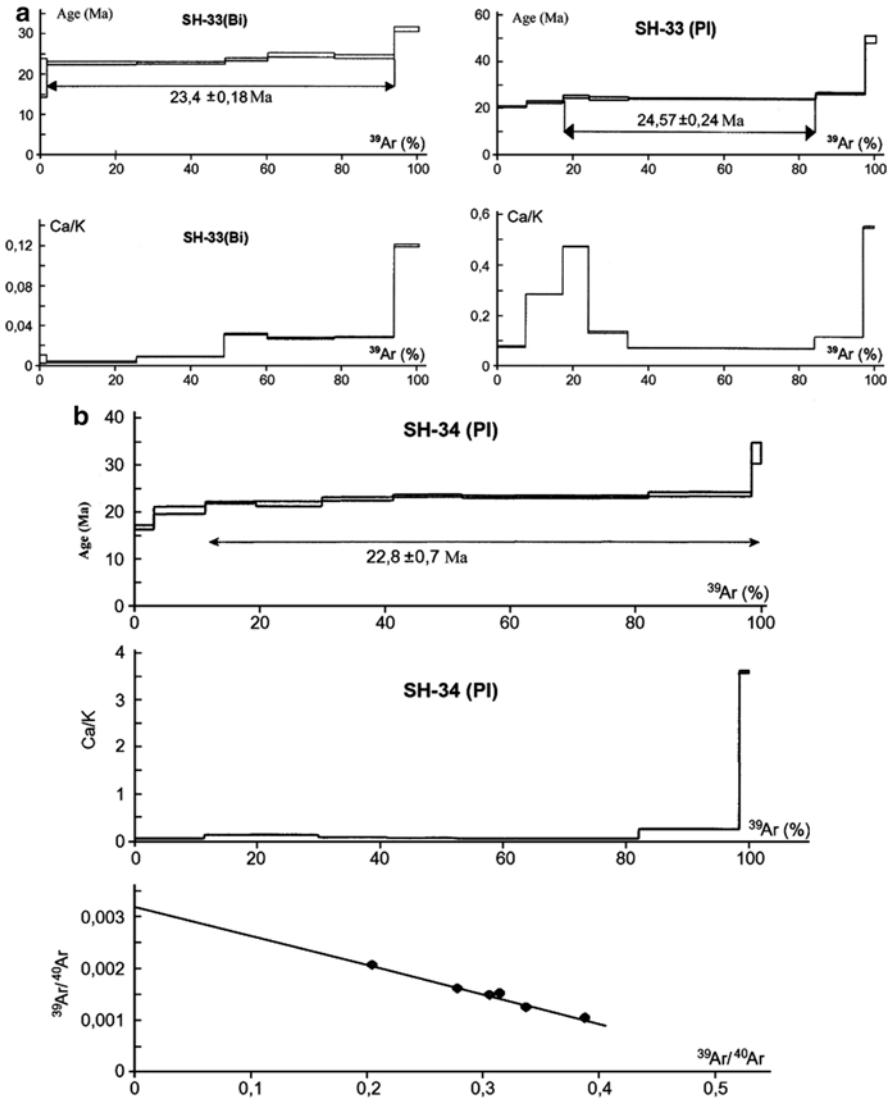

Fig. 8.20 Plateau ages of Red River leucogranite; (**a**) Trung Tam block, (**b**) Tan Huong block

8.3.5 Source Origin and Formation Conditions

The presence of undeformed (or weakly deformed), high pressure, Oligocene-Miocene Tan Huong-type granite in the Red River zone suggests a complexity in geological development and evolution of the Red River shear zone. The fact that the granitoids not being involved in the Cenozoic deformation indicates that the scale of motion along the Red River fault zone was limited or the magnitude of motion had been decreased considerably during 24–22 Ma.

Besides, although the allochthonous nature of the granite is undeniable there are questions on their formation mechanisms needed to answer, including (1) magma source, depth of melt generation along with the related geodynamic parameters; (2) relationship between the magma generation and the Red River geodynamics in Oligocene – Miocene.

Based on the rock-forming mineral assemblage of Q + Fsp + Pl + Bi ± Mus ± Gr in biotite granite and leucogranite from Long Khanh, Trung Tam and Tan Huong blocks it may suggest that the study granite is comparable to one of high-Al granitoidic series (e.g. S-type). Additional evidence supporting S-type granite includes the popularity of high- Al garnet minerals as well as high $^{87}Sr/^{86}Sr$ (0.7277) and low $\varepsilon_{Nd(0)}$ (−9.79), indicating a crustal source, also a protolith from which the granite melts generated may be of low maturity. A protolith neodymium model age T_{DM} calculated for the biotite granite and leucogranite in the Red River zone shows 1.57 Ga, apparently younger as compared with T_{DM} in Permian – Triassic high-Al granite in northeastern Viet Nam at 1.79–2.19 Ga.

What was the source substance that produced the Tan Huong –type granite melts in the Red River fault zone? For this high-Al metamorphic metapelite in the Red River complex may not be a candidate as high pressure melting model for the Tan Huong-type biotite granite would not explain the difference in age of the gneiss at 770–925 Ma (after Thi and Quan 1997) or at 838 Ma (after Lan et al. 2001) and a neodymium model age T_{DM} at 1570 Ma calculated for granite at the Trung Tam block. However, following the above argument the gneiss and crystalline schist of Song Chay complex may be appropriate for the primary source substance for Tan Huong –type granite melts. This melting source problem is thus needed further investigation to clarify.

Thus, along with the anatexis melting process related to elastic deformation to generate coarse-grained granite and pegmatite and leucogranite – aplite (stress granite as defined by Tapponnier et al. 1990), high pressure, high-Al, −K, poor-Nb and Ta granites are also popular in the Red River fault zone. These granites are also distributed in the high grade metamorphosed gneiss in the fault zone; however, the timing and formation of weakly deformed Tan Huong-type granites may represent a quiescence period of the Red River fault zone. The spatial (and possibly temporal) association of stress-granite and high pressure granite has been reported at collision-related orogeny within Asian continent such as south Pamir (Vladimirov et al. 1992), Andan and Sain (south Siberia) (Nojzkin 1997), but the difference is, the south Pamir is early Mesozoic (Triassic) and Andan and Sain is Preproterozoic.

8.4 Summary on Cenozoic Magmatic Activities

Cezonoic magmtic activities in northern Viet Nam mostly occurred in the northeastern regions, in structures adjacent to Cenozoic boundary between Indochina and Viet Nam – China composite terrane in the framework of India – Eurasian collision. The Paleogene potassic and ultrapotassic alkaline magmas in the northeastern wing of Song Da rift zone may be classified into ultrapotassic, high-Mg and low-Ti mafic magmas which are, according to their mineralogical, geochemical and isotopic

characteristics, may be comparable to the low-Ti Mediterranean-type lamproites. The similarity in the occurrence, compositional characteristics (including enrichment of LILE and REE, and depletion of Ti, Nb and Ta, etc.) of northeastern Vietnam lamproites as well as other Paleogene alkaline magmas and those similar magma types outcropped in structures distributed along boudanries of the India – Eurasian collision-induced terranes. The formation of these magmatic associations is a result of fractional crystallization from primary melts having compositions analogous to lamproites, produced by metasomatosed mantle melting, whose appearance may be related to lithosphere extension following the India – Eurasian collision. With formation ages determined between 42 and 35 Ma the magmatic associations may occur before the major, strong motion phase of the Indochina block along the Red River fault zone.

In the nearby Phan Si Pan uplift massif sub-alkaline granitoids shoing geochemical indications analogous to high-K calc-alkaline magmatics series were occurred between 35 and 32 Ma, coincident with the timing of an early strong shear motion along the Red River zone. A primarily crustal source of the magmas is supported by high-Al, –alkaline, relatively low Nb, Ta and Zr, and high initial $^{87}Sr/^{86}Sr$ isotopic ratios. On the other hand, the contemporaneous occurrence of the granite magmatism and start of the major shear motion phase suggests that the magmas can be viewed as syn-kinetic.

The syn-kinetic magmatism in the Red River shear zone formed an uniform association including small intrusive bodies comprised of lherzolite, websterite and gabbro, which were subsequently turned into shear boudinage in later stages. The magmas occurred in two major stages at 35 and 25 Ma. The presence of clinopyroxene with high fassaite component and the popularity of garnet in early-stage gabbroids indicate their higher pressure (deep level) crystallization relative to magmas occurred in later stages. These observations suggest that the formation of mafic – ultramafic magmas in the early stage may be associated with the exhumation process, while the later magmas may be related to post-gneiss exhumation activities along the Red River shear zone. However, the magmas of two stages are geochemically similar, suggesting their common source. Mafic and ultramafic magmatism during the period of 35 Ma, contemporaneous with potassic and ultrapotassic mafic and ultramafic in nearby structures (such as the Song Da rift zone) suggest there were various geological substrates (even in the same region) for each individual magma type.

The occurrence of high-Al, –alkaline and high-pressure melting granite during 24–22 Ma is a specific character of the Red River shear zone. The undeformity or weak deformity feature of the granite indicates that magnitude of shear motion in the Red River zone decreased after the peak time between 35 and 22 Ma. Note that the occurrence of granite aplite and pegmatite in gneiss in the Red River zone is not related to the nature of Tan Huong –type granite generation. This is evident by their spatially separated distribution as well as the large difference in their initial strontium isotopic ratios as mentioned earlier.

References

Allen CR, Gillespie AR, Han Yuan, Sieh KE, Zhang Buchue, Zhu Chenghan (1984) Red River and associated faults, Yunnan Province, China. Quaternary geology, slip rates and seismic hazard. Bull Geol Soc Am 95:6686–6700

Anczkiewicz R, Viola G, Mu¨ntener O, Thirlwall M, Quong NQ (2007) Structure and shearing conditions in the Day Nui Con Voi massif, northern Vietnam: implications for the evolution of the Red River fault. Tectonics 26, TC2002. doi:10.1029/2006TC-001972

Bonin B (1990) From orogenic to anorogenic settings: evolution of granite suites after a major orogenesis. Geogr J 25:261–270

Briais A, Patriat P, Tapponnier P (1993) Updated interpretation of magnetic anomalies and seafloor spreading stages in the South China Sea, implications for the Tertiary tectonics of SE Asia. J Geophys Res 98:6299–6328

Chung SL, Lee TY, Lo CH, Wang PL, Chen CY, Nguyen TY, Tran TH, Wu GY (1997) Intraplate extension prior to continental extrusion along the Ailao Shan – Red River shear zone. Geology 25:311–314

Cox KG, Bell JD, Pankhurst RJ (1979) The interpretation of igneous rocks. George Allen & Unwin, London, 445 pp

Dao Dinh Thuc, Huynh Trung (eds) (1995) Geology of Viet Nam, P. II: magmatic formations. Science and Technology Publishing, Hanoi, 359 p

Dewey JF, Cande S, Pitman WCI (1989) Tectonic evolution of the India/Eurasia collision zone. Eclogae Geol Helv 82:717–734

Dovjikov (ed) (1965) Geology of Northern Viet Nam. Science and Technology Publ. Hanoi 668 p

England P, Molnar P (1990) Surface uplift, uplift of rocks, and exhumation of rocks. Geology 18:1173–1177

Frost CD, Bell JM, Frost BR, Chamberiain KR (2001) Crustal growth by magmatic underplating: isotopic evidence from the northern Sherman batholith. Geology 29:515–518

Garnier V, Giuliani G, Maluski H, Ohnenstetter D, Phan Trong Trinh, Hoang Quang Vinh, Pham van Long, Vu Van Tich, Schwarz D (2002) Ar-Ar ages phlogopites from marble-hosted ruby deposits in Northern Vietnam: evidence for Cenozoic ruby formation. Chem Geol 188:33–49

Gilley LD, Harrison TM, Leloup PH, Ryerson FJ, Lovera OM, Wang J (2003) Direct dating of left-lateral deformation along the Red River shear zone, China and Vietnam. J Geophys Res 108(B2):2127. http://dx.doi.org/10.1029/20-01JB001726

Harrison TM, Leloup PH, Ryerson FJ, Tapponnier P, Lacassin R, Chen Wenji (1996) Diachronous initiation of transtension along the Ailao Shan-Red River Shear Zone, Yunnan and Vietnam. Tectonic evolution of Asia, World and regional geology series. Cambridge University Press, New York, pp 208–226

Hoang Thai Son (ed) (1997) Geological map-sheets Lao Cai – Kim Binh (at scale 1: 50,000). Center for Information and Archives of Geology, Hanoi

Izokh AE, Tran Trong Hoa, Polyakov GV, Ngo Thi Phuong, Tran Tuan Anh, Travin AV (2004) Syn-kinematic ultramafic-mafic magmatism in the Red River shear zone. J Geol Series B 23:26–41

Izokh AE, Polyakov GV, Tran Trong Hoa, Balykin PA, Ngo Thi Phuong (2005) Permian-Triassic ultramafic-mafic magmatism of Northern Vietnam and Southern China as expression of plume magmatism. Russ Geol Geophys 46(9):942–951

Lan CY, Chung S-L, Jason Jiun-San Shen, Lo CH, Wang PL, Tran Trong Hoa, Hoang Huu Thanh, Mertzman SA (2000) Geochemical and Sr-Nd isotopic characteristics of granitic rocks from Northern Vietnam. J Asia Earth Sci 18:267–280

Lan CY, Chung SL, Lo CH, Lee TY, Wang PL, Li H, Dinh Van Toan (2001) First evidence for Archean continental crust in northern Vietnam and its implications for crustal and tectonic evolution in Southeast Asia. Geology 29(3):222–219

Lazko EE, Sarkov EV (1988) Magmatic rocks. Ultramafic rocks. Nauka, Moscow, 488 pp

Leloup PH, Kienast JK (1993) High temperature metamorphism in a major tertiary ductile continental strike-slip shear zone: the Ailao Shan-Red River (P.R.C). Earth planet. Sci Lett 118:213–234

Leloup PH, Lacassin R, Tapponnier P, Scharer U, Zhong Dalai, Liu Xaohan, Zhang Shan, Ji Shaocheng, Phan Trong Trinh (1995) The Ailao Shan – Red river shear zone (Yunnan, China), Tertiary transform boundary of Indochina. Tectonophysics 251:3–84

Leloup PH, Arnau N, Lacassin R, Kienast JR, Harrison TM, Phan Trong Trinh (2001) New constraints on the structure, thermochronology and timing of the Ailao Shan-Red Rivershear zone, SE Asia J GR 106:6657–6671

Ludwig KR (2003) Isoplot v. 3.0: a geochronological toolkit for microsoft excel, special publication, No 4, Berkeley Geochronology Center, 70 pp

Maluski H, Lepvrier C, Jolivet L, Carter A, Roques D, Beyssac O, Ta Trong Thang, Nguyen Duc T, Avigad D (2001b) Ar-Ar and fission track ages in the song Chay massif: early Triassic and Cenozoic tectonics in Northern Vietnam. J Asia Earth Sci 19(1–2):233–248

Molnar P, Gipson JM (1996) A bound on the rheology of continental lithosphere using very long baseline interferometry: the velocity of south China with respect to Eurasia. J Geophys Res 101:545–553

Murphy MA, Yin A, Harrison TM, Dürr SB, Chen Z, Ryerson FJ, Kidd WSF, Wang X, Zhou X (1997) Did the Indo-Asian collision alone create the Tibetan plateau? Geology 25:719–722. doi:10.1130/0091-7613(1997)0252.3.CO;2

Ngo Thi Phuong, Tran Trong Hoa, Tran Tuan Anh (2001) Petro-minerallogical characteristics of the P2-T1 basalts-komatiite association in the Ta Khoa Anticline, Song Da Zone (NW Vietnam). J Geol Ser B 17–18:10–19

Nguyen Kinh Quoc (ed) (1995) Origin, distribution and potential of gemstones and technical stones in Vietnam. Final report of National project, Code KT-01-09, Archives in National Agency for Science and Technology Information (NASTI), Hanoi (in Vietnamese)

Nguyen Trung Chi (ed) (2003) Petrology and mineralization of alkaline magma formations in northern Viet Nam. Final report of ministerial project (Ministry of Natural Resources and Environment), Center for Information and Literature Archives, Department of Geology and Minerals, Hanoi (in Vietnamese)

Nguyen Quoc Cuong, Takarski AK, Swierczewska A, Zuchiewicz W, Nguyen Trong Yem (2009) Late Tertiary tectonics of the Red River fault zone (Vietnam part) based on studies of sedimentary rocks. In: Cenozoic Geodynamics of North Vietnam, The proceedings of Vietnam-Poland symposium. Academy of Science and Technology, 50–78 pp (in Vietnamese with English abstract)

Nojzkin AD (1997) Petrochemistry of pre-Cambrian complexes in the south Siberia. Dissertation of Dr. of Science, Novosibirsk (in Russian)

Pearce JA, Harris NBW, Tindle AG (1984) Trace element discrimination diagrams for the tectonic interpretation of granitic rocks. J Petrol 25:956–983

Pham Thi Dung, Tran Trong Hoa, Lan CY, Tadashi Usuki, Tran Tuan Anh, Ngo Thi Phuong, Vu Hoang Ly, Tran Van Hieu, Nguyen Thi Mai (2013) Cenozoic granite in the Phan Si Pan uplift, Northwest Vietnam. Extend. In: Abstract of the volume of international symposium "large igneous provinces of Asia: mantle plume and metallogeny" LIPs, Hanoi, 7 Nov 2013, p. 152

Phan Truong Thi, Dang Tran Quan (1997) Dynamic role of the Red River Fault: orogenic uplift and basin subsidence. J Geol Ser B 9–10:33–46

Phan Trong Trinh, Hoang Quang Vinh, Leloup H, Giuliani G, Garnier V, Tapponnier P (2004a) Deformation, evolution and thermal kinetics of Red River shear zone and ruby mineralization during the Cenozoic. In: Monograph of Red River fault zone: geodynamics, mineralization and natural hazards. Science and Technology Publication, Hanoi, 532 p (in Vietnamese)

Phan Trong Trinh, Hoang Quang Vinh, Leloup H, Tapponier P (2004b) Deformation and thermal kinetics evolution of Phan Si Pan zone in Cenozoic. J Geol A 285:57–68

Rangin C, Huchon P, Le Pichon X, Bellon H, Levrier C, Roques D, Hoe ND, Quynh PV (1995) Cenozoic deformation of central and south. Tectonophysics (special issue), 251:180–196

Rozen OM, Phedorovsky VS (2001) Collisional granitoids and crust delamination (Cenozoic, Paleozoic and Proterozoic collisional systems), vol 545. Publication of GIN RAS, Nauchnyi Mir, Moscow, 188 pp (in Russian)

Searle MP (2006) Role of the Red River Shear Zone, Yunnan and Vietnam, in the continental extrusion of SE Asia. J Geol Soc Lond 163:1025–1036

Sun SF, McDonough WF (1989) Chemical and isotopic systematics of oceanic basalts: implication for mantle composition and processes. In: Saunders AD, Norry NJ (eds) Magmatism in ocean basins, vol 42. Geological Society Special Publication, Oxford, pp 313–345

Tran Duc Luong, Nguyen Xuan Bao (1989) Geology of Vietnam, P I: stratigraphy. Science and Technology Publishing, Hanoi, 378 p (in Vietnamese)

Tran Trong Hoa (2007) Intraplate magmatism in North Vietnam and related metallogeny. Dissertation of Dr. of Science. Institute of Geology and Mineralogy, Siberian Branch, RAS, Novosibirsk, 382 p

Tran Ngoc Nam TM, Itaya T (1998) P-T-t paths and post-metamorphic exhumation of the Dãy Núi Con Voi shear zonein Vietnam. Tectonophysics 1998(290):299–318

Tran Tat Thang, Tran Tuan Anh (2000) Indications of granulite metamorphic facies in the Red River zone. J Earth Sci 22(4):410–419 (in Vietnamese with English abstract)

Tran Van Tri, Truong Cam Bao (eds) (1977) Geology of Vietnam, northern part. Institute of Geology and Mineral Resources (in Vietnamese)

Tran Trong Hoa, Tran Tuan Anh, Ngo Thi Phuong, Phan Luu Anh, Hoang Huu Thanh (2000a) Origin of ultramafic rocks in the Red River zone on the basis of new results of mineralogical, geochemical and isotopic analyses. J Geol Ser B 2000(15–16):62–75

Tran Trong Hoa, Phan Luu Anh, Ngo Thi Phuong, Nguyen Van The (2000b) Cenozoic granitoids in the Red River fault zone. J Earth Sci 22(4):306–318 (in Vietnamese with English abstract)

Tran Tuan Anh, Tran Trong Hoa, Pham Thi Dung (2002) Granites of the Ye Yensun complex and their significances in tectonic interpretation of the early Cenozoic stage in West Bac Bo. J Geol Ser B 19–20:43–53

Tran Trong Hoa, Tran Tuan Anh, Ngo Thi Phuong, Pham Thi Dung, Tran Viet Anh, Izokh AE (2004) Mesozoic – Cenozoic magmatic formations in the Phan Si Pang – Red River uplift block, northwest Viet Nam. In: The Red River fault zone, geodynamics, mineralization and natural hazards. Science and Technology Publ, Hanoi, pp 297–372 (in Vietnamese)

Tran Trong Hoa, Tran Tuan Anh, Ngo Thi Phuong, Pham Thi Dung, Tran Viet Anh (2005) Permian – Triassic magmatic activities in Viet Nam and prospect of associated rare and precious metal (Pt, Au) mineralization. In: Proceedings of 60-Anniversary of Geology of Viet Nam, pp 63–79 (in Vietnamese)

Tran Trong Hoa, Tran Tuan Anh, Pham Thi Dung, Pham Ngoc Can, Andrzej Zelazniewicz (2009) Cenozoic magmatism in the Northwest Vietnam and their relation with Red River Shear Zone. In: Cenozoic Geodynamics of North Vietnam, Proceedings of Vietnam-Poland symposium, Academy of Science and Technology, 137–149 pp (in Vietnamese with English abstract)

Tran My Dung, Liu Junlai, Nguyen Quang Luat (2010) Cenozoic high-K magmatism and Cu-Mo-Au metallogeny in the Jinping – Phan Si Pan mineralization zone. In: Proceedings of the 19th science conference, Hanoi University of Mining and Geology, 11 Nov 2010, pp 3–16 (in Vietnamese with English abstract)

Tran Trong Hoa (ed), Polyakov GV, Tran Tuan Anh, Borisenko AS, Izokh AE, Balykin PA, Ngo Thi Phuong, Pham Thi Dung (2011). Intraplate magmatism and metallogeny of North Vietnam. Science & Technology Publication House (Vietnam Academy of Science and Technology), 368 pp

Tran Trong Hoa, Pham Thi Dung, Tran Tuan Anh, Ching – Ying Lan, Tadashi Usuki, Tran Van Hieu, Vu Hoang Ly (2012) New U-Pb zircon ages of Ye Yen Sun complex granite in the Phan Si Pan uplift and their relationship with Red River Shear Zone. J Earth Sci 34(4):453–464

Tran Trong Hoa, Ching–Ying Lan, Tadashi Usukib, Gregory Shellnutt J, Pham Thi Dung, Tran Tuan Anh, Pham Ngoc Can, Ngo Thi Phuong, Izokh AE, Borisenko AS (2015) Petrogenesis of

Late Permian silicic rocks of Tu Le Basin and Phan Si Pan Uplift (NW Vietnam) and their association with the Emeishan large igneous province. J Earth Sci 109(2015):1–19

Tapponnier P, Peltzer G, Le Dain AY, Armijio R, Cobbold P (1982) Propagating extrusion tectonics in Asia: new insights from simple experiment with plasticine. Geology 7:611–616

Tapponnier P, Peltzer G, Armijo R (1986) On the mechanics of the collision between India and Asia. In: Coward MP, Ries AC (eds) Collision tectonics, vol 19, Geological Society Special Publication, pp 115–157

Tapponnier P, Lacassin R, Leloup H, Scharer U, Zhong Dalai, Liu Xaohan, Shaocheng J, Zhang Lian Shang, Zhong Jiayou (1990) The Ailao Shan – Red River metamorphic belt: Tertiary left-lateral shear between Indochina and South China. Nature 343:431–437

Vladimirov AG, Malykh MM, Dronov VI et al (1992) Indosinian igneous activity and geodynamics of the South Pamir Region, Novosibirsk, 228 pp

Wang PL, Lo CH, Lee TY, Chung SL, Lan CY, Nguyen Trong Yem (1998) Thermochronological evidence for the movement of the Ailao Shan – Red river shear zone. Geology 26:887–890

Wang PL, Lo CH, Chung SL, Lee TY, Lan CY, Tran Van Thang (2000) Onset timing of lateral movement along the Ailao Shan-Red river shear zone: Ar-Ar dating constraint from the Nam Dinh area, northeastern Vietnam. J Asia Earth Sci 18:281–292

Wang J-H, An Yin, Mark Harrison T, Marty Grove, Yu-Quan Zhang, Guang-Hong Xie (2001) A tectonic model for Cenozoic igneous activities in the eastern Indo-Asian collision zone. Earth Planet Sci Lett 188(2001):123–133

Whalen JB, Currie KL, Chappell BW (1987) A-type granite: geochemical characteristics, discrimination and petrogenesis. Contrib Mineral Petrol 95:407–419

Wilson M (1989) Igneous petrogenesis: a gobal tectonic approach. Springer, 466 pp

Zelazniewicz Andrzey, Hoa Trong Tran, Larionov AN (2012) The significance of geological and zircon age data derived from the wall rocks of the Ailao Shan–Red River Shear Zone, NW Vietnam. J Geodyn 69:122–139

Zhang Lian-Sheng, Scharer U (1999) Age and origin of magmatism along the Cenozoic Red River shear belt, China. Contrib Mineral Petrol 134:67–85

Chapter 9
Metallogeny in the Cenozoic

Abstract The Cenozoic mineralization in structures associated with the Red River shear zone (RRSZ) in northern Viet Nam includes the following mineralized ore types TR- (U-Th)-Pb-Zn and TR- (U-Th) –Ba-F, Au-Cu in the Song Da rift zone. The origin of the mineralizations is spatially and (possibly) temporally related to the formation of Paleogene potassic mafic – ultramafic and silisic associations. Molybdenum –precious metals (Mo-W-Cu-Au) in the along with Cu-Au mineralization in the Phan Si Pan uplift are related to Paleogene granitoidic magmatism in the Ye Yen Sun complex. Beside, Cu-(Au – REE) mineralizationsin the Phan Si Pan Uplift are described.

The Cenozoic mineralization in structures associated with the Red River shear zone (RRSZ) in northern Vietnam includes the following mineralized ore types: TR-(U-Th)-Pb-Zn and TR- (U-Th) –Ba-F (Nam Xe and Dong Pao deposit fields) (Tri 2000), Au-Cu (Chinh Sang) (Chi 2003) all in the Song Da rift zone. The origin of the mineralizations is spatially and (possibly) temporally related to the formation of Paleogene potassic mafic and ultramafic associations. Molybdenum –precious metals (Mo-W-Cu-Au) in the O Quy Ho, Thac Bac and Ban Khoang areas along with Cu-Au mineralization in the Phan Si Pan uplift are related to Paleogene granitoidic magmatism in the Ye Yen Sun complex. In the Red River high-grade metamorphic belts aside from gemstones (ruby and sapphire) there are indications (such as quartz – sulfide ore) of precious metal mineralization, which has not been studied. In the Phan Si Pan uplift area, Cu-(Au – TR), Cu and Au (in Sin Quyen, Lung Po and Lang Phat) ores are discovered in Proterozoic – Paleozoic sediment – metamorphic formations within a length of about 100 km. Their formation age and origin in relation to the regional magmatic activities have not yet been studied. Some of the above ore- deposits are classified as Cu – Fe – Au – REE type (Sin Quyen) (Tri 2000) or hydrothermal – metasomatic type (Lang Phat) (The et al. 1999). But there is possibility that these ore types are analogous to the Ni-Mo-Cu-PGE-Au mineralized complex occurred elsewhere in the Yangtze craton, having been metamorphosed in later periods, even during the Cenozoic. There are indications of certain impact on the ore types by the Red River shear motion activities, however, these are not yet studied. In a Chinese metallogenic map, some sediment – hydrothermal-origin ore belts reported be 534 Ma (by Re-Os) (Mao et al. 2002; Wang et al. 2004)

T.-H. Tran et al., *Intraplate Magmatism and Metallogeny of North Vietnam*,
Modern Approaches in Solid Earth Sciences 11,
DOI 10.1007/978-3-319-25235-3_9

show indications of continuation from the craton to northern Vietnam, where the similar ore types have been metamorphosed following shear motion activities in the Red River zone. Note that, the Ta Phoi deposit (southeast of the Sin Quyen deposit) is described as Cu-porphyry type (Dien et al. 2005). The Sin Quyen and Ta Phoi Cu-Fe-Au-REE mineralizations are not presented in this book since lacking ore-formation ages. Classification of Cenozoic ore complexes is given in Table 6.1 (Chap. 3, Part II), and distribution of the major ore fields are given in the metallogenic map of northern Vietnam (Fig. 6.1; Chap. 3, Part II)

9.1 TR – F – Ba Ore Complex

There are two sub-type being established in the TR-F-Ba complex: TR-(Th)-U-F in the Dong Pao area and TR-(Th)-Pb-Zn in the Nam Xe area; the formation of both sub-types is spatially and temporally related to Pu Sam Cap ultrapotassic magmas dated from 42 to 35 Ma (see Chap. 1). The TR-F-Ba-U-(Th) deposits are estimated to be highly industrial values. Mineralization forms zones having up to 70 km long in the northeast of the Song Da metallogenic belt. There are two deposit groups are recognized in the metallogenic belt, including Nam Xe to the northwest and Dong Pao to southeast, comprising rare earths and U-Th, Ta, Nb, Pb-Zn, F and Ba-bearing minerals (Fig. 6.1). The ore bodies are hosted by Paleogene volcanic and sub-volcanic alkaline felsic magmas commonly associated with ultrapotassic mafic formations (such as lamproite, minette and absarokite), in some case also by aegirine-pyrochlorite-calcite dykes described by Chi (2003) as carbonatite. Thus, the genetic relation between the ore formation and Paleogene alkaline magmatic activities in the region is undebatable.

There are two ore types being identified in the Nam Xe deposit, including weathered ore having RE_2O_3 between 4 and 5 wt% and primary ore showing RE_2O_3 about 1.4 wt%, the latter contains bastnasite, parasite, small amount of magnetite, uranopyrochlorite, purite, apatite, barite and fluorite (Tri 2009). Basing on the percentage of useful ore components for ore types are subsequently being classified, (REE) rare earth-rich barite – carbonate, REE – niobium – tantalum- uranium (minor), rare earth, and rare earth alluvial and deluvian in weathering crust (Xinh et al. 1988).

The total reserve and natural resource of RE_2O_3 is about 7.8 million tons, in which certain reserve is (121) 1.74 million tons, confident resource is (222) 5.5 million tons and forecasting reserve (334a) is 2 million tons in northern Vietnam. Accompanying components include (in ton) U_3O_8: 76,000, ThO_2: 59,000, Nb_2O_5: 38,000 and RE_2O_3: 940,000; the latter contains (ton) Y_2O_3: 3,200, Gd_2O_3: 5,500, U_3O_8: 320, Th: 3,200, Sr: 2,200 and barite: 55,000. The resource is estimated to be about 3 million tons for southern Vietnam (ESCAP 1990).

There are 60 ore bodies in the form of pocket, lens or vein being discovered in a diagenesis belt surrounding Paleogene syenite blocks in the Dong Pao deposit,

among these 16 bodies reach industrial levels for mining. The Dong Pao rare earth ore is belonged to fluorite-carbonate group having major minerals of bastnasite, parasite, fluorite and barite. Depending on ratios between minerals ores may be divided into separate types such as rare earth RE_2O_3>5 wt%, rare earth – RE_2O_3-bearing barite about 0.5–30 wt%, rare earth – barite – fluorite having RE_2O_3 about 0.5–30 wt% and fluorite-bearing rare earth with RE_2O_3 about 1–5 wt% (Tri and Khuc 2011). Confident resource (222) of RE_2O_3 is estimated at 645,000 t, while forecasting reserve (333) suggests seven million tons, with CaF_2 at 9.4 million tons and $BaSO_4$ about 288 million tons (ESCAP 1990).

9.2 Au-Cu Complex

Au-Cu-sulfide complex is observed only at the Chinh Sang ore site (Binh Lu district, Lai Chau province). The mineralization is distributed in Paleogene trachyrhyolite, granosyenite and syenite magmas in the northeastern wing of Song Da rift zone. The gold-copper ore type is volcano- hydrothermal origin, consisted mainly of chalcopyrite-galenite-pyrite and arsenopyrite (Chi 2003). However, the ore mineralogy and geochemistry have only been briefly studied even though the ore has been exploited for many years by a private mining company. The company may have conducted exploration work but related geological and ore mineralization results have not yet been published.

9.3 Mo-(Cu-Au) Complex

Recent mineral exploration reports about 40 MO-bearing deposits and ore spots in Lao Cai province, scattered in the areas of Y Ty, Sa Pa, Lung Po and Bat Xat, with those in the Sa Pa area being most significant (Tri and Khuc 2011). Fifteen Mo-ore bodies estimated to reserve about 15,000 t (of Mo) are discovered in the O Quy Ho and neighboring areas. Ore mineralization is occurred mostly as veins, molybdenum-bearing quartz dispersed veins along with chalcopyrite, pyrite and other essential minerals. According to exploration reports by Geological Division No 3 (1994) Mo-bearing ore distribution in the Sa Pa area has been discovered and mapped by geophysical, geochemical anomalies along with trench and drilling survey. The Division No 3 also reported that hydrothermal Mo-mineralization ore in Sa Pa is dominant, while other accompanying minerals are not valuable (Combined report on mineral resources of Sa Pa district, Lao Cai province) (after Tri 2000).

Ore samples were collected by the authors of this monograph at several mineralized sites in the O Quy Ho and Ban Khoang areas. The ore sites are being described below.

9.3.1 Mo-(Cu-Au) Mineralization of O Quy Ho

Mo- (Cu, Au) mineralization in the O Quy Ho area may be found at a number of locations along National route 4 from Sa Pa to Thac Bac waterfall. Expression of the mineralization at various locations is mostly similar, including quartzitized zone or quartz veins containing sulfides filled in fractured zones and tectonic channels in biotite granite (Photo 9.1), showing various metamorphosed rates. The granite show petrologic and mineralogical features that are vastly similar to Permian sub-alkaline granite outcropped elsewhere in the area. It is notable that the Mo-Cu mineralization is commonly developed in areas where quartzitization and K-feldsparization being well-developed (Photo 9.2). This is the typical expression of Mo-Cu porphyry mineralization worldwide. Therefore, the Mo-Cu- mineralization in O Quy Ho is needed further detailed investigation. The Mo- ore contains molybdenite and pyrite, and a minor amount of chalcopyrite and other sulfide minerals. Forming age of the Mo mineralization in the O Quy Ho – Ban Khoang areas dated by Re-Os method is 36 ± 1 Ma (Dung et al. 2009).

9.3.2 Mineralization at Suoi Lanh (Ban Khoang)

The Suoi Lanh mineralization is distributed in Phan Si Pan Permian granite (see Sect. 3.3.1, Chap. 3, Part II). The mineralization occurred as dispersed molybdenum in feldsparized granite and in quartz – feldspar veins, having thickness about 30–40 cm. The ore minerals are mainly molybdenite, chalcopyrite, pyrite and magnetite, appeared as dispersed or cumulated forms.

The ore is surrounded by granite consisted mainly of K-feldspar and plagioclase (50–55 vol.%), quartz (25–30 vol.%), biotite (ca. 5 vol.%) and a minor amount of accessory minerals (up to 10 vol.%) such as sphene, epidote, apatite and ore miner-

Photo 9.1 Quartzitized zone in granitoid containing molybdenite, chalcopyrite and pyrite; O Quy Ho site

Photo 9.2 Mo-Cu mineralization occurred at well-developed quartzitization and K-feldsparization areas; O Quy Ho site

als. The granite is porphyritic with feldspar and plagioclase in the phenocryst. The biotite is brownish green, commonly associated with ore minerals and sphene, filling interstitials between quartz grains or surrounding feldspar phenocrysts.

Fine-grained (0.1–0.4 mm) quartz and K-feldspar veins in granite lie gently with a dip angle about 20–30°. Whereas, biotite and ore minerals form separate phenocrysts or concentrate as lenses. The quartz veins, having a dip angle from 80 to 90°, are comprised of quartz gains with sizes from 0.1–0.3 to 1–1.5 mm.

The mineralized cumulate is normally distributed directly in feldsparized zones in biotite granite and in quartz-feldspar and quartz veins. K-feldsparized zones host mainly dispersed minerals in the form of magnetite-pyrite-molybdenite and chalcopyrite veins (Photo 9.3). The pyrite is found in veins and small disseminated mass (0.1–5 mm). The pyrite aggregate are commonly cracked and developed along fractures rich in hydrous iron substances. Marcasite (ca. 0.3 mm), sometimes having up to 10 wt% of iron sulfide, is commonly found in pyrite crystals. Pyrrhotite is also commonly occurred in the pyrite. Fluorite-bearing small-scaled quartz-sulfide veins are often found in bright colored, fine-grained granite seen at Thac Bac wall.

Molybdenite is formed as association of single grains having length up to 1.5 mm, sometimes associated with chalcopyrite (up to 0.3 mm). Basically, ore minerals are about 5–7 vol.%, where pyrite being dominant (80–90 vol.%), molybdenite (5–7 vol.%), magnetite (7–1 vol.%) and chalcopyrite (3–5 vol.%).

Quartz, and quartz-feldspar veins (Photo 9.4) contains mostly mineral association of molybdenite-pyrite-magnetite. The molybdenite is made up by tabular, easy-peeled single crystals. The mineral associations are normally distributed along the vein direction. The pyrite is made up by irregular-formed, porous grains surrounding quartz crystals. Both the pyrite and magnetite are often cracked, forming fractures where hydrous iron minerals (such as limonite, hematite and goethite) are well developed, sometimes completely replacing magnetite. In general, ore minerals in the veins reach 3–5 %, where molybdenite is about 20 % (of the ore).

Photo 9.3 Sulfide mineralization in feldsparized zones in granite; Suoi Lanh, Ban Khoang

9.3.3 Mineralogical, Geochemical and Isotopic Characteristics

The chemical compositions of molybdenite and pyrite at mineralization occurrences in the Ban Khoang and O Quy Ho areas show highly variable although within theoretical ranges (Tables 9.1 and 9.2). The amount of associated impure elements is insignificant (under EPMA detection limit). Natural gold grains were found in some ground and sieved samples. The chemical composition of gold shows high Au (89–91 wt%), Ag (8.5–11.06 wt%) and low Hg (0.12–0.13 wt%) (Hoa et al. 2010)

According to previous studies, the average of chemical composition of molybdenum ore in the Sa Pa area is Mo: 0.3 % and Cu: 0.1–0.3 % (Tri and Khuc 2011). Concentrations of other accompanying elements are insignificant; however, Au was reported to show 0.3–0.5 g/T (Hoa et al. 2006). Recent quantitative spectral analysis conducted by the monograph's authors on molybdenum ore in the Ban Khoang and O Quy Ho areas showed Mo varying between 200 and 500 ppm. Besides, the analysis also showed relatively high concentrations of Pb, Zn, Cu, Ba, and La especially high in samples from the O Quy Ho area, up to 100 ppm (Hoa. 2010).

Preliminary study of isotopic and melt inclusion suggested that the mineralization may occur at mild to high temperature (>290 °C, based on temperature of inclusion synchronization). And that the mineralization may have a intrusive magma link ($\delta^{34}S = 2.1–3.7$; total salinity based on equivalent NaCl% =11.7–9.2) (Hoa 2006).

Photo 9.4 Molybdenite mineralization in quartz-feldspar veins in granite; Suoi Lanh, Ban Khoang

The above descriptions suggest that the occurrence of Mo mineralization at Ban Khoang and O Quy Ho in the Phan Si Pan zone may be viewed as a Mo (Cu, Au) porphyry type, having the main features as follows: (1) molybdenite, chalcopyrite, gold mineralization type and hydrothermal alteration (K-feldsparization, sericitization, quartzitization and pyritization); (2) characterized mineralization (Mo, Cu, Au) and inclusion (salt level equivalent to NaCl); (3) mineralization related to intrusive magma activity (spatial, formation age, sulfur isotopes), most likely, Paleogen granitoid of Ye Yen Sun complex (35–30 Ma, see Chap. 3). Besides, the presence of sub-volcanic adakitic dykes is characterized for the development of Cu (Mo, Au) porphyry mineralization along the Ailao Shan – Red River shear zone. However, in order to consolidate better practical evidence it is needed to carry out detailed geochemical, isotopic and melt inclusion research with regards to Mo and Cu mineralization in magma formations in the Phan Si Pan zone.

According to research documentation of Cu (Mo, Au) mineralization worldwide, mineral associations commonly occur in the following order: pyrite, chalcopyrite, molybdenite, magnetite, hematite, sheelite, wolframite- to- galenite, sphalerite, tetradimite, bornite, chalcosine enargite- to- cinnabar, fluorite, barite and bismuth minerals. This mineralization order reflects process of ore mineral separation and

Table 9.1 Chemical compositions of molybdenite in Ban Khoang (BK) and O Quy Ho (OQH) mineralized zones

Sample ID	Mo	S	Total
BK-3-1	58.54	38.32	97.07
BK-3-2	60.95	39.39	100.33
BK-4	59.57	39.31	98.87
BK-5-2	58.50	39.02	97.02
OQH-2-1	59.44	40.00	99.44
OQH-2-2	60.37	39.31	99.68
OQH-4-2	59.81	39.64	99.45
OQH-5-1	60.15	38.57	98.72
OQH-5-2	60.26	39.59	99.86

Data were acquired by EPMA at Analytical Center, Institute of Geology and Mineralogy, Russian Academy of Science, Siberian Branch

Table 9.2 Chemical compositions of pyrite in Ban Khoang (BK) and O Quy Ho (OQH) mineralized zones

Sample ID	Analyzed point	MET	MAC	Fe	Co	As	S	Ni	Cu	Total
BK-3	4-5-1	F	M	46.97	0	0	52.9	0.01	0.009	99.9
BK-3	4-5-2	F	M	47.13	0	0	53.14	0.015	0.014	100.29
BK-4	4-6-1	F	M	46.42	0	0	52.9	0.006	0.017	99.35
BK-5	4-7-1	F	M	46.74	0	0	52.59	0.016	0.024	99.36
BK-5	4-7-2	F	M	46.82	0	0	53.06	0	0.039	99.92
OQH-4	5-2-1	F	M	46.96	0.014	0	53.83	0	0.02	100.82
OQH-4	5-2-2	F	M	47.38	0	0	53.98	0.004	0.01	101.37
OQH-5	5-3-1	F	M	47.36	0.008	0	53.75	0.02	0.009	101.14
OQH-5	5-3-2	F	M	47.24	0	0	53.38	0.011	0	100.63

Data were acquired by EPMA at Analytical Center, Institute of Geology and Mineralogy, Russian Academy of Science, Siberian Branch

zonation both horizontally and vertically. In addition, this type of mineralization is well exposed at the first two stages of mineral formation, forming, respectively, inner zone (Cu, Mo) and outer zone (polymetallic). Therefore, Pb- Zn- and Ba- rich phenomenon at Ban Khoang and O Quy Ho may reflect an outer mineral zone, while an inner zone rich in Mo, Cu (Au) may not yet be discovered.

The tight association of Cu, Cu-(Au-TR) and Cu-(Au)-Mo mineralization in the Phan Si Pan area with various magmatic activities having occurred at different periods (from Late Proterozoic – Early Paleozoic (?) to Cenozoic) implies that Phan Si Pan may be viewed as a Cu, Au-Cu and Cu-(Au)-Mo metallogenic belt. The similar mineralization was discovered in Yunnan (China), as mentioned above, along the two wings of Ailao Shan – Red River Shear zone (e.g. Zheng et al. 2004) believed to link to Cenozoic (35–40 Ma) alkaline monzonitoid, syenite, lamproite and

minette. The majority of this mineralization type are classified as porphyry deposits. Therefore, in order to carry out a general evaluation of Cu (Au), Cu (Mo, Au), Mo (Cu, Au) porphyry mineralization in relation to the formation and evolution of Cenozoic Red River shear zone in northwestern Vietnam it is recommended that Au (Cu) or Cu (Au) mineralization on the boundary between Phan Si Pan and Song Da zones, where Cenozoic mafic and K-alkaline felsic and ultra-K alkaline magmas are well-spread, should be detailedly studied.

9.4 Ruby – Sapphire Mineralization

The ruby – sapphire mineralization in the Red River shear zone includes a series of deposits distributed in high-pressured metamorphic rocks, among these is Tan Huong mine, Luc Yen district (Yen Bai province) considered as one of the clearest mineralization expressions and the most valuable ruby – sapphire mines. Two ruby-saphire deposit types are identified as mable-hosted and gneiss-hosted (Huong et al. 2012). The Cenozoic age of 27 – 24 Ma for the mine formation is based on radiometric dating of phlogopite coexisted with ruby in host marbles (Trinh et al. 2004). The ruby mineralization is closely associated with a 35 – 25 Ma gabbro-websterite formation (see above). Ruby exploration drilled core descriptions revealed a clear transition zone in the following order: corundum-bearing marble – sapphirine – websterite (see Chap. 3), this appears to indicate that the mineralization was genetically related to the Red River mafic – ultramafic magmas, from where chrome (Cr) and heat were supplied for the ruby formation. However, this matter is required more detailed investigation in the future.

References

Dinh Van Dien, Bui Xuan Anh, Đinh Thanh Binh (2005) Cu-porphyry mineralization in the Ta Phoi area (Lao Cai province). Proceedings of the 60-year anniversary of geology of Viet Nam, pp 610–621 (in Vietnamese)

ESCAP (1990) Atlas of mineral resources of the ESCAP Region, 6, Vietnam. United Nations Publication, Bangkok, p 124

Le Thac Xinh (ed) (1988) Geology and mineral resources of Vietnam. Vietnam General Department of Geology and Mineral Resources, Hanoi, Vietnam

Le Thi Thu Huong, Tobias Häger, Wolfgang Hofmeister, Christoph Hauzenbeger, Dietmar Shwarz, Pham Van Long, Ursula Whemeister, Nguyen Ngoc Khoi, Nguy Tuyet Nhung (2012) Gemstone from Vietnam: an update. Gem Gemol 48:3

Mao J, Qui Y, Goldfarb JR (2002) Geology, distribution, and classification of gold deposits in the western Quinling belt, central China. Miner Deposita 37:352–377

Nguyen Van The (ed) (1999) Geology and mineral resources of the Luc Yen map sheet of 1:50,000. Archives of the Center of Geology Information and Literature Hanoi

Nguyen Trung Chi (ed) (2003) Petrology and mineralization of alkaline magma formations in northern Viet Nam. Final report of Ministerial Project (Ministry of Natural Resources and

Environment), Center for Information and Literature Archives, Department of Geology and Minerals, Hanoi (in Vietnamese)

Phan Trong Trinh, Hoang Quang Vinh, Leloup H, Giuliani G, Garnier V, Tapponnier P (2004) Deformation, evolution and thermal kinetics of Red River shear zone and ruby mineralization during the Cenozoic. In: Monograph of Red River fault zone: geodynamics, mineralization and natural hazards. Science and Technology Publ, Hanoi, p 532 (in Vietnamese)

Tran Van Tri (ed) (2000) Mineral Resources of Viet Nam Department of Geology and Minerals of Viet Nam Publication 214 p (in Vietnamese)

Tran Van Tri, Vu Khuc (eds) (2011) Geology and earth resources of Việt Nam. Publ. House for Science and Technology, Hanoi

Tran Trong Hoa (ed), Borisenko AS, Ngo Thi Phuong, Izokh AE, Tran Tuan Anh, Hoang Huu Thanh, Vu Van Van, Bui An Nien, Hoang Viet Hang, Tran Hong Lam (2006) Study and definition of new Au –mine type (Au-Sb-Hg) related to magmatic activities in northern Viet Nam. Final report to International collaboration sponsored by Viet Nam Academy of Science and Technology (2005–2006). Archives of the Institute of Geological Sciences, 51 p (in Vietnamese)

Tran My Dung, Liu Junlai, Nguyen Quang Luat, Đao Thai Bac (2009) Re-Os dating of molipdenite from the O Quy Ho-Ban Khoang molipdenum mineralization: belt and its geological significance. J Geol A 7–8

Tran Trong Hoa (ed), Tran Tuan Anh, Ngo Thi Phuong, Bui An Nien, Phan Luu Anh, Tran Quoc Hung, Pham Thi Dung, Pham Ngoc Can, Tran Van Hieu, Tran Hong Lam, Polyakov GV, Borisenko AS, Izokh AE, Gaskov IV, Shelepaev RA, Nevolko PA (2010) Study on origin, formation conditions of Pt-Au- and Ti-V-perspective ore-magmatic systems. Final report to International collaboration Project Vietnam-Russia (2007–2009). Archives of the National Agency for Science and Technology Information, 217 p (in Vietnamese)

Wang DH, Qu WJ, Li ZW, Ying HL, Chen YC (2004) The metallogenic concentrating epoch of the Porphyry Copper (molybdenum) deposits in Jinshajiang–Red River metallogenic belt: Re–Os isotope dating. Sci China D 34:345–349 (in Chinese)

Zheng Pusheng HZ, Mo Xuanxue, Yu Xuehui, Gao Yongfeng (2004) The Cenozoic Cu-Au mineralization of the alkali-rich porphyries under a background of strike-slip in west Yunnan. Abs. of IGCP-430 continental dynamics workshop, May 2004, pp 23–31, Kunming, China

Conclusions

There are two intraplate magmatic stages being determined in northern Vietnam, including Paleozoic -Mesozoic (mainly Permian – Triassic) and Cenozoic (mostly Paleogene). The magmas are distinguishable in terms of coexisting mineral assemblages, chemical compositions, geodynamic settings and mineralization processes.

The early stage may be related to Emeishan super-plume, to which the Permian – Triassic magmatic activities in northern Viet Nam may be viewed as southwestern and southeastern margins of the Emeishan large igneous province, having been extruded southeasterly along the Ailao Shan – Red River shear zone in the Cenozoic. This period is characterized by wide occurrence of mafic – ultramafic and felsic magmas including the wide presence of picritic magma (high-Ti komatiite and picrite in the Song Da rift zone and low-Ti picrite in the Song Hien belt). Geochemical and isotopic characteristics of the Permian – Triassic mafic and ultramafic magmas suggest their parental melts were generated from a highly heterogeneous lithospheric mantle. And that the low-Ti, high-Mg magma associations in the Song Da rift zone were derived from a depleted sub-oceanic-like lithospheric mantle, while the high-Ti magma series were generated in a sub-continental-like lithospheric mantle above a subduction- associated mantle wedge.

The redetermination of formation age of Permian – Triassic for felsic volcano – intrusive magmas in the Tu Le basin and Phan Si Pang uplift block suggests that the magma occurrence was related to geodynamic activities of the Song Da rifting, on the one hand, and the continental nature of the rifting activities, on the other. Therefore, the geological history of northwest Viet Nam in particular and northern Viet Nam in general has been rewritten to become closer to what happened. It may suggest that the previously determined separate structures such as Song Da rift and Tu Le basin were basically belonged to an actual continental rift system developed in marginal zones of the Yangtze craton. The presence of picrites in the Song Hien structure similar to those in the Shizong – Mile belt in southeastern margin of the craton indicates that Permian – Triassic magmatism in the Song Hien belt occurred synchronously with a rifting activity in cratonic marginal areas.

T.-H. Tran et al., *Intraplate Magmatism and Metallogeny of North Vietnam*,
Modern Approaches in Solid Earth Sciences 11,
DOI 10.1007/978-3-319-25235-3

The above-subduction mantle geochemical characteristics observed in Song Hien volcano-plutonic magma associations are not in conflict with intraplate nature of the magmatism; in contrast, they suggest the nature of above-subduction lithospheric mantle under southern margin of the Yangtze craton in late Paleozoic – early Mesozoic. The Song Hien volcano-plutonic magmatic melts reflect mantle – crust interaction, showing the difference between these and other Emeishan mantle plume-related magmas in other geological structures in northern Viet Nam, on the one hand, and provide new evidence, more reliable in explaining the nature of tectonic settings with regard to Permian – Triassic mafic – ultramafic and felsic magmas in nearby Phu Ngu – Lo Gam structure.

The Cenozoic magmatic activities were associated with India – Eurasian collision. Detailed studies show that Eocene – Oligocene volcano-plutonic mafic and felsic magmatism in northern Vietnam were produced as a result of mantle upwelling melting under the impact of geodynamic activities of the Indochina and Vietnam – China blocks following India – Eurasian collision. Meanwhile potassic and ultra-potassic alkaline mafic and felsic magmas along the border between Song Da rift and Phan Si Pang uplift are viewed as products related to intraplate extension occurred prior to the extrusion of Indochina block along the Red River shear zone. This is a regional tectonic event that occurred in entire collision-effected zone and extended further to the east of Asian continent. The mantle-derived magmas also include syn-extrusion mafic and ultramafic intrusions in the Red River zone, showing features different from those of deep mantle origin, which are explained by the fact that they were produced in a high-pressure and temperature metamorphic belt.

Review of mineralization activities during the Permian – Triassic and Cenozoic stages in northern Vietnam shows the following results:

1. The Permian – Triassic ore formations are classified and their temporally forming order was established. These serve as basics for division of regional mineralized ore types for Permian – Triassic period, where the Song Da – Song Hien mineralized belt is most detailedly reported. Besides, the Au-sulfur and Sn-sulfur ore sites have been systematized with regard to the magma – ore systems
2. For the first time, comparison of magma – ore formation age has been conducted; also the wide development of various Au-mineralization types was determined, including the determination of highly potential ore types (Au-As, Au-Sb-Hg, Au-Cu) related to magma – ore systems which appear to be highly ore-productive in the Permian – Triassic period.
3. Confirmation has been made on highly potential Cu-Ni-PGM and Ti-V mineralization in Permian – Triassic mafic and ultramafic magmas in the Song Da, Song Hien and Lo Gam – Phu Ngu ore belts along with newly determined Au-mineralized ore, especially the non-conventional such as Au-Sb-Hg type that is related to Permian – Triassic magmatism. Given such criteria northern Viet Nam may be considered as a new ore province having high potential of this mineralization type in southeast Asia.

4. The fact that Permian – Triassic magmatism in rifting structures northern Viet Nam was influenced by a mantle plume there is a high possibility that Ni-Co-As and Cu-(Mo)-Au ore mineralization may occur, especially in Ta Khoa and Suoi Cun- type intrusive magmas.
5. Magma generation modeling for gabbro – peridotite intrusions in the Phu Ngu – Lo Gam belt has provided evidence on contemporaneous Cu-Ni-PGM ores in the differentiated magmas and Ti-Fe-V mineralized products in pegmatoidic series in the magmatic intrusions. Besides the modeling also provides reasonable fact for expanding investigation of Ti-V ore mineralization in satellite gabbroic bodies of Nui Chua-type magmas.
6. The prospect of Cu-(Mo)-Au and Cu-Au ore mineralization along with new porphyry- type ore may be expected to discover in Permian – Triassic felsic volcanic (rhyolite) and sub-volcanic silicic (granite porphyry) magmas in the Song Hien structure and trachy-rhyolite – granosyenite in the Tu Le zone, and in trachyte and syenite porphyry as well as in Paleogene alkaline mafic magmas in the border between Song Da and Phan Si Pang structures.

Index

T.-H. Tran et al., *Intraplate Magmatism and Metallogeny of North Vietnam*,
Modern Approaches in Solid Earth Sciences 11,
DOI 10.1007/978-3-319-25235-3